# UC Berkeley

## UC Berkeley Electronic Theses and Dissertations

### Title

Skeletal morphology of early Homo sapiens from the Middle Awash study area, Ethiopia

### Permalink

https://escholarship.org/uc/item/4586h0xx

### Author

Brasil, Marianne F

### Publication Date

2020

Peer reviewed|Thesis/dissertation

eScholarship.org Powered by the California Digital Library
University of California

# Skeletal morphology of early *Homo sapiens* from the Middle Awash study area, Ethiopia

By

Marianne F. Brasil

A dissertation submitted in partial satisfaction of the

requirements for the degree of

Doctor of Philosophy

in

Integrative Biology

in the

Graduate Division

of the

University of California, Berkeley

Committee in charge:

Professor Leslea J. Hlusko, Chair
Professor Tim D. White
Professor Craig T. Miller

Spring 2020

Skeletal morphology of early *Homo sapiens* from the Middle Awash study area, Ethiopia

Copyright © 2020
by
Marianne F. Brasil

Abstract

Skeletal morphology of early *Homo sapiens* from the Middle Awash study area, Ethiopia

by

Marianne F. Brasil

Doctor of Philosophy in Integrative Biology

University of California, Berkeley

Professor Leslea J. Hlusko, Chair

The timing, location, and circumstances of the origin of anatomically modern humans has long been of interest, and ongoing studies continue to refine our understanding of early modern human evolution. However, research efforts are constrained by the available fossil evidence, which is predominantly comprised of geographically and chronologically disparate craniodental remains. Considering these limitations, new fossil evidence, particularly associated skeletons, is critically important to the study of modern human origins.

The Middle Awash research project has recovered a relatively complete early *Homo sapiens* partial skeleton (HAL-VP-9/1) from a Middle Stone Age archaeological context in the Halibee region of the Middle Awash study area of Ethiopia, preliminarily dated to ca. 54-106 ka. This dissertation includes the original description of the skeletal anatomy of this partial skeleton, as well as additional, more fragmentary hominid postcranial fossil material recovered from the same stratigraphic interval.

Understanding how Middle and Late Pleistocene hominid fossils relate to one another and to recent modern humans has been hindered by the sparseness of the Pleistocene fossil record, and by the variable combinations of plesiomorphic and derived traits displayed by the known fossil specimens. The chronological and geographic position of the Halibee fossils places them within a population ancestral or closely related to anatomically modern humans. These fossils therefore provide a lens through which we can examine the evolution of modern human anatomy.

The specific objectives of this dissertation include the qualitative and quantitative characterization of the skeletal anatomy of the Halibee fossils, via an assessment of the fossil morphologies relative to recent modern humans and our closest fossil relatives (particularly the Neanderthal lineage and other premodern sets of fossils). Accordingly, the Halibee fossils are described with reference to five recent modern human comparative samples and are systematically compared with fossils of Pleistocene *Homo*.

The morphologies exhibited by the Halibee fossils fall within the range of recent modern human variation in nearly all respects, albeit often near the margins of the range, but they do exceed the sampled range in a few features. The HAL-VP-9/1 partial skeleton, in particular, exceeds the sampled recent modern range in the absolute size of some elements, the sizes of articular surfaces, and the unusual proportions between the long bone ends and shaft cross-sectional sizes. Relative to other fossils of Pleistocene *Homo*, the Halibee fossils are similar to

other early modern humans (i.e., Omo I, Skhul, and Qafzeh) in most respects, but exhibit several anatomical features that are more similar to the conditions described for Neanderthals.

The results of this dissertation contribute to our understanding of how early modern human anatomy varied and evolved. The anatomies preserved by the Halibee fossils reinforce previous calls to reconsider the polarity and dichotomy of traits historically treated as diagnostically modern human or Neanderthal. The results of this study also reinforce the need for better sampling of the Late and Middle Pleistocene African fossil record to better characterize the morphology ancestral to the modern human and Neanderthal lineages.

Given the relative scarcity of associated postcranial material in the African Pleistocene fossil record, the HAL-VP-9/1 partial skeleton constitutes a notable addition to the sample available for study. The Halibee fossils contribute to an emerging image of a morphologically heterogeneous segment of the modern human lineage in the Middle and Late Pleistocene of Africa. These fossils increase the available sample size for frequency-based anatomical studies that will be important for interpreting variation in the postcranial skeleton during the Middle Pleistocene, and consequently, for clearer insight into the evolution of modern humans.

*Dedico esta dissertação à minha mãe e ao meu pai, com gratidão e amor.*

## Table of Contents

Dedication ..... i
Table of Contents ..... ii
List of Tables and Figures ..... vi
Acknowledgements ..... ix

**Chapter 1: Introduction ..... 1**
1.1 Background to the dissertation ..... 1
1.1.1 A definition for "modern human" ..... 1
1.1.2 Emergence of modern humans ..... 2
1.1.2.1 Models of modern human origins ..... 2
1.1.2.2 The Middle to Late Pleistocene fossil record ..... 5
1.1.2.3 Interpreting morphological heterogeneity ..... 7
1.1.2.4 Mode and tempo of modern human "emergence" ..... 8
1.1.2.5 Archaeological evidence ..... 9
1.1.2.6 Genetic evidence ..... 10
1.1.3 Significance of the Halibee Middle Stone Age fossils ..... 11
1.2 Organization of the dissertation ..... 12

**Chapter 2: Middle Stone Age hominid fossils from the Middle Awash study area ..... 14**
2.1 *Homo sapiens* fossils from the Middle Awash ..... 14
2.2 Geography ..... 15
2.3 History of visitation/collection ..... 16
2.4 Chronostratigraphic placement ..... 16
2.5 Archaeology ..... 17
2.6 Taxonomy ..... 17
2.7 Taphonomy ..... 18
2.7.1 HAL-VP-9/1 ..... 18
2.7.2 HAL-VP-9/1520 ..... 20
2.7.3 HAL-VP-3/15 ..... 20
2.8 Conclusions ..... 20
Table ..... 22
Figures ..... 23

**Chapter 3: Materials and methods ..... 33**
3.1 Comparative materials ..... 33
3.1.1 Recent modern human comparative samples ..... 33
3.1.1.1 Southern Africa (Zulu) ..... 33
3.1.1.2 Northeastern Africa (Egypt) ..... 33
3.1.1.3 Levant (Jordan) ..... 34
3.1.1.4 Western Europe (Portugal) ..... 34
3.1.1.5 North America (California, U.S.A.) ..... 35
3.1.2 Comparative fossil specimens ..... 35
3.1.2.1 Modern humans ..... 36
3.1.2.2 Neanderthals ..... 36

3.1.2.3 African Pleistocene....36
3.1.2.4 Asian Pleistocene....36
3.1.2.5 European Pleistocene....37
3.2 Data collection methods....37
3.2.1 Data collection from Middle Awash fossils....37
3.2.1.1 Metric and nonmetric data....38
3.2.1.2 Photography....38
3.2.1.3 Laser scans....38
3.2.1.4 Micro computed tomography scans....38
3.2.2 Comparative fossil data collection....39
3.2.3 Comparative recent modern human data collection....39
3.3 Analytical methods....40
3.4 Research questions....40
Table....42

**Chapter 4: Estimation of sex, age, stature, and mass of HAL-VP-9/1....43**
4.1 Age estimation....43
4.1.1 Cranial sutures....43
4.1.2 Pubic symphyseal surface and acetabulum....43
4.1.3 Auricular surface of the ilium....44
4.1.4 Composite age estimate....44
4.2 Sex estimation....44
4.2.1 Cranium and mandible....44
4.2.1.1 Mastoid process....45
4.2.1.2 Supraorbital margin....45
4.2.1.3 Glabellar region....45
4.2.1.4 Nuchal crest....45
4.2.1.5 Mental eminence....45
4.2.2 Pelvis....45
4.2.2.1 Greater sciatic notch....45
4.2.2.2 Subpubic angle....45
4.2.2.3 Ventral arc....46
4.2.2.4 Subpubic concavity....46
4.2.2.5 Medial aspect of the ischiopubic ramus....46
4.2.2.6 Preauricular sulcus....46
4.2.2.7 Size of acetabulum, obturator foramen, and os coxae....46
4.2.3 Composite sex estimation....46
4.3 Stature estimation....46
4.3.1 Tibial length....47
4.3.2 Additional postcranial metrics....48
4.4 Mass estimation....48
4.4.1 Femoral head....49
4.5 Summary....49
Tables....51
Figures....54

**Chapter 5: The Halibee fossils in the context of modern human variation ..... 61**
5.1 Axial skeleton ..... 61
5.1.1 Vertebrae ..... 61
5.1.2 Ribs and sternum ..... 62
5.2 Appendicular skeleton ..... 62
5.2.1 Shoulder girdle ..... 62
5.2.2 Arm ..... 62
5.2.3 Hand ..... 64
5.2.4 Pelvic girdle ..... 65
5.2.5 Leg ..... 65
5.2.6 Foot ..... 67
5.3 Body size comparisons ..... 67
5.3.1 Stature ..... 67
5.3.2 Mass ..... 68
5.4 Conclusions ..... 68
Figures ..... 70

**Chapter 6: The Halibee fossils in the context of the Pleistocene fossil record ..... 108**
6.1 Axial skeleton ..... 109
6.1.1 Vertebrae ..... 109
6.1.1.1 Cervical and thoracic ..... 109
6.1.1.2 Lumbar ..... 110
6.1.2 Ribs ..... 111
6.2 Appendicular skeleton ..... 111
6.2.1 Shoulder girdle ..... 111
6.2.1.1 Clavicle ..... 111
6.2.1.2 Scapula ..... 111
6.2.2 Arm ..... 112
6.2.2.1 Humerus ..... 112
6.2.2.2 Ulna ..... 115
6.2.2.3 Radius ..... 116
6.2.3 Hand ..... 116
6.2.3.1 Carpals ..... 116
6.2.3.2 Metacarpals ..... 117
6.2.3.3 Hand phalanges ..... 118
6.2.4 Pelvic girdle ..... 119
6.2.4.1 Sacrum ..... 119
6.2.4.2 Os coxae ..... 119
6.2.5 Leg ..... 121
6.2.5.1 Femur ..... 121
6.2.5.2 Patella ..... 122
6.2.5.3 Tibia ..... 123
6.2.5.4 Fibula ..... 124
6.2.6 Foot ..... 124
6.2.6.1 Talus ..... 124
6.2.6.2 Calcaneus ..... 125

6.2.6.3 Cuboid and navicular ..... 125
6.2.6.4 Metatarsals ..... 125
6.2.6.5 Foot phalanges ..... 127
6.3 Body size and shape comparisons ..... 127
6.3.1 Stature and mass ..... 128
6.3.2 Skeletal proportions ..... 128
6.3.3 Cortical thickness and entheseal changes ..... 129
6.4 Conclusions ..... 130
Figures ..... 132

**Chapter 7: Conclusions ..... 167**
7.1 Introduction ..... 167
7.2 Key findings ..... 167
7.3 Future directions ..... 168

References ..... 172

Appendix 1: Inventory of HAL-VP-9/1 skeletal elements ..... 199
Appendix 2: Catalog of Middle Stone Age hominid fossils with postcranial material from the Halibee Member, Dawaitoli Formation, Middle Awash study area ..... 205
Appendix 3: Brief description of salient preservation and general morphology of the hominid fossils from the Halibee Member, Dawaitoli Formation, Middle Awash study area ..... 206
Appendix 4: Comparative fossil samples with data sources ..... 249
Appendix 5: Measurements of the fossils from the Halibee Member, Dawaitoli Formation, Middle Awash study area ..... 253
Appendix 6: Definitions and sources of measurements ..... 285
Appendix 7: Measurement protocols for comparative data collection ..... 299
Appendix 8: Nonmetric observations for the HAL-VP-9/1 partial skeleton ..... 328
Appendix 9: Summary statistics for comparative modern human measurements ..... 330

## List of Tables and Figures

**Tables:**

**Chapter 2:**

**Table 2.1** Middle Stone Age hominid postcranial fossils from the Halibee Member, Dawaitoli Formation, Middle Awash study area ..... 22

**Chapter 3:**

**Table 3.1** Recent modern human comparative samples ..... 42

**Chapter 4:**

**Table 4.1** Stature estimates based on tibial length ..... 51
**Table 4.2** Stature estimates based on various postcranial measurements ..... 52
**Table 4.3** Mass estimates based on femoral head diameter ..... 53

**Chapter 7:**

**Table 7.1** Neanderthal-like features exhibited by the HAL-VP-9/1 partial skeleton ..... 171

**Figures:**

**Chapter 2:**

**Figure 2.1** Inventory of preserved anatomy on the HAL-VP-9/1 partial skeleton ..... 23
**Figure 2.2** Map of the Middle Awash study area ..... 24
**Figure 2.3** Stratigraphic placement of the partial skeletons from Halibee ..... 25
**Figure 2.4** HAL-VP-9/1 cranial vault ..... 26
**Figure 2.5** HAL-VP-9/1 mandible ..... 27
**Figure 2.6** Mandibles recovered from HAL-VP-9, Halibee Member, Dawaitoli Formation ..... 27
**Figure 2.7** HAL-VP-9/1 femoral pilaster ..... 28
**Figure 2.8** Insect damage to HAL-VP-9/1 ..... 29
**Figure 2.9** Calcium carbonate deposits on HAL-VP-9/1 ..... 30
**Figure 2.10** Examples of likely carnivore damage to HAL-VP-9/1520 ..... 31
**Figure 2.11** Examples of burning damage to HAL-VP-3/15 ..... 32

**Chapter 4:**

**Figure 4.1** HAL-VP-9/1 cranial vault sutures ..... 54
**Figure 4.2** HAL-VP-9/1 pubic symphyseal surface ..... 55
**Figure 4.3** HAL-VP-9/1 auricular surface ..... 56
**Figure 4.4** HAL-VP-9/1 mastoid processes ..... 57

**Figure 4.5** HAL-VP-9/1 greater sciatic notch....58
**Figure 4.6** HAL-VP-9/1 right os coxae....59
**Figure 4.7** Tibial length regression plot....60

**Chapter 5:**

**Figure 5.1** Bivariate plots of body dimensions for cervical vertebrae....70
**Figure 5.2** Bivariate plots of body and pedicle dimensions for cervical vertebrae....71
**Figure 5.3** Bivariate plots of body dimensions for lumbar vertebrae....72
**Figure 5.4** Distal humeral remains of HAL-VP-9/1, TAL-VP-7/36, and HAL-VP-9/1520....73
**Figure 5.5** Bivariate plots of humeral dimensions....74
**Figure 5.6** Box plots of humeral dimensions....75
**Figure 5.7** Radial heads of HAL-VP-9/1 and HAL-VP-2/16....76
**Figure 5.8** Bivariate and box plots of radial dimensions....77
**Figure 5.9** Proximal ulna of HAL-VP-9/1....78
**Figure 5.10** Bivariate and box plots of ulnar dimensions....79
**Figure 5.11** Hand of HAL-VP-9/1 in dorsal view....80
**Figure 5.12** Bivariate plots of lunate, triquetral, and trapezium dimensions....82
**Figure 5.13** Bivariate plots of capitate dimensions....83
**Figure 5.14** Bivariate plots of hamate dimensions....84
**Figure 5.15** Bivariate plots of first and second metacarpal dimensions....85
**Figure 5.16** Third metacarpal of HAL-VP-9/1....86
**Figure 5.17** Bivariate plots of third metacarpal dimensions....87
**Figure 5.18** Bivariate plots of fourth and fifth metacarpal dimensions....88
**Figure 5.19** Os coxae of HAL-VP-9/1....89
**Figure 5.20** Bivariate plots of os coxae dimensions....89
**Figure 5.21** Proximal femur of HAL-VP-9/1....90
**Figure 5.22** Bivariate plots of femoral dimensions....91
**Figure 5.23** Patellae of HAL-VP-9/1....92
**Figure 5.24** Bivariate plots of patellar dimensions....93
**Figure 5.25** Tibial remains of HAL-VP-9/1 and HAL-VP-9/1520....94
**Figure 5.26** Bivariate plots of tibial dimensions....95
**Figure 5.27** Box plots of tibial shaft dimensions....96
**Figure 5.28** Distal fibulae of HAL-VP-9/1....97
**Figure 5.29** Bivariate plots of fibular dimensions....98
**Figure 5.30** Tali of HAL-VP-9/1....99
**Figure 5.31** Bivariate plots of talar dimensions....100
**Figure 5.32** Calcanei of HAL-VP-9/1....101
**Figure 5.33** Bivariate plots of calcaneal dimensions....102
**Figure 5.34** Cuboid and navicular of HAL-VP-9/1....103
**Figure 5.35** Bivariate plots of cuboid dimensions....104

**Figure 5.36** Bivariate plots of navicular dimensions ..... 105
**Figure 5.37** Metatarsals of HAL-VP-9/1 ..... 106
**Figure 5.38** Bivariate plots of first, third, fourth, and fifth metatarsal dimensions ..... 107

**Chapter 6:**

**Figure 6.1** Cervical vertebral remains of HAL-VP-9/1 and Omo I ..... 132
**Figure 6.2** Upper thoracic vertebra of HAL-VP-9/1 ..... 133
**Figure 6.3** Lumbar vertebrae of HAL-VP-9/1 ..... 134
**Figure 6.4** Clavicular remains of HAL-VP-9/1 ..... 135
**Figure 6.5** Scapular remains of HAL-VP-9/1 ..... 136
**Figure 6.6** Proximal humeri of HAL-VP-9/1, HAL-V-9/930, and Omo I ..... 137
**Figure 6.7** Distal humeri of HAL-VP-9/1, TAL-VP-7/36, HAL-VP-9/1520, and Omo I ..... 138
**Figure 6.8** Humeral remains of HAL-VP-9/1 ..... 139
**Figure 6.9** Proximal ulnae of HAL-VP-9/1, HAL-VP-3/1, HAL-VP-9/930, HAL-VP-9/1520, and Omo I ..... 140
**Figure 6.10** Distal ulnae of HAL-VP-9/1, HAL-VP-9/930, and Omo I ..... 141
**Figure 6.11** Proximal radii of HAL-VP-9/1, HAL-VP-2/16, and Omo I ..... 142
**Figure 6.12** Distal radius of TAL-VP-7/36 ..... 143
**Figure 6.13** Trapezium of HAL-VP-9/1 ..... 144
**Figure 6.14** Hamate of HAL-VP-9/1 and Omo I ..... 145
**Figure 6.15** Lunate of HAL-VP-9/1 and Omo I ..... 146
**Figure 6.16** Triquetra of HAL-VP-9/1 ..... 147
**Figure 6.17** Capitate of HAL-VP-9/1 ..... 148
**Figure 6.18** First metacarpal head of HAL-VP-9/1 and Omo I ..... 149
**Figure 6.19** Second metacarpal base of HAL-VP-9/1 and Omo I ..... 150
**Figure 6.20** Third metacarpal of HAL-VP-9/1 and Omo I ..... 151
**Figure 6.21** Fourth metacarpal of HAL-VP-9/1 ..... 152
**Figure 6.22** Fifth metacarpal of HAL-VP-9/1 ..... 153
**Figure 6.23** Terminal hand phalanges of HAL-VP-9/1, HAL-VP-3/15, and Omo I ..... 154
**Figure 6.24** Sacral remains of HAL-VP-9/1 ..... 155
**Figure 6.25** Os coxae of HAL-VP-9/1 and Omo I ..... 156
**Figure 6.26** Femoral shaft of BOU-VP-16/100 and HAL-VP-9/1520 ..... 157
**Figure 6.27** Distal femur of HAL-VP-9/1 and Omo I ..... 158
**Figure 6.28** Left tibia of HAL-VP-9/1 and Kib 158-1a ..... 159
**Figure 6.29** Talus of HAL-VP-9/1 and Omo I ..... 160
**Figure 6.30** Navicular of HAL-VP-9/1 and Omo I ..... 161
**Figure 6.31** First metatarsal of HAL-VP-9/1 and Omo I ..... 162
**Figure 6.32** Third metatarsal base of HAL-VP-9/1 and Omo I ..... 163
**Figure 6.33** Fourth metatarsal of HAL-VP-9/1 and Omo I ..... 164
**Figure 6.34** Fifth metatarsal of HAL-VP-9/1 ..... 165
**Figure 6.35** Proximal and intermediate foot phalanges of HAL-VP-9/1 ..... 166

**Acknowledgements**

I thank my dissertation committee for their guidance and support over the course of this project. I am deeply grateful to my advisor, Leslea Hlusko, who has been unwavering in her support at every stage of my graduate career and has challenged me in the best ways possible. I owe the better part of my intellectual, professional, and personal growth over the last several years to her advice and example as my mentor. I am also deeply thankful to Tim White, without whom I would not have found human paleobiology as an undergraduate student many years ago, and would never have had the incredible opportunity to work on this project. Craig Miller deserves many thanks for his thoughtful review of previous drafts, his patience, and his advice throughout my graduate career from my qualifying exam to the completion of this dissertation.

I also thank Tony Barnosky and Tom Carlson for their guidance through my qualifying exam, and the many enjoyable conversations that preceded it and provided valuable context for pursuing this dissertation. I am also thankful to Fred Grine, Marc Meyer, Osbjorn Pearson, and Erik Trinkaus for helpful discussion in the early phases of this project.

I thank the National Museum of Ethiopia, the Authority for Research and Conservation of Cultural Heritage, and the Middle Awash research project (Berhane Asfaw, Yonas Beyene, Tim White, and Giday WoldeGabriel) for access to the Halibee fossils. I also thank Metasebia Endalamaw, Sahle Melaku, and Yared Assefa for facilitating access to the fossils at the National Museum of Ethiopia. I am grateful to the many members of the Middle Awash research project for their work in the field and the laboratory that made this study possible. I am especially thankful to Teodros GebreMedhin and Wegen Amerga for their support and friendship in the field and the lab. I also thank Gen Suwa and Tomohiko Sasaki for their time and effort in CT scanning the Halibee fossils in Addis Ababa, and for helpful discussions in the early phases of this project. Many thanks also go to the Afar people of the Middle Awash for their collaboration and contributions to the fieldwork that yielded this fossil assemblage, especially H. Elema for his support to the project and for his camaraderie in the field. I am also grateful to the Middle Awash research project leadership for the opportunity to contribute to the 2015 and 2017 field seasons and to the many project members who made my field experience especially enjoyable and memorable.

Many individuals and institutions deserve thanks for allowing access to skeletal remains in their care. Thanks to Natasha Johnson at the Phoebe A. Hearst Museum of Anthropology, Eugénia Cunha and Catarina Coelho at the Coimbra 21st Century Identified Skeletal Collection, Brendon Billings and Nicholas Bacci at the Raymond A. Dart Collection, and David Hunt at the Smithsonian's National Museum of Natural History.

I am sincerely grateful to the funding organizations that valued and supported this project. This work was partially supported by the National Science Foundation (DDRIG-1732221) and a Leakey Foundation Research Grant. The Portuguese Studies Program at UC Berkeley supported data collection at the Coimbra 21st Century Identified Skeletal Collection through a Student Research Award and provided repeated support through Pinto Fellowships. The Institute of International Studies at UC Berkeley supported an early visit to the National Museum of Ethiopia with a Pre-Dissertation Research Grant. A Summer Research Award from the Department of Integrative Biology at UC Berkeley also partially supported travel to the National Museum of Ethiopia. Paul Renne and the Berkeley Geochronology Center provided guidance and support. The John Templeton Foundation supported the final phase of writing. Lastly, I am grateful for the repeated support from the Human Evolution Research Center,

especially in the form of the Desmond Clark Graduate Fellowship that repeatedly supported travel to study the original fossils in Ethiopia.

Measurement protocol development and data collection were significantly aided by four exceptional undergraduate students, to whom I am deeply grateful. Fiona Chatterjee, John Francis, Nick Shepetuk, and Emma Thatcher were enthusiastic, careful, and thoughtful research assistants who made many hours of data collection much more enjoyable and less lonesome. Thanks also to Alyssa Case for her help with developing measurement protocols. I am thankful to each of these students for helping me grow as a mentor.

I have been very fortunate over the course of my graduate career to have been part of a supportive and stimulating lab group, and there are many members of the Hlusko Lab and the broader Human Evolution Research Center group to whom I am grateful. These include Whitney Reiner, Tara Lepore, Peter Kloess, and Ryan Yohler. Joshua Carlson has also always been generous with his encouragement and support. Catherine Taylor has been a wonderful collaborator and has become a dear friend. Special thanks go to Tesla Monson for her mentorship, patience, and friendship over the full course of my graduate career, and for the many adventures we've shared along the way.

Elizabeth Niespolo deserves special thanks for being my counterpart in the "two lady village" in the Middle Awash and for being an inspiration and a true friend. I am also grateful to Laurie Wilkie for her constant encouragement and shared enthusiasm for Portuguese history and culture.

I owe this dissertation to the example and encouragement of my parents, Antonio and Rosalia Brasil, whose work and sacrifice made this opportunity possible for me, and to whom this dissertation is dedicated. Without their example of a strong work ethic, self-discipline, and meticulous attention to detail, I would not have made it here. I am also grateful to my sisters, Dina Brasil and Delia Teixeira, for always encouraging me to take the less practical route in life, and for supporting me along the way with long trail runs, home-cooked meals, and unfailing love. Many friends deserve thanks for providing balance and for reminding me of the wonder that got me into this science in the first place: Kevin Roth, Zosha Kandel, Mahya Krause, Joh and Susy Schoeneberg, Kate Wilsterman, and Kathryn Rieck. Lastly, I cannot adequately express my gratitude to my partner, Austin Peck, for his inexhaustible patience, encouragement, and love, and for co-parenting our sweet pup, Tater, who contributed joy and calm as she slept on my feet during the final stages of writing this dissertation.

# Chapter 1: Introduction

## 1.1 Background to the dissertation

The emergence of anatomically modern humans has long been of great interest and importance to the study of human evolution, but despite improved datasets across paleontology, archaeology, and genetics, the details of our species' origins remain obscured by a sparse and geographically disparate Middle Pleistocene fossil record (Pope, McNabb, & Gamble, 2017; Rightmire, 2008; Schwartz & Tattersall, 2010). Overcoming these limitations requires increasing the samples available for study, a goal met only with the recovery, preparation, and description of original fossils.

The Middle Awash research project has recovered a relatively complete *Homo sapiens* partial skeleton from a Middle Stone Age archaeological context preliminarily dated to ca. 54-106 ka (Morgan, Renne, Taylor, & WoldeGabriel, 2009). This partial skeleton from Halibee (HAL-VP-9/1; see Appendix 1), and other more fragmentary hominid postcranial fossils from the same sedimentary package (see Appendix 2), create a unique opportunity to better understand the emergence of modern human postcranial anatomy ("hominid" here taken as all taxa on the human side of the chimp/human split). The addition of new African fossils is crucially important to advancing the rich body of research focused on the evolution of *Homo sapiens*. The geographic and chronological position of these fossils makes them especially pertinent to this field of research, as it places them within a population ancestral or closely related to more recent humans.

This chapter will provide a brief introduction to the literature pertaining to modern human origins. The quantity of literature engaged with various aspects of this field of study reflects the historical depth and intense activity that characterizes this research area. Because a comprehensive review of the massive body of literature in this field is beyond the scope of this dissertation, the review below focuses primarily on the more recent literature. Subsequent chapters will delve into the description and comparative analysis of the Middle Stone Age postcranial fossils recovered from the Middle Awash research area.

### 1.1.1 A definition for "modern human"

Explicit diagnosis is necessary prior to any discussion of *Homo sapiens* evolution. The definition set forth by Linnaeus (to "know thyself," 1758), while adequate for recognizing living humans as distinct from other extant animals, is impractical and ambiguous in the case of the fossil record. Although the present-day species definition for humans seems much more scientific, there is essentially still no agreement among researchers about what constitutes an anatomically modern human. Positions on this matter range widely with respect to how much morphological and chronological breadth *Homo sapiens* should encompass diachronically. Some researchers, following a classic multiregional concept, would go so far as to include *Homo erectus* within *Homo sapiens* (Wolpoff & Caspari, 1997), whereas others would restrict our species nomen to include only fossils that display a minimum number of derived features shared exclusively with extant humans (Tattersall & Schwartz, 2008).

A strictly cladistic classificatory scheme recognizes *Homo sapiens* as a monophyletic clade, extending back into the fossil record prior to 0.5 Ma, to the point of divergence between the Neanderthal and modern human lineages (Meyer et al., 2016). By contrast, an anatomical

approach includes in *Homo sapiens* only fossils that display derived features shared with living modern humans (Stringer, 2016). These features include curved parietals, a flexed braincase, a tall cranium, and a vertically oriented forehead, which, taken together comprise the characteristically modern human "globular braincase" (Lahr & Foley, 2016; Stringer, 2016). Additional cranial features include reduced facial size and prognathism, a canine fossa, discontinuous supraorbital tori, and a mental eminence (Stringer, 2016). Comparatively fewer postcranial features have been included in attempts to define modern human anatomy, but the few that have include a narrow trunk, slender limb bones, a short pelvis, and short superior pubic rami (Pearson, 2000; Stringer, 2016). A ventrally-placed or bisulcate sulcus on the axillary border of the scapula and a femoral pilaster are also both sometimes regarded as modern human features, but their diagnostic utility is compromised by their variable expression across modern human populations (Pearson, 2000; Trinkaus, 1976a, 1977).

Agreement on a species diagnosis, and therefore which fossils to include within *Homo sapiens*, is further complicated by the continuously varying nature of skeletal features. Skeletal traits displayed by Middle Pleistocene African fossils range between "primitive" and "derived," making discrete categorization of these fossils (particularly fragmentary ones) difficult (Stringer, 2002). A fossil may be assigned to *Homo sapiens* if it displays a certain number of modern traits, but the number of traits deemed sufficient varies according to researcher preference. For example, as mentioned above, some researchers propose encompassing fossils classified by most researchers as *Homo erectus* within *Homo sapiens*, in part because of the combination of "primitive" and "derived" features observed in Middle Pleistocene fossils across Africa and Eurasia and the perceived continuity between them (Thorne & Wolpoff, 1992). By contrast, Braüer (2008) contends that the retention of certain archaic features does not mean that a particular fossil does not belong to a "more derived" species. An even more contrasting position is that of Tattersall and Schwartz (2008), who argue that only specimens that display a strict suite of modern features should be included in *Homo sapiens.* While the latter approach is seemingly more straightforward to apply than the more moderate approach of Braüer (2008), the resulting taxonomic atomization of the modern human lineage creates unproductive boundaries (Stringer & Buck, 2014).

I employ an anatomical definition for *Homo sapiens* following Stringer (2002, 2016), including only specimens that are nearly universally considered members of *Homo sapiens* because they share a significant number of derived skeletal features with living humans. Under this definition, the earliest securely dated fossil evidence most clearly attributable to *Homo sapiens* includes Omo I, Herto, and possibly Jebel Irhoud following previous classifications (Grine, 2016; Hublin et al., 2017; Stringer, 2016). Fossils considered directly ancestral to *Homo sapiens* are treated here as chronospecies or chronosubspecies, as discussed below, pending increased resolution of the fossil record (Sahle et al., 2019b). The use of "modern humans" herein is equivalent to "anatomically modern humans," also taken here to be equivalent to *Homo sapiens*, contrary to the *sensu lato* use of the name (e.g., Bräuer, 2008). "Recent humans" is used to mean only populations from the Holocene to the present (Kidder, Jantz, & Smith, 1992).

### 1.1.2 Emergence of modern humans

#### 1.1.2.1 Models of modern human origins

Extensive attention has been paid to developing inferences about modern human evolution that can be evaluated and reviewed in light of archaeological, paleontological and genetic data (Aiello, 1993; Holliday, 1997; Lahr & Foley, 1998; Reyes-Centeno, Hubbe, Hanihara, Stringer, & Harvati, 2015; Stringer & Andrews, 1988). These inferences have helped frame hypotheses regarding the ancestral condition for our species and the details of our species' origin. They are primarily concerned with the geographical position and timing of events during later human evolution. Such inferences or "models" can be conceptualized as fitting into three main groups. The two original, and somewhat diametrically opposed models are the recent African origin and multiregional models (Stringer & Andrews, 1988; Wolpoff, 1989). Between these is a group of intermediate models, including the assimilation model and the hybridization and replacement model. These intermediate models differ primarily in the extent to which interbreeding is allowed between expanding modern human populations and the non-modern populations they encountered (Stringer, 2014). Each of these models is described below, followed by a discussion of which is best supported by the available evidence.

The recent African origin model posits that modern humans evolved in Africa ca. 100-200 ka and then expanded their geographic range beyond Africa between 30-100 ka, replacing local populations as they expanded, with little to no interbreeding with the hominid populations already living across Africa and Eurasia (Cann, Stoneking, & Wilson, 1987; Stringer, 2002; Stringer & Andrews, 1988). This model has gone by several names, including 'out of Africa' and 'African replacement' (Stringer, 2001, 2014). The model predicts that modern morphology should be first observed in Africa, and that the gradual evolution from premodern to modern forms should be observed only in the African fossil record. These grades of evolution should not be observed outside of Africa, where modern morphology is expected to appear abruptly in the fossil record as modern humans replaced the non-modern local populations as they expanded their geographic range (Stringer & Andrews, 1988). The single recent origin model is similar in most details, differing only in that it does not require that Africa be the location of earliest modern human evolution. Some have suggested that Levantine fossils (i.e., Skhul and Qafzeh) make likely ancestors to modern humans on the basis of morphological similarities (Stringer, 1992; Waddle, 1994).

By contrast, under the multiregional model, Africa is not seen as central to modern human evolution. Instead, modern humans are proposed to have evolved across a much broader geographic region that encompasses Africa, Europe, and Asia. According to this model, interbreeding populations gradually coalesced toward modern human morphology across the Old World (Wolpoff, 1989). The predictions of this model differ from those of recent African origin in that intermediate forms, spanning premodern to modern morphologies, should be observed across all regions of the Old World at approximately the same time, allowing for minor regional variations in the appearance timing of modern morphology (Stringer, 2001).

The assimilation model accepts an African origin for modern humans, but emphasizes gene flow and selection as key processes, instead of replacement (Aiello, 1993; Smith, Falsetti, & Donnelly, 1989). Genes underlying modern human morphology were passed into Europe and Asia via interbreeding, and subsequently rose in frequency as the result of directional selection (Aiello, 1993). As a result, morphological continuity should be observed through time across regions outside of Africa (Smith, 2002). This model can approximate either the recent African origin or multiregional models, depending on the extent of interbreeding between modern and non-modern populations. In a version tending toward the multiregional model, modern human features are seen as having been assimilated into non-modern populations, whereas in the version

tending toward recent African origin, non-modern features were assimilated into expanding modern human populations (Stringer, 2014).

The latter version of the assimilation model, in which non-modern features were assimilated into modern human populations, is essentially equivalent to the recent African origin with hybridization model. This model, also known as the hybridization and replacement model, is a variant of the recent African origin model that allows a small degree of interbreeding between expanding modern human populations and the non-modern populations they encountered (Stringer, 2002). This model is essentially equivalent to Bräuer's 'Afro-European *sapiens*' model (1984a, 1984b), but with additional emphasis on hybridization (Smith, 2002). Under this model, modern humans expanded beyond Africa and largely replaced groups they encountered, but with some interbreeding. This model is seen as consistent with the perceived continuity in cranial morphology across fossils from Africa, Europe, and Asia (Bräuer, 1984a, 1984b).

In light of new genetic and fossil data, models of human origins have been modified since their first formulations (Stringer, 2014). Whereas the recent African origin hypothesis originally specified little to no hybridization, this paradigm has been updated to allow for larger degrees of admixture following evidence of interbreeding between modern human and non-modern groups, including Neanderthals (Sánchez-Quinto & Lalueza-Fox, 2015; Skoglund & Mathieson, 2018; Wolf & Akey, 2018). With this evidence of interbreeding between modern human and "archaic" populations outside of Africa, the multiregional model was reassessed (Disotell, 2012; Stringer, 2014). In a strict sense, a model that allows admixture between non-modern groups in Eurasia and modern groups expanding beyond Africa can be classified as a multiregional model (Relethford, 2001; Wolpoff, 2002). However, following this logic extends the category of multiregional model to include vastly different degrees of gene flow.

Recent African origin is a more appropriate classification for models that emphasize an African origin for modern humans followed by range expansion, allowing for some admixture (Weaver, 2012). Because the amount of introgression is small and the fossil evidence does not evince morphological continuity outside of Africa as is expected under the multiregional model, the available data taken together support a version of the recent African origin model (Stringer, 2014), perhaps the recent African origin with hybridization model, or possibly even the latter version of the assimilation model described above. Stringer (2014) considers a situation with a modest degree of "archaic" assimilation into modern humans to be more appropriately considered as "mostly out of Africa", which he classifies as a version of recent African origin. It is worth noting, however, that the evolutionary dynamics were not necessarily the same across all regions of Africa and Eurasia, but may well have entailed components of the different models depending on the local circumstances. The semantics of which specific model is considered the most appropriate is secondary to the general consensus that the evidence supports a recent African origin with a small degree of interbreeding between modern humans expanding beyond Africa and the non-modern populations they encountered (Henn, Cavalli-Sforza, & Feldman, 2012; Stringer, 2014).

Inherent to many of these models is the primary question: where did modern humans evolve? Since there is now general consensus that some version of the recent African origin model best fits the available evidence for modern human evolution, attention has turned to developing and testing models for modern human evolution that are focused on dynamics within the African continent (Henn, Steele, & Weaver, 2018). One such model is African multiregionalism, in which populations across Africa are connected during the evolution of early

modern humans. This model is argued to be more consistent with the fossil and archaeological records, which evince modern anatomical features and archaeological innovations across the continent between ca. 100-300 ka (Gunz et al., 2009; Hublin et al., 2017; Lahr & Foley, 1998; McBrearty & Brooks, 2000; Scerri et al., 2018).

The second and third are variants of a single origin range expansion model (i.e., a recent African origin model, but restricted to a single region of Africa). Under the single origin range expansion with local extinctions model, a single population of modern humans expands across Africa and replaces all other populations (Chan et al., 2019; Henn et al., 2011). By contrast, under the single origin range expansion with regional persistence model, there is limited gene flow between the source population of modern humans and populations in other regions of Africa. Lastly, the archaic "hominin" admixture in Africa model includes admixture with more distantly-related populations of *Homo*, having diverged prior to 500 ka. Each of these models makes specific predictions that can be tested with data from genetics, archaeology, and the fossil record, and the integration of data from these disciplines will be critical to revealing which of these models best characterizes the evolutionary history of early *Homo sapiens* within the African continent (Henn et al., 2018). I now turn to a discussion of what the paleontological record currently entails.

#### 1.1.2.2 The Middle to Late Pleistocene fossil record

The earliest securely-dated specimens that are nearly universally classified as *Homo sapiens* are from ca. 200-150 ka in eastern Africa (Aubert et al., 2012; Brown, McDougall, & Fleagle, 2012; Clark et al., 2003; Fleagle, Assefa, Brown, & Shea, 2008; McDougall, Brown, & Fleagle, 2008; Sahle et al., 2019a; Sahle et al., 2019b; White et al., 2003) and, arguably, ca. 315 ka in northern Africa (Hublin et al., 2017; Richter et al., 2017; but see Sahle et al., 2019b). These fossils are recognized as modern human on the basis of derived morphological features shared with extant humans, despite variably displaying primitive features. The mix of primitive and derived features displayed by these fossils has led to their perception as constituting a morphological bridge between earlier "archaic" fossils and later modern humans (Hublin et al., 2017; White et al., 2003). This time period between ca. 200-60 ka in the African hominid (and indeed, faunal) fossil record is characterized by a large degree of morphological variation encompassing archaic and derived features, not only in these eastern and northern African fossils, but particularly in those from southern Africa and the adjacent Near East (Harvati et al., 2011; Pearson & Grine, 1997; Trinkaus, 2005).

Whereas the fossil record suggests that modern humans evolved in Africa, the patterns and processes of this evolutionary history are much more elusive. This is in large part because interpreting variation in the Middle Pleistocene African fossil record remains a complicated and contentious endeavor. This difficulty arises mostly from the unfortunate facts that the fossil evidence preceding modern humans is particularly sparse and the dating nearly universally inadequate (Grine, 2016; Lahr & Foley, 2016; Sahle et al., 2019b). Despite the limited fossil evidence, the dominant paradigm that has emerged is that of a single human lineage, with stages of evolution leading to anatomically modern humans (Grine, 2016). This lineage is often divided into a group of earlier fossils (ca. 700-400 ka, e.g., Bodo and Saldanha), intermediate fossils (ca. 400-200, e.g., Florisbad and Eliye Springs), and a group attributed to *Homo sapiens* (ca. 200-100 ka, e.g., Herto, Omo I, Skhul, and Qafzeh). There is general consensus about the overarching pattern as trending toward enlarged brains and anatomical features that more closely approximate

recent human morphology, but there is far less agreement about the specific details of the evolutionary process. Different phylogenetic interpretations and taxonomic schemes among researchers have resulted in differences in the names of these different "grades" or "stages" and the fossils assigned to each.

Some researchers propose that all hominids chronologically intermediate to *Homo erectus* and *Homo sapiens*, including both African and Eurasian fossils, should be recognized as a single group, which is ancestral to both *Homo sapiens* and *Homo neanderthalensis* (Endicott, Ho, & Stringer, 2010; Rightmire, 1996, 2009; Stringer, 2002). This scheme therefore recognizes a single widespread population in the Middle Pleistocene, and is invoked to explain similarities between penecontemporaneous African (e.g., Bodo and Kabwe) and European (e.g., Ceprano and Petralona) fossils (Rightmire, 1998; Stringer, 2012). This widespread population is called *Homo heidelbergensis* if it is taken to also include the holotype Mauer mandible, or *Homo rhodesiensis* by those who do not (Stringer, 2012). Others propose an earlier divergence between distinct African and European lineages, recognizing *Homo rhodesiensis* as an exclusively African taxon ancestral to modern humans, and *Homo heidelbergensis* as a chronospecies of the Neanderthal lineage in Europe (Carretero, Haile-Selassie, Rodriguez, & Arsuaga, 2009; Hublin, 2009; Manzi, 2004).

Some researchers have advocated recognizing a segment of the lineage (ca. 200-300 ka) between *Homo heidelbergensis* sensu lato and *Homo sapiens* as a separate chronospecies, *Homo helmei*, which is proposed to be ancestral to both *Homo sapiens* and *Homo neanderthalensis* (Foley & Lahr, 1997; Lahr & Foley, 2001). However, recent divergence timing estimates for the Neanderthal and modern human lineages at ca. 520-765 make this phylogenetic hypothesis untenable (Meyer et al., 2016; 2017; Prüfer et al., 2014). All of these taxonomic schemes and phylogenetic hypotheses infer that evolution by cladogenesis was the mode by which modern humans and Neanderthals arose, with a Middle Pleistocene species splitting and giving rise to the two species lineages. *Homo antecessor* from ca. 800 ka in Atapuerca, Spain has been proposed as the last common ancestor of the Neanderthal and modern human lineages, shifting the last common ancestor to Europe (Arsuaga et al., 1999b; Bermúdez de Castro et al., 1997; 2004). Subsequent studies failed to support this phylogenetic and taxonomic hypothesis, leading some to question the validity of *Homo antecessor* (Bräuer, 2008), but additional fossil material has prompted a reconsideration of the taxon's validity and phylogenetic placement (Bermúdez de Castro, Martinón-Torres, Arsuaga, & Carbonell, 2017; Martinón-Torres et al., 2019).

An alternative to classifying these pre-modern fossils as a taxon distinct from modern humans (i.e., *H. heidelbergensis* and/or *H. rhodesiensis*) has been proposed by Braüer (2008, 2012), who divides them into "grades" of *H. sapiens* that correspond to segments along a single evolving lineage. Under this scheme, three grades of *Homo sapiens* are recognized as approximately diachronic segments of a single lineage, grouped according to similarity in a set of anatomical criteria (Bräuer, 2008). Following "developed *Homo erectus*" is "early archaic *Homo sapiens*," then "late archaic *Homo sapiens*" (or "pre-modern"), and lastly, "anatomically modern *Homo sapiens.*" This scheme is intended as a means of describing the phyletic and mosaic evolution of modern morphology, or "modernization," by which modern traits are seen to accumulate over the modern human lineage's evolutionary course (Bräuer, 2008).

The introduction of these terms, however, has produced further confusion to the definition of the species, especially in light of earlier, even less precise uses of "archaic" as a descriptor for a stage of *H. sapiens* evolution (Stringer, Howell, & Melentis, 1979). This issue is even more apparent when we consider the more recent variable use of "archaic," with some

using "archaic *Homo sapiens*" to refer only to the fossils included in Braüer's "late archaic" grade (Stringer, 2002). These names reflect an effort to recognize and describe a largely phyletic evolution of the modern human lineage, but it remains unclear whether these "grades" are meaningful in terms of paleobiological differences between what are perhaps more appropriately characterized as paleodemes (Howell, 1999) or even chronospecies (Sahle et al., 2019b; White et al., 2003). As Bräuer (2008) himself notes, paleodemes, a useful classification device that groups fossils into spatially and temporally bounded groups below the species level (Howell, 1999), are consistent with his suggested sequence. While the proposed grades serve to shift the focus away from a typological approach on individual specimens, the expanded breadth of *Homo sapiens* and introduction of various degrees of "archaic" as a means of classification have unfortunately produced the unintended consequences of confusion and imprecise communication.

In contrast to the scheme above (in which specimens that span over half a million years of the fossil record are subsumed into *Homo sapiens*), other researchers are far more restrictive in their use of the species name. According to this restrictive diagnosis, a fossil must share a particular set of morphological features and is only permitted to lack one or two in order to still be included in *Homo sapiens* (Tattersall & Schwartz, 2008). This interpretation of the variation evinced by the fossil record has led these researchers to claim that repeated occurrences of speciation must have characterized the Pleistocene (Tattersall & Schwartz, 2008).

It is clear that the field is far from agreeing on a taxonomic classification or phylogenetic framework for Middle Pleistocene fossils. The state of this issue is aptly summarized by Braüer (2008, p. 34): "…how to define species and how many species or morphs… appears to be largely subjective." Key to this apparent subjectivity is the wide range of opinions researchers have as to how morphological variation should be interpreted. Consequently, I now turn to the topic of morphological heterogeneity.

#### 1.1.2.3 Interpreting morphological heterogeneity

The sparse and geographically scattered nature of the fossil record and the poor chronometric control of Middle and Late Pleistocene African fossils pose significant challenges to interpreting the fossil evidence for modern human evolution, and to revealing what we increasingly perceive to be a spatially and temporally complex evolutionary history (Grine, 2016; Lahr & Foley, 2016; Millard, 2008). The evidence from the African Pleistocene record is limited, with only approximately 50 sites known from between 200-10 ka. Only half of these have so far yielded postcranial fossils (Grine, 2016).

The available evidence suggests a pattern of cranial and postcranial morphological evolution characterized by considerable morphological heterogeneity (Carretero et al., 2009; Pearson, Fleagle, Grine, & Royer, 2008a; Pearson & Grine, 1997). The combination of plesiomorphic and derived traits has made interpreting the limited available fossil evidence difficult (Bräuer, 2008; Pearson, 2000). There are multiple interpretations as to why some contemporaneous specimens have archaic morphologies and others derived, and why some individual specimens have both primitive and derived features. This combination of features has been interpreted as indicating either the existence of multiple morphologically distinct groups across Africa, or the existence of one highly-variable population (Lahr & Foley, 2016). In the former interpretation, there was overlap in time between morphologically distinct archaic and modern groups as archaic groups persisted alongside their modern relatives, with possible admixture among them (Bräuer, 1992), or with eventual replacement of the archaic population

by the modern one (Stringer & Andrews, 1988). Alternatively, populations on a lineage between archaic and derived populations may have had a mosaic distribution of morphologies, as is expected in an evolving lineage (Smith et al., 1989). The combination of archaic and derived morphologies in the Late Pleistocene record has been posited to be the result of admixture between archaic and derived populations. Genetic studies of modern Africans have suggested archaic admixture (Hammer, Woerner, Mendez, Watkins, & Wall, 2011; Lachance et al., 2012) and have been invoked as evidence supporting that hypothesis (Harvati et al., 2011). However, the combination is more parsimoniously explained as reflecting polymorphism in these populations, with the combination of plesiomorphic and derived alleles resulting in increased phenotypic variability (Grine, 2016).

Features usually attributed to Neanderthals have been identified in *Homo sapiens* fossils such as those from Skhul, Qafzeh (McCown & Keith, 1939; Vandermeersch, 1981), and Omo I (Pearson et al., 2008a). The different combinations of features distinguishing African and Levantine Pleistocene samples from recent humans, and the presence of "Neanderthal traits" among early *Homo sapiens* and earlier taxa suggest considerable anatomical variation in these groups (Carretero et al., 2009). These findings have forcefully raised the possibility that the "Neanderthal traits" in Eurasian early modern humans may have been ancestral retentions rather than traits derived in the Neanderthal lineage (Bermúdez de Castro et al., 2012; Pearson et al., 2008a). This contrasts with a more traditionally accepted view that the ancestor of modern humans and Neanderthals lacked the derived features seen in the descendant taxa, and suggests that an ancestral population may have had a combination of these archaic and derived traits that were then differentially passed onto their descendants (Stringer, 2016).

Ancient DNA studies have indicated several episodes of introgression between modern human, Neanderthal, and Denisovan lineages (Green et al., 2010; Prüfer et al., 2014; Reich et al., 2010) and the results of these studies have influenced interpretations of archaic morphology observed in fossil and modern humans (e.g., Bailey, Hublin, & Antón, 2019, but see also Scott, Irish, & Martinón-Torres, 2020). The mixture of archaic and derived features observed in early modern humans in Europe and Africa has been interpreted as the result of admixture between modern and archaic human groups (Trinkaus, 2005), or as reflecting deep population substructure (Crevecoeur, Brooks, Ribot, Cornelissen, & Semal, 2016; Harvati et al., 2011). However, it is also possible that these archaic polymorphisms have not yet been sampled by our limited early modern human fossil sample from eastern Africa, such that the actual ancestral variation remains unknown. Parsing how much of this archaic morphology is the result of inheritance from a modern human ancestor and how much is the result of admixture will remain unresolved until the ancestral population is better sampled.

#### 1.1.2.4 Mode and tempo of modern human "emergence"

The evolution leading to modern humans is often either inferred to have been lengthy, occurring over several hundreds of thousands of years following divergence from the lineage that eventually led to Neanderthals, or one characterized by a discrete event ca. 200 ka, when we generally recognize modern humans in the fossil record (Weaver, 2012). A consensus emerging from the available fossil and genetic evidence is that a discrete event ca. 200 ka produced modern humans (Weaver, 2012). In the case of the genetic evidence, the coalescence estimate for mitochondrial DNA haplotypes in living humans is ca. 200 ka (Behar et al., 2008; Cann et al., 1987; Ingman, Kaessmann, Pääbo, & Gyllensten, 2000). However, this coalescence estimate

need not correspond to the origin of modern human anatomies, and there is no reason to expect that it did (Weaver, 2012).

The earliest fossil evidence generally classified as anatomically modern human appears near this time (i.e., Herto and Omo I), with mosaics of primitive and derived features observed in the earlier fossils (Bräuer, 2008; Stringer, 2016). The manner in which observed anatomical variation is interpreted and parsed patterns our perception of how evolution proceeded. Was emergence via a discrete event (i.e., punctuated event) in the evolution of modern humans, or through a longer period of gradual transition that occurred over several hundreds of thousands of years (Weaver, 2012)? In the case of the Neanderthal lineage it is generally agreed that features have accumulated in a mosaic pattern (Hublin, 2009; Stringer, 2002). The disagreement about the pattern of late human evolution may be at least in part due to the poorer nature of the African relative to the European record (Weaver, 2012). Further testing these two hypothetical modes of evolution (i.e., discrete event or gradual shift) will be satisfactory only when the sparse nature of the African fossil record is improved (Rightmire, 2009).

But even an improved record cannot fix the problem that classificatory systems are static and discontinuous, whereas evolution is dynamic and continuous. The nature of the evolutionary process is inconsistent with the use of common terms such as "origins" and "emergence," which are misleading in that they imply a discrete transition from one thing to another. As the fossil record becomes increasingly populated and geographic and chronological gaps are filled, it is certain that we will increasingly have to contend with the issue that "Origins disappear in continuity" (Foley, Martin, Lahr, & Stringer, 2016, p. 1). This makes the focus on claims of the "earliest" evidence of modern humans (Fleagle et al., 2008; Groucutt et al., 2018; Hershkovitz et al., 2018; Hublin et al., 2017; Liu et al., 2015) a distraction from more meaningful questions about evolutionary process and products (Sahle et al., 2019b).

#### 1.1.2.5 Archaeological evidence

Fossil evidence of the emergence of modern human anatomy is often evaluated relative to the emergence of modern human behavior, or "behavioral modernity" (Henshilwood et al., 2003; McBrearty & Brooks, 2000). This evaluation, however, is made difficult by the disagreement surrounding which set of behaviors are uniquely and "fully" modern, because different researchers prioritize different elements of behavior (Henshilwood et al., 2003; Nowell, 2010). The discussion about the mode and pace of the emergence of "behavioral modernity" is similar to the discussion concerned with the fossil evidence. Some have claimed that human behavior only arose ca. 40-50 ka near the Middle to Upper Paleolithic transition, and that this behavior appears rapidly (Klein, 2000), whereas others maintain that indicators of this behavior are preserved in the record much earlier and accrued in a more gradual and piecewise fashion, perhaps as early as ca. 300 ka (Brooks et al., 2018; McBrearty & Brooks, 2000). It remains unclear whether the change to "behavioral modernity" was abrupt and geographically restricted, or gradual and broadly distributed (Marean, 2015).

The perceived non-synchronous appearance of behavioral and anatomical modernity has led some researchers to conclude that anatomical and behavioral evidence should be decoupled, and that they do not necessarily correspond (Nowell, 2010; Tattersall, 2009). This suggestion makes sense considering that the evolution of technology and organisms should not be treated as the same, and that there is no reason that the definitions for behavioral and anatomical modernity should correspond. Indeed, integrating evidence across genetics, archaeology, and paleontology

is difficult because definitions of modernity do not necessarily match and the data across these disciplines likely often sample different populations and may therefore yield different results (Henn et al., 2018).

The origin of modern humans has been broadly linked to the appearance, in the Middle Pleistocene, of archaeological assemblages referred to as Middle Stone Age (MSA, McBrearty & Brooks, 2000). However, the MSA appears at different times in different places. The oldest MSA predates the earliest known modern humans, and there is no single point in time when the MSA appears and the Acheulean disappears (Clark, 1988; Morgan & Renne, 2008; Sahle et al., 2019b). The traditional model outlining three discrete technological phases (Early, Middle, and Late Stone Ages) with clear boundaries between each is not supported by the behavioral evidence, which demonstrates overlap between these "technologies" and a spatially and temporally complex "transition" between them (e.g., Blegen, Jicha, & McBrearty, 2018; Clark et al., 2003). Despite the evidence otherwise, some researchers still advance the notion of a transition from one to another "technology", with the Middle Stone Age replacing the Acheulean over a discrete period between ca. 300-500 ka (e.g., Brooks et al., 2018; Deino et al., 2018). Furthermore, these typological units (i.e., Acheulean and Middle Stone Age) do not appear to correspond to the appearance (or disappearance) of any specific hominid (Blegen et al., 2018). This evidence calls into question the practice of attributing particular "technologies" to hominid species and using behavioral evidence as a proxy for their presence (Armitage et al., 2011). In a similar vein, the lack of correspondence between typological units and hominid taxa makes including associated "technologies" in taxonomic definitions particularly problematic (e.g., *H. helmei* and "mode 3", Lahr & Foley, 1998).

#### 1.1.2.6 Genetic evidence

Genetic data from living humans and Middle and Late Pleistocene fossils have been applied to several questions regarding early modern human evolution, including inferences about the geographic origin of *Homo sapiens*, estimations of the timing of the coalescence of modern human lineages, and estimates of the divergence age between *Homo sapiens* and Neanderthals. The fields of modern human population genetics and ancient DNA have grown rapidly in the last few decades, and are producing and reporting data at a seemingly accelerating rate. Here I provide a very cursory overview of the research focused on the questions outlined above. Several recent review papers provide much more comprehensive overviews of the historical and recent progress across genetic studies focused on human evolution (e.g., Beltrame, Rubel, & Tishkoff, 2016; Llamas, Willerslev, & Orlando, 2017; Nielsen et al., 2017; Schlebusch & Jakobsson, 2018; Skoglund & Mathieson, 2018).

Genetic data have repeatedly supported a recent African origin for modern humans (Underhill et al., 2001; but see also Árnason, 2016; 2017; Behar et al., 2008; Cann et al., 1987; Gonder, Mortensen, Reed, de Sousa, & Tishkoff, 2006; Henn et al., 2011; Ingman et al., 2000; Li et al., 2008; Salas et al., 2002; Tishkoff et al., 2009). Initial studies consistently inferred an African origin for *Homo sapiens* (Cann et al., 1987; Ingman et al., 2000). More recent studies suggest a complex evolutionary scenario that involved multiple regions of Africa (Schlebusch et al., 2012; 2017) or a southern African origin (Chan et al., 2019; Henn et al., 2011). The southern African distribution of modern populations with genetic signatures of the deepest divergence has been taken as evidence supporting a southern African origin for modern humans (Grine, 2016), but this assumes that these populations have not moved in over 100 ka (Lahr & Foley, 2016). It

has been noted that this inference may be biased by sparse sampling across Africa and the spatial distribution of the few surviving hunter-gatherer populations (Henn et al., 2011; Lahr & Foley, 2016). The general consensus is that human anatomical and behavioral and genetic emergence largely occurred within the African continent, and future studies will likely clarify where, when, and how (Henn et al., 2018; Schlebusch & Jakobsson, 2018).

Mitochondrial DNA and Y-chromosome data point to a coalescence of all extant human lineages to the most recent common ancestor sometime between 200 and 80 ka, with Y-chromosome-based analyses typically pointing to a younger coalescence (Behar et al., 2008; Cann et al., 1987; Garrigan & Hammer, 2006; Gonder et al., 2006; Underhill et al., 2000). This does not necessarily correspond to the origin of modern humans (Weaver, 2012), but provides an upper limit on modern human population divergence, and has been taken to indicate that prior to this coalescence there existed a common ancestral population (Grine, 2016).

Newly-recovered genetic evidence from the Neanderthal fossil record has permitted estimation of the divergence date between the Neanderthal and modern human lineages. Estimates based on mitochondrial genomes from five dated Neanderthals initially suggested a divergence ca. 410-440 (Endicott et al., 2010). A more recent estimate based on nuclear DNA from Sima de los Huesos, Spain, dated to ca. 430 ka, places the divergence between ca. 550-765 ka (Meyer et al., 2016). This estimate is in agreement with those derived from more recent (ca. 50 ka) high-coverage Neanderthal genomes from Denisova Cave, Russia, and Vindija Cave, Croatia, which are ca. 550-765 ka and ca. 520-630 ka, respectively (Prüfer et al., 2014; 2017). These more recent estimates taken together suggest that the divergence between the modern human and Neanderthal lineages occurred between ca. 520-765 ka.

### 1.1.3 Significance of the Halibee Middle Stone Age fossils

Improvements in many aspects of our understanding of human origins and evolution rely on the fossil record, as described above. This primary description of the Halibee postcranial remains from the Middle Awash study area contributes new data for broader studies. The significance of these fossil remains can be well appreciated in the words of senior colleagues working on the emergence of *Homo sapiens*, who have made calls for the acquisition and publication of additional original fossil material:

> *"The state of adequate published paleontological description of most early modern human and many late archaic human fossils, even for the time periods in which they were discovered, is pathetic. A concerted effort needs to be made to integrate fully the morphology and paleobiology of the known sample into the field."* (Trinkaus, 2005, p. 222)

> *"More fossils are needed, particularly postcranial remains of Middle and early Late Pleistocene African hominids."* (Carretero et al., 2009, p. 29)

The human skeletal remains described in this dissertation represent one answer to this call. These fossils improve the resolution of when and where aspects of modern human anatomy evolved, and enable the reassessment of the polarity of traits that have historically been treated as Neanderthal apomorphies. Because these fossils fit chronologically between early modern humans in eastern Africa (i.e., Herto and Omo I) and recent humans, they stand to contribute to

our knowledge of morphological evolution between this early ancestral population and recent African populations. These early modern African fossils, as an expanding sample, are robust relative to living people, and it is not until ca. 35 ka that the gracile morphology more closely resembling living people emerges (Rightmire 2009; Grine 2016). The state of our understanding of this process is well-summarized as follows:

> *"We think we know that our species emerged somewhere in sub-Saharan Africa close to 200 ka, and we know something about the people and their archaeological traditions in the Holocene, but the mechanisms and processes that were involved over the past two hundred millennia are frustratingly opaque.*"
> (Grine, 2016, pp. 363-364)

Increased resolution of the fossil record is necessary to reveal these mechanisms and processes. The fossils described here accordingly contribute additional data from a crucial time period and place.

### 1.2 Organization of the dissertation

The framework for this dissertation is as follows. Chapter Two provides an introduction to the fossils recovered from the Halibee Member of the Upper Dawaitoli Formation, in the Middle Awash study area, described herein for the first time. This introduction reviews the Middle and Late Pleistocene evidence from the study area to provide context for the description of these new fossils. It introduces the fossils, and outlines the history of recovery as well as their geographic and chronostratigraphic positions. The archaeological context, taxonomic classification, and notable taphonomic features are also reported. Chapter Three presents the comparative materials used in the analysis, including the five recent modern human samples and fossil specimens. The latter are primarily organized according to geographic region and time. Data collection methods are described, including those relevant to both the Middle Awash fossils and the comparative materials. The analytical methods employed in this study are also described, followed by a discussion of the research questions that the fossils are poised to address. Chapter Four details the individual characteristics of the HAL-VP-9/1 partial skeleton, including estimation of age, sex, stature, and mass. The following two chapters are dedicated to systematic anatomical comparisons with closely related groups, whereby the evolutionary significance of the Halibee fossils is assessed. Chapters Five and Six evaluate the Halibee fossils in the context of modern human variation and the Middle to Late Pleistocene fossil record, respectively. In the final chapter I review the results of this study and discuss their bearing on current hypotheses about modern human evolution. I conclude by reviewing questions arising from the results and outlining future research directions.

Detailed morphological description and comparative study of the craniodental fossils from Halibee and other Middle Stone Age deposits within the Middle Awash study area will be published elsewhere. The craniodental fossils are described briefly in Chapters Two and Four, with respect to taxonomic classification and estimation of age and sex of associated postcranial remains. The fossils described comprehensively herein will be restricted to the postcranial elements. In the chapters that follow, the Halibee partial skeleton (HAL-VP-9/1) will be treated first, followed by the other individuals where applicable. The descriptions included in the text of Chapters Five and Six will be comparative in nature, and will focus on functionally and/or

evolutionarily informative aspects of the skeletal anatomy. Preservational descriptions are included in Appendix Three and will be referenced where relevant. Measurements of the Halibee fossils will be reported in tabular or figure format as part of quantitative comparisons with modern humans and fossil specimens in Chapters Five and Six, respectively. Appendices Five and Eight will be referenced for additional measurements and observations not included in the text of the chapters.

## Chapter 2: Middle Stone Age hominid fossils from the Middle Awash study area

### 2.1 *Homo sapiens* fossils from the Middle Awash

Advancement in our understanding of the emergence of anatomically modern humans has been hindered by a sparse and geographically scattered Middle and Late Pleistocene African fossil record, particularly between ca. 300-50 ka. The often fragmentary and isolated elements available provide a glimpse of regionally-patterned morphological variation. But making sense of these regional patterns and the evolutionary processes they reflect is made especially difficult by the poorly-chronologically constrained nature of the fossil record (Grine, 2016; Lahr & Foley, 2016; Pearson, 2000; Trinkaus, 2005). Regardless, it is clear that both the archaeological and fossil evidence increasingly suggest a spatially and temporally complex 'transition' to anatomical modernity (see Chapter 1).

Evidence from the Middle Awash study area in Ethiopia has contributed significantly to this anatomical and behavioral record by providing chronologically-constrained fossils representing critical points in hominid evolution. Segments of what appears to be an evolving lineage culminating in anatomically modern humans have been sampled at 1.0 Ma at Daka (Asfaw et al., 2002; de Heinzelin, Clark, Schick, & Gilbert, 2000; Gilbert & Asfaw, 2008), 600 ka at Bodo (Asfaw, 1983; Carretero et al., 2009; Clark et al., 1994; Conroy, Jolly, Cramer, & Kalb, 1978; de Heinzelin et al., 2000; White, 1986), 154-160 ka at Herto (Clark et al., 2003; White et al., 2003), and ca. 80-100 ka at Aduma (Haile-Selassie, Asfaw, & White, 2004; Yellen et al., 2005). In particular, the chronological and geographic positions of Herto and Aduma make them central to studies of early modern human evolution in the late Middle and Late Pleistocene, and the associated archaeological assemblages contribute to our understanding of the behavioral contexts in which this evolution took place (Clark et al., 2003).

The fossil evidence from Herto includes one immature and two adult crania, all securely dated to between 160 ± 2 ka and 154 ± 7 ka (Clark et al., 2003, Sahle et al., 2019). The Herto fossils are intermediate in morphology and chronology to anatomically modern Late Pleistocene humans (e.g., Klasies River Mouth and Qafzeh), and pre-modern Middle Pleistocene African fossils (e.g., Bodo and Kabwe). They are very likely ancestral to anatomically modern humans, as they appear to sample a portion of the lineage intermediate to *Homo rhodesiensis* and later *Homo sapiens* (White et al., 2003). Because of the differences between the Herto fossils and a set of other penecontemporary fossil hominids, and their position just beyond the range of variation observed in extant human populations, the Herto hominids were assigned the chronosubspecies name *Homo sapiens idaltu* (White et al., 2003). The Herto fossils are associated with archaeological assemblages that contain elements of both Acheulean and MSA technocomplexes, and they display evidence of post-mortem mortuary practice (Clark et al., 2003). The Herto fossils and their associated behavioral evidence lend strong support to an African origin for modern humans (White et al., 2003).

The evidence from Aduma includes portions of four hominid crania, one of which is considerably more complete than the others (Haile-Selassie et al., 2004). These remains from Aduma are the youngest hominid fossils yet recovered from the sedimentary succession in the Middle Awash study area. Dates derived from multiple techniques yielded inconsistent results, but the majority of the results lie between 79-105 ka (Haile-Selassie et al., 2004). The archaeological evidence suggests a later stage of the Middle Stone Age for most of the Aduma occurrences (Yellen et al., 2005). The Aduma hominid remains contribute to the fossil and

archaeological records at a poorly sampled but critical time and place. Similar to the pattern observed in the Herto fossils, the Aduma cranium displays a combination of pre-modern and modern features. The Aduma cranium most closely resembles ca. 100-300 ka specimens from Africa and the Middle East (e.g., Omo I, Skhul, and Qafzeh) and is therefore interpreted as sampling a portion of the modern human lineage subsequent to that sampled by the Herto fossils (Haile-Selassie et al., 2004).

As with the evidence from Herto and Aduma, the geographic and chronological position of the Halibee fossils and the associated archaeological assemblages make them central to research questions focused on evolutionary changes in early modern human behavior and biology. The paucity of postcranial relative to craniodental remains in the African Middle and Late Pleistocene record makes the Halibee assemblage, and particularly the partial skeletons from Halibee vertebrate paleontology locality 9, important for understanding modern human evolution from the perspective of the whole organism (Table 2.1).

The majority of the postcranial material in the sample described herein belongs to a single partial skeleton from Halibee (HAL-VP-9/1; Figure 2.1). In order to illustrate the percentage of the skeleton preserved on this individual, Omo I is included in Figure 2.1 as an example of the most complete previously known partial skeleton from eastern Africa from between 150 and 200 Ka. The HAL-VP-9/1 partial skeleton preserves portions of all long bone elements, as well as much of the hands and feet, the vertebral column, and the shoulder and pelvic girdles. Most of the cranial vault is also preserved, as well as small fragments of the facial skeleton and the mandible (see Appendix 1 for inventory).

There are an additional eight hominid individuals represented by fossils, most of them known from isolated skeletal elements. These include a proximal radius (HAL-VP-2/16) and ulna (HAL-VP-3/1), a terminal hand phalanx (HAL-VP-3/15), a partial femoral condyle (HAL-V-14/44), and a proximal femur shaft (BOU-VP-16/100). The latter specimen constitutes the only postcranial evidence yet recovered from the Upper Herto Member deposits. Two individuals are represented by multiple arm elements, including a proximal humerus, and proximal and distal ulna (HAL-VP-9/930), as well as a distal humerus and radius (TAL-VP-7/36; see Appendix 2 for inventory of associated cranial remains). The final individual included here is a fragmentary partial skeleton that includes cranial fragments and shaft fragments of the upper and lower limbs (HAL-VP-9/1520; see Appendix 2 for inventory). Another partial skeleton was recovered in 2018 from MSA-bearing Pleistocene deposits in the Goboli area, east of the modern Awash River. Chronostratigraphic analyses are underway, as are cleaning and restoration of this individual's skeletal parts, so it is not included in the present study.

All of the original fossils from the Middle Awash research area are housed in laboratories of the Cultural Heritage Collection and Laboratory Service Directorate, Ethiopian Authority for Research and Conservation of Cultural Heritage, on the premises of the National Museum of Ethiopia in Addis Ababa.

## 2.2 Geography

The fossils described here for the first time were recovered from the Middle Awash study area in the Afar depression of Ethiopia (Figure 2.2). They derive from three geographic areas west of the modern Awash River, ranging from near the northern to the southern extent of the study area in the following order: Talalak, Halibee, and Bouri. According to Middle Awash project nomenclatural practice, these geographic areas are each designated by a three-letter

abbreviation: TAL, HAL, and BOU, respectively. Vertebrate paleontology (VP) localities within each geographic area are numbered sequentially, as are the fossil specimens recovered from each VP locality. Details of field and laboratory methods and conventions are described in deHeinzelin et al. (2000), Gilbert (2008), and Haile-Selassie & WoldeGabriel (2009).

### 2.3 History of visitation/collection

All of the fossils described here were recovered during fieldwork operations between 2003 and 2015. Surface finds were followed by intensive crawls and comprehensive sieving of loose sediment. The stratigraphic position for each was securely placed based on spatial distribution of the fossils, geomorphological considerations, preservation characteristics, and in most cases, adhering matrix. Field (discovery) year, discoverer, and element inventories are reported in Table 2.1. For all fossils except one (the HAL-VP-9/1 partial skeleton), all elements were recovered during a single field year. In the case of HAL-VP-9/1, the discovery and initial collection took place during the 2003 field season when project co-director and geologist, Dr. Giday WoldeGabriel discovered a cranial vault fragment. A systematic recovery operation followed for four days, during which the ~ 20 meter x 20 meter area was crawled intensively, swept, and sieved. None of the skeleton was found to be *in situ*, but the distribution of elements securely indicated that the original stratigraphic position was immediately above the 'basaltic tuff' of Morgan et al. (2009; Figure 2.3). The collection site was revisited during the 2004 field season, during which a temporal bone fragment, cranial fragment, rib fragments and foot phalanx were recovered. A revisit to the collection site in the 2010 did not yield any additional remains. In 2015, the site was revisited once more, yielding another rib fragment and the head of a left fifth metatarsal.

### 2.4 Chronostratigraphic placement

The majority of the fossils, including the partial skeleton, derive from sediments in the Halibee Member of the Dawaitoli Formation in the Middle Awash study area and were recovered between 2003 and 2015. The fossils from HAL-VP-9 and HAL-VP-2 are constrained by a minimum radiocarbon age of >54 ka and a maximum $^{40}Ar/^{39}Ar$ obsidian age of 106 ± 20 ka (Morgan et al., 2009; Figure 2.3). HAL-VP-3 lies stratigraphically approximately two meters below HAL-VP-9 and HAL-VP-2, placing it chronologically marginally older. TAL-VP-7 is in direct stratigraphic association with a Middle Stone Age assemblage, but the exact chronostratigraphic position relative to the other localities is unknown. There is one specimen from Herto included in this study, from the same locality and stratigraphic horizon as the Herto cranial individuals (Sahle et al., 2019a; White et al., 2003). It derives from the Upper Herto Member, which has been securely dated to between ca. 154 and 160 ka (Clark et al., 2003; Sahle et al., 2019a). The single specimen from HAL-VP-14 derives from sediments below a volcanic horizon that yielded an $^{40}Ar/^{39}Ar$ age of 148 ± 34 ka (Morgan et al., 2009; additional dating in progress). In sum, with the exception of the single specimen from HAL-VP-14, the entire sample described here is technically stratigraphically constrained to between >54 ka and 160 ka in age, and the partial skeleton is between >54 ka and ca. 106 ka, but faunally, lithostratigraphically, and archaeologically likely to be far closer to the older bound. Geochronological efforts to further constrain these Halibee Member localities are currently underway, the results of which will be published elsewhere.

## 2.5 Archaeology

The Halibee archaeological assemblages are easily attributable to the Middle Stone Age. They include abundant Levallois cores, flakes, and points, across varied lithologies (e.g., basalt, chalcedony, jasper, and obsidian). In contrast to the evidence known from Herto, the Halibee assemblages are exclusively Middle Stone Age in their compositions, and do not contain artifacts that are typologically attributed to the Acheulean technocomplex (Clark et al., 2003; Sahle et al., 2019a). The Middle Stone Age lithics observed at Halibee are typologically intermediate to the Herto (Clark et al., 2003) and upper Aduma (Yellen et al., 2005, not including ADU-A1 which is likely roughly contemporary with Halibee) assemblages (Morgan et al., 2009).

As with the Herto and Aduma remains, because the Halibee fossil remains were discovered in association with exceptionally rich lithic and faunal assemblages, they stand to contribute to the holistic understanding of modern human emergence.

## 2.6 Taxonomy

Considering the geographic position of the Halibee fossils and their antiquity, the null taxonomic hypothesis is that these fossils represent anatomically modern humans (i.e., *Homo sapiens*). Several salient portions of the anatomy are preserved on the Halibee partial skeletons that make testing this hypothesis a relatively straightforward endeavor. The preserved portion of the HAL-VP-9/1 supraorbital region includes the lateral half of the right supraciliary arch, which is gracile, unprojecting, and exhibits a bipartite brow with separate medial and lateral supraciliary portions (Figure 2.4), anatomy closely duplicated by the frontal fragment associated with the more fragmentary HAL-VP-9/1520 skeleton. This morphology is similar to recent modern humans and unlike earlier Middle Pleistocene crania known from Africa (Grine, 2016; Rightmire, 2008). The HAL-VP-9/1 frontal is tall and vertically oriented, consistent with the derived modern human pattern (Stringer, 2016). The small preserved midline portion of its mandible has a clear mental eminence (Figure 2.5), which is one of the few features widely agreed to be a diagnostically modern human feature (Lahr & Foley, 1998; Schwartz & Tattersall, 2000, 2010; Stringer, 2016). Three additional mandibles recovered from the same locality (HAL-VP-9) also display clear mental eminences (Figure 2.6).

In contrast to the cranial skeletal features, only a few features of the postcranial skeleton have been recognized and agreed upon as diagnostically modern human (Pearson, 2000). The femoral pilaster is one of the few postcranial features identified as such, although it should be noted that its expression across modern humans is variable and therefore alone not sufficient for such diagnosis (Hrdlička, 1934; Pearson, 2000). Nonetheless, a very well-developed pilaster is present on the HAL-VP-9/1 individual, further failing to reject the null hypothesis that this individual is an anatomically modern human (Figure 2.7). Taking all of these anatomical features together, the null hypothesis that this individual belongs to *Homo sapiens* cannot be rejected. Based on the anatomical similarity of the additional fossils in this postcranial sample, their chronological and geographic position, and the lack of any phylogenetically informative features indicating otherwise (see Chapter 5), the most parsimonious inference is that they also represent *Homo sapiens*. Considering their geographic and chronological proximity, these fossils are likely members of the same, or closely-related populations.

## 2.7 Taphonomy

The following three Halibee skeletal individuals include associated sets of elements: HAL-VP-9/1, HAL-VP-9/1520, and HAL-VP-3/15. For all three individuals, the first fragments were found on the surface. The surface was then assessed for geomorphological circumstances, bounded, and systematically crawled. All loose surface sediment was sieved. The eroding *in situ* sediments were then closely inspected for any additional parts. For the first two individuals (the partial skeletons from Halibee: HAL-VP-9/1 and HAL-VP-9/1520), none of the skeletal parts were found *in situ*. Skeletal fragments of the third individual (HAL-VP-3/15) were found *in situ*, and will be described in greater detail elsewhere.

The skeletal parts for all individuals were prepared and conjoined in the laboratory at the National Museum of Ethiopia, and full inventories of all identifiable elements were completed. Fragments resulting from ancient postmortem damage to HAL-VP-9/1520 were not permanently conjoined. In each case below, the elements were judged to be associated based on matching adhering matrix, geographic position, pattern of conjoining across breaks, and compatibility across all elements in terms of size, morphology, non-duplication of element side and portion, and estimated age.

### 2.7.1 HAL-VP-9/1

The HAL-VP-9/1 partial skeleton from Halibee is generally very well-fossilized, although it was discovered in a highly fragmented state. The post-fossilization fracture pattern across the skeleton indicates that it fragmented when erosion reached the sedimentary stratum in which the skeleton was embedded. There are several additional important taphonomic features on the skeleton.

There is extensive evidence of insect modification affecting both cortical and cancellous bone across the skeleton, with particularly noteworthy examples on the external surface of the cranial vault, both left and right calcaneal tubers, and the external surfaces of most long bone shafts (Figure 2.8). Of the four groups of insects known to impact bone (Britt, Scheetz, & Dangerfield, 2008), the pattern of damage to the bone is most consistent with that documented for species of Isoptera (i.e., termites), although other insects may also have contributed to the damage. The calcaneal tubers display bore holes (e.g., Fig. 8 in Backwell, Parkinson, Roberts, d'Errico, & Huchet, 2012), whereas the damage to most affected areas of cortical bones is more consistent with “termite pitting” (e.g., Fig. 7 in Tappen, 1994), but lacking the extensive edge striations documented by Backwell et al. (2012). The presence of termite damage is not necessarily surprising, since it has also been reported for other Middle and Late Stone Age African fossils (Backwell et al., 2012). Osteophagy in termites has been reported repeatedly (Derry, 1911; Tappen, 1994; Thorne & Kimsey, 1983; Wylie, Walsh, & Yule, 1987), including in archaeological (Huchet, Deverly, Gutiérrez, & Chauchat, 2011; Wrobel & Biggs, 2018) and fossil (Backwell et al., 2012; Fejfar & Kaiser, 2005; Kaiser, 2000) contexts. The ectocortical furrows inferred to have been made by termites after the skeleton had been embedded in sediment often retain adherent calcium carbonate matrix deposited subsequent to the insect damage.

Several additional lines of evidence are informative about the depositional history of this skeleton. Many of the hand and foot elements retain thin (<0.1mm - 5mm) calcium carbonate deposits on their external surfaces. During preparation, much of this adhering matrix was

removed by air scribe to reveal bone anatomy. During this work, it was recognized that the subchondral surfaces of the opposing bone articulating at the joint also retained such adhering calcium carbonate matrix. These examples of inter-articular matrix are revealing in that they often preserve negative impressions that are likely of the opposing joint elements (19 of 31 manual fragments and five of 19 pedal fragments; see Appendix 3 for further details).

Four examples are particularly illustrative in this regard (see Figure 2.9). The first is a thin calcium carbonate deposit on the surface of the facet for the talar head of the left navicular (HAL-VP-9/1-192), preserving what is likely a negative impression of the left talar head (HAL-VP-9/1-190). The second is a thin deposit on the proximal articular facet of a proximal hand phalanx that is likely from the left fourth ray (HAL-VP-9/1-148), preserving a likely negative impression of the head of the left fourth metacarpal (HAL-VP-9/1-141). A thin plate of bone is adhered to the surface of the carbonate deposit; both the bone spall and the underlying carbonate deposit correspond in contour to the fourth metacarpal head (HAL-VP-9/1-141). The third example is a thin deposit on the radial facet of the right proximal ulna (HAL-VP-9/1-121), which preserves what is likely the negative impression of the right radial head (HAL-VP-9/1-119). Lastly, the lateral articular facet of the right patella (HAL-VP-9/1-186) has a thin calcium carbonate deposit that preserves a negative impression likely to be of the patellar surface of the right lateral femoral condyle (HAL-VP-9/1-161).

These natural casts of adjacent skeletal elements are found across the skeleton, and constitute strong evidence that the skeleton was articulated or semi-articulated within the sediment, its elements only disarticulating when the erosional surface reached the specimen and the well-preserved individual elements broke away from one another across the weaker thin carbonate interface between them. Evidence of this post-depositional, post-fossilization disarticulation goes well beyond the natural casts within the carbonate matrix described above. In many instances, when the elements disarticulated at the matrix interface, bone from one element or the other exfoliated into the matrix. For example, the left distal ulna has a small fragment of bone cemented to the medial surface of the ulnar head, with the trabeculae of the adhering fragment exposed. Particularly among the hand elements, there are several examples of bone spall adhering to the carbonate. This same pattern is also seen in the vertebral column and thorax. The right inferior articular facet of an upper thoracic vertebra has the right superior costal facet of the inferiorly adjacent vertebra cemented to it. In a similar case, a left superior articular facet and left inferior articular facet of thoracic vertebrae are cemented to each other along the articular surfaces, and together these fragments are cemented to a left rib head. There are three additional instances where a rib fragment is cemented to a transverse process of a thoracic vertebra, and two instances where small unidentifiable bone fragments are cemented to rib fragments.

The combined evidence of negative impressions and spalled bone from adjacent articulating elements across the skeleton, along with instances in which separate elements were still cemented together upon recovery (HAL-VP-9/1-30, -44, -46, -47, -79), indicate that this individual's skeleton was largely articulated when the calcium carbonate was deposited on the external and articular surfaces of bony elements after burial and termite furrowing. In other words, skeletal elements must have been in articulation for a period of time long enough for carbonate to precipitate between them. Furthermore, the representation of small distal elements (i.e., hand and foot) and the lack of evidence of carnivore or rodent damage, suggests that this individual was buried rapidly, soon after death. This is also consistent with the extensive termite damage, although it should be noted that this alone does not constitute evidence of burial, since

termites are capable of colonizing both buried and exposed skeletal remains (Adam, Mitchell, & van der Westhuizen, 2008; Huchet et al., 2011). The question of whether the burial was intentional unfortunately cannot be definitively answered, since none of the skeleton was found *in situ*. It is certainly possible that the HAL-VP-9/1 individual was buried intentionally, but the details of the recovery of this individual preclude ruling out natural depositional processes as accounting for the rapid nature of the burial. The evidence for articulation, alone, is inadequate for drawing firm conclusions about intentionality (Gargett, 1999).

### 2.7.2 HAL-VP-9/1520

In contrast to the taphonomic evidence described above, HAL-VP-9/1520 displays evidence of damage prior to being embedded in sediment and fossilized. These bones display ancient postmortem fractures, presenting longitudinal and spiral fractures with sharp edges typical of fragmentation that occurs when the bone retains its organic content (Figure 2.10, White, Black, & Folkens, 2012). The pattern of damage and the representation of elements and portions is consistent with damage resulting from carnivore activity (Haglund, 2006; Haglund, Reay, & Swindler, 1988). Only cortical portions of the skeleton are preserved, including primarily long bone shaft and cranial vault fragments. None of the vertebrae, epiphyses, or other trabecular portions are preserved. These portions are the softest, and the most nutritionally attractive since they contain the more easily accessed marrow, and are therefore the most often affected by carnivores (Haglund et al., 1988). Spiral fractures often result from carnivores gnawing the epiphyses and breaking into the bone shaft to access trabecular bone and marrow (Haynes, 1980). Spiral fractures can also be produced by trampling (Haynes, 1983), but the pattern of fracture exhibited by this skeleton and the representation of element portions makes this interpretation less likely. Even more convincingly, the left frontal fragment preserves a single linear mark with a smooth contour oriented obliquely across the supraorbital region, likely produced by a carnivore canine or premolar (Figure 2.10, Fernandez-Jalvo & Andrews, 2016).

### 2.7.3 HAL-VP-3/15

The final of the three individuals from this assemblage that display notable taphonomic features are the remains of a very fragmentary individual that include a third molar, a terminal hand phalanx, and many small unidentifiable cranial and postcranial fragments. This individual displays evidence of burning, including extensive cracking and discoloration, ranging between shades of white, blue, gray, and black (White et al., 2012). The terminal hand phalanx, as with the other fragments, displays warping and surficial reticular cracks (Figure 2.11, Whyte, 2001). Measurements of this element were only taken in cases where warping was judged not to have significantly affected the dimensions. A more detailed taphonomic investigation of this individual is currently underway and will be reported elsewhere.

## 2.8 Conclusions

The Halibee Middle Stone Age postcranial fossils described here, in addition to the contextual information of fauna, flora, geology, and archaeology, constitute a rich body of new evidence. Whereas the skeletal remains are suggestive of mortuary practices, ongoing studies and additional remains are necessary to elucidate their behavioral significance. I now turn to a

detailed consideration of how these fossils relate to recent modern humans and other Pleistocene fossils in order to understand their place in human evolutionary studies.

**Table 2.1** Middle Stone Age hominid postcranial fossils from the Halibee Member, Dawaitoli Formation, Middle Awash study area (as of 2017; suffixes in parentheses). [1]Derives from the Upper Herto Member, Bouri Formation. [2]Individuals with associated cranial remains.

| Full specimen number | Field year | Discoverer | Postcranial element(s) |
|---|---|---|---|
| BOU-VP-16/100[1] | 2012 | Kampiro Kayrento | Proximal femur shaft |
| HAL-VP-2/16 | 2003 | Awoke Amzay | Proximal radius |
| HAL-VP-3/1 | 2003 | Same | Proximal ulna |
| HAL-VP-3/15 (A-N)[2] | 2015 | Wegeno Amerga | Terminal hand phalanx |
| HAL-VP-9/1 (-1 to -206)[2] | 2003 | Giday WoldeGabriel | Partial skeleton (see Appendix 1) |
| HAL-VP-9/930 (A-C) | 2004 | Kampiro Kayrento | Proximal humerus; proximal and distal ulna |
| HAL-VP-9/1520 (A-M)[2] | 2015 | Alemayehu Asfaw | Skeletal parts (see Appendix 2) |
| HAL-VP-14/44 | 2004 | Tim White | Femoral condyle |
| TAL-VP-7/36 (A-J)[2] | 2010 | Onder Ozkurt | Distal humerus; distal radius |

**Figure 2.1** Inventory of preserved anatomy on HAL-VP-9/1 (**A**). All element portions preserved that are identifiable to side and specific portion are shaded in gray. Omo I (**B**) included on the right for comparison, modified from Pearson et al. (2008a).

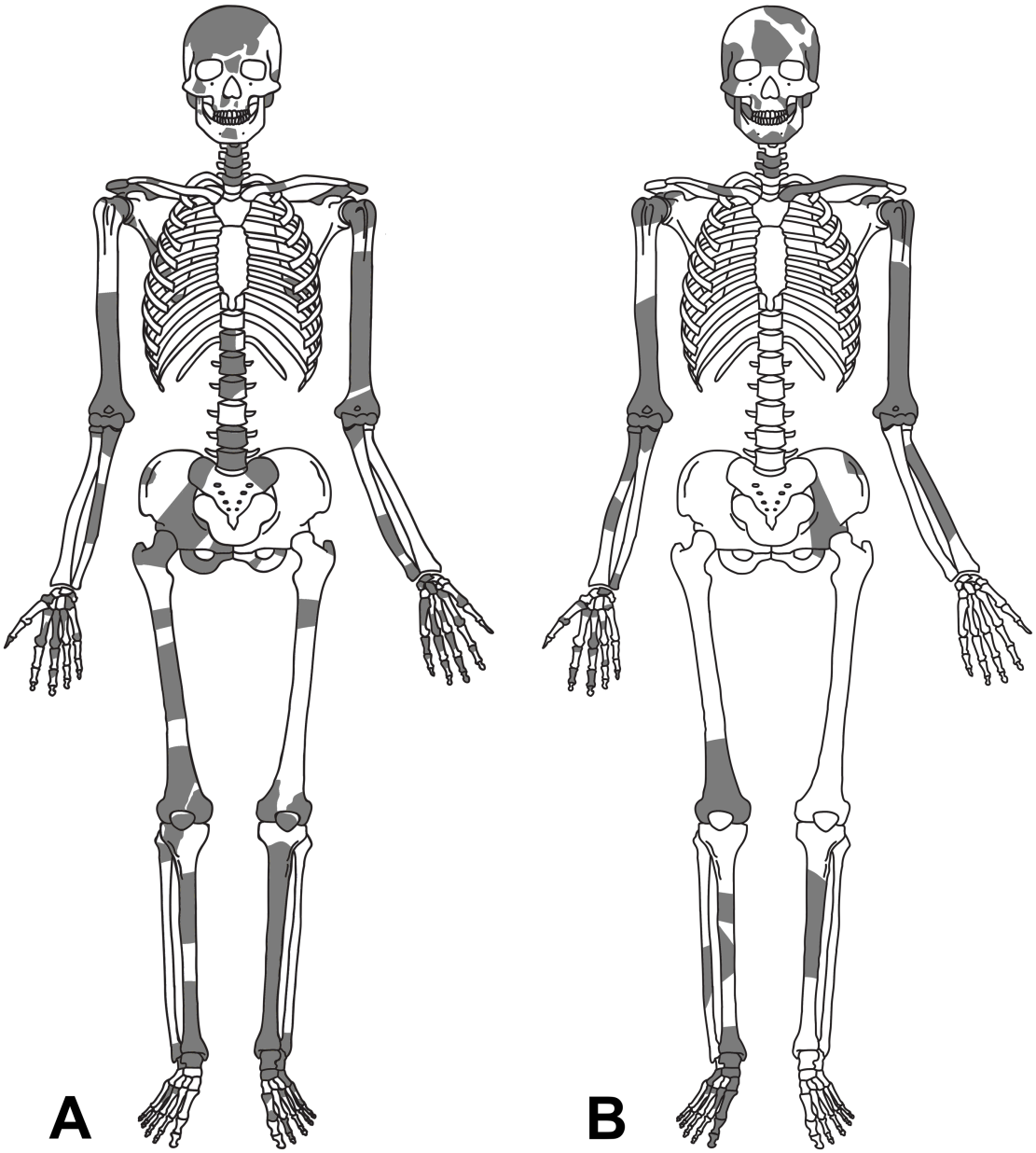


**Figure 2.2** Map showing the location of the Middle Awash study area, indicated on the left by the grey rectangle. The research area is enlarged in the inset map on the right with the locations of the Talalak, Halibee, and Bouri areas indicated. The modern Awash River is visible as the dark green strip of vegetation running approximately north-south. Map data ©2018 Google.

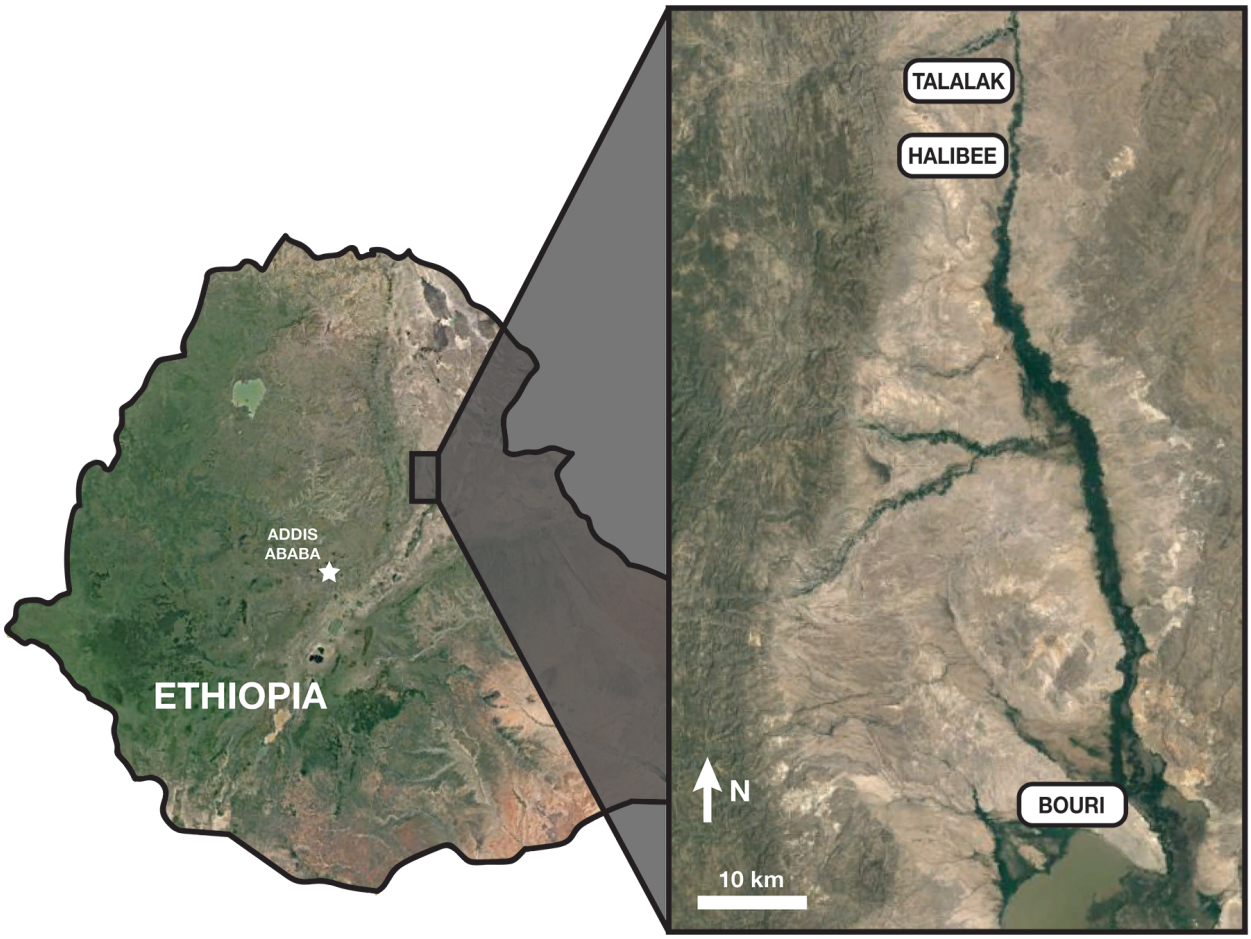


**Figure 2.3** HAL-VP-9/1 collection site at top (**A**). Yellow flags mark the fragments identified as hominid that were exposed on the surface. Blue flags mark the perimeter of the distribution of hominid fragments. Photo courtesy of Tim White. Stratigraphic position of the two Halibee partial skeletons at bottom (**B**). Radiocarbon and $^{40}Ar/^{39}Ar$ ages are from Morgan (2009). Triangles indicate the possible stratigraphic position of the obsidian sampled for $^{40}Ar/^{39}Ar$ age determination. Ongoing work will more firmly establish the position of the dated obsidian sample.



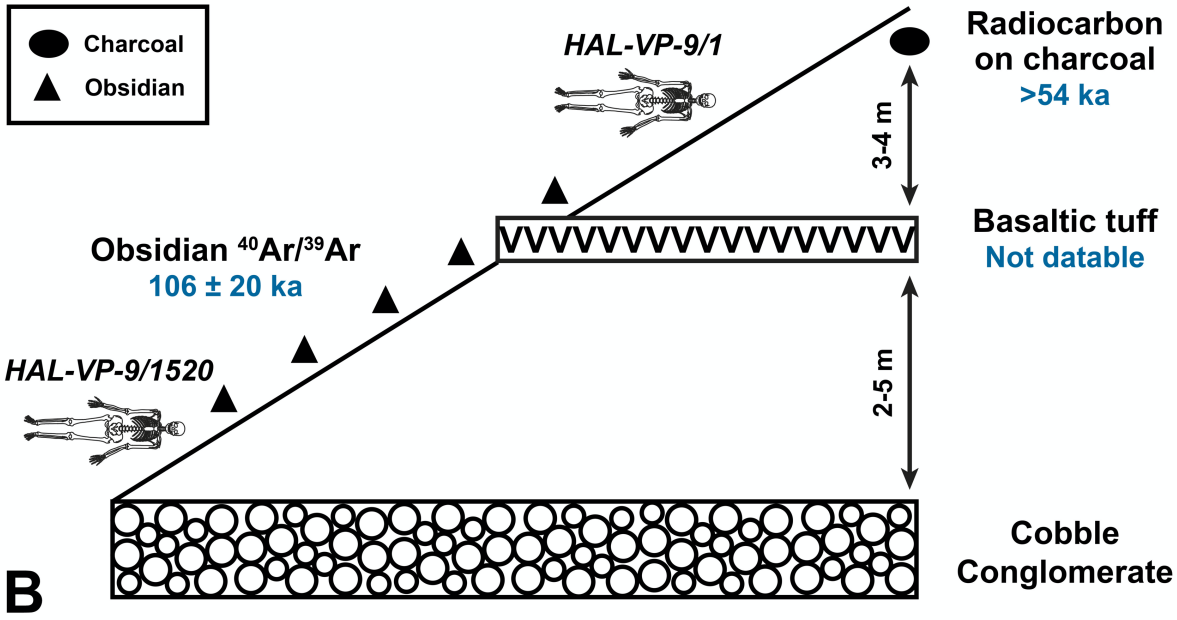



**Figure 2.4** HAL-VP-9/1 cranial vault in (**A**) anterior, (**B**) posterior, (**C**) superior, (**D**) inferior, (**E**) left lateral, and (**F**) right lateral views. In superior and inferior views, anterior is left. White arrow in anterior view indicates the point of division between the medial and lateral portions of the supraciliary arch.

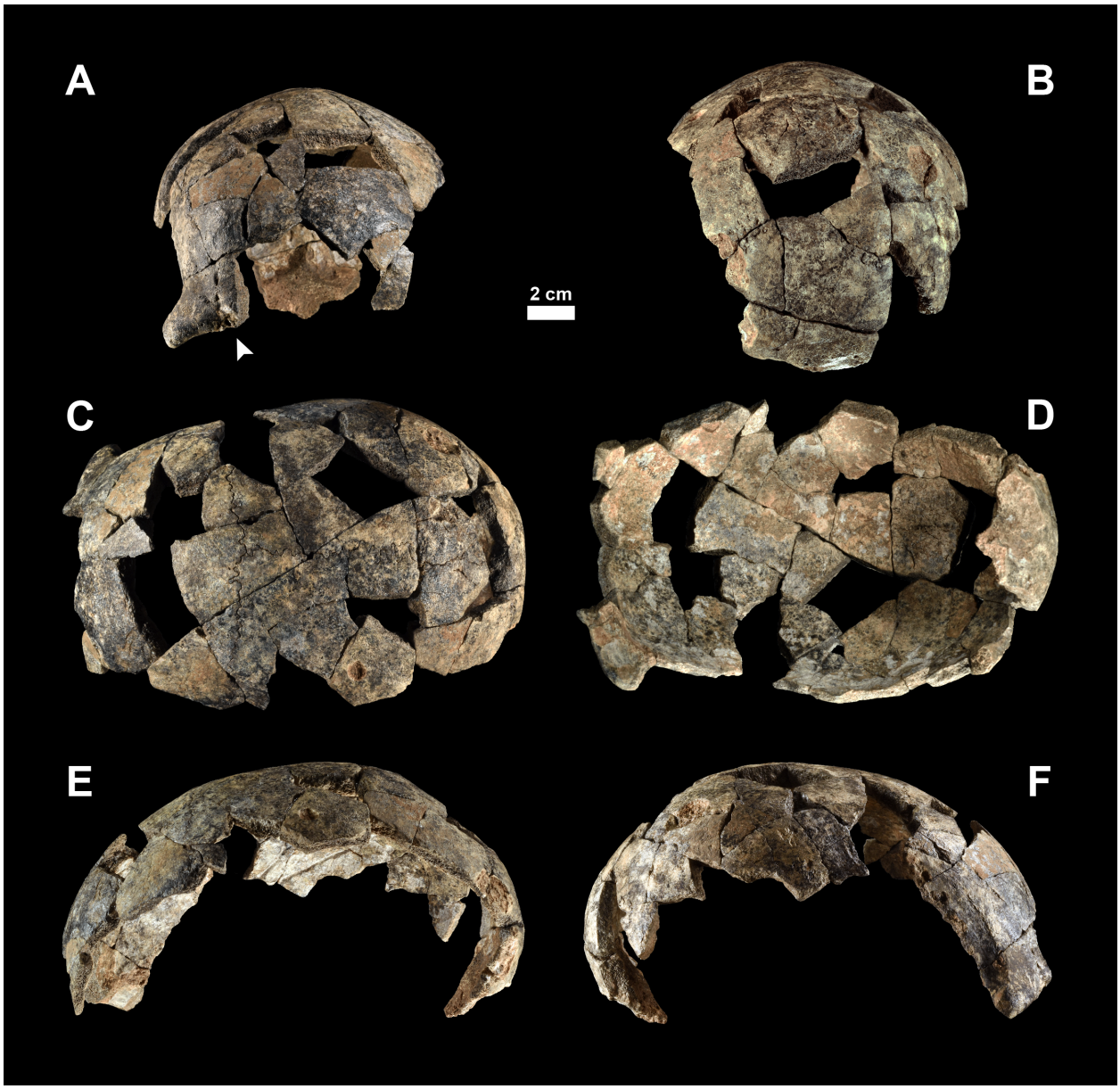


**Figure 2.5** HAL-VP-9/1 mandible in superior view, anterior is up. White arrow indicates the presence of a mental eminence.

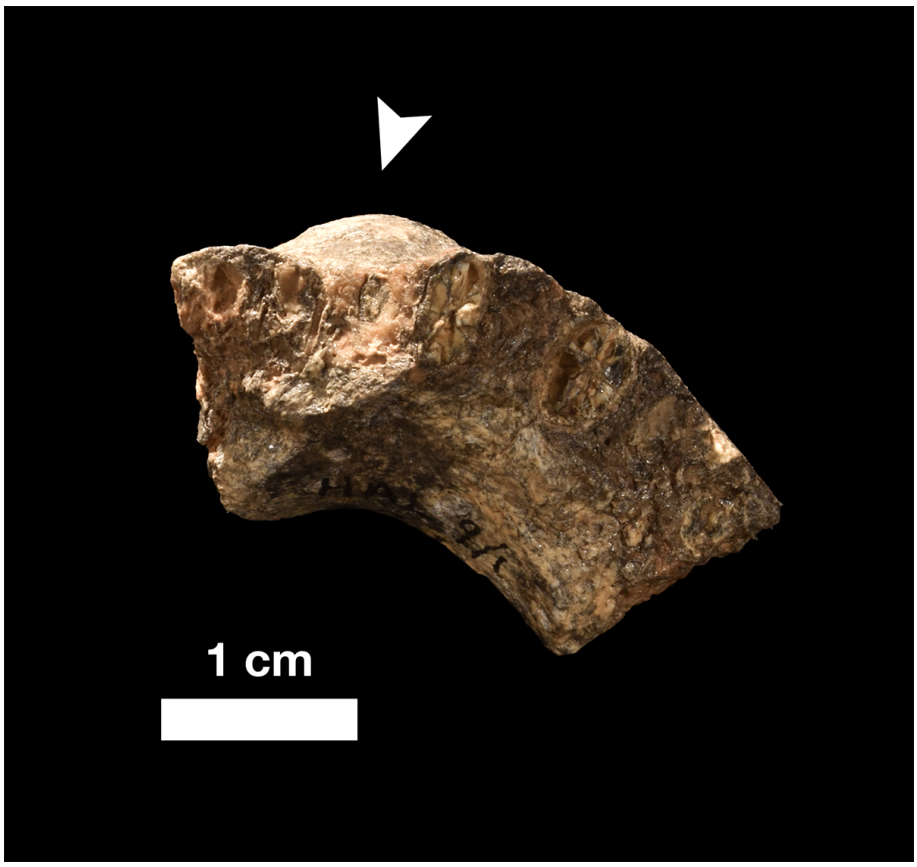



**Figure 2.6** Mandibles recovered from HAL-VP-9, Halibee Member, Dawaitoli Formation, Middle Awash study area, in left lateral view. **A**: HAL-VP-9/4, right side, reversed. **B**: HAL-VP-9/987. **C**: HAL-VP-9/400-B. White arrows indicate the presence of a mental eminence.

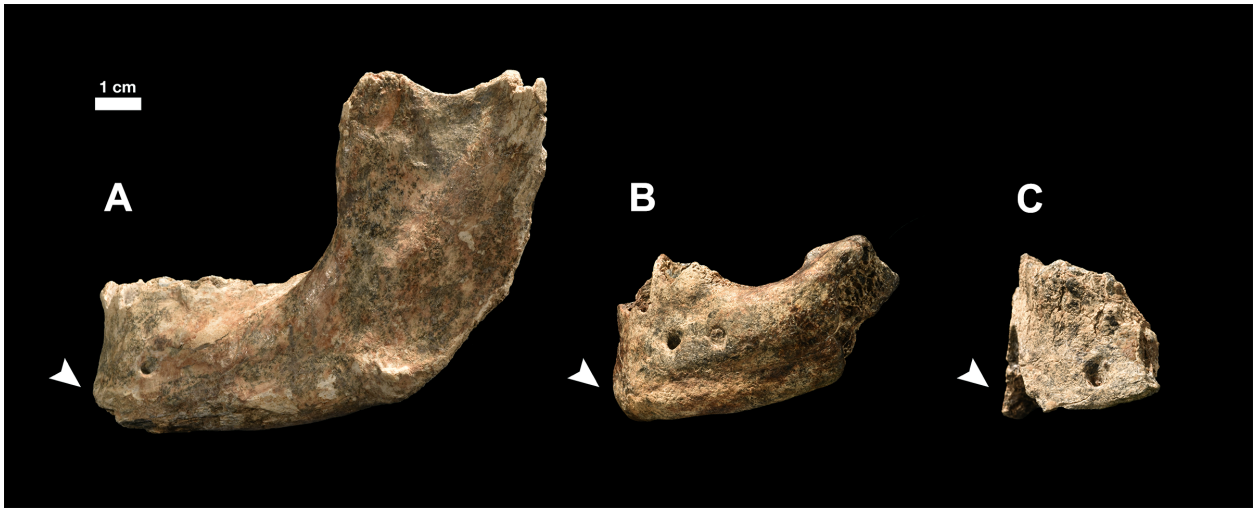


**Figure 2.7** HAL-VP-9/1 left femoral shaft fragment displaying a pilaster. **A**: Posterior view, proximal end is up. **B**: Distal view, anterior is up. Note that insect damage has modified the outer shaft surface, minimizing the apparent size of the pilaster at its proximal extent in posterior view.

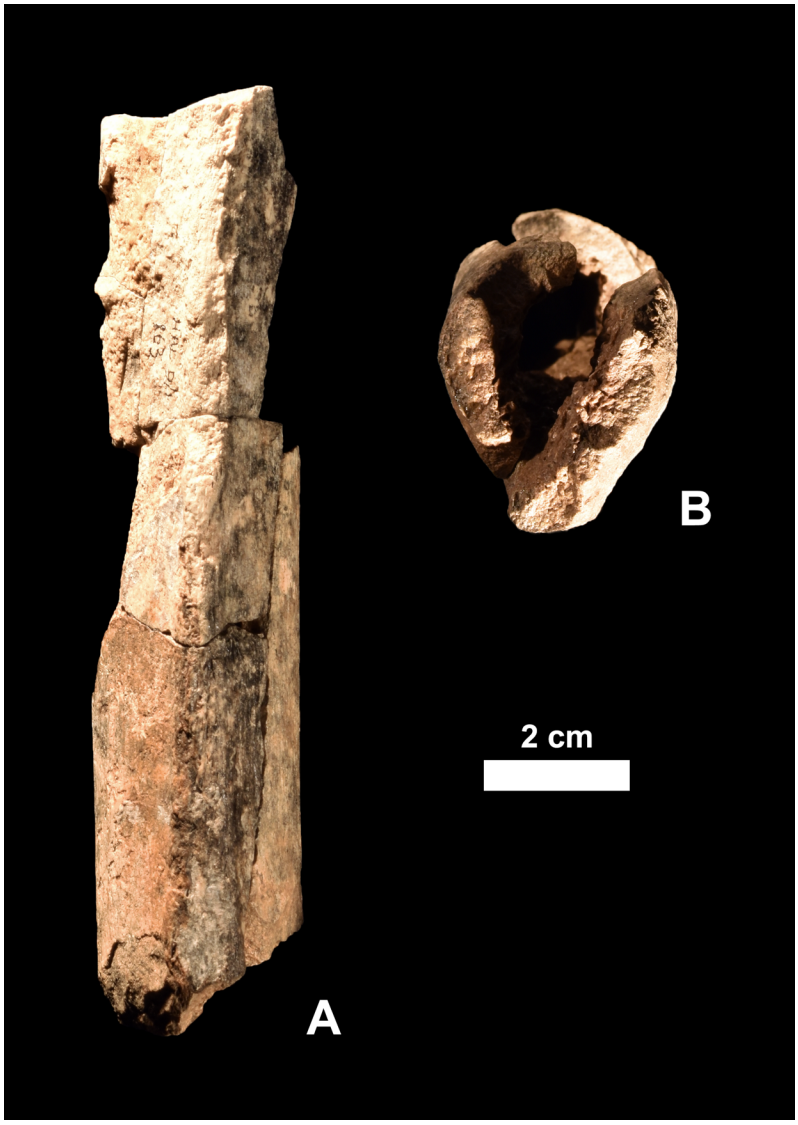


**Figure 2.8** Examples of insect damage to HAL-VP-9/1. **A**: Cranial vault (HAL-VP-9/1-1A+1B) in superior view, anterior is right. White arrows indicate large pits on the external vault surface. **B**: Left calcaneus (HAL-VP-9/1-191) in lateral view. White arrow indicates the presence of a large bore hole on the lateral surface of the calcaneal tuber. **C**: Right calcaneus (HAL-VP-9/1-189) in posterior view. White arrow indicates the presence of a bore hole on the inferomedial surface of the calcaneal tuber. **D**: Thoracic vertebra (HAL-VP-9/1-32) in oblique right superolateral view. White arrow indicates the presence of a bore hole. **E**: Right radial head (HAL-VP-9/1-119) in proximal view. White arrow indicates insect pitting. **F**: Right ulnar shaft (HAL-VP-9/1-122) in lateral view. Note the $CaCO_3$ adhering to the insect-modified surface. **G**: Proximal shaft fragment of the left femur (HAL-VP-9/1-168) in posterior view. As with (**F**), note the $CaCO_3$ overlying the insect-modified surface.

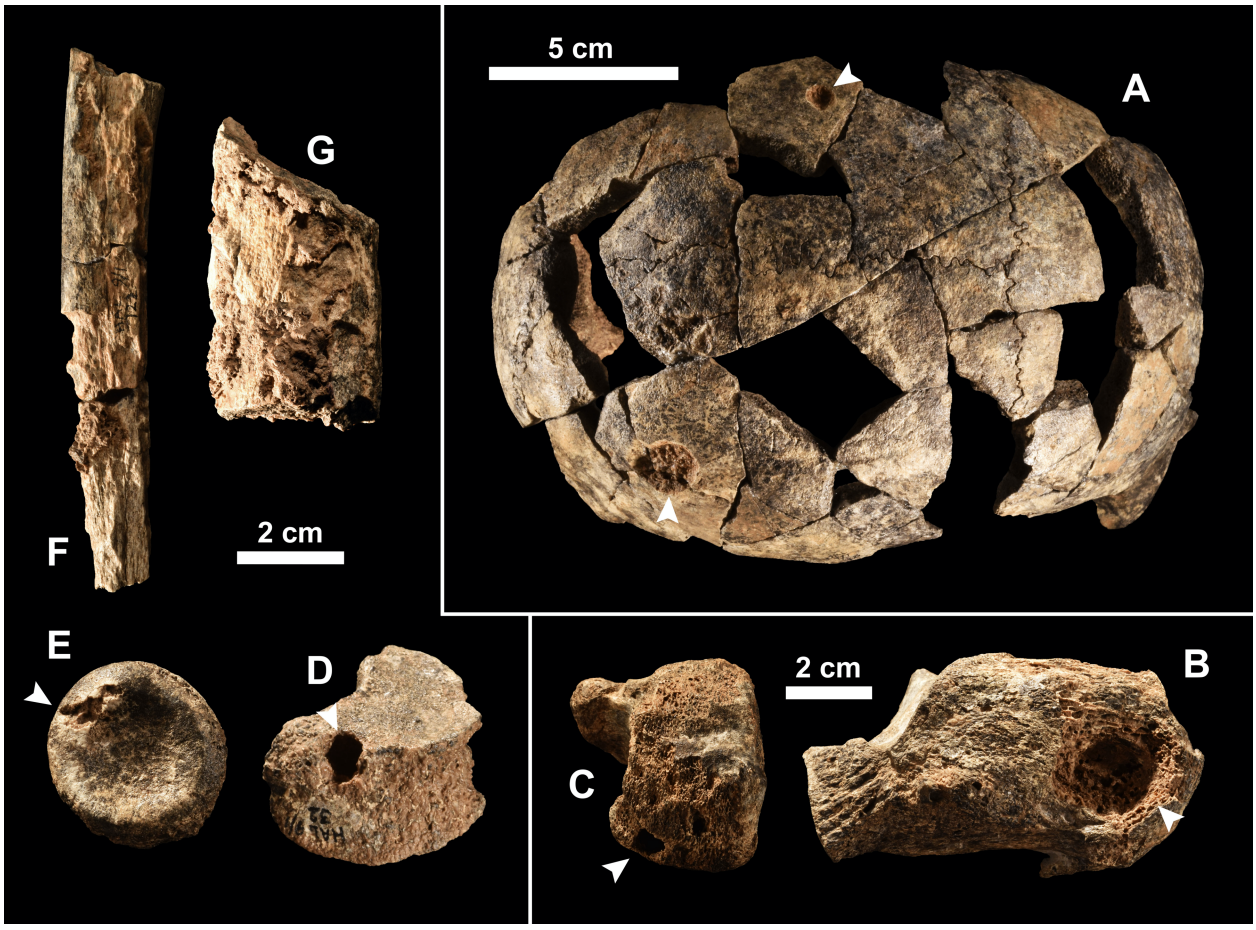


**Figure 2.9** Examples of calcium carbonate deposits on HAL-VP-9/1. **A**: Proximal end of the right ulna (HAL-VP-9/1-121) in lateral view. White arrow indicates a $CaCO_3$ matrix "skin" adhering to the radial notch. **B**: Right patella (HAL-VP-9/1-186) in posterior view. White arrow indicates a $CaCO_3$ "skin" adhering to the lateral articular facet. **C**: Distal end of the left ulna (HAL-VP-9/1-124) in anteromedial view. White arrow indicates the presence of bone cemented to the medial surface of the ulnar head, with trabeculae exposed. **D**: Left navicular (HAL-VP-9/1-192) in proximal view. White arrow indicates a $CaCO_3$ "skin" of matrix adhering to facet for the talar head, preserving the negative impression of the left talar head. **E**: Proximal hand phalanx, likely from left ray IV (HAL-VP-9/1-148), in proximal view. White arrow indicates the presence of a $CaCO_3$ "skin" adhering to the proximal articular facet. Note the thin concave plate of bone adhering to the surface of the "skin," likely from the head of the articulating metacarpal.

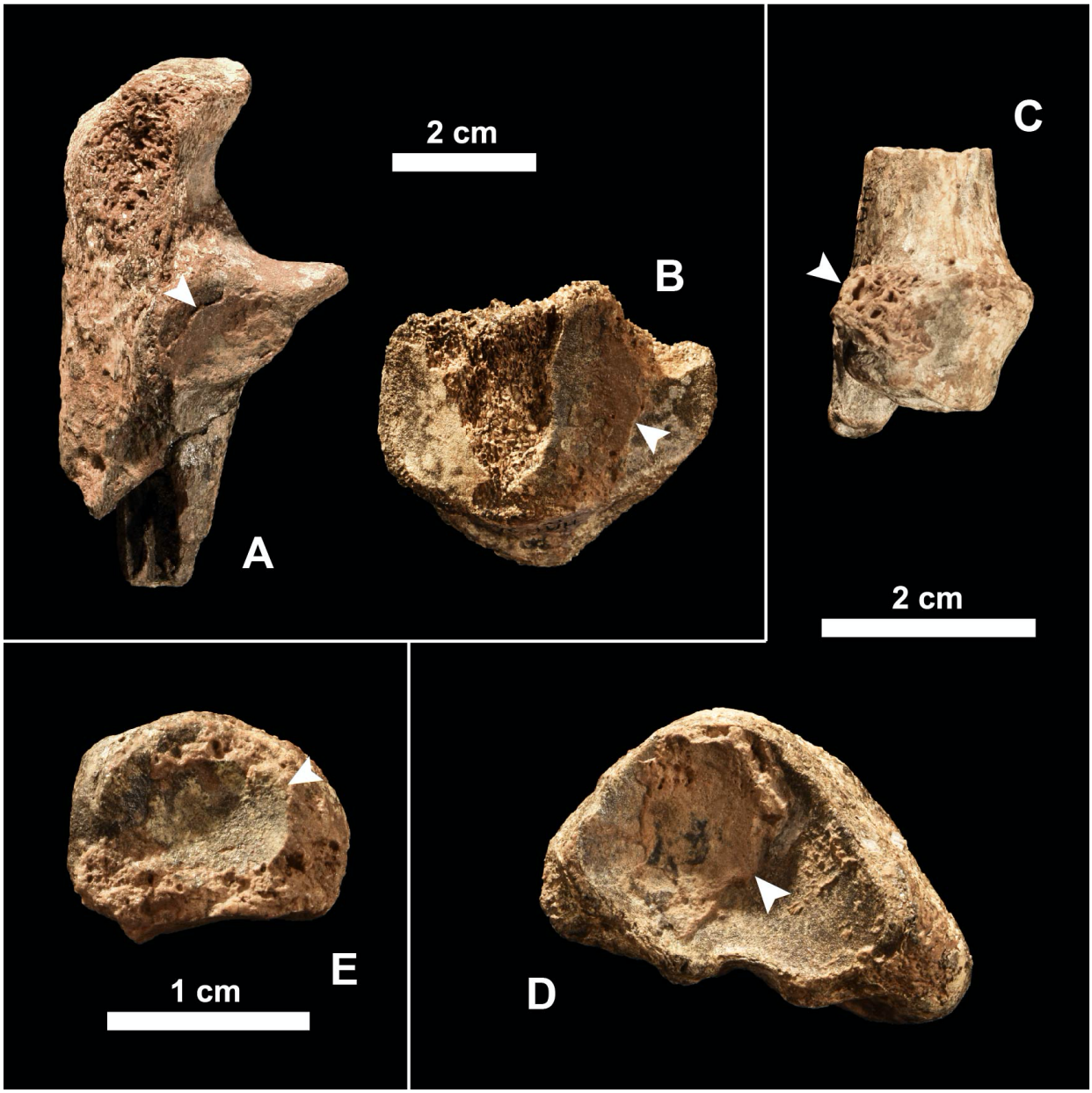


**Figure 2.10** Examples of likely carnivore damage to HAL-VP-9/1520. **A**: Left frontal (HAL-VP-9/1520-A) in anterior view. White arrows indicate the approximate superior and inferior margins of a linear mark, likely produced by a carnivore tooth. Arrows are approximately perpendicular to the long axis of the linear mark. **B**: Right tibial shaft (HAL-VP-9/1520-D) in anterior view. White arrows indicate a point of refit at a step fracture. Fragments resulting from ancient postmortem fracturing have not been conjoined. **C**: Proximal shaft of the left femur (HAL-VP-9/1520-I) in posterior view. **D**: Distal shaft fragment of the right humerus (HAL-VP-9/1520-F) in anterior view. **E**: Proximal shaft fragment of the right ulna (HAL-VP-9/1520-E) in lateral view. The latter three fragments (C, D, E) exemplify a skeleton-wide pattern, where only cortical portions are preserved and all epiphyses are absent.

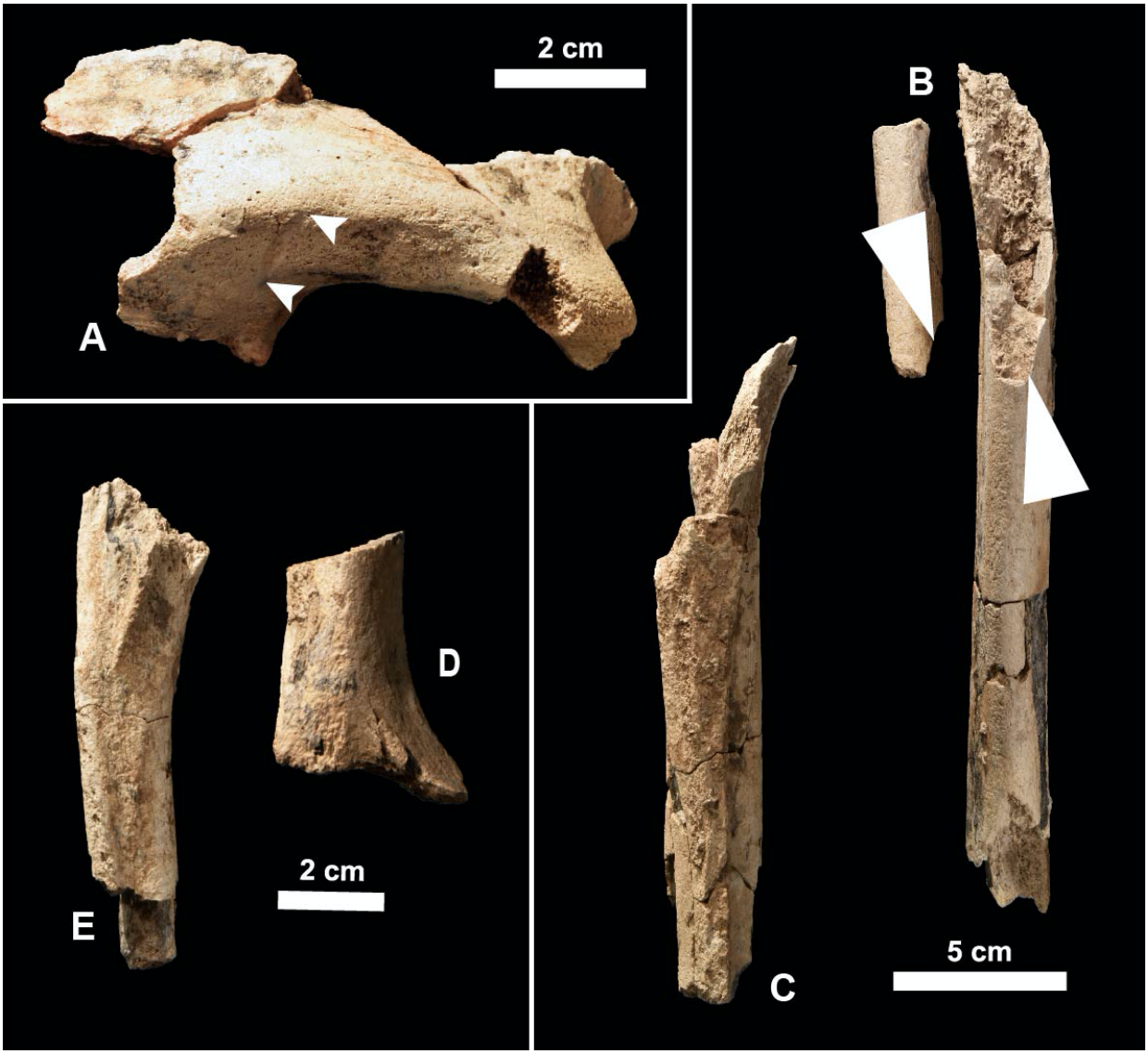
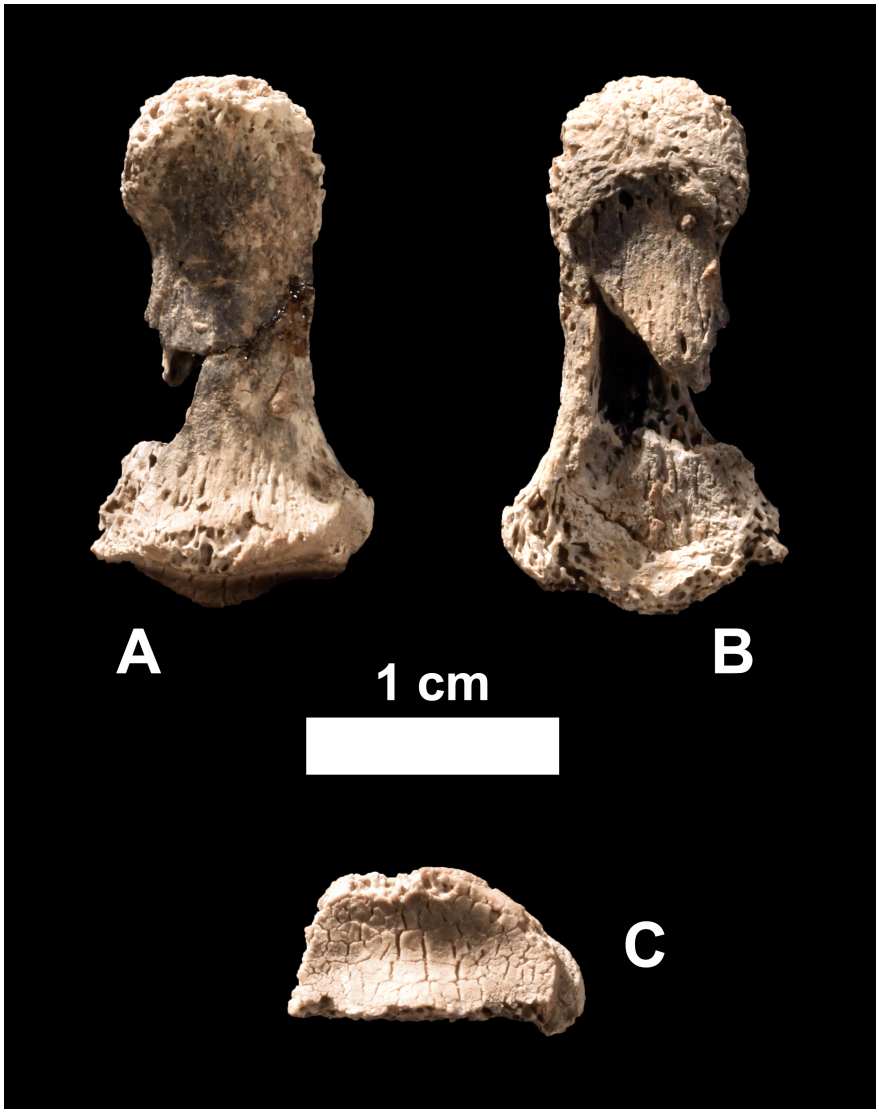


**Figure 2.11** Examples of burning damage to HAL-VP-3/15. **A**: Terminal hand phalanx in dorsal view. **B**: Terminal hand phalanx in palmar view. **C**: Terminal hand phalanx in proximal view (palmar is down).



## Chapter 3: Materials and methods

The Halibee Middle Stone Age hominid fossils introduced in Chapter 2 were studied in a comparative context, the results of which are reported in Chapters 5 and 6. The current chapter details the recent modern human and Pleistocene fossil comparative samples employed, followed by a description of data collection and analytical methods. The chapter concludes by laying out the research aims and questions to be addressed in the subsequent chapters.

### 3.1 Comparative materials

The comparative materials for this study fall into two categories: recent modern human skeletal remains and Pleistocene fossil specimens. Recent modern human is taken here to mean populations spanning the Holocene to the present. Five recent modern human comparative samples were selected to capture a range of modern human variation that spans geography, climate, and subsistence. Each of the samples is approximately sex-balanced and includes only adult individuals (i.e., all epiphyses completely fused). Three samples are archaeological in origin, whereas the remaining two samples derive from cadaver dissections and cemetery exhumations (see Table 3.1). Comparative fossil specimens range between ca. 1.8 Ma and ca. 12 ka, and geographically span Africa, Europe, Asia, and Australia (see Appendix 4 for sample details and references).

#### 3.1.1 Recent modern human comparative samples

##### 3.1.1.1 Southern Africa (Zulu)

A sample of individuals (n=34) of southern African ancestry (Zulu population group) was measured from original osteological remains in the Raymond A. Dart Collection of Human Skeletons housed in the School of Anatomical Sciences at the University of the Witwatersrand in Johannesburg, South Africa. Because the skeletons in this collection are cadaver-derived, they are well-preserved and are nearly all complete. The collected sample includes n=17 females and n=17 males, spanning ages at death of 22-65 (mean age of 38), with death dates ranging between 1925-1953. All skeletons in the Dart Collection included in this study were collected prior to 1958, and were acquired from unclaimed bodies at regional hospitals in South Africa (Dayal, Kegley, Štrkalj, Bidmos, & Kuykendall, 2009). As a result, some of the documented details (e.g., population group and age at death) are estimates (Dayal et al., 2009). It has been noted that age data are questionable for some of the individuals (Dayal et al., 2009), but for the purposes of the present study, age at death more specific than an age class of "adult" is unnecessary. Some individual data were derived from death certificates, and in some cases, population group was estimated based on an individual's surname. Sex was determined from medical records and soft tissue inspection.

##### 3.1.1.2 Northeastern Africa (Egypt)

A sample of individuals (n=32, sex-balanced) of Egyptian origin was measured from original archaeological remains housed at the Smithsonian's National Museum of Natural History in Washington, D.C. The sample encompasses three collection localities, with a large

majority derived from Lisht (n=25) and smaller contingents derived from Kharga Oasis (n=4) and Luxor (n=3). The remains from Lisht and Kharga Oasis were collected in the early 20th century as part of an expedition led by the Metropolitan Museum of Art, New York (Lythgoe, 1907, 1908, 1909). Lisht is located in Middle Egypt, and is inferred to span 2061-333 BCE (Raxter et al., 2008). Kharga Oasis is located in the Western Desert of Egypt, and is estimated to span ca. 30 BCE-640 AD (White, Longstaffe, & Law, 1999). The accession records for two of the skeletons from Luxor indicate that they originate from the "Monastery of Epiphanos and Psau," and the crania are physically labeled "Coptic Monk… About 600 AD" (pers. observation). It is likely that these two individuals were collected by the same expedition, based on records of expedition efforts focused in the area from which these crania were collected (Phillips, 2007). The remains from Luxor are from ca. 337-642 CE (Raxter et al., 2008). The most complete and well-preserved skeletons from each of these localities were selected for inclusion in this study. The majority of the skeletal remains in this sample are well-preserved, and often have desiccated soft tissue still attached.

#### 3.1.1.3 Levant (Jordan)

A sample of individuals of Jordanian origin was measured from original archaeological remains housed at the Smithsonian's National Museum of Natural History in Washington, D.C. The sample was collected from the archaeological site Bâb edh-Dhrâ, Jordan, dated to ca. 3300-2000 BCE (Ortner & Frohlich, 2007). The population sampled is inferred to have been either sedentary or comprised of nomadic pastoralists; the latter interpretation is considered more likely (Ortner & Frohlich, 2007). The majority of the skeletal remains were recovered from secondary burials. Unfortunately, some elements, particularly smaller ones, were not recovered from the primary burial site, and others were broken during transfer to the secondary burial site. The secondary burial process, which included interring multiple individuals in a single tomb chamber, resulted in mixing of the postcranial bones. Since each chamber contained only a few individuals, it was possible to associate the major long bones with a particular skull. In a few cases, the burials were interred with soft tissue still holding the bones together, and in these cases the association of skeletal parts is known (Ortner & Frohlich, 2007). Of the collected sample, 39 individuals comprise associated remains (i.e, partial skeletons of single individuals). Because of the issues posed by secondary burial and uncertain association between smaller skeletal elements recovered, n=150 unassociated hand and foot elements were also measured to increase sample size for these measurements. Some of these isolated hand and foot elements certainly belong to the individuals measured as associated sets of elements, but making certain associations between them is not currently possible.

#### 3.1.1.4 Western Europe (Portugal)

A sample of individuals (n=30, sex-balanced) of Portuguese nationality was measured from original osteological remains housed at the 21st Century Identified Skeletal Collection in the Department of Life Sciences at the University of Coimbra, Portugal. This collection consists of recently-exhumed unclaimed skeletal remains from the Capuchos Cemetery. In Portugal, it is permissible to exhume remains three years after burial, thereby making the burial ground available for reuse. Following exhumation, skeletons that are unclaimed by relatives remain under the protection of the cemetery (Ferreira et al., 2014). At that point, the unclaimed remains

from the Capuchos Cemetery are transferred to the 21st Century Identified Skeletal Collection. This arrangement is the result of a collaboration between the Department of Life Sciences and the City Council of Santarém, which oversees the Capuchos Cemetery from which the remains are exhumed. With the transfer of remains, inhumation and exhumation documents and death certificates are provided, which includes individual details such as sex, age at death, and nationality. The cleaning of remains is finalized in the Collection laboratory (Ferreira et al., 2014). The remains are very well-preserved, and include nearly all elements. Some individuals are missing smaller elements (e.g., carpals and phalanges) as a result of incomplete recovery during the exhumation. The age at death of the sample measured spans 27-94 (mean age of 75) and the death date spans 1998-2011. All individuals are of Portuguese nationality. This comparative sample is the most recent sample included in the present study.

#### 3.1.1.5 North America (California, U.S.A.)

A sample of Native Californian individuals (n=41; n=20 females, n=21 males) was measured from original archaeological remains housed at the Phoebe A. Hearst Museum of Anthropology at the University of California, Berkeley. The human remains studied are unaffiliated under The Native American Graves Protection and Repatriation Act (NAGPRA) of 1990. This sample spans two archaeological sites in San Joaquin County, within the California Central Valley: CA-SJO-68 (n=29) and CA-SJO-56 (n=12). Both of these sites represent the Early Period (ca. 5000-2500 BP) in the sequence of broad temporal units recognized in the central Californian archaeological record (Bennyhoff & Hughes, 1987; Moratto, 1984). The site SJO-68 (Blossom Mound) was excavated in 1921 by E. J. Dawson, and in 1938 and 1947 by the University of California (Heizer, 1949; Ragir, 1972). It has been dated to >3450-2450 BP on the basis of radiocarbon dating results, artifact composition, and obsidian hydration results (Schwitalla, 2010). The site SJO-56, just 1.75 miles southeast of SJO-68, was excavated in 1938 by F. Fenenga for Sacramento Junior College (Heizer, 1949; Ragir, 1972). The same date range has been produced for SJO-56 (Phelps Mound) as for SJO-68, based on radiocarbon results and artifact composition (Schwitalla, 2010). Both of these sites have been recognized as belonging to the "Windmiller" culture of the Early Period, based primarily on the burial tradition observed at each (Heizer, 1949). The inclusion of this comparative sample of robust hunter-gatherers is particularly appropriate considering similarities in subsistence between these Native Californian Holocene populations and the Halibee remains (Davies, Pomeroy, Shaw, & Stock, 2014; Larsen, 1981).

### 3.1.2 Comparative fossil specimens

Comparative fossil data were selected to sample the hominid postcranial fossil record between ca. 1.8 Ma and 12 ka and were primarily culled from the published literature (see Appendix 4). The taxonomic status for many of the Middle and Late Pleistocene fossils is contentious, and the classification scheme that applies to fossils from this time period is in flux (see Chapter 1). As such, only two groups are organized according to taxonomic classification, modern humans and Neanderthals, and they include only specimens for which general consensus regarding classification has emerged. Beyond these two taxa, all other fossils are organized first according to geographic region and then according to time period. In cases where samples are very limited (<2 individuals), time bins are pooled. Within Africa, samples include *Homo*

specimens from the Late, Middle, and Early Pleistocene. Asian samples include a pooled Late and Middle Pleistocene *Homo* sample, and an Early Pleistocene group. Finally, Early and Middle Pleistocene *Homo* from Europe are pooled into a single group.

#### 3.1.2.1 Modern humans

The modern human fossil sample includes early evidence spanning northern and eastern Africa (Jebel Irhoud and Omo 1) and the Levant (Skhul and Qafzeh). Several fossils younger than 50 ka are also included to sample the latter part of the Late Pleistocene record in Africa, Australia, and Europe (e.g., Nazlet Khater, Lake Mungo, and Sunghir). These recent samples were selected for completeness of fossils and availability of data. However, because of their geographic and chronological proximity, and relative completeness, the Halibee partial skeleton will be described in the greatest detail relative to the earlier modern specimens of Omo I, Skhul, and Qafzeh.

#### 3.1.2.2 Neanderthals

The Neanderthal sample spans Europe and the Near East, and is comprised of the most complete and abundant specimens for which published descriptions and metrics are available (e.g., Krapina, Kebara, La Chapelle-aux-Saints 1).

#### 3.1.2.3 African Pleistocene

The African Late Pleistocene sample includes mostly southern African fossils from imprecisely dated contexts that display a combination of primitive and derived features, and whose status as "modern" remains contentious (Grine, 2016; Stringer, 2016).

The African Middle Pleistocene includes a broad assemblage of very fragmentary postcranial remains from eastern and southern Africa, variably ascribed to *H. rhodesiensis*, *H. heidelbergensis*, and/or some version of "archaic" *Homo sapiens.* It is noted here that the postcranial associations for Kabwe remain tenuous (Trinkaus, 2009; Woodward, 1921).

African Early Pleistocene *Homo* includes specimens from eastern Africa that are older than 781 ka (Gibbard, Head, Walker, & Subcommision on Quaternary Stratigraphy, 2010), and have been assigned to *Homo erectus*. This sample does not include Early *Homo* fossils (e.g., *Homo habilis*, *Homo rudolfensis*), for which taxonomic and phylogenetic positions remain contested (Villmoare, 2018). The evidence from this portion of the record is very fragmentary, with the exception of the partial skeleton from West Turkana (KNM-WT-15000). Although this specimen is a subadult, it provides the most complete information about pre-modern postcranial skeletal anatomy from this period in Africa and is therefore included here, although with consideration of the potential impact of its subadult status on skeletal morphology.

#### 3.1.2.4 Asian Pleistocene

The Asian Late and Middle Pleistocene *Homo* sample includes specimens from China and Indonesia. Taxonomic affinity of these specimens is contentious, and it is likely that this group samples early modern humans, late *Homo erectus*, and in the case of the Jinniushan partial

skeleton, an anatomically intermediate pre-modern group (Antón, 2003; Etler, 1996; Lu, Meldrum, Huang, He, & Sarmiento, 2011; Rosenberg, Zuné, & Ruff, 2006).

The Asian Early Pleistocene *Homo* sample also includes specimens from Indonesia, as well as the sample from Dmanisi, Georgia. The fossils in this group are generally regarded as belonging to *Homo erectus* (*sensu lato*, Antón, 2002; Lordkipanidze et al., 2013).

#### 3.1.2.5 European Pleistocene

Lastly, the European Early and Middle Pleistocene *Homo* sample primarily contains specimens that share derived features with later Neanderthals. This sample includes the roughly contemporaneous specimens from Sima de Los Huesos (Spain), Arago (France), and Boxgrove (UK), and the earlier fossils from Gran Dolina (referred to by some researchers as *H. antecessor*, e.g., Arsuaga et al., 1999b; Bermúdez de Castro et al., 1997; 2004). Among the European Middle Pleistocene comparative materials, the large well-documented sample from Sima de los Huesos, for which many published data are available, will be considered in the greatest detail relative to the Halibee remains.

### 3.2 Data collection methods

Data collection was guided by the availability of metrics on the Halibee postcranial sample. Three distinct but largely overlapping sets of metric data were collected. The first includes all standard measurements for the Halibee fossils, with non-standard measurements added to provide a more comprehensive metric description of the remains (see Appendix 5). The second set is the comparative modern human data, which includes nearly all standard measurements and a subset of non-standard measurements collected from the Halibee fossils (see Appendix 6). The third set includes data for comparative fossils, mostly culled from the literature (see Appendix 4). Postcranial measurement definitions largely from Arsuaga et al. (2015) and Pearson (1997) were followed with some standard and non-standard additions (see Appendix 6a). The set of measurements collected includes those that capture anatomical features noted as of potential interest in elucidating the evolution of modern human skeletal form. For example, distal tufts of hand phalanges, third metacarpal styloid length, depth and width of the olecranon fossa, width of medial pillar on the humerus, femoral neck-shaft angle, and the shape of the superior articular surface on the talus (Bermúdez de Castro et al., 2012; Carretero, Arsuaga, & Lorenzo, 1997; Pablos et al., 2013b; Weaver, 2009).

Measurement equipment included digital sliding calipers (6”, 8” and 12”), 6” digital sliding caliper equipped with inner points, spreading caliper, osteometric board, cloth measuring tape, digital protractor, and USB cable for data input. All metric observations were recorded and saved in an Excel spreadsheet (.xlsx).

Standard nonmetric data were collected according to established protocols (see Appendix 6b). Scoring systems were developed for each non-standard nonmetric observation (see Appendix 7b for non-standard measurement definitions and scoring systems). All standard nonmetric features were recorded for the Middle Awash fossils (see Appendix 8), in addition to the subset of nonmetric features recorded for the modern comparative specimens. All nonmetric observations were recorded and saved in an Excel spreadsheet (.xlsx).

#### 3.2.1 Data collection from Middle Awash fossils

#### 3.2.1.1 Metric and nonmetric data

All metric and nonmetric data were collected from the original fossil specimens at the National Museum of Ethiopia using the equipment described above and following the definitions and protocols outlined in Appendices 6 and 7. Appendices 5 and 8 include all metric and nonmetric data, respectively, collected from the fossils.

#### 3.2.1.2 Photography

High-resolution photographs of the Middle Awash fossils were produced and saved as JPEG and NEF (Nikon's RAW image format) files. Photographic equipment used includes a Nikon D5500 DSLR camera, Nikon 60 mm macro lens, black velvet cloth backdrop, portable photography lights (incandescent and LED), light reflectors, sand bags, photography props (e.g., rubber washers), reference scale and stand, and a photography stand. Specimens were stabilized in the appropriate orientation using props, with a scale bar raised to the focal plane. Directional lighting was applied to highlight bony anatomy and surface detail, and reflectors were used to illuminate dark shadows (White et al., 2012). Photographs were processed in Adobe Photoshop CC 2018 and Adobe Illustrator CC 2018 (Adobe, Inc.).

#### 3.2.1.3 Laser scans

A subset of the Halibee fossils was scanned using a NextEngine Desktop 3D Scanner from NextEngine, Inc. and the proprietary ScanStudio software (NextEngine, Inc., 2006-2015). Two or three scans were recorded for each element portion at different orientations. All scans were recorded in the "Neutral" target setting and the "360" positioning setting, with between 6-12 divisions, and either 1.1k or 4.4k points/in.$^2$. The range setting was "Macro" for all element portions except the cranial vault, where the setting was necessarily adjusted to "Wide" to capture the entire surface. The number of scans taken, as well as the number of divisions and points/in.$^2$ settings were adjusted for each element portion according to the complexity of the surface topography to minimize scanning time and maximize the total anatomical information captured from the skeleton.

The scans were processed using ScanStudio software. Scans were trimmed to remove extraneous objects (e.g., rotating base and securing arm) and then manually aligned using landmarks clearly distinguishable across the multiple scans (Sholts, Wärmländer, Flores, Miller, & Walker, 2010). Once data processing was complete, the final composite scan was exported as an OBJ file.

#### 3.2.1.4 Micro computed tomography scans

Micro-computed tomography of the most complete and potentially informative elements among the Halibee fossils was completed while a micro-CT machine (Dr. G. Suwa, U. Tokyo) was at the National Museum of Ethiopia during late 2016. Raw data files were produced and saved as TIFF files. These micro-CT scans provide a means of capturing and communicating high resolution external and internal anatomy such as diaphyseal cross-sectional profiles. The

scans serve a basic descriptive purpose in the present study; a comprehensive comparative study of endostructural pattern is beyond the scope of this primary description.

### 3.2.2 Comparative fossil data collection

Measurements were collected and qualitative observations made from the original Omo I specimen at the National Museum of Ethiopia. All other fossil data included in the present study were culled from the published literature (see Appendix 4 for comparative fossil specimens and published data sources).

The partial nature of this comparative dataset reflects the fragmentary nature of Halibee fossil specimens, and the availability of published data. Published measurements were only collected in cases where equivalency between measurement definitions could be established. Qualitative morphological descriptions of comparative fossil specimens were also culled from the published literature and compiled in a database (Filemaker Pro 11, Filemaker, Inc.) for use as a comparative reference in describing the Halibee fossils. The inclusion of this large database is beyond the scope of this dissertation but was an important resource for the description reported in Chapter 6, and will be valuable for future studies of Pleistocene hominid evolution.

### 3.2.3 Comparative recent modern human data collection

Measurements collected from modern human comparative samples were selected based on an inventory of all skeletal measurements that could be reliably collected on the Halibee remains. A total of 366 metric observations were collected for the comparative modern samples, including, but not limited to, all standard measurements that can be reliably taken from the Halibee remains (see Appendix 7a for measurement protocols). These measurements span nearly all elements of the vertebral column (C3-L5; n=112 measurements), shoulder girdle and arm (n=41), hand (n=100), pelvic girdle and leg (n=40), and foot (n=73).

All data for the recent modern human comparative samples were collected by one observer (M. Brasil), save for the individuals from the Native Californian sample housed at the Phoebe A. Hearst Museum of Anthropology, where four undergraduate researchers assisted in data collection. Each undergraduate was assigned a particular set of elements to measure, with no overlap between them so as to minimize potential inter-observer error. Written protocols were developed, following published sources where possible (see Appendix 6), and revised for clarity and replicability following an initial "practice" trial. Once the protocols had been tested and revised, both intra- and inter-observer error were assessed. Three trials of measurements were collected on a sample of eight individuals, with a minimum of three days between trials. Of the 336 total measurements, 61 returned inter-observer error values above five percent (assessed between each research assistant and M. Brasil). Unsurprisingly, this included almost exclusively measurements of the vertebrae, hands, and feet, where dimensions are small and minor deviations result in significant inflation of error magnitudes and rates. The 61 measurements with inter-observer error values above five percent, and the select few where intra-observer error for the undergraduate researchers exceeded 5%, were re-collected by a single observer (M. Brasil). The intra-observer error rate for M. Brasil exceeded 5% for three of the 336 measurements: pedicle height of L5 (7.0%), lateral malleolar breadth of the talus (7.0%), and trochlear height of the talus (5.2%). These measurements were not included in analyses.

A total of eleven nonmetric traits were evaluated for the recent modern human comparative samples (see Appendix 7b for collection protocols). All nonmetric observations were made by M. Brasil. To calculate intra-observer error, five trials of nonmetric observations were collected on a sample of eight individuals, with a minimum of three days between trials. Measurement error rates for each of the eleven nonmetric traits are as follows: axillary sulcus (0%), humeral head shape (0%), olecranon fossa relative size (8.6%), olecranon fossa depth (14.3%), ulnar trochlear notch form (10%), ulnar trochlear notch orientation (5%), squatting facets on the tibia (2.5%), squatting facets on the talus (2.5%), talar trochlear shape (0%), inferior talar articular surface (0%), and anterior calcaneal facets (0%).

Adult status was confirmed for all individuals measured across all recent modern human comparative samples. For samples where sex was not known from a death record, sex estimation was made based on sexually-diagnostic cranial and pelvic characteristics (e.g., Buikstra & Ubelaker, 1994; Coleman, 1969; Phenice, 1969; White et al., 2012) and checked against the collection record.

### 3.3 Analytical methods

All statistical analyses and graphical representations were produced in the open source R statistical environment (*v3.6.1*, R Core Team, 2019). Reduced Major Axis regression was employed to estimate the stature of the HAL-VP-9/1 individual, and was completed using the package *lmodel2* (*v1.7.3*, Legendre, 2018). All graphical data visualizations were produced using the package *ggplot2* (*v3.2.1*, Wickham, 2016). Descriptive statistics were produced in Microsoft Excel.

For the HAL-VP-9/1 partial skeleton stature and body mass were estimated using regression formulae specific to the most appropriate modern comparative group. In order not to make an *a priori* judgment, stature and body mass were first estimated using several available comparative samples to evaluate how the estimates compared. The sample that was most likely to yield the most accurate estimates was then selected to produce a final estimate. This was the comparative sample most likely to have the most similar body size and proportions to the HAL-VP-9/1 partial skeleton (Feldesman & Lundy, 1988; Grine, Jungers, Tobias, & Pearson, 1995).

### 3.4 Research questions

The fossils described herein for the first time are well-positioned to further clarify how the modern human and Neanderthal lineages have evolved anatomically. With this goal in mind, this dissertation addresses two questions:

> (1) How does the skeletal anatomy represented in this assemblage compare to recent *Homo sapiens* populations?
> (2) How does the skeletal anatomy represented in this assemblage compare to their closest fossil relatives, including Neanderthals, *Homo erectus*, and chronologically intermediate groups?

Three research objectives follow directly from these research aims:

(1) To qualitatively and quantitatively characterize the skeletal anatomy of early modern *Homo sapiens* skeletal remains.
(2) To explore how these fossil morphologies compare to the range of variation observed in recent anatomically modern human comparative samples.
(3) To make systematic anatomical comparisons among the Halibee early *Homo sapiens* remains, and fossils of Pleistocene *Homo* (particularly Neanderthals and other "archaic" sets of fossils). This is an essential step in understanding the morphological evolution of our lineage and closest fossil relatives.

The second research objective will be the topic of Chapter 5, where the fossils are described relative to the five modern human samples introduced above. The third research objective is the focus of Chapter 6, where the fossils are placed in the context of the Pleistocene fossil evidence. Prior to addressing these specific objectives, however, the necessary groundwork is laid in Chapter 4, where the individual details of the HAL-VP-9/1 partial skeleton are reported. Taken together, the following three chapters comprehensively address the first of the objectives outlined above.

**Table 3.1** Recent modern human comparative samples included in this study.

| Geography | Collection type | Repository | Sample size (N) | Age |
|---|---|---|---|---|
| Southern Africa (Zulu) | Anatomical | Raymond A. Dart Collection | 34 | 20th Century |
| Northeastern Africa (Egypt) | Archaeological | National Museum of Natural History | 32 | ca. 2061 BCE-642 CE |
| Levant (Jordan) | Archaeological | National Museum of Natural History | 39+ (see text) | ca. 3300-2000 BCE |
| Western Europe (Portugal) | Cemetery | 21st Century Identified Skeletal Collection | 30 | 21st Century |
| North America (California, U.S.A.) | Archaeological | Phoebe A. Hearst Museum of Anthropology | 41 | ca. 5000-2500 BP |

## Chapter 4: Estimation of age, sex, stature, and mass of HAL-VP-9/1

This chapter presents basic details about the HAL-VP-9/1 partial skeleton, which must be established prior to assessment in a comparative context. This discussion begins with an estimation of biological age, using multiple skeletal indicators for which estimation methods have been established. An estimation of sex follows, discussing the cranial and then postcranial indicators. Lastly, estimations of stature and mass are reported. Although the description and analysis in the subsequent chapters is restricted to the postcranial evidence, associated cranial remains are considered in this chapter for the purposes of age and sex estimation.

### 4.1 Age estimation

All epiphyses on the HAL-VP-9/1 skeleton are fused, and there is no indication that this individual was subadult. There are several key aspects of the morphology that permit a more specific age estimate within the "adult" age class. Prior to moving onto these methods of age estimation, it is worth noting that tests of the various available methods indicate that the accuracy of the results vary by population and sex (Galera, Ubelaker, & Hayek, 1998; Hoppa, 2000; Key, Aiello, & Molleson, 1994; Martrille et al., 2007). However, otherwise lacking methods that are appropriately specific to Late Pleistocene African populations, these estimation methods are the best available and are applied here where preservation allowed. Because approaches that consider all of the available evidence for age at death result in more accurate estimates of age than those focusing on a single indicator (Baccino, Ubelaker, Hayek, & Zerilli, 1999; Saunders, Fitzgerald, Rogers, Dudar, & McKillop, 1992), here I consider the multiple skeletal indicators displayed on the HAL-VP-9/1 skeleton in order to make an integrated age estimation.

#### 4.1.1 Cranial sutures

Age-related changes in the degree of ectocranial suture closure have been used to develop a method for estimating age-at-death in modern humans (Meindl & Lovejoy, 1985). The HAL-VP-9/1 partial cranium does not preserve all suture segments required to calculate a composite score using the Meindl and Lovejoy (1985) method. However, four positions are preserved and can be assessed, including: anterior sagittal, bregma, midcoronal, and midlambdoid (Figure 4.1). The degree of closure was scored for each of these four positions; the first three positions were scored as zero (open) and the last was assigned a score of one (minimal closure). The midcoronal position was scored on the left side, and the position was estimated since the coronal suture is only partially preserved, missing the lateralmost portion on both the left and right sides. The portion including the midlambdoid position is not preserved, but the medially adjacent portion on the right side is preserved and was scored to serve as an approximation. The mean ages that correspond to these scores at each position are, in the order above: 31.3, 33.6, 33.8, and 40.5, with reported standard deviations for mean ages at each position ranging between 10 and 11.2 years (Meindl & Lovejoy, 1985).

The endocranial sutures are almost completely obliterated, and are only visible along the posterior third of the sagittal suture as a thin fissure. Partial preservation of the cranium precludes the application of composite scoring systems (e.g., Acsádi & Nemeskéri, 1970).

#### 4.1.2 Pubic symphyseal surface and acetabulum

The pubic symphyseal surface is widely regarded as one of the most reliable skeletal indicators of age (Brooks & Suchey, 1990; Brooks, 1955; Garvin & Passalacqua, 2012; Meindl, Lovejoy, Mensforth, & Walker, 1985; Todd, 1920). Unfortunately, the degree of post-depositional erosion to the pubic symphyseal surface is too great (Figure 4.2) for it to be used as a reliable indicator of age using established methods (e.g., Brooks & Suchey, 1990; Todd, 1920). Similarly, too little of the acetabular morphology is preserved for this region to be useful in age estimation (e.g., Rissech, Estabrook, Cunha, & Malgosa, 2006).

#### 4.1.3 Auricular surface of the ilium

The majority of the auricular surface of the right ilium is preserved, permitting the application of the Buckberry and Chamberlain (2002) and Lovejoy et al. (1985) age estimation methods (Figure 4.3). In both cases, because of the partial preservation of the auricular surface and erosional modifications to the surface texture, scores for each aspect considered were produced conservatively to reflect the uncertainty introduced by the state of preservation. The result of this conservative approach is a broad possible age range that spans multiple phases defined by these methods.

Following the Buckberry and Chamberlain (2002) method, five features of the auricular surface were scored: transverse organization, surface texture, microporosity, macroporosity, and apical changes. The ranges of scores assigned for each feature (2-4, 1-2, 1, 1, and 1-2, respectively) result in a composite score ranging from six to ten, and corresponding to age stages one through three. The mean ages of these three stages are 17.33, 29.33, and 37.86, and the ranges for each are 16-19, 21-38, and 16-65.

The reduced billowing, presence of striae, and granularity displayed by the auricular surface aligns most closely with phase three as defined by Lovejoy et al. (1985), corresponding to 30-34 years. However, a more conservative estimate that takes into account the partial preservation of the surface spans phases two through four, which range from 25 to 39 years at the upper and lower ends of these age phases.

#### 4.1.4 Composite age estimate

The mean ages corresponding to the degree of closure seen on the ectocranial sutures range between 31 and 41 years. Age range estimates based on the auricular surface include 17-38 (Buckberry & Chamberlain, 2002) and 25-39, or more likely 30-34 years (Lovejoy et al., 1985). These estimates, taken together, suggest a probable age at death in the range of 25-40 years for this individual.

### 4.2 Sex estimation

There are several key elements preserved that permit the reliable estimation of the sex of HAL-VP-9/1. Cranial and mandibular features that typically exhibit sexual dimorphism will be discussed first, followed by informative aspects of the pelvic anatomy.

#### 4.2.1 Cranium and mandible

#### 4.2.1.1 Mastoid process

Both the left and right mastoid processes are preserved, and display approximate symmetry (Figure 4.4). They are very large in absolute volume, length, and relative size compared to the external auditory meatus, and are therefore more consistent with male morphology (score of 4 or 5 following the system in Buikstra & Ubelaker, 1994).

#### 4.2.1.2 Supraorbital margin

The segment of the supraorbital margin just lateral to the supraorbital foramen is preserved, including the zygomatic process. This portion of the margin is thick and rounded, as is typical of male individuals (score of 4 or 5 following the system in Buikstra & Ubelaker, 1994).

#### 4.2.1.3 Glabellar region

The glabellar region is poorly preserved, with the external surface missing on the left side (exposing underlying trabecular bone) and the right side affected by distortion. The poor state of preservation precludes reliable scoring by the standard system (Buikstra & Ubelaker, 1994). However, despite the distortion to the right side, it appears that the glabella is large and projecting.

#### 4.2.1.4 Nuchal crest

The external surface of this region of the occipital is not preserved, precluding the use of this feature for sex estimation.

#### 4.2.1.5 Mental eminence

Only the superior part of the mental eminence is preserved. This portion is well-developed, suggesting that the mental eminence as a whole would have been large. Because the inferior portion of the symphyseal region is not preserved, this feature cannot be reliably scored according to standard criteria (Buikstra & Ubelaker, 1994). Nonetheless, the available evidence is more consistent with male morphology.

### 4.2.2 Pelvis

#### 4.2.2.1 Greater sciatic notch

The right os coxae preserves the greater sciatic notch, although the anterior and posterior margins are eroded (Figure 4.5). Despite the state of preservation, it can be determined that the greater sciatic notch is intermediate to narrow in curvature (score between 3 and 5, Buikstra & Ubelaker, 1994). These scores are consistent with intermediate to male.

#### 4.2.2.2 Subpubic angle

The preservation of the right pubis and ischiopubic ramus allows for the estimation of the subpubic angle, based on mirroring of the right side (Figure 4.6a). The estimated subpubic angle is small, more consistent with male morphology (Coleman, 1969; White et al., 2012).

#### 4.2.2.3 Ventral arc

The ventral surface of the pubis is preserved on the right os coxae (Figure 4.6a,b). There is an elevated ridge in the region where the ventral arc is typically observed, but it does not take the course that is characteristic of female pelves (Phenice, 1969; White et al., 2012).

#### 4.2.2.4 Subpubic concavity

The medial edge of the of the ischiopubic ramus is preserved on the right os coxae, displaying a very slight subpubic concavity. Although the presence of a subpubic concavity is typical of female morphology, a very slight concavity can also be observed in males (Phenice, 1969; White et al., 2012). The very slight degree of concavity displayed is more consistent with male morphology (Phenice, 1969; White et al., 2012).

#### 4.2.2.5 Medial aspect of the ischiopubic ramus

As with the features discussed above, the medial margin of the ischiopubic ramus is only preserved on the right side (Figure 4.6b,c). There is slight erosion to this region and a small segment of bone is missing, but nonetheless the morphology can still be assessed as broad and blunt, which is more often observed in males (Phenice, 1969).

#### 4.2.2.6 Preauricular sulcus

The right os coxae displays a very shallow hollowing in the area in which a true preauricular sulcus is found. A true sulcus and/or pitting in this area are related to parturition (Kelley, 1979), and therefore used as a criterion in sex estimation (Bruzek, 2002; Rogers & Saunders, 1994). Although the preauricular sulcus is most often observed in females, it can also be present in males (White et al., 2012).

#### 4.2.2.7 Size of acetabulum, obturator foramen, and os coxae

The very large acetabular diameter, obturator foramen, os coxae and overall skeletal size, make a male sex estimation highly probable for the HAL-VP-9/1 individual (Rogers & Saunders, 1994; White et al., 2012).

### 4.2.3 Composite sex estimation

The cranial and pelvic features considered above all strongly indicate that this skeletal individual is male, and this finds confirmation across the size variables introduced in the further analysis of other postcranial elements presented below.

## 4.3 Stature estimation

Because of the fragmentary nature of all of the long bones, a "mathematical" approach is taken in estimating the stature of the HAL-VP-9/1 partial skeleton, where a stature estimate is produced by using the relationship between skeletal measurements and living stature in a human reference sample (Auerbach & Ruff, 2010). This approach is limited by its requirement of a reference sample of known stature, and known length of the element used to make the estimation. Furthermore, the reference sample must be an "appropriate" reference, which has been taken to mean that it is bears some resemblance to the target individual being assessed (e.g., in terms of geography, chronology, phylogeny, etc., Ruff et al., 2012). This becomes particularly challenging in cases concerned with individuals sampling ancient populations, where the relationship between limb length and stature is unknown. Several available formulae have been employed here (Tables 4.1 and 4.2) to estimate stature, and the concordance in stature and body shape between HAL-VP-9/1 and the various reference samples is discussed.

### 4.3.1 Tibial length

Although the HAL-VP-9/1 skeleton does not preserve any complete major long bone, the left tibia is nearly complete, preserving the bone from the top of the tibial tuberosity to the complete distal end. Because many stature estimation formulae have been developed for the tibia, maximum tibial length was estimated for HAL-VP-9/1 from the preserved portion. The total length from the distal most point on the medial malleolus to the proximal most point of the tibial tuberosity was measured from HAL-VP-9/1. The same measurement was collected from n=31 individuals in the modern comparative sample of Native Californian individuals. Reduced Major Axis (RMA) regression was applied to generate an equation for maximum tibial length based on tibial length to the tuberosity. RMA regression was employed instead of Least Squares regression because the latter has been noted to underestimate values for larger individuals, and overestimate for smaller individuals (Ruff, Burgess, Squyres, Junno, & Trinkaus, 2018; Sjøvold, 1990). Considering the large size of the HAL-VP-9/1 individual, RMA regression is likely to produce a less biased estimate.

RMA regression was completed in the R statistical environment (version 3.6.1) using the package *lmodel2* (*v1.7.3*, note that RMA is equal to SMA in this package), and visualized using the package *ggplot2* (*v3.2.1*). The two tibial length measurements are strongly correlated ($r = 0.992$, $p < 0.001$; Figure 4.7). The regression formula yields a maximum length estimate of 430.86 mm for the tibia, based on the measured length (from the tibial tuberosity) of 405 mm. The formulae at the upper and lower bounds of the 95% confidence interval yield estimates of 468.90 mm and 393.06 mm, respectively, the latter of which is not possible since it is smaller than the length measurement taken from the tuberosity.

Stature was estimated using several available regression formulae derived from modern human samples of varied compositions (Table 4.1). Stature estimates reported in Table 4.1 are based on the maximum tibial length estimate of 430.86 mm (M1a in Martin System, Bräuer, 1988). The formulae employed are specific to male samples in all cases but one, where a sex-specific formula was not available (i.e., Sjøvold, 1990). Using a sex-specific equation is preferred when possible, since allometric scaling of limb lengths has been found to vary by sex (Sylvester, Kramer, & Jungers, 2008) and directional bias is reduced by using sex-specific rather than combined-sex equations (Ruff et al., 2012).

It should be noted that several of the available stature estimation equations are based on lateral tibial length (M1 in the Martin System, Bräuer, 1988), which does not include the proximal intercondylar tubercles. The stature estimates produced by these equations, using the maximum length estimate, are therefore slight overestimates. Although the size and proximal projection of the intercondylar tubercles varies, the spines usually constitute less than 10 mm of the maximum length (personal observation based on modern humans included in this study). This length has a small effect on the stature estimates, which is made clear by examining the results yielded from the formulae of Raxter (2008), where one is based on maximum length and the other on lateral length (i.e., not including the intercondylar tubercles). The difference between the estimates produced using these two equations is less than a centimeter (Table 4.1).

Stature estimates based on tibial length range from 173 to 189 cm (Table 4.1). However, because of the longer distal limbs characteristic of populations at lower latitudes, using an equation derived for a higher latitude population or pooled sample often results in overestimates of stature (Ruff et al., 2012). The estimates produced reflect this trend, with the formulae derived from European and mixed-geography samples producing larger estimates (Table 4.1). Stature estimates based on the tibia should utilize regression equations that are based on 'appropriate' reference samples (Ruff et al., 2012), meaning that body proportions of the reference sample closely resemble those of the target sample, or in this case, individual. Of the populations for which stature estimation formulae have been produced, Ancient Egyptians and Nigerians are most likely to be similar in body size and shape to HAL-VP-9/1 (Didia, Nduka, & Adele, 2009; Raxter et al., 2008), making an estimate derived using these equations less likely to be biased. Because one of the equations reported by Raxter et al. (2008) is based on a maximum tibial length measurement (i.e., including the intercondylar tubercles), the estimate of 179.25 ± 3 cm yielded by that equation is considered here to be the best available.

### 4.3.2 Additional postcranial metrics

A number of additional postcranial measurements were employed to produce stature estimations (Table 4.2). Estimates range from 157 to 189 centimeters, based on several postcranial measurements and regression formulae developed for various reference populations. However, the estimates at the lower end of this range are almost certainly underestimates, because as with stature estimates based on tibial length, the measurements employed do not scale with height consistently across the reference samples (Pablos et al., 2013a). These estimates, particularly those at the greater end of the range that are likely to be the least biased, taken together with those reported above based on tibial length, firmly indicate that the HAL-VP-9/1 individual was tall-statured. The position of this individual among recent modern humans and fossil taxa in terms of stature will be assessed in the following chapters.

## 4.4 Mass estimation

Mass estimations permit comparative size analyses between fossil specimens, in addition to stature comparisons, and contribute to our understanding of body size changes through time (Grabowski, Hatala, Jungers, & Richmond, 2015; McHenry, 1992; 2018; Ruff, Trinkaus, & Holliday, 1997). Mass estimates are also useful for scaling other morphological aspects, such as limb strength, measures of robusticity, and relative brain size (Ruff et al., 1997; 2000). Two main types of approaches exist for mass estimation, and have been shown to produce concordant

results (Auerbach & Ruff, 2004). The first, a mechanical approach, is taken here, which relies on the association between body mass and weight-bearing elements, such as articular surfaces of long bones (Auerbach & Ruff, 2004). A morphometric approach, which is based on measured pelvic breadth and estimated stature (e.g., Ruff, 1994), is not applicable in this case since bi-iliac breadth cannot be measured or reliably estimated for the HAL-VP-9/1 partial skeleton.

### 4.4.1 Femoral head

Mass estimates produced using measures of articular area, such as the commonly-used femoral head measurements, are limited by their assumption of a constant mechanical relationship between mass and articular size (Ruff et al., 2012). The relationship between body mass and femoral head size is complicated by allometric effects, making necessary size-specific regression formulae for mass estimation (Kurki, Ginter, Stock, & Pfeiffer, 2010; Ruff, 2010). Considering the large size of HAL-VP-9/1, formulae developed using large-bodied reference samples are likely to yield the most accurate estimates (e.g., Grine et al., 1995). However, as with stature, in order to assess the variation among estimates produced using different formulae, mass has been estimated using several available formulae derived using different reference populations (Table 4.3).

Most mass estimation formulae based on femoral head size use superoinferior breadth (see Table 4.3). Erosion to the inferior surface of the femoral head of HAL-VP-9/1 precludes taking this measurement. One possible alternative approach is to estimate the superoinferior dimension from the size of the acetabulum (Ruff, 2010), but this individual does not preserve the regions of the acetabular margin required to take this measurement. Fortunately, anteroposterior breadth of the HAL-VP-9/1 femoral head can be reliably measured. Anteroposterior head diameter has been used previously in place of superoinferior diameter, which has been justified by citing an average difference between these two measurements of less than 0.5% (Ruff et al., 2018). Anteroposterior breadth can also be corrected to superoinferior breadth by using the relationship observed between these two measurements across modern humans: superoinferior breadth = 1.004 x anteroposterior breadth (Ruff et al., 2006). This correction was applied to HAL-VP-9/1, which has an anteroposterior head diameter of 51.3 mm. The equation above yields an estimate of 51.5 mm for superoinferior breadth, which was used to estimate body mass (Table 4.3).

Estimates range from 60 to 89 kg, with the majority of estimates in the 75-89 kg range. The two estimates produced using the formulae published by Grabowski et al. (2015) are the lowest by far, which is unsurprising considering that their reference sample was deliberately selected to include humans of small stature and mass. This formula may work well for small-bodied hominids, which was indeed the target sample of the authors, but is likely to produce gross underestimates for an individual as large as HAL-VP-9/1.

By contrast, Grine et al. (1995) deliberately selected large-bodied human samples to produce a mass estimation formula that would be appropriate for use on the large proximal femur from Berg Aukas, Namibia. For this reason, Auerbach and Ruff (2004) recommend using this formula for large-bodied individuals. The formula of Grine et al. (1995) produces a mass estimate of 80.3 ± 4.3 kg, which is considered the most likely accurate estimate because of the greater similarity in body size between the target individual and the reference sample.

## 4.5 Summary

Based on the available evidence discussed above, this individual was very likely male and was between 25-40 years of age at the time of death. This individual was tall-statured, estimated to have stood at 179.25 ± 3 cm, and with an estimated mass of 80.3 ± 4.3 kg. These estimates provide the basic details necessary for their further consideration and evaluation of the HAL-VP-9/1 partial skeleton relative to modern humans and the Pleistocene fossil evidence, which will be the focus of the subsequent chapters.

**Table 4.1** Stature estimates based on tibial length.

| Measurement | Reference | Population | Sex | Equation | Standard Error | Estimate (in cm) | Imperial |
|---|---|---|---|---|---|---|---|
| Tibial lateral total length (M1) | Sjøvold, 1990 | Multiple | Combined | 3.29a + 47.34 (in cm) | 4.15 cm | 189.09 | 6’ 2.44” |
| Tibial maximum length (M1a) | Raxter et al., 2008 | Ancient Egyptians | Males | 2.554a + 69.21 (in cm) | 3.00 cm | 179.25 | 5’ 10.57” |
| Tibial lateral total length (M1) | Raxter et al., 2008 | Ancient Egyptians | Males | 2.552a + 70.18 (in cm) | 3.06 cm | 180.14 | 5’ 10.92” |
| Tibial lateral total length (M1) | Ross & Konigsberg, 2002 | Eastern Europeans | Males | 2.5712a + 751.85 (in mm) | 33.9 mm | 185.97 | 6’ 1.22” |
| Tibial medial total length | Duyar & Pelin, 2003 | Turkish (medium stature group) | Males | 2.057a + 944.82 (in mm) | 36.14 mm | 183.11 | 6’ 0.09” |
| Tibial medial total length | Duyar & Pelin, 2003 | Turkish (tall stature group) | Males | 1.530a + 1224.15 (in mm) | 35.08 mm | 188.34 | 6’ 2.15” |
| Tibial maximum length (M1a) | Ruff et al., 2012 | Southern European samples | Males | 2.78a + 60.76 (in cm) | 3.05 cm | 180.54 | 5’ 11.08” |
| Tibial medial total length | Didia et al., 2009 | Nigerians | Males | 2.9289a + 46.8421 (in cm) | None reported | 173.04 | 5’ 8.13” |

**Table 4.2** Stature estimates based on various postcranial measurements.

| Measurement | Reference | Population | Sex | Equation | Standard Error | Estimate (in cm) | Imperial |
|---|---|---|---|---|---|---|---|
| Ulna (distal breadth) | Badkur & Nath, 1990 | Indians | Males | 4.63a + 1587.17 (in mm) | 35.49 mm | 167.53 | 5’ 5.96” |
| Femur (lateral condyle length) | Bidmos, 2008b | South Africans of European descent | Males | 1.31a + 72.32 (in cm) | 5.31 cm | 169.82 | 5’ 6.86” |
| Femur (lateral condyle length) | Bidmos, 2008a | Indigenous South Africans | Males | 0.96a + 90.86 (in cm) | 4.36 cm | 162.31 | 5’ 3.9” |
| Femur (lateral condyle height) | Simmons, Jantz, & Bass, 1990 | American blacks | Males | 1.34a + 113.23 (in cm) | 6.91 cm | 170.11 | 5’ 6.97” |
| Femur (lateral condyle height) | Simmons et al., 1990 | American whites | Males | 1.47a + 107.09 (in cm) | 6.24 cm | 169.49 | 5’ 6.73” |
| Calcaneus (body height) | Bidmos & Asala, 2005 | South African blacks | Males | 0.75a + 118.67 (in cm) | 5.47 cm | 157.07 | 5’ 1.84” |
| Calcaneus (length) | Bidmos & Asala, 2005 | South African blacks | Males | 0.63a + 100.87 (in cm) | 5.34 cm | 159.69 | 5’ 2.87” |
| MC3 (length) | Meadows & Jantz, 1992 | American blacks | Males | 1.279a + 81.61 (in cm) | 5.36 cm | 172.59 | 5’ 7.95” |
| Calcaneus (maximum calcaneal length (a) and posterior calcaneal length (b)) | Holland, 1995 | American blacks | Males | 0.373a + 0.790b +98.38 (in cm) | 4.75 cm | 189.43 | 6’ 2.58” |
| Calcaneus (maximum calcaneal length (a) and maximum talar length (b)) | Holland, 1995 | American blacks | Males | 0.362a + 0.707b + 103.27 (in cm) | 4.59 cm | 180.31 | 5’ 10.99” |
| Calcaneus (posterior calcaneal length (a) and maximum talar length (b)) | Holland, 1995 | American blacks | Males | 0.792a + 0.709b + 85.28 (in cm) | 4.38 cm | 185.01 | 6’ 0.84” |
| Calcaneus (maximum length) | Pablos et al., 2013a | American blacks | Males | 9.789a + 965.838 (in mm) | 33.49 mm | 187.97 | 6’ 2” |
| Talus (maximum length) | Pablos et al., 2013a | American blacks | Males | 14.765a + 858.359 (in mm) | 33.49 mm | 176.14 | 5’ 9.35” |

**Table 4.3** Mass estimates based on femoral head diameter.

| Measurement | Reference | Population | Sex | Equation | Standard Error (in kg) | Estimate (in kg) |
|---|---|---|---|---|---|---|
| Femoral head diameter (superoinferior breadth) | Ruff et al., 2018 | Multiple | Combined | 2.262a - 38.7 (in mm) | 5.3 | 77.793 |
| Femoral head diameter (superoinferior breadth) | Grabowski et al., 2015 | Multiple | Combined | 1.574a - 2.10269 (natural log-transformed) | 0.249 (natural log-transformed) | 60.422 |
| Femoral head diameter (anteroposterior breadth) | Grabowski et al., 2015 | Multiple | Combined | 1.528a -1.91619 (natural log-transformed) | 0.250 (natural log-transformed) | 60.377 |
| Femoral head diameter (superoinferior breadth) | Ruff, Scott, & Liu, 1991 | American blacks | Combined | 2.015a -15.2 (in mm) | 18.3 | 88.573 |
| Femoral head diameter (superoinferior breadth) | Ruff et al., 1991 | American blacks and whites | Males | 2.741a - 54.9 (in mm) | 13.7 | 86.262 |
| Femoral head diameter (superoinferior breadth) | Ruff et al., 1997 | Multiple | Combined | 2.239a - 39.9 (in mm) | Not reported | 75.409 |
| Femoral head diameter (superoinferior breadth) | McHenry, 1992 | Multiple | Combined | 1.7125a - 1.0480 (least squares; log-transformed) | 0.033 (log-transformed) | 76.466 |
| Femoral head diameter (superoinferior breadth) | McHenry, 1992 | Multiple | Combined | 1.7538a - 1.1137 (reduced major axis; log-transformed) | Not reported | 77.351 |
| Femoral head diameter (superoinferior breadth) | Ruff et al., 2012 | Multiple European regions | Males | 2.8a - 66.70 (in mm) | 6.84 kg | 77.5 |
| Femoral head diameter (superoinferior breadth) | Grine et al., 1995 | Multiple | Combined | 2.268a - 36.5 (in mm) | 4.3 kg | 80.302 |

**Figure 4.1** HAL-VP-9/1 cranial vault in (A) superior and (B) posterior views. Anterior is to the left in superior view. White circles indicate suture positions assessed for age estimation and discussed in the text.

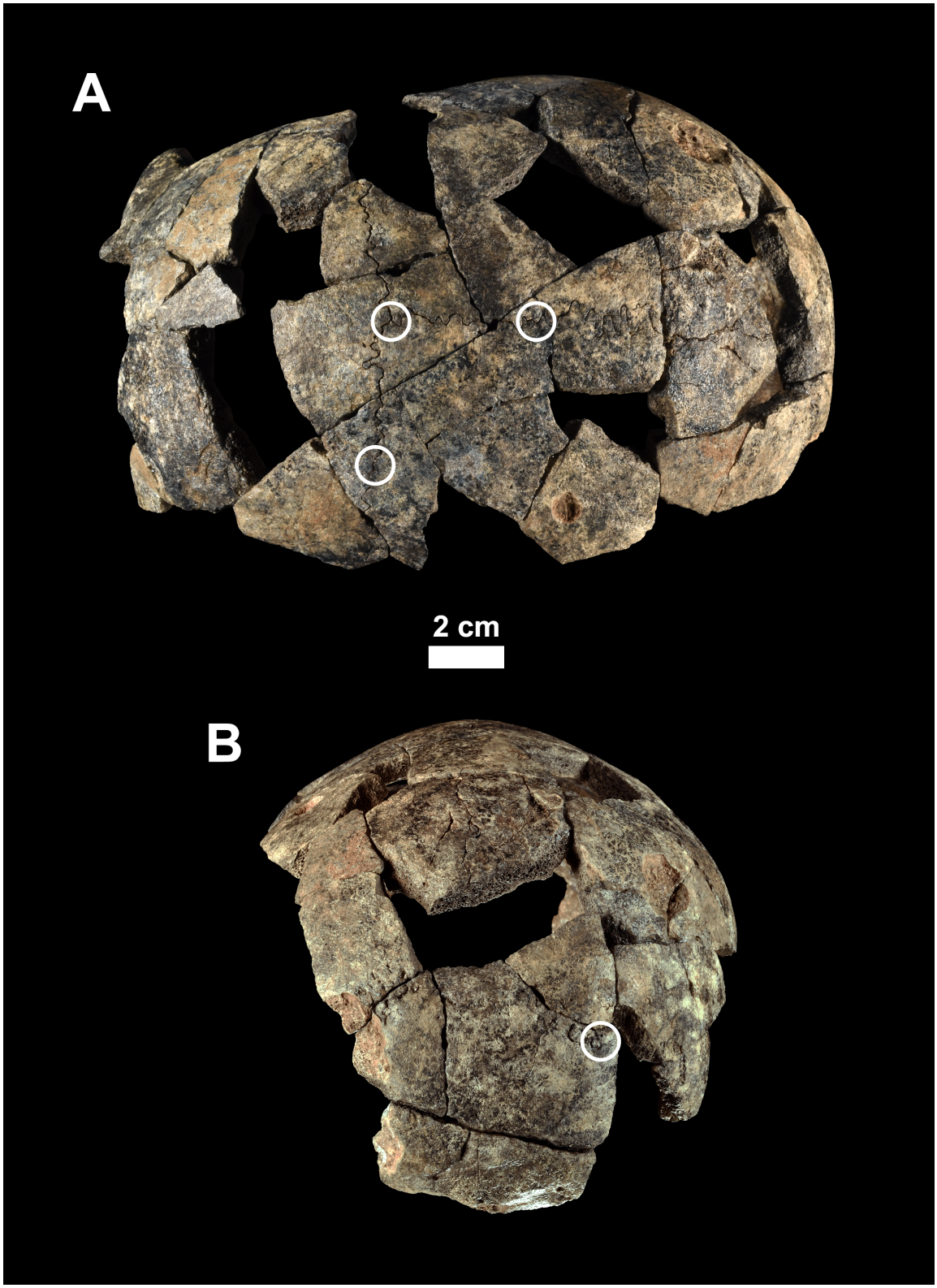


**Figure 4.2** HAL-VP-9/1 right pubic symphyseal surface in medial view (superior is up and ventral is to the left). Erosion to the surface precludes the use of this region as a reliable indicator of age.



**Figure 4.3** HAL-VP-9/1 right auricular surface in medial view (posterior is down).



**Figure 4.4** HAL-VP-9/1 (A) right and (B) left mastoid processes in lateral view. Anterior is to the right in (A) and to the left in (B).

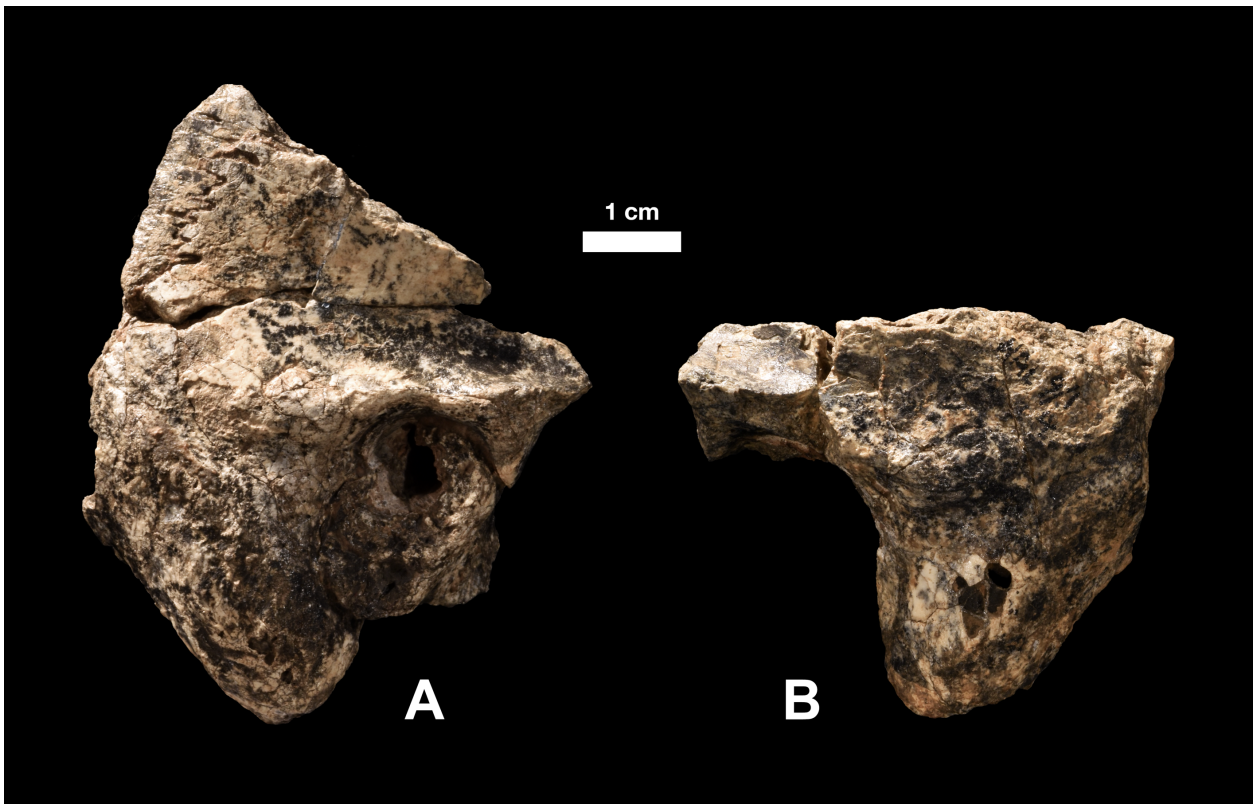


**Figure 4.5** HAL-VP-9/1 right greater sciatic notch in medial view. The white curve reflects an estimation of the true curvature that accounts for erosion to the anterior and posterior portions of the greater sciatic notch.



**Figure 4.6** HAL-VP-9/1 right os coxae in (A) anterior, (B) medial, and (C) oblique anterior views. Superior is up. Note the absence of a ventral arc (A, B) and the broad and blunt medial margin of the ischiopubic ramus (B, C).

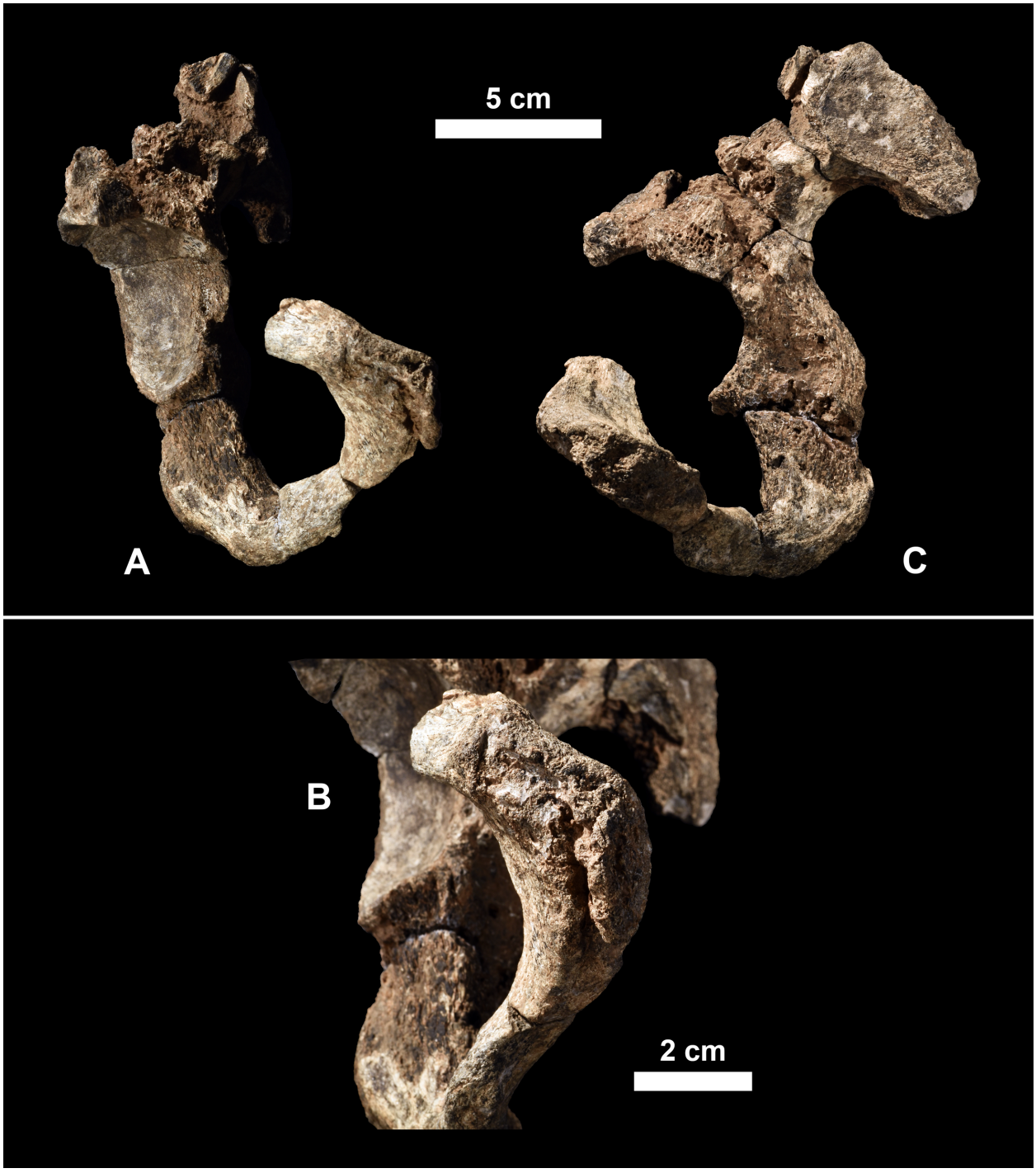
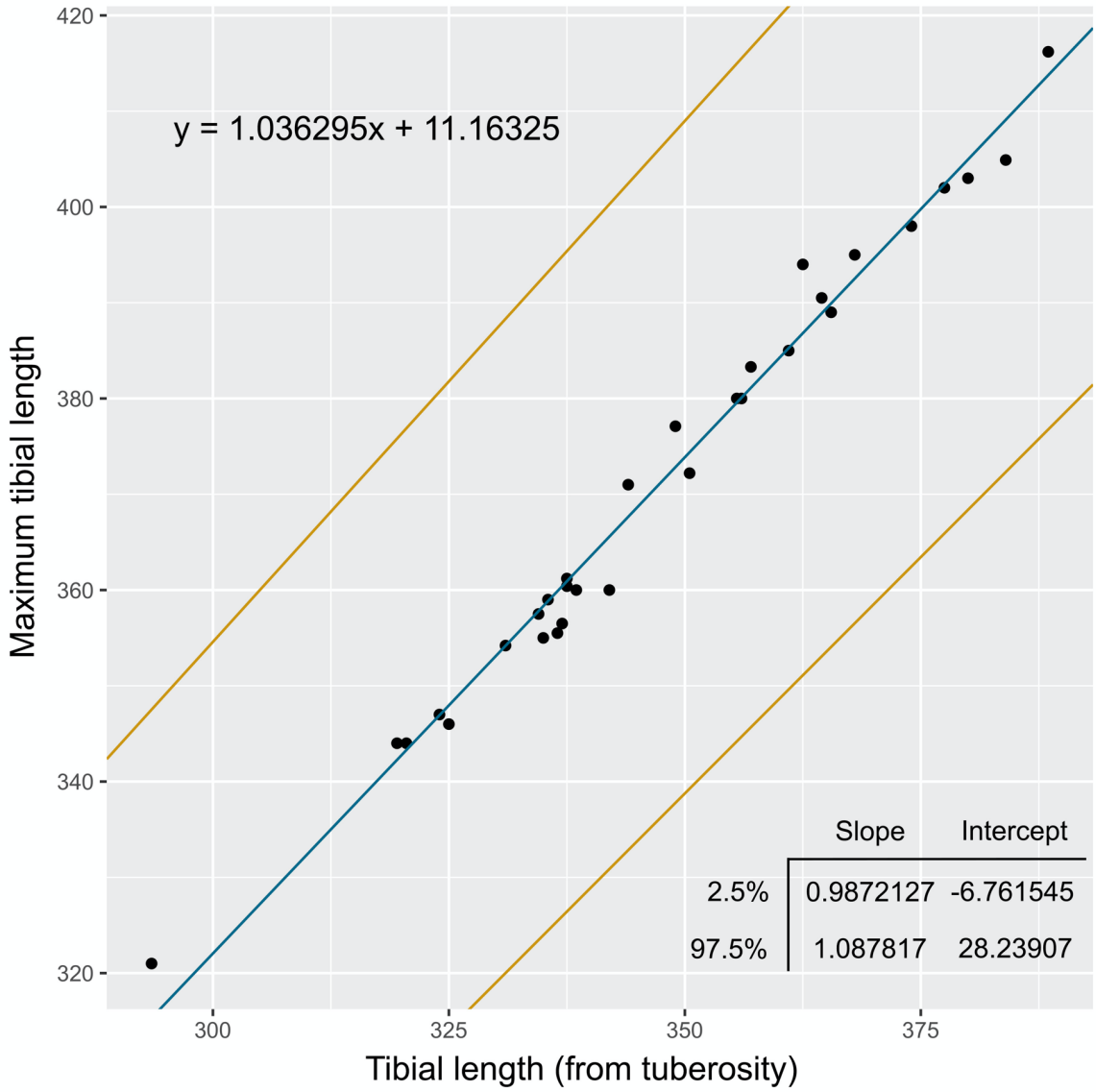


**Figure 4.7** Reduced Major Axis (RMA) regression between maximum tibial length (in mm) and tibial length between the top of the tuberosity and the distal most point on the medial malleolus (in mm). The RMA line is plotted in blue, and the 95% confidence intervals are plotted in yellow.



## Chapter 5: The Halibee fossils in the context of modern human variation

Having established that the Halibee postcranial fossils meet the diagnostic criteria for inclusion in *Homo sapiens* (see Chapter 2), the present chapter describes the skeletal anatomies relative to recent modern humans. The skeletal anatomy of the fossils is characterized in qualitative and quantitative terms by comparing these fossils with five recent modern human samples. Considering the ca. 100 ka between recent modern humans and the Halibee fossils, and the varied morphologies chronologically preceding the fossils as reported for Herto and Omo I (Pearson, Royer, Grine, & Fleagle, 2008b; White et al., 2003), it is reasonable to expect that some aspects of skeletal anatomy will differ between the fossils described herein and recent modern humans.

Comparisons in this chapter are centered on HAL-VP-9/1 because of the completeness of this skeletal individual. Metrics and qualitative descriptions of additional fossils from the postcranial sample are included where available and relevant. The comparative description is primarily metric, with qualitative descriptions included where quantitative measures cannot reliably capture morphologies of interest. Because of the small fossil sample size (n=1 for most metrics), comparisons are presented visually as bivariate and box plots, rather than as statistical assessments.

The results are organized first by anatomical region and then by element. The comparative descriptions are limited to the most complete and informative elements; detailed preservational descriptions are reported in Appendix 3 for all preserved portions. The most complete portions of each element are introduced in-text (and identified by suffix) at the start of each section, followed by a comparative description of the most informative portions. Following the comparative descriptions presented by anatomical region, the stature and mass of HAL-VP-9/1 relative to recent modern humans is presented.

Measurements of the fossils are reported in tabular format in Appendix 5. Measurement definitions and sources are reported in Appendix 6, and measurement protocols are detailed in Appendix 7. Nonmetric observations of the fossils are reported in Appendix 8. Summary statistics for the comparative modern human samples are reported in Appendix 9.

### 5.1 Axial skeleton

#### 5.1.1 Vertebrae

All regions of the vertebral column of HAL-VP-9/1 are partially represented. The cervical vertebrae include the anterior midline portion of the axis (lacking the dens; HAL-VP-9/1-23) and bodies of the fourth through seventh vertebrae (HAL-VP-9/1-24 through -27). The thoracic vertebrae include a single nearly complete upper vertebra, likely first or second in the sequence (HAL-VP-9/1-30), as well as five partial bodies spanning the upper to lower portions of the column (HAL-VP-9/1-31 through -35). The lumbar vertebrae include partial first, second, and third vertebrae (HAL-VP-9/1-49 through -51) and complete bodies of the fourth and fifth (HAL-VP-9/1-52 and -53).

The fourth through seventh cervical vertebrae fall within the modern human range for ventral height of the body and superior dorsoventral height (Figure 5.1), with the lowest two vertebrae in this sequence falling at the edge of the bivariate distribution (C-7; Figure 5.1D) or just beyond it (C-6; Figure 5.1C). The transverse shape of the fourth and fifth cervical bodies is

also within the modern range, and falls within the range of the Native Californian sample, which tends to have greater transverse relative to dorsoventral body diameters (Figure 5.2A,B). Pedicle height could be measured for the fourth and sixth vertebrae, and is at the upper end of the range for the fourth (Figure 5.2C) and well beyond the upper end of the range for the sixth (Figure 5.2D).

Measurements of the first, fourth and fifth lumbar vertebral bodies fall well within the modern human range, and not far from mean values for most metrics (Figure 5.3). The moderate size of the vertebral bodies is unusual, considering the large size of the cervical vertebrae and the exceptional size of much of the appendicular skeleton, which will be described below and in the subsequent chapter.

### 5.1.2 Ribs and sternum

The costal skeleton of HAL-VP-9/1 is highly fragmented, with only small fragments preserved (HAL-VP-9/1-61 through -95; see Appendix 3 for inventory). None of the sternum is preserved.

## 5.2 Appendicular skeleton

### 5.2.1 Shoulder girdle

The clavicle is represented by three small shaft fragments (HAL-VP-9/1-96 through -98). Both left and right scapulae are present, although fragmentary. Scapular remains include both acromial processes and the right scapular spine (HAL-VP-9/1-100 and -104), fragments of both inferior angles (HAL-VP-9/1-103 and -105), partial right glenoid (HAL-VP-9/1-101), and the axillary border of the right side (HAL-VP-9/1-102).

### 5.2.2 Arm

The right humerus is represented by a complete head (HAL-VP-9/1-112), and complete distal end with most of the shaft (HAL-VP-9/1-113). Of the left humerus, the complete head (HAL-VP-9/1-115), partial distal end (HAL-VP-9/1-116), and shaft portion with the deltoid tuberosity (HAL-VP-9/1-117) are preserved. The radial head (HAL-VP-9/1-119), most likely from the right side, and a radial shaft fragment (HAL-VP-9/1-120) are preserved. Of the ulna, the right side includes the complete proximal end (HAL-VP-9/1-121) and midshaft portion (HAL-VP-9/1-122). The left side includes the partial proximal end (HAL-VP-9/1-123), complete distal end (HAL-VP-9/1-124) and a distal shaft fragment (HAL-VP-9/1-125).

In addition to the HAL-VP-9/1 individual, four other individuals preserve arm elements. The first includes a complete right distal humerus (TAL-VP-7/36-H) and a right distal radius (TAL-VP-7/36-I), the latter of which is deeply eroded on most surfaces. The second individual is known from a single fragment, a complete radial head, likely from the left side (HAL-VP-2/16). The third individual is known from three portions of right arm elements: a complete proximal humerus (HAL-VP-9/930-A), proximal ulna (HAL-VP-9/930-B), and distal ulnar epiphysis (HAL-VP-9/930-C). The former two portions are badly eroded, the humeral head also having been affected by expanding matrix distortion (as defined in White, 2003). The distal ulnar epiphysis had not completely fused at the time of death, indicating that the individual was likely

an adolescent between the ages of 14-20 (White et al., 2012). The fourth individual is the second partial skeleton from Halibee (HAL-VP-9/1520; see Chapter 2), which includes a partial right distal humerus, shaft fragment with possible deltoid (HAL-VP-9/1520-H), and right ulnar shaft (HAL-VP-9/1520-M).

The humerus of HAL-VP-9/1 is striking in its proportions, with massive proximal and distal ends at the upper edge of the modern range (Figure 5.4 and 5.5A) but moderate cross-sectional dimensions at midshaft (Figure 5.5B). The relationship between the humeral ends and shaft dimensions is most similar to the proportions observed for the Native Californian sample (Figure 5.5C,D). The morphology of the distal end of the humerus is unusual in some respects, relative to modern humans. For example, the bicondylar breadth alone is striking in size, falling at the upper end of the modern range, but when considered relative to the thickness of the medial pillar, falls outside of the modern bivariate distribution (Figure 5.5E). A similar, although less pronounced pattern is also observed when considering the thickness of the medial pillar relative to the medial epicondyle width (Figure 5.5F). The olecranon fossa breadth of HAL-VP-9/1 relative to the medial pillar thickness is also at the edge of modern variation (5.5G). The HAL-VP-9/1 individual is also at the edge of the bivariate distribution for relative thicknesses of the medial and lateral pillars (Figure 5.5H), a feature which, as with olecranon fossa breadth, has been suggested to differentiate Neanderthals from modern humans (Carretero et al., 1997), and will also be considered in the following chapter. As with the proportional relationship between the humeral ends and the shaft dimensions, the distal morphology HAL-VP-9/1 falls closest to the Native Californian sample.

The additional postcranial remains in the sample mirror the position of HAL-VP-9/1 relative to modern variation in some aspects, and differ in others. For example, whereas HAL-VP-9/1 falls at the edge of modern variation, the distal end dimensions of TAL-VP-7/36 fall well within range (Figure 5.5E-H). The vertical head diameter for HAL-VP-9/930 is above all modern human sample averages, but is not as extreme in size as HAL-VP-9/1 (Figure 5.6A). Both HAL-VP-9/1 and HAL-VP-9/1520 have moderate humeral shaft circumferences, either near or just above the modern human sample averages (Figure 5.6B). Thickness of the medial pillar is the most variable dimension sampled by the Halibee fossils, with relatively thin pillars in HAL-VP-9/1520 and especially HAL-VP-9/1, and a much thicker pillar in TAL-VP-7/36 (Figure 5.5E-H and 5.6C).

The radius, like the humerus, is characterized by a massive proximal end (Figures 5.7 and 5.8A,B), which is particularly notable when considered relative to the moderate shaft dimensions (Figure 5.8B). Because the radial portions are limited to the head and a small shaft fragment of indeterminate side and placement, the ulnar shaft is used here to compare end and shaft dimensions. Similar to the proportions observed in the humerus, whereas the anteroposterior diameter of the ulnar shaft is just above the mean for the modern range, the radial head circumference exceeds the greatest values recorded for the modern comparisons (Figure 5.8B). However, as with the distal humerus, there is variation in this dimension, with HAL-VP-2/16 measuring above modern sample means but within range (Figure 5.8D). In contrast with the generally large dimensions of HAL-VP-9/1, the distal radius of TAL-VP-7/36 is moderate in breadth, but thin in anteroposterior diameter, placing it at the edge of the modern bivariate distribution (Figure 5.8C).

As with the other arm elements, the ulna is characterized by a very large proximal end both in absolute terms and relative to shaft dimensions (Figures 5.9 and 5.10A,F). The ulnar trochlea is very long, reflecting a large articular surface. The distal end is also at the upper end of

the modern range, as is the shaft minimum circumference (although the latter may be slightly inflated since only a small portion of the distal shaft is preserved, and may not include the point with the smallest circumference; Figure 5.10B).

The radial notch is very large (Figure 5.10C), consistent with the large articular surfaces observed elsewhere, such as the proximal radius discussed above. The coronoid process is tall in absolute terms and relative to the height of the olecranon process, aligning it more closely with the Native Californian, Portuguese, and South African samples (Figure 5.10D). The trochlea is very thick, and the length of the olecranon process is moderate (Figure 5.10E). However, as with the humeral dimensions, the fossil sample captures variation in the trochlear thickness between HAL-VP-9/1 and HAL-VP-3/1, corresponding roughly to the upper and lower bounds of the Native Californian sample (Figure 5.10G). If a modern human sample is taken as a reference for population-level variation, then the fossils appear to be sampling the ends of that range in a Late Pleistocene population. Ulnar shaft minimum circumference is above average but within range for both HAL-VP-9/1 and HAL-VP-9/1520 (Figure 5.10H).

### 5.2.3 Hand

Carpals of the right hand include a complete hamate (HAL-VP-9/1-128), complete trapezium (HAL-VP-9/1-129), and complete triquetral (HAL-VP-9/1-130). The right second metacarpal is represented by the base (HAL-VP-9/1-134) and head with shaft (HAL-VP-9/1-135). The complete right third metacarpal (HAL-VP-9/1-136) is preserved, as is the right fourth metacarpal base with shaft (HAL-VP-9/1-137).

Carpals of the left hand include a complete lunate (HAL-VP-9/1-131), complete capitate (HAL-VP-9/1-132), and complete triquetral (HAL-VP-9/1-133). The head of the first metacarpal (HAL-VP-9/1-138) and the base (HAL-VP-9/1-139) and head (HAL-VP-9/1-140) of the second metacarpal are preserved, as well as the shaft of the third metacarpal (HAL-VP-9/1-144), the head and shaft of the fourth metacarpal (HAL-VP-9/1-141), and the base with shaft (HAL-VP-9/1-142) and head (HAL-VP-9/1-143) of the fifth metacarpal.

Phalangeal elements are represented by a complete proximal hand phalanx (HAL-VP-9/1-145), four partial proximal hand phalanges (HAL-VP-9/1-146 through 149), a complete intermediate hand phalanx (HAL-VP-9/1-150), five partial intermediate hand phalanges (HAL-VP-9/1-151 through 155), a complete terminal hand phalanx (HAL-VP-9/1-157), and the base of the terminal hand phalanx of ray I (HAL-VP-9/1-158). In addition to the HAL-VP-9/1 individual, there is a single terminal hand phalanx in the sample, likely of a first ray (HAL-VP-3/15).

All of the carpals are large, with some exceeding the modern range in some dimensions (Figure 5.11). The lunate is long (in approximate proximodistal dimension) relative to its breadth (approximately corresponding to dorsopalmar height; Figure 5.12A). The triquetral follows a similar pattern, sitting just outside of the modern bivariate distribution for width (approximately corresponding to the dorsopalmar diameter) and maximum length (Figure 5.12B). The trapezium is very long, and follows the same pattern of large articular surfaces observed elsewhere in having a long facet for the first metacarpal (Figure 5.12C,D). Large articular surfaces are also reflected in the large size of the capitate base and especially head, with the latter exceeding the modern range (Figure 5.13). The height of the hamate (approximately dorsopalmar) is at the upper end of the modern range, whereas the width (approximately proximodistal) is moderate (Figure 5.14A). The hamulus is very large, both in terms of width and height (i.e., projection of

the hamulus above the body), exceeding the heights observed in the modern samples (Figure 5.14B,C). Because the hamulus serves as an attachment point for the transverse carpal ligament that bridges the carpal tunnel, the size of the hamulus reflects the depth of the tunnel (Trinkaus, 1983b). The potential functional and evolutionary implications of this morphology will be discussed in the subsequent chapter.

The metacarpals display a similar pattern to the arm elements described above in having large proximal and distal ends relative to shaft cross-sectional dimensions. The distal end of the first metacarpal is broad relative to its height (Figure 5.15A), whereas the second is at the upper end of the modern range for both dimensions (Figure 5.15B). The second metacarpal base is wide and especially tall, falling beyond the upper end of the modern range (Figure 5.15C). The third metacarpal base is both wider and taller than all modern humans in the comparative sample (Figures 5.16 and 5.17A), and the head, as with the first metacarpal, is broad relative to its height (Figure 5.17B). The shaft follows this same pattern, with a midshaft that is broad relative to its height (Figure 5.17C). The third metacarpal is long and has a large base and head relative to the height at midshaft, falling just beyond the bivariate distribution of these traits (Figure 5.17D-G). The proximal facet (for the capitate) falls closer to the upper end of the distribution for the palmar and dorsal widths, but well within range (Figure 5.17H). The fourth and fifth metacarpals follow a similar pattern to the others in having large dimensions of the base and head (Figure 5.18A,B,D,E), and for the fourth metacarpal, a broad midshaft relative to its height (Figure 5.18C).

### 5.2.4 Pelvic girdle

The right os coxae preserves most of the lower portion, including the ischium, pubis, acetabulum, and posteroinferior part of the ilium (HAL-VP-9/1-106A+B). Much of the right iliac blade is missing. The left os coxal portion includes the ischium with a small part of the acetabulum (HAL-VP-9/1-108). Only small portions of the sacrum are present, including partial alae and bodies (HAL-VP-9/1-57 through -59). None of the coccyx is preserved.

The right os coxae has a very large acetabulum, an absolutely elongate ischium, and a long ischiopubic ramus, falling near the upper end of the modern range for these metrics, and closest to the Native Californian sample (Figure 5.19 and 5.20A,B). The acetabulum and femoral head, as the two articulating parts of the hip joint, correspond closely in size (Plavcan, Hammond, & Ward, 2014). This relationship is clear in the HAL-VP-9/1 individual, where the very large acetabulum matches the very large size of the femoral head described in the following section. As pelvic size and body size are also known to be correlated in humans (Tague, 2000), the overall large pelvic dimensions are attributable at least in part to the general large body size of this individual. The proportions and qualitative features of the os coxae will be discussed in detail in the subsequent chapter, particularly those that have been described as differing significantly between Neanderthals and modern humans (e.g., superior pubic ramus length and cross-sectional shape, Arsuaga et al., 1999a; Rosenberg, 1988; Trinkaus, 1976b).

### 5.2.5 Leg

Portions of both right and left legs are preserved. The right femoral remains include the complete proximal femur (HAL-VP-9/1-160) and partial distal end with shaft (HAL-VP-9/1-161+167). The left femur is known from a portion of the shaft and condyle fragments (HAL-VP-

9/1-163 through -166, -168). Both the right (HAL-VP-9/1-186) and left (HAL-VP-9/1-187) patellae are nearly complete. The right tibial remains include a partial distal end with shaft (HAL-VP-9/1-173) and a midshaft portion (HAL-VP-9/1-174+175). The complete distal end with much of the shaft of the left tibia is preserved, the proximal extent of the preserved portion corresponding to the top of the tibial tuberosity (HAL-VP-9/1-177+178). Both the right (HAL-VP-9/1-180) and left (HAL-VP-9/1-182) distal fibular ends are preserved.

In addition to the HAL-VP-9/1 individual, the second partial skeleton from Halibee (HAL-VP-9/1520; see Chapter 2) preserves elements of the leg, including the left (HAL-VP-9/1520-I) and right (HAL-VP-9/1520-J) femoral shafts, and the right tibial shaft (HAL-VP-9/1520-D).

Mirroring the large size of the acetabulum, the proximal femur of HAL-VP-9/1 is massive, at the upper edge of modern variation for vertical head diameter and beyond it for biomechanical neck length and anteroposterior head diameter (Figure 5.21 and 5.22A,B). The shaft dimensions at midshaft for HAL-VP-9/1520 are near the upper end of the modern range (Figure 5.22C). The femoral neck angle of HAL-VP-9/1 is below the modern mean, and at the edge of the bivariate distribution with anteroposterior head diameter (Figure 5.22B). Femoral neck-shaft angle is known to vary considerably across modern humans, but the factors underlying this variation are still under debate. On one hand, some studies propose that variation in neck-shaft angle is primarily the result of differences in habitual activities during ontogeny, with higher neck-shaft angles typically associated with decreased levels of mobility (Anderson & Trinkaus, 1998; Child & Cowgill, 2017; Trinkaus, 1993a). On the other hand, others have proposed that variation in this trait is most closely tied to variation in climate-induced body proportions, with lower angles generally observed in colder climates (Gilligan, Chandraphak, & Mahakkanukrauh, 2013; Weaver, 2003). The femoral neck-shaft angle of HAL-VP-9/1 (122.5º) is toward the lower end of expected values for an individual from a warm climate, and well below the approximate global mean of 127º based on 100 modern groups, but is within the reported range of most modern samples (Gilligan et al., 2013).

The patellae of HAL-VP-9/1 are moderate in height, and are at the upper end of the modern range for breadth (Figure 5.23 and Figure 5.24A). They are notable in their thickness, where they exceed the greatest modern human measurements (Figure 5.24B,C).

The tibia of HAL-VP-9/1 is striking in its length, the estimated value exceeded by only three of 145 modern human individuals in the comparative sample (Figures 5.25A,B and 5.26A,B). The maximum shaft diameter is similarly at the edge of the modern distribution (Figure 5.26A), while the mediolateral shaft diameter is moderate (Figures 5.25A,B and 5.26B). The tibia of HAL-VP-9/1520 follows a similar pattern, with a large maximum shaft diameter in absolute terms and relative to the mediolateral shaft diameter (Figures 5.25G-I and 5.26D). At midshaft, the anteroposterior diameter of HAL-VP-9/1 exceeds the modern range, and for HAL-VP-9/1520 is at the upper end (Figure 5.27A). The large shaft circumference reflects the large anteroposterior shaft diameter that characterizes both HAL-VP-9/1 and HAL-VP-9/1520, as does the low platycnemic index (Figure 5.26C and Figure 5.27C). The significance of these shaft dimensions will be discussed in the subsequent chapters. Similarly to the other long bones, the size of the tibial distal end of HAL-VP-9/1 is striking (Figure 5.26E,F). This is particularly true relative to mediolateral shaft diameter, where HAL-VP-9/1 falls at the upper end of the Native Californian range (Figure 5.26F).

The distal fibular end of HAL-VP-9/1 is only moderate in size, falling near the center of the modern human distribution (Figures 5.28 and 5.29A). This moderate size stands in contrast to

the large size observed for the other long bone ends (e.g., the tibial distal end; Figure 5.29C,D). However, in terms of the distal articular surface, the large articular surface size of HAL-VP-9/1 places it at the edge of the modern range (Figure 5.29B).

### 5.2.6 Foot

Remains of the right foot include a complete talus (HAL-VP-9/1-188) and calcaneus (HAL-VP-9/1-189), base of the third metatarsal (HAL-VP-9/1-194), and base with shaft of the fourth metatarsal (HAL-VP-9/1-195). The left foot remains include a complete talus (HAL-VP-9/1-190), calcaneus (HAL-VP-9/1-191), navicular (HAL-VP-9/1-192), and cuboid (HAL-VP-9/1-193), as well as the base (HAL-VP-9/1-196) and head (HAL-VP-9/1-197) of the first metatarsal, base of the third metatarsal (HAL-VP-9/1-198), and base (HAL-VP-9/1-199) and head (HAL-VP-9/1-200) of the fifth metatarsal. Pedal phalangeal remains (side indeterminate) include a complete proximal foot phalanx (HAL-VP-9/1-203) and a complete intermediate foot phalanx (HAL-VP-9/1-204).

The talus of HAL-VP-9/1 falls beyond the modern human range in several features. The talus is long, tall, and very wide (Figures 5.30 and 5.31A,B). The talar head and neck are short relative to total talar length, and the talar head is narrow relative to its length (Figure 5.31C,D). As with the distal fibula, the articular surfaces of the talus are large (Figure 5.31E,F). The most notable example is the posterior subtalar facet, which surpasses the upper end of the modern range by several millimeters (Figure 5.31F). The large articular surfaces observed here and elsewhere throughout the HAL-VP-9/1 skeleton are to be expected, considering the close relationship between body mass and articular surface size of the long bones observed in primates (Ruff, 2003) and between body mass and talar articular surface size in hominoids at both the inter- and intra-specific levels (Parr, Chatterjee, & Soligo, 2011).

The calcaneus is similarly large in most dimensions, including in maximum length, breadth, and height (Figures 5.32 and 5.33A,B). The calcaneal tuber is massive, as is apparent from the position of HAL-VP-9/1 at the upper end of the modern human range for calcaneal body height, and beyond it for posterior length (Figure 5.33B). These large dimensions, however, stand in slight contrast to the minimum breadth of the calcaneal body, which is more moderate in size (Figure 5.33C,D).

The cuboid is near the upper end of the modern range in both breadth and height, and is moderately long (Figures 5.34 and 5.35A,B). As observed on the talus and distal fibula, the articular surfaces are very large, particularly the facet for the calcaneus, which exceeds the modern range (Figure 5.35C). The navicular is also long, broad, and moderately tall, with a large facet for the talar head that is at the upper end of the modern range (Figures 5.34 and 5.36).

The metatarsals mirror the metacarpals in terms of the large size of the ends. The proximal ends of the first, third, fourth, and especially fifth metatarsals are strikingly large, and are at the upper end or just beyond the modern range (Figures 5.37 and 5.38A,C-E). Only the heads of the first and fifth metatarsals are preserved, and while the first metatarsal head is broad relative to its height and moderate in size, the fifth metatarsal head is very large and particularly broad, falling well above the modern range (Figure 5.38B,F).

## 5.3 Body size comparisons

### 5.3.1 Stature

The best available stature estimate for HAL-VP-9/1 is 179.25 ± 3 cm (see Chapter 4 for details). This estimate falls at the upper end of a previously reported male eastern African range (including individuals from Kenya and Uganda) of 146-185 cm (mean of 166.4 cm), and well above the male Pecos Pueblo Native American range (155-168 cm, mean of 161.2, Ruff, 2000). Among reported statures for other modern samples, the HAL-VP-9/1 estimate falls above average and close to the upper end of the estimated range for most, with the exception of the Skhul/Qafzeh sample (Gallagher, 2013). The HAL-VP-9/1 estimate also exceeds the range (mean ± two SDs) reported by Auerbach (2012) for several modern samples and falls at the upper end of the ranges for samples from Nubia, Medieval Germany, and Medieval Scotland, emphasizing the tall stature of this individual.

The estimated stature range for HAL-VP-9/1 spans the "tall" (170-179.9 cm) and "very tall" (180-199.9 cm) categories for male modern humans, falling short of "giant" (>200 cm) as defined by Martin and Saller (1957). This aligns HAL-VP-9/1 with what has been called the "derived biotype" within genus *Homo*, following a change ca. 200 ka from shorter and broader bodies to taller and more slender ones (Carretero et al., 2012). The evolution of human stature and position of HAL-VP-9/1 relative to other fossil taxa will be discussed in the subsequent chapter.

### 5.3.2 Mass

The best available mass estimate for HAL-VP-9/1 is 80.3 ± 4.3 kg (see Chapter 4 for details). This estimate falls above the range reported for a male eastern African sample (same sample as above) and a male Pecos Pueblo Native American sample (Ruff, 2000). This mass estimate also exceeds several other reported modern sample ranges, and is at the upper end of the range for European early Upper Paleolithic, Poundbury, and Medieval Hungarian samples (Gallagher, 2013). Similarly, of the mass estimates reported by Auerbach (2012), the estimate for HAL-VP-9/1 falls above almost all samples, with the exception of a Medieval German sample for which the HAL-VP-9/1 estimate falls at the uppermost end of the reported range. These comparisons with modern human samples demonstrate that the HAL-VP-9/1 individual was very large-bodied, not just in terms of stature but also in mass.

## 5.4 Conclusions

This chapter places the Halibee postcranial fossils in the context of modern human variation. The results of the comparisons to recent modern humans fall into two general categories. The first set of results demonstrates aspects of the fossil morphologies that fall within the recent modern range of variation, albeit often at the edge of the range, as represented by the five comparative samples. The second set of results highlights aspects of the anatomy that fall beyond the sampled range of modern variation.

Particularly striking aspects of the anatomy of HAL-VP-9/1 include this individual's very large size (in terms of stature, mass, and individual elements), the unusual proportional relationship of the long bone ends to shaft cross-sectional dimensions, and the large absolute and relative size of the articular surfaces. In most measures of absolute size, HAL-VP-9/1 falls at the upper end of, or just beyond, the recent modern human range. In several cases, the skeletal proportions and size of articular surfaces of this individual exceed the sampled range of recent

modern variation. Having established how the fossils conform to and deviate from modern morphologies, I now turn to how these findings relate to the fossil record and thereby inform our understanding of human postcranial evolution.

**Figure 5.1** Bivariate plots of vertebral body dimensions for the fourth through seventh cervical vertebrae of HAL-VP-9/1.

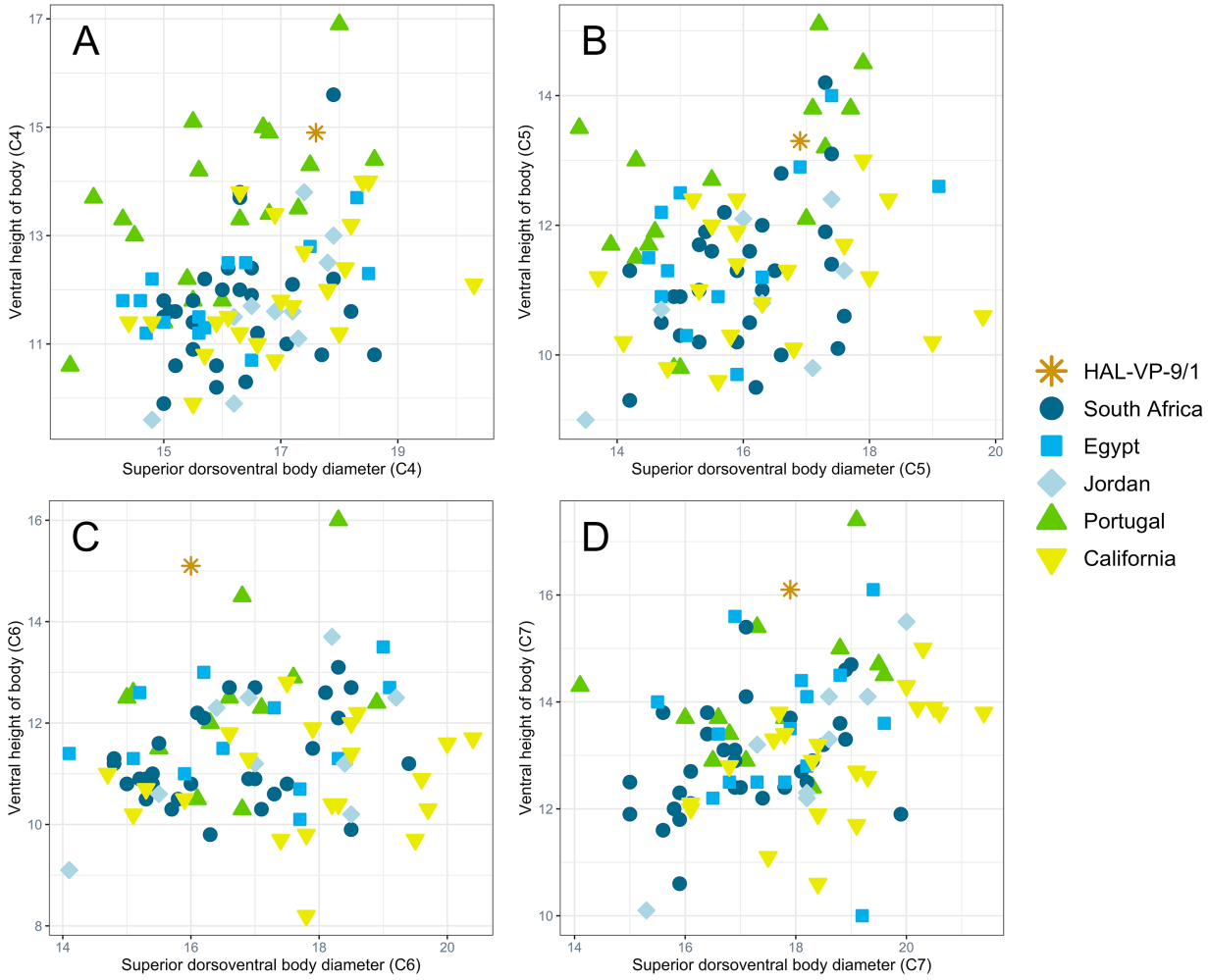


**Figure 5.2** Bivariate plots of vertebral body dimensions (**A, B**) and pedicle height relative to body height (**C, D**) for the fourth through sixth cervical vertebrae of HAL-VP-9/1.

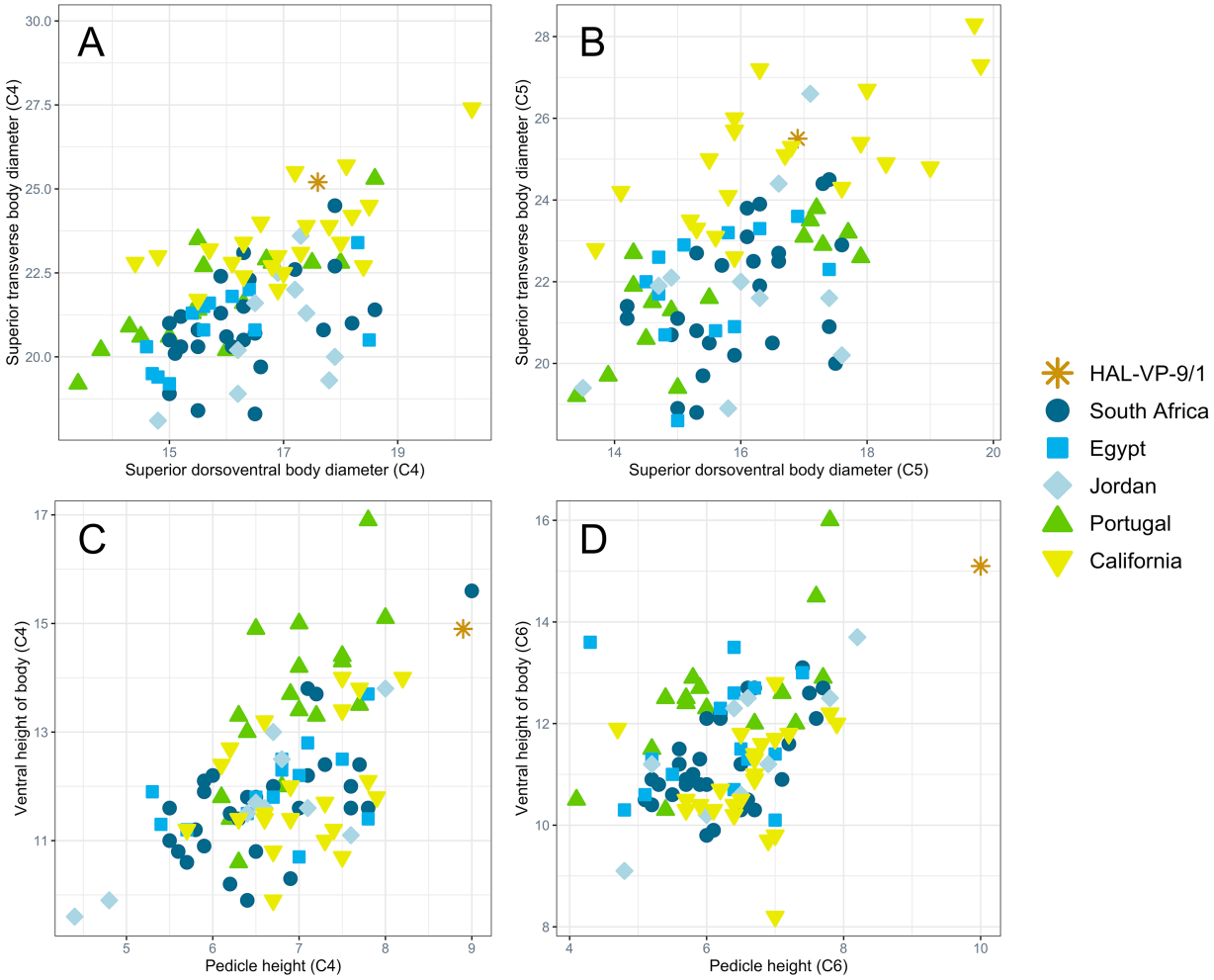


**Figure 5.3** Bivariate plots of vertebral body dimensions for the first (**A**), fourth (**B, D**), and fifth (**C, E**) lumbar vertebrae of HAL-VP-9/1.

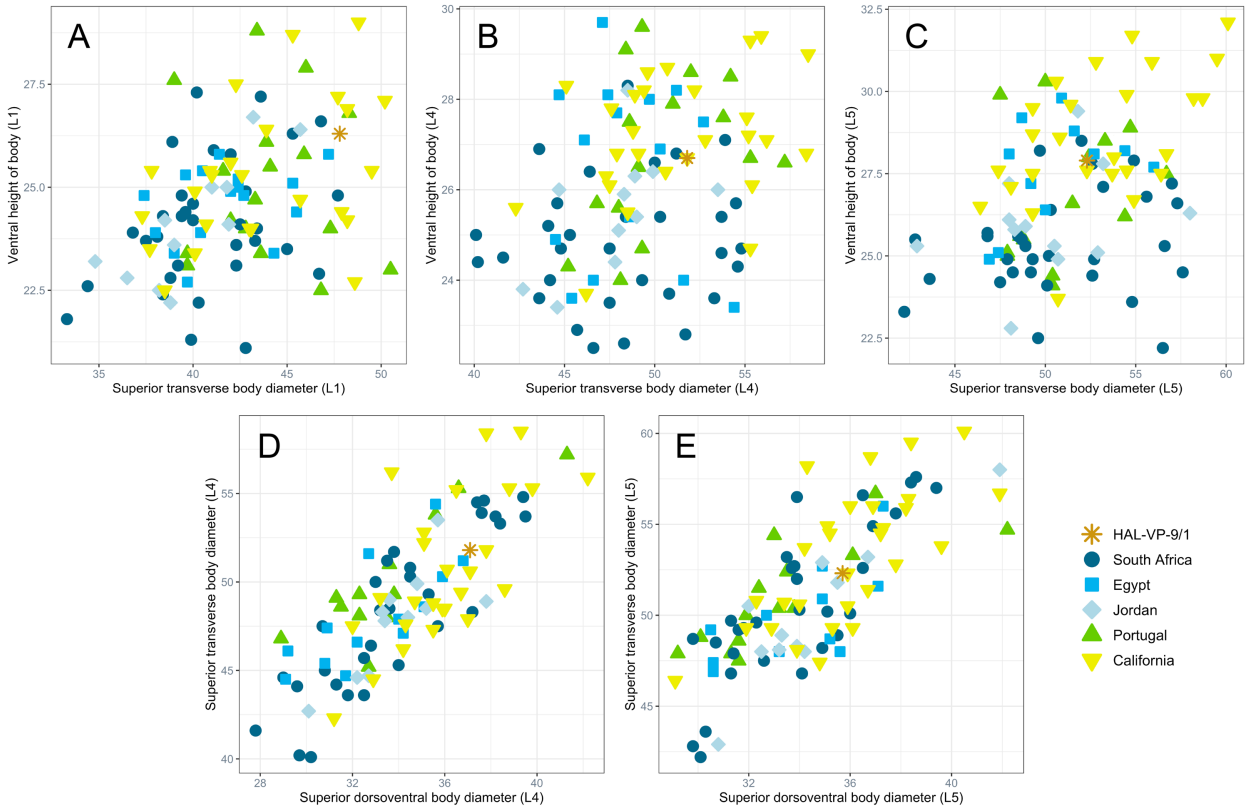


**Figure 5.4** Right distal humerus (HAL-VP-9/1-113) in anterior (**A**) and posterior (**B**) views. Right distal humerus (TAL-VP-7/36-H) in anterior (**C**) and posterior (**D**) views. Partial right distal humerus (HAL-VP-9/1520-F) in anterior (**A**) and posterior (**B**) views.



**Figure 5.5** Bivariate plots of humeral dimensions for HAL-VP-9/1 (**A-H**) and TAL-VP-7/36 (**E-H**). Legend as in (**A**).

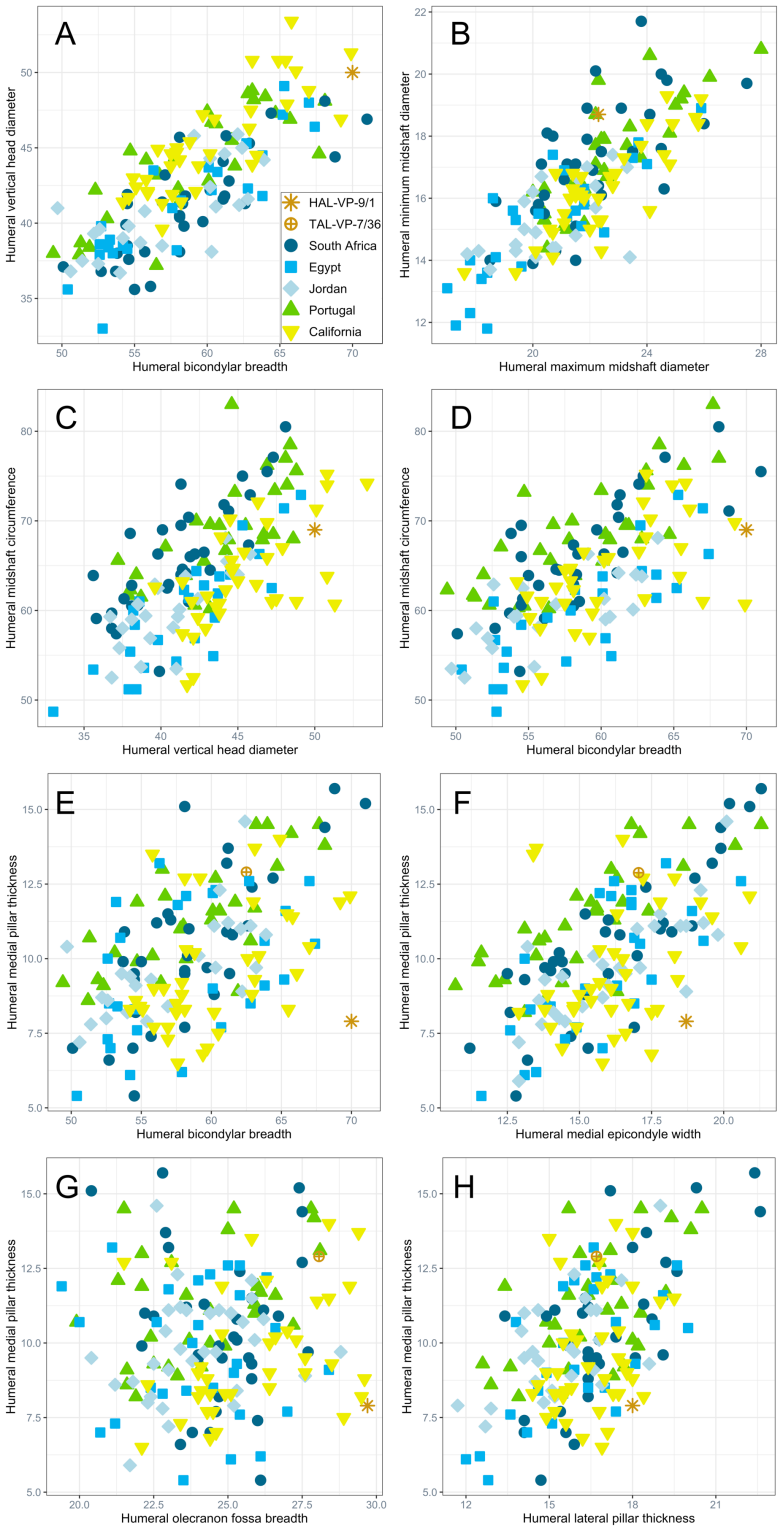


**Figure 5.6** Box plots of humeral dimensions for HAL-VP-9/1 (**A-C**), HAL-VP-9/930 (**A**), HAL-VP-9/1520 (**B, C**) and TAL-VP-7/36 (**C**).

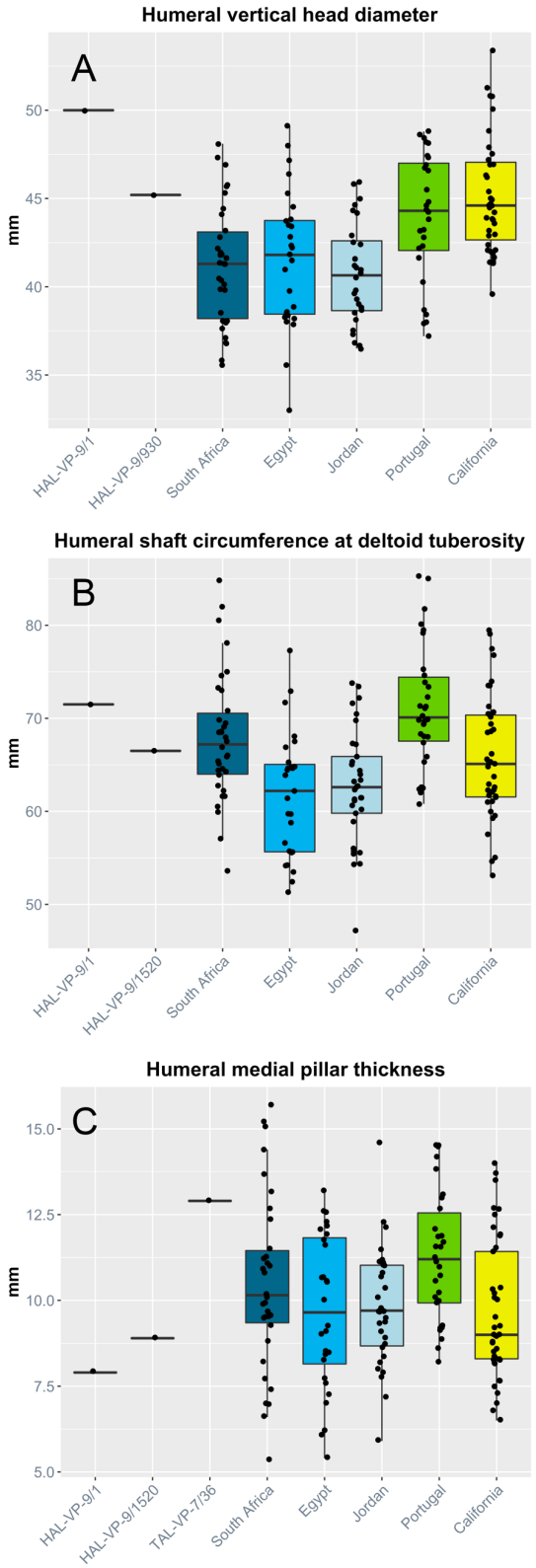


**Figure 5.7** Radial head of HAL-VP-9/1 (HAL-VP-9/1-119; **A**) and HAL-VP-2/16 (**B**) in proximal view.



**Figure 5.8** Bivariate and box plots of radial dimensions for HAL-VP-9/1 (**A, B, D**), TAL-VP-7/36 (**C**), and HAL-VP-2/16 (**D**). Ulnar dimensions are also included in (**A**) and (**B**).

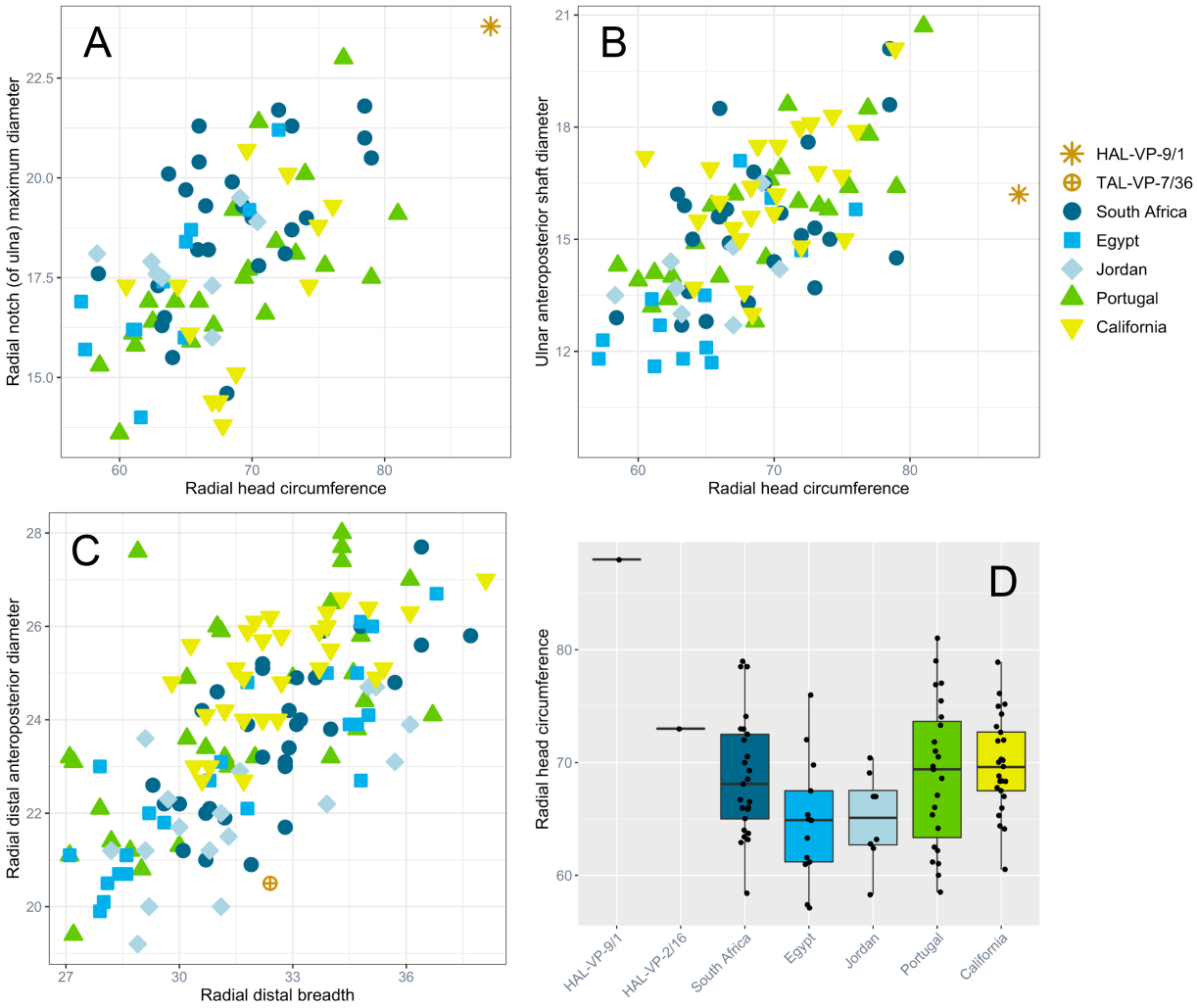


**Figure 5.9** Right proximal ulna (HAL-VP-9/1-121) in anterior (**A**), lateral (**B**), and medial (**C**) views.

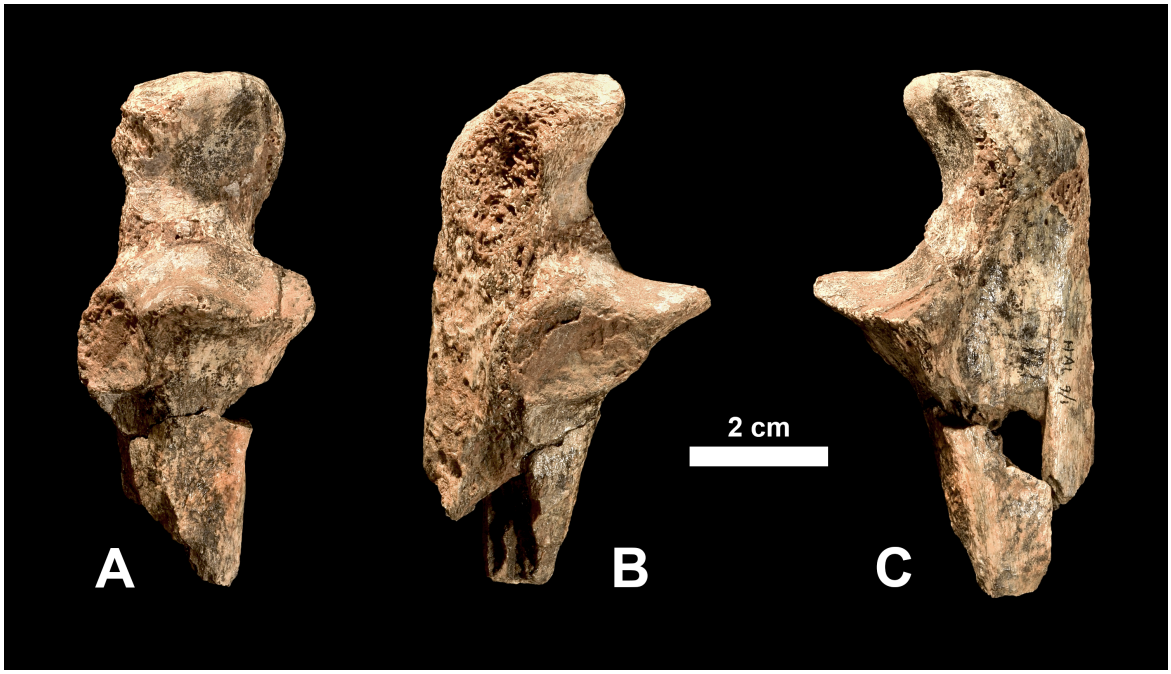


**Figure 5.10** Bivariate and box plots of ulnar dimensions for HAL-VP-9/1 (**A-H**), HAL-VP-3/1 (**G**), and HAL-VP-9/1520 (**H**). Legend as in (**B**).

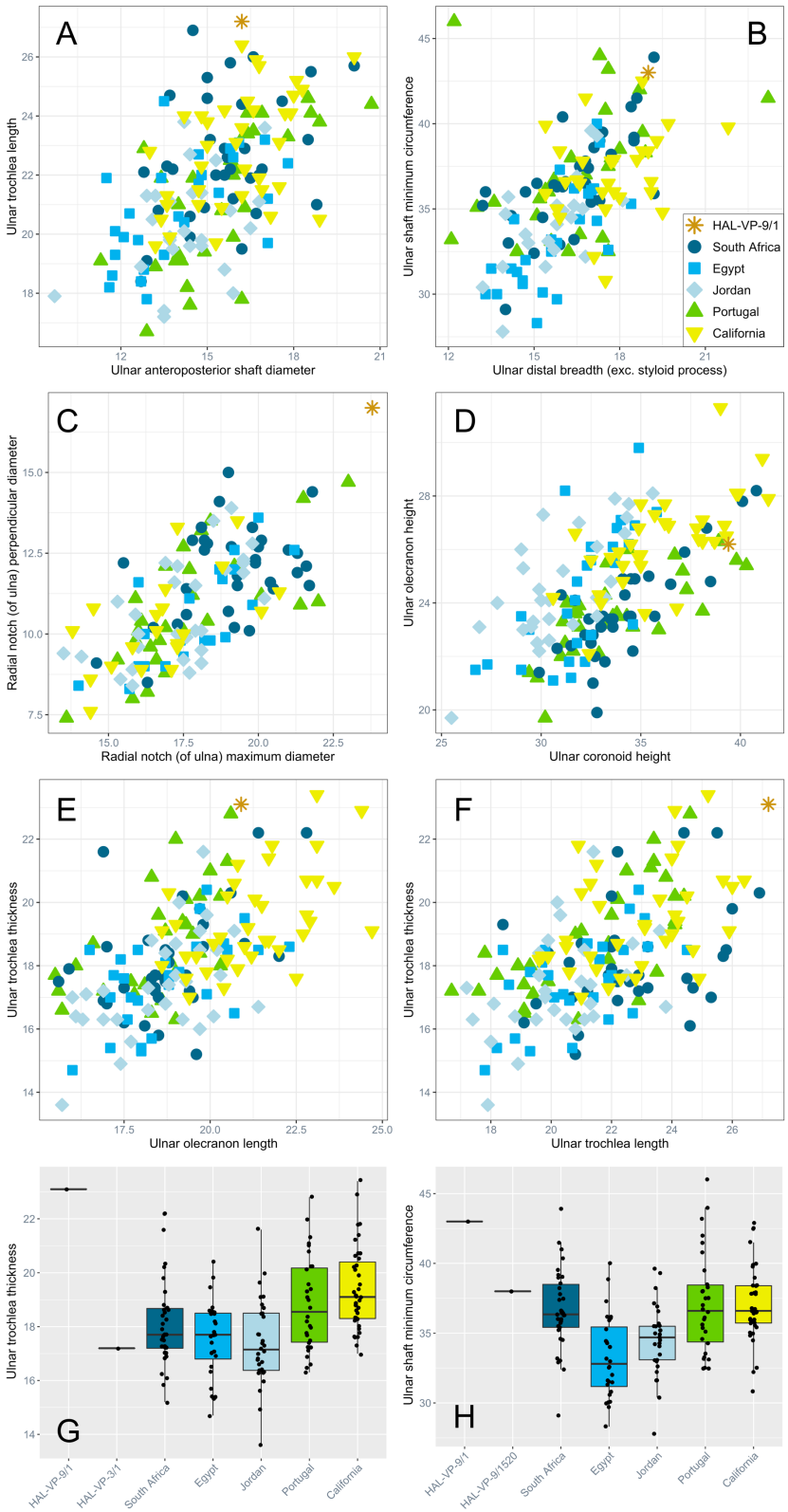


**Figure 5.11** Hand of HAL-VP-9/1 in dorsal view. Bottom row, from left to right: triquetral (HAL-VP-9/1-133) and lunate (HAL-VP-9/1-131). Second row from the bottom, from left to right: hamate (HAL-VP-9/1-128), capitate (HAL-VP-9/1-132), and trapezium (HAL-VP-9/1-129). Third row from the bottom, from left to right: fifth metacarpal head (HAL-VP-9/1-143) and base with shaft (HAL-VP-9/1-142), fourth metacarpal head with shaft (HAL-VP-9/1-141), complete third metacarpal (HAL-VP-9/1-136), second metacarpal head with shaft (HAL-VP-9/1-135) and base (HAL-VP-9/1-134), and first metacarpal head (HAL-VP-9/1-138). Fourth row from the bottom, from left to right: complete proximal hand phalanx of ray V (HAL-VP-9/1-145), base and shaft of a proximal hand phalanx likely of ray IV (HAL-VP-9/1-148+149), and base and shaft of a proximal hand phalanx likely of ray III (HAL-VP-9/1-146). Second row from the top, from left to right: base of an intermediate hand phalanx of ray V (HAL-VP-9/1-154), base of an intermediate hand phalanx of ray IV (HAL-VP-9/1-153), complete intermediate hand phalanx of ray III (HAL-VP-9/1-150), base of an intermediate hand phalanx of ray II (HAL-VP-9/1-152), and base of a terminal hand phalanx of ray I (HAL-VP-9/1-158). Top row: complete terminal hand phalanx of ray II, III, or IV (HAL-VP-9/1-157; side indet., positioned as ray III). All elements are from the left side (or likely from the left side, in the case of the phalanges), except the following, which have been mirrored: hamate (HAL-VP-9/1-128), trapezium (HAL-VP-9/1-129), second metacarpal head with shaft (HAL-VP-9/1-135) and base (HAL-VP-9/1-134), third metacarpal (HAL-VP-9/1-136), fourth metacarpal head with shaft (HAL-VP-9/1-141), fifth metacarpal head (HAL-VP-9/1-143), and base of a terminal hand phalanx of ray I (HAL-VP-9/1-158).

**See next page for Figure 5.11.**

**See previous page for Figure 5.11 legend.**



**Figure 5.12** Bivariate plots of dimensions of the lunate (**A**), triquetral (**B**) and trapezium (**C, D**) of HAL-VP-9/1.

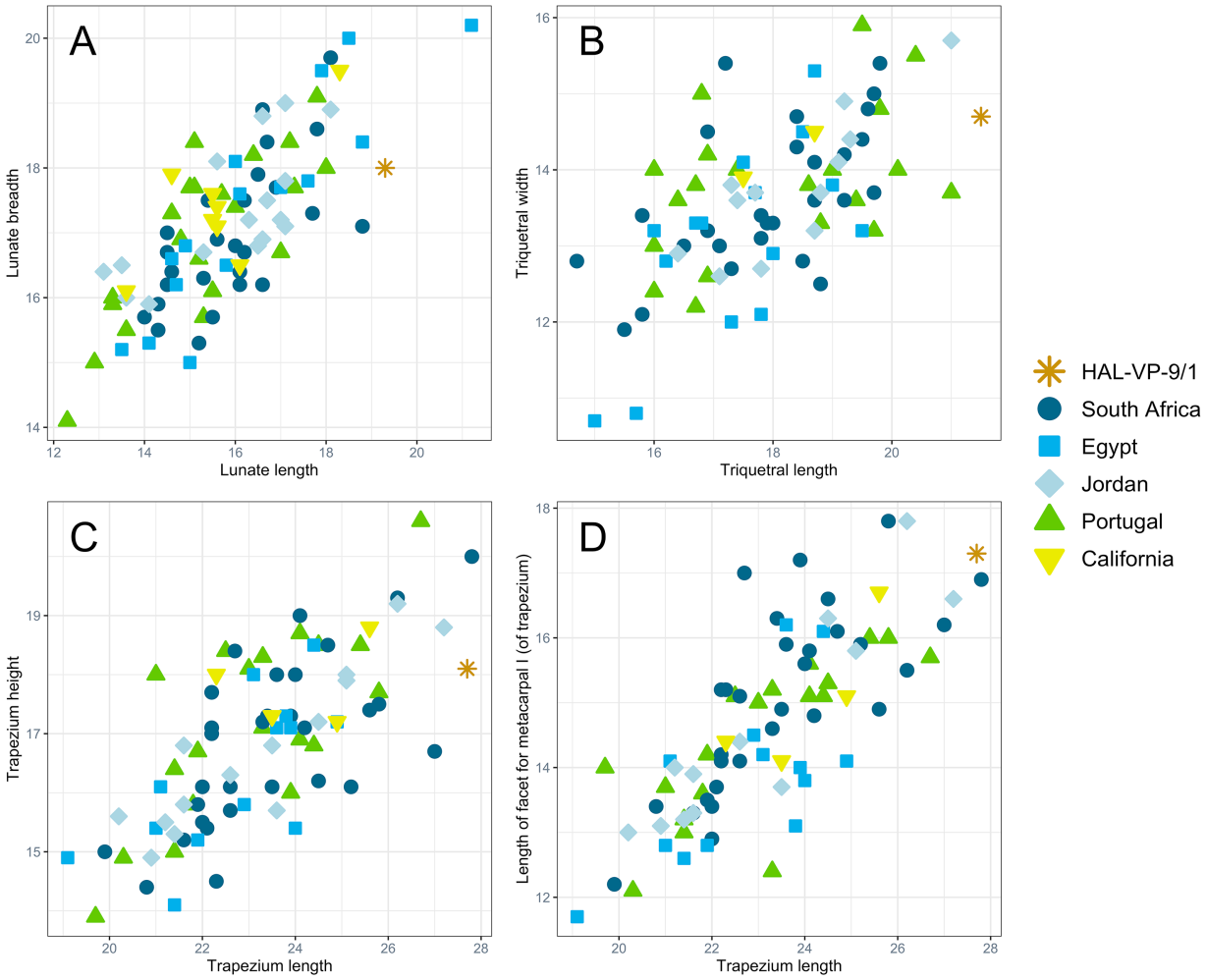


**Figure 5.13** Bivariate plots of capitate dimensions of HAL-VP-9/1.

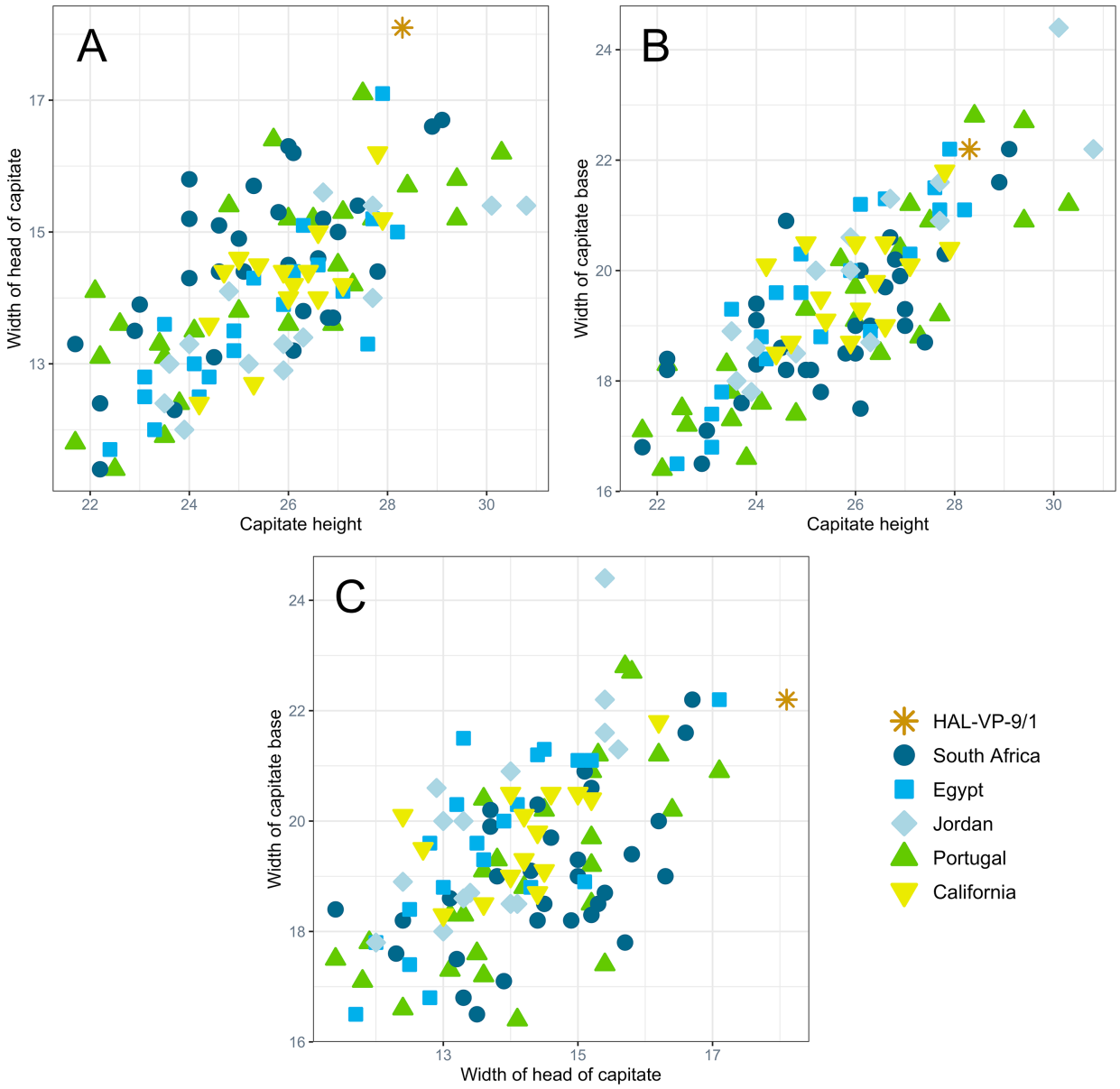


**Figure 5.14** Bivariate plots of hamate dimensions of HAL-VP-9/1.

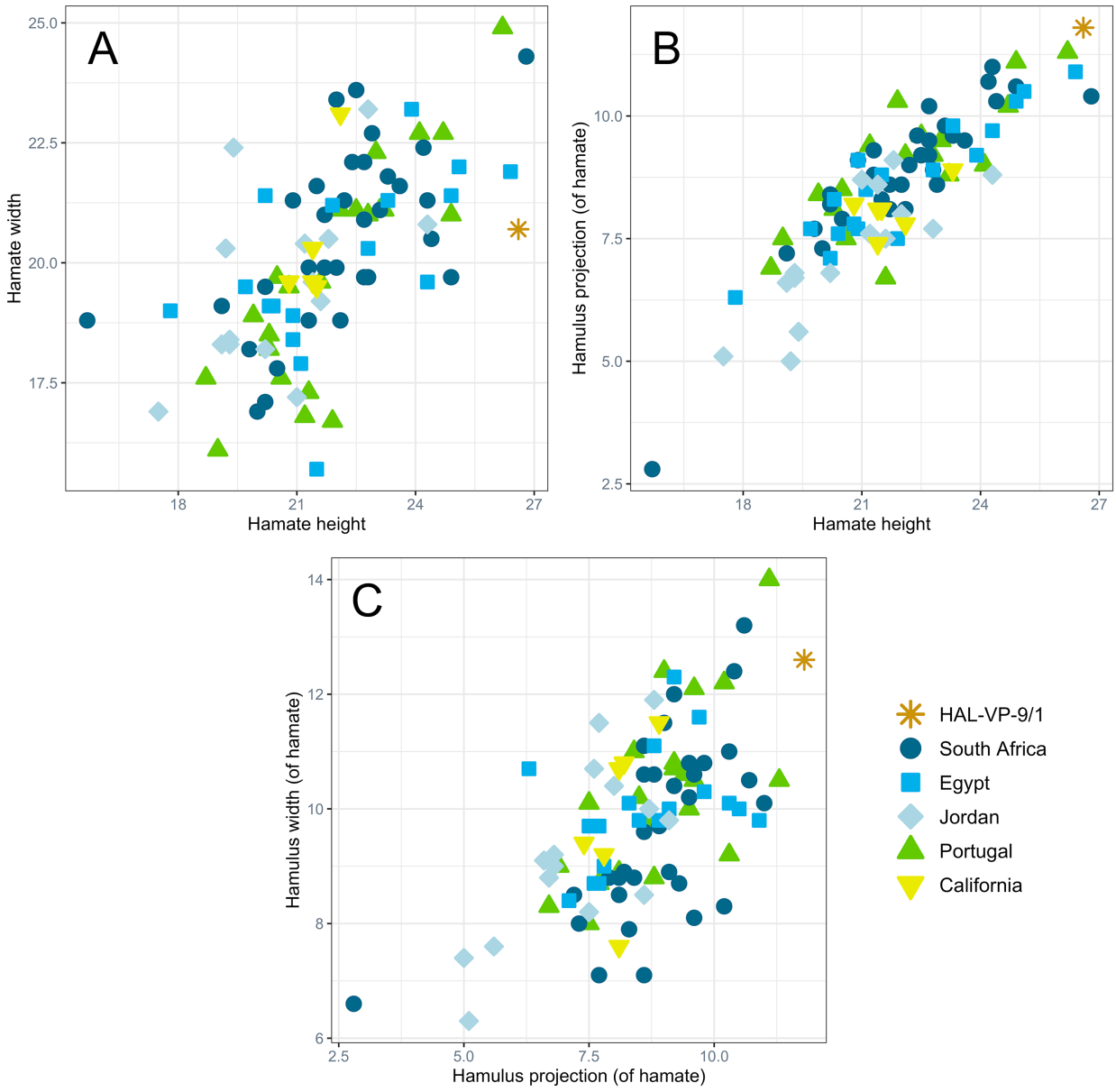


**Figure 5.15** Bivariate plots of first (**A**) and second (**B, C**) metacarpal dimensions of HAL-VP-9/1.

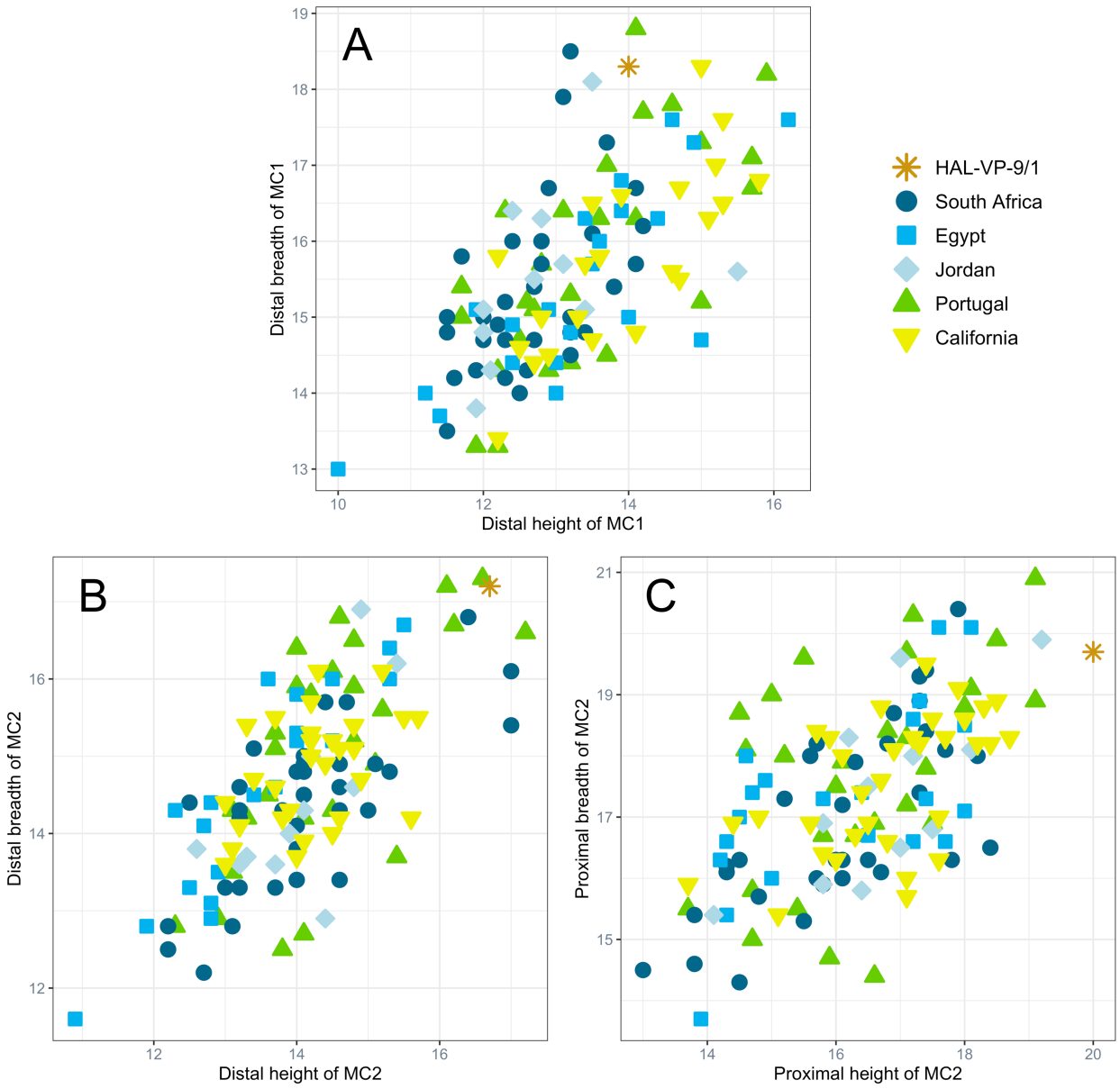


**Figure 5.16** Right third metacarpal (HAL-VP-9/1-136) in dorsal (**A**), palmar (**B**), and medial (**C**) views.



**Figure 5.17** Bivariate plots of third metacarpal dimensions of HAL-VP-9/1. Legend as in (**A**).

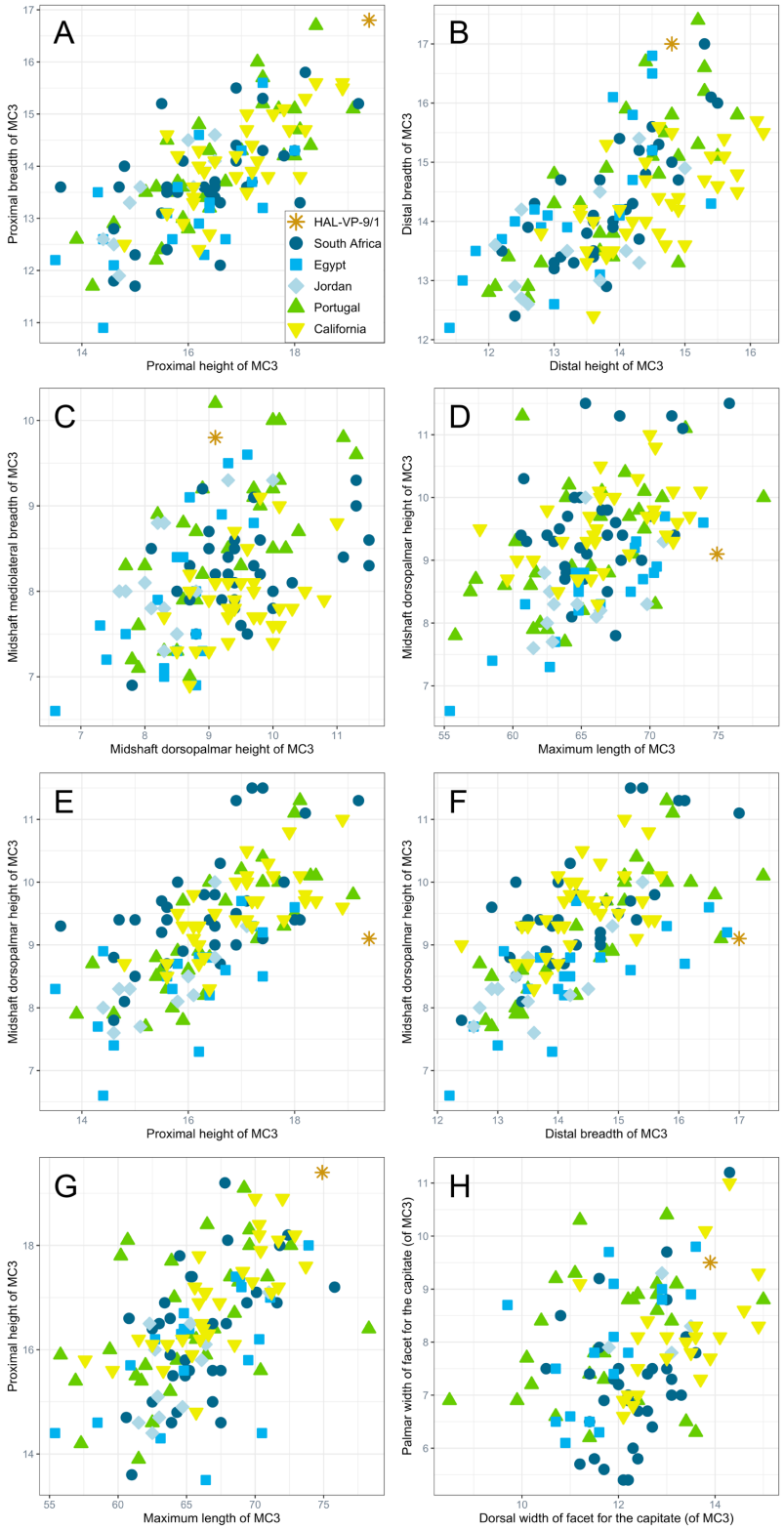


**Figure 5.18** Bivariate plots of fourth (**A-C**) and fifth (**D, E**) metacarpal dimensions of HAL-VP-9/1.

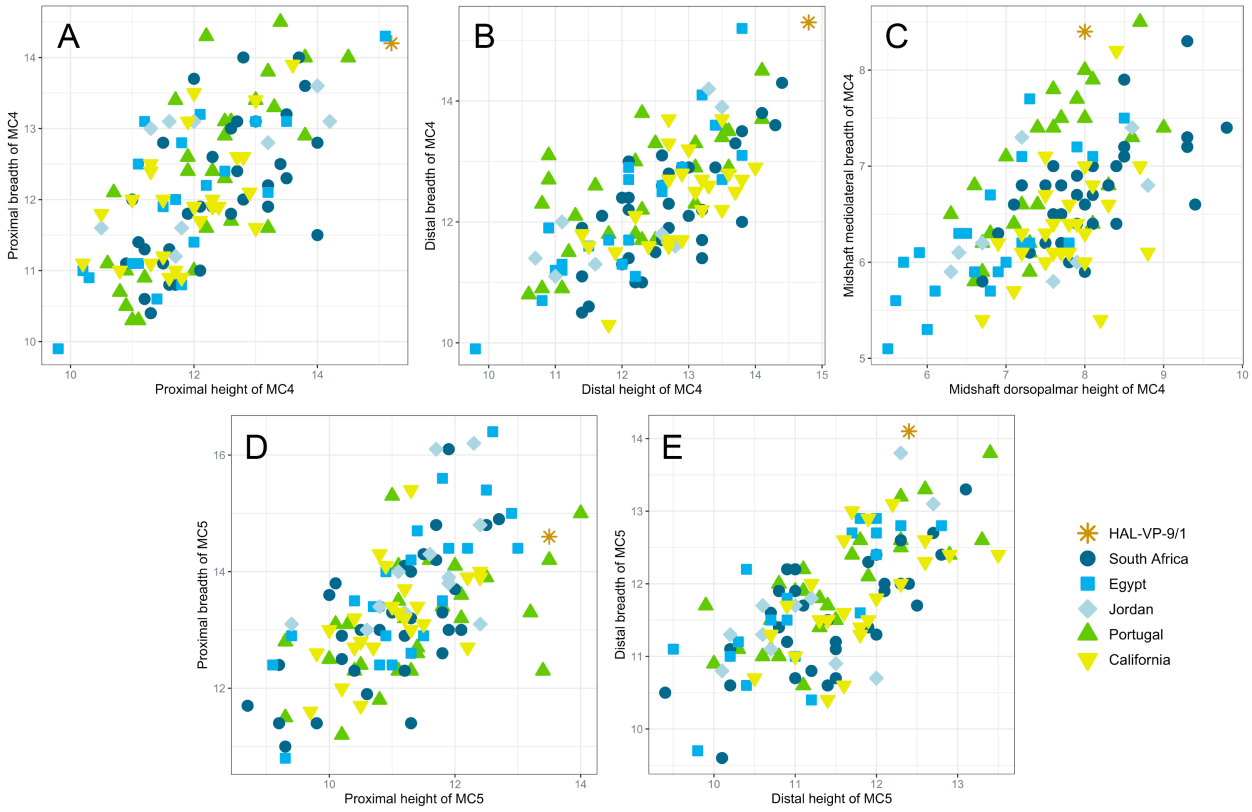


**Figure 5.19** Right os coxae (HAL-VP-9/1-106) in anterior (**A**) and lateral (**B**) views.

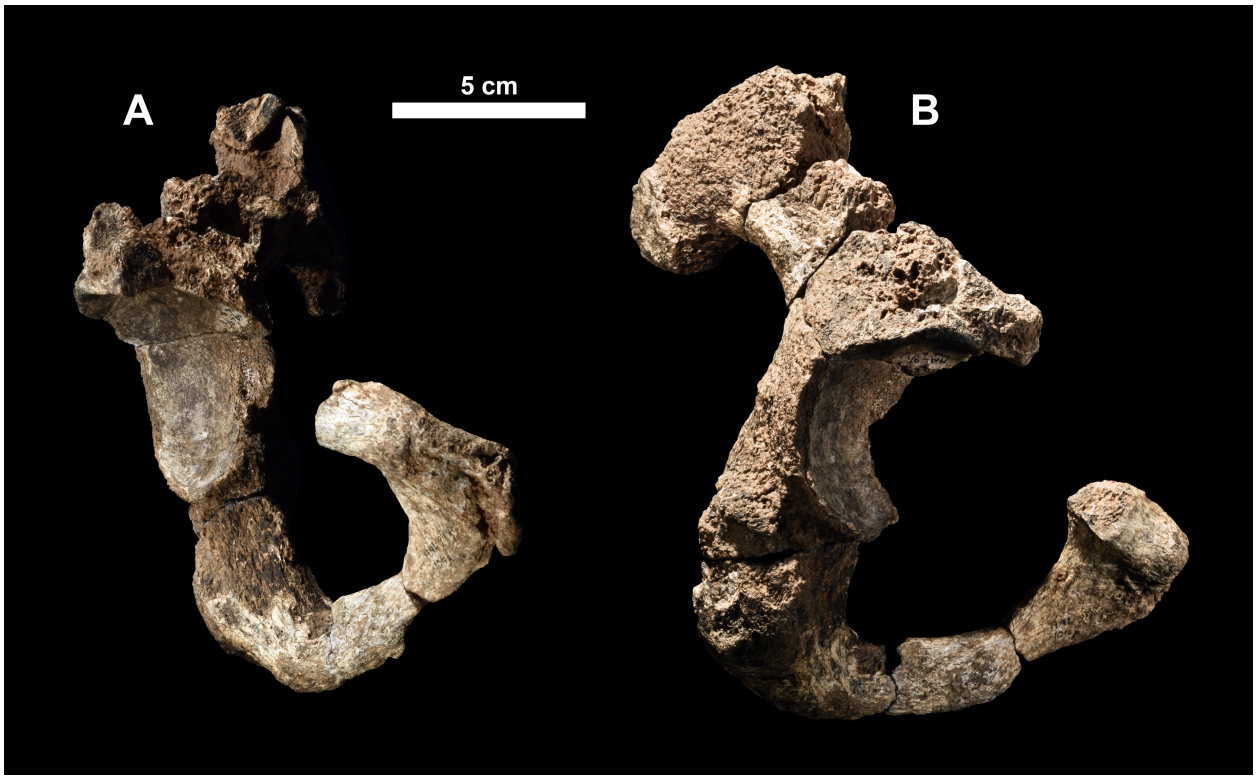



**Figure 5.20** Bivariate plots of os coxae dimensions of HAL-VP-9/1.

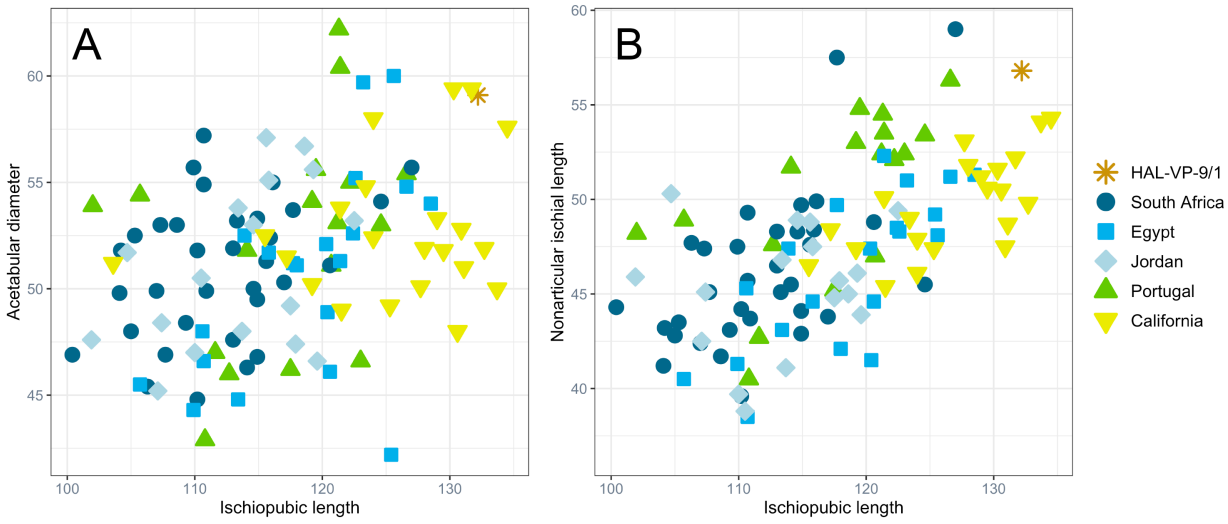


**Figure 5.21** Right proximal femur (HAL-VP-9/1-160) in anterior (**A**) and posterior (**B**) views.



**Figure 5.22** Bivariate plots of femoral dimensions for HAL-VP-9/1 (**A, B**) and HAL-VP-9/1520 (**C**).

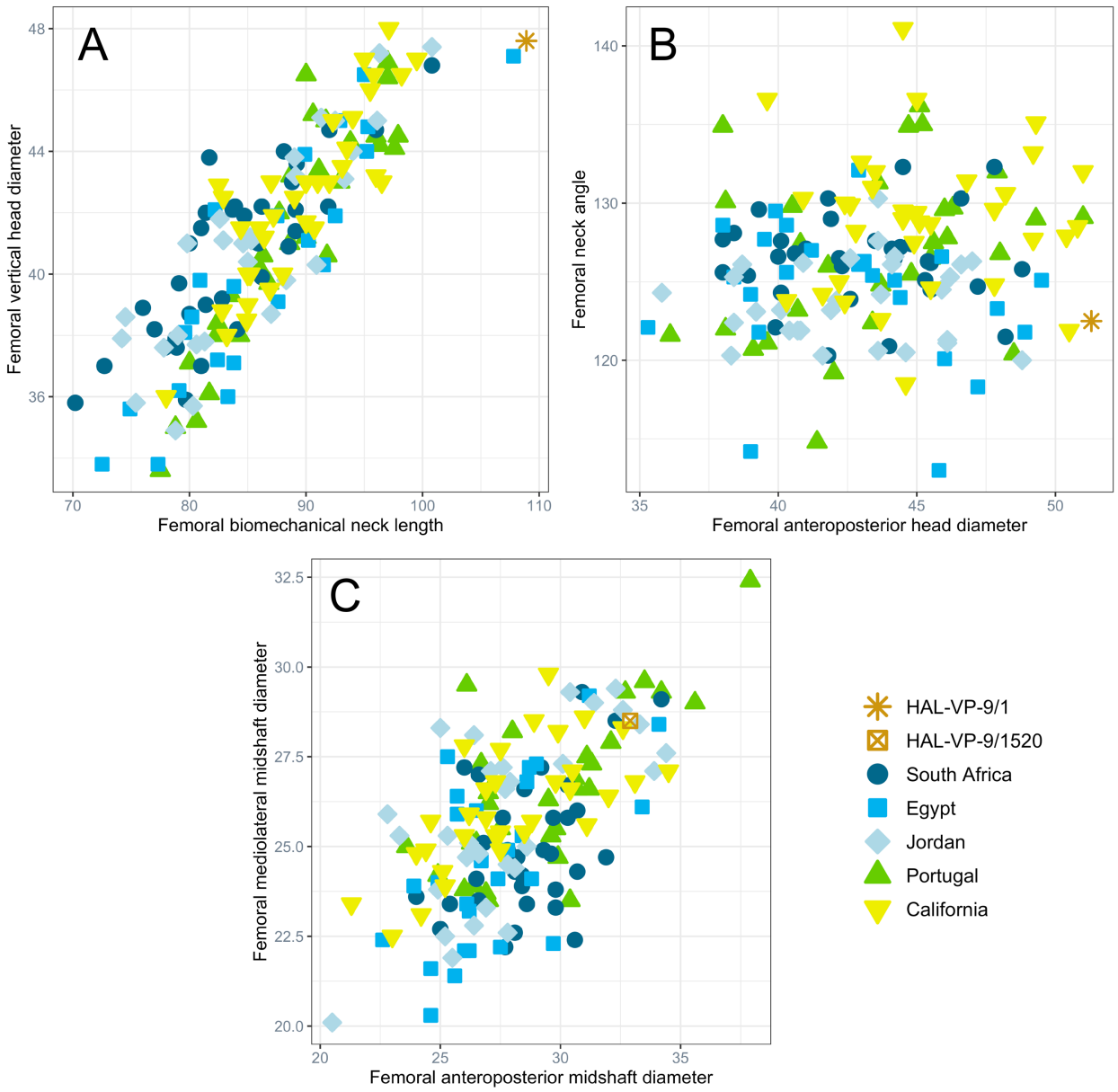


**Figure 5.23** Left (HAL-VP-9/1-187) and right (HAL-VP-9/1-186) patellae in anterior (**A, B**), posterior (**C, D**), lateral (**E, F**), and superior (**G, H**) views. The left patella is presented in the left column (**A, C, E, G**) and the right patella in the right column (**B, D, F, H**).

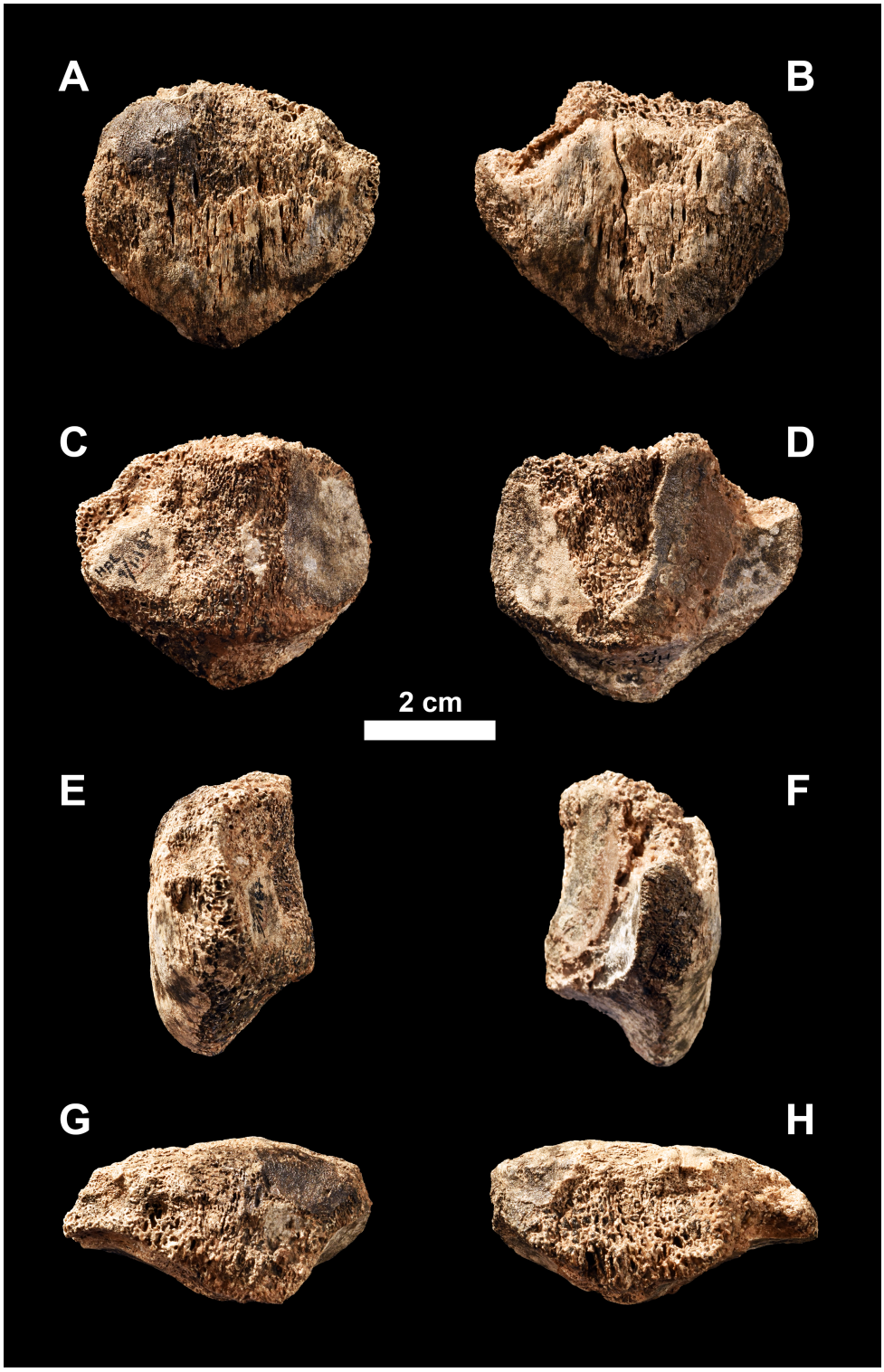


**Figure 5.24** Bivariate plots of patellar dimensions of HAL-VP-9/1.

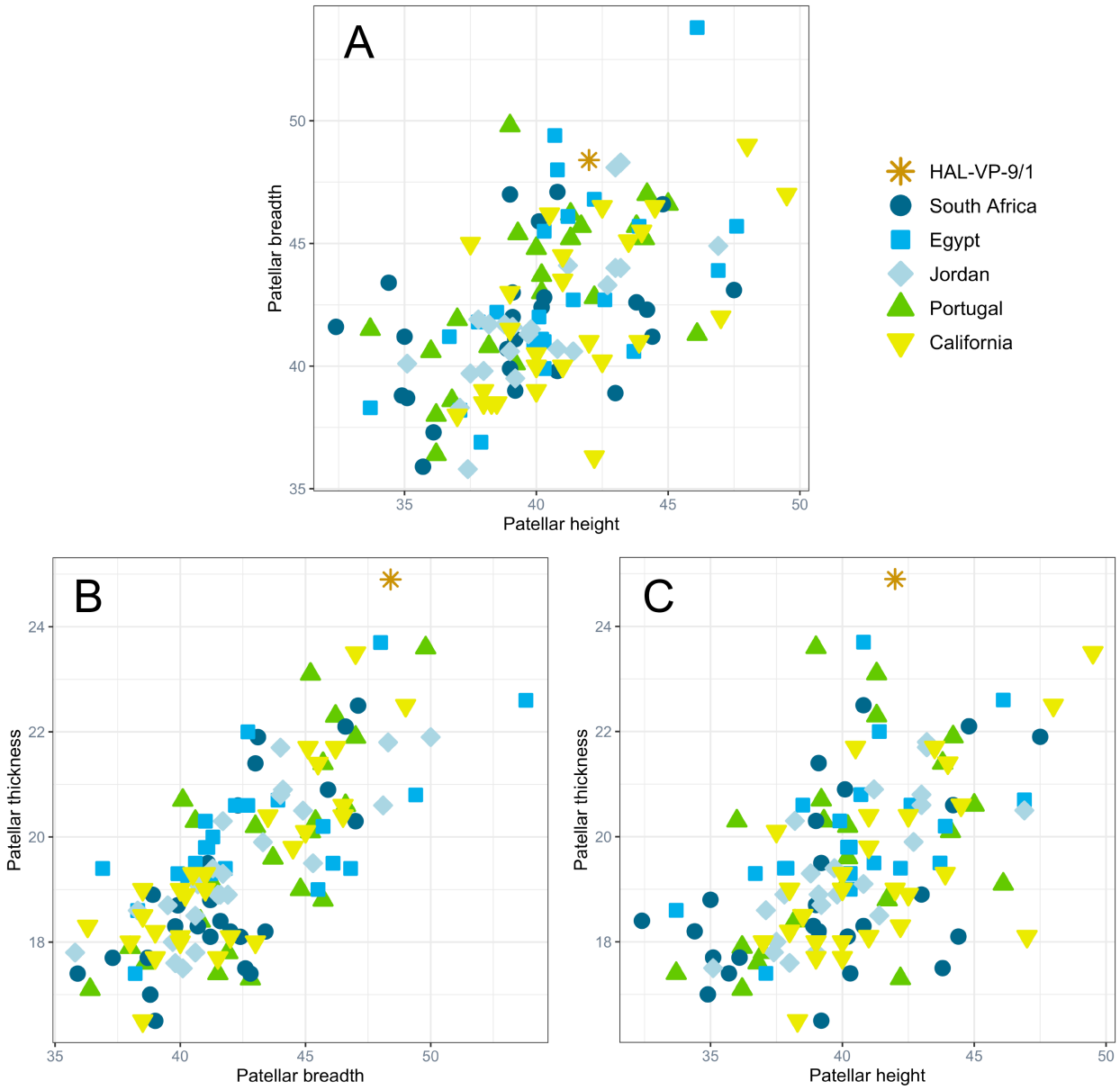


**Figure 5.25** Left tibia (HAL-VP-9/1-177+178) in anterior (**A**) and posterior (**B**) views. Right proximal tibial shaft (HAL-VP-9/1-174+175) in anterior (**C**) and lateral (**D**) views. Distal end of right tibia (HAL-VP-9/1-173) in anterior (**E**) and posterior (**F**) views. Right tibia (HAL-VP-9/1520-D) in anterior (**G**), posterior (**H**), and lateral (**I**) views. The blue tape (visible in **G, I**) indicates a point of refit at an ancient postmortem step fracture.

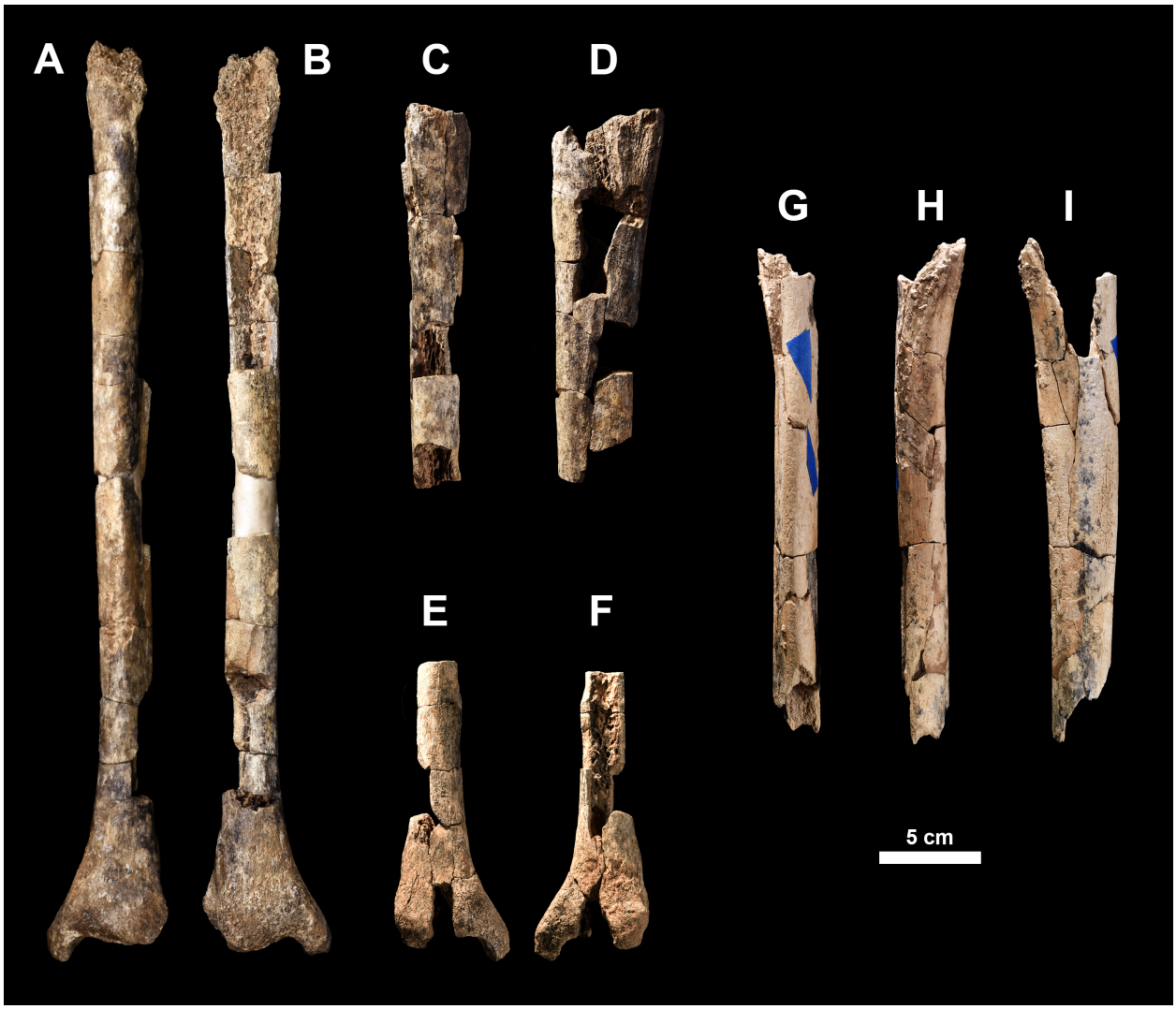


**Figure 5.26** Bivariate plots of tibial dimensions for HAL-VP-9/1 (**A-F**) and HAL-VP-9/1520 (**C, D**). Legend as in (**A**).

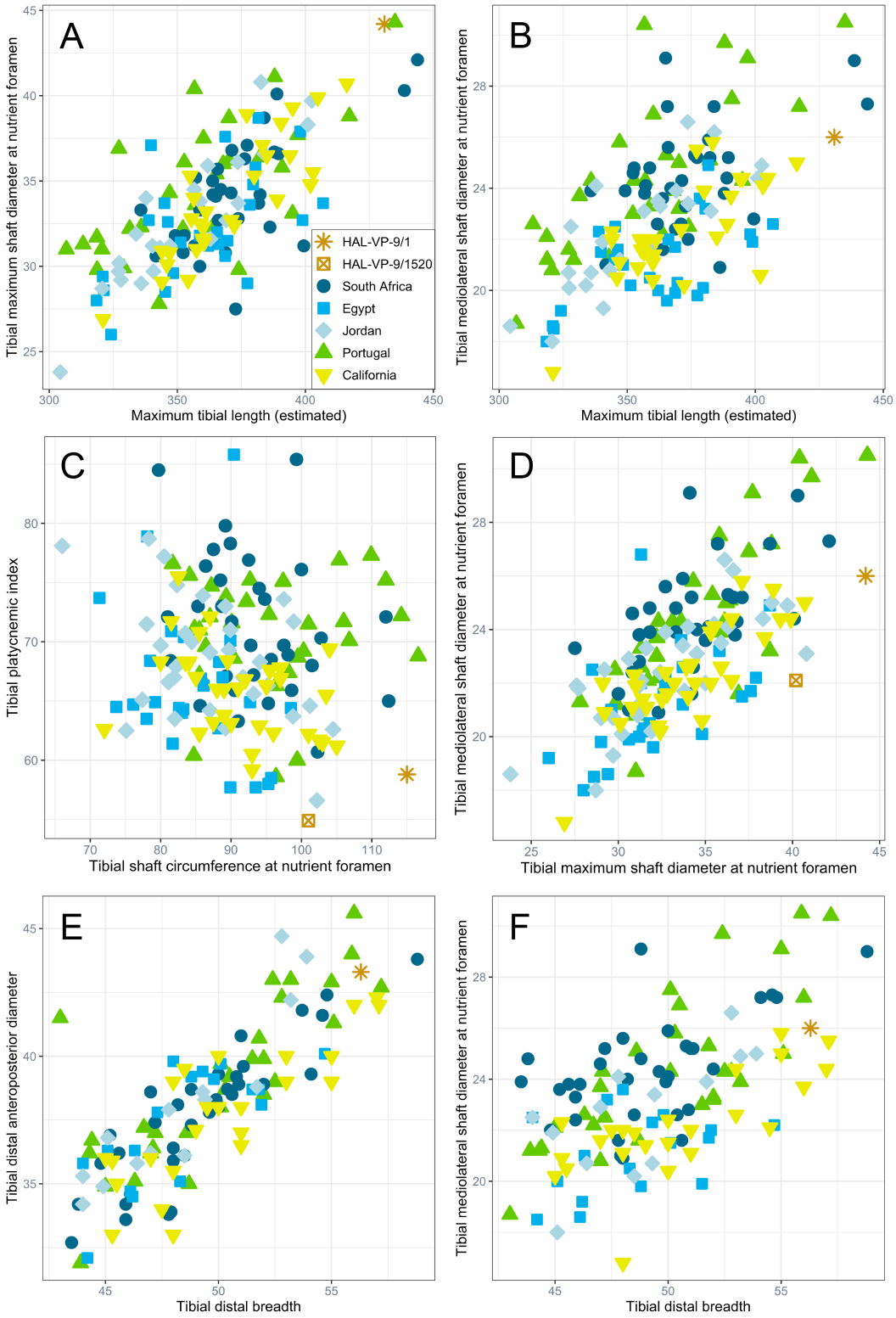


**Figure 5.27** Box plots of tibial shaft dimensions for HAL-VP-9/1 and HAL-VP-9/1520.

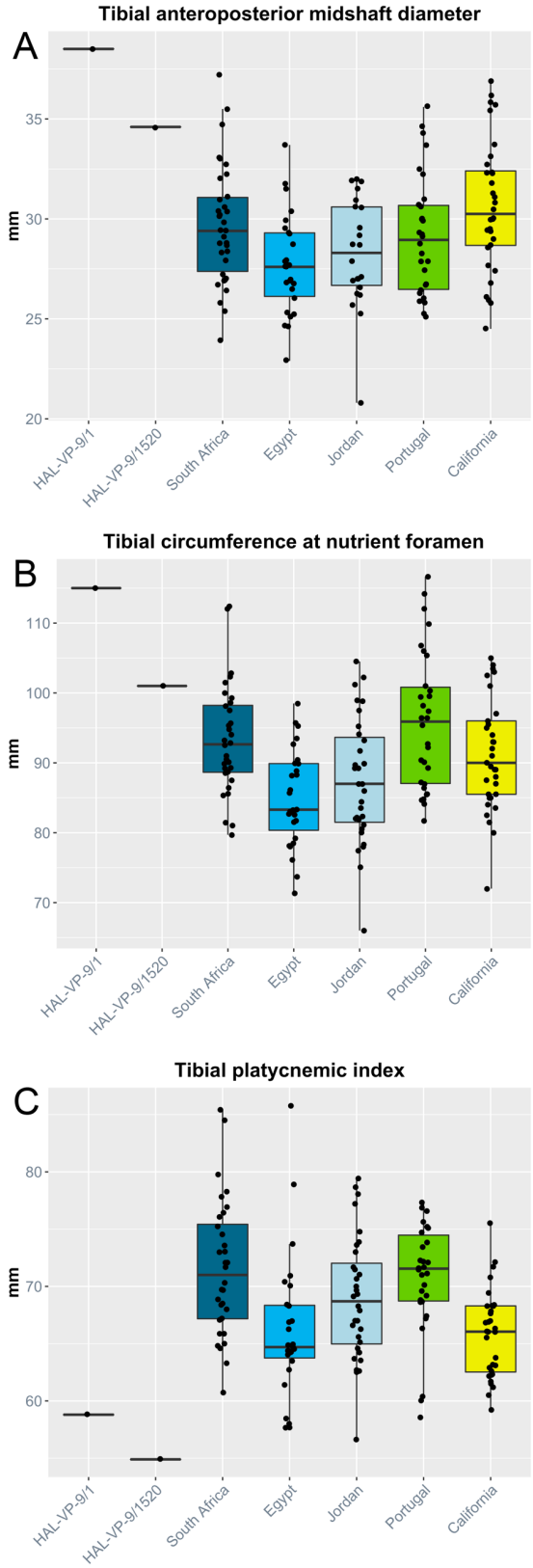


**Figure 5.28** Left (HAL-VP-9/1-182) and right (HAL-VP-9/1-180) distal fibulae in medial (**A, B**) and lateral (**C, D**) views. The left fibula is presented in the left column (**A, C**) and the right fibula in the right column (**B, D**).

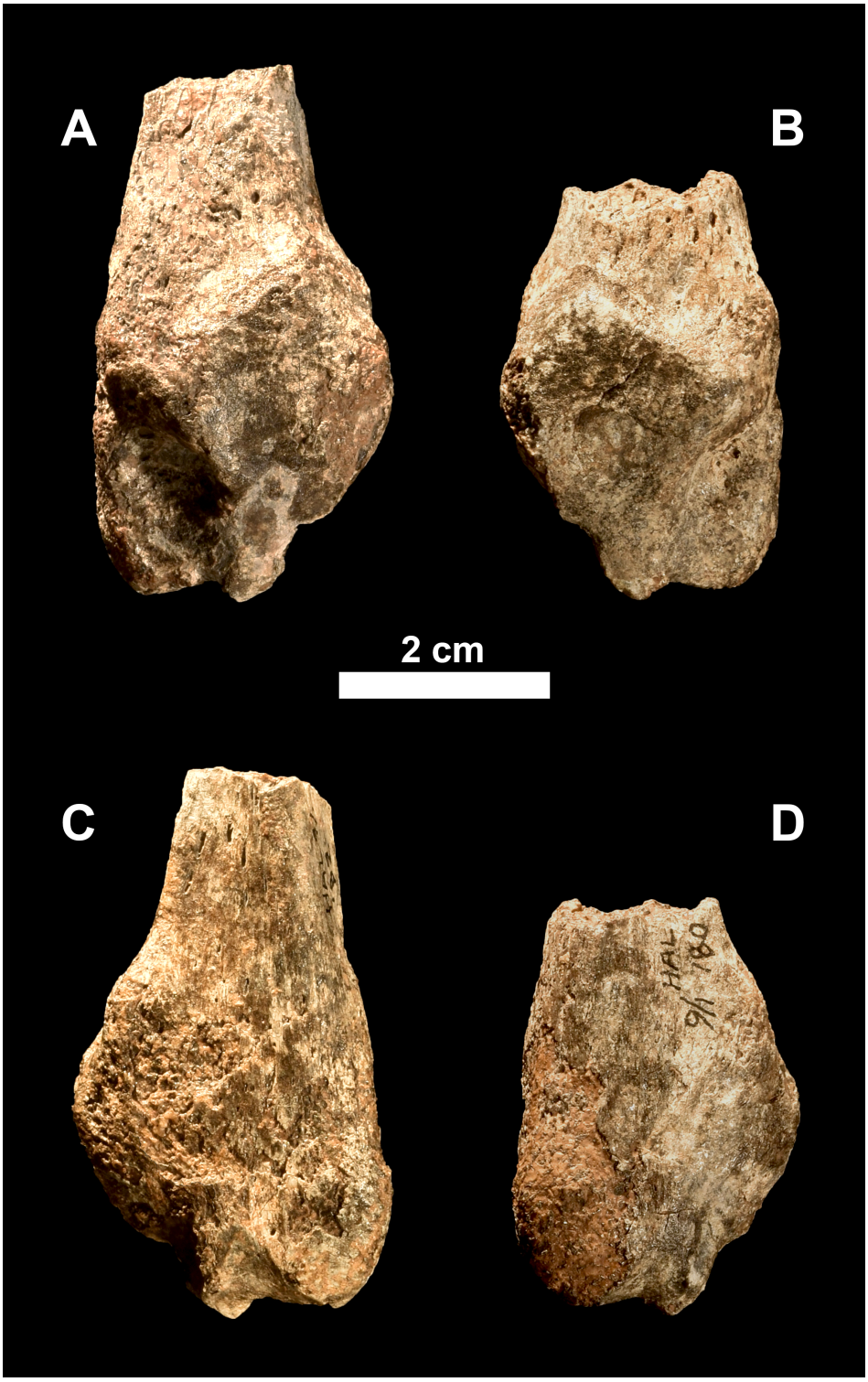


**Figure 5.29** Bivariate plots of fibular dimensions of HAL-VP-9/1. Tibial measurements are also included in (**C**) and (**D**).

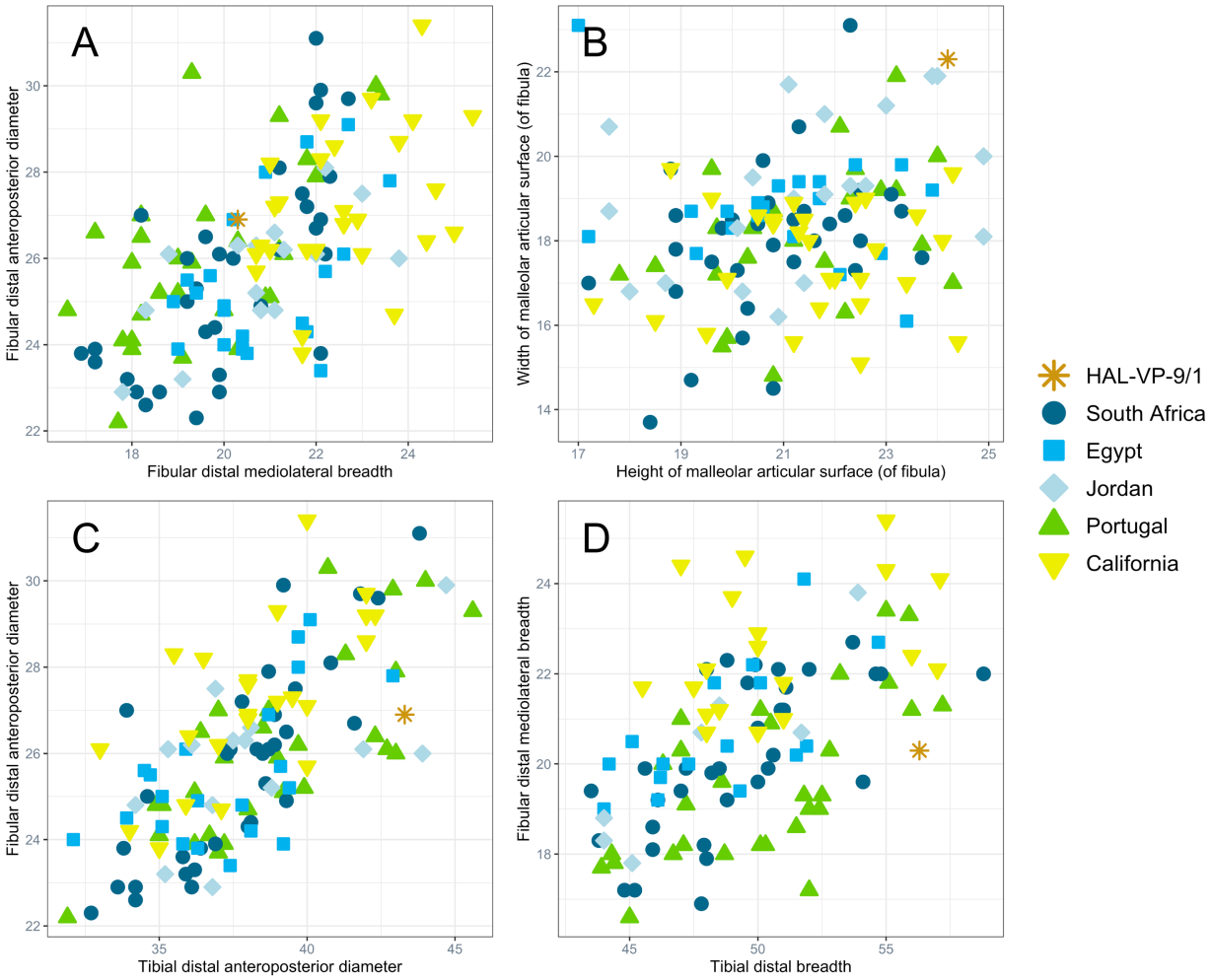


**Figure 5.30** Left (HAL-VP-9/1-190) and right (HAL-VP-9/1-188) tali in superior (**A, B**) and inferior (**C, D**) views. The left talus is presented in the left column (**A, C**) and the right talus in the right column (**B, D**).

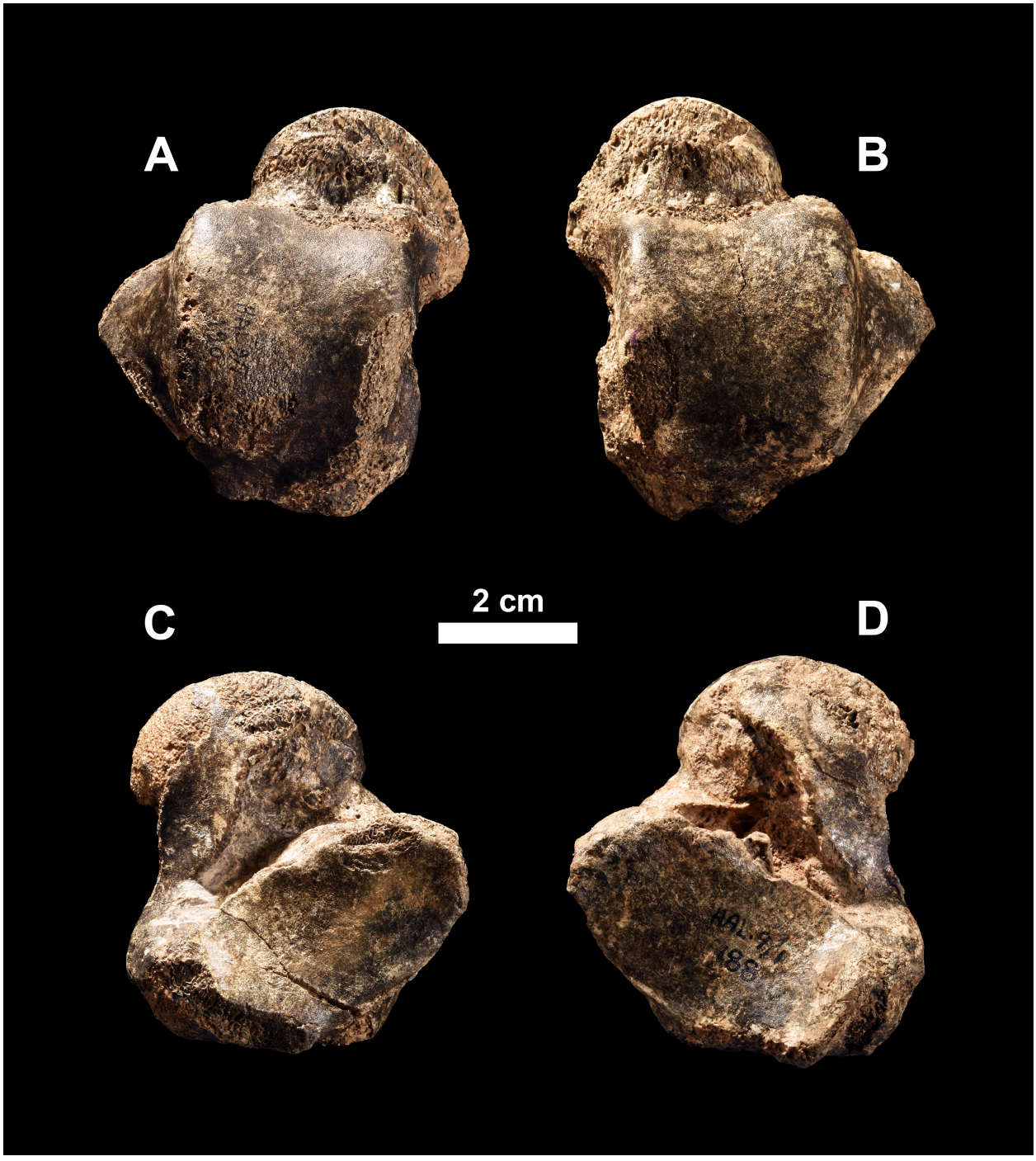


**Figure 5.31** Bivariate plots of talar dimensions of HAL-VP-9/1. Legend as in (**A**).

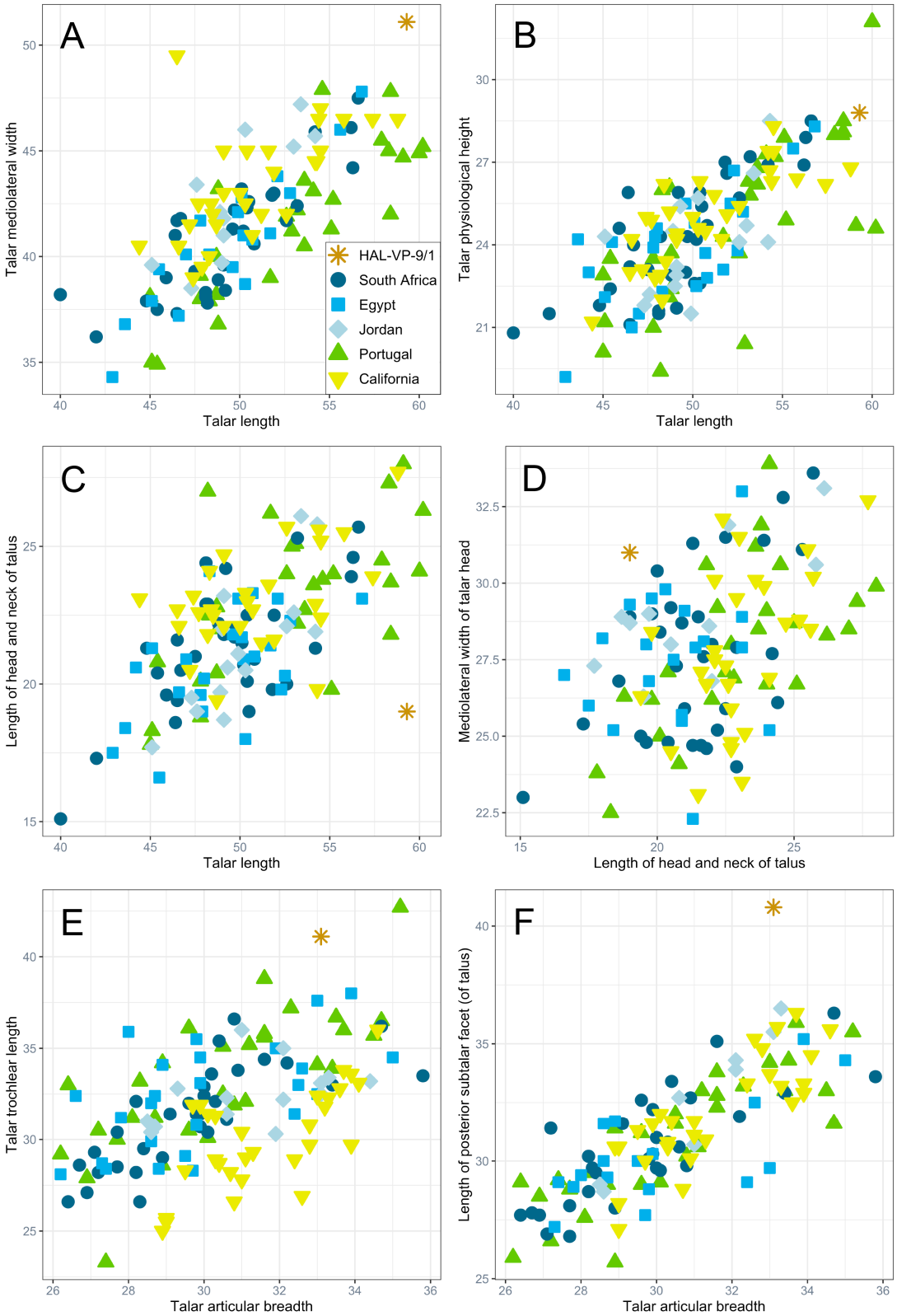


**Figure 5.32** Left (HAL-VP-9/1-191) and right (HAL-VP-9/1-189) calcanei in superior (**A, B**) and medial (**C, D**) views. The left calcaneus is presented in the left column (**A, C**) and the right calcaneus in the right column (**B, D**).

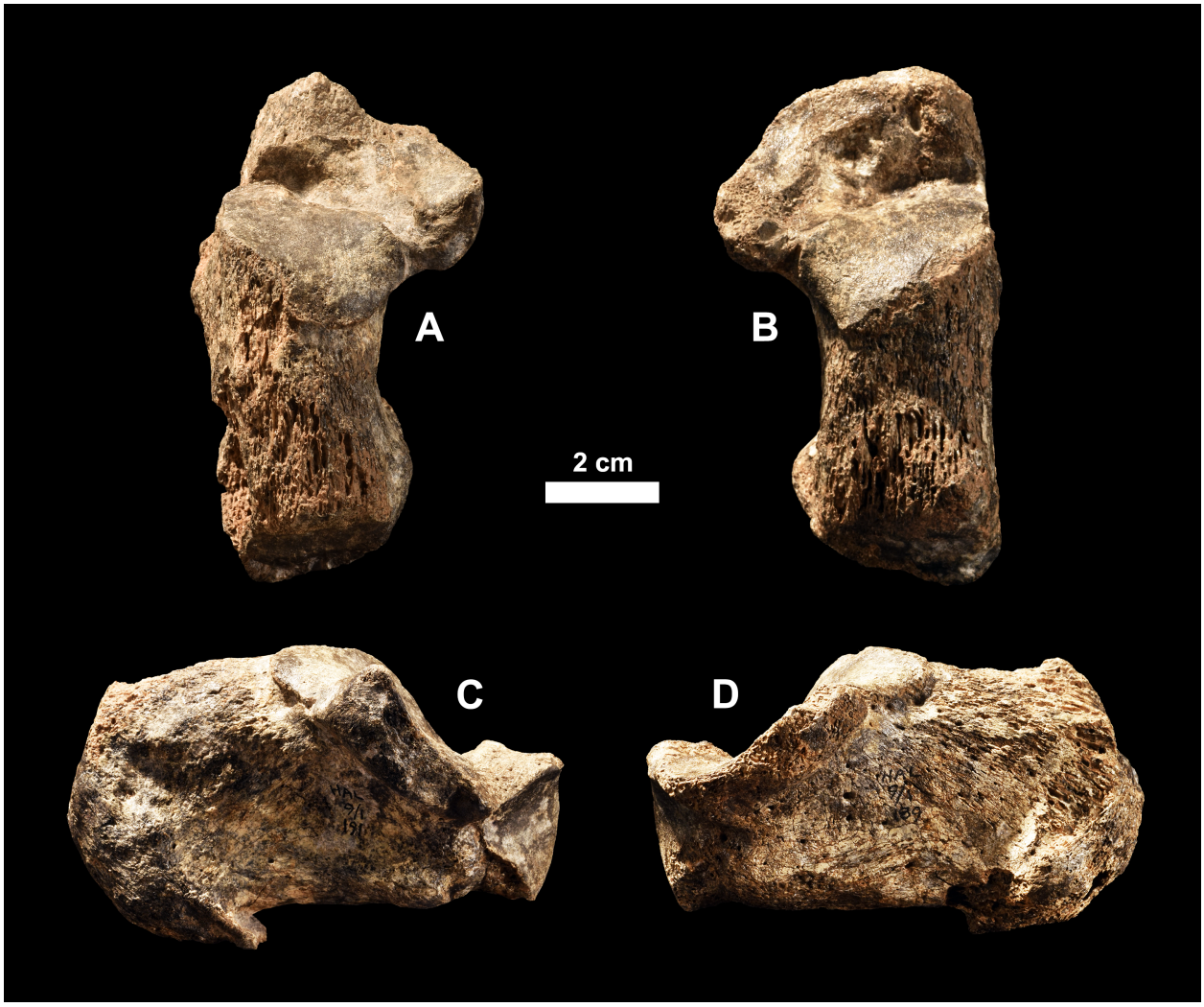


**Figure 5.33** Bivariate plots of calcaneal dimensions of HAL-VP-9/1.

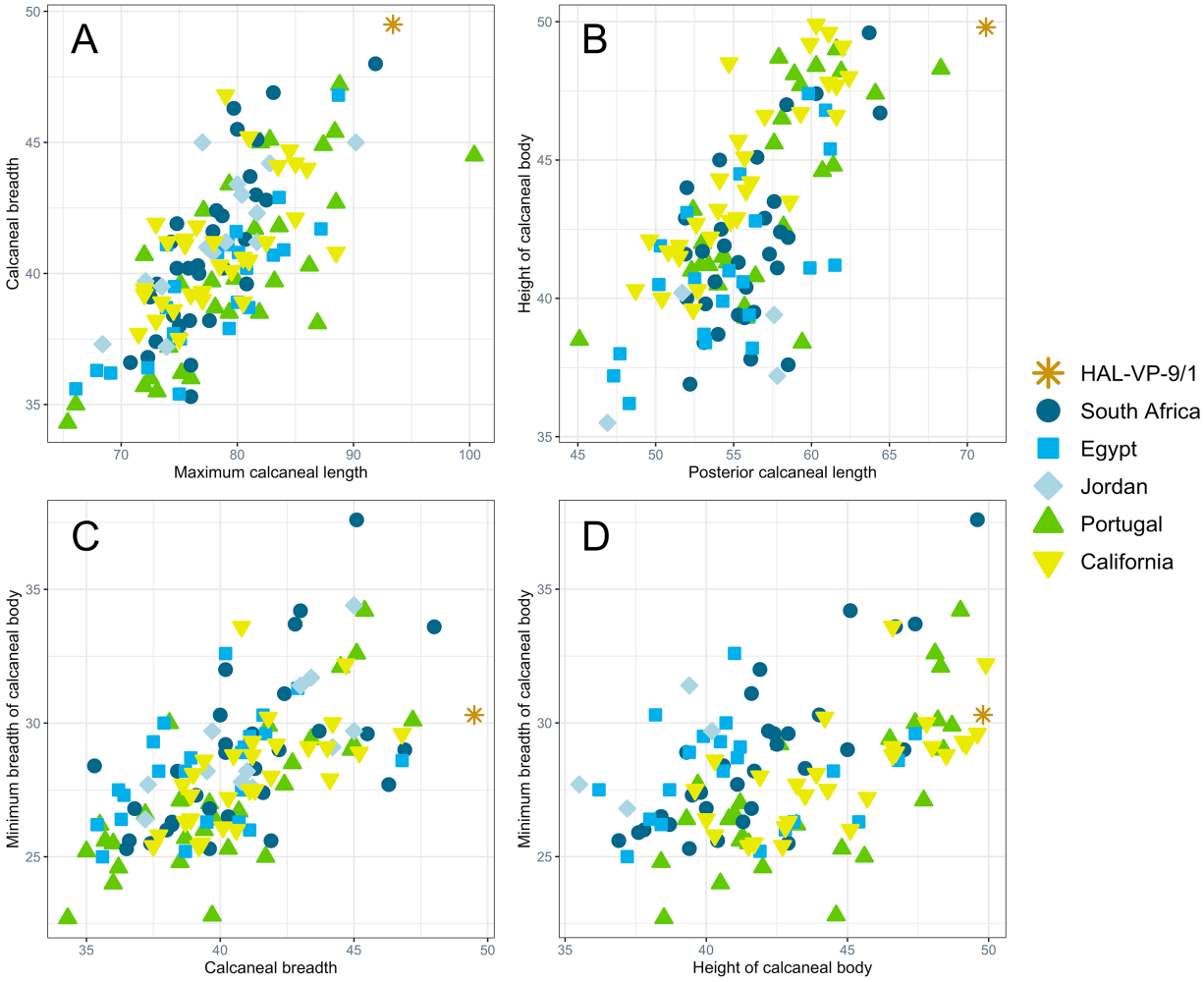


**Figure 5.34** Left navicular (top; HAL-VP-9/1-192) and left cuboid (bottom; HAL-VP-9/1-193) in distal (**A**), proximal (**B**), dorsal (**C**), and plantar (**D**) views.

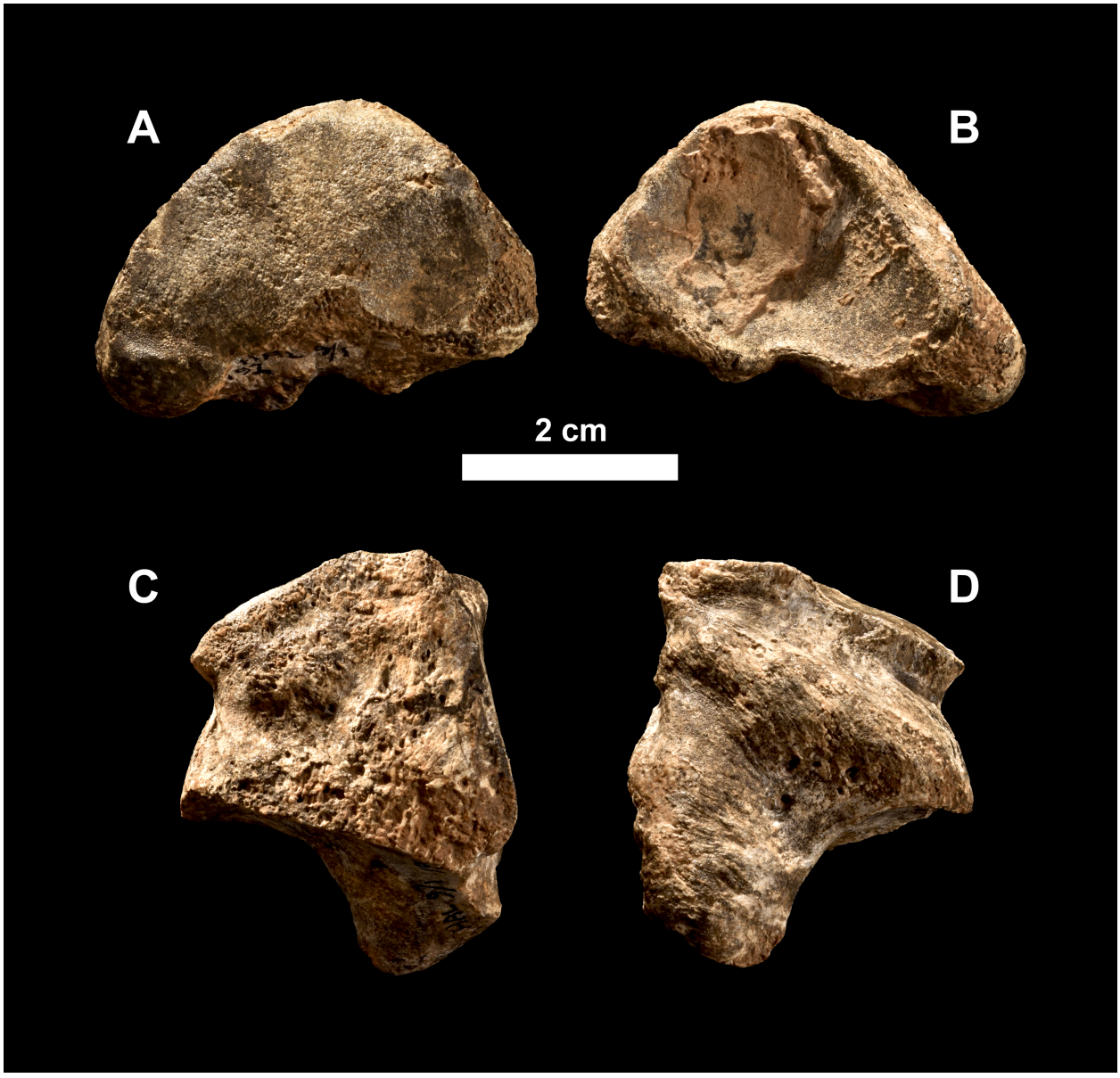


**Figure 5.35** Bivariate plots of cuboid dimensions of HAL-VP-9/1.

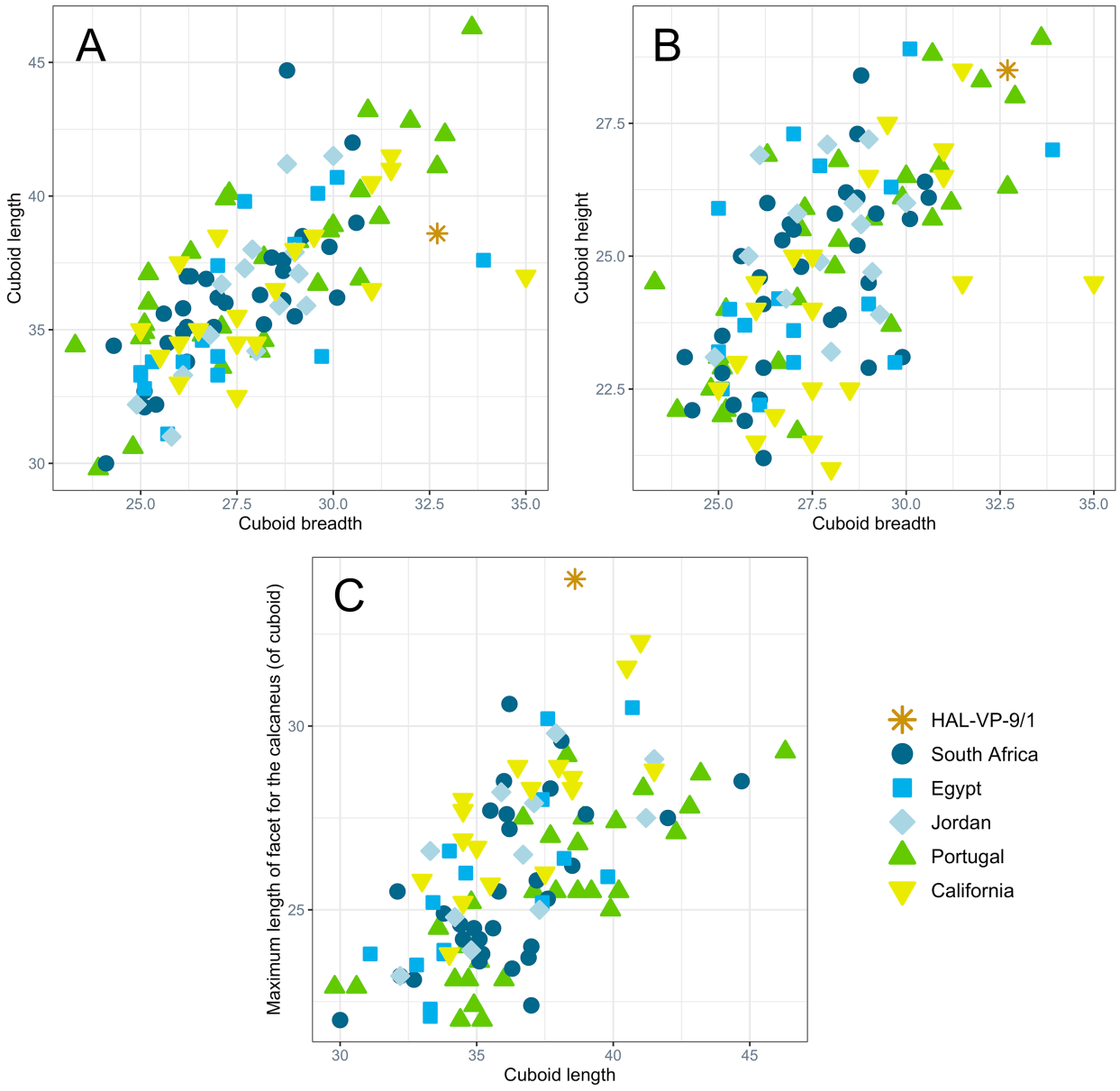


**Figure 5.36** Bivariate plots of navicular dimensions of HAL-VP-9/1.

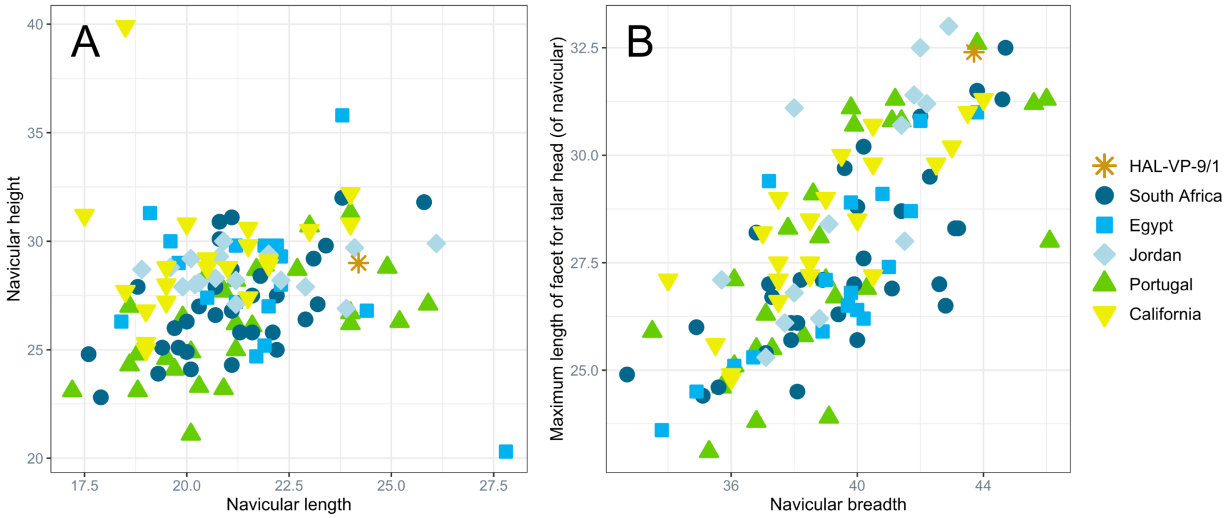
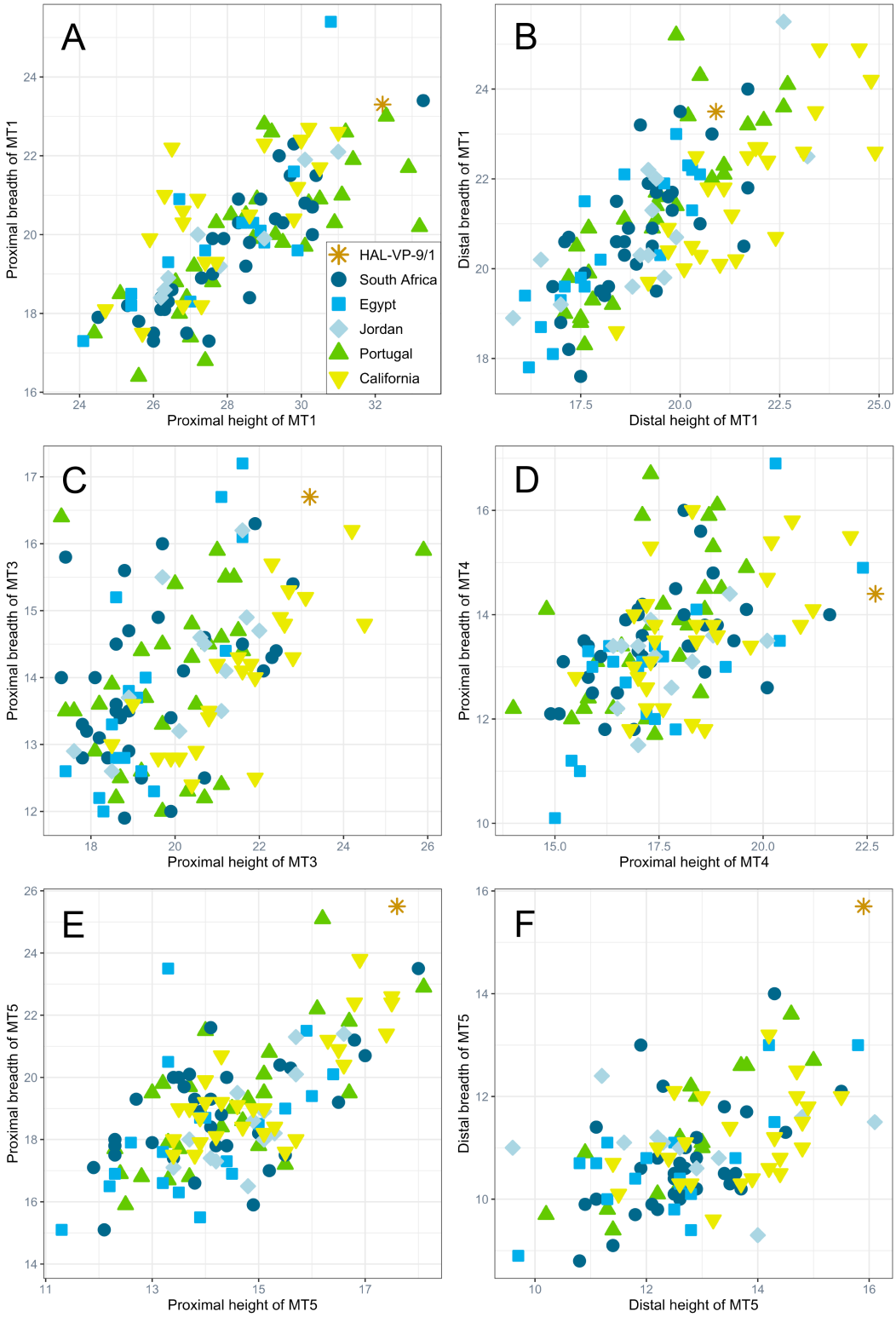


**Figure 5.37** Metatarsals of HAL-VP-9/1 in dorsal (top) and proximal (bottom) views. From left to right: head of fifth metatarsal (at top; HAL-VP-9/1-200), base of fifth metatarsal (middle row; HAL-VP-9/1-199), base of fourth metatarsal (HAL-VP-9/1-195), base of third metatarsal (HAL-VP-9/1-198), head of first metatarsal (at top; HAL-VP-9/1-197), and base of first metatarsal (middle row; HAL-VP-9/1-196). All elements are from the left side except the fourth metatarsal (HAL-VP-9/1-195), which has been mirrored here.



**Figure 5.38** Bivariate plots of first (**A, B**), third (**C**), fourth (**D**), and fifth (**E, F**) metatarsal dimensions of HAL-VP-9/1. Legend as in (**A**).



## Chapter 6: The Halibee fossils in the context of the Pleistocene fossil record

The previous chapter introduced the Halibee postcranial fossils and described them relative to recent modern human skeletal variation. The present chapter further describes the fossils by comparatively assessing the anatomies relative to known Pleistocene fossils (see Chapter 3 and Appendix 4 for sample details).

As discussed in detail in the introductory chapter, the sparse Middle Pleistocene postcranial fossil record has obscured details of the evolution of *H. sapiens* (Carretero et al., 2009). Historically, Neanderthals have been considered a representative of the primitive condition (Hublin, 2009), and a suite of morphological traits have been described as differing between modern humans and Neanderthals (Arsuaga et al., 2015). However, many of these purported differences are based on comparisons with recent modern humans, with limited comparisons to early modern humans owing to the sparseness of the fossil record. Although there have been calls to evaluate these anatomical differences with greater focus on modern human evidence (e.g., Trinkaus, 2006b), the poor representation of early modern humans in the fossil record has continued to obscure the evolutionary history of many of these presumed distinguishing characteristics. Study of the Halibee fossils permits a much needed assessment of claims regarding the distribution of purported primitive and derived features between and within both the modern human and the Neanderthal lineages. Results of the global skeletal sampling presented in Chapter 5 help to build upon what Pearson (2000) has called an "operational definition" of modern human postcranial anatomy.

The fossil record hints at a variable mix of traits in early modern humans. Fossil specimens of comparable antiquity to the sample described here have been described as displaying a combination of derived modern human-like and Neanderthal-like traits (e.g., Omo I, Skhul, and Qafzeh, McCown & Keith, 1939; Pearson et al., 2008a; Vandermeersch, 1981). The Skhul and Qafzeh fossils in particular have been noted as having characteristics that are shared with Neanderthals, to the exclusion of modern humans (McCown & Keith, 1939; Vandermeersch, 1981). Even within the Skhul sample, the number of Neanderthal-like traits varies by specimen (McCown & Keith, 1939). Based on these previous observations, it is reasonable to hypothesize that the Halibee fossils, although geologically slightly younger than the aforementioned samples, will display skeletal traits typically regarded as Neanderthal-like. With the aim of testing this hypothesis, this chapter focuses on aspects of skeletal anatomy that bear on our understanding of Neanderthal and modern human anatomical variation and evolution.

As in Chapter 5, the present chapter is organized by anatomical region and element, but foregoes an element-by-element description, instead focusing on evolutionarily informative morphology. Comparisons in this chapter are centered on the HAL-VP-9/1 partial skeleton; descriptions of additional fossils from the postcranial sample are included where available and relevant to the discussion. The chapter concludes with a brief discussion of the stature, mass, skeletal proportions, and cortical thickness of the HAL-VP-9/1 individual relative to other fossils of Pleistocene *Homo*.

Only adult individuals are included in the comparative fossil samples, with the exception of KNM-WT 15000, which is included even though it is a juvenile individual because it is the most complete pre-modern individual known from genus *Homo* in eastern Africa and thereby provides valuable insight to ancestral morphology. Metric comparisons are included in cases where they significantly aid in comparison, but otherwise the comparative description is

primarily qualitative. Because the large and well-documented fossil sample from the Spanish Middle Pleistocene site of Sima de los Huesos is referenced often throughout this chapter, it is referred to from here on as the "Sima hominids" for brevity. Although the comparative description below does not include juvenile individuals (with the exception of KNM-WT-15000), it should be noted the several of the features assessed are known to vary in their expression throughout ontogeny (Dodo, Kondo, Muhesen, & Akazawa, 2002; Tompkins & Trinkaus, 1987; Trinkaus, 2008; Trinkaus, Mednikova, & Cowgill, 2016). While it is beyond the scope of this initial assessment, further study of the ontogenetic course of these features promises to provide further insight about their etiology and systematic valence.

As described in the study methods (Chapter 3), a comprehensive literature review aimed at identifying anatomical features used for systematic and functional assessments was an important step in this comparative analysis of the Halibee fossils. The key features identified in this literature review were organized as a database. The inclusion of this large database is beyond the scope of this dissertation but was an important resource for the description reported below and will be valuable for ongoing studies of Pleistocene hominid evolution.

Preservational descriptions of the Halibee fossils are reported in Appendix 3. Comparative fossil specimens and data sources are listed in Appendix 4. Measurements of the fossils are reported in tabular format in Appendix 5. Nonmetric data are reported in Appendix 8.

## 6.1 Axial skeleton

### 6.1.1 Vertebrae

#### 6.1.1.1 Cervical and thoracic

The cervical vertebral morphology of modern humans and Neanderthals is generally similar, with the clearest differences being in the length and orientation of the spinous processes. The spinous processes of Neanderthals, particularly of the lower cervical vertebrae, are generally longer and more horizontally oriented relative to modern humans (Carretero, Lorenzo, & Arsuaga, 1999; Gómez-Olivencia, 2009; Gómez-Olivencia, Been, Arsuaga, & Stock, 2013; Gómez-Olivencia et al., 2007; Trinkaus, 1983b). The increased length of the spinous process in Neanderthals is inferred to be the derived condition, whereas the horizontal orientation is shared with earlier *Homo* fossils and is considered ancestral (Arsuaga et al., 2015).

The thoracic vertebrae of modern humans and Neanderthals are also indistinguishable in most respects. A more laterally oriented transverse process has been reported for some Neanderthal fossils (e.g., La Chapelle-aux-Saints 1 and La Ferrassie 1, Heim, 1976), but this anatomy is not characteristic of all Neanderthals (e.g., the transverse processes of the Shanidar individuals are more dorsolaterally oriented, as in recent modern humans, Trinkaus, 1983b).

Unfortunately, the vertebral features of greatest interest and potential systematic utility are not preserved among the Halibee fossils. The preserved portions indicate that the cervical vertebrae of HAL-VP-9/1 are similar to recent modern humans (see Chapter 5) and are at the upper end of the recent modern human range for most metrics. The cervical bodies are also large in absolute dimensions relative to Omo I (Figure 6.1). The single nearly-complete thoracic vertebra of HAL-VP-9/1 (suffixed portion -30, likely a first or second thoracic vertebra, Figure 6.2) does not preserve a complete transverse processes, but the root of the right process suggests an orientation similar to a recent modern human first or second thoracic vertebra.

#### 6.1.1.2 Lumbar

As with the cervical and thoracic vertebrae, the lumbar vertebrae of Neanderthals and modern humans (particularly robust modern humans) are generally similar, with a few exceptions. The lumbar transverse processes tend to be longer in Neanderthals than in modern humans, and those of the second and third vertebrae are more laterally oriented. The polarity of the transverse process length remains unresolved, but the lateral orientation more typical of Neanderthals appears to be derived (although it is not shared with the Sima hominids, which are more similar to modern humans in this respect, Arsuaga et al., 2015; Been, Peleg, Marom, & Barash, 2010; Bonmatí et al., 2010; Gómez-Olivencia, 2009; Trinkaus, 1983b).

The vertebral canal shape of the lower lumbar vertebrae (L4-5) is also reported as differing between modern humans and Neanderthals. The canal is dorsoventrally elongate in Neanderthals relative to modern humans, and this elongate morphology is interpreted as derived (Bonmatí et al., 2010; Gómez-Olivencia, 2009). This shape is not shared with the Sima hominids, which more closely match the modern human morphology (Arsuaga et al., 2015).

One of the most notable differences in the lumbar part of the spine is the degree of lordosis. Modern humans have a lordotic lumbar spine, whereas Neanderthals and the Sima hominids generally have a lower degree of lumbar lordosis (as interpreted from pattern of wedging across the bodies of the lumbar sequence, Been et al., 2010; Bonmatí et al., 2010; Gómez-Olivencia, 2009). This morphology does vary, however, among Neanderthals (e.g., the wedged fifth lumbar vertebra of Shanidar 3 that fits within recent modern human variation, and the more recent description of a lordotic lumbar spine in La Chapelle-aux-Saints 1, Haeusler et al., 2019; Trinkaus, 1983b). The low degree of lordosis observed in Neanderthals and the Sima hominids relative to modern humans and earlier *Homo* suggests that the Neanderthal lineage is derived in this regard (Arsuaga et al., 2015; Been, Gómez-Olivencia, & Kramer, 2012, 2014; Lordkipanidze et al., 2007).

The lumbar transverse processes of HAL-VP-9/1 are too incomplete to be assessed for length and orientation (Figure 6.3), but enough of the vertebral canal of L4 is preserved to suggest that the shape of the canal is similar to modern humans, and not dorsoventrally elongate as in Neanderthals. Complete or nearly-complete bodies of L1-2 and L4-5 are preserved for HAL-VP-9/1 (Figure 6.3), and the pattern of body wedging indicates a lordotic lumbar spine similar to the recent modern human pattern and unlike the pattern reported for some Neanderthals and the Sima hominids.

The first and second lumbar vertebrae of HAL-VP-9/1 exhibit extensive degenerative changes to the superior and inferior surfaces of the bodies (Figure 6.3). Similar degenerative changes are also seen in recent modern humans (Battié, Videman, & Parent, 2004; Pye et al., 2004; Wang, Videman, & Battié, 2012) and Neanderthals (e.g., La Chapelle-aux-Saints 1, Dawson & Trinkaus, 1997; Haeusler et al., 2019). Several of the inferior and superior surfaces of the bodies (e.g., see the superior body surface of L5 in Figure 6.3) exhibit lesions that may be the result of intervertebral disc herniation (i.e., Schmorl's nodes). These lesions are common in recent modern humans (Wang et al., 2012; Williams, Manek, Sambrook, Spector, & Macgregor, 2007), most often occur in the lower thoracic and lumbar regions (Hilton, Ball, & Benn, 1976), and may be related to vertebral shape (Plomp, Dobney, Weston, Viðarsdóttir, & Collard, 2019). Clinical studies suggest that this condition likely would have been painful for this individual (Faccia & Williams, 2008).

### 6.1.2 Ribs

Perhaps the most commonly noted difference between the ribs of modern humans and Neanderthals is related to the overall size and shape of the thorax. The thorax is generally larger and wider toward its inferior end in Neanderthals relative to modern humans, and the vertebrae are positioned more deeply within the thorax (Gómez-Olivencia, 2009; Gómez-Olivencia, Eaves-Johnson, Franciscus, Carretero, & Arsuaga, 2009). The ribs of Neanderthals are also described as thicker, on average, than those of modern humans (Trinkaus, 1983b).

As noted in the preceding chapter, the costal skeleton of HAL-VP-9/1 is highly fragmented, with only small fragments preserved (HAL-VP-9/1-61 through -95; see Appendix 3 for inventory). In all observable aspects of morphology, the ribs of HAL-VP-9/1 fall within modern human variation.

## 6.2 Appendicular skeleton

### 6.2.1 Shoulder girdle

#### 6.2.1.1 Clavicle

Modern human clavicles are thought to be derived in their shorter relative length and pattern of curvature (Carretero et al., 1997; Carretero et al., 1999; Voisin, 2001, 2008; Weaver, 2009). In Neanderthals and other earlier *Homo* individuals (e.g., Carretero et al., 1997; Carretero et al., 1999), clavicles are generally long relative to other long bones, such as the humerus (although this is variable among Neanderthals, e.g., Shanidar 1 and 3, Trinkaus, 1983b). There has been considerable discussion of variation in curvature patterns, particularly the type of curvature in the coronal and transverse planes (Voisin, 2001, 2006b, 2008). In general, modern humans differ from Neanderthals and other *Homo* taxa (including *H. habilis, H. ergaster*, and *H. antecessor*) in having only one inferior curvature or two slight curvatures in dorsal view (i.e., curvature in the coronal plane), rather than the two distinct curvatures that are interpreted as the ancestral configuration (Voisin, 2006b, 2008). This modern human pattern is thought to be associated with a scapula that is positioned lower on the thorax than in taxa with two pronounced curvatures (Voisin, 2006a, 2006b). The clavicle of Omo I falls within the modern human range of variation for curvature in the coronal plane (i.e., in dorsal view), and the pattern of weak lateral curvature and strong medial curvature in the transverse plane is also within the modern range (Pearson et al., 2008b; Voisin, 2008).

The clavicular remains of HAL-VP-9/1 (Figure 6.4) are too fragmentary to permit a reliable assessment of either relative length or complete curvature pattern. One feature that is preserved and can be assessed is the conoid tubercle, which is similar to the well-developed tubercle of Omo I (Pearson et al., 2008b). Otherwise, there is little available morphology that can be brought to bear on questions of modern human clavicular anatomy.

#### 6.2.1.2 Scapula

The position of the axillary sulcus has figured prominently in discussions of anatomical differences between the scapulae of modern humans and Neanderthals (see Trinkaus, 2008 for a

historical review of this literature). In Neanderthals, the axillary sulcus is most often located on the dorsal surface of the axillary border (i.e., *sulcus axillaris teretis*), or is bisulcate (i.e., *facies axillaris bisulcata*), meaning that it is distributed between both the dorsal and ventral surfaces (Trinkaus, 1977). In contrast, recent modern human groups have considerably higher frequencies of a ventrally-positioned sulcus (i.e., *sulcus axillaris subscapularis*, Trinkaus, 1977). Various functional hypotheses have been proposed to explain this variation in the position of the axillary sulcus (Churchill & Trinkaus, 1990; Heim, 1982; Trinkaus, 1977). On the other hand, others have suggested that study of this feature in recent modern humans and immature Neanderthals and earlier *Homo* implies a greater genetic than functional influence (Bermúdez de Castro et al., 2020; Carretero et al., 1997; Frayer, 1992, 1993). Although the factors underlying the development of this feature are not yet well understood, the variants of this feature are clearly at different frequencies in modern humans and Neanderthals (Carretero et al., 1997; Trinkaus, 1977, 2006a).

The axillary margin of the right scapula of the HAL-VP-9/1 individual is preserved (suffixed portion -102, Figure 6.5), and exhibits a dorsally-positioned axillary sulcus (Figure 6.5G-I), as is most commonly observed in Neanderthals and the Sima hominids. The dorsal axillary sulcus morphology is rare in recent modern humans (Trinkaus, 1977, 1983b), and early modern human samples exhibit bisulcate sulci (i.e., Skhul and Qafzeh, Carretero et al., 1997). The significance of this feature remains unclear, but its presence in the HAL-VP-9/1 individual, along with the Levantine evidence, suggests that this feature is morphologically variable in early modern humans.

In addition to the morphology of the axillary border, several other aspects of the scapula have been described as differing between modern humans and Neanderthals. These varying features include the shape of the glenoid cavity and coracoid process, and the relative orientations of the scapular spine, axillary border, and glenoid fossa (Carretero et al., 1997; Trinkaus, 1983b; Weaver, 2009). The fragmentary status of the scapular remains of HAL-VP-9/1 precludes assessment of these features (Figure 6.5, and see Appendix 3 for preservational descriptions).

### 6.2.2 Arm

#### 6.2.2.1 Humerus

A number of humeral features have been proposed as varying taxonomically within genus *Homo*, and they are discussed here more or less from the proximal to the distal end (and pictured for HAL-VP-9/1 in Figures 6.6, 6.7, and 6.8). The shape of the humeral head has been described as more transversely (i.e., horizontally) ovoid in Neanderthals, and more vertically ovoid in modern humans, although the polarity of this trait is unresolved (Arsuaga et al., 2015; Carretero et al., 1997). The humeral head of HAL-VP-9/1 is vertically ovoid and is slightly larger than that of Omo I. Direct comparison of the head shape with Omo I is unreliable, since the humeral head of Omo I is anteroposteriorly crushed and distorted. The second humeral head in the Halibee sample (HAL-VP-9/930-A) is similar to HAL-VP-9/1 and the described modern human morphology in having a vertically ovoid head (Figure 6.6). The lesser tubercles of modern humans have been characterized as narrow and flat, whereas those of Neanderthals are more projecting and massive (although it should be noted that modern humans vary significantly in this region, Carretero et al., 1997; Tanaka, Lestrel, Uetake, Kato, & Ohtsuki, 2000). In both

HAL-VP-9/1 and Omo I, the greater and lesser tubercles are well-developed and moderately projecting (Figure 6.6, Pearson et al., 2008b). The tubercles are slightly larger in absolute terms in HAL-VP-9/1, but erosion to this area of the humerus of Omo I makes it difficult to assess the degree of this difference.

Variation in the form and size of the hominid deltoid tuberosity has received significant attention in the literature (Carretero et al., 1997; Churchill & Smith, 2000; Endo, 1971; Endo & Kimura, 1970; Gómez et al., 2020). Neanderthals are typically described as having a narrow tuberosity in the form of two crests, whereas modern humans have a wider tuberosity with three crests (Arsuaga et al., 2015; Carretero et al., 1997; Endo, 1971). Neanderthals have also been noted as having a very well-developed deltoid tuberosity, among well-developed muscular attachment sites in general (Trinkaus, 1983b; Vandermeersch & Trinkaus, 1995). However, deltoid tuberosity morphology varies considerably within and across modern human groups (Arsuaga, Carretero, Martínez, & Gracia, 1991). The shape and size of the deltoid tuberosity have been often used to make inferences about upper limb function and capabilities within and between various hominid taxa (Trinkaus, 1983b; Trinkaus, Churchill, Ruff, & Vandermeersch, 1999a). As with the axillary sulcus of the scapula discussed above, the etiology of the deltoid tuberosity in humans is not yet well understood, although studies in model organisms are yielding more general insights about the developmental basis of this attachment site (Blitz et al., 2009; Zelzer, Blitz, Killian, & Thomopoulos, 2014). The deltoid tuberosity of the right humerus of HAL-VP-9/1 is only partially preserved (suffixed portion -113, see Appendix 3). Insect damage to the lateral surface near midshaft limits full assessment of the tuberosity, but despite the damage to the shaft surface, it appears to be very weakly developed. The tuberosity is a thin and poorly-defined segment of roughened shaft surface, angling anteriorly toward its distal extent, with its inferior extent at approximately the estimated midshaft position (Figure 6.8).

The humeral shafts of Neanderthals (and the shafts of the other long bones, as discussed below) are characterized as robust relative to most modern humans (Trinkaus, 1983b; Trinkaus et al., 1999a; Vandermeersch & Trinkaus, 1995). The humeral remains of HAL-VP-9/1 clearly deviate from this typical Neanderthal morphology in being very slender and straight, with weakly-developed muscular attachment sites. The humeral shaft of Omo I is similar, but even more slender in absolute terms. The straight and slender shape of the HAL-VP-9/1 humeral shaft is particularly striking when considered relative to the massive proximal and distal ends (as demonstrated relative to recent modern humans in the preceding chapter, Figures 5.5 and 5.6); this pattern is not as pronounced in Omo I. The humeral diaphyseal dimensions of Omo I reveal a low degree of asymmetry (Pearson et al., 2008b), and the humeri of HAL-VP-9/1 similarly display a low degree of asymmetry in size as well as development of attachment sites.

Moving to the morphology of the distal humerus, the olecranon fossa of Neanderthals (as well as the Sima hominids and the earlier Spanish remains from Gran Dolina) is described as relatively broad and deep, whereas the fossa of modern humans is more narrow and shallow (Bermúdez de Castro et al., 2012; Carretero et al., 1997; Weaver, 2009). In this respect, the humerus of HAL-VP-9/1 more closely matches the typical Neanderthal morphology in having a markedly large and deep olecranon fossa, both in absolute and relative terms (Figure 6.7). The absolute fossa breadth is 29.7 mm for HAL-VP-9/1, placing it most closely to Middle Pleistocene *Homo,* early modern human, and the Gran Dolina humeral remains (range of 28.5-31.0 mm) and above recent modern human averages (Carretero et al., 2009).

Another feature that has been described as differing between modern humans and Neanderthals, and is likely correlated with the olecranon fossa morphology, is the relative

mediolateral thickness of the medial and lateral pillars that frame the olecranon fossa. The medial pillar is described as relatively thin in Neanderthals, and thicker in modern humans (Bermúdez de Castro et al., 2012; Carretero et al., 1997; Weaver, 2009). The Sima hominids and the much smaller samples from Gran Dolina fit the Neanderthal pattern, as does the distal humerus from the Middle Pleistocene sediments at Bodo in Ethiopia (Bermúdez de Castro et al., 2012; Carretero et al., 1997; Carretero et al., 2009). In contrast, earlier *Homo* from Africa (i.e., KNM-WT 15000, Walker & Leakey, 1993) as well as the poorly-provenienced but probably Middle Pleistocene humerus from Kabwe (Trinkaus, 2009; Yokley & Churchill, 2006) more closely match the modern human morphology. The polarity of this trait remains unresolved, but it clearly exhibits a large degree of variation within and between groups (Arsuaga et al., 2015; Carretero et al., 2009).

The relative thickness of the medial pillar of HAL-VP-9/1 is small, aligning it more closely with the described Neanderthal pattern, as with the olecranon fossa. The absolute medial pillar thickness of HAL-VP-9/1 is 7.9 mm and is closest to the values for the Gran Dolina humerus (ATD6-148, thickness: 7.0 mm), the Bodo humerus (BOD-VP-1/2, thickness: 9.0 mm) and Neanderthals (mean: 7.7 mm), and well below recent modern human averages (reported averages range between 9.7-12.7 mm, Bermúdez de Castro et al., 2012). Following a similar pattern, the pillar index (ratio of medial to lateral pillar thickness) of HAL-VP-9/1 is 43.9 and is closest to the values for the Gran Dolina humerus (ATD6-148, index: 50.0), the Bodo humerus (BOD-VP-1/2, index: 50.0) and Neanderthals (mean: 51.0), and well below recent modern human averages (reported averages range between 61.4-70.8, Bermúdez de Castro et al., 2012).

The morphology of the HAL-VP-9/1 humeral distal end is generally similar to Omo I, including in the relative widths of the medial and lateral pillars and the size and depth of the olecranon fossa (Pearson et al., 2008b). The most notable difference between these two individuals is the straighter shape of the distal portion of the shaft of HAL-VP-9/1, which contrasts with the slightly more sinuous shape of Omo I. The additional distal humeral remains from the Halibee sample (TAL-VP-7/36-H and HAL-VP-9/1520-F, Figure 6.7) demonstrate variation in the olecranon fossa breadth and the relative thickness of the medial pillar. The depth of the olecranon fossa of TAL-VP-7/36-H is similar to HAL-VP-9/1, but the fossa is slightly narrower. As for the medial pillar, whereas HAL-VP-9/1520-F is similar to HAL-VP-9/1 in having a very thin medial pillar (at least in absolute terms), the medial pillar of TAL-VP-7/36-H is considerably thicker (see Figures 5.5 and 5.6 in the preceding chapter).

The shape of the capitulum of Neanderthals is characterized as rectangular and broad (larger width than height) relative to modern humans, which more often have a capitulum that is taller than it is wide (Carretero, 1994). In this respect, HAL-VP-9/1 is more similar to modern humans with a capitulum width of 21.0 mm and height of 25.8 mm (see Appendix 5 for measurements of the fossils). The distal articular size, in general, has been described as relatively large for most Neanderthals, flanked by robust medial and lateral condyles (Trinkaus, 1983b; Vandermeersch & Trinkaus, 1995). The medial epicondyle of HAL-VP-9/1 is strikingly large and medially projecting, with an approximately rectangular shape. The proportions of these features of the distal end are more striking in HAL-VP-9/1 than in Omo I, and the capitulum is much taller in absolute and relative terms. The distal end of the Omo I humerus is described as "showing a dramatic flare" in its mediolateral width just above the condyles (Pearson et al., 2008b, p. 425), and HAL-VP-9/1 is similarly flared.

The humeral remains of HAL-VP-9/1 reveal a mix of what have historically been regarded as typically modern human and Neanderthal features, echoing previous reports of a

morphologically variable Middle and Late Pleistocene record (Carretero et al., 2009; Pearson et al., 2008b). Similar examples are detailed below throughout other regions of the skeleton, and the implications of this pattern are discussed in the concluding section and in the subsequent chapter.

#### 6.2.2.2 Ulna

The majority of the ulnar features that have been described as varying between modern humans and Neanderthals are concentrated at the proximal end. The olecranon size and shape, for example, is described as large and broad in Neanderthals, and smaller and narrower in modern humans (Aiello & Dean, 1990; Trinkaus, 1983b). Contrary to the expectations for a modern human individual, the olecranon process of Omo I is very broad and has been described as massive (Pearson et al., 2008b). The olecranon of HAL-VP-9/1 is similarly large, and is similar in overall shape to Omo I (Figure 6.9).

The orientation of the trochlear notch has received considerable attention and is described as anteriorly oriented in Neanderthals (and the Sima hominids) and more superoanteriorly oriented in modern humans (Thoma, 1975; Trinkaus, 1983b). However, this morphology is variable, especially in early modern human samples (e.g., Skhul 2 and 7, McCown & Keith, 1939). The ulnae from the Late Pleistocene sites in South Africa (Klasies River and Border Cave) also exhibit a mix of ancestral and derived features, including a low coronoid relative to the olecranon (i.e., an anteriorly-oriented trochlear notch, Churchill, Pearson, Grine, Trinkaus, & Holliday, 1996; Pearson & Grine, 1996; Rightmire & Deacon, 1991). The low coronoid relative to olecranon process condition is somewhat frequent among Middle Stone Age early human fossils but is at low frequencies in most modern human groups (Pearson & Grine, 1996). The coronoid process projects more anteriorly relative to the olecranon in Omo I than in the Klasies River or Border Cave ulnae, or the Middle Pleistocene Baringo Kapthurin ulna (Pearson et al., 2008b; Solan & Day, 1992). The trochlear notch orientation of HAL-VP-9/1 is similar to Omo I in being oriented superoanteriorly, matching the described modern human morphology. The notch of Omo I is oriented only slightly more anteriorly than in HAL-VP-9/1. The orientation of the trochlear notch can be quantified as the ratio of the olecranon to coronoid height (Thoma, 1975; Trinkaus, 1983b). Higher indices indicate a more anteriorly facing notch, as in most Neanderthals (range of 85.5-88.7 in the Shanidar sample, and a mean index of 82.2 for European Neanderthals, Trinkaus, 1983b). Lower indices indicate a more superiorly facing notch, as in the Skhul sample (range of 70.6-82.8), and recent modern humans (mean index of 71.4, Trinkaus, 1983b). The HAL-VP-9/1 index is 66.5, reflecting a superoanterior orientation of the trochlear notch that is most similar to early and recent modern humans.

The additional proximal ulnar remains from the Halibee sample (HAL-VP-3/1, HAL-VP-9/930-B, and HAL-VP-9/1520-E, Figure 6.9) are less well-preserved than the ulnae of HAL-VP-9/1, but in their preserved morphologies fall within the modern human range. The trochlear notch of HAL-VP-3/1 opens slightly more anteriorly than HAL-VP-9/1 (i.e., more similar to the described Neanderthal configuration), although erosion to the anterior margins of the coronoid and olecranon processes make it difficult to assess the extent of this difference.

The shape of the modern human radial notch is described as longer in horizontal dimension versus the vertically longer notch of Neanderthals (and the Sima hominids, Arsuaga et al., 2015; Trinkaus, 1983b). The absolutely and relatively large radial notch of HAL-VP-9/1 is similar to Omo I in being horizontally elongate. The HAL-VP-9/1 supinator crest extends

distally from posteroinferior corner of radial notch, and is long and thin. This crest morphology is more similar to the long and sharp crest described as typical of modern humans, and less so to the short and blunt crest described for most Neanderthals (Arsuaga et al., 2015).

The cross-sectional shape at midshaft of the HAL-VP-9/1 ulna is approximately triangular, as is common in modern humans, and less like the round and gracile midshaft of Neanderthals (Trinkaus, 1983b). There is little evolutionarily or functionally informative anatomy in the distal ulna of *Homo* taxa (Hlusko, Reiner, & Njau, 2015). The distal ulna of HAL-VP-9/1, other than its remarkably large size and tall articular surface, is well within modern human variation. The slightly smaller second distal ulna in the Halibee sample (HAL-VP-9/930-C) also matches modern human morphology (Figure 6.10).

#### 6.2.2.3 Radius

As with the ulna, most of the radial features that have been shown to vary between Neanderthals and modern humans are concentrated at the proximal end. The neck of modern human radii are short and thick in absolute and relative terms (as compared to radial head size), in contrast to the longer and more slender necks of Neanderthal radii (Carretero et al., 1999; Weaver, 2009). The position of the radial tuberosity has also received considerable attention because it tends to be more anteriorly placed in modern humans and more medially placed in Neanderthals (Carretero et al., 1999; Trinkaus & Churchill, 1988; Walker, Ortega, Parmová, López, & Trinkaus, 2011; Weaver, 2009). In early modern humans, however, the radial orientation varies, with medially placed tuberosities reported for Omo I, some of the Skhul and Qafzeh individuals, and the Cave of Hearths radius (Pearson & Grine, 1997; Pearson et al., 2008b). In terms of the radial shaft, Neanderthals typically exhibit greater lateral convexity, whereas modern human shafts are less curved (but with exceptions, e.g., Shanidar, Carretero et al., 1999; Trinkaus, 1983b).

Most of the radial features described above are not preserved for HAL-VP-9/1. A small portion of the radial shaft is preserved, but it is not adequately long to permit an assessment of shaft curvature. The radial head is preserved but the fragment does not include the neck (Figure 6.11). However, the cross-section of the neck immediately below the radial head is visible and suggests a very slender neck relative to radial head size, more similar to the more frequent condition in Neanderthals. This head to neck proportion is likely driven by the very large absolute and relative head size of HAL-VP-9/1, which is beyond the modern range (see Figure 5.8 in the preceding chapter). The neck of the smaller second proximal radius (HAL-VP-2/16) does not appear particularly slender relative to the size of its head and is otherwise indistinguishable from modern human morphology (Figure 6.11). The distal radial end is generally similar in modern humans and Neanderthals, and the morphology discernible from the eroded distal radius of TAL-VP-7/36 (suffixed portion -I, Figure 6.12) falls within expected modern human morphology.

### 6.2.3 Hand

#### 6.2.3.1 Carpals

The carpals of modern humans and Neanderthals are generally similar, but notable differences have been reported for aspects of the trapezium, hamate, lunate, and triquetral. For

the trapezium, the palmar tubercle is described as less projecting in modern humans relative to Neanderthals (and the Sima hominids, Arsuaga et al., 2015; Lorenzo, 2007; Lorenzo, Arsuaga, & Carretero, 1999). The more projecting tubercle of Neanderthals and the Sima hominids is associated with a deep carpal tunnel (Arsuaga et al., 2015). The metacarpal facet on the trapezium is reportedly more concave in modern humans and flatter in Neanderthals. The Sima hominids are more similar to modern humans in having a more saddle-shaped carpo-metacarpal articulation of the thumb, interpreted as reflecting a high mobility of the first metacarpal (Arsuaga et al., 2015). The trapezium of HAL-VP-9/1 (Figure 6.13) exhibits a moderately projecting tubercle relative to the overall size of the element and a saddle-shaped facet for the first metacarpal, as is most common for recent modern humans.

Similarly to the palmar tubercle of the trapezium, the palmarly-projecting hamulus of the hamate tends to be more strongly projecting in Neanderthals and the Sima hominids, and less so in modern humans (Arsuaga et al., 2015; Lorenzo, 2007; Lorenzo et al., 1999; Trinkaus, 1983b; Walker et al., 2011b). The projection of the hamulus has been reported as an index (hamulus projection/maximum height of the hamate bone, Trinkaus, 1983b), and as with the tubercle of the trapezium, above, a large and projecting hamulus is associated with a deep carpal tunnel (Arsuaga et al., 2015). The relative enlargement of the palmar tuberosities of the trapezium, hamate, and scaphoid of Neanderthals has been hypothesized as reflecting hypertrophy of the flexor muscles of the hand that attach to them (Trinkaus, 1983b, 2016). The hamulus of HAL-VP-9/1 (Figure 6.14) is large in absolute terms, but only moderate in relative size, aligning with the proportions observed recent modern humans (see Figure 5.14 in the preceding chapter, Shang & Trinkaus, 2010; Trinkaus, 2016).

In terms of lunate shape, modern humans are similar to Neanderthals in having relatively long lunates in proximodistal dimension, but differ from the Sima hominids, who have relatively short lunates. The HAL-VP-9/1 lunate (Figure 6.15) is slightly elongate in proximodistal length relative to its dorsopalmar width, falling at the edge of the recent modern human distribution (see Figure 5.12 in the preceding chapter). The lunate of HAL-VP-9/1 differs notably in both size and shape from the Omo I lunate, which is unusually small and short in its proximodistal dimension (Pearson et al., 2008b).

The triquetra of modern humans, in contrast to the lunates, differ from both Neanderthals and the Sima hominids in being relatively narrow in radioulnar dimension (Lorenzo, 2007). The triquetra of HAL-VP-9/1 (Figure 6.16), as with the other carpals, are large in absolute size. They are proximodistally long relative to their dorsopalmar width, falling at the edge of modern human variation (see Figure 5.12 in preceding chapter), but otherwise are unremarkable in their proportions. The capitate does not vary notably between modern humans and Neanderthals, and the capitate of HAL-VP-9/1 is as expected for modern human morphology (Figure 6.17).

#### 6.2.3.2 Metacarpals

The majority of the reported differences between the metacarpals of modern humans and Neanderthals are concentrated on the first, second, and third metacarpals. The proximal articulation of the first metacarpal, as with the articulating facet on the trapezium, is more saddle-shaped in modern humans than Neanderthals (Arsuaga et al., 2015; Trinkaus, 2016). This saddle-shaped morphology is shared with the Sima hominids, and as mentioned above, is thought to reflect higher mobility of the first metacarpal relative to the flatter articulations more often found in Neanderthals (Arsuaga et al., 2015). The Omo I proximal articular surface is only

slightly saddle-shaped and is less concave in dorsopalmar contour than many modern humans, more similar to Neanderthals and some early modern humans (e.g., Skhul 5 and Qafzeh 9, Pearson et al., 2008b; Trinkaus, 1983b). The HAL-VP-9/1 individual does not preserve the base of the first metacarpal, and so cannot be brought to bear on the distribution of this anatomy. The head of the first metacarpal is preserved (Figure 6.18), and matches modern human morphology, which has not been reported to deviate significantly from Neanderthals.

The capitate facet on the base of the second metacarpal is described as parasagittally oriented in Neanderthals and more obliquely oriented in recent modern humans (Niewoehner, 2001; Niewoehner, Weaver, & Trinkaus, 1997). The second metacarpal base of HAL-VP-9/1 (Figure 6.19) exhibits an obliquely oriented facet for the capitate, similar to the common morphology in recent modern humans. The second metacarpal base of Omo I is similar to HAL-VP-9/1 in these observable aspects of its anatomy, but it is crushed and distorted (and likely for this reason was previously misidentified as a "Metatarsal II or cuneiform II?, base", KHS 1-44, Pearson et al., 2008b, p. 429).

The base of the third metacarpal is reported to vary between modern humans and Neanderthals in the following features. The facet for the second metacarpal tends to be more concave and the styloid projection greater in modern humans relative to Neanderthals (Niewoehner, 2001; Niewoehner et al., 1997). The degree of proximal projection of the styloid process is intermediate in most of the Skhul and Qafzeh bases and is not quite as strongly projecting as in most modern humans (Niewoehner, 2001). The facet for the second metacarpal of HAL-VP-9/1 is similarly concave to modern humans, and the styloid projection is within modern human variation (Figure 6.20). The styloid process of Omo I is similarly well-developed (Pearson et al., 2008b), and projects even more strongly relative to its size compared to HAL-VP-9/1. The base of the third metacarpal, as in nearly all skeletal dimensions, is absolutely larger in HAL-VP-9/1 than Omo I. The shape of the proximal articular facet is similar, but the facet tapers more toward its palmar end in the Omo I metacarpal.

The fourth and fifth metacarpal morphologies of modern humans and Neanderthals do not deviate notably. The fourth (Figure 6.21) and fifth (Figure 6.22) metacarpal remains of HAL-VP-9/1 conform to modern human morphology in all respects, beyond their remarkably large size in most dimensions (see Chapter 5).

Most descriptions of metacarpal proportions have focused on relative lengths among the rays and among the segments within each ray. In these respects, modern humans and Neanderthals are indistinguishable (Trinkaus, 1983b, 2016). Within-element assessments of the metacarpals indicate that the shaft and articular end sizes are large relative to total length in Neanderthals compared to modern humans, but with considerable overlap between Neanderthals and some recent modern human samples (Smith, 2000). Modern human variation in relative metacarpal length and shaft thickness appears to be correlated with climate (with relatively shorter and thicker metacarpals in populations inhabiting colder environments) and Neanderthals also appear to conform to this cold-adapted pattern in their metacarpal morphology, as with their limb bones more broadly (Betti, Lycett, von Cramon-Taubadel, & Pearson, 2015). The single complete metacarpal of HAL-VP-9/1 (from the third ray) differs from this Neandertal-like cold adapted pattern in its large absolute length and moderate relative length, and moderate relative shaft dimensions (although the shaft cross-sectional shape is at the edge of the modern human range, see Figure 5.17 in the preceding chapter).

#### 6.2.3.3 Hand phalanges

The proximal and intermediate hand phalanges of modern humans and Neanderthals are indistinguishable in most respects. They are non-curved in both groups, which is the ancestral morphology within genus *Homo* (Lorenzo, 2007). The trochleae of the proximal and intermediate hand phalanges tend to be broader in Neanderthals and the Sima hominids than in modern humans (Arsuaga et al., 2015; Musgrave, 1973). The HAL-VP-9/1 phalanges, unsurprisingly, are non-curved, and the trochleae do not appear particularly broad.

The most notable difference between the phalanges of modern humans and Neanderthals is the breadth of the distal tuberosities of the terminal hand phalanges. In modern humans, the tuberosity is relatively narrow, while in Neanderthals it is relatively broad and sometimes appears circular in dorsal or palmar view (Lorenzo, 2007; Musgrave, 1973; Trinkaus, 1983b; Trinkaus, Haduch, Valde-Nowak, & Wojtal, 2014). This Neanderthal anatomy has been hypothesized to reflect a functional adaptation affecting grip capabilities (Trinkaus, 1983b) or thermoregulation of these distalmost extremities in a cold climate via increased vascularization (Musgrave, 1971). However, more recent comparative work assessing distal tuberosity morphology across primates fails to support the latter hypothesis, and cautions against making functional interpretations until the relative roles of the multiple underlying factors affecting this morphology are better understood (Mittra, Smith, Lemelin, & Jungers, 2007). The narrow distal tuberosity of the terminal hand phalanges of HAL-VP-9/1 (Figure 6.23) is consistent with modern human morphology, and stands apart from the broad tuberosities of Neanderthals and the Sima hominids (Arsuaga et al., 2015).

### 6.2.4 Pelvic girdle

#### 6.2.4.1 Sacrum

The sacra of modern humans and Neanderthals are generally similar, with only a few described distinctions (Arsuaga et al., 2015; Trinkaus, 1983b). The modern human sacrum is similar in absolute and relative size and shape to that of Neanderthals, but is notably shorter and narrower than the Sima hominids (Arsuaga et al., 2015). The sacral remains of HAL-VP-9/1 are too fragmentary to provide information on the shape and total size of the sacrum, but the available morphology (including the sacroiliac joint size) matches that of modern humans (Figure 6.24).

#### 6.2.4.2 Os coxae

Several features of the os coxae have been described as differing significantly between Neanderthals and modern humans. These differences include aspects of pelvic shape, most notably the transverse shape of the pelvic canal and the degree of lateral flaring of the iliac blade. Modern humans generally have a rounder transverse shape of the pelvic canal, whereas Neanderthals, the Sima hominids, and African *Homo erectus* exhibit the ancestral trait of a more elliptical transverse canal shape (i.e., mediolaterally broad, Bonmatí et al., 2010; Rosenberg et al., 2006; Ruff, 2010; Simpson et al., 2008). Neanderthal pelvic remains, on average, are broader than modern humans, but are narrower than the markedly broad and robust pelves of the Sima individuals (Arsuaga et al., 2015; Arsuaga et al., 1999a). Modern humans are also considered derived in their small degree of iliac flaring relative to Neanderthals, the Sima hominids, and

earlier African *Homo* (Arsuaga et al., 1999a; Bonmatí et al., 2010; Simpson et al., 2008; Walker & Leakey, 1993). The pelvic remains of HAL-VP-9/1 are too fragmentary to provide information on these more global aspects of shape without a detailed digital reconstruction of the pelvis that is beyond the scope of this dissertation.

There are, however, a few other pelvic features of interest on which HAL-VP-9/1 can be brought to bear, and they primarily include aspects of the superior pubic ramus morphology. The inferred ancestral morphology for the superior pubic ramus in genus *Homo* is a thin and plate-like shape (as observed in the Sima hominids, and Early and Middle Pleistocene *Homo* fossils, Arsuaga et al., 1999a; Bonmatí et al., 2010; Rosenberg, 1988, 1998; Trinkaus, 1976b). Both modern humans and Neanderthals appear to be derived in this respect, but in different ways. The Neanderthal ramus is described as extremely craniocaudally flattened and plate-like with a distinct crest-like ventral border, whereas the modern human ramus is thick and bar-like (Arsuaga et al., 2015; Bonmatí et al., 2010; Trinkaus, 1976b). Unlike the Neanderthal morphology and more similar to recent humans, HAL-VP-9/1 has a thick and bar-like superior pubic ramus (Figure 6.25).

In terms of the length of the superior pubic ramus, Neanderthals and the Sima hominids present the inferred ancestral condition of having a relatively long ramus, whereas the ramus of humans tends to be shorter (Arsuaga et al., 2015; Arsuaga et al., 1999a; Rosenberg, 1998; Trinkaus, 1984). However, this Neanderthal-like morphology is also observed in some early modern humans (e.g., the long superior pubic ramus of Skhul 9, Pearson, 1997). The long superior pubic rami and the resulting greater anterior breadth of Neanderthal pelves have been interpreted as a less energetically efficient configuration for walking (Trinkaus, 1983b). Most researchers have interpreted this configuration as advantageous during childbirth, but the precise significance of this feature has seen considerable debate (Dean, Stringer, & Bromage, 1986; Friedlander & Jordan, 1994; Rak & Arensburg, 1987; Rosenberg, 1988, 1998; Trinkaus, 1984). Neanderthal pelves are also characterized by a suite of features that are associated with the long superior pubic ramus morphology, including a relatively large mediolateral size of the obturator foramen and greater subpubic angles in both males and females (Trinkaus, 1983b). The superior pubic ramus of HAL-VP-9/1 appears to be absolutely elongate but is more similar to the common modern human morphology in being only moderately long when considered relative to overall size. The medial portion of the acetabulum and most of the superior pubic ramus are unfortunately not preserved, precluding measurement of the acetabulosymphyseal length that is most commonly used in assessments of pubic ramus relative length (Rak & Arensburg, 1987; Rosenberg, 1988).

Additional features that are preserved on the HAL-VP-9/1 pelvic remains include a shallow supracetabular sulcus (although only the anterior part is preserved). A shallow sulcus is common among modern humans and thought to be the derived condition, whereas Neanderthals exhibit the ancestral morphology in having a relatively well-developed sulcus, sharing this condition with Early and Middle Pleistocene *Homo* (Bonmatí et al., 2010; Endo & Kimura, 1970; Heim, 1982; Sigmon, 1982; Stringer, 1986). The anterior inferior iliac spine, adjacent to this sulcus, is most often medially twisted in Neanderthals relative to the anterior margin of the iliac blade and is thought to be the ancestral morphology (Arsuaga et al., 1999a; Endo & Kimura, 1970). The Sima hominids exhibit a similar morphology to Neanderthals, and distinct from the untwisted or only slightly twisted anterior inferior iliac spine of modern humans (Bonmatí & Arsuaga, 2007; Endo & Kimura, 1970; Meyer, Bruzek, Couture, Madelaine, & Maureille, 2011;

Rose, 1984). The os coxal remains of HAL-VP-9/1 unfortunately do not preserve the anterior inferior iliac spine.

The acetabulum of the Sima hominids is notable in its large average size relative to modern humans and Neanderthals (Arsuaga et al., 2015). The acetabulum of HAL-VP-9/1 is strikingly large in absolute dimensions (59.1 mm), placing it above the reported mean for the Sima hominids (56.7 mm, range: 50-60 mm) and at the upper end of the Neanderthal and modern human ranges (Neanderthal mean: 56.2 mm, range: 41-62 mm, modern human mean: 52.7 mm, range: 41.7-62 mm, Arsuaga et al., 2015). The acetabulum of HAL-VP-9/1 is considerably larger than Omo I (Figure 6.25). The hollowing in the area of the preauricular sulcus is shallower in HAL-VP-9/1, and the sciatic notch is more tightly curved than in Omo I. These differences support the previously reported tentative sex estimation of female for Omo I (Pearson et al., 2008b, see Chapter 4 for discussion of sex estimation).

### 6.2.5 Leg

#### 6.2.5.1 Femur

Several femoral features vary between modern humans and Neanderthals, and as with the humerus above, they are described here from the proximal to distal end. The relative length of the femoral neck is generally longer in Neanderthals and Early and Middle Pleistocene *Homo* (with exceptions, e.g., the femur from Berg Aukas, Grine et al., 1995), whereas modern humans more often exhibit the inferred derived condition of a relatively shorter neck (Arsuaga et al., 2015). The neck of HAL-VP-9/1 is very long in absolute terms (see Figure 5.22 in the preceding chapter), but moderate in its relative length and within modern human variation.

The angle of the neck relative to the shaft is, on average, lower in Neanderthals than in most modern human groups, and modern humans are considered derived in this respect (Lordkipanidze et al., 2007; Trinkaus, 1983b; Walker & Leakey, 1993; Weaver, 2009). Most of the fossils from Skhul and Qafzeh exhibit high neck-shaft angles (except Skhul 4), whereas the limited evidence from the African Middle Pleistocene shows variation in this morphology (i.e., the high angle of KNM-ER 999 and low angle of the Berg Aukas femur, Grine et al., 1995; Trinkaus, 1993b). The femoral neck-shaft angle varies considerably across modern human groups, and as discussed in the preceding chapter, the factors that underlie this variation are still debated (e.g., Anderson & Trinkaus, 1998; Child & Cowgill, 2017; Gilligan et al., 2013; Weaver, 2003). The low neck-shaft angles of Neanderthals are interpreted by some as reflecting high levels of mobility and physical activity (Trinkaus, 1993b), whereas others interpret the low angles as a correlate of a cold-adapted body form (Weaver, 2003). The femoral neck-shaft angle of HAL-VP-9/1 (122.5º) is below the mean for the modern human comparative samples included in this study (see Figure 5.22 in preceding chapter, and Appendix 9 for modern human summary statistics) and similar to reported values for some Neanderthals (Trinkaus, 1993b), but is still within the range of modern humans considered here and in previous studies of global variation in this trait (Gilligan et al., 2013).

The proximal femoral shafts of Early and Middle Pleistocene members of genus *Homo* have been often described as platymeric (Arsuaga et al., 2015; Gilbert, 2008; Weidenreich, 1941). The proximal shaft of HAL-VP-9/1 is not preserved, but those of HAL-VP-9/1520 and BOU-VP-16/100 exhibit varying degrees of platymeria, with the latter femur being slightly more anteroposteriorly flattened but still well within modern human variation. Platymeria is likely

associated with the attachment site morphology of the *gluteus maximus*, including, for example, the presence of a third trochanter or a hypotrochanteric fossa (Lovejoy, Meindl, Ohman, Heiple, & White, 2002). Hypotrochanteric fossae are exhibited at higher frequencies in fossils of earlier *Homo* relative to modern humans (Arsuaga et al., 2015; Carretero et al., 1999). None of the fossils in the Halibee sample described here preserve the complete proximal shaft, and therefore cannot bear on the frequency of this trait in early modern humans. The gluteal tuberosities of Neanderthals have been described as larger than modern humans, on average, and have been interpreted by some as indicating hypertrophy of the *gluteus maximus* (Trinkaus, 1983b). The gluteal tuberosity of HAL-VP-9/1 is not preserved, but those of HAL-VP-9/1520 and BOU-VP-16/100 are moderately developed (Figure 6.26).

Although the *linea aspera* is well-developed in early *Homo* (Lordkipanidze et al., 2007) and Neanderthals (Trinkaus, 1983b), the presence of a true pilaster is derived in, and nearly exclusive to, modern humans (Gilbert, 2008; Weaver, 2009). Because they lack a pilaster, fossils of Neanderthals and earlier *Homo* generally exhibit a rounder femoral midshaft in cross-section, with particularly robust shafts described for most Neanderthals (Trinkaus, 1983b; Trinkaus et al., 1999a; Trinkaus & Ruff, 2012). However, it should be noted that although the presence of a pilaster is nearly exclusive to modern humans, the expression of this feature varies within modern humans (Hrdlička, 1934; Pearson, 2000). The femur of HAL-VP-9/1 exhibits a clear pilaster, as does the femur of the second partial skeleton from Halibee, HAL-VP-9/1520 (Figure 6.26). The third individual that includes femoral shaft remains, BOU-VP-16/100, preserves only the superior portion of the *linea aspera*, and can therefore not be assessed for pilastric morphology (see preservational description in Appendix 3).

Relatively few features of the distal femur have been described as varying significantly between modern humans and Neanderthals (Trinkaus, 1983b). Relative to Omo I, the distal femur is considerably larger in absolute dimensions (Figure 6.27) but is otherwise similar in morphology. Both femora exhibit a laterally positioned lateral lip of the anterior patellar surface, and the patellar lip of HAL-VP-9/1 on the lateral side is tall (i.e., extends proximally). The height of the lateral patellar lip in Omo I cannot be determined due to erosion to this surface.

#### 6.2.5.2 Patella

The patellae of Neanderthals have been characterized as absolutely and relatively large and thick relative to modern humans, but they overlap the upper part of the recent modern human range in size and shape (Trinkaus, 1983b). The patellar shape of Neanderthals, usually described via the height/breadth index, is most often wider than tall (corresponding to a low index, Trinkaus, 1983b; Trinkaus & Rhoads, 1999). The Sima hominids share this tendency with Neanderthals, whereas the earlier Spanish fossils from Gran Dolina tend to be taller than wide (corresponding to a high index), and modern humans very widely in their patellar shapes (see Figure 5.24 in preceding chapter, Arsuaga et al., 2015; Carretero et al., 1999).

In addition to their large size and wide shape, Neanderthal patellae are described as thick in absolute and relative terms. Some have suggested this to reflect a hypertrophied *quadriceps femoris* muscle (Trinkaus, 1983b), but recent work suggests that patellar shape and thickness may be more directly associated with body size and shape (Rosas et al., 2020). The relative widths of the medial and lateral facets are variable in Neanderthals and modern humans, and in early modern humans (e.g., Qafzeh 9 and Skhul 4) the lateral facet tends to be wider (Trinkaus, 1983b, 2000). The patellae of HAL-VP-9/1 are wider than they are tall and are moderately thick

relative to their overall size (see Figure 5.23 in the preceding chapter). As with the patellae of other early modern humans, the lateral facet is wider than the medial facet.

#### 6.2.5.3 Tibia

Tibial features that have been described as varying between modern humans and Neanderthals are described here more or less from the proximal to distal end, as with the humerus and femur, above. Two aspects of the proximal end have been reported to vary between these two groups: the retroversion angle and the placement of the tibial condyles. The retroversion angle (the inclination of the tibial plateau relative to the shaft axis) is described as higher, on average, in Neanderthals relative to most modern human groups, meaning that Neanderthals have a more posteroinferiorly inclined tibial plateau (Trinkaus & Rhoads, 1999). The tibial condyles of Neanderthals are also described as more posteriorly displaced relative to the shaft axis, compared to most recent modern humans (Trinkaus, 1983b; Trinkaus & Rhoads, 1999). Only a small fragment of the proximal tibial end of HAL-VP-9/1 is preserved (suffixed portion -176, see Appendix 3), and is inadequate to assess either of these features.

Considerable attention has been given to the cross-sectional shape of the tibial shaft across hominid taxa, and more specifically within modern humans (Lovejoy & Trinkaus, 1980; Pearson, Petersen, Sparacello, Daneshvari, & Grine, 2014; Ruff & Larsen, 2014; Trinkaus & Ruff, 2012; Trinkaus et al., 1999c). Despite these efforts, the etiology of tibial shaft cross-sectional geometry is still not well understood. Previous studies have suggested that the cross-sectional geometry of the tibial shaft is influenced by habitual activity, with greater anteroposterior mechanical strain (as is induced by running) being associated with greater bony reinforcement in the anteroposterior axis (i.e., higher degrees of platycnemia, Pearson et al., 2014; Ruff et al., 2006; Shaw & Stock, 2009). However, the role of climate-influenced body proportions on the cross-sectional geometry of the lower limb bones may also influence tibial shaft cross-sectional shape (Pearson et al., 2014; Ruff & Larsen, 2014).

The tibia of Omo I is described as very platycnemic, and the newly-recovered tibia from broadly contemporaneous deposits within the Kibish Formation is described as slightly less platycnemic (Kib 158-1a, Pearson et al., 2008a; Pearson et al., 2008b). The HAL-VP-9/1 tibia is larger than the Omo I and Kib 158-1a tibiae, as is the case with nearly all other dimensions, but all three individuals share very slender and platycnemic tibial shaft morphology (see Figure 6.28 and Figures 5.26 and 5.27 in the preceding chapter). In contrast to this shaft morphology, Neanderthals are described as typically having relatively wide and exceptionally robust shafts that are amygdaloid in cross-sectional shape (Endo & Kimura, 1970; Trinkaus, 1983b). The significance of differences in cross-sectional geometry of the tibial shaft, and the other long bones, is still a matter of debate (Davies & Stock, 2014; Pearson et al., 2014; Ruff, 2000; Shaw & Stock, 2011; Trinkaus & Ruff, 2012).

Fewer differences have been described for the distal end of modern human and Neanderthal tibiae. The medial malleolus tends to be well-developed in Neanderthals and the Sima hominids relative to modern humans (Arsuaga et al., 2015; Trinkaus, 1983b). Other than its large absolute size, the tibial distal end of HAL-VP-9/1 is unremarkable. The medial malleolus of HAL-VP-9/1 is moderate in size relative to the overall size of the distal end and is otherwise similar to modern human morphology. The right tibial distal end of HAL-VP-9/1 exhibits a very slight lateral squatting facet, with the distal articular surface extending slightly onto the anterior surface of the distal tibia at the lateral edge. The left side does not exhibit a squatting facet.

Squatting facets are also present on Kib 158-1a, but erosion precludes assessment of Omo I for this trait (Pearson et al., 2008a). The presence of squatting facets is variable in Neanderthals and recent modern humans, as well as in the Sima hominids (Arsuaga et al., 2015; Boulle, 2001; Trinkaus, 1975b, 1983b). The presence of squatting facets is related to hyperdorsiflexion of the ankle joint, which occurs when a squatting position is assumed (Trinkaus, 1975a).

The distal articular surface for the talus is rectangular in HAL-VP-9/1, as is typical for modern humans, and differs from the unusual triangular talar facet reported for Omo I, which has a considerably shorter medial relative to lateral margin (however, this shape may be at least partly the result of erosion to the anteromedial surface of the distal end, Pearson et al., 2008b).

The tibiae of HAL-VP-9/1 and Kib 158-1a are both strikingly long (Pearson et al., 2008a), suggesting a high crural index for these two individuals. The relative tibial length of HAL-VP-9/1 will be further discussed below.

#### 6.2.5.4 Fibula

The fibular morphology of modern humans and Neanderthals is generally similar, with the only notable differences being the more robust shafts and distal ends of most Neanderthals (Trinkaus, 1983b). Similarly, the fibular robusticity of the Sima hominids is at the upper end of the modern human range (Arsuaga et al., 2015). The absolute dimensions of the distal fibular end of HAL-VP-9/1 are moderate relative to recent modern humans, but the size of the articular surface is at the upper end of the range (see Figures 5.28 and 5.29 in the preceding chapter). The few preserved fibular shaft fragments (see Appendix 3) are not particularly robust.

### 6.2.6 Foot

#### 6.2.6.1 Talus

Several aspects of the talus have also been reported to vary between modern humans and Neanderthals. The talar head, for example, tends to be absolutely and relatively narrow in fossils of Early Pleistocene *Homo* and in the Sima hominids (Pablos et al., 2013b; Rhoads & Trinkaus, 1977). In contrast, the talar head of Neanderthals is absolutely and relatively broad, whereas modern humans are more intermediate in their talar head morphology (Pablos et al., 2013b; Rhoads & Trinkaus, 1977). The talar head of HAL-VP-9/1 is large and broad in absolute terms, but only moderately so relative to its overall size. The talar head of Omo I is described as "disproportionately large", but does not appear to be remarkably so, relative to the proportions observed in HAL-VP-9/1 (see Figure 6.29, Pearson et al., 2008b, p. 431).

The lateral malleolar facet is generally mediolaterally broad (i.e., projecting laterally) in Neanderthals, and even moreso in the Sima hominids, but is relatively narrow in modern humans (Gambier, 1982; Pablos et al., 2019; Pablos, Pantoja-Pérez, Martínez, Lorenzo, & Arsuaga, 2017; Rhoads & Trinkaus, 1977; Rosas et al., 2017; Trinkaus, 1983b). However, there is considerable overlap in this feature between Neanderthals and some modern human groups (Trinkaus, 1983b), likely at least in part because this feature appears to be associated with general postcranial robusticity (Pablos et al., 2017). Pearson et al. (2008b) describe the lateral malleolar facet of Omo I as laterally projecting, similarly to Neanderthals, some Skhul and Qafzeh individuals, and some recent human groups (e.g., Khoe-San), and suggest that this may be an ancestral feature inherited from an African ancestor. The evidence from the HAL-VP-9/1

talus further supports this hypothesis, as it has a similarly broad and projecting lateral process (Figure 6.29).

The narrow and posteriorly wedged trochlear shape described as characteristic of modern humans differs from the rectangular and broad shape of Neanderthals, the Sima hominids, and earlier *Homo* (Pablos et al., 2019; Pablos et al., 2012; Pablos et al., 2013b; Rosas et al., 2017). The talus of HAL-VP-9/1 conforms more closely to the typical Neanderthal morphology in its rectangular and broad trochear shape. The trochlea of Omo I tapers more posteriorly than HAL-VP-9/1 (i.e., is more wedged), more like the morphology described as characteristic of modern humans. It should be noted, however, that trochlear shape is widely variable within modern humans (Kidd & Oxnard, 2002; Sorrentino et al., 2020), and varies within Neanderthals as well (e.g., the slightly wedged trochleae of Shanidar 1 and 3, Trinkaus, 1983b).

#### 6.2.6.2 Calcaneus

The calcaneal shape of modern humans has been described as narrow relative to the broader calcanei of Neanderthals and the Sima hominids (Pablos et al., 2014; Trinkaus, 1983b). Similarly, Neanderthals and the Sima hominids share a strongly projecting sustentaculum tali relative to modern humans (Pablos et al., 2014; Pablos et al., 2017; Trinkaus, 1983b). The calcaneal tuber of Neanderthals is also described as long relative to overall calcaneal length (Pablos et al., 2017; Raichlen, Armstrong, & Lieberman, 2011; Trinkaus, 1983b). The calcaneus of HAL-VP-9/1 is moderately broad, and aside from its exceptional size, is similar in its proportions to recent modern humans (see Figure 5.33 in the preceding chapter). The sustentaculum tali appears to be strongly projecting, but is only moderately so relative to overall calcaneal size (see Figure 5.32 in the preceding chapter). The calcaneal body similarly appears remarkably long, but is only moderately so relative to overall length, and is within the expected proportions for modern humans.

#### 6.2.6.3 Cuboid and navicular

The anterior tarsals of modern humans and Neanderthals, including the cuboid and navicular, are generally very similar (Trinkaus, 1975a, 1983b). Both the cuboid and navicular of HAL-VP-9/1 are preserved (Figure 6.30), and both elements fall within modern human variation in nearly all respects (see Figures 5.35 and 5.36 in the preceding chapter). The articular surface for the calcaneus on the cuboid of Omo I is described as large (Pearson et al., 2008b), and this morphology is even more exaggerated for HAL-VP-9/1, for which the maximum dimension of this facet is the only measurement of the cuboid that exceeds the modern human range (see Figure 5.35 in the preceding chapter). Both the cuboid and the navicular are larger in absolute terms in HAL-VP-9/1 than Omo I.

#### 6.2.6.4 Metatarsals

Similar to the pattern described for the metacarpals, the overall proportions of the metatarsals are generally similar between Neanderthals and modern humans (Trinkaus, 1983a). The most notable difference in their proportions is that the metatarsals of Neanderthals tend to have thicker shafts relative to their lengths (Mersey, Jabbour, Brudvik, & Defleur, 2013; Trinkaus, 1983a). Contrary to the pattern observed in the metacarpals where shorter and thicker

elements are associated with colder climates, the metatarsals appear to follow this pattern only in terms of their thicknesses, but not their relative lengths (at least for the first ray, Betti et al., 2015). The HAL-VP-9/1 foot remains do not preserve any complete metatarsals, thereby precluding an assessment of their relative lengths. However, the preserved shaft portions do not indicate particularly thick metatarsal shafts, unlike the condition more typically observed in Neanderthals.

The cross-sectional shape of the first metatarsal shaft of HAL-VP-9/1 is similar to that of the Klasies River human first metatarsal, which is flat on its lateral surface and approximately triangular in cross-section (Rightmire, Deacon, Schwartz, & Tattersall, 2006). This cross-sectional shape is also shared with Neanderthals (Trinkaus, 1983b). Aside from its heightened robusticity, the Klasies River first metatarsal is reportedly similar to recent Africans and does not exhibit any significant proportional differences. It is, however, small relative to the early modern humans from Skhul and Qafzeh (Rightmire et al., 2006). This stands in contrast to Omo I, which falls within the Skhul and Qafzeh range for all dimensions except length, for which it exceeds the range (Pearson et al., 2008b). Only the proximal and distal ends of the first metatarsal of HAL-VP-9/1 are preserved (Figure 6.31). Their size relative to Omo I suggests that the first metatarsal of HAL-VP-9/1 is longer in absolute length, placing it well above the Skhul and Qafzeh individuals for this dimension (Pearson et al., 2008b).

The midshaft shape of the second metatarsal varies subtly between modern humans and Neanderthals. In the Klasies River human second metatarsal, and in most recent modern humans, the dorsoplantar dimension of the shaft is large relative to its breadth (Rightmire et al., 2006). This shape differs from Neanderthal shaft shape, which tends to be broad relative to shaft height (i.e., more circular in cross-section, Rightmire et al., 2006). The second metatarsal of HAL-VP-9/1 is not preserved, but the remains of the fourth metatarsal suggest a similarly dorsoplantarly tall midshaft for the metatarsals of the middle rays.

Aside from general robusticity, few notable differences have been described for the third metatarsals of modern humans and Neanderthals. The HAL-VP-9/1 third metatarsal base (Figure 6.32) is unremarkable outside of its large size, and in all other respects conforms to modern human morphology.

The base of the fourth metatarsal is described as absolutely broad in Neanderthals and the Sima hominids relative to the narrower base of modern humans (Pablos et al., 2012). In this respect humans are considered to present the ancestral morphology shared with earlier *Homo* (e.g., Gran Dolina, Pablos et al., 2012). The fourth metatarsal base of HAL-VP-9/1 (Figure 6.33) is at the edge of recent modern human variation in its absolute height and width dimensions (see Figure 5.38 in preceding chapter), but otherwise matches the described modern human morphology in having a tall and narrow base.

Few differences have been noted between modern human and Neanderthal fifth metatarsals, beyond degree of robusticity in the shaft and especially the base (Pablos et al., 2019; Trinkaus, 1975a, 1983b). The human fifth metatarsal from the Klasies River site has a smaller base than the Skhul and Qafzeh individuals (Rightmire et al., 2006). The Klasies River specimen also has a flattened shaft similar to recent modern human populations, and different from the shape of the Skhul and Qafzeh individuals in which the midshaft shape is tall relative to its breadth (Rightmire et al., 2006). The fifth metatarsal of HAL-VP-9/1 shares the shaft shape of the Klasies River specimen, exhibiting a mediolaterally broad shaft that appears dorsoplantarly flattened (Figure 6.34). The Klasies River specimen is also described as very large compared to Holocene humans and recent South Africans, exceeding averages for recent modern human

groups in all dimensions but still within range (Rightmire et al., 2006). The fifth metatarsal of HAL-VP-9/1 is also similar to the Klasies River specimen in this respect, falling near the recent modern human upper limit, or beyond it, in dimensions of the head and base (see Figure 5.38 in the preceding chapter). As described above, the lateral metatarsals (rays III-IV) of modern humans and Neanderthals are generally similar, but the bases of Neanderthals, and the Sima hominids, are described as absolutely broader than modern humans (Arsuaga et al., 2015). However, the limited available fossil evidence for the foot in the African Early and Middle Pleistocene makes it difficult to assess whether these traits are specific to the Neanderthal lineage or more generally associated with overall robusticity and body proportions (Pablos et al., 2019).

#### 6.2.6.5 Foot phalanges

There are few notable differences between modern humans and Neanderthals in foot phalangeal morphology. The clearest distinction mirrors the pattern observed in the terminal hand phalanges; the distal tuberosity on the distal foot phalanges is more expanded in Neanderthals and the Sima hominids relative to modern humans (Arsuaga et al., 2015; Trinkaus, 1983b). The terminal foot phalangeal morphology cannot be assessed for HAL-VP-9/1, since the only foot phalanges preserved include one proximal and one intermediate phalanx (Figure 6.35). The morphology of these two foot phalanges is unremarkable and fits well within modern human variation.

## 6.3 Body size and shape comparisons

The Plio-Pleistocene African fossil record demonstrates changes in hominid stature and limb proportions in fossils of *Homo erectus* relative to earlier hominid taxa (Holliday, 2012; McHenry, 1992; Walker & Leakey, 1993). The stature and proportions of *H. erectus* appear to lie within the range of humans (Ruff, 2002; Walker & Leakey, 1993), and the efficiency of upright walking is inferred to have been equivalent to humans (Lordkipanidze et al., 2007). Between this large increase in body size at 1.5-2 million years ago and approximately 50 thousand years ago, body size remained largely constant as far as the limited record reveals, but between 50 and 10 thousand years ago it is argued to have decreased on average (Carretero et al., 2012; Ruff, 2002; Ruff et al., 1997). It is also during this most recent time period that much of the variation we see today in human body size and proportions across the globe was shaped, both by climatic influences on and population history of different human groups (Roseman & Auerbach, 2015; Stulp & Barrett, 2016).

The recovery and study of associated skeletons is particularly valuable, not only because they typically preserve more of the total skeletal anatomy, but because they also permit the study of body shape and size changes through time (e.g., KNM-WT-15000 and Jinnuishan, Rosenberg et al., 2006; Walker & Leakey, 1993). Study of associated remains avoids the limitations posed by reconstructing individual size and shape based on isolated elements (e.g., Carretero et al., 2012; Sawyer & Maley, 2005), or describing body shape using proportions that span elements from multiple individuals. The HAL-VP-9/1 skeleton thereby provides a window into the stature, mass, and body proportions of early modern humans in the Late Pleistocene of eastern Africa, building on the previous report of the geographically proximate Omo I partial skeleton (Pearson et al., 2008b).

### 6.3.1 Stature and mass

The best available stature estimate for HAL-VP-9/1 is 179.25 ± 3 cm (see Chapter 4 for details). As discussed in the preceding chapter, the tall stature of this individual aligns it with what has been called the "derived biotype" within genus *Homo* (Carretero et al., 2012). This "derived biotype" appears in the fossil record ca. 200 ka, as body shape changes from shorter and broader bodies to taller and more slender ones (Carretero et al., 2012). Stature estimates for early modern humans (i.e., Skhul and Qafzeh individuals) are well above those of Neanderthals and the Sima hominids (pooled sex means of 177.4 cm, 160.6 cm, and 163.6 cm, respectively, Arsuaga et al., 2015). The stature estimate of HAL-VP-9/1 aligns it most closely to the male early modern humans from Skhul and Qafzeh (185.1 cm, Arsuaga et al., 2015), indicating that this individual, like other early modern humans, was tall by recent average modern human standards. The estimate for HAL-VP-9/1 is within a centimeter of the estimate for the Kabwe individual (178.9 cm, Trinkaus, 2009), and slightly above the Boxgrove estimate (175.3 cm, Stringer, Trinkaus, Roberts, Parfitt, & Macphail, 1998). The stature estimates for Omo I and the Kib 158-1a tibia are slightly lower than for HAL-VP-9/1, but the estimate ranges overlap (Pearson et al., 2008a; Pearson et al., 2008b). The estimate for HAL-VP-9/1 sets it apart from Neanderthals (except for the Amud individual, which is unusually tall for a Neanderthal, Carretero et al., 2012; Endo & Kimura, 1970) and earlier *Homo*. Several selective pressures have been proposed to explain the increased stature and narrow physique of modern humans, and it remains unclear how much of a role obstetrical, mechanical, or physiological factors may have each played in this evolutionary trend (Carretero et al., 2012; Churchill, 2006; Holliday, 1997; Tague, 2000; Weaver, 2009).

The best available mass estimate for HAL-VP-9/1 is 80.3 ± 4.3 kg (see Chapter 4 for details). The comparisons with recent modern humans reported in the preceding chapter indicate that the HAL-VP-9/1 individual had a very large body mass. Recent average modern human body mass is large relative to most earlier *Homo* taxa; several body mass increases are inferred to have occurred throughout the evolutionary history of the human genus. Body mass increases are generally observed in early *Homo*, throughout the record of *H. erectus*, and then in Middle Pleistocene *Homo*, followed by a relatively stable period until the late Upper Paleolithic, after which body size variably decreased across modern human groups (Holliday, 2015; Ruff et al., 2018). Body mass in recent modern humans appears to generally follow ecogeographical rules, with higher body masses on average in higher latitude populations (Holliday, 2015; Ruff, 1994). Neanderthal body mass estimates are greater than those of early modern humans (i.e., Skhul and Qafzeh) and Upper Paleolithic humans, but similar to estimates for Middle Pleistocene African *Homo* (Gallagher, 2013). Neanderthal mass estimates are also similar to those for the Sima hominids (pooled sex weighted means of 72.1 kg and 69.1 kg, respectively, Arsuaga et al., 2015). The body mass estimate of HAL-VP-9/1 places it near the estimate based on the Kabwe tibia, and at the upper end of the Sima hominid and the male Neanderthal ranges (Arsuaga et al., 2015; Ruff et al., 2018).

### 6.3.2 Skeletal proportions

Although a large percentage of the HAL-VP-9/1 skeleton is preserved, the long bones are unfortunately too fragmentary to provide reliable intra- and intermembral indices. However, some aspects of the postcranial proportions can still be observed, or at least inferred from the

preserved portions. For example, although the femoral remains are too fragmentary to provide a maximum length, the strikingly long tibia of HAL-VP-9/1 nonetheless suggests a high crural index (i.e., long distal to proximal segments of the lower limb, Carretero et al., 2012). The limited African Pleistocene fossil evidence suggests that early modern humans and preceding taxa may have had ecogeographically patterned limb proportions (i.e., relatively long distal limb segments, as seen in Omo I, for example, Holliday, 1997; Pearson et al., 2008a; Pearson et al., 2008b; Trinkaus, 2009; Walker & Leakey, 1993), and the evidence from the HAL-VP-9/1 skeleton further supports this notion.

One of the most striking aspects of the HAL-VP-9/1 skeleton is the intra-element proportions of the limb bones. For most of the long bones, including the metacarpals and metatarsals, the ends are notably large relatively to the thickness of the shafts, which are slender for an individual of such large size. For many of the limb elements, this proportional relationship places HAL-VP-9/1 at the edge of recent modern human variation or beyond it (see Chapter 5). The proportional relationships between the ends and shaft dimensions of the humerus and tibia align HAL-VP-9/1 most closely with Native Californians among the recent modern human sample (see Figures 5.5 and 5.26 in the preceding chapter), although at the edge of the sampled variation for this group.

Although Neanderthals have been described as having relatively large epiphyses and articular surfaces, these large ends are associated with robust shafts, unlike the pattern that characterizes HAL-VP-9/1 (Trinkaus, 1983b; Trinkaus et al., 1999a; Vandermeersch & Trinkaus, 1995). The end-to-shaft proportions exhibited by HAL-VP-9/1 also do not appear to characterize the humerus or tibia from Kabwe (Trinkaus, 2009, 2012). The long bone shafts of Omo I are similarly slender to HAL-VP-9/1, but the ends are not as massive relative to the shaft dimensions. Although this pattern is not as pronounced in Omo I as in HAL-VP-9/1, the variation between these two individuals in these proportions does not exceed that observed in recent modern human samples. The etiology of the pattern observed in HAL-VP-9/1 is unclear, but may be related to developmental variation and sets up an interesting avenue of future study, which will be outlined in the next and final chapter.

### 6.3.3 Cortical thickness and entheseal changes

Early and Middle Pleistocene *Homo* generally exhibit very thick cortices in the long bones of their limbs. The cortical bone of Neanderthals and the Sima hominids is generally also quite thick and is on average considerably thicker than in modern humans (Arsuaga et al., 2015; Trinkaus, 1983b). African Late Pleistocene fossils exhibit moderately, but not remarkably thick cortical bone (Pearson & Grine, 1996; Rightmire et al., 2006). The cortical thickness of the limb bones of HAL-VP-9/1, as observed at the breaks across the long bone shafts, is moderate, unlike the thicker cortices of Middle and Early Pleistocene *Homo* (Ruff, Trinkaus, Walker, & Larsen, 1993; Trinkaus & Ruff, 2012; Trinkaus, Ruff, & Conroy, 1999b). Cortical thickness variation in modern humans, and its evolution in hominids, has received considerable attention (Ruff, 2005; Ruff et al., 1993; Trinkaus, 1997; Trinkaus & Churchill, 1999; Trinkaus & Ruff, 2012). However, despite this extensive literature, the relative contributions of various factors (e.g., biomechanical forces, climatic influences, and population history) are still debated; this area of study will be further considered in the subsequent and final chapter.

Differences between modern humans and Neanderthals in the robusticity of muscular and ligamentous attachment sites have also been documented (Belcastro, Mariotti, Facchini, &

Bonfiglioli, 2006; Mariotti & Belcastro, 2011; Trinkaus, 1983b, 1997). However, the systematic description of modifications to entheseal surfaces requires adherence to standardized methods (Belcastro et al., 2020; Davis, Shuler, Danforth, & Herndon, 2013) and very good preservation of the bone surface, which is often not the case in fossil specimens. While a systematic assessment of entheseal expression is beyond the scope of the present study, the attachment sites on the HAL-VP-9/1 can be described in a broad sense. The attachment sites of the HAL-VP-9/1 individual are not particularly rugose relative to recent modern humans, and are generally surprisingly gracile for an individual of such large size (see Appendix 3 for descriptions). While attachment site morphology has been interpreted as a reflection of activity patterns, it is increasingly clear that many factors influence these markers (Belcastro et al., 2020; Lovejoy et al., 2002; Milella, 2014; Villotte & Knüsel, 2013).

## 6.4 Conclusions

This chapter has characterized the postcranial skeletal anatomy of the Halibee fossils in an evolutionary comparative framework by describing them relative to the most relevant known fossils. Echoing the results of the preceding chapter, the Halibee postcranial fossils conform to expectations for modern human anatomy in most respects but deviate in a few interesting ways. Several features of the postcranium align more closely with traditional characterizations of Neanderthal anatomy. Notable examples from the shoulder and upper limb of HAL-VP-9/1 include the dorsally-placed sulcus of the scapular axillary border, the broad and deep humeral olecranon fossa, and the relatively thin medial pillar of the distal humerus. Among the pelvis and the lower limb of HAL-VP-9/1, the acetabular height is above the mean of the very large Sima hominids and well above the modern human and Neanderthal means. This skeleton's femoral neck-shaft angle is similar to those reported for Neanderthals but is still within the lower part of the modern human range. Characteristics of the HAL-VP-9/1 foot remains that are traditionally considered Neanderthal-like include the flaring lateral malleolar facet, the broad and rectangular trochlea, and the strikingly broad base of the fifth metatarsal.

The presence of these Neanderthal-like features adds to the morphological heterogeneity observed in early modern humans. The Neanderthal-like features in this sample, and particularly in HAL-VP-9/1, build on previous reports that suggest a mixture of Neanderthal-like and modern human-like traits in a population ancestral to these two lineages. It would appear that traits variably sorted across and within both lineages, and changed in relative frequencies over the course of the last half a million years, with possible influences from gene flow (Pearson et al., 2008a; Stringer, 2016; Trinkaus, 2005). The Halibee fossils thereby help to fill in a major gap in the Late and Middle Pleistocene record of Africa. This gap has significantly limited our understanding of anatomy and its variation in the population ancestral to early modern humans and Neanderthals (see Introduction).

The results of body stature and mass comparisons of the HAL-VP-9/1 individual relative to fossil samples reinforce conclusions from the previous chapter. This individual was undeniably large in stature and mass relative to modern humans, Neanderthals, and other representatives of genus *Homo*. Despite this large size, however, the cortical thickness of the limb bones is moderate, and muscular and ligamentous attachment areas are only moderately developed. The skeletal proportions support previous suggestions that early human variation was patterned ecogeographically, given the likely high crural index suggested by the strikingly long tibia. The HAL-VP-9/1 individual appears to have had a long, linear physique, with long distal

limb segments, which is in accordance with inferences made from the Omo I and the Kabwe tibial remains (Pearson et al., 2008b; Trinkaus, 2009).

The HAL-VP-9/1 skeleton exhibits intra-element proportions of the long bones that are unusual relative to recent modern humans, Neanderthals, and what we can discern of Late and Middle Pleistocene *Homo.* Most of the long bones have very large ends relative to the thicknesses of their shafts. This pattern is striking, although its significance is unclear. Insights from evolutionary developmental biological studies may inform hypotheses about what underlies this peculiar morphological pattern, and this promises to be an important future avenue of study, as does the study of developmental patterns observed in modern humans and Neanderthals (the latter are well represented by infant, child, and juvenile individuals whose assessment lies beyond the scope of the present study).

Many of the skeletal features considered in this chapter that appear to have systematic valence also appear to be at least moderately correlated (e.g., the olecranon of the proximal ulna, and the olecranon fossa and medial pillar of the distal humerus), but the significance of most of these correlations remains unclear. This fact is particularly problematic for cladistic analyses assuming character independence, a concern which has been repeatedly raised (Hlusko, 2004; McCollum & Sharpe, 2001; Trinkaus, 1990). Several of the skeletal anatomies that have been shown to vary among modern humans and other *Homo* taxa have received considerable attention (e.g., patellar shape and thickness, tibial cross-sectional shape, and robusticity of the lateral metatarsals), but the relative roles of biomechanical forces, body size and shape, and underlying patterning mechanisms are not well understood. Many inferences about behavior have been made based on such skeletal variation, but these are better characterized as hypotheses than findings. The importance of studies aimed at parsing out the various factors underlying variation in these postcranial skeletal traits will be emphasized in the next chapter.

**Figure 6.1** Cervical vertebrae of HAL-VP-9/1 (left) and Omo I (right) in superior view. Dorsal is up. HAL-VP-9/1 cervical vertebrae include, from top to bottom, C4 (HAL-VP-9/1-24), C5 (HAL-VP-9/1-25), C6 (HAL-VP-9/1-26), and C7 (HAL-VP-9/1-27). Omo I cervical vertebrae positions are indeterminate (Pearson et al., 2008b). The vertebrae pictured here are, from top to bottom: KHS 1-55-V3, KHS 1-55-V4, and KHS 1-55-V5.

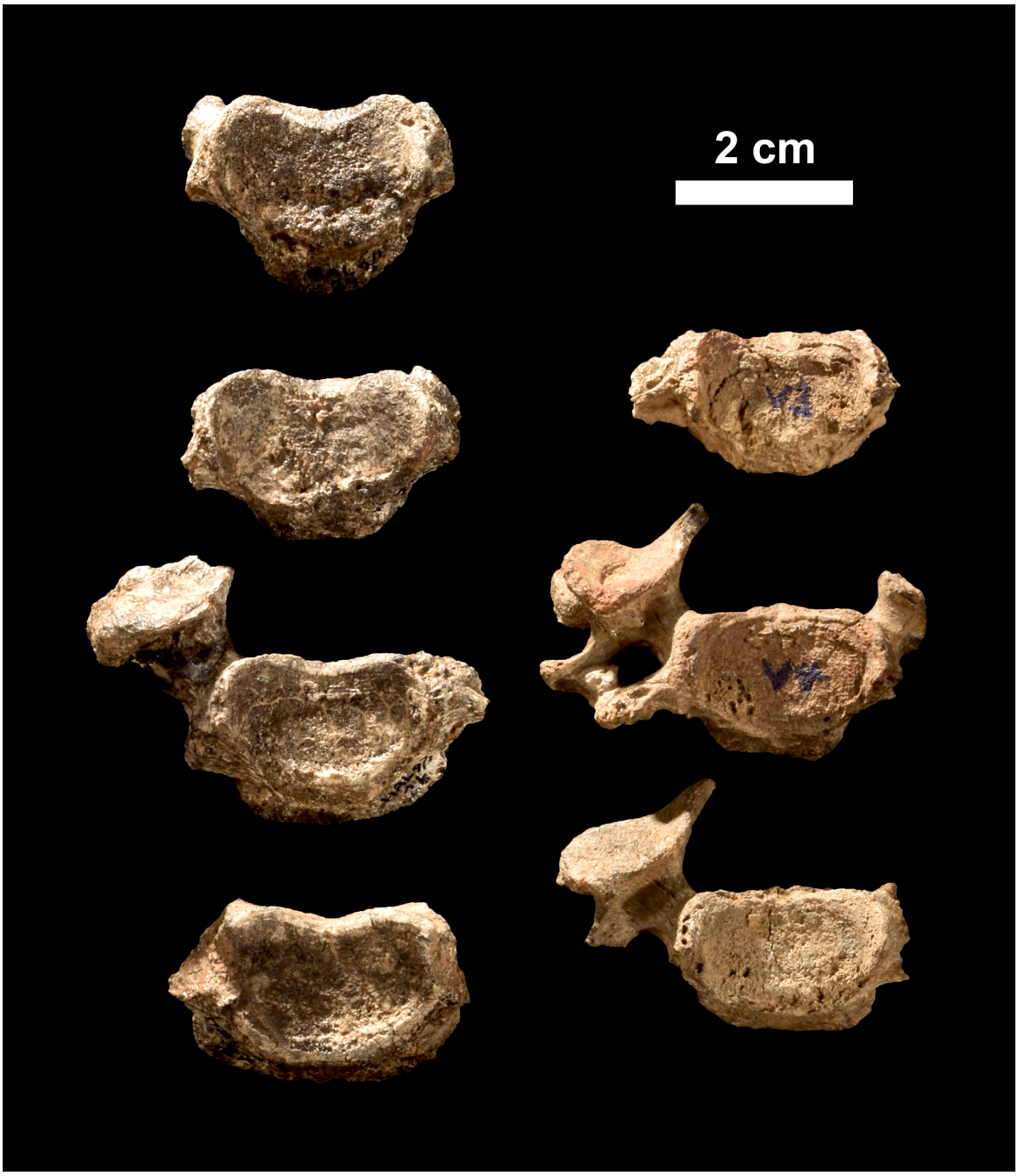


**Figure 6.2** Upper thoracic vertebra (probably first or second) of HAL-VP-9/1 (suffixed portion -30). Views are, clockwise from top: anterior (superior is up), inferior, right lateral (ventral is right), left lateral (ventral is left), and superior.



**Figure 6.3** Lumbar vertebrae of HAL-VP-9/1. From top to bottom: first lumbar vertebra (HAL-VP-9/1-50), second lumbar vertebra (HAL-VP-9/1-49), fourth lumbar vertebra (HAL-VP-9/1-52), and fifth lumbar vertebra (HAL-VP-9/1-53). The vertebrae are presented in superior view in the left column, inferior view in the center column, and right lateral view in the right column (ventral is to the right). The white arrow indicates a small lesion that may be the result of intervertebral disc herniation.

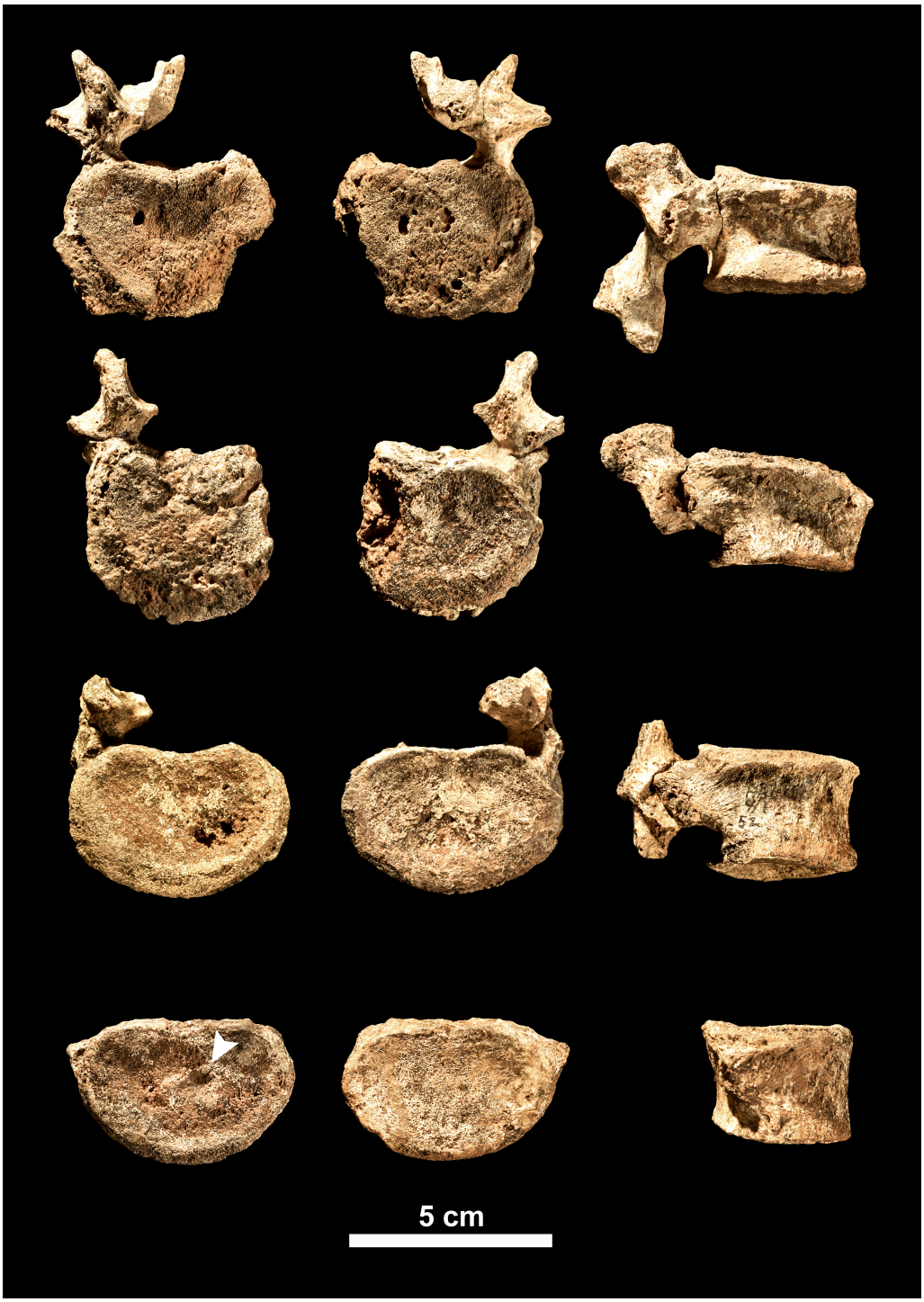


**Figure 6.4** Clavicle of HAL-VP-9/1. The shaft portion near the acromial end of the right clavicle (HAL-VP-9/1-96) is pictured in the top panel in superior (top) and inferior (bottom) views. In superior view, anterior is up and lateral is toward the right. In inferior view, anterior is up and lateral is toward the left. The medial shaft portion of the left clavicle (HAL-VP-9/1-97) is pictured in the bottom panel in superior (top) and inferior (bottom) views. In superior view, anterior is up and lateral is toward the left. In inferior view, anterior is up and lateral is toward the right.



**Figure 6.5** Scapular remains of HAL-VP-9/1. Right acromion and scapular spine (HAL-VP-9/1-100) in posterior (**A**), lateral (**B**), and anterior (**C**) views. Lateral is to the right in **A**, anterior is to the right in **B**, and lateral is to the left in **C**. Partial right glenoid fossa (HAL-VP-9/1-101) in anterior (**D**), posterior (**E**), and lateral (**F**) views. Lateral is to the left in **D** and to the right in **E**, anterior is to the right in **F**. Partial axillary border of right scapula (HAL-VP-9/1-102) in lateral (**G**), anterior (**H**), and posterior (**I**) views. Anterior is to the right in **G**, lateral is to the left in **H** and to the right in **I**. Inferior angle of left scapula (HAL-VP-9/1-105) in posterior (**J**) and anterior (**K**) views. Lateral is to the left in **J** and to the right in **K**. Partial left acromion (HAL-VP-9/1-104) in superoposterior view (**L**), anterior is up. Scale is the same for all panels.

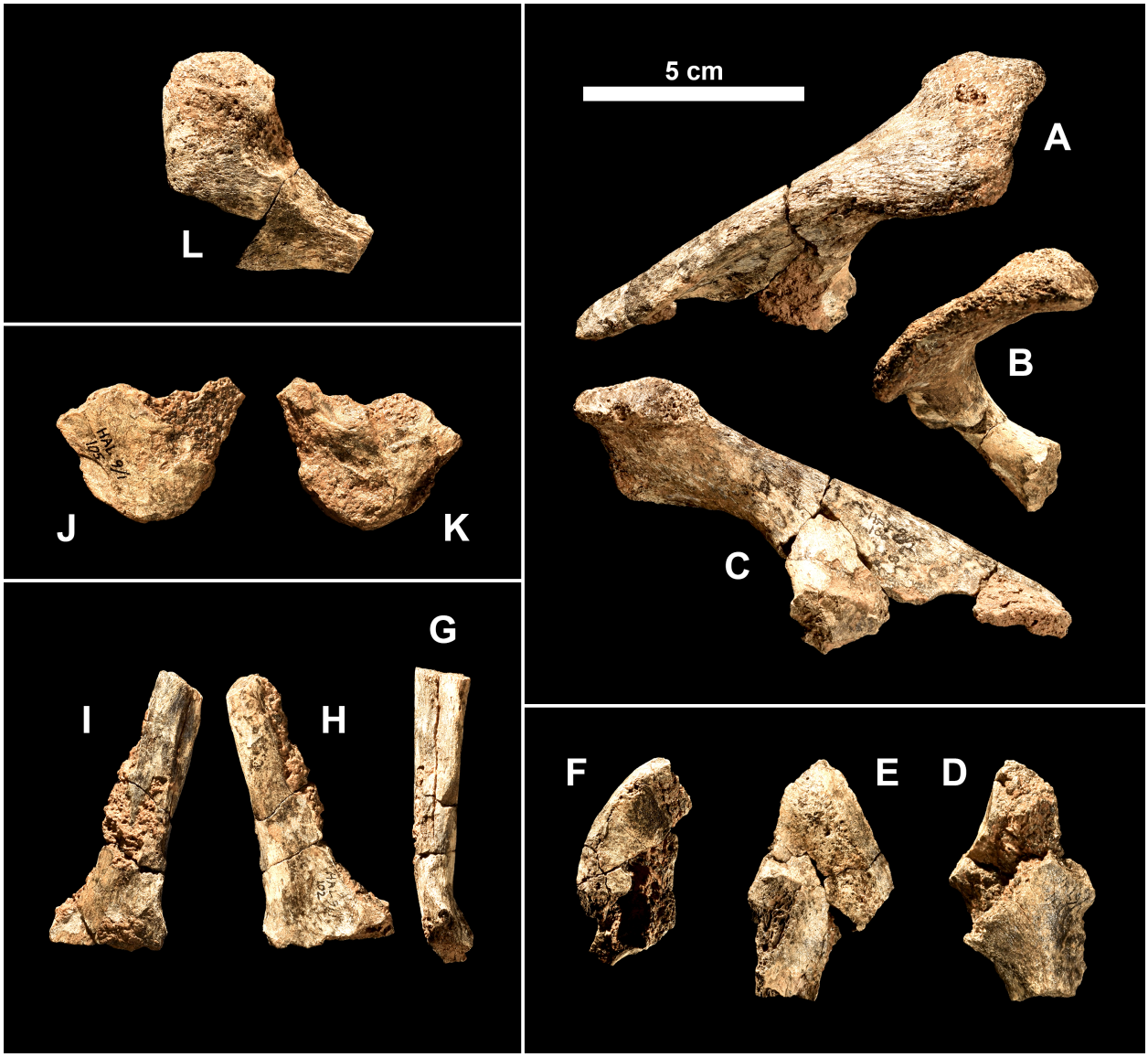


**Figure 6.6** Proximal humeri in anterior view. **A:** Left proximal humerus of HAL-VP-9/1 (suffixed portion -115). **B:** Right proximal humerus of HAL-VP-9/930 (suffixed portion -A). **C:** Left proximal humerus of Omo I (KHS 1-34). **D:** Right proximal humerus of Omo I (KHS 1-33).

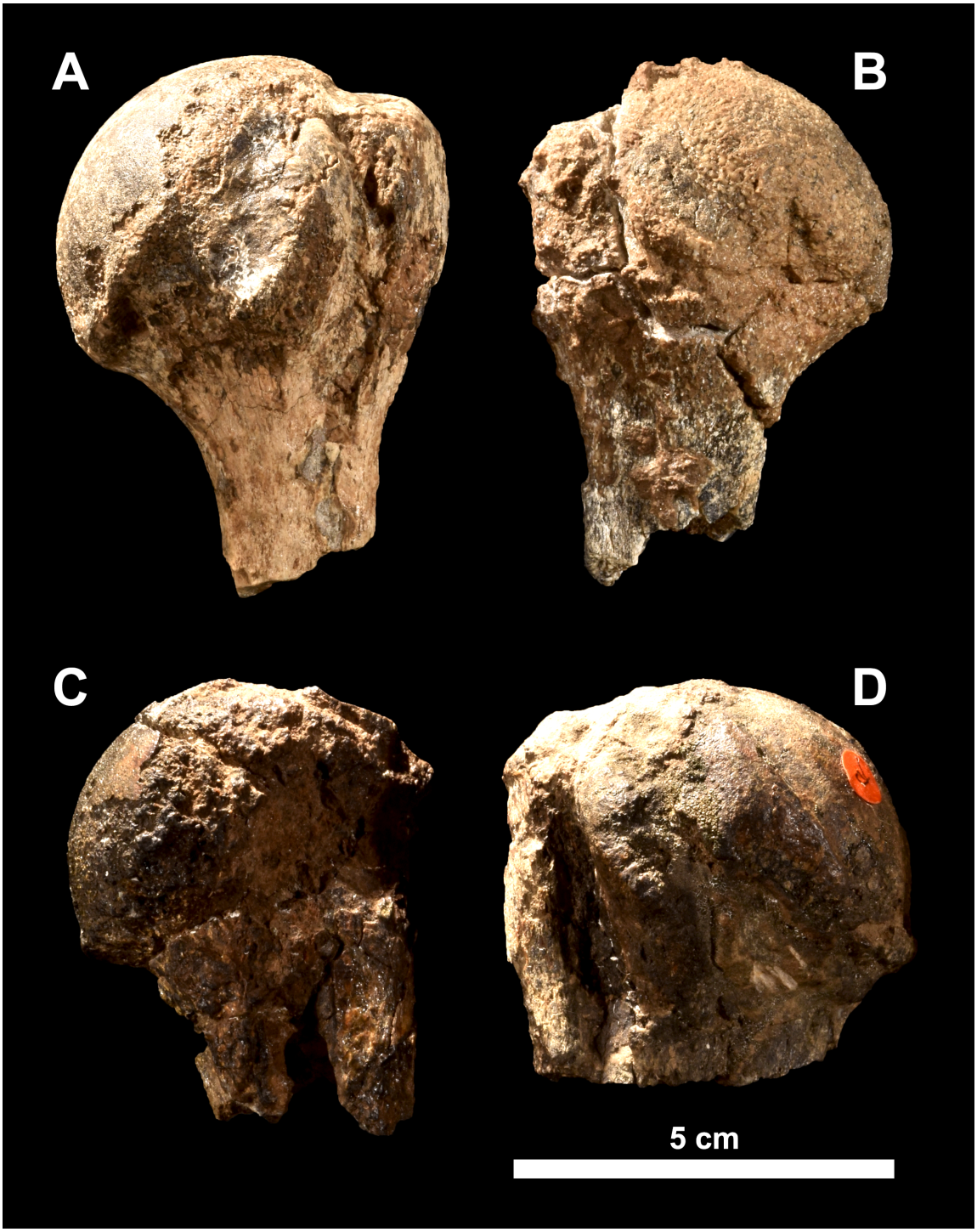


**Figure 6.7** Distal humeri in anterior (top) and posterior (bottom) views. **A:** Right distal humerus of Omo I (KHS 1-30). **B:** Left distal humerus of Omo I (KHS 1-31). **C:** Right distal humerus of HAL-VP-9/1 (suffixed portion -113). **D:** Left distal humerus of HAL-VP-9/1 (suffixed portion -116). **E:** Right distal humerus of TAL-VP-7/36 (suffixed portion -H). **F:** Right distal humerus of HAL-VP-9/1520 (suffixed portion -F). Scale is the same for all panels.

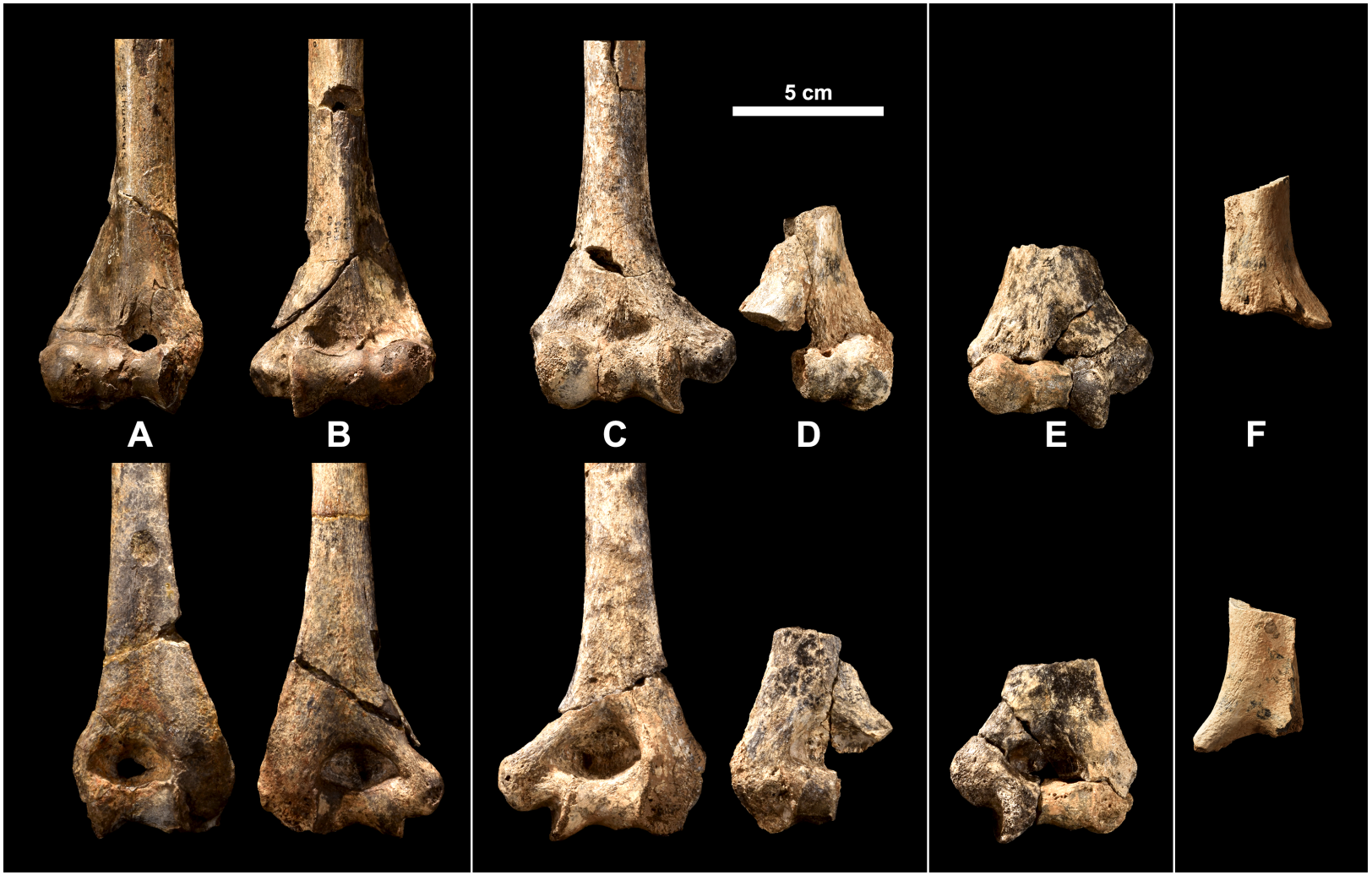


**Figure 6.8** Humeral remains of HAL-VP-9/1. **A**: Right humeral head (HAL-VP-9/1-112) in anterior view, medial is to the right. **B**: Right distal end and shaft (HAL-VP-9/1-113) in anterior view, medial is to the right. **C**: Left proximal end (HAL-VP-9/1-115) in anterior view, medial is to the left. **D**: Left humeral shaft (HAL-VP-9/1-117) in anterior view, medial is to the left. **E**: Left partial distal end (HAL-VP-9/1-116) in anterior view, medial is to the left. **F**: Left humeral shaft (same as pictured in **D** and **G**, HAL-VP-9/1-117) in posterior view, medial is to the right. **G**: Left humeral shaft (same as pictured in **D** and **F**, HAL-VP-9/1-117) in lateral view, anterior is to the left. Scale is the same for both panels.

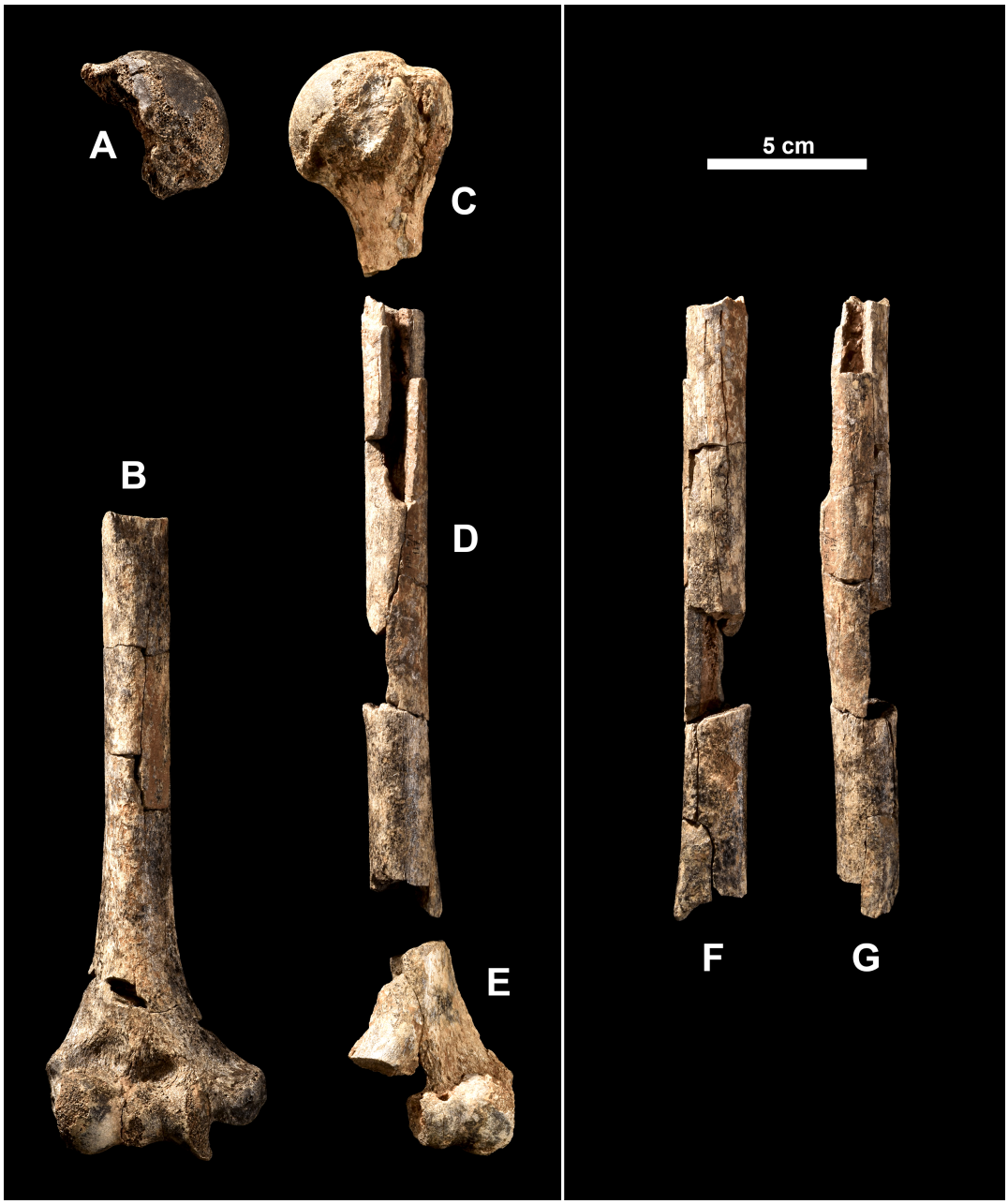


**Figure 6.9** Proximal right ulnae in lateral (top row), medial (middle row), anterior (bottom left panel) and posterior (bottom right panel) views. Pictured in the top two rows, from left to right: Omo I (KHS 1-39), HAL-VP-9/1-121, HAL-VP-3/1, HAL-VP-9/930-B, and HAL-VP-9/1520-E. Each of the bottom two panels picture Omo I (KHS 1-39) on the left and HAL-VP-9/1-121 on the right. Scale is the same for all panels.



**Figure 6.10** Distal ulnae in distal (top row), lateral (middle row), and medial (bottom row) views. In distal view (top row), anterior is up. Left column: left distal ulna of HAL-VP-9/1 (suffixed portion -124). Center column: right distal ulnar epiphysis of HAL-VP-9/930 (suffixed portion -C). Right column: right distal ulna of Omo I (KHS 1-9).



**Figure 6.11** Proximal radii in proximal (top) and approximately anterior (bottom) views. Left column: right proximal radius of HAL-VP-9/1 (suffixed portion -119). Center column: proximal radius of HAL-VP-2/16. Right column: right proximal radius of Omo I (KHS 1-19).



**Figure 6.12** Right distal radius of TAL-VP-7/36 (suffixed portion -I). Views pictured in the top row, from left to right, are: anterior, medial, lateral, and posterior. Proximal view is pictured at the bottom, dorsal is up.



**Figure 6.13** Right trapezium of HAL-VP-9/1 (suffixed portion -129). Left: view from the base of the second metacarpal, palmar is up. Middle: view from the lateral scaphoid end, palmar is up. Right: approximately medial view (from the scaphoid-trapezoid boundary), distal is to the right.



**Figure 6.14** Hamate of HAL-VP-9/1 (left) and Omo I (right). The HAL-VP-9/1 hamate (suffixed portion -128) is from the right side. The Omo I hamate (KHS 1-41) is also from the right side, and only preserves the hamulus. Top: approximately lateral view, palmar is up. Middle: approximately medial view, palmar is up. Bottom: approximately palmar view, distal is to the right.



**Figure 6.15** Lunate of HAL-VP-9/1 (left) and Omo I (right). The HAL-VP-9/1 lunate (suffixed portion -131) is from the left side. The Omo I lunate (KHS 1-22) is from the right side. Top: view from the triquetral, palmar is up. Middle: view from the scaphoid, palmar is up. Bottom: view from the capitate, dorsal is up.



**Figure 6.16** Left and right triquetra of HAL-VP-9/1. The left triquetral (HAL-VP-9/1-133) is on the left and the right triquetral (HAL-VP-9/1-130) is on the right. Top: palmar view, lateral is up. Bottom: view from the hamate, palmar is up.



**Figure 6.17** Left capitate of HAL-VP-9/1 (suffixed portion -132). Top left: distal view, palmar is up. Top right: proximal view, palmar is up. Middle left: medial view, proximal is up. Middle right: lateral view, proximal is up. Bottom left: palmar view, proximal is up. Bottom right: dorsal view, proximal is up.



**Figure 6.18** First metacarpal head of HAL-VP-9/1 (left) and Omo I (right). The HAL-VP-9/1 first metacarpal head (suffixed portion -138) is from the left side. The Omo I first metacarpal head (KHS 1-16) is from the right side. Top: distal view, dorsal is up. Middle: dorsal view, distal is up. Bottom: palmar view, distal is up.

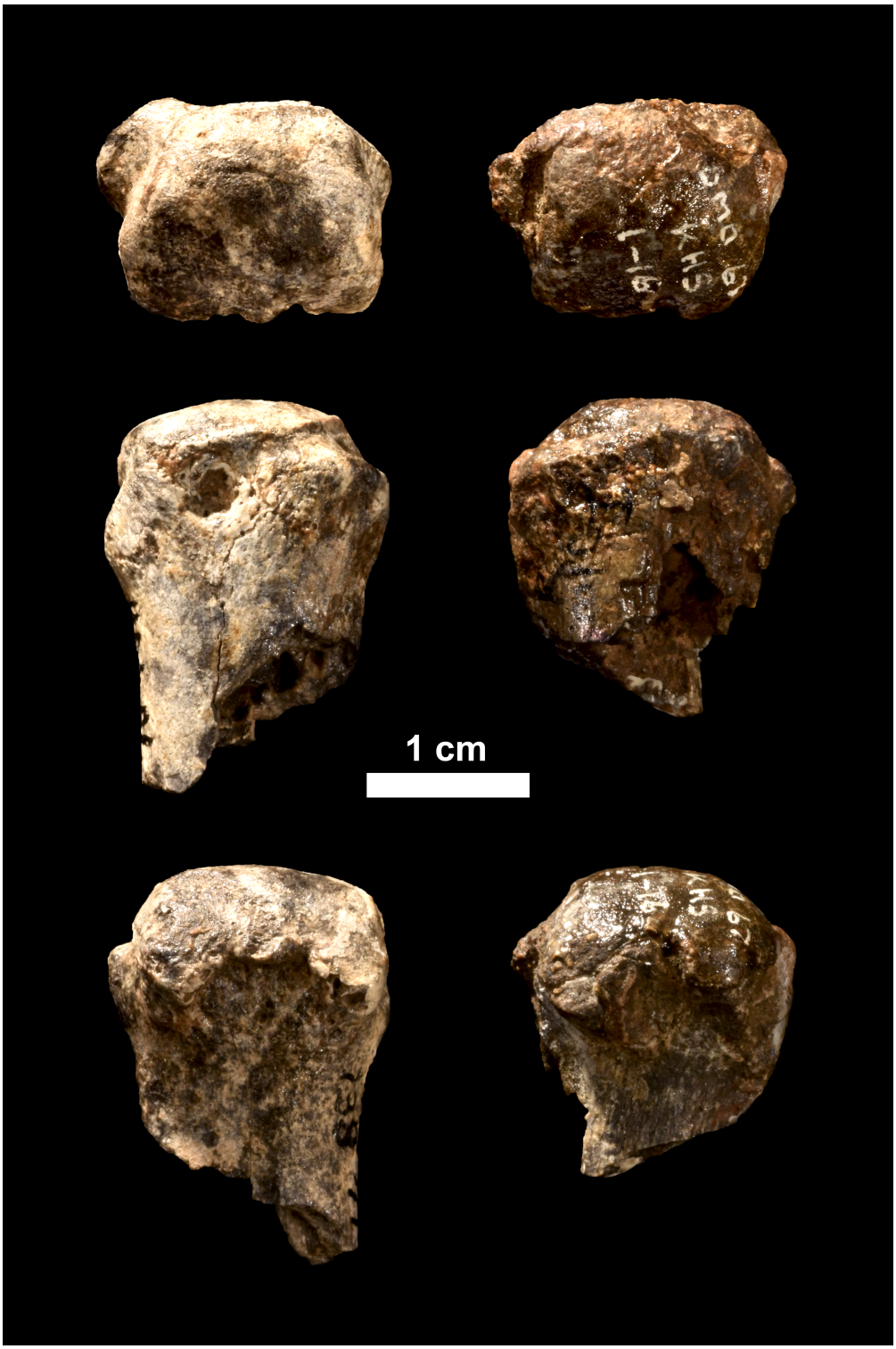


**Figure 6.19** Second metacarpal base of HAL-VP-9/1 (left) and Omo I (right). The HAL-VP-9/1 second metacarpal base (suffixed portion -134) is from the right side. The Omo I second metacarpal base (KHS 1-44) is also from the right side. Top: dorsal view, distal is up. Middle: palmar view, distal is up. Bottom: proximal view, dorsal is up.

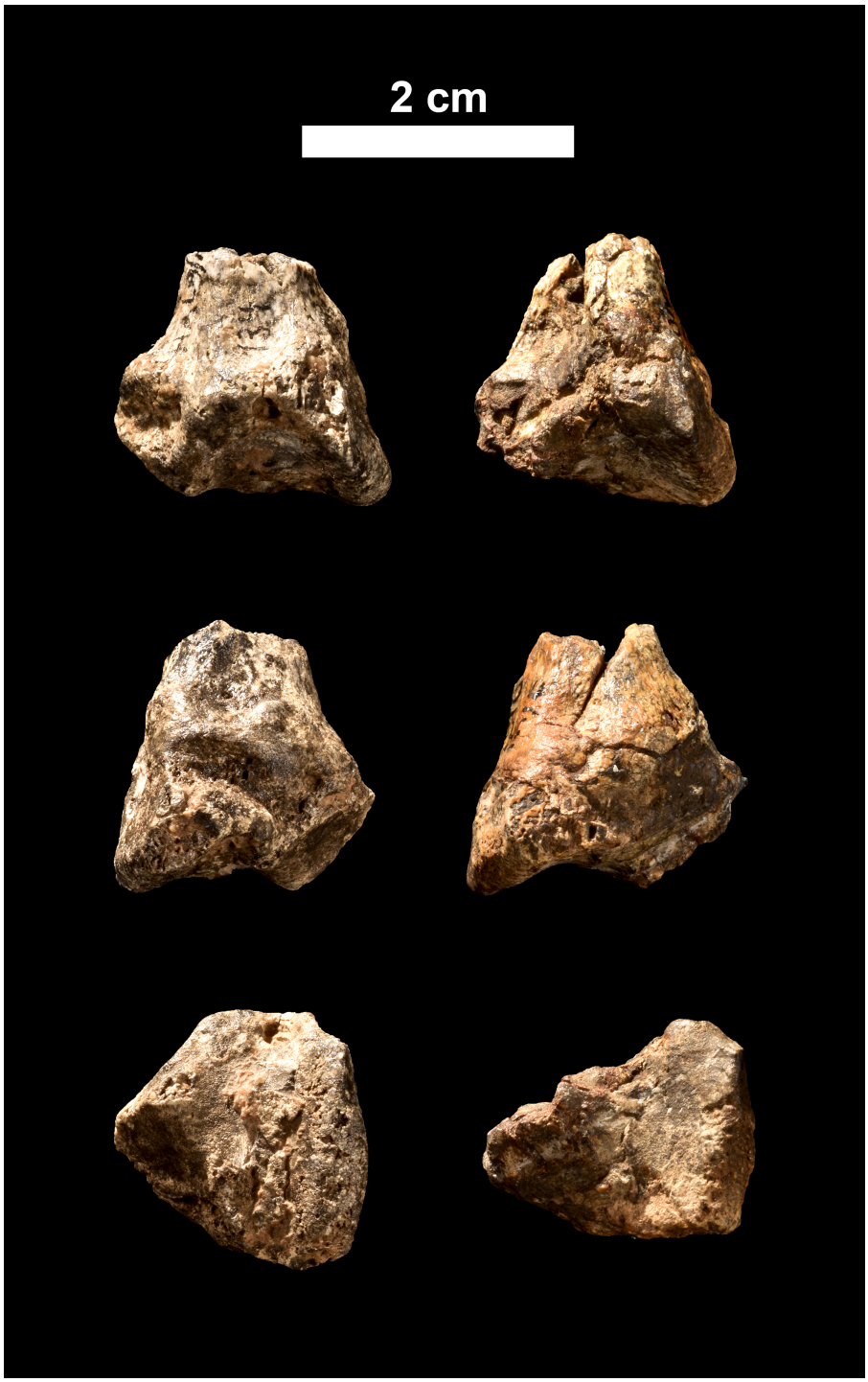


**Figure 6.20** Third metacarpal of HAL-VP-9/1 and Omo I. For each paired set, HAL-VP-9/1 is on the left and Omo I is on the right. The HAL-VP-9/1 third metacarpal (suffixed portion -136) is from the right side. The Omo I third metacarpal head (KHS 1-18) and base (KHS 1-28) are also from the right side. Top panel: *left pair,* distal view, dorsal is up; *right pair*, proximal view, dorsal is up. Middle panel: *left pair*, dorsal view, distal is up; *right pair*, palmar view, distal is up. Bottom panel: *left pair*, medial view, distal is up; *right pair*, lateral view, distal is up. Scale is the same for the bottom two panels.



**Figure 6.21** Fourth metacarpal remains of HAL-VP-9/1. Top row: left fourth metacarpal head with shaft (HAL-VP-9/1-141). Bottom row: right fourth metacarpal base with shaft (HAL-VP-9/1-137). Views, from left to right: dorsal, palmar, lateral, medial, distal (top) and proximal (bottom). Dorsal is up in distal and proximal views.



**Figure 6.22** Fifth metacarpal remains of HAL-VP-9/1. Top row: right fifth metacarpal head (HAL-VP-9/1-143) in dorsal (left) and palmar (right) views. Bottom row: left fifth metacarpal base with shaft (HAL-VP-9/1-142). Views, from left to right: dorsal, palmar, lateral, medial, and proximal. Dorsal is up in proximal view.



**Figure 6.23** Terminal hand phalanges of HAL-VP-9/1, HAL-VP-3/15, and Omo I in dorsal (top) and palmar (bottom) views. From left to right: right ray I (HAL-VP-9/1-158); ray II, III, or IV, side indet. (HAL-VP-9/1-157); probably ray I, side indet. (HAL-VP-3/15-11); ray and side indet. (KHS 1-36); probably ray V, side indet. (KHS 1-57).



**Figure 6.24** Sacral remains of HAL-VP-9/1. The left (HAL-VP-9/1-58) and right (HAL-VP-9/1-57) sacral portions are pictured in the left and right columns, respectively. Views, from top to bottom: posterior, approximately lateral, and superior. In superior view, posterior is up.

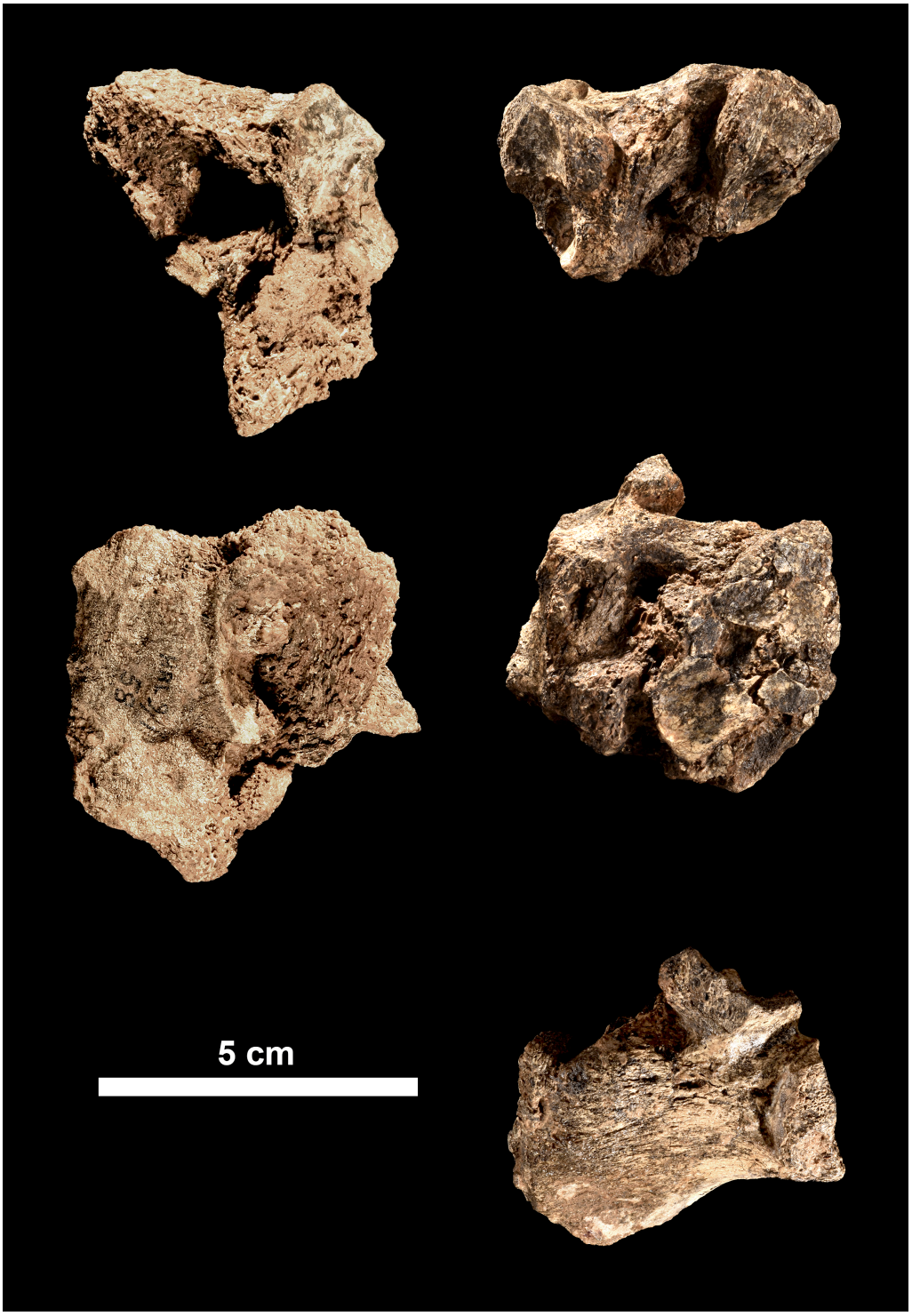


**Figure 6.25** Os coxae of HAL-VP-9/1 (top) and Omo I (bottom). The HAL-VP-9/1 os coxae (suffixed portion -106A+B) is from the right side. The Omo I os coxae (KHS 1-60A) is from the left side, but has been mirrored for ease of comparison between the two individuals. Anterior, lateral, and medial views are pictured from left to right.



**Figure 6.26** Left proximal femoral shaft of BOU-VP-16/100 (top) and HAL-VP-9/1520 (bottom, suffixed portion -I). Views in the left panel, from left to right: anterior, medial, lateral, and posterior. Shaft cross-sectional shape is presented in the right panel in inferior view, anterior is up. It should be noted that the external shape of the BOU-VP-16/100 shaft has been modified by erosion to portions the shaft surface, particularly on the anterior and anteromedial aspects.



**Figure 6.27** Distal femur of HAL-VP-9/1 and Omo I. For each paired set, HAL-VP-9/1 is on the left and Omo I is on the right. The HAL-VP-9/1 distal femur (suffixed portion -161+167) is from the right side. The Omo I distal femur (KHS 1-29A+B) is also from the right side. Top row: *left pair,* anterior view; *right pair*, posterior view. Bottom row: *left pair*, lateral view, anterior is to the right; *right pair*, distal view, anterior is up. Scale is the same for all panels.



**Figure 6.28** Left tibia of HAL-VP-9/1 (suffixed portion -177+178) and Kib 158-1a. For each paired set, HAL-VP-9/1 is on the left and Kib 158-1a is on the right. Views in the top panel, from left to right: anterior, medial, lateral, and posterior. Bottom panel: distal view, anterior is up.



**Figure 6.29** Talus of HAL-VP-9/1 and Omo I. For each paired set, HAL-VP-9/1 is on the left and Omo I is on the right. The HAL-VP-9/1 talus (suffixed portion -188) is from the right side. The Omo I talus (KHS 1-59) is also from the right side. Left panel: *top pair*, distal view, dorsal is up; *middle pair*, dorsal view, distal is up; *bottom pair*, medial view, dorsal is up. Right panel: *top pair*, proximal view, dorsal is up; *middle pair*, plantar view, distal is up; *bottom pair*, lateral view, dorsal is up. Scale is the same for all panels.

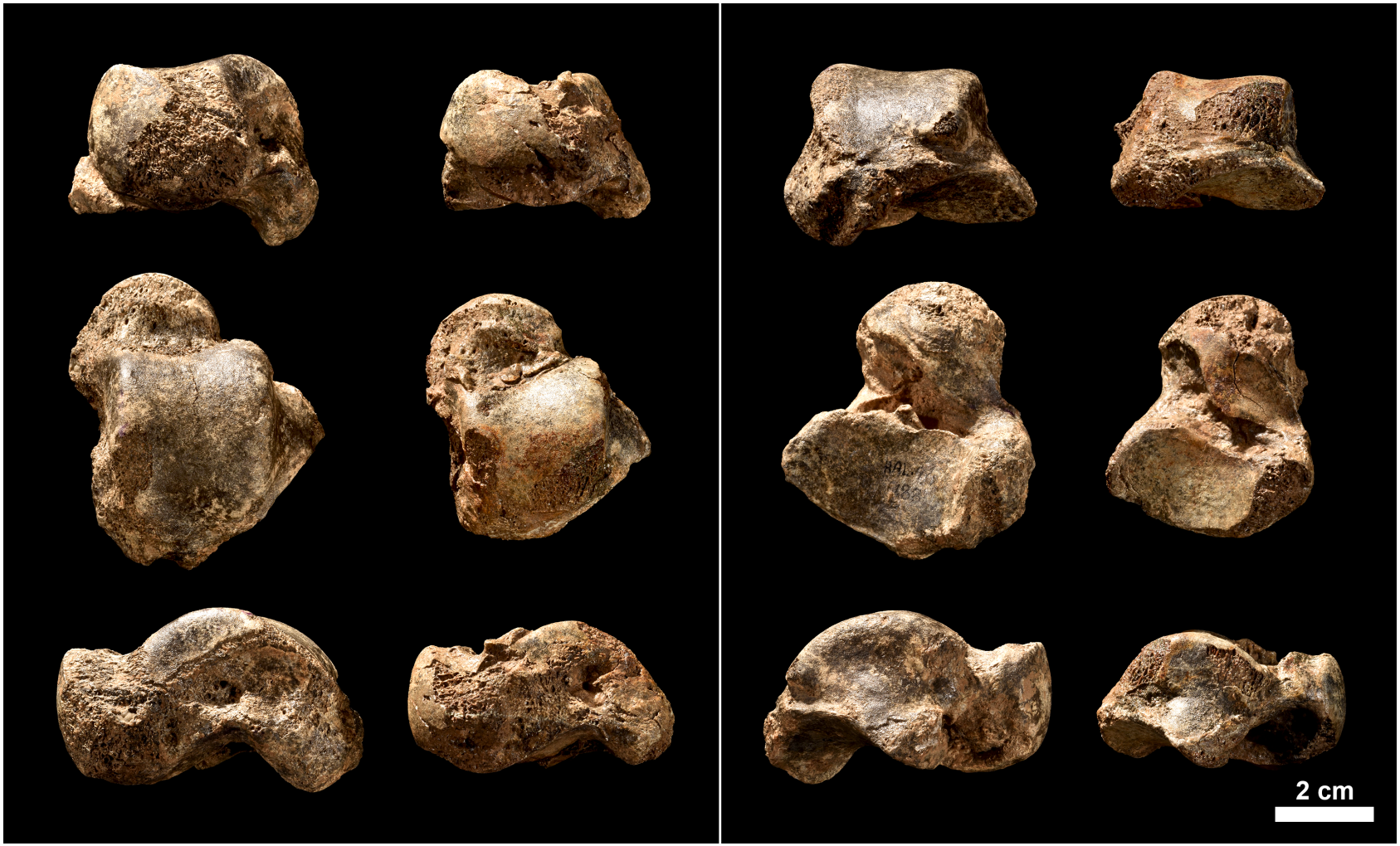


**Figure 6.30** Navicular of HAL-VP-9/1 (left) and Omo I (right). The HAL-VP-9/1 navicular (suffixed portion -192) is from the left side. The Omo I navicular (KHS 1-45) is from the right side. Top: proximal view, dorsal is up. Middle: distal view, dorsal is up. Bottom: superomedial view, distal is up.



**Figure 6.31** First metatarsal of HAL-VP-9/1 and Omo I. For each paired set, HAL-VP-9/1 is on the left and Omo I is on the right. The HAL-VP-9/1 first metatarsal head (suffixed portion -197) and base (suffixed portion -196) are from the left side. The Omo I first metatarsal (KHS 1-21) is from the right side. Top row: *left pair,* distal view, dorsal is up; *right pair*, proximal view, dorsal is up. Middle row: *left pair*, dorsal view, distal is up; *right pair*, plantar view, distal is up. Bottom row: *left pair*, medial view, distal is up; *right pair*, lateral view, distal is up. Scale is the same for all panels.



**Figure 6.32** Third metatarsal base of HAL-VP-9/1 (left) and Omo I (right). The HAL-VP-9/1 third metatarsal base (suffixed portion -194) is from the right side. The Omo I third metatarsal base (KHS 1-52) is also from the right side. Top row: proximal view, dorsal is up. Second row from top: dorsal view, distal is up. Third row from top: medial view, dorsal is right. Bottom row: lateral view, dorsal is left.

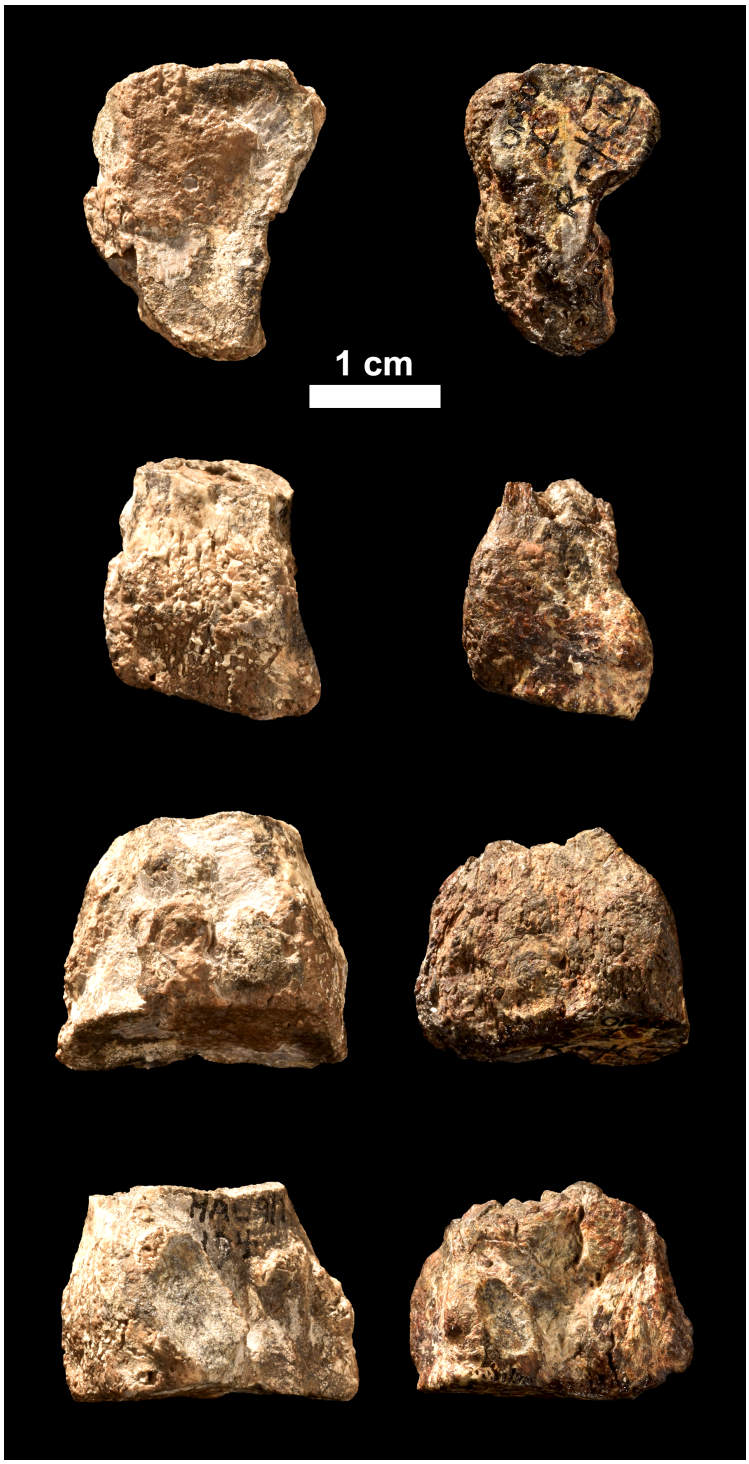


**Figure 6.33** Fourth metatarsal of HAL-VP-9/1 and Omo I. For each paired set, HAL-VP-9/1 is on the left and Omo I is on the right. The HAL-VP-9/1 fourth metatarsal (suffixed portion -195) is from the right side. The Omo I fourth metatarsal (KHS 1-14) is also from the right side. Top row: *left pair,* dorsal view, distal is up; *right pair*, proximal view, dorsal is up. Bottom row: *left pair*, medial view, dorsal is right; *right pair*, lateral view, dorsal is left. Scale is the same for all panels.



**Figure 6.34** Fifth metatarsal remains of HAL-VP-9/1. The left fifth metatarsal head (HAL-VP-9/1-200) is pictured at the top, and the left fifth metatarsal base is pictured at the bottom (HAL-VP-9/1-199). Views, from left to right: dorsal, plantar, lateral, medial, distal (top), and proximal (bottom). In proximal and distal views, dorsal is up.



**Figure 6.35** Proximal and intermediate foot phalanges of HAL-VP-9/1. The proximal foot phalanx (HAL-VP-9/1-203) is pictured at the bottom, and the intermediate foot phalanx (HAL-VP-9/1-204) is pictured at the top. Ray and side are indeterminate, but their size suggests that they are likely from ray II or III. Views, from left to right: dorsal, plantar, right, and left.



# Chapter 7: Conclusions

## 7.1 Introduction

This dissertation described the skeletal anatomy of recently recovered hominid postcranial fossils (n=9 individuals) from Middle Stone Age deposits in the Halibee region of the Middle Awash study area of Ethiopia. The described sample includes a partial skeleton (HAL-VP-9/1) that preserves portions of nearly all postcranial elements, and for this reason was the central focus of the comparative description. Several other more fragmentary hominid postcranial fossils from the same sedimentary package are also described, including a second partial skeleton (HAL-VP-9/1520), two individuals with associated postcranial elements (HAL-VP-9/930 and TAL-VP-7/36), and five individuals that preserve only a single postcranial element (HAL-VP-2/16, HAL-VP-3/1, HAL-VP-3/15, HAL-VP-14/44, and BOU-VP-16/100).

The geographic and chronological position of these fossils make them particularly valuable to studies of early modern human anatomical variation and evolution because they fill in a critical gap in the fossil record of the modern human lineage in Africa, after its divergence from the Neanderthal lineage (see Chapter 1). They thereby provide a small but significant window into the anatomy of early modern humans in eastern Africa and permit comparison to modern human variation observed today, as well as to the variation observed in the Pleistocene hominid fossil record. Prior to describing the anatomy preserved by the fossils, Chapter 2 provided brief introductions to their geographic provenience, chronostratigraphic placement, Middle Stone Age archaeological context, history of collection, taxonomic identification, and key taphonomic features. Chapter 3 detailed the materials and study methods for the comparative description of the fossils. Chapter 4 then presented basic details about the HAL-VP-9/1 partial skeleton, including an estimation of sex, biological age, stature, and mass. Having established these basics, Chapters 5 and 6 then described the Halibee fossils in the context of modern human variation and the Pleistocene fossil record, respectively. Together, the results reported in these latter two chapters address the research objectives laid out in Chapter 3:

> (1) To qualitatively and quantitatively characterize the skeletal anatomy of early modern *Homo sapiens* skeletal remains.
> (2) To explore how these fossil morphologies compare to the range of variation observed in recent anatomically modern human comparative samples.
> (3) To make systematic anatomical comparisons among the Halibee early *Homo sapiens* remains, and fossils of Pleistocene *Homo* (particularly Neanderthals and other "archaic" sets of fossils). This is an essential step in understanding the morphological evolution of our lineage and closest fossil relatives.

## 7.2 Key findings

According to recent modern human standards, the available anatomy on the HAL-VP-9/1 partial skeleton indicates that this individual was most likely male and between 25-40 years of age at the time of death. The best available stature estimate (based on the estimated tibial length) is 179.25 ± 3 cm, indicating that this individual was tall-statured by recent modern human standards. The estimated mass for this individual is 80.3 ± 4.3 kg.

The HAL-VP-9/1 individual is tall relative to most recent modern human averages and is at the upper end of an eastern African sample range. Among fossils for which stature estimates are available, this individual is most similar to other early modern humans (i.e., Omo I, Skhul, and Qafzeh) and the limited Middle Pleistocene evidence from Africa (i.e., Kabwe). The mass of this individual is similarly very large relative to recent modern human averages, falling at the upper end of or above most modern human samples. Relative to other fossils, the estimated mass of this individual is most similar to Kabwe and is at the upper end of the Sima de los Huesos and Neanderthal ranges. The intra-limb skeletal proportions of HAL-VP-9/1 appear to follow ecogeographic predictions, if the strikingly long tibia is taken to indicate long distal relative to proximal limb segments.

The results of the comparative assessment relative to the five recent modern human groups indicate that the morphologies exhibited by the Halibee fossils fall within the range of recent modern human variation in nearly all respects, albeit often near the margins of the range. In some features the fossils (particularly HAL-VP-9/1) do exceed the sampled recent modern human variation, including in terms of absolute size of some elements, the sizes of articular surfaces, and the unusual proportions between the long bone ends and shaft cross-sectional sizes.

Relative to other Pleistocene fossils assessed in this study, the Halibee fossils present some interesting although not entirely unexpected anatomies. Following a similar pattern as the comparisons to recent modern humans, the Halibee fossils (and particularly HAL-VP-9/1) are similar to other early modern humans in most respects (i.e., Omo I, Skhul, and Qafzeh). However, there are several anatomical features that deviate from those reported for recent modern humans, and are closer to the conditions described for Neanderthals (Table 7.1).

These results, taken together, make two clear contributions to the study of early modern human variation and evolution. First, they contribute to an emerging image of a morphologically heterogeneous segment of the modern human lineage in the Middle and Late Pleistocene of Africa. This heterogeneity has made establishing definitional criteria for modern human anatomy difficult and makes it clear that these criteria must consider anatomical features in terms of frequencies rather than as discrete states across taxa. It is clear that modern human anatomy does not suddenly appear in a leap from a pre-modern configuration, but instead appears asynchronously and through a patchwork of modern and ancestral anatomical features. Second, and related to the first point, the Halibee fossils echo previous calls to reconsider the polarity and dichotomy of traits historically treated as diagnostically modern human or Neanderthal. The Halibee fossils reinforce the need for better sampling of the Late and Middle Pleistocene African fossil record to better characterize the morphology ancestral to the modern human and Neanderthal lineages. This ancestral morphology increasingly appears to encompass Neanderthal and modern human-like traits, the frequencies of which vary across time and space throughout the last half a million years.

This dissertation has completed the primary description of the Halibee fossils and in so doing it has generated many anatomical observations. These observations can now be leveraged to generate hypotheses that can be tested with a wide variety of approaches. I now turn to a brief discussion of future avenues of research that are raised by this study.

### 7.3 Future directions

The large amount of anatomy preserved by the HAL-VP-9/1 partial skeleton provides valuable data for further studies, and the assessment of this individual's anatomy relative to

recent modern humans and Pleistocene *Homo* suggests several interesting avenues of productive research. While studies during the last two decades have characterized patterns of integration and modularity in the hominid cranium, relatively fewer studies have focused on postcranial anatomy. Those that have were most often restricted to anatomical regions or functional complexes within the skeleton. Some of these recent studies have focused on the pelvis (Fischer & Mitteroecker, 2015; Grabowski, Polk, & Roseman, 2011), the long bones (Arias-Martorell, Potau, Bello-Hellegouarch, & Pérez-Pérez, 2014; Holliday & Ruff, 2001; Lozanoff, Sciulli, & Schneider, 1985), and the hands and feet (Morrish & Hlusko, 2014; Reno et al., 2008; Rolian, Lieberman, & Hallgrímsson, 2010). These studies have advanced our understanding of patterns of correlation within regions of the skeleton, and are critical for interpreting variation among modern humans, and even more so in the fossil record where the evidence is much more scarce (Ackermann, 2002, 2009; Hlusko, 2004). A broader-scale analysis of patterns of correlation in the human postcranial skeleton promises to further contribute to future analyses of skeletal variation and evolution through an improved understanding of how aspects of skeletal anatomy are interrelated (Savell, Auerbach, & Roseman, 2016). Specific questions of interest include, for example, (1) What are the broad patterns of correlation that characterize the skeleton across modern humans? (2) Are patterns of correlation in the skeleton consistent across modern human groups? (3) How do aspects of human skeletal anatomy correlate with overall body size? Beyond gaining a better understanding of the patterns of correlation that characterize the modern human skeleton, addressing these questions will allow us to interpret variation in the fossil record with a better sense of how variation is patterned in extant humans, and which aspects of skeletal anatomy tend to be more variable within and among groups.

Differences in the pattern of correlation across modern human groups may be informative about evolutionary history (i.e., carry signals of natural selection or neutral evolution, Betti, Cramon-Taubadel, & Lycett, 2012; Hubbe, Hanihara, & Harvati, 2009) and/or environmental contributions to morphology (i.e., osteogenic responses to activity-related mechanical stress, Ruff, 1987; Stock & Pfeiffer, 2001; von Cramon-Taubadel, 2011). Many studies over the last few decades have examined the relationship between cross-sectional geometric properties of long bone shafts and habitual behavior across different human groups (Bridges, 1989; Ruff & Larsen, 2014; Sparacello & Marchi, 2008; Stock & Pfeiffer, 2001). Although these studies generally propose that signatures of behavior can be detected from diaphyseal cross-sectional anatomy, the pattern of these signatures and the best anatomical positions at which to detect them remains unclear (Davies & Stock, 2014; Stock, 2006). Additionally, aspects of body size and shape have been found to significantly affect cross-sectional anatomy, thereby complicating the extrapolation of behavior from anatomy, and requiring that researchers control for these relationships when trying to infer behavior from cross-sectional properties (Ruff, 2000; Ruff & Larsen, 2014). However, studies focusing on the relationship between cross-sectional geometry and aspects of body size and shape (often stature and body breadth), have found that these relationships are not consistent across elements and element segments (Pearson et al., 2014; Shaw & Stock, 2011).

Beyond calling into question the practice of drawing direct inferences about behavior from cross-sectional anatomy, these findings also raise the question: how do these cross-sectional properties relate to other aspects of skeletal anatomy? At least some of the inconsistency observed in cross-sectional anatomy across different limb segments may be due to other factors, such as shared developmental underpinnings. Indeed, correlation patterns observed in a previous study suggest that cross-sectional properties may be integrated with epiphyseal

dimensions (Davies & Stock, 2014). Previous work considering the effects of body size and shape on cross-sectional geometry also found similar scaling of upper and lower limbs in the relationship of bending strength to body mass, which was noted as surprising since upper limbs are not weight-bearing (Ruff, 2000). It should be considered, however, that this pattern need not be related to habitual activity but may be due to integration resulting from other factors.

It is increasingly clear that hominid skeletal anatomical traits are not independent, discrete features, but are actually interrelated because of shared genetic, developmental, and/or functional factors (Ackermann, 2009; González-José, Van der Molen, González-Pérez, & Hernández, 2004; Klingenberg, 2013; Weiss, 2017; Young, Wagner, & Hallgrímsson, 2010). Recent work in developmental biology has repeatedly underscored the incredibly complicated and carefully integrated processes that underlie adult limb bone morphology at the molecular, cellular, histological, and gross morphological levels of organization (Lui et al., 2018; Rolian, 2020; Tickle, 2015). Various signaling pathways are involved in a series of hierarchical processes that overlap spatially and temporally over the course of limb development, including, for example, Sonic Hedgehog (Tickle & Towers, 2017), Fibroblast Growth Factor (Ornitz & Marie, 2019), and Wnt (Tickle, 2015). The Wnt pathway appears to also be involved in skeletal homeostasis, and recent work suggests that it may also play a role in regulating cortical bone thickness (Gori, Lerner, Ohlsson, & Baron, 2015).

One of the most notable features of the HAL-VP-9/1 skeleton, as detailed in Chapters 5 and 6, is the proportional relationship between the long bone ends and shaft cross-sectional sizes, in which the ends are remarkably large relative to the slender shaft. Whereas many studies have focused on the developmental processes underlying the relative lengths of limb segments (see Lui et al., 2018; Rolian, 2016, 2020), comparatively fewer have focused explicitly on the relationship between epiphyseal and diaphyseal dimensions. The moderate cortical thickness of the HAL-VP-9/1 long bones also stands in contrast to the thick cortices observed in earlier *Homo*, and raises questions about the significance of this change from the morphology preceding modern humans, and whether this cortical thickness change may be correlated with other aspects of the bony anatomy. Both of these observations merit additional study aimed at understanding their etiology and significance, and such understanding also promises to reveal more about the peculiar biology of the Neanderthal skeleton.

A careful review of the developmental, genetic, and biomedical literature promises to yield hypotheses that can be tested with large modern human skeletal collections and the Halibee fossils, particularly the HAL-VP-9/1 partial skeleton, and the subadult skeletons available for both extant humans and Neanderthals. The insights gleaned from these complementary fields will also permit a better assessment of how much of the skeletal variation observed is due to intrinsic determinants (i.e., genetic and developmental factors), versus extrinsic factors (i.e., environmental contributions). Recent studies have demonstrated a way forward for generating hypotheses from evolutionary developmental insights and testing them with anatomical data, and while these kinds of studies are clearly not straightforward, their value to studies of anatomical variation and evolution is clear (Reno, 2016; Young & Capellini, 2016). Future studies informed by insights from developmental and genetic studies will be invaluable for interpreting the fossilized skeletal anatomy of early humans and of the expanding fossil samples from the Middle Pleistocene gap in Africa, which are in turn crucial for understanding the evolution of modern humans.

**Table 7.1** Neanderthal-like features and proportions exhibited by the HAL-VP-9/1 partial skeleton

| Anatomical feature | Modern humans | Neanderthals | HAL-VP-9/1 |
|---|---|---|---|
| Axillary sulcus position | Ventral | Dorsal | Dorsal |
| Olecranon fossa relative size | Narrow | Broad | Broad |
| Olecranon fossa relative depth | Shallow | Deep | Deep |
| Medial pillar relative thickness | Thick | Thin | Thin |
| Radial neck relative thickness | Thick | Thin | Thin |
| Femoral neck-shaft angle | Higher | Lower | Lower |
| Lateral malleolar facet | Narrow | Broad | Broad |
| Trochlear shape | Narrow and wedged | Broad and rectangular | Broad and rectangular |
| Fifth metatarsal base | Narrow | Broad | Broad |

**References**


Ackermann, R. R. (2002). Patterns of covariation in the hominoid craniofacial skeleton: implications for paleoanthropological models. *Journal of Human Evolution, 43*(2), 167-187.

Ackermann, R. R. (2009). Morphological integration and the interpretation of fossil hominin diversity. *Evolutionary Biology, 36*, 149-156.

Acsádi, G., & Nemeskéri, J. (1970). *History of human life span and mortality*. Budapest: Akadémiai Kiadó.

Adam, R., Mitchell, J., & van der Westhuizen, M. (2008). Aspects of foraging in the harvester termite, *Trinervitermes trinervoides* (Sjöstedt) (Termitidae: Nasutitermitinae). *African Entomology, 16*(2), 153-161.

Aiello, L., & Dean, C. (1990). *An Introduction to Human Evolutionary Anatomy*. London: Academic Press.

Aiello, L. C. (1993). The fossil evidence for modern human origins in Africa: a revised view. *American Anthropologist, 95*(1), 73-96.

Anderson, J. E. (1968). Late Paleolithic skeletal remains from Nubia. In F. Wendorf (Ed.), *The prehistory of Nubia* (2 ed., pp. 996-1040).

Anderson, J. Y., & Trinkaus, E. (1998). Patterns of sexual, bilateral and interpopulational variation in human femoral neck-shaft angles. *The Journal of Anatomy, 192*(2), 279-285.

Antón, S. C. (2002). Evolutionary significance of cranial variation in Asian *Homo erectus*. *American Journal of Physical Anthropology, 118*(4), 301-323.

Antón, S. C. (2003). Natural history of *Homo erectus*. *American Journal of Physical Anthropology, 122*(S37), 126-170.

Arias-Martorell, J., Potau, J. M., Bello-Hellegouarch, G., & Pérez-Pérez, A. (2014). Brief communication: developmental versus functional three-dimensional geometric morphometric-based modularity of the human proximal humerus. *American Journal of Physical Anthropology, 154*(3), 459-465.

Armitage, S. J., Jasim, S. A., Marks, A. E., Parker, A. G., Usik, V. I., & Uerpmann, H.-P. (2011). The southern route "out of Africa": evidence for an early expansion of modern humans into Arabia. *Science, 331*(6016), 453-456.

Árnason, Ú. (2016). The Out of Africa hypothesis and the ancestry of recent humans: cherchez la femme (et l'homme). *Gene, 585*(1), 9-12.

Árnason, Ú. (2017). A phylogenetic view of the Out of Asia/Eurasia and Out of Africa hypotheses in the light of recent molecular and palaeontological finds. *Gene, 627*, 473-476.

Arsuaga, J. L., & Carretero, J. M. (1994). Multivariate analysis of the sexual dimorphism of the hip bone in a modern human population and in early hominids. *American Journal of Physical Anthropology, 93*(2), 241-257.

Arsuaga, J. L., Carretero, J.-M., Lorenzo, C., Gómez-Olivencia, A., Pablos, A., Rodríguez, L., . . . Carbonell, E. (2015). Postcranial morphology of the middle Pleistocene humans from Sima de los Huesos, Spain. *Proceedings of the National Academy of Sciences USA, 112*(37), 11524-11529.

Arsuaga, J. L., Carretero, J. M., Martínez, I., & Gracia, A. (1991). Cranial remains and long bones from Atapuerca/Ibeas (Spain). *Journal of Human Evolution, 20*(3), 191-230.

Arsuaga, J. L., Lorenzo, C., Carretero, J.-M., Gracia, A., Martínez, I., García, N., . . . Carbonell, E. (1999a). A complete human pelvis from the Middle Pleistocene of Spain. *Nature, 399*(6733), 255-258.

Arsuaga, J. L., Martínez, I., Lorenzo, C., Gracia, A., Muñoz, A., Alonso, O., & Gallego, J. (1999b). The human cranial remains from Gran Dolina lower Pleistocene site (Sierra de Atapuerca, Spain). *Journal of Human Evolution, 37*(3-4), 431-457.

Asfaw, B. (1983). A new hominid parietal from Bodo, Middle Awash Valley, Ethiopia. *American Journal of Physical Anthropology, 61*(3), 367-371.

Asfaw, B., Gilbert, W. H., Beyene, Y., Hart, W. K., Renne, P. R., WoldeGabriel, G., . . . White, T. D. (2002). Remains of *Homo erectus* from Bouri, Middle Awash, Ethiopia. *Nature, 416*, 317-320.

Aubert, M., Pike, A. W., Stringer, C., Bartsiokas, A., Kinsley, L., Eggins, S., . . . Grün, R. (2012). Confirmation of a late middle Pleistocene age for the Omo Kibish 1 cranium by direct uranium-series dating. *Journal of Human Evolution, 63*(5), 704-710.

Auerbach, B. M. (2012). Skeletal variation among early Holocene North American humans: implications for origins and diversity in the Americas. *American Journal of Physical Anthropology, 149*(4), 525-536.

Auerbach, B. M., & Ruff, C. B. (2004). Human body mass estimation: A comparison of "morphometric" and "mechanical" methods. *American Journal of Physical Anthropology, 125*(4), 331-342.

Auerbach, B. M., & Ruff, C. B. (2010). Stature estimation formulae for indigenous North American populations. *American Journal of Physical Anthropology, 141*(2), 190-207.

Baccino, E., Ubelaker, D. H., Hayek, L.-A., & Zerilli, A. (1999). Evaluation of seven methods of estimating age at death from mature human skeletal remains. *Journal of Forensic Sciences, 44*(5), 931-936.

Backwell, L. R., Parkinson, A. H., Roberts, E. M., d'Errico, F., & Huchet, J.-B. (2012). Criteria for identifying bone modification by termites in the fossil record. *Palaeogeography, Palaeoclimatology, Palaeoecology, 337-338*, 72-87.

Badkur, P., & Nath, S. (1990). Use of regression analysis in reconstruction of maximum bone length and living stature from fragmentary measures of the ulna. *Forensic Science International, 45*(1-2), 15-25.

Bailey, S. E., Hublin, J.-J., & Antón, S. C. (2019). Rare dental trait provides morphological evidence of archaic introgression in Asian fossil record. *Proceedings of the National Academy of Sciences, 116*(30), 14806-14807.

Bar-Yosef, O., & Vandermeersch, B. (1991). *Le squelette Moustérien de Kébara 2*. Paris: CNRS.

Bass, W. M. (2005). *Human osteology: a laboratory and field manual* (5th ed.). Springfield, MO: Missouri Archaeological Society.

Battié, M. C., Videman, T., & Parent, E. (2004). Lumbar disc degeneration: epidemiology and genetic influences. *Spine, 29*(23), 2679-2690.

Been, E., Gómez-Olivencia, A., & Kramer, P. A. (2012). Lumbar lordosis of extinct hominins. *American Journal of Physical Anthropology, 147*(1), 64-77.

Been, E., Gómez-Olivencia, A., & Kramer, P. A. (2014). Brief communication: lumbar lordosis in extinct hominins: implications of the pelvic incidence. *American Journal of Physical Anthropology, 154*(2), 307-314.

Been, E., Peleg, S., Marom, A., & Barash, A. (2010). Morphology and function of the lumbar spine of the Kebara 2 Neandertal. *American Journal of Physical Anthropology, 142*(4), 549-557.

Behar, D. M., Villems, R., Soodyall, H., Blue-Smith, J., Pereira, L., Metspalu, E., . . . Consortium, T. G. (2008). The dawn of human matrilineal diversity. *American Journal of Human Genetics, 82*(5), 1130-1140.

Belcastro, M. G., Mariotti, V., Facchini, F., & Bonfiglioli, B. (2006). Musculoskeletal stress and adult age markers in the Krapina hominid collection: the study of femora 213 Fe.1 and 214 Fe.2. *Periodicum Biologorum, 108*(3), 319-329.

Belcastro, M. G., Mariotti, V., Pietrobelli, A., Sorrentino, R., García-Tabernero, A., Estalrrich, A., & Rosas, A. (2020). The study of the lower limb entheses in the Neanderthal sample from El Sidrón (Asturias, Spain): How much musculoskeletal variability did Neanderthals accumulate? *Journal of Human Evolution, 141*, 102746.

Beltrame, M. H., Rubel, M. A., & Tishkoff, S. A. (2016). Inferences of African evolutionary history from genomic data. *Current Opinion in Genetics & Development, 41*, 159-166.

Bennyhoff, J. A., & Hughes, R. E. (1987). Shell Bead and Ornament Exchange Networks Between California and the Western Great Basin. In *Anthropological Papers of the American Museum of Natural History* (Vol. 64). New York.

Bermúdez de Castro, J., Arsuaga, J. L., Carbonell, E., Rosas, A., Martínez, I., & Mosquera, M. (1997). A hominid from the Lower Pleistocene of Atapuerca, Spain: possible ancestor to Neandertals and modern humans. *Science, 276*(5317), 1392-1395.

Bermúdez de Castro, J., Martinón-Torres, M., Carbonell, E., Sarmiento, S., Rosas, A., van der Made, J., & Lozano, M. (2004). The Atapuerca sites and their contribution to the knowledge of human evolution in Europe. *Evolutionary Anthropology, 13*(1), 25-41.

Bermúdez de Castro, J. M., Carretero, J. M., García-González, R., Rodríguez-García, L., Martinón-Torres, M., Rosell, J., . . . Carbonell, E. (2012). Early Pleistocene human humeri from the Gran Dolina-TD6 site (Sierra de Atapuerca, Spain). *American Journal of Physical Anthropology, 147*(4), 604-617.

Bermúdez de Castro, J. M., Martínez de Pinillos, M., López-Polín, L., Martín-Francés, L., García-Campos, C., Modesto-Mata, M., . . . Martinón-Torres, M. (2020). A descriptive and comparative study of two Early Pleistocene immature scapulae from the TD6.2 level of the Gran Dolina cave site (Sierra de Atapuerca, Spain). *Journal of Human Evolution, 139*, 102689.

Bermúdez de Castro, J. M., Martinón-Torres, M., Arsuaga, J. L., & Carbonell, E. (2017). Twentieth anniversary of *Homo antecessor* (1997-2017): a review. *Evolutionary Anthropology, 26*(4), 157-171.

Betti, L., Cramon-Taubadel, N. V., & Lycett, S. J. (2012). Human pelvis and long bones reveal differential preservation of ancient population history and migration out of Africa. *Human Biology, 84*(2), 139-152.

Betti, L., Lycett, S. J., von Cramon-Taubadel, N., & Pearson, O. M. (2015). Are human hands and feet affected by climate? A test of Allen's rule. *American Journal of Physical Anthropology, 158*(1), 132-140.

Bidmos, M., & Asala, S. (2005). Calcaneal measurement in estimation of stature of South African blacks. *American Journal of Physical Anthropology, 126*(3), 335-342.

Bidmos, M. A. (2008a). Estimation of stature using fragmentary femora in indigenous South Africans. *International Journal of Legal Medicine, 122*(4), 293-299.

Bidmos, M. A. (2008b). Stature reconstruction using fragmentary femora in South Africans of European descent. *Journal of Forensic Sciences, 53*(5), 1044-1048.
Blegen, N., Jicha, B. R., & McBrearty, S. (2018). A new tephrochronology for early diverse stone tool technologies and long-distance raw material transport in the Middle to Late Pleistocene Kapthurin Formation, East Africa. *Journal of Human Evolution, 121*, 75-103.
Blitz, E., Viukov, S., Sharir, A., Shwartz, Y., Galloway, J. L., Price, B. A., . . . Zelzer, E. (2009). Bone ridge patterning during musculoskeletal assembly is mediated through SCX regulation of Bmp4 at the tendon-skeleton junction. *Developmental cell, 17*(6), 861-873.
Bonmatí, A., & Arsuaga, J. (2007). The innominate bone sample from Krapina. *Periodicum Biologorum, 109*(4), 335-361.
Bonmatí, A., Gómez-Olivencia, A., Arsuaga, J. L., Carretero, J. M., Gracia, A., Martínez, I., . . . Carbonell, E. (2010). Middle Pleistocene lower back and pelvis from an aged human individual from the Sima de los Huesos site, Spain. *Proceedings of the National Academy of Sciences USA, 107*(43), 18386-18391.
Boulle, E. L. (2001). Evolution of two human skeletal markers of the squatting position: a diachronic study from antiquity to the modern age. *American Journal of Physical Anthropology, 115*(1), 50-56.
Bräuer, G. (1984a). The "Afro-European *sapiens* hypothesis" and hominid evolution in East Asia during the late Middle and Upper Pleistocene. In P. Andrews & G. Frazen (Eds.), *The Early Evolution of Man* (Vol. 69, pp. 145-165): Courier Forschungsinstitut Senckenberg.
Bräuer, G. (1984b). A craniological approach to the origin of anatomically modern *Homo sapiens* in Africa and implications for the appearance of modern Europeans. In F. H. Smith & F. Spencer (Eds.), *The origins of modern humans: A world survey of the fossil evidence* (pp. 327-410). New York: Alan R. Liss.
Bräuer, G. (1988). Osteometrie. In R. Knussman (Ed.), *Anthropologie: Handbuch der vergleichenden biologie des menschen I* (pp. 160-232). Stuttgart: Fischer Verlag.
Bräuer, G. (1992). The origins of modern Asians: by regional evolution or by replacement. In T. Akazawa, K. Aoki, & T. Kimura (Eds.), *The evolution and dispersal of modern humans in Asia* (pp. 401-413). Tokyo: Kokusen-sha.
Bräuer, G. (2008). The origin of modern anatomy: by speciation or intraspecific evolution? *Evolutionary Anthropology, 17*(1), 22-37.
Bräuer, G. (2012). Middle Pleistocene diversity in Africa and the origin of modern humans. In J.-J. Hublin & S. P. McPherron (Eds.), *Modern Origins* (pp. 221-240): Springer.
Bridges, P. S. (1989). Changes in activities with the shift to agriculture in the southeastern United States. *Current Anthropology, 30*(3), 385-394.
Britt, B. B., Scheetz, R. D., & Dangerfield, A. (2008). A suite of dermestid beetle traces on dinosaur bone from the Upper Jurassic Morrison Formation, Wyoming, USA. *Ichnos, 15*(2), 59-71.
Brooks, A. S., Yellen, J. E., Potts, R., Behrensmeyer, A. K., Deino, A. L., Leslie, D. E., . . . Clark, J. B. (2018). Long-distance stone transport and pigment use in the earliest Middle Stone Age. *Science, 360*(6384), 90-94.
Brooks, S., & Suchey, J. M. (1990). Skeletal age determination based on the os pubis: a comparison of the Acsádi-Nemeskéri and Suchey-Brooks methods. *Human Evolution, 5*(3), 227-238.
Brooks, S. T. (1955). Skeletal age at death: the reliability of cranial and pubic age indicators. *American Journal of Physical Anthropology, 13*(4), 567-597.

Brown, F. H., McDougall, I., & Fleagle, J. G. (2012). Correlation of the KHS Tuff of the Kibish Formation to volcanic ash layers at other sites, and the age of early *Homo sapiens* (Omo I and Omo II). *Journal of Human Evolution, 63*(4), 577-585.
Bruzek, J. (2002). A method for visual determination of sex, using the human hip bone. *American Journal of Physical Anthropology, 117*(2), 157-168.
Buckberry, J. L., & Chamberlain, A. T. (2002). Age estimation from the auricular surface of the ilium: a revised method. *American Journal of Physical Anthropology, 119*(3), 231-239.
Buikstra, J. E., & Ubelaker, D. H. (1994). *Standards for data collection from human skeletal remains*. Fayetteville, Arkansas: Arkansas Archaeological Survey.
Bush, M. E., Lovejoy, C. O., Johanson, D. C., & Coppens, Y. (1982). Hominid carpal, metacarpal, and phalangeal bones recovered from the Hadar Formation: 1974–1977 collections. *American Journal of Physical Anthropology, 57*, 651–677.
Cann, R. L., Stoneking, M., & Wilson, A. C. (1987). Mitochondrial DNA and human evolution. *Nature, 325*, 31-36.
Carretero, J. M. (1994). *Estudio del esqueleto de las dos cinturas y el miembro superior de los homínidos de la Sima de los Huesos, Sierra de Atapuerca, Burgos.* (Ph.D.). Universidad Complutense de Madrid, Madrid,
Carretero, J. M., Arsuaga, J. L., & Lorenzo, C. (1997). Clavicles, scapulae and humeri from the Sima de los Huesos site (Sierra de Atapuerca, Spain). *Journal of Human Evolution, 33*(2-3), 357-408.
Carretero, J. M., Haile-Selassie, Y., Rodriguez, L., & Arsuaga, J. L. (2009). A partial distal humerus from the Middle Pleistocene deposits at Bodo, Middle Awash, Ethiopia. *Anthropological Science, 117*(1), 19-31.
Carretero, J. M., Lorenzo, C., & Arsuaga, J. L. (1999). Axial and appendicular skeleton of *Homo antecessor*. *Journal of Human Evolution, 37*(3-4), 459-499.
Carretero, J. M., Rodríguez, L., García-González, R., Arsuaga, J.-L., Gómez-Olivencia, A., Lorenzo, C., . . . Quam, R. (2012). Stature estimation from complete long bones in the Middle Pleistocene humans from the Sima de los Huesos, Sierra de Atapuerca (Spain). *Journal of Human Evolution, 62*(2), 242-255.
Chan, E. K. F., Timmermann, A., Baldi, B. F., Moore, A. E., Lyons, R. J., Lee, S.-S., . . . Hayes, V. M. (2019). Human origins in a southern African palaeo-wetland and first migrations. *Nature, 575*, 185-189.
Child, S. L., & Cowgill, L. W. (2017). Femoral neck-shaft angle and climate-induced body proportions. *American Journal of Physical Anthropology, 164*(4), 720-735.
Churchill, S. E. (2006). Bioenergetic perspectives on Neanderthal thermoregulatory and activity budgets. In *Neanderthals Revisited: New Approaches and Perspectives* (pp. 113-133). Dordrecht: Springer.
Churchill, S. E., Berger, L. R., & Parkington, J. E. (2000). A Middle Pleistocene human tibia from Hoedjiespunt, Western Cape, South Africa. *South African Journal of Science, 96*(7), 367-368.
Churchill, S. E., Pearson, O. M., Grine, F. E., Trinkaus, E., & Holliday, T. W. (1996). Morphological affinities of the proximal ulna from Klasies River main site: archaic or modern? *Journal of Human Evolution, 31*(3), 213-237.
Churchill, S. E., & Smith, F. H. (2000). A modern human humerus from the early Aurignacian of Vogelherdhöhle (Stetten, Germany). *American Journal of Physical Anthropology, 112*(2), 251-273.

Churchill, S. E., & Trinkaus, E. (1990). Neandertal scapular glenoid morphology. *American Journal of Physical Anthropology, 83*(2), 147-160.
Clark, J. D. (1988). The Middle Stone Age of East Africa and the beginnings of regional identity. *Journal of World Prehistory, 2*(3), 235-305.
Clark, J. D., Beyene, Y., WoldeGabriel, G., Hart, W. K., Renne, P. R., Gilbert, H., . . . White, T. D. (2003). Stratigraphic, chronological and behavioural contexts of Pleistocene *Homo sapiens* from Middle Awash, Ethiopia. *Nature, 423*, 747-752.
Clark, J. D., de Heinzelin, J., Schick, K. D., Hart, W. K., White, T. D., WoldeGabriel, G., . . . Vrba, E. (1994). African *Homo erectus*: old radiometric ages and young Oldowan assemblages in the Middle Awash Valley, Ethiopia. *Science, 264*(5167), 1907-1910.
Coleman, W. H. (1969). Sex differences in the growth of the human bony pelvis. *American Journal of Physical Anthropology, 31*(2), 125-151.
Conroy, G. C., Jolly, C. J., Cramer, D., & Kalb, J. E. (1978). Newly discovered fossil hominid skull from the Afar depression, Ethiopia. *Nature, 276*, 67-70.
Crevecoeur, I. (2008). Étude anthropologique du squelette du Paléolithique supérieur de Nazlet Khater 2 (Égypte). In. Belgium: Leuven University Press.
Crevecoeur, I. (2012). The Upper Paleolithic human remains of Nazlet Khater 2 (Egypt) and past modern human diversity. In J.-J. Hublin & S. McPherron (Eds.), *Modern Origins* (pp. 205-219). Dordrecht: Springer.
Crevecoeur, I., Brooks, A., Ribot, I., Cornelissen, E., & Semal, P. (2016). Late Stone Age human remains from Ishango (Democratic Republic of Congo): new insights on Late Pleistocene modern human diversity in Africa. *Journal of Human Evolution, 96*, 35-57.
Davies, T. G., Pomeroy, E., Shaw, C. N., & Stock, J. T. (2014). Mobility and the skeleton: a biomechanical view. In J. Leary (Ed.), *Past mobilities* (pp. 129-153). Surrey, England: Ashgate.
Davies, T. G., & Stock, J. T. (2014). The influence of relative body breadth on the diaphyseal morphology of the human lower limb. *American Journal of Human Biology, 26*(6), 822-835.
Davis, C. B., Shuler, K. A., Danforth, M. E., & Herndon, K. E. (2013). Patterns of interobserver error in the scoring of entheseal changes. *International Journal of Osteoarchaeology, 23*(2), 147-151.
Dawson, J. E., & Trinkaus, E. (1997). Vertebral osteoarthritis of the La Chapelle-aux-Saints 1 Neanderthal. *Journal of Archaeological Science, 24*(11), 1015-1021.
Day, M. H. (1969). Early *Homo sapiens* remains from the Omo River region of south-west Ethiopia: Omo human skeletal remains. *Nature, 222*, 1135-1138.
Day, M. H. (1971). Postcranial remains of *Homo erectus* from bed IV, Olduvai Gorge, Tanzania. *Nature, 232*, 383-387.
Day, M. H., & Leakey, R. E. F. (1974). New evidence of the genus *Homo* from East Rudolf, Kenya (III). *American Journal of Physical Anthropology, 41*(3), 367-380.
Dayal, M. R., Kegley, A. D., Štrkalj, G., Bidmos, M. A., & Kuykendall, K. L. (2009). The history and composition of the Raymond A. Dart Collection of human skeletons at the University of the Witwatersrand, Johannesburg, South Africa. *American Journal of Physical Anthropology, 140*(2), 324-335.
de Heinzelin, J., Clark, J. D., Schick, K. D., & Gilbert, W. H. (Eds.). (2000). *The Acheulean and the Plio-Pleistocene deposits of the Middle Awash Valley, Ethiopia*. Tervuren, Belgium: Royal Museum of Central Africa.

Dean, M. C., Stringer, C. B., & Bromage, T. G. (1986). Age at death of the Neanderthal child from Devil's Tower, Gibraltar and the implications for studies of general growth and development in Neanderthals. *American Journal of Physical Anthropology, 70*(3), 301-309.

Deino, A. L., Behrensmeyer, A. K., Brooks, A. S., Yellen, J. E., Sharp, W. D., & Potts, R. (2018). Chronology of the Acheulean to Middle Stone Age transition in eastern Africa. *Science, 360*(6384), 95-98.

Derry, D. E. (1911). Damage done to skulls and bones by termites. *Nature, 86*(2164), 245-246.

Didia, B. C., Nduka, E. C., & Adele, O. (2009). Stature estimation formulae for Nigerians. *Journal of Forensic Sciences, 54*(1), 20-21.

Disotell, T. R. (2012). Archaic human genomics. *American Journal of Physical Anthropology, 149*(S55), 24-39.

Dodo, Y., Kondo, O., Muhesen, S., & Akazawa, T. (2002). Anatomy of the Neandertal infant skeleton from Dederiyeh Cave, Syria. In T. Akazawa, K. Aoki, & O. Bar-Yosef (Eds.), *Neandertals and modern humans in Western Asia* (pp. 323-338): Springer.

Durband, A. C., Rayner, D. R. T., & Westaway, M. (2009). A new test of the sex of the Lake Mungo 3 skeleton. *Archaeology in Oceania, 44*(2), 77-83.

Duyar, I., & Pelin, C. (2003). Body height estimation based on tibia length in different stature groups. *American Journal of Physical Anthropology, 122*(1), 23-27.

Endicott, P., Ho, S. Y. W., & Stringer, C. (2010). Using genetic evidence to evaluate four palaeoanthropological hypotheses for the timing of Neanderthal and modern human origins. *Journal of Human Evolution, 59*(1), 87-95.

Endo, B. (1971). Some characteristics of the deltoid tuberosity of the humerus in the West Asian and the European "Classic" Neanderthals. *Journal of the Anthropological Society of Nippon, 79*(3), 249-258.

Endo, B., & Kimura, T. (1970). Postcranial skeleton of the Amud Man. In H. Suzuki & F. Takai (Eds.), *The Amud man and his cave site* (pp. 231-406). Tokyo: Academic Press of Japan.

Etler, D. A. (1996). The fossil evidence for human evolution in Asia. *Annual Review of Anthropology, 25*, 275-301.

Faccia, K. J., & Williams, R. C. (2008). Schmorl's nodes: clinical significance and implications for the bioarchaeological record. *International Journal of Osteoarchaeology, 18*(1), 28-44.

Fejfar, O., & Kaiser, T. M. (2005). Insect bone-modification and paleoecology of Oligocene mammal-bearing sites in the Doupov Mountains, northwestern Bohemia. *Palaeontologia Electronica, 8*(1), 1-11.

Feldesman, M. R., & Lundy, J. K. (1988). Stature estimates for some African Plio-Pleistocene fossil hominids. *Journal of Human Evolution, 17*(6), 583-596.

Fernandez-Jalvo, Y., & Andrews, P. (2016). *Atlas of taphonomic identifications: 1001+ images of fossil and recent mammal bone modification*. Dordrecht: Springer.

Ferreira, M. T., Vicente, R., Navega, D., Gonçalves, D., Curate, F., & Cunha, E. (2014). A new forensic collection housed at the University of Coimbra, Portugal: the 21st Century Identified Skeletal Collection. *Forensic Science International, 245*, 202.e201-202.e205.

Finnegan, M. (1978). Non-metric variation of the infracranial skeleton. *Journal of Anatomy, 125*(1), 23-37.

Fischer, B., & Mitteroecker, P. (2015). Covariation between human pelvis shape, stature, and head size alleviates the obstetric dilemma. *Proceedings of the National Academy of Sciences, 112*(18), 5655-5660.
Fleagle, J. G., Assefa, Z., Brown, F. H., & Shea, J. J. (2008). Paleoanthropology of the Kibish Formation, southern Ethiopia: introduction. *Journal of Human Evolution, 55*(3), 360-365.
Foley, R., & Lahr, M. M. (1997). Mode 3 technologies and the evolution of modern humans. *Cambridge Archaeological Journal, 7*(1), 3-36.
Foley, R. A., Martin, L., Lahr, M. M., & Stringer, C. (2016). Major transitions in human evolution. *Philosophical Transactions of the Royal Society B, 371*(1698), 20150229.
Frayer, D. W. (1992). The persistence of Neanderthal features in post-Neanderthal Europeans. In G. Bräuer & F. H. Smith (Eds.), *Continuity or replacement: Controversies in Homo sapiens evolution* (pp. 179-188). Rotterdam: A. A. Balkema.
Frayer, D. W. (1993). Evolution at the European edge: Neanderthal and Upper Paleolithic relationships. *Préhistore Européenne, 2*, 9-69.
Friedlander, N. J., & Jordan, D. K. (1994). Obstetric implications of Neanderthal robusticity and bone density. *Human Evolution, 9*, 331-342.
Galera, V., Ubelaker, D. H., & Hayek, L.-A. C. (1998). Comparison of macroscopic cranial methods of age estimation applied to skeletons from the Terry Collection. *Journal of Forensic Science, 43*(5), 933-939.
Gallagher, A. (2013). Stature, body mass, and brain size: A two-million-year odyssey. *Economics & Human Biology, 11*(4), 551-562.
Gambier, D. (1982). Etude ostéométrique des astragales néandertaliens du Regourdou (Montignac, Dordogne). *Comptes Rendus de l'Academie des Sciences Paris, série III, 295*, 279-282.
Gargett, R. H. (1999). Middle Palaeolithic burial is not a dead issue: the view from Qafzeh, Saint-Césaire, Kebara, Amud, and Dederiyeh. *Journal of Human Evolution, 37*(1), 27-90.
Garrigan, D., & Hammer, M. F. (2006). Reconstructing human origins in the genomic era. *Nature Reviews Genetics, 7*, 669-680.
Garvin, H. M., & Passalacqua, N. V. (2012). Current practices by forensic anthropologists in adult skeletal age estimation. *Journal of Forensic Sciences, 57*(2), 427-433.
Gibbard, P. L., Head, M. J., Walker, M. J. C., & Subcommission on Quaternary Stratigraphy (2010). Formal ratification of the Quaternary System/Period and the Pleistocene Series/Epoch with a base at 2.58 Ma. *Journal of Quaternary Science, 25*(2), 96-102.
Gilbert, W. H. (2008). Daka Member hominid postcranial remains. In W. H. Gilbert & B. Asfaw (Eds.), *Homo erectus: Pleistocene evidence from the Middle Awash, Ethiopia* (pp. 373-390). Berkeley, CA: University of California Press.
Gilbert, W. H., & Asfaw, B. (2008). *Homo erectus: Pleistocene evidence from the Middle Awash, Ethiopia* (Vol. 1). Berkeley, CA: University of California Press.
Gilligan, I., Chandraphak, S., & Mahakkanukrauh, P. (2013). Femoral neck-shaft angle in humans: variation relating to climate, clothing, lifestyle, sex, age and side. *Journal of Anatomy, 223*(2), 133-151.
Gómez, M., Casado, A., De Diego, M., Arias-Martorell, J., Pastor, J. F., & Potau, J. M. (2020). Quantitative shape analysis of the deltoid tuberosity of modern humans (*Homo sapiens*) and common chimpanzees (*Pan troglodytes*). *Annals of Anatomy, 230*, 151505.

Gómez-Olivencia, A. (2009). *Estudios paleobiológicos sobre la columna vertebral y la caja torácica de los humanos fósiles del Pleistoceno, con especial referencia a los fósiles de la Sierra de Atapuerca.* (Ph.D. Ph.D.). Universidad de Burgos, Burgos.

Gómez-Olivencia, A. (2013). Back to the old man's back: Reassessment of the anatomical determination of the vertebrae of the Neandertal individual of La Chapelle-aux-Saints. *Annales de Paléontologie, 99*(1), 43-65.

Gómez-Olivencia, A., Been, E., Arsuaga, J. L., & Stock, J. T. (2013). The Neandertal vertebral column 1: The cervical spine. *Journal of Human Evolution, 64*(6), 608-630.

Gómez-Olivencia, A., Carretero, J. M., Arsuaga, J. L., Rodríguez-García, L., García-González, R., & Martínez, I. (2007). Metric and morphological study of the upper cervical spine from the Sima de los Huesos site (Sierra de Atapuerca, Burgos, Spain). *Journal of Human Evolution, 53*(1), 6-25.

Gómez-Olivencia, A., Couture-Veschambre, C., Madelaine, S., & Maureille, B. (2013b). The vertebral column of the Regourdou 1 Neandertal. *Journal of Human Evolution, 64*(6), 582-607.

Gómez-Olivencia, A., Eaves-Johnson, K. L., Franciscus, R. G., Carretero, J. M., & Arsuaga, J. L. (2009). Kebara 2: new insights regarding the most complete Neandertal thorax. *Journal of Human Evolution, 57*(1), 75-90.

Gonder, M. K., Mortensen, H. M., Reed, F. A., de Sousa, A., & Tishkoff, S. A. (2006). Whole-mtDNA genome sequence analysis of ancient African lineages. *Molecular Biology and Evolution, 24*(3), 757-768.

González-José, R., Van der Molen, S., González-Pérez, E., & Hernández, M. (2004). Patterns of phenotypic covariation and correlation in modern humans as viewed from morphological integration. *American Journal of Physical Anthropology, 123*(1), 69-77.

Gori, F., Lerner, U., Ohlsson, C., & Baron, R. (2015). A new WNT on the bone: WNT16, cortical bone thickness, porosity and fractures. *BoneKEy Reports, 4*, 669.

Grabowski, M., Hatala, K. G., Jungers, W. L., & Richmond, B. G. (2015). Body mass estimates of hominin fossils and the evolution of human body size. *Journal of Human Evolution, 85*, 75-93.

Grabowski, M. W., Polk, J. D., & Roseman, C. C. (2011). Divergent patterns of integration and reduced constraint in the human hip and the origins of bipedalism. *Evolution, 65*(5), 1336-1356.

Green, R. E., Krause, J., Briggs, A. W., Maricic, T., Stenzel, U., Kircher, M., . . . Pääbo, S. (2010). A Draft Sequence of the Neandertal Genome. *Science, 328*, 710-722.

Grine, F. E. (2016). The Late Quaternary hominins of Africa: the skeletal evidence from MIS 6-2. In S. C. Jones & B. A. Stewart (Eds.), *Africa from MIS 6-2* (pp. 323-381). Dordrecht: Springer.

Grine, F. E., Jungers, W. L., Tobias, P. V., & Pearson, O. M. (1995). Fossil *Homo* femur from Berg Aukas, northern Namibia. *American Journal of Physical Anthropology, 97*(2), 151-185.

Grine, F. E., & Klein, R. G. (1993). Late Pleistocene human remains from the Sea Harvest site, Saldanha Bay, South Africa. *South African Journal of Science, 89*, 145-152.

Groucutt, H. S., Grün, R., Zalmout, I. A. S., Drake, N. A., Armitage, S. J., Candy, I., . . . Petraglia, M. D. (2018). *Homo sapiens* in Arabia by 85,000 years ago. *Nature Ecology & Evolution, 2*(5), 800-809.

Gunz, P., Bookstein, F. L., Mitteroecker, P., Stadlmayr, A., Seidler, H., & Weber, G. W. (2009). Early modern human diversity suggests subdivided population structure and a complex out-of-Africa scenario. *Proceedings of the National Academy of Sciences USA, 106*(15), 6094-6098.

Haeusler, M., Trinkaus, E., Fornai, C., Müller, J., Bonneau, N., Boeni, T., & Frater, N. (2019). Morphology, pathology, and the vertebral posture of the La Chapelle-aux-Saints Neandertal. *Proceedings of the National Academy of Sciences, 116*(11), 4923-4927.

Haglund, W. D. (2006). Forensic taphonomy: the postmortem fate of human remains. In W. D. Haglund & M. H. Sorg (Eds.), *Forensic taphonomy: the postmortem fate of human remains* (pp. 367-381). Boca Raton, FL: CRC Press.

Haglund, W. D., Reay, D. T., & Swindler, D. (1988). Tooth mark artifacts and survival of bones in animal scavenged human skeletons. *Journal of Forensic Sciences, 33*(4), 985-997.

Haile-Selassie, Y., & WoldeGabriel, G. (Eds.). (2009). *Ardipithecus kadabba: Late Miocene evidence from the Middle Awash, Ethiopia* (Vol. 2). Berkeley, CA: University of California Press.

Haile-Selassie, Y., Asfaw, B., & White, T. D. (2004). Hominid cranial remains from upper Pleistocene deposits at Aduma, Middle Awash, Ethiopia. *American Journal of Physical Anthropology, 123*(1), 1-10.

Hammer, M. F., Woerner, A. E., Mendez, F. L., Watkins, J. C., & Wall, J. D. (2011). Genetic evidence for archaic admixture in Africa. *Proceedings of the National Academy of Sciences USA, 108*(37), 15123–15128.

Harris, S. M., & Case, D. T. (2012). Sexual dimorphism in the tarsal bones: implications for sex determination. *Journal of Forensic Sciences, 57*(2), 295-305.

Harvati, K., Stringer, C., Grün, R., Aubert, M., Allsworth-Jones, P., & Folorunso, C. A. (2011). The Later Stone Age calvaria from Iwo Eleru, Nigeria: morphology and chronology. *PLoS ONE, 6*(9), e24024.

Haynes, G. (1980). Evidence of carnivore gnawing on Pleistocene and recent mammalian bones. *Paleobiology, 6*(3), 341-351.

Haynes, G. (1983). Frequencies of spiral and green-bone fractures on ungulate limb bones in modern surface assemblages. *American antiquity, 48*(1), 102-114.

Heim, J. L. (1976). *Les hommes fossiles de La Ferrassie. Tome I. Le gisement. Les squelettes adultes (crâne et squelette du tronc)*. Paris: Masson.

Heim, J. L. (1982). *Les hommes fossiles de La Ferrassie. Tome II. Les squelettes adultes (squelette des membres)*. Paris: Masson.

Heizer, R. F. (1949). The archaeology of central California. I: The Early Horizon. *University of California Anthropological Records, 12*, 1-84.

Henn, B. M., Cavalli-Sforza, L. L., & Feldman, M. W. (2012). The great human expansion. *Proceedings of the National Academy of Sciences USA, 109*(44), 17758-17764.

Henn, B. M., Gignoux, C. R., Jobin, M., Granka, J. M., Macpherson, J., Kidd, J. M., . . . Feldman, M. W. (2011). Hunter-gatherer genomic diversity suggests a southern African origin for modern humans. *Proceedings of the National Academy of Sciences USA, 108*(13), 5154-5162.

Henn, B. M., Steele, T. E., & Weaver, T. D. (2018). Clarifying distinct models of modern human origins in Africa. *Current Opinion in Genetics & Development, 53*, 148-156.

Henshilwood, C. S., Marean, C. W., Chase, P., Davidson, I., Gamble, C., Holliday, T. W., . . . Henshilwood, C. S. (2003). The origin of modern human behavior: critique of the models and their test implications. *Current Anthropology, 44*(5), 627-651.
Hershkovitz, I., Weber, G. W., Quam, R., Duval, M., Grün, R., Kinsley, L., . . . Weinstein-Evron, M. (2018). The earliest modern humans outside Africa. *Science, 359*(6374), 456-459.
Hilton, R., Ball, J., & Benn, R. (1976). Vertebral end-plate lesions (Schmorl's nodes) in the dorsolumbar spine. *Annals of the rheumatic diseases, 35*(2), 127-132.
Hlusko, L. J. (2004). Integrating the genotype and phenotype in hominid paleontology. *Proceedings of the National Academy of Sciences, 101*(9), 2653-2657.
Hlusko, L. J., Reiner, W. B., & Njau, J. K. (2015). A one-million-year-old hominid distal ulna from Olduvai Gorge, Tanzania. *American Journal of Physical Anthropology, 158*(1), 36-42.
Holland, T. D. (1995). Estimation of adult stature from the calcaneus and talus. *American Journal of Physical Anthropology, 96*(3), 315-320.
Holliday, T. W. (1997). Body proportions in Late Pleistocene Europe and modern human origins. *Journal of Human Evolution, 32*(5), 423-448.
Holliday, T. W. (2012). Body size, body shape, and the circumscription of the genus *Homo*. *Current Anthropology, 53*(S6), S330-S345.
Holliday, T. W. (2015). Population affinities of the Jebel Sahaba skeletal sample: Limb proportion evidence. *International Journal of Osteoarchaeology, 25*(4), 466-476.
Holliday, T. W. (2015). The significance of changes in body mass in human evolution. *BMSAP, 27*(3-4), 101-109.
Holliday, T. W., & Ruff, C. B. (2001). Relative variation in human proximal and distal limb segment lengths. *American Journal of Physical Anthropology, 116*(1), 26-33.
Hoppa, R. D. (2000). Population variation in osteological aging criteria: an example from the pubic symphysis. *American Journal of Physical Anthropology, 111*(2), 185-191.
Howell, F. C. (1999). Paleo-demes, species clades, and extinctions in the Pleistocene hominin record. *Journal of Anthropological Research, 55*(2), 191-243.
Hrdlička, A. (1934). Contributions to the study of the femur: the crista aspera and the pilaster. *American Journal of Physical Anthropology, 19*(1), 17-37.
Hubbe, M., Hanihara, T., & Harvati, K. (2009). Climate signatures in the morphological differentiation of worldwide modern human populations. *The Anatomical Record, 292*(11), 1720-1733.
Hublin, J.-J. (2009). The origin of Neandertals. *Proceedings of the National Academy of Sciences USA, 106*(38), 16022-16027.
Hublin, J.-J., Ben-Ncer, A., Bailey, S. E., Freidline, S. E., Neubauer, S., Skinner, M. M., . . . Gunz, P. (2017). New fossils from Jebel Irhoud, Morocco and the pan-African origin of *Homo sapiens*. *Nature, 546*, 289-292.
Huchet, J. B., Deverly, D., Gutiérrez, B., & Chauchat, C. (2011). Taphonomic evidence of a human skeleton gnawed by termites in a Moche-civilisation grave at Huaca de la Luna, Peru. *International Journal of Osteoarchaeology, 21*(1), 92-102.
Ingman, M., Kaessmann, H., Pääbo, S., & Gyllensten, U. (2000). Mitochondrial genome variation and the origin of modern humans. *Nature, 408*, 708-713.

Kaiser, T. M. (2000). Proposed fossil insect modification to fossil mammalian bone from Plio-Pleistocene hominid-bearing deposits of Laetoli (Northern Tanzania). *Annals of the Entomological Society of America, 93*(4), 693-700.
Kelley, M. A. (1979). Parturition and pelvic changes. *American Journal of Physical Anthropology, 51*(4), 541-545.
Key, C. A., Aiello, L. C., & Molleson, T. (1994). Cranial suture closure and its implications for age estimation. *International Journal of Osteoarchaeology, 4*(3), 193-207.
Kidd, R. S., & Oxnard, C. E. (2002). Patterns of morphological discrimination in selected human tarsal elements. *American Journal of Physical Anthropology, 117*(2), 169-181.
Kidder, J. H., Jantz, R. L., & Smith, F. H. (1992). Defining modern humans: a multivariate approach. In G. Bräuer & F. H. Smith (Eds.), *Continuity or replacement: Controversies in Homo sapiens evolution* (pp. 157-177). Rotterdam: A. A. Balkema.
King, W. (1864). The reputed fossil man of the Neanderthal. *Quarterly Journal of Science, 1*, 88-97.
Klein, R. G. (2000). Archeology and the evolution of human behavior. *Evolutionary Anthropology, 9*(1), 17-36.
Klingenberg, C. P. (2013). Cranial integration and modularity: insights into evolution and development from morphometric data. *Hystrix, the Italian Journal of Mammalogy, 24*(1), 43-58.
Kurki, H. K., Ginter, J. K., Stock, J. T., & Pfeiffer, S. (2010). Body size estimation of small-bodied humans: applicability of current methods. *American Journal of Physical Anthropology, 141*(2), 169-180.
Lachance, J., Vernot, B., Elbers, C. C., Ferwerda, B., Froment, A., Bodo, J.-M., . . . Tishkoff, S. A. (2012). Evolutionary history and adaptation from high-coverage whole-genome sequences of diverse African hunter-gatherers. *Cell, 150*(3), 457-469.
Lahr, M. M., & Foley, R. A. (1998). Towards a theory of modern human origins: geography, demography, and diversity in recent human evolution. *American Journal of Physical Anthropology, 107*(S27), 137-176.
Lahr, M. M., & Foley, R. A. (2001). Mode 3, *Homo helmei*, and the pattern of human evolution in the Middle Pleistocene. In L. Barham & K. R. Brown (Eds.), *Human roots: Africa and Asia in the Middle Pleistocene* (pp. 23-39). Bristol: CHERUB, Western Academic and Specialist Press.
Lahr, M. M., & Foley, R. A. (2016). Human evolution in late Quaternary eastern Africa. In S. C. Jones & B. A. Stewart (Eds.), *Africa from MIS 6-2* (pp. 215-231). Dordrecht: Springer.
Larsen, C. S. (1981). Functional implications of postcranial size reduction on the prehistoric Georgia coast, USA. *Journal of Human Evolution, 10*(6), 489-502.
Legendre, P. (2018). *lmodel2: Model II Regression. R package version 1.7.3*. Retrieved from https://CRAN.R-project.org/package=lmodel2
Li, J. Z., Absher, D. M., Tang, H., Southwick, A. M., Casto, A. M., Ramachandran, S., . . . Myers, R. M. (2008). Worldwide human relationships inferred from genome-wide patterns of variation. *Science, 319*(5866), 1100-1104.
Linnaeus, C. (1758). *Systema naturae per regna tria naturae: secundum classes, ordines, genera, species, cum characteribus, differentiis, synonymis, locis*. Stockholm: Laurentii Salvii.

Liu, W., Martinón-Torres, M., Cai, Y.-j., Xing, S., Tong, H.-w., Pei, S.-w., . . . Wu, X.-j. (2015). The earliest unequivocally modern humans in southern China. *Nature, 526*(7575), 696-699.

Llamas, B., Willerslev, E., & Orlando, L. (2017). Human evolution: a tale from ancient genomes. *Philosophical Transactions of the Royal Society B: Biological Sciences, 372*, 20150484.

Lordkipanidze, D., Jashashvili, T., Vekua, A., Ponce de León, M. S., Zollikofer, C. P. E., Rightmire, G. P., . . . Rook, L. (2007). Postcranial evidence from early *Homo* from Dmanisi, Georgia. *Nature, 449*(7160), 305-310.

Lordkipanidze, D., Ponce de León, M. S., Margvelashvili, A., Rak, Y., Rightmire, G. P., Vekua, A., & Zollikofer, C. P. E. (2013). A complete skull from Dmanisi, Georgia, and the evolutionary biology of early *Homo*. *Science, 342*(6156), 326-331.

Lorenzo, C. (2007). *Evolución de la mano en los homínidos: análisis morfológico de los fósiles de la Sierra de Atapuerca.* (Ph.D.). Universidad Complutense de Madrid, Madrid.

Lorenzo, C., Arsuaga, J. L., & Carretero, J. M. (1999). Hand and foot remains from the Gran Dolina Early Pleistocene site (Sierra de Atapuerca, Spain). *Journal of Human Evolution, 37*(3-4), 501-522.

Lovejoy, C. O., Meindl, R. S., Ohman, J. C., Heiple, K. G., & White, T. D. (2002). The Maka femur and its bearing on the antiquity of human walking: applying contemporary concepts of morphogenesis to the human fossil record. *American Journal of Physical Anthropology, 119*(2), 97-133.

Lovejoy, C. O., Meindl, R. S., Pryzbeck, T. R., & Mensforth, R. P. (1985). Chronological metamorphosis of the auricular surface of the ilium: a new method for the determination of adult skeletal age at death. *American Journal of Physical Anthropology, 68*(1), 15-28.

Lovejoy, C. O., & Trinkaus, E. (1980). Strength and robusticity of the Neandertal tibia. *American Journal of Physical Anthropology, 53*(4), 465-470.

Lozanoff, S., Sciulli, P. W., & Schneider, K. N. (1985). Third trochanter incidence and metric trait covariation in the human femur. *Journal of Anatomy, 143*, 149-159.

Lu, Z. E. (2003). The Jinniushan hominid in anatomical, chronological, and cultural context. In C. Shen & S. G. Keates (Eds.), *Current Research in Chinese Pleistocene Archaeology* (Vol. 1179, pp. 127-136). British Archaeological Reports International Series.

Lu, Z., Meldrum, D. J., Huang, Y., He, J., & Sarmiento, E. E. (2011). The Jinniushan hominin pedal skeleton from the late Middle Pleistocene of China. *HOMO-Journal of Comparative Human Biology, 62*(6), 389-401.

Lui, J. C., Jee, Y. H., Presley Garrison, J. R. I., Yue, S., Ad, M., Nguyen, Q., . . . Baron, J. (2018). Differential aging of growth plate cartilage underlies differences in bone length and thus helps determine skeletal proportions. *PLoS Biology, 16*(7), e2005263.

Lythgoe, A. M. (1907). The Egyptian Expedition. *The Metropolitan Museum of Art Bulletin, 2*(4), 61-63.

Lythgoe, A. M. (1908). The Egyptian Expedition. *The Metropolitan Museum of Art Bulletin, 3*(5), 83-86.

Lythgoe, A. M. (1909). The Egyptian Expedition. *The Metropolitan Museum of Art Bulletin, 4*(7), 119-123.

Manzi, G. (2004). Human evolution at the Matuyama-Brunhes boundary. *Evolutionary Anthropology, 13*(1), 11-24.

Marean, C. W. (2015). An evolutionary anthropological perspective on modern human origins. *Annual Review of Anthropology, 44*, 533-556.

Mariotti, V., & Belcastro, M. G. (2011). Lower limb entheseal morphology in the Neandertal Krapina population (Croatia, 130 000 BP). *Journal of Human Evolution, 60*(6), 694-702.
Martin, H. (1923). *L'homme fossile de la Quina*. Paris: Librairie Octave Doin.
Martin, R., & Saller, K. (1957). *Lehrbuch der Anthropologie*. Stuttgart: Gustav Fischer.
Martinón-Torres, M., Bermúdez de Castro, J. M., Martínez de Pinillos, M., Modesto-Mata, M., Xing, S., Martín-Francés, L., . . . Liu, W. (2019). New permanent teeth from Gran Dolina-TD6 (Sierra de Atapuerca). The bearing of *Homo antecessor* on the evolutionary scenario of Early and Middle Pleistocene Europe. *Journal of Human Evolution, 127*, 93-117.
Martrille, L., Ubelaker, D. H., Cattaneo, C., Seguret, F., Tremblay, M., & Baccino, E. (2007). Comparison of four skeletal methods for the estimation of age at death on white and black adults. *Journal of Forensic Sciences, 52*(2), 302-307.
Mastrangelo, P., De Luca, S., Alemán, I., & Botella, M. C. (2011). Sex assessment from the carpals bones: discriminant function analysis in a 20th century Spanish sample. *Forensic Science International, 206*(1-3), 216.e211-216.e210.
McBrearty, S., & Brooks, A. S. (2000). The revolution that wasn't: a new interpretation of the origin of modern human behavior. *Journal of Human Evolution, 39*(5), 453-563.
McCollum, M. A., & Sharpe, P. T. (2001). Developmental genetics and early hominid craniodental evolution. *BioEssays, 23*(6), 481-493.
McCown, T. D., & Keith, A. (1939). *The Stone Age of Mt. Carmel* (Vol. 2). Oxford: Clarendon Press.
McDougall, I., Brown, F. H., & Fleagle, J. G. (2008). Sapropels and the age of hominins Omo I and II, Kibish, Ethiopia. *Journal of Human Evolution, 55*(3), 409-420.
McHenry, H. M. (1992). Body size and proportions in early hominids. *American Journal of Physical Anthropology, 87*(4), 407-431.
McHenry, H. M., & Corruccini, R. S. (1978). The femur in early human evolution. *American Journal of Physical Anthropology, 49*(4), 473-487.
McHenry, H. M., Corruccini, R. S., & Howell, F. C. (1976). Analysis of an early hominid ulna from the Omo Basin, Ethiopia. *American Journal of Physical Anthropology, 44*(2), 295-304.
Meadows, L., & Jantz, R. L. (1992). Estimation of stature from metacarpal lengths. *Journal of Forensic Sciences, 37*(1), 147-154.
Meindl, R. S., & Lovejoy, C. O. (1985). Ectocranial suture closure: a revised method for the determination of skeletal age at death based on the lateral-anterior sutures. *American Journal of Physical Anthropology, 68*(1), 57-66.
Meindl, R. S., Lovejoy, C. O., Mensforth, R. P., & Walker, R. A. (1985). A revised method of age determination using the os pubis, with a review and tests of accuracy of other current methods of pubic symphyseal aging. *American Journal of Physical Anthropology, 68*(1), 29-45.
Mersey, B., Jabbour, R. S., Brudvik, K., & Defleur, A. (2013). Neanderthal hand and foot remains from Moula-Guercy, Ardèche, France. *American Journal of Physical Anthropology, 152*(4), 516-529.
Meyer, M., Arsuaga, J.-L., de Filippo, C., Nagel, S., Aximu-Petri, A., Nickel, B., . . . Pääbo, S. (2016). Nuclear DNA sequences from the Middle Pleistocene Sima de los Huesos hominins. *Nature, 531*, 504-507.

Meyer, V., Bruzek, J., Couture, C., Madelaine, S., & Maureille, B. (2011). Un nouveau bassin néandertalien: description morphologique des restes pelviens de Regourdou 1 (Montignac, Dordogne, France). *PALEO. Revue d'archéologie préhistorique, 22*, 207-222.

Milella, M. (2014). The influence of life history and sexual dimorphism on entheseal changes in modern humans and African great apes. *PLoS ONE, 9*(9), e107963.

Millard, A. R. (2008). A critique of the chronometric evidence for hominid fossils: I. Africa and the Near East 500–50 ka. *Journal of Human Evolution, 54*(6), 848-874.

Mittra, E. S., Smith, H. F., Lemelin, P., & Jungers, W. L. (2007). Comparative morphometrics of the primate apical tuft. *American Journal of Physical Anthropology, 134*(4), 449-459.

Moratto, M. J. (1984). *California Archaeology*. Orlando, Florida: Academic Press.

Morgan, L. E., & Renne, P. R. (2008). Diachronous dawn of Africa's Middle Stone Age: new $^{40}Ar/^{39}Ar$ ages from the Ethiopian Rift. *Geology, 36*(12), 967-970.

Morgan, L. E., Renne, P. R., Taylor, R., & WoldeGabriel, G. (2009). Archaeological age constraints from extrusion ages of obsidian: Examples from the Middle Awash, Ethiopia. *Quaternary Geochronology, 4*(3), 193-203.

Morris, A. G. (1992). Biological relationships between Upper Pleistocene and Holocene populations in southern Africa. In G. Bräuer & F. H. Smith (Eds.), *Continuity or replacement: Controversies in Homo sapiens evolution* (pp. 131-144). Rotterdam: Balkema.

Morrish, K. R., & Hlusko, L. J. (2014). Modularity and sexual dimorphism in human metacarpals. *PaleoBios, 31*(2), 1-20.

Musgrave, J. H. (1971). How dextrous was Neanderthal man? *Nature, 233*, 538-541.

Musgrave, J. H. (1973). The phalanges of Neanderthal and Upper Palaeolithic hands. In M. H. Day (Ed.), *Human Evolution* (Vol. 11, pp. 59-85). London: Taylor & Francis.

Nielsen, R., Akey, J. M., Jakobsson, M., Pritchard, J. K., Tishkoff, S., & Willerslev, E. (2017). Tracing the peopling of the world through genomics. *Nature, 541*, 302-310.

Niewoehner, W. A. (2001). Behavioral inferences from the Skhul/Qafzeh early modern human hand remains. *Proceedings of the National Academy of Sciences USA, 98*(6), 2979-2984.

Niewoehner, W. A., Weaver, A. H., & Trinkaus, E. (1997). Neandertal capitate-metacarpal articular morphology. *American Journal of Physical Anthropology, 103*(2), 219-233.

Nowell, A. (2010). Defining behavioral modernity in the context of Neandertal and anatomically modern human populations. *Annual Review of Anthropology, 39*, 437-452.

Ornitz, D. M., & Marie, P. J. (2019). Fibroblast growth factors in skeletal development. *Current Topics in Developmental Biology, 133*, 195-234.

Ortner, D. J., & Frohlich, B. (2007). The EB IA tombs and burials of Bâb edh-Dhrâ, Jordan: A bioarchaeological perspective on the people. *International Journal of Osteoarchaeology, 17*(4), 358-368.

Pablos, A., Gómez-Olivencia, A., García-Pérez, A., Martínez, I., Lorenzo, C., & Arsuaga, J. L. (2013a). From toe to head: Use of robust regression methods in stature estimation based on foot remains. *Forensic Science International, 226*(1-3), 299.e1-299.e7.

Pablos, A., Gómez-Olivencia, A., Maureille, B., Holliday, T. W., Madelaine, S., Trinkaus, E., & Couture-Veschambre, C. (2019). Neandertal foot remains from Regourdou 1 (Montignac-sur-Vézère, Dordogne, France). *Journal of Human Evolution, 128*, 17-44.

Pablos, A., Lorenzo, C., Martínez, I., Bermúdez de Castro, J. M., Martinón-Torres, M., Carbonell, E., & Arsuaga, J. L. (2012). New foot remains from the Gran Dolina-TD6

Early Pleistocene site (Sierra de Atapuerca, Burgos, Spain). *Journal of Human Evolution, 63*(4), 610-623.
Pablos, A., Martínez, I., Lorenzo, C., Gracia, A., Sala, N., & Arsuaga, J. L. (2013b). Human talus bones from the Middle Pleistocene site of Sima de los Huesos (Sierra de Atapuerca, Burgos, Spain). *Journal of Human Evolution, 65*(1), 79-92.
Pablos, A., Martínez, I., Lorenzo, C., Sala, N., Gracia-Téllez, A., & Arsuaga, J. L. (2014). Human calcanei from the Middle Pleistocene site of Sima de los Huesos (Sierra de Atapuerca, Burgos, Spain). *Journal of Human Evolution, 76*, 63-76.
Pablos, A., Pantoja-Pérez, A., Martínez, I., Lorenzo, C., & Arsuaga, J. L. (2017). Metric and morphological analysis of the foot in the Middle Pleistocene sample of Sima de los Huesos (Sierra de Atapuerca, Burgos, Spain). *Quaternary International, 433*, 103-113.
Parr, W. C. H., Chatterjee, H. J., & Soligo, C. (2011). Inter-and intra-specific scaling of articular surface areas in the hominoid talus. *Journal of Anatomy, 218*(4), 386-401.
Pearson, O. M. (1997). *Postcranial morphology and the origin of modern humans.* (PhD). State University of New York at Stony Brook.
Pearson, O. M. (2000). Appendix 8: Human remains from Twin Rivers. In *The Middle Stone Age of Zambia, South Central Africa* (pp. 281-282). Bristol: Western Academic and Specialist Press.
Pearson, O. M. (2000). Postcranial remains and the origin of modern humans. *Evolutionary Anthropology, 9*(6), 229-247.
Pearson, O. M., Fleagle, J. G., Grine, F. E., & Royer, D. F. (2008a). Further new hominin fossils from the Kibish Formation, southwestern Ethiopia. *Journal of Human Evolution, 55*(3), 444-447.
Pearson, O. M., & Grine, F. E. (1996). Morphology of the Border Cave hominid ulna and humerus. *South African Journal of Science, 92*(5), 231-236.
Pearson, O. M., & Grine, F. E. (1997). Re-analysis of the hominid radii from Cave of Hearths and Klasies River Mouth, South Africa. *Journal of Human Evolution, 32*(6), 577-592.
Pearson, O. M., Grine, F. E., Barham, L., & Stringer, C. (2000). Human remains from the Middle and Later Stone Age of Mumbwa Caves. In L. Barham (Ed.), *The Middle Stone Age of Zambia, South Central Africa* (pp. 149-164). Bristol: Western Academic and Specialist Press.
Pearson, O. M., Petersen, T. R., Sparacello, V. S., Daneshvari, S. R., & Grine, F. E. (2014). Activity,"body shape," and cross-sectional geometry of the femur and tibia. In K. Carlson & D. Marchi (Eds.), *Reconstructing Mobility* (pp. 133-151). Boston, MA: Springer.
Pearson, O. M., Royer, D. F., Grine, F. E., & Fleagle, J. G. (2008b). A description of the Omo I postcranial skeleton, including newly discovered fossils. *Journal of Human Evolution, 55*(3), 421-437.
Pfeiffer, S., & Zehr, M. K. (1996). A morphological and histological study of the human humerus from Border Cave. *Journal of Human Evolution, 31*(1), 49-59.
Phenice, T. W. (1969). A newly developed visual method of sexing the os pubis. *American Journal of Physical Anthropology, 30*(2), 297-301.
Phillips, S. R. (2007). *Cranial anomaly, pathology, or normal variant? Thin parietal bones in ancient Egyptian human remains.* (Ph.D.). University of Pennsylvania.
Plavcan, J. M., Hammond, A. S., & Ward, C. V. (2014). Brief Communication: Calculating hominin and nonhuman anthropoid femoral head diameter from acetabular size. *American Journal of Physical Anthropology, 155*(3), 469-475.

Plomp, K. A., Dobney, K., Weston, D. A., Viðarsdóttir, U. S., & Collard, M. (2019). 3D shape analyses of extant primate and fossil hominin vertebrae support the ancestral shape hypothesis for intervertebral disc herniation. *BMC Evolutionary Biology, 19*, 226.

Pope, M., McNabb, J., & Gamble, C. (2017). *Crossing the human threshold: dynamic transformation and persistent places during the Middle Pleistocene*. Abingdon: Routledge.

Prüfer, K., de Filippo, C., Grote, S., Mafessoni, F., Korlević, P., Hajdinjak, M., . . . Pääbo, S. (2017). A high-coverage Neandertal genome from Vindija Cave in Croatia. *Science, 358*(6363), 655-658.

Prüfer, K., Racimo, F., Patterson, N., Jay, F., Sankararaman, S., Sawyer, S., . . . Pääbo, S. (2014). The complete genome sequence of a Neanderthal from the Altai Mountains. *Nature, 505*, 43-49.

Pye, S. R., Reid, D. M., Smith, R., Adams, J. E., Nelson, K., Silman, A. J., & O'Neill, T. W. (2004). Radiographic features of lumbar disc degeneration and self-reported back pain. *The Journal of Rheumatology, 31*(4), 753-758.

R Core Team. (2019). *R: A language and environment for statistical computing*. Retrieved from https://www.R-project.org/

Ragir, S. (1972). The early horizon in central California prehistory. *Contributions of the University of California Archaeological Research Facility, 15*.

Raichlen, D. A., Armstrong, H., & Lieberman, D. E. (2011). Calcaneus length determines running economy: implications for endurance running performance in modern humans and Neandertals. *Journal of Human Evolution, 60*(3), 299-308.

Rak, Y., & Arensburg, B. (1987). Kebara 2 Neanderthal pelvis: first look at a complete inlet. *American Journal of Physical Anthropology, 73*(2), 227-231.

Raxter, M. H., Ruff, C. B., Azab, A., Erfan, M., Soliman, M., & El-Sawaf, A. (2008). Stature estimation in ancient Egyptians: A new technique based on anatomical reconstruction of stature. *American Journal of Physical Anthropology, 136*(2), 147-155.

Reich, D., Green, R. E., Kircher, M., Krause, J., Patterson, N., Durand, E. Y., . . . Pääbo, S. (2010). Genetic history of an archaic hominin group from Denisova Cave in Siberia. *Nature, 468*, 1053-1060.

Relethford, J. H. (2001). *Genetics and the search for modern human origins*. New York: Wiley-Liss.

Reno, P. L. (2016). Evo-devo sheds light on mechanisms of human evolution: limb proportions and penile spines. In J. C. Boughner & C. Rolian (Eds.), *Developmental approaches to human evolution* (pp. 77-99). Hoboken, NJ: Wiley.

Reno, P. L., McCollum, M. A., Cohn, M. J., Meindl, R. S., Hamrick, M., & Lovejoy, C. O. (2008). Patterns of correlation and covariation of anthropoid distal forelimb segments correspond to Hoxd expression territories. *Journal of Experimental Zoology Part B: Molecular and Developmental Evolution, 310B*(3), 240-258.

Reyes-Centeno, H., Hubbe, M., Hanihara, T., Stringer, C., & Harvati, K. (2015). Testing modern human out-of-Africa dispersal models and implications for modern human origins. *Journal of Human Evolution, 87*, 95-106.

Rhoads, J. G., & Trinkaus, E. (1977). Morphometrics of the Neandertal talus. *American Journal of Physical Anthropology, 46*(1), 29-43.

Richter, D., Grün, R., Joannes-Boyau, R., Steele, T. E., Amani, F., Rué, M., . . . McPherron, S. P. (2017). The age of the hominin fossils from Jebel Irhoud, Morocco, and the origins of the Middle Stone Age. *Nature, 546*, 293-296.
Rightmire, G. P. (1996). The human cranium from Bodo, Ethiopia: evidence for speciation in the Middle Pleistocene? *Journal of Human Evolution, 31*(1), 21-39.
Rightmire, G. P. (1998). Human evolution in the Middle Pleistocene: the role of *Homo heidelbergensis*. *Evolutionary Anthropology, 6*(6), 218-227.
Rightmire, G. P. (2008). *Homo* in the Middle Pleistocene: hypodigms, variation, and species recognition. *Evolutionary Anthropology, 17*(1), 8-21.
Rightmire, G. P. (2009). Middle and later Pleistocene hominins in Africa and Southwest Asia. *Proceedings of the National Academy of Sciences USA, 106*(38), 16046-16050.
Rightmire, G. P., & Deacon, H. J. (1991). Comparative studies of late Pleistocene human remains from Klasies River Mouth, South Africa. *Journal of Human Evolution, 20*(2), 131-156.
Rightmire, G. P., Deacon, H. J., Schwartz, J. H., & Tattersall, I. (2006). Human foot bones from Klasies River main site, South Africa. *Journal of Human Evolution, 50*(1), 96-103.
Rissech, C., Estabrook, G. F., Cunha, E., & Malgosa, A. (2006). Using the acetabulum to estimate age at death of adult males. *Journal of Forensic Sciences, 51*(2), 213-229.
Roberts, M. B., Stringer, C. B., & Parfitt, S. A. (1994). A hominid tibia from Middle Pleistocene sediments at Boxgrove, UK. *Nature, 369*, 311-313.
Rodríguez, L., Carretero, J. M., García-González, R., Lorenzo, C., Gómez-Olivencia, A., Quam, R., . . . Arsuaga, J. L. (2016). Fossil hominin radii from the Sima de los Huesos Middle Pleistocene site (Sierra de Atapuerca, Spain). *Journal of Human Evolution, 90*, 55-73.
Rogers, T., & Saunders, S. (1994). Accuracy of sex determination using morphological traits of the human pelvis. *Journal of Forensic Sciences, 39*(4), 1047-1056.
Rolian, C. (2016). Tinkering with growth plates: a developmental simulation of limb bone evolution in hominoids. In J. C. Boughner & C. Rolian (Eds.), *Developmental approaches to human evolution* (Vol. 6, pp. 139-165).
Rolian, C. (2020). Endochondral ossification and the evolution of limb proportions. *Wiley Interdisciplinary Reviews: Developmental Biology*, e373.
Rolian, C., Lieberman, D. E., & Hallgrímsson, B. (2010). The coevolution of human hands and feet. *Evolution, 64*(6), 1558-1568.
Rosas, A., Agustina, B. L., García-Martínez, D., Torres-Tamayo, N., García-Tabernero, A., Pastor, J. F., . . . Bastir, M. (2020). Analyses of the neandertal patellae from El Sidrón (Asturias, Spain) with implications for the evolution of body form in *Homo*. *Journal of Human Evolution, 141*, 102738.
Rosas, A., Ferrando, A., Bastir, M., García-Tabernero, A., Estalrrich, A., Huguet, R., . . . de la Rasilla, M. (2017). Neandertal talus bones from El Sidrón site (Asturias, Spain): A 3D geometric morphometrics analysis. *American Journal of Physical Anthropology, 164*(2), 394-415.
Rosas, A., Martínez-Maza, C., Bastir, M., García-Tabernero, A., Lalueza-Fox, C., Huguet, R., . . . Fortea, J. (2006). Paleobiology and comparative morphology of a late Neandertal sample from El Sidrón, Asturias, Spain. *Proceedings of the National Academy of Sciences, 103*(51), 19266-19271.
Rose, M. D. (1984). A hominine hip bone, KNM-ER 3228, from East Lake Turkana, Kenya. *American Journal of Physical Anthropology, 63*(4), 371-378.

Roseman, C. C., & Auerbach, B. M. (2015). Ecogeography, genetics, and the evolution of human body form. *Journal of Human Evolution, 78*, 80-90.
Rosenberg, K. R. (1988). The functional significance of Neandertal pubic length. *Current Anthropology, 29*(4), 595-617.
Rosenberg, K. R. (1998). Morphological variation in West Asian postcrania. In T. Akazawa, K. Aoki, & O. Bar-Yosef (Eds.), *Neandertals and modern humans in Western Asia* (pp. 367-379). New York: Plenum Press.
Rosenberg, K. (2002). A Late Pleistocene human skeleton from Liujiang, China suggests regional population variation in sexual dimorphism in the human pelvis. *Variability and Evolution, 10*, 5-17.
Rosenberg, K. R., Zuné, L., & Ruff, C. B. (2006). Body size, body proportions, and encephalization in a Middle Pleistocene archaic human from northern China. *Proceedings of the National Academy of Sciences USA, 103*(10), 3552-3556.
Ross, A. H., & Konigsberg, L. W. (2002). New formulae for estimating stature in the Balkans. *Journal of Forensic Sciences, 47*(1), 165-167.
Ruff, C. (1987). Sexual dimorphism in human lower limb bone structure: relationship to subsistence strategy and sexual division of labor. *Journal of Human Evolution, 16*(5), 391-416.
Ruff, C. B. (1994). Morphological adaptation to climate in modern and fossil hominids. *American Journal of Physical Anthropology, 37*(S19), 65-107.
Ruff, C. B. (2000). Body size, body shape, and long bone strength in modern humans. *Journal of Human Evolution, 38*(2), 269-290.
Ruff, C. B. (2002). Variation in human body size and shape. *Annual Review of Anthropology, 31*, 211-232.
Ruff, C. B. (2003). Long bone articular and diaphyseal structure in Old World monkeys and apes. II: Estimation of body mass. *American Journal of Physical Anthropology, 120*(1), 16-37.
Ruff, C. B. (2005). Mechanical determinants of bone form: insights from skeletal remains. *Journal of Musculoskeletal and Neuronal Interactions, 5*(3), 202-212.
Ruff, C. B. (2010). Body size and body shape in early hominins – implications of the Gona pelvis. *Journal of Human Evolution, 58*(2), 166-178.
Ruff, C. B., Burgess, M. L., Squyres, N., Junno, J.-A., & Trinkaus, E. (2018). Lower limb articular scaling and body mass estimation in Pliocene and Pleistocene hominins. *Journal of Human Evolution, 115*, 85-111.
Ruff, C. B., Holt, B. M., Niskanen, M., Sladék, V., Berner, M., Garofalo, E., . . . Tompkins, D. (2012). Stature and body mass estimation from skeletal remains in the European Holocene. *American Journal of Physical Anthropology, 148*(4), 601-617.
Ruff, C. B., Holt, B. M., Sládek, V., Berner, M., Murphy Jr, W. A., zur Nedden, D., . . . Recheis, W. (2006). Body size, body proportions, and mobility in the Tyrolean "Iceman". *Journal of Human Evolution, 51*(1), 91-101.
Ruff, C. B., & Larsen, C. S. (2014). Long bone structural analyses and the reconstruction of past mobility: a historical review. In K. Carlson & D. Marchi (Eds.), *Reconstructing Mobility* (pp. 13-29). Boston, MA: Springer.
Ruff, C. B., Scott, W. W., & Liu, A. Y. C. (1991). Articular and diaphyseal remodeling of the proximal femur with changes in body mass in adults. *American Journal of Physical Anthropology, 86*(3), 397-413.

Ruff, C. B., Trinkaus, E., & Holliday, T. W. (1997). Body mass and encephalization in Pleistocene *Homo*. *Nature, 387*(6629), 173-176.

Ruff, C. B., Trinkaus, E., Walker, A., & Larsen, C. S. (1993). Postcranial robusticity in *Homo*. I: Temporal trends and mechanical interpretation. *American Journal of Physical Anthropology, 91*(1), 21-53.

Sahle, Y., Beyene, Y., Defleur, A., Asfaw, B., WoldeGabriel, G., Hart, W. K., . . . White, T. D. (2019a). Revisiting Herto: new evidence of *Homo sapiens* from Ethiopia. In Y. Sahle, H. Reyes-Centeno, & C. Bentz (Eds.), *Modern human origins and dispersal*. Tübingen, Germany: Kerns Verlag.

Sahle, Y., Beyene, Y., Defleur, A., Asfaw, B., WoldeGabriel, G., Hart, W. K., . . . White, T. D. (2019b). Human emergence: perspectives from Herto, Afar Rift, Ethiopia. In Y. Sahle, H. Reyes-Centeno, & C. Bentz (Eds.), *Modern human origins and dispersal*. Tübingen, Germany: Kerns Verlag.

Salas, A., Richards, M., De la Fe, T., Lareu, M.-V., Sobrino, B., Sánchez-Diz, P., . . . Carracedo, Á. (2002). The making of the African mtDNA landscape. *American Journal of Human Genetics, 71*(5), 1082-1111.

Sánchez-Quinto, F., & Lalueza-Fox, C. (2015). Almost 20 years of Neanderthal palaeogenetics: adaptation, admixture, diversity, demography and extinction. *Philosophical Transactions of the Royal Society B: Biological Sciences, 370*(1660), 20130374.

Santa Luca, A. P. (1980). The Ngandong fossil hominids: a comparative study of a far eastern *Homo erectus* group. *78*, 1-175.

Saunders, S. R., Fitzgerald, C., Rogers, T., Dudar, C., & McKillop, H. (1992). A test of several methods of skeletal age estimation using a documented archaeological sample. *Canadian Society of Forensic Science Journal, 25*(2), 97-118.

Savell, K. R. R., Auerbach, B. M., & Roseman, C. C. (2016). Constraint, natural selection, and the evolution of human body form. *Proceedings of the National Academy of Sciences USA, 113*(34), 9492-9497.

Sawyer, G., & Maley, B. (2005). Neanderthal reconstructed. *The Anatomical Record, 283B*(1), 23-31.

Scerri, E. M., Thomas, M. G., Manica, A., Gunz, P., Stock, J. T., Stringer, C., . . . Chikhi, L. (2018). Did our species evolve in subdivided populations across Africa, and why does it matter? *Trends in Ecology & Evolution, 33*(8), 582-594.

Schlebusch, C. M., & Jakobsson, M. (2018). Tales of human migration, admixture, and selection in Africa. *Annual Review of Genomics and Human Genetics, 19*, 405-428.

Schlebusch, C. M., Malmström, H., Günther, T., Sjödin, P., Coutinho, A., Edlund, H., . . . Jakobsson, M. (2017). Southern African ancient genomes estimate modern human divergence to 350,000 to 260,000 years ago. *Science, 358*(6363), 652-655.

Schlebusch, C. M., Skoglund, P., Sjödin, P., Gattepaille, L. M., Hernandez, D., Jay, F., . . . Jakobsson, M. (2012). Genomic variation in seven Khoe-San groups reveals adaptation and complex African history. *Science, 338*, 374-379.

Schwartz, J. H., & Tattersall, I. (2000). The human chin revisited: what is it and who has it? *Journal of Human Evolution, 38*(3), 367-409.

Schwartz, J. H., & Tattersall, I. (2010). Fossil evidence for the origin of *Homo sapiens*. *American Journal of Physical Anthropology, 143*(S51), 94-121.

Schwitalla, A. W. (2010). *The Medieval Climatic Anomaly in central California: Environmental imperatives reconsidered from a bioarchaeological perspective.* (M.A.). California State University, Sacramento.
Scott, G. R., Irish, J. D., & Martinón-Torres, M. (2020). A more comprehensive view of the Denisovan 3-rooted lower second molar from Xiahe. *Proceedings of the National Academy of Sciences, 117*(1), 37-38.
Shang, H., Tong, H., Zhang, S., Chen, F., & Trinkaus, E. (2007). An early modern human from Tianyuan Cave, Zhoukoudian, China. *Proceedings of the National Academy of Sciences, 104*(16), 6573-6578.
Shang, H., & Trinkaus, E. (2010). *The early modern human from Tianyuan Cave, China*. College Station: Texas A&M University Press.
Shaw, C. N., & Stock, J. T. (2009). Intensity, repetitiveness, and directionality of habitual adolescent mobility patterns influence the tibial diaphysis morphology of athletes. *American Journal of Physical Anthropology, 140*(1), 149-159.
Shaw, C. N., & Stock, J. T. (2011). The influence of body proportions on femoral and tibial midshaft shape in hunter-gatherers. *American Journal of Physical Anthropology, 144*(1), 22-29.
Sholts, S. B., Wärmländer, S. K. T. S., Flores, L. M., Miller, K. W. P., & Walker, P. L. (2010). Variation in the measurement of cranial volume and surface area using 3D laser scanning technology. *Journal of Forensic Sciences, 55*(4), 871-876.
Sigmon, B. A. (1982). Comparative morphology of the locomotor skeleton of *Homo erectus* and the other fossil hominids, with special reference to the Tautavel innominate and femora. In *1er Congrès International de Paléontologie Humaine, Nice L'Homo erectus et la place de l'homme de Tautavel parmi les Hominidés fossiles* (pp. 422-446). Nice: CNRS.
Simmons, T., Jantz, R. L., & Bass, W. (1990). Stature estimation from fragmentary femora: A revision of the Steele method. *Journal of Forensic Sciences, 35*(3), 628-636.
Simpson, S. W., Quade, J., Levin, N. E., Butler, R., Dupont-Nivet, G., Everett, M., & Semaw, S. (2008). A female *Homo erectus* pelvis from Gona, Ethiopia. *Science, 322*, 1089-1092.
Sjøvold, T. (1990). Estimation of stature from long bones utilizing the line of organic correlation. *Human Evolution, 5*(5), 431-447.
Skoglund, P., & Mathieson, I. (2018). Ancient genomics of modern humans: the first decade. *Annual Review of Genomics and Human Genetics, 19*, 381-404.
Smith, F. H. (2002). Migrations, radiations and continuity: Patterns in the evolution of Middle and Late Pleistocene humans. In W. C. Hartwig (Ed.), *The primate fossil record* (pp. 437-456). Cambridge: Cambridge University Press.
Smith, F. H., Falsetti, A. B., & Donnelly, S. M. (1989). Modern human origins. *American Journal of Physical Anthropology, 32*(S10), 35-68.
Smith, S. L. (2000). Shape variation of the human pollical distal phalanx and metacarpal. *American Journal of Physical Anthropology, 113*(3), 329-348.
Soficaru, A., Doboş, A., & Trinkaus, E. (2006). Early modern humans from the Peştera Muierii, Baia de Fier, Romania. *Proceedings of the National Academy of Sciences USA, 103*(46), 17196-17201.
Solan, M., & Day, M. (1992). The Baringo (Kapthurin) ulna. *Journal of Human Evolution, 22*(4-5), 307-313.

Sorrentino, R., Stephens, N. B., Carlson, K. J., Figus, C., Fiorenza, L., Frost, S., . . . Benazzi, S. (2020). The influence of mobility strategy on the modern human talus. *American Journal of Physical Anthropology, 171*(3), 456-469.
Sparacello, V., & Marchi, D. (2008). Mobility and subsistence economy: a diachronic comparison between two groups settled in the same geographical area (Liguria, Italy). *American Journal of Physical Anthropology, 136*(4), 485-495.
Stock, J., & Pfeiffer, S. (2001). Linking structural variability in long bone diaphyses to habitual behaviors: foragers from the southern African Later Stone Age and the Andaman Islands. *American Journal of Physical Anthropology, 115*(4), 337-348.
Stock, J. T. (2006). Hunter-gatherer postcranial robusticity relative to patterns of mobility, climatic adaptation, and selection for tissue economy. *American Journal of Physical Anthropology, 131*(2), 194-204.
Stringer, C. (1986). An archaic character in the Broken Hill innominate E. 719. *American Journal of Physical Anthropology, 71*(1), 115-120.
Stringer, C. (1992). Reconstructing recent human evolution. *Philosophical Transactions of the Royal Society B, 337*(1280), 217-224.
Stringer, C. (2001). Modern human origins—distinguishing the models. *African Archaeological Review, 18*(2), 67-75.
Stringer, C. (2002). Modern human origins: progress and prospects. *Philosophical Transactions of the Royal Society B, 357*(1420), 563-579.
Stringer, C. (2012). The status of *Homo heidelbergensis* (Schoetensack 1908). *Evolutionary Anthropology, 21*(3), 101-107.
Stringer, C. (2014). Why we are not all multiregionalists now. *Trends in Ecology & Evolution, 29*(5), 248-251.
Stringer, C. (2016). The origin and evolution of *Homo sapiens*. *Philosophical Transactions of the Royal Society B, 371*(1698), 20150237.
Stringer, C., & Andrews, P. (1988). Genetic and fossil evidence for the origin of modern humans. *Science, 239*(4845), 1263-1268.
Stringer, C., & Buck, L. T. (2014). Diagnosing *Homo sapiens* in the fossil record. *Annals of Human Biology, 41*(4), 312-322.
Stringer, C., Howell, F. C., & Melentis, J. K. (1979). The significance of the fossil hominid skull from Petralona, Greece. *Journal of Archaeological Science, 6*(3), 235-253.
Stringer, C., Trinkaus, E., Roberts, M. B., Parfitt, S. A., & Macphail, R. I. (1998). The Middle Pleistocene human tibia from Boxgrove. *Journal of Human Evolution, 34*(5), 509-547.
Stulp, G., & Barrett, L. (2016). Evolutionary perspectives on human height variation. *Biological Reviews, 91*(1), 206-234.
Sulzmann, C. E., Buckberry, J. L., & Pastor, R. F. (2008). The utility of carpals for sex assessment: a preliminary study. *American Journal of Physical Anthropology, 135*(3), 252-262.
Sylvester, A. D., Kramer, P. A., & Jungers, W. L. (2008). Modern humans are not (quite) isometric. *American Journal of Physical Anthropology, 137*(4), 371-383.
Tague, R. G. (2000). Do big females have big pelves? *American Journal of Physical Anthropology, 112*(3), 377-393.
Tanaka, H., Lestrel, P. E., Uetake, T., Kato, S., & Ohtsuki, F. (2000). Sex differences in proximal humeral outline shape: elliptical Fourier functions. *Journal of Forensic Science, 45*(2), 292-302.

Tappen, M. (1994). Bone weathering in the tropical rain forest. *Journal of Archaeological Science, 21*(5), 667-673.
Tattersall, I. (2009). Human origins: out of Africa. *Proceedings of the National Academy of Sciences USA, 106*(38), 16018-16021.
Tattersall, I., & Schwartz, J. H. (2008). The morphological distinctiveness of *Homo sapiens* and its recognition in the fossil record: clarifying the problem. *Evolutionary Anthropology, 17*(1), 49-54.
Thoma, A. (1975). Were the Spy fossils evolutionary intermediates between classic Neandertal and modern man? *Journal of Human Evolution, 4*(5), 387-410.
Thoma, A. (1984). Morphology and affinities of the Nazlet Khater man. *Journal of Human Evolution, 13*(3), 287-296.
Thorne, A. G., & Wolpoff, M. H. (1992). The multiregional evolution of humans. *Scientific American, 266*(4), 76-83.
Thorne, B. L., & Kimsey, R. B. (1983). Attraction of neotropical *Nasutitermes* termites to carrion. *Biotropica, 15*(4), 295-296.
Tickle, C. (2015). How the embryo makes a limb: determination, polarity and identity. *Journal of Anatomy, 227*(4), 418-430.
Tickle, C., & Towers, M. (2017). Sonic hedgehog signaling in limb development. *Frontiers in Cell and Developmental Biology, 5*, 14.
Tishkoff, S. A., Reed, F. A., Friedlaender, F. R., Ehret, C., Ranciaro, A., Froment, A., . . . Williams, S. M. (2009). The genetic structure and history of Africans and African Americans. *Science, 324*(5930), 1035-1044.
Tobias, P. V. (1971). Human skeletal remains from the Cave of Hearths, Makapansgat, northern Transvaal. *American Journal of Physical Anthropology, 34*(3), 335-367.
Todd, T. W. (1920). Age changes in the pubic bone. I. The male white pubis. *American Journal of Physical Anthropology, 3*(3), 285-334.
Tompkins, R. L., & Trinkaus, E. (1987). La Ferrassie 6 and the development of Neandertal pubic morphology. *American Journal of Physical Anthropology, 73*(2), 233-239.
Trinkaus, E. (1975a). *A functional analysis of the Neanderthal foot.* (Ph.D.). University of Pennsylvania, Pennsylvania.
Trinkaus, E. (1975b). Squatting among the Neandertals: a problem in the behavioral interpretation of skeletal morphology. *Journal of Archaeological Science, 2*(4), 327-351.
Trinkaus, E. (1976a). The evolution of the hominid femoral diaphysis during the Upper Pleistocene in Europe and the Near East. *Zeitschrift für Morphologie und Anthropologie, 67*(3), 291-319.
Trinkaus, E. (1976b). The morphology of European and Southwest Asian Neandertal pubic bones. *American Journal of Physical Anthropology, 44*(1), 95-103.
Trinkaus, E. (1977). A functional interpretation of the axillary border of the Neandertal scapula. *Journal of Human Evolution, 6*(3), 231-234.
Trinkaus, E. (1978). Les métarsiens et les phalanges du pied des Néandertaliens de Spy. *Bulletin de l'Institut Royale Science Naturelle de Belgique, 51*(7), 1-18.
Trinkaus, E. (1983a). Functional aspects of Neandertal pedal remains. *Foot & Ankle, 3*(6), 377-390.
Trinkaus, E. (1983b). *The Shanidar Neandertals*. New York: Academic Press.
Trinkaus, E. (1984). Neandertal pubic morphology and gestation length. *Current Anthropology, 25*(4), 509-514.

Trinkaus, E. (1990). Cladistics and the hominid fossil record. *American Journal of Physical Anthropology, 83*(1), 1-11.
Trinkaus, E. (1993a). Femoral neck-shaft angles of the Qafzeh-Skhul early modern humans, and activity levels among immature Near Eastern Middle Paleolithic hominids. *Journal of Human Evolution, 25*(5), 393-416.
Trinkaus, E. (1993b). A note on the KNM-ER 999 hominid femur. *Journal of Human Evolution, 24*(6), 493-504.
Trinkaus, E. (1997). Appendicular robusticity and the paleobiology of modern human emergence. *Proceedings of the National Academy of Sciences USA, 94*(24), 13367-13373.
Trinkaus, E. (2000). Human patellar articular proportions: recent and Pleistocene patterns. *The Journal of Anatomy, 196*(3), 473-483.
Trinkaus, E. (2005). Early modern humans. *Annual Review of Anthropology, 34*, 207-230.
Trinkaus, E. (2006a). The Krapina scapulae. *Periodicum Biologorum, 108*(3), 341-351.
Trinkaus, E. (2006b). Modern human versus Neandertal evolutionary distinctiveness. *Current Anthropology, 47*(4), 597-620.
Trinkaus, E. (2008). Kiik-Koba 2 and Neandertal axillary border ontogeny. *Anthropological Science, 116*(3), 231-236.
Trinkaus, E. (2009). The human tibia from Broken Hill, Kabwe, Zambia. *PaleoAnthropology, 2009*, 145-165.
Trinkaus, E. (2011). The postcranial dimensions of the La Chapelle-aux-Saints 1 Neandertal. *American Journal of Physical Anthropology, 145*(3), 461-468.
Trinkaus, E. (2012). Brief communication: the human humerus from the Broken Hill Mine, Kabwe, Zambia. *American Journal of Physical Anthropology, 149*(2), 312-317.
Trinkaus, E. (2016). The evolution of the hand in Pleistocene Homo. In T. L. Kivell, P. Lemelin, B. G. Richmond, & D. Schmitt (Eds.), *The Evolution of the Primate Hand* (pp. 545-571): Springer.
Trinkaus, E. (2016). *The Krapina human postcranial remains: morphology, morphometrics and paleopathology*. Zagreb: FF Press.
Trinkaus, E., Buzhilova, A. P., Mednikova, M. B., & Dobrovolskaia, M. V. (2014). *The people of Sunghir: burials, bodies, and behavior in the earlier Upper Paleolithic*. New York: Oxford University Press.
Trinkaus, E., & Churchill, S. E. (1988). Neandertal radial tuberosity orientation. *American Journal of Physical Anthropology, 75*(1), 15-21.
Trinkaus, E., & Churchill, S. E. (1999). Diaphyseal cross-sectional geometry of Near Eastern Middle Palaeolithic humans: the humerus. *Journal of Archaeological Science, 26*(2), 173-184.
Trinkaus, E., Churchill, S. E., Ruff, C. B., & Vandermeersch, B. (1999a). Long bone shaft robusticity and body proportions of the Saint-Césaire 1 Châtelperronian Neanderthal. *Journal of Archaeological Science, 26*(7), 753-773.
Trinkaus, E., Haduch, E., Valde-Nowak, P. W., & Wojtal, P. (2014). The Obłazowa 1 early modern human pollical phalanx and Late Pleistocene distal thumb proportions. *Homo, 65*, 1-12.
Trinkaus, E., Mednikova, M. B., & Cowgill, L. W. (2016). The appendicular remains of the Kiik-Koba 2 Neandertal infant. *PaleoAnthropology*, 185-210.

Trinkaus, E., & Rhoads, M. L. (1999). Neandertal knees: power lifters in the Pleistocene? *Journal of Human Evolution, 37*(6), 833-859.
Trinkaus, E., & Ruff, C. B. (2012). Femoral and tibial diaphyseal cross-sectional geometry in Pleistocene *Homo*. *PaleoAnthropology*, 13-62.
Trinkaus, E., Ruff, C. B., & Conroy, G. C. (1999b). The anomalous archaic *Homo* femur from Berg Aukas, Namibia: a biomechanical assessment. *American Journal of Physical Anthropology, 110*(3), 379-391.
Trinkaus, E., Smith, F. H., Stockton, T. C., & Shackelford, L. L. (2006). The human postcranial remains from Mladeč. In *Early modern humans at the Moravian gate* (pp. 385-445). Vienna: Springer Verlag.
Trinkaus, E., Stringer, C. B., Ruff, C. B., Hennessy, R. J., Roberts, M. B., & Parfitt, S. A. (1999c). Diaphyseal cross-sectional geometry of the Boxgrove 1 Middle Pleistocene human tibia. *Journal of Human Evolution, 37*(1), 1-25.
Underhill, P. A., Passarino, G., Lin, A. A., Shen, P., Lahr, M. M., Foley, R. A., . . . Cavalli-Sforza, L. L. (2001). The phylogeography of Y chromosome binary haplotypes and the origins of modern human populations. *Annals of Human Genetics, 65*(1), 43-62.
Underhill, P. A., Shen, P., Lin, A. A., Jin, L., Passarino, G., Yang, W. H., . . . Oefner, P. J. (2000). Y chromosome sequence variation and the history of human populations. *Nature Genetics, 26*, 358-361.
Vandermeersch, B. (1981). *Les hommes fossiles de Qafzeh (Israël)*. Paris: Centre National de la Recherche Scientifique.
Vandermeersch, B., & Trinkaus, E. (1995). The postcranial remains of the Régourdou 1 Neandertal: the shoulder and arm remains. *Journal of Human Evolution, 28*(5), 439-476.
Villmoare, B. (2018). Early *Homo* and the role of the genus in paleoanthropology. *American Journal of Physical Anthropology, 165*(S65), 72-89.
Villotte, S., & Knüsel, C. J. (2013). Understanding entheseal changes: definition and life course changes. *International Journal of Osteoarchaeology, 23*(2), 135-146.
Voisin, J. L. (2001). Évolution de la morphologie claviculaire au sein du genre *Homo*. Conséquences architecturales et fonctionnelles sur la ceinture scapulaire. *L'Anthropologie, 105*(4), 449-468.
Voisin, J. L. (2006a). Clavicle, a neglected bone: morphology and relation to arm movements and shoulder architecture in primates. *The Anatomical Record, 288A*(9), 944-953.
Voisin, J. L. (2006b). Krapina and other Neanderthal clavicles: A peculiar morphology? *Periodicum Biologorum, 108*(3), 331-339.
Voisin, J. L. (2008). The Omo I hominin clavicle: archaic or modern? *Journal of Human Evolution, 55*(3), 438-443.
von Cramon-Taubadel, N. (2011). Global human mandibular variation reflects differences in agricultural and hunter-gatherer subsistence strategies. *Proceedings of the National Academy of Sciences, 108*(49), 19546-19551.
Waddle, D. M. (1994). Matrix correlation tests support a single origin for modern humans. *Nature, 368*(6470), 452-454.
Walker, A., & Leakey, R. (1993). *The Nariokotome Homo erectus skeleton*. Cambridge: Harvard University Press.
Walker, M. J., Ortega, J., López, M. V., Parmová, K., & Trinkaus, E. (2011a). Neandertal postcranial remains from the Sima de las Palomas del Cabezo Gordo, Murcia, southeastern Spain. *American Journal of Physical Anthropology, 144*(4), 505-515.

Walker, M. J., Ortega, J., Parmová, K., López, M. V., & Trinkaus, E. (2011b). Morphology, body proportions, and postcranial hypertrophy of a female Neandertal from the Sima de las Palomas, southeastern Spain. *Proceedings of the National Academy of Sciences, 108*(25), 10087-10091.
Wang, Q., Tobias, P. V., Roberts, D. L., & Jacobs, Z. (2008). A re-examination of a human femur found at the Blind River Site, East London, South Africa: Its age, morphology, and breakage pattern. *Anthropological Review, 71*, 43-61.
Wang, Y., Videman, T., & Battié, M. C. (2012). Lumbar vertebral endplate lesions: prevalence, classification, and association with age. *Spine, 37*(17), 1432-1439.
Weaver, T. D. (2003). The shape of the Neandertal femur is primarily the consequence of a hyperpolar body form. *Proceedings of the National Academy of Sciences, 100*(12), 6926-6929.
Weaver, T. D. (2009). The meaning of Neandertal skeletal morphology. *Proceedings of the National Academy of Sciences USA, 106*(38), 16028-16033.
Weaver, T. D. (2012). Did a discrete event 200,000–100,000 years ago produce modern humans? *Journal of Human Evolution, 63*(1), 121-126.
Weidenreich, F. (1941). The extremity bones of *Sinanthropus pekinensis*. *Palaeontologica Sinica, New Series D, 5*, 1-150.
Weiss, K. (2017). What is a biological 'trait'? *Building Bones: Bone Formation and Development in Anthropology*, 13-25.
Wells, L. H. (1935). A fossilized human femur from East London. *South African Journal of Science, 32*(7), 596-600.
White, C. D., Longstaffe, F. J., & Law, K. R. (1999). Seasonal stability and variation in diet as reflected in human mummy tissues from the Kharga Oasis and the Nile Valley. *Palaeogeography, Palaeoclimatology, Palaeoecology, 147*(3-4), 209-222.
White, T. D. (1986). Cut marks on the Bodo cranium: a case of prehistoric defleshing. *American Journal of Physical Anthropology, 69*(4), 503-509.
White, T. D. (2003). Early Hominids--Diversity or Distortion? *Science, 299*(5615), 1994-1997.
White, T. D., Asfaw, B., DeGusta, D., Gilbert, H., Richards, G. D., Suwa, G., & Howell, F. C. (2003). Pleistocene *Homo sapiens* from Middle Awash, Ethiopia. *Nature, 423*, 742-747.
White, T. D., Black, M. T., & Folkens, P. A. (2012). *Human Osteology*. San Diego: Academic Press.
Whyte, T. R. (2001). Distinguishing remains of human cremations from burned animal bones. *Journal of Field Archaeology, 28*(3-4), 437-448.
Wickham, H. (2016). *ggplot2: elegant graphics for data analysis*. New York: Springer.
Williams, F. M. K., Manek, N. J., Sambrook, P. N., Spector, T. D., & Macgregor, A. J. (2007). Schmorl's nodes: common, highly heritable, and related to lumbar disc disease. *Arthritis Care & Research, 57*(5), 855-860.
Wolf, A. B., & Akey, J. M. (2018). Outstanding questions in the study of archaic hominin admixture. *PLoS Genetics, 14*(5), e1007349.
Wolpoff, M. H. (1989). Multiregional evolution: the fossil alternative to Eden. In P. Mellars & C. Stringer (Eds.), *The human revolution* (pp. 62-108). Edinburgh: Edinburgh University Press.
Wolpoff, M. H. (2002). Comment on A diffusion wave out of Africa: the mechanism of the modern human revolution? *Current Anthropology, 43*(5), 768-769.

Wolpoff, M. H., & Caspari, R. (1997). *Race and human evolution*. New York: Simon and Schuster.
Woo, J.-K. (1959). Human fossils found in Liukiang, Kwangsi, China. *Vertebrata PalAsiatica, 3*(3), 109-118.
Woodward, A. S. (1921). A new cave man from Rhodesia, South Africa. *Nature, 108*, 371-372.
Wrobel, G. D., & Biggs, J. (2018). Osteophageous insect damage on human bone from Je'reftheel, a Maya mortuary cave site in west-central Belize. *International Journal of Osteoarchaeology, 28*(6), 745-756.
Wu, X., & Poirier, F. E. (1995). *Human evolution in China: a metric description of the fossils and a review of the sites*. New York: Oxford University Press.
Wylie, F. R., Walsh, G. L., & Yule, R. A. (1987). Insect damage to aboriginal relics at burial and rock-art sites near Carnarvon in central Queensland. *Australian Journal of Entomology, 26*(4), 335-345.
Yellen, J., Brooks, A., Helgren, D., Tappen, M., Ambrose, S., Bonnefille, R., . . . Stewart, K. (2005). The archaeology of Aduma Middle Stone Age sites in the Awash Valley, Ethiopia. *PaleoAnthropology, 10*, 25-100.
Yokley, T. R., & Churchill, S. E. (2006). Archaic and modern human distal humeral morphology. *Journal of Human Evolution, 51*(6), 603-616.
Young, N. M., & Capellini, T. D. (2016). Out on a limb: development and the evolution of the human appendicular skeleton. In J. C. Boughner & C. Rolian (Eds.), *Developmental approaches to human evolution* (pp. 101-138). Hoboken, NJ: Wiley.
Young, N. M., Wagner, G. P., & Hallgrímsson, B. (2010). Development and the evolvability of human limbs. *Proceedings of the National Academy of Sciences USA, 107*(8), 3400-3405.
Zelzer, E., Blitz, E., Killian, M. L., & Thomopoulos, S. (2014). Tendon-to-bone attachment: from development to maturity. *Birth Defects Research Part C: Embryo Today: Reviews, 102*(1), 101-112.

**Appendix 1** Inventory of HAL-VP-9/1 skeletal elements

A "Y" in the right-hand column indicates specimens with evidence that adjacent elements remained in postmortem articulation until surface exposure, erosion, and surface scattering. Subchondral joint surfaces in such specimens retain adhering carbonate with the natural impression (mold) of the opposing articulating element. Some such specimens actually even retain exfoliated bone from the originally articulating element embedded in the interarticular matrix. Where determinable, the number of the element originally articulated is provided in parentheses.

| Suffix | Element | Element portion | $CaCO_3$ cast or bone of adjacent element |
|---|---|---|---|
| 1A | R. + L. FRO | – | |
| 1B | R. + L. FRO + PAR + OCC | – | |
| 2 | R. TEM + PAR | Frag. | |
| 3 | R. TEM + SPH | w/ TMJ | |
| 4 | L. TEM | Frag. | |
| 5 | L. TEM | Lat. TMJ | |
| 6 | L. OCC | Frag. | |
| 7 | L. OCC | Basioccipital? | |
| 8 | OCC or SPH | Frag. | |
| 9 | SPH | Frag. | |
| 10 | R + L. FRO + NAS | Frag. | |
| 11 | L. TEM + PAR | Frag. | |
| 12 | R. ZYG + MAX | Frag. | |
| 13 | R. MAX | Roots I2-M1 | |
| 14 | R. MAX + SPH | Roots M2-3 | |
| 15 | L. MAX | I roots | |
| 16 | L. MAX + PAL | M1-3 roots | |
| 17 | R. MAN | Condyle | |
| 18 | R. MAN | Gonial angle | |
| 19 | R. MAN | Ramus frag. | |
| 20 | R. MAN | Lateral corpus | |
| 21 | R. + L. MAN | Corpus w/ R. I1-2 roots and mentum osseum | |
| 22 | CRA frags. | N = 24 | |
| 23 | Axis VER | Ant. midline, no dens | |
| 24 | Cervical VER | Body | |
| 25 | Cervical VER | Body | |
| 26 | Cervical VER | Body with R. pedicle | |
| 27 | Cervical VER | Body | |
| 28 | R. cervical VER | Partial pedicle and lamina | |
| 29 | Cervical VER (?7) | Spinous process | |
| 30 | Thoracic VER (upper) | Body | Y |

| Suffix | Element | Element portion | $CaCO_3$ cast or bone of adjacent element |
|---|---|---|---|
| 31 | Thoracic VER | Body | |
| 32 | Thoracic VER | Body | Y |
| 33 | Thoracic VER | Body, partial | |
| 34 | Thoracic VER | Body, partial | |
| 35 | Thoracic VER | R. body, pedicle | |
| 36 | Thoracic VER | Body frag. | |
| 37 | Thoracic VER | Body frag. | |
| 38 | Thoracic VER | Partial spinous process | |
| 39 | Thoracic VER | Partial spinous process (R. lamina) | |
| 40 | Thoracic VER | Spinous process (R. lamina) | |
| 41 | Thoracic VER | Spinous process terminus | |
| 42 | Thoracic VER | Spinous process terminus | |
| 43 | Thoracic VER | L. partial transverse process | |
| 44 | Thoracic VER | R. transverse process, partial lamina | Y |
| 45 | Thoracic VER | R. partial transverse process | |
| 46 | Thoracic VER + R. rib head | Root of R. transverse process | Y |
| 47 | Thoracic VER | Root of L. transverse process w/ rib frag. | Y |
| 48 | Thoracic VER | R. partial transverse process | |
| 49 | Lumbar VER | Body, R. pedicle | |
| 50 | Lumbar VER | Body, R. arch | |
| 51 | Lumbar VER | Partial body | |
| 52 | Lumbar VER | Body, R. partial arch | |
| 53 | Lumbar VER | Body | |
| 54 | Lumbar VER | L. partial lamina w/ inferior facet | |
| 55 | Lumbar VER | Partial spinous process | |
| 56 | Lumbar VER | R. partial inferior facet | |
| 57 | Sacral VER | R. partial ala | |
| 58 | Sacral VER | L. partial ala | |
| 59 | Sacral VER | Partial bodies (n=2) | |
| 60 | VER fragments | N = 6 | |
| 61 | R. rib | Head | |
| 62 | R. rib | Head | |
| 63 | R. rib | Neck | |
| 64 | R. rib | Neck | |
| 65 | R. rib | Neck | |
| 66 | R. rib | Neck | |
| 67 | R. rib | Shaft at costal angle | Y |
| 68 | R. rib | Shaft at costal angle | |
| 69 | R. rib | Shaft at costal angle | |
| 70 | R. rib | Shaft frag. | |
| 71 | R. rib | Shaft frag. | |

| Suffix | Element | Element portion | $CaCO_3$ cast or bone of adjacent element |
|---|---|---|---|
| 72 | R. rib | Shaft frag. | |
| 73 | R. rib | Shaft frag. | |
| 74 | R. rib | Shaft frag. | |
| 75 | R. rib | Shaft frag. | |
| 76 | R. rib | Sternal end | |
| 77 | R. rib | Sternal end | |
| 78 | R. rib | Sternal end | |
| 79 | L. rib | Head | Y |
| 80 | L. rib | Shaft at costal angle | |
| 81 | L. rib | Shaft at costal angle | Y |
| 82 | L. rib | Shaft at costal angle | |
| 83 | L. rib | Shaft at costal angle | |
| 84 | L. rib | Shaft frag. | |
| 85 | L. rib | Shaft frag. | |
| 86 | L. rib | Shaft frag. | |
| 87 | L. rib | Shaft frag. | |
| 88 | L. rib | Shaft frag. | |
| 89 | L. rib | Shaft frag. | |
| 90 | L. rib | Shaft frag. | |
| 91 | L. rib | Shaft frag. | |
| 92 | L. rib | Shaft frag. | |
| 93 | L. rib | Sternal end | |
| 94 | L. rib | Sternal end | |
| 95 | Rib shaft frags; side indet. | N = 62 | |
| 96 | R. CLA | Acromial end | |
| 97 | L. CLA | Shaft near sternal end | |
| 98 | CLA | Shaft frag. | |
| 99 | ? CLA | Shaft frag. | |
| 100 | R. SCA | Acromion and spine | |
| 101 | R. SCA | Partial glenoid | |
| 102 | R. SCA | Axillary border | |
| 103 | R. SCA | Inferior angle | |
| 104 | L. SCA | Partial acromion | |
| 105 | L. SCA | Inferior angle | |
| 106A | R. OCX | Lower portion | |
| 106B | R. OCX | Upper portion | |
| 107 | R. OCX | Top of Iliac pillar, with gluteal line | |
| 108 | L. OCX | Ischium with acetabular frag. | |
| 109 | L. OCX | Ischiopubic ramus | |
| 110 | OCX | Acetabular frag. | |
| 111 | ?R. OCX | Iliac blade frag. | |

| Suffix | Element | Element portion | $CaCO_3$ cast or bone of adjacent element |
|---|---|---|---|
| 112 | R. HUM | Head | |
| 113 | R. HUM | Dist. end with shaft | |
| 114 | ? L. HUM | Shaft frag. w/deltoid | |
| 115 | L. HUM | Prox. end | |
| 116 | L. HUM | Partial distal end | |
| 117 | L. HUM | Partial shaft | |
| 118 | HUM | Shaft frag. | |
| 119 | R. RAD | Head | |
| 120 | RAD | Shaft frag. | |
| 121 | R. ULN | Proximal end | Y (-119) |
| 122 | R. ULN | Shaft | |
| 123 | L. ULN | Partial proximal end | |
| 124 | L. ULN | Distal end | Y |
| 125 | L. ULN | Partial shaft | |
| 126 | ULN | Shaft frag. | |
| 127 | ? ULN | Shaft frag. | |
| 128 | R. HAM | – | Y (-130) |
| 129 | R. Trapezium | – | Y |
| 130 | R. TRI | – | |
| 131 | L. LUN | – | Y (-132) |
| 132 | L. CAP | – | Y |
| 133 | L. TRI | – | |
| 134 | R. MC2 | Base | Y |
| 135 | R. MC2 | Head + partial shaft | Y |
| 136 | R. MC3 | – | Y |
| 137 | R. MC4 | Base + shaft | Y |
| 138 | L. MC1 | Head | |
| 139 | L. MC2 | Base | Y |
| 140 | L. MC2 | Head | |
| 141 | L. MC4 | Head + shaft | Y |
| 142 | L. MC5 | Base + shaft | |
| 143 | R. MC5 | Head | Y |
| 144 | L. MC3 | Shaft frag. | |
| 145 | PHP | Complete | Y |
| 146 | PHP | Base + shaft | Y |
| 147 | PHP | Base + shaft | Y |
| 148 | PHP | Base | Y (-141) |
| 149 | PHP | Shaft frag. | |
| 150 | IHP | Complete | Y |
| 151 | IHP | Base + shaft | |
| 152 | IHP | Base + shaft | |

| Suffix | Element | Element portion | $CaCO_3$ cast or bone of adjacent element |
|---|---|---|---|
| 153 | IHP | Base + shaft | |
| 154 | IHP | Base + shaft | Y |
| 155 | IHP | Head | Y |
| 156 | ? IHP | Shaft frag. | |
| 157 | THP | Complete | |
| 158 | THP Ray 1 | Base + shaft | Y |
| 159 | MTT | Shaft frag. | |
| 160 | R. FEM | Proximal end | |
| 161 | R. FEM | Partial distal end (lateral condyle) | |
| 162 | R. FEM | Medial condyle | |
| 163 | L. FEM | Partial shaft | |
| 164 | L. FEM | Lateral condyle (partial) | |
| 165 | L. FEM | Medial condyle (partial) | |
| 166 | L. FEM | Lateral condyle frag. | |
| 167 | R. FEM | Shaft frag. | |
| 168 | L. FEM | Shaft frag. | |
| 169 | FEM | Shaft frag. | |
| 170 | L. FEM | Trochanteric frag. | |
| 171 | ? L. FEM | Trochanteric frag. | |
| 172 | FEM shaft fragments | N = 6 | |
| 173 | R. TIB | Distal end + shaft | |
| 174 | R. TIB | Post. midshaft | |
| 175 | R. TIB | Anterior part, proximal shaft | |
| 176 | ? R. TIB | Part of proximal plateau | Y |
| 177 | L. TIB | Distal end + shaft | |
| 178 | L. TIB | Anterior proximal shaft | |
| 179 | TIB shaft fragments | N = 6 | |
| 180 | R. FIB | Distal end | |
| 181 | ? R. FIB | Proximal shaft | |
| 182 | L. FIB | Distal end | |
| 183 | FIB | Shaft frag. | |
| 184 | FIB | Shaft frag. | |
| 185 | FIB shaft fragments | N = 2 | |
| 186 | R. PAT | – | Y (-161) |
| 187 | L. PAT | – | |
| 188 | R. TAL | – | Y (-189) |
| 189 | R. CAL | – | |
| 190 | L. TAL | – | |
| 191 | L. CAL | – | |
| 192 | L. NAV | – | Y (-190) |
| 193 | L. CUB | – | |

| Suffix | Element | Element portion | $CaCO_3$ cast or bone of adjacent element |
|---|---|---|---|
| 194 | R. MT3 | Base | Y |
| 195 | R. MT4 | Base + shaft | Y |
| 196 | L. MT1 | Base | |
| 197 | L. MT1 | Head | |
| 198 | L. MT3 | Base | Y |
| 199 | L. MT5 | Base | |
| 200 | L. MT5 | Head | |
| 201 | L. MTT | Head | |
| 202 | MTT | Shaft frag. | |
| 203 | PFP | Complete | |
| 204 | IFP | Complete | |
| 205 | MTT | Shaft frag. | |
| 206 | OCX | Acetabular frag. | |
| 207 | ? R. OCC | – | |

**Appendix 2** Catalog of Middle Stone Age hominid fossils with postcranial material from the Halibee Member, Dawaitoli Formation, Middle Awash study area

| Specimen # | Suffix | Element | Element portion |
|---|---|---|---|
| BOU-VP-16/100 | – | L. FEM | Shaft frag. |
| HAL-VP-2/16 | – | RAD | Proximal frag. |
| HAL-VP-3/1 | – | R. ULN | Proximal frag. |
| HAL-VP-3/15 | A-N | CRA + M + THP + skeletal parts | – |
| HAL-VP-9/1 | See Appendix 1 | Partial skeleton | – |
| HAL-VP-9/930 | A | R. HUM | Proximal frag. |
| HAL-VP-9/930 | B | R. ULN | Proximal frag. |
| HAL-VP-9/930 | C | R. ULN | Distal frag. |
| HAL-VP-9/1520 | A | FRO | Frag. |
| HAL-VP-9/1520 | B | OCC | Frag. |
| HAL-VP-9/1520 | C | OCC | Frag. |
| HAL-VP-9/1520 | D | R. TIB | Shaft frag. |
| HAL-VP-9/1520 | E | R. ULN | Shaft frag. |
| HAL-VP-9/1520 | F | R. HUM | Shaft frag. |
| HAL-VP-9/1520 | G | R. CLA | Frag. |
| HAL-VP-9/1520 | H | R. CLA | Frag. |
| HAL-VP-9/1520 | I | L. FEM | Shaft frag. |
| HAL-VP-9/1520 | J | R. FEM | Shaft frag. |
| HAL-VP-9/1520 | K | HUM | Shaft frag. |
| HAL-VP-9/1520 | L | FIB | Shaft frag. |
| HAL-VP-9/1520 | M | R. ULN | Shaft frag. |
| HAL-VP-14/44 | – | FEM | Condyle frag. |
| TAL-VP-7/36 | A | L. FRO | Frag. |
| TAL-VP-7/36 | B | FRO + R. + L. NAS | Frag. |
| TAL-VP-7/36 | C | R. ZYG | Frag. |
| TAL-VP-7/36 | D | R. MAX | Frontal process |
| TAL-VP-7/36 | E | OCC | Frag. |
| TAL-VP-7/36 | F | R. TEM | Frag. |
| TAL-VP-7/36 | G | CRA | Frag. |
| TAL-VP-7/36 | H | R. HUM | Distal frag. |
| TAL-VP-7/36 | I | R. RAD | Distal frag. |
| TAL-VP-7/36 | J | OCC | Basioccipital |

**Appendix 3** Brief description of salient preservation and general morphology of the hominid fossils from the Halibee Member, Dawaitoli Formation, Middle Awash study area

Descriptions of the preserved portions for each of the hominid fossils are included in the tables below, in the following order: (**3a**) HAL-VP-9/1, (**3b**) HAL-VP-9/1520, (**3c**) HAL-VP-9/930, (**3d**) TAL-VP-7/36, and (**3e**) the five individuals represented by a single postcranial element. The descriptions include an inventory of the preserved anatomy, as well as morphological observations for the more complete portions. The comparative adjectives employed (e.g., large, thick, deep) are based on the comparative recent modern human samples assessed for this study and a close reading of published anatomical descriptions. Preservational descriptions for cranial elements are only included for HAL-VP-9/1. The following individuals have associated cranial material that is not described here: HAL-VP-3/15, HAL-VP-9/1520, and TAL-VP-7/36. An inventory of associated cranial remains is included in Appendix 2.

**3a**. HAL-VP-9/1

| Suffix | Element | Element portion | Preservational description |
|---|---|---|---|
| 1A | R. + L. FRO | | This portion joins with HAL-VP-9/1-1B. The preserved portion includes the lateral part of the right supraorbital margin with the root of the zygomatic process, the anterolateral portion of the pars orbitalis, and the superiormost part of the frontal crest. The right temporal line is preserved and is weakly developed. The lateral portion of the supraorbital margin is not particularly robust (especially considering the size of the individual); the medial portion of the supraorbital margin is not preserved. The vault is thick and thickens posteriorly. When joined with 1B, the frontal is closer to the vertical orientation typical of modern humans than the low and sloping morphology that characterizes Neanderthals and premodern hominids. |
| 1B | R. + L. FRO + PAR + OCC | | This portion joins with HAL-VP-9/1-1A. The preserved portion includes the posterior part of the right and left frontals, the anterolateral part of the left frontal, the medial parts of the right and left parietals, the lateral part of the right parietal nearly reaching the squamous suture, and the superomedial part of the occipital planum. The medial part of the coronal suture is preserved, as are the superolateral parts of the lambdoid suture. The sagittal suture is almost completely preserved, missing only the posteriormost part at the point of contact with the lambdoid suture. The coronal, sagittal, and occipital sutures are visible on the external vault surface; small portions of the occipital suture are obliterated, and the coronal and sagittal sutures are closed but not obliterated. None of the sutures are visible on the endocranial surface. The sagittal sulcus is visible near the posterior part of the parietals, with small foramina on and near the sulcus (the sulcus is eroded along the anterior part of the parietals and the superior part of the occipital, but a bony thickening at midline is still visible). The lateral part of the right parietal thins laterally, with two deep meningeal grooves on the internal surface. The external surface of the superomedial portion of occipital planum preserves a moderately developed external occipital protuberance and superior nuchal line; the vault is very thick near the external occipital protuberance relative to other preserved portions. The internal surface |

| | | | |
|---|---|---|---|
| | | | of the occipital planum preserves the superior portion of the cruciform eminence (the point where the transverse and sagittal sulci intersect is eroded). |
| **Suffix** | **Element** | **Element portion** | **Preservational description** |
| 2 | R. TEM + PAR | Frag. | The posteroinferior portion of the temporal is preserved, with the posteroinferior portion of the squamous suture (near the parietal notch), and a small portion of the parietal. The external acoustic meatus and the inferior portion of the temporal squama are preserved. The lateralmost portion of the petrous pyramid is preserved, as well as the lateral wall of the mastoid notch, the lateral wall of the carotid canal, the stylomastoid foramen, and the postglenoid process. The tympanic part is very thick and thickens considerably inferoposteriorly. The root of the styloid process is preserved, as well as the mastoid process, although the latter exhibits minor erosion to the lateral surface and near the apex. The suprameatal and supramastoid crests are preserved; the latter is weakly developed. The posterior part of the root of the zygomatic process is partially preserved. The anterior part of this portion nearly joins with HAL-VP-9/1-3. |
| 3 | R. TEM + SPH | w/ TMJ | The preserved portion includes the anterior part of the temporal with partial temporal squama, the anterior part of the articular eminence (the anterior extent of the articular eminence is eroded), and the anterior part of the root of the zygomatic process. The anterior part of the squamous suture is preserved, along with the posterolateral part of the greater wing of the sphenoid with the lateral part of the orbital surface. |
| 4 | L. TEM | Frag. | The posteroinferior portion of the temporal is preserved, including the mastoid process; the lateral, anteromedial, and inferior portions are eroded, exposing the mastoid cells. The posterior part of the root of the zygomatic process is partially preserved, as is the postglenoid process and the lateral wall of the mastoid notch. As with right temporal, the supramastoid crest is weakly developed. |
| 5 | L. TEM | Lat. TMJ | The preserved portion includes the lateral part of the articular eminence with the posterior part of the zygomatic process. |
| 6 | L. OCC | Frag. | The exact identity of this portion is uncertain, but it is possibly an inferolateral part of the nuchal planum. |
| 7 | L. OCC | Basioccipital? | This portion preserves a foramen and possible suture, but the exact position is indeterminate. |
| 8 | OCC or SPH | Frag. | – |
| 9 | SPH | Frag. | The preserved portion includes the left lesser wing, the root of the anterior clinoid process, and the optic canal. |
| 10 | R + L. FRO + NAS | Frag. | This portion preserves the glabellar region, with the inferomedial portions of the right and left frontals (including partial sinuses on both sides), partial frontonasal, internasal, and nasomaxillary sutures, and the superior portions of the right and left nasals. The bone is very thick, and the external surface is eroded and distorted. On the internal surface, the inferior part of the frontal crest is preserved, although partially eroded. |
| 11 | L. TEM + PAR | Frag. | The superoposterior portion of the temporal squama is preserved, with the squamous suture and a small portion of the parietal. The bone thickens near the posterior edge of the preserved portion. |
| 12 | R. ZYG + MAX | Frag. | This portion preserves the inferomedial part of the zygomatic, with the zygomaticomaxillary suture and the inferolateral part of the zygomatic process of the maxilla. The zygomaticofacial foramen is preserved, as well as a |

| | | | |
|---|---|---|---|
| | | | small portion of the inferolateral orbital margin, a small lateral portion of the inferior surface of the orbit, and the medial part of the masseteric origin (which is slightly eroded). |
| **Suffix** | **Element** | **Element portion** | **Preservational description** |
| 13 | R. MAX | Roots I2-M1 | This portion preserves the inferomedial part of the maxilla with the roots of I2-M1, the inferolateral margin of the nasal aperture, a small segment of the intermaxillary suture, and part of the palate. The canine jugum is eroded, exposing the canine root. The canine fossa is also preserved, although the bone surface is eroded. |
| 14 | R. MAX + SPH | Roots M2-3 | This portion preserves the inferolateral portion of the posterior part the maxilla (with maxillary sinus), with the posterolateral portion of the palate. The roots of M2 and M3 are partially preserved. The lateral wall of the greater palatine foramen and the anterior part of the lateral pterygoid plate of the sphenoid are preserved. |
| 15 | L. MAX | I roots | The inferomedial portion of the maxilla is preserved. The root of I2 and the anteromedial surface of the palate are preserved. |
| 16 | L. MAX + PAL | M1-3 roots | This portion preserves the inferolateral portion of the posterior part the maxilla, with the posterolateral margin of the palate. The roots of M1-3 and the anterolateral portion of the palatine with the greater palatine foramen are preserved. |
| 17 | R. MAN | Condyle | The mandibular condyle with the condylar neck and the posterior portion of the mandibular notch are preserved. The condyle is strikingly large in absolute size and relative to the thickness of the superoposterior margin of the ascending ramus; the condyle projects considerably medially. |
| 18 | R. MAN | Coronoid process | The anterior portion of the coronoid process is preserved and is strikingly large, particularly in its anteroposterior dimension. The apex is eroded and the posterior portion is broken. |
| 19 | R. MAN | Ramus frag. | The portion of the root of the ascending ramus immediately superior and posterior to the extramolar sulcus is preserved. The endocoronoid ridge is well-developed. A very small portion of the superiormost part of the lingula is preserved. |
| 20 | R. MAN | Lateral corpus | This portion preserves the posterior part of the corpus with partial margins of the molar alveoli (either M1-2 or M2-3) and part of the root of the ascending ramus. |
| 21 | R. + L. MAN | Corpus w/ R. I1-2 roots and mentum osseum | The midline portion of the corpus with the partial roots of I1-C is preserved. The inferior margin is not preserved. The superior part of the mental eminence is preserved, and suggests the eminence is well-developed. |
| 22 | CRA frags. | N = 24 | – |
| 23 | Axis VER | Ant. midline, no dens | The anterior midline portion is preserved, including the body and the superior articular facets, which are nearly complete but eroded along their margins. The dens is broken at the level of the superior facets. |
| 24 | Cervical VER | Body | The complete body of the fourth cervical vertebra is preserved. The uncinate processes and the anterior part of the root of the right pedicle are preserved. The body slopes inferiorly towards the ventral end, especially the inferior surface. The bone on the ventral part of the superior surface is porous and appears remodeled. The left half of the ventral margin of the superior surface is thickened and bulges ventrally. |
| 25 | Cervical VER | Body | The complete body of the fifth cervical vertebra is preserved. The uncinate processes are preserved. The body slopes inferiorly toward the ventral end, particularly the inferior surface. The ventral margin of the superior surface |

| | | | |
|---|---|---|---|
| | | | is porous with bony remodeling. The right half of the ventral margin of the superior surface is thickened and bulges ventrally. There is bony lipping (extending inferiorly) on the ventral margin of the inferior surface. |
| **Suffix** | **Element** | **Element portion** | **Preservational description** |
| 26 | Cervical VER | Body with R. pedicle | The complete body of the sixth cervical vertebra is preserved. The uncinate processes are preserved but are both partially eroded. The right pedicle is preserved, along with the posteromedial wall of the right transverse foramen, and the right superior and inferior articular facets (facet margins are eroded). There is a small tubercle immediately inferolateral to the superior articular facet. The inferior articular facet curves anteriorly toward the lateral margin. The body slopes slightly inferiorly toward the ventral end, although to a lesser degree than in the fourth and fifth cervical vertebrae. There is a slight bony lip on the ventral margin of the superior surface of the body. There is a bony thickening along the ventral margin of the inferior surface, especially on the right side. |
| 27 | Cervical VER | Body | The complete body of the seventh cervical vertebra is preserved. The uncinate processes are preserved but are both partially eroded. The margin of the inferior surface is eroded. The body slopes slightly inferiorly toward the ventral end, although to a lesser degree than in the sixth cervical vertebra (HAL-VP-9/1-26). The ventral margin of the inferior surface is thickened and slightly elevated. The dorsal margin of the inferior surface is mostly eroded. |
| 28 | R. cervical VER | Partial pedicle and lamina | This portion preserves the lateral portion of the pedicle and lamina, the posterior wall of the transverse foramen, and the superior and inferior articular facets (there is slight erosion at the facet margins). This portion is likely part of the third, fourth, or fifth cervical vertebra. |
| 29 | Cervical VER (?7) | Spinous process | This portion preserves a complete spinous process. The process is very short and symmetrical and is not bifurcated. The posterior tip is eroded. The inferior surface exhibits considerable relief. The inferior portion of the ventral wall of the spinous process (at midline) is preserved. This portion is likely part of a lower cervical vertebra (probably the sixth or seventh). |
| 30 | Thoracic VER (upper) | Body | A nearly complete upper thoracic vertebra is preserved, mostly likely the first or second in the thoracic sequence. The complete body is preserved, with most of the vertebral arch. The superior costal facets are preserved and are between demi and complete facets in their shape (facet margins are eroded). A very small right inferior costal facet is preserved (the same portion on the left side is eroded and cannot be assessed). The right pedicle is complete, and the left pedicle is partially preserved. The laminae are complete and are very tall in superoinferior dimension. A small inferomedial portion of the right superior articular facet is preserved. The left inferior articular facet is complete (although the margins are slightly eroded). The spinous process is partially preserved (lacking the posterior tip), and the surface is eroded. The root of the right transverse process is preserved. The right superior costal facet of the inferiorly adjacent vertebra is cemented to the right inferior articular facet of this portion. |
| 31 | Thoracic VER | Body | This portion preserves a nearly complete upper thoracic vertebral body. The superior surface and circumferential surfaces are very badly eroded. |
| 32 | Thoracic VER | Body | This portion preserves an upper or middle thoracic vertebral body. The margins of the superior and inferior surfaces and the circumferential surfaces are badly eroded. The body exhibits very slight ventral wedging. There is a round and deep cavity on the right superolateral margin of the body, most likely the result of insect activity. There is a flat plate of bone adhering to the left side of the inferior surface. This portion fits well above HAL-VP-9/1-33 and appears likely to be the superiorly adjacent vertebra. |

| Suffix | Element | Element portion | Preservational description |
|---|---|---|---|
| 33 | Thoracic VER | Body, partial | This portion preserves a partial upper or middle thoracic vertebral body. Most of the left half is missing (especially the inferior portion). The right superior costal demifacets are preserved, although the margins are eroded. The inferior and circumferential surfaces are badly eroded. This portion fits well below HAL-VP-9/1-32 and appears likely to be the inferiorly adjacent vertebra. |
| 34 | Thoracic VER | Body, partial | This portion preserves a partial middle thoracic vertebral body. Almost all of the left side is missing. The superior surface is partially preserved, and a small portion of the inferior surface is preserved. The root of the right pedicle is preserved. |
| 35 | Thoracic VER | R. body, pedicle | The right portion of a lower thoracic body with the right pedicle is preserved. The superior articular facet is preserved (but partially eroded). Small portions of the superior and inferior surfaces of the body are preserved. The circumferential surfaces are badly eroded. There is a bony thickening on the superior portion of the dorsolateral surface of right side of body, extending ventrally from the lateral surface of the pedicle. The pedicle is very tall in superoinferior dimension (nearly extending along the full height of the body). The transverse process is broken at its base, but the base nonetheless indicates that the transverse process would have been oriented posteriorly, suggesting that this portion likely belongs to an eleventh or twelfth thoracic vertebra. |
| 36 | Thoracic VER | Body frag. | This portion preserves part of a thoracic vertebral body. This portion likely belongs to a lower thoracic vertebra, based on the superoinferior height of the body. All surfaces are badly eroded. |
| 37 | Thoracic VER | Body frag. | This portion preserves part of a thoracic vertebral body. This portion likely belongs to a middle thoracic vertebra, based on the superoinferior height of the body. All surfaces are badly eroded. |
| 38 | Thoracic VER | Partial spinous process | This portion preserves the anterior part of a spinous process, including the portion where the left and right laminae meet at the midline. This portion very likely belongs to an upper thoracic vertebra based on the anteroposterior dimension along the midline, the height of the laminae, the mediolateral thickness of the spinous process, and the angle of the spinous process. |
| 39 | Thoracic VER | Partial spinous process (R. lamina) | This portion preserves the anterior part of a spinous process, including the portion where the left and right laminae meet at the midline. The right lamina is also preserved. This portion very likely belongs to an upper or middle thoracic vertebra (lower in the sequence than HAL-VP-9/1-38) based on the height of the lamina and the angle of the spinous process. The lamina is much shorter in superoinferior dimension than the lamina of HAL-VP-9/1-30. |
| 40 | Thoracic VER | Spinous process (R. lamina) | This portion preserves the anterior part of a spinous process. The inferior part of the right lamina and the right inferior articular facet are preserved, although the latter is partially eroded. This portion very likely belongs to a middle thoracic vertebra based on the angle of the spinous process and the position of the inferior articular facet. |
| 41 | Thoracic VER | Spinous process terminus | This portion preserves the posterior tip of a spinous process. This portion likely belongs to a lower thoracic vertebra based on the superoinferior height of the process tip and its rounded outline in lateral view. |
| 42 | Thoracic VER | Spinous process terminus | This portion preserves the posterior tip of a spinous process. This portion likely belongs to a middle thoracic vertebra based on the small mediolateral dimension and the inferior extension of the bone at the very tip of the process (resulting in a hook-like shape at the terminus). The posterior tip of the spinous process is tall in superoinferior dimension. |

| Suffix | Element | Element portion | Preservational description |
|---|---|---|---|
| 43 | Thoracic VER | L. partial transverse process | This portion preserves the lateral part of a left transverse process, with a transverse costal facet on the inferolateral surface of the process (facet margins are partially eroded). The end of the process is bulbous. This portion is unlikely to be from a lower thoracic vertebra based on the placement and orientation of the transverse costal facet. The transverse costal facet is concave and small relative to the size of the transverse process. |
| 44 | Thoracic VER | R. transverse process, partial lamina | This portion preserves a right transverse process with the right lamina. The right inferior articular facet is preserved, although the inferior margin is eroded. The base of the superior articular facet is visible, but the surface of the articular facet itself is missing. The transverse costal facet is partially preserved (but is eroded) and is placed inferiorly on the transverse process. This portion likely belongs to a middle or lower thoracic vertebra based on the height of the lamina and the angle of the transverse process. The transverse process appears superoinferiorly tall and thin (in anterolateral to posteromedial dimension), although this appearance is likely due in part to distortion. A sliver of the margin of a rib is cemented to the transverse process, superomedially adjacent to the transverse costal facet. |
| 45 | Thoracic VER | R. partial transverse process | This portion preserves the lateral part of a right transverse process. The transverse costal facet is preserved (although it is partially eroded and distorted) and is inferiorly placed. The superoinferior dimension of the transverse process is greater than in HAL-VP-9/1-43 and -44. |
| 46 | Thoracic VER + R. rib head | Root of R. transverse process | This portion preserves the root of a right transverse process with the posterior portion of the pedicle and a small inferolateral portion of the superior articular facet. This portion likely belongs to a middle thoracic vertebra based on the height of the pedicle and the angle of the transverse process. The head of a right rib is cemented to the anterolateral surface of the transverse process in a nearly vertical orientation, with the rib head at the superior end. The partial right inferior articular facet of the superiorly adjacent vertebra is cemented to the right superior articular facet, with a thin calcium carbonate deposit visible between the two facets. |
| 47 | Thoracic VER | Root of L. transverse process w/ rib frag. | This portion preserves the root of a left transverse process with the left superior articular facet (margins eroded) and the posterior portion of the pedicle. This portion likely belongs to an upper or middle thoracic vertebra based on the pedicle cross-sectional shape (which is short and broad) and the angle of transverse process. A fragment of rib shaft is cemented (in a horizontal orientation) to the anterolateral surface of the superior articular facet. |
| 48 | Thoracic VER | R. partial transverse process | The medial portion of a right transverse process is preserved. The transverse process is smaller in superoinferior dimension than HAL-VP-9/1-45. |
| 49 | Lumbar VER | Body, R. pedicle | This portion preserves a nearly complete lumbar body, missing the inferior portion of the left side. This body likely belongs to the second lumbar vertebra; the position is likely between HAL-VP-9/1-50 (superiorly adjacent) and HAL-VP-9/1-51 (inferiorly adjacent; based on goodness of fit, facet position and orientation, and the cross-sectional shape of the root of the pedicle). The right pedicle is preserved, along with the medial part of the transverse process, the right superior articular facet (margins eroded), and the right mammillary process. The superior surface of the body has undergone considerable remodeling and is highly irregular with small nodular outgrowths. The ventral surface of the body is superoinferiorly compressed, with the ventral portion of the superior margin of the body depressed inferiorly and small nodules along the depressed margin near the midline. The inferior and especially superior margins of the body exhibit bony lipping; erosion to the inferior margin may have reduced the apparent |

| | | | |
|---|---|---|---|
| | | | degree of lipping. The ventral compression and bony lipping around the margins of the body have resulted in a waisted appearance. |
| **Suffix** | **Element** | **Element portion** | **Preservational description** |
| 50 | Lumbar VER | Body, R. arch | This portion preserves a nearly complete lumbar body, missing the ventral portion of the left half. This body likely belongs to the first lumbar vertebra, based on goodness of fit above HAL-VP-9/1-49 (including corresponding remodeled surfaces and osteophytic lipping), the position of the superior and inferior facets, the position of the root of the pedicle, and the orientation of the superior articular facet (less curved than HAL-VP-9/1-49). The right pedicle is preserved, along with the medial part of the right transverse process, the right lateral part of the spinous process, the right superior and inferior articular facets (margins eroded), and the right mammillary process. The inferior articular process is long and thin, and the inferior articular facet has small bony outgrowths (irregular lipping) along the inferior margin. The body is superoinferiorly compressed toward its ventral end. There is a great degree of bony lipping on the inferior and superior margins of the right side of the body (the corresponding areas on the left side are eroded). On the right of the body, the lipping is offset inferiorly from the superior margin of the ventral surface of the body, and superiorly from the inferior margin. The inferior surface of the body has undergone remodeling and is highly irregular. The body has a severely waisted appearance. |
| 51 | Lumbar VER | Partial body | This portion preserves the posterolateral part of a lumbar body with the superior and inferior surfaces; most surfaces have been eroded. This portion likely belongs to the third lumbar vertebra, based on the height of the body relative to the other lumbar remains and the superoinferior height of the root of the pedicle. This partial body has a slightly waisted appearance, although to a lesser degree than HAL-VP-9/1-49 and -50. |
| 52 | Lumbar VER | Body, R. partial arch | This portion preserves a complete lumbar body with the right pedicle and the medial part of the right superior articular facet. This body likely belongs to the fourth lumbar vertebra, based on the size and shape of the body relative to the other lumbar remains, goodness of fit above HAL-VP-9/1-53, the position and cross-sectional shape of the root of the pedicle, and the position of the superior articular facet. The ventral edge is the tallest part of the body. The superior margin of the body exhibits slight bony lipping and is depressed slightly inferiorly. The body has a slightly waisted appearance (especially on the lateral surfaces of the body). The anterior half of the left side of the superior surface exhibits pathological changes. There is a bony lesion on this surface, and the bone in this area is porous. This lesion may be the result of intervertebral disc herniation (i.e., a Schmorl's node, see Chapter 6). |
| 53 | Lumbar VER | Body | This portion preserves a complete lumbar body. This body likely belongs to a fifth lumbar vertebra based on goodness of fit below HAL-VP-9/1-53, the relative shape and height of the body (e.g., the ventral height is taller than HAL-VP-9/1-52), and the position and cross-sectional shape of the root of the pedicle (which slopes from superomedial to inferolateral, as is common in the lowest lumbar vertebrae). The lateral surface has a slightly waisted appearance. Unlike the other lumbar remains, this body does not exhibit bony lipping along its margins (it is possible that erosion has affected this appearance slightly, but if bony lipping was present it would have been very minimal). The body is wedged dorsally (i.e., is taller on the ventral side), and the inferior surface of the body slopes inferiorly toward the ventral edge. There is a small pit-like depression near the center of the superior surface of the body, which may be the result of intervertebral disc herniation (i.e., a Schmorl's node, see Chapter 6), as with HAL-VP-9/1-52. |

| Suffix | Element | Element portion | Preservational description |
|---|---|---|---|
| 54 | Lumbar VER | L. partial lamina w/ inferior facet | This portion preserves the inferolateral part of a left lamina and a partial inferior articular facet. This portion likely belongs to a middle lumbar vertebra, based on the shape of the inferior articular facet (superoinferiorly long and mediolaterally thin), and the distance of the facet from midline (as determined by the mediolateral width of the lamina between the facet and the base of the spinous process). It is unlikely to belong to the first lumbar vertebra; the inferior facet does not match the right inferior facet of HAL-VP-9/1-50. |
| 55 | Lumbar VER | Partial spinous process | This portion preserves the posterior tip of a slightly asymmetrical spinous process. The portion is very thick along its inferior margin. |
| 56 | Lumbar VER | R. partial inferior facet | This portion preserves a partial right inferior facet with the lateral part of the lamina. This portion likely belongs to a middle lumbar vertebra based on the shape of the inferior articular facet (superoinferiorly long and mediolaterally thin). This facet may be the antimere of HAL-VP-9/1-54, but erosion makes it difficult to be certain. |
| 57 | Sacral VER | R. partial ala | The superior portion of the right sacral ala is preserved. This portion includes the posterolateral edge of the first sacral body and the partial right superior articular facet (margins eroded). The auricular surface has been affected by distortion; the surface is displaced posteromedially and the superior part is distorted and eroded. The preserved portion of the superior articular facet indicates that this facet is large. |
| 58 | Sacral VER | L. partial ala | The posterolateral portion of the left ala is preserved. This portion includes most of the auricular surface (missing the inferior and superior portions) and a small fragment of the left superior articular facet. All surfaces except the auricular surface are either broken or deeply eroded. |
| 59 | Sacral VER | Partial bodies (n=2) | This portion preserves the ventral parts of two sacral vertebrae. The two bodies likely belong to upper or middle sacral vertebrae, based on the heights and widths of the preserved portions of each. The line of fusion between the two bodies is visible on the ventral surfaces as a thin gap filled with calcium carbonate. The ventral surfaces of the bodies are eroded. |
| 60 | VER fragments | N = 6 | – |
| 61 | R. rib | Head | This portion preserves a head with a superiorly placed articular facet (it does not appear to have a second articular facet, although this area is slightly eroded). The medial extent of the crest of the neck is weakly developed. There is a sharp crest on the inferior margin of the neck, terminating in a small beak-like shape. This portion does not belong to a first, second, or twelfth rib. |
| 62 | R. rib | Head | This portion preserves a head with two articular facets. The posterior surface exhibits considerable relief. The articular facet of the tubercle is preserved and has a very porous surface (slightly eroded). The inferior margin of the tubercle extends inferiorly into a crest along the inferior margin of the rib. The distance between the margin of the articular surface of the head and the facet of the tubercle is short. The head is tall in superoinferior dimension. This portion is likely from one of the middle ribs, based on the height of the head. |
| 63 | R. rib | Neck | This portion preserves the crest of the neck (slightly eroded) and the tubercle, the latter of which is large in superoinferior and mediolateral dimensions. The superior part of the articular facet of the tubercle is preserved. This portion is likely from one of the middle ribs, based on its cross-sectional dimensions. |

| Suffix | Element | Element portion | Preservational description |
|---|---|---|---|
| 64 | R. rib | Neck | This portion preserves the part of the neck immediately adjacent to the head and includes a small anteroinferior portion of the head. There is a rugosity on the posteroinferior surface. The medial portion of the crest of the neck is preserved. This portion is likely from one of the upper (but not the first or second) or the lower ribs, based on the cross-sectional dimensions of the neck. |
| 65 | R. rib | Neck | This portion preserves the part of the neck just lateral to the tubercle. The lateral margin of the tubercle is preserved. There is a deep and wide groove on the inferior surface. Lateral to the tubercle there is a rugosity extending from superomedial to inferolateral. This portion is likely from one of the upper ribs (but not the first rib). |
| 66 | R. rib | Neck | This portion preserves part of the neck, possibly medial to the tubercle (position is uncertain). This portion is likely from one of the middle ribs, based on the large superoinferior dimension. |
| 67 | R. rib | Shaft at costal angle | This portion preserves part of the shaft at the costal angle. There is a groove on the anteroinferior surface that deepens laterally, with small crests along the anterior and posterior margins. There is a small piece of bone cemented to the posteroinferior surface that likely belongs to a rib based on the very thin cortical bone. This portion does not belong to a first, eleventh, or twelfth rib. |
| 68 | R. rib | Shaft at costal angle | This portion preserves part of the shaft at the costal angle, with the costal groove. There is a weak crest along the superior margin of the shaft, with a wide and shallow groove anterior to it along the medial part. The inferior margin is eroded. This portion is likely from one of the middle ribs (not a first, second, eleventh, or twelfth rib). |
| 69 | R. rib | Shaft at costal angle | This portion preserves part of the shaft at the costal angle. There is a very deep costal groove on the anteroinferior surface, and a slight rugosity on the inferior surface of the medial part. The inferior margin is eroded. This portion is likely from one of the upper ribs (but not the first or second), based on the anteroposterior relative to superoinferior thickness. |
| 70 | R. rib | Shaft frag. | This portion preserves part of the shaft near the sternal end. The costal groove is very weak. The shaft is slender with smooth surfaces. The posteroinferior surface is eroded. |
| 71 | R. rib | Shaft frag. | This portion preserves part of the shaft, likely from near the midshaft position. The shaft surfaces are smooth and the costal groove is moderately deep. The inferior margin is eroded. This portion does not belong to a first or second rib. |
| 72 | R. rib | Shaft frag. | This portion preserves part of the shaft, likely from near the midshaft position. The shaft surfaces are smooth and the costal groove is moderately deep. The inferior margin is eroded. This portion is likely from one of the middle ribs based on the large superoinferior height. |
| 73 | R. rib | Shaft frag. | This portion preserves part of the shaft near the costal angle. The costal groove is very deep. The shaft surfaces are smooth, with the exception of a bony elevation on the posteroinferior part. The inferior margin is eroded. This portion is likely from one of the middle ribs based on the large superoinferior height. |
| 74 | R. rib | Shaft frag. | This portion preserves part of the shaft near the costal angle. The costal groove is very deep. The shaft surfaces are smooth, with the exception of a slight bony elevation on the posteroinferior part, and a very slight groove adjacent to the superior margin on the posterior side. The inferior margin is eroded. This portion is likely from one of the middle ribs based on the large superoinferior height. |

| Suffix | Element | Element portion | Preservational description |
|---|---|---|---|
| 75 | R. rib | Shaft frag. | This portion preserves part of the shaft near the costal angle. The costal groove is deep and deepens laterally. The shaft surfaces are smooth. Portions of the superior and inferior margins are eroded. A small inferomedial fragment is displaced anteriorly, with calcium carbonate filling the resulting fissure on the posterior surface. This portion is likely from one of the middle ribs based on the large superoinferior height. |
| 76 | R. rib | Sternal end | This portion preserves part of the shaft near the sternal end. The superior margin is thin. The superior surface on the inner part of the shaft is smooth and slightly hollowed. There is a shallow groove on the inferior surface, flanked on both sides by slight ridges. The superior margin is eroded. This portion does not belong to a first, second, eleventh, or twelfth rib. |
| 77 | R. rib | Sternal end | This portion preserves a complete sternal end. The superior margin is thin and is eroded at the lateral end. There is a shallow groove on the inferior part of the inner surface. The middle part of the internal surface has a rounded appearance (bulges inward). The shaft flares (widens in both superficial-deep and superoinferior dimensions) near the sternal end. The outline of the sternal end is teardrop-shaped; the margins are eroded. There is a very slight bony tubercle on the inferior margin immediately adjacent to the sternal end. This portion does not belong to a first, second, eleventh, or twelfth rib. |
| 78 | R. rib | Sternal end | This portion preserves a complete sternal end. Both the superior and inferior margins are very thin, and the inferior margin is sharp. The shaft is thin in superficial-deep dimension. The shaft thins in superoinferior dimension and thickens very slightly in superficial-deep dimension at the sternal end. The margin of the sternal end and the shaft surfaces are slightly eroded. This portion is likely from a tenth or eleventh rib based on the size and the tapered shape of the end, or possibly from a second rib, but the latter is less likely considering the tapered shape and thickness. This portion is likely the antimere of HAL-VP-9/1-94. |
| 79 | L. rib | Head | This portion preserves a head with two articular facets. The superior facet is larger; the inferior facet is partially eroded. There is slight relief on the inferior margin of the lateral part of the fragment, and on the small part of the posterior surface that this portion preserves. The inferolateral portion of the shaft is slightly displaced superoposteriorly. This portion is likely from one of the middle ribs based on the large superoinferior height of the head. Two fragments of bone are cemented to the superoposterior surface immediately adjacent to the superior articular facet on the head. These two fragments include a left superior articular facet of a thoracic vertebra and a left inferior articular facet of a thoracic vertebra, and they are cemented to each other along the facet surfaces. |
| 80 | L. rib | Shaft at costal angle | This portion preserves part of the shaft at the costal angle. The costal groove is deep. The superior part of the internal surface is rounded (bulges inward). There is a slight bony thickening on the inferior part of the posterior surface, on the medial portion of the fragment. The inferior margin is eroded. A small sliver of the lateral part of the shaft is slightly displaced and the resulting gap is filled with calcium carbonate. This portion is likely from one of the middle ribs (not a first, second, eleventh, or twelfth rib). |
| 81 | L. rib | Shaft at costal angle | This portion preserves part of the shaft at the costal angle, just lateral to the tubercle. There is a groove along the length of the inferior surface, flanked by ridges on both sides. This portion is likely from one of the upper ribs (but not the first or second). There is a small bone fragment cemented to the posterior surface near the medial end of this portion. |

| Suffix | Element | Element portion | Preservational description |
|---|---|---|---|
| 82 | L. rib | Shaft at costal angle | This portion preserves part of the shaft at the costal angle, near the lateral part of the angle. The costal groove is deep and is inferior to a sharp ridge running along the middle part of the inner surface of the shaft. The superior and inferior margins are eroded, and there is insect damage to the medial part of the posterior surface. This portion does not belong to a first, second, or twelfth rib. |
| 83 | L. rib | Shaft at costal angle | This portion preserves part of the shaft at the costal angle. The costal groove is very deep. There is a slight thickening on the inferior part of the posterior surface near the middle of the fragment. The superior and inferior margins are eroded. This portion is likely from one of the middle ribs (not a first, second, eleventh, or twelfth rib). |
| 84 | L. rib | Shaft frag. | This portion preserves part of the middle segment of the shaft. The costal groove is deep, the shaft surfaces are smooth, and the inferior margin is very sharp. The medial and lateral portions of the inferior margin are eroded. This portion is likely from one of the middle ribs (not a first, second, eleventh, or twelfth rib). |
| 85 | L. rib | Shaft frag. | This portion preserves part of the middle segment of the shaft, closer to the costal angle than to the sternal end. The costal groove is shallow. The shaft is very tall in superoinferior dimension. The superior and inferior margins are eroded, and there is slight insect damage to the inner shaft surface. This portion is likely from one of the middle ribs (not a first, second, eleventh, or twelfth rib). |
| 86 | L. rib | Shaft frag. | This portion preserves part of the middle segment of the shaft. The costal groove is deep and the superior margin is angular, taking the form of a corner superiorly adjacent to the groove. This portion is distorted and the surfaces are eroded. The inner table of bone at the medial end is displaced inward, and the resulting gap is filled with calcium carbonate. This portion is likely from one of the middle ribs (not a first, second, eleventh, or twelfth rib). |
| 87 | L. rib | Shaft frag. | This portion preserves part of the middle segment of the shaft. The costal groove is very shallow and the shaft surfaces are smooth. The shaft is very tall in superoinferior dimension. Portions of the superior and inferior margins are eroded. This portion is likely from one of the middle ribs (not a first, second, eleventh, or twelfth rib). |
| 88 | L. rib | Shaft frag. | This portion preserves part of the middle segment of the shaft. The costal groove is very shallow and the shaft surfaces are smooth. The shaft increases laterally in superoinferior dimension. There is a slight bulge along the length of the shaft at the middle of the external shaft surface. Most of the superior and inferior shaft surfaces are eroded. This portion is likely from one of the middle ribs (not a first, second, eleventh, or twelfth rib). |
| 89 | L. rib | Shaft frag. | This portion preserves part of the middle segment of the shaft. The costal groove is very shallow and the shaft surfaces are smooth. The shaft increases in superoinferior dimension toward the lateral end. Portions of the superior and inferior margins are eroded. This portion is likely from one of the middle ribs (not a first, second, eleventh, or twelfth rib). |
| 90 | L. rib | Shaft frag. | This portion preserves part of the shaft near the costal angle. The costal groove is deep and the superior margin is angular, taking the form of a corner superiorly adjacent to the groove. The inferior margin is very sharp. The shaft is short in superoinferior dimension and the height is approximately constant along the length of the fragment. Portions of the superior and inferior margins are eroded. A sliver of bone at the medial end of the fragment is displaced inward from the inner surface of the shaft. This portion is likely from one of the upper to middle ribs (not a first, second, eleventh, or twelfth rib). |

| Suffix | Element | Element portion | Preservational description |
|---|---|---|---|
| 91 | L. rib | Shaft frag. | This portion preserves part of the shaft near the costal angle. The medial part of the superior margin is thick and flattened. The superficial-deep dimension is large. The inferior margin is eroded. This portion is likely from one of the middle to lower ribs (but not an eleventh or twelfth rib), based on thickness and curvature. |
| 92 | L. rib | Shaft frag. | This portion preserves part of the shaft near the sternal end. The costal groove is thin and very shallow, and the shaft surfaces are smooth. The shaft increases in superoinferior dimension towards its lateral end and is weakly curved. Portions of the superior and inferior margins are eroded. This portion is likely from one of the middle ribs (not a first, second, eleventh, or twelfth rib). |
| 93 | L. rib | Sternal end | This portion preserves a complete sternal end. The superior margin is thin and is partially eroded. There is a shallow groove on the inferior part of the internal surface. The middle portion of the internal surface is rounded (bulges inward). The shaft flares in both superficial-deep and superoinferior dimensions near the sternal end. The outline of the sternal end is teardrop-shaped (the margins are eroded). There is a slight bony thickening on the inferior margin, immediately adjacent to the sternal end. This portion does not belong to a first, second, eleventh, or twelfth rib. |
| 94 | L. rib | Sternal end | This portion preserves a complete sternal end. The superior and inferior margins are thin. The shaft is thin in its superficial-deep dimension. The shaft tapers in superoinferior dimension and thickens slightly in superficial-deep dimension near at the sternal end. The margin of the sternal end is eroded. This portion is likely from a tenth or eleventh rib based on the size and the tapered shape of the end, or possibly from a second rib, but the latter is less likely considering the tapered shape and thickness. This portion is likely the antimere of HAL-VP-9/1-78. |
| 95 | Rib shaft frags; side indet. | N = 62 | – |
| 96 | R. CLA | Acromial end | This portion preserves part of the shaft near the acromial end, just medial to the depth of the lateral curve. The rugosity for the *deltoideus* is preserved on the anterior surface of the lateral part of the fragment, taking the form of two crests that slant inferolaterally, separated by a narrow and deep groove. A shallow subclavian sulcus is preserved on the medial part of this portion. The sulcus is not observable toward its lateral end due to insect damage. The superior and inferior shaft surfaces exhibit insect damage. |
| 97 | L. CLA | Shaft near sternal end | This portion preserves the medial part of the shaft, near (but not including) the sternal end. The costoclavicular impression is well-defined, taking the form of an oval-shaped depression with a small elevated island of bone in the center, and with a tubercle at the medial margin of the oval depression. The anterior surface above the costoclavicular impression is slightly hollowed. The subclavian sulcus is shallow. The shaft is slender and the dorsoventral curvature appears wide. There is a very slight rugosity for the *pectoralis major* in the form of a slight ridge. The medial end exhibits considerable insect damage. |
| 98 | CLA | Shaft frag. | This portion preserves part of middle segment of the shaft. The shaft surfaces are smooth. There is a shallow sulcus running along the length of the shaft on the inferior surface. The dorsoventral dimension of the shaft is greater than the superoinferior dimension. There is deep insect damage on the superior and especially inferior surfaces, extending through the cortical bone and into the cancellous bone. |
| 99 | ? CLA | Shaft frag. | This portion preserves part of a shaft that is possibly clavicular. This portion is distorted and exhibits insect damage. |

| Suffix | Element | Element portion | Preservational description |
|---|---|---|---|
| 100 | R. SCA | Acromion and spine | The scapular spine is nearly completely preserved, missing the medialmost portion where the spine begins to expand to meet the medial border. The acromion is complete. The clavicular facet appears to have undergone pathological changes. The facet surface is very porous and has an irregular margin. The scapular spine is thick, and the thickness is nearly constant along its middle segment, between its expansion toward the acromion and thinning toward the medial border. There is a rugosity along the length of posterior surface of the spine, with one sharp ridge along the superior margin of the spine (giving it a corner-like appearance) and another ridge along the center of the posterior surface of the spine. A shallow groove separates the two ridges. The acromion is large and rectangular, with angular anterolateral and posterolateral corners. The surfaces of the supraspinous and infraspinous fossae exhibit insect damage. |
| 101 | R. SCA | Partial glenoid | The superior two-thirds of the posterior part of the glenoid fossa, including the margin, are preserved (but slightly eroded). The medial part of the scapular neck is preserved, along with the root of the scapular spine. The superior part of a bony pillar is preserved on the ventral surface of the bone, running along the preserved part of the axillary border. There is a slight hollowing on the ventral surface, immediately lateral to the bony pillar. There is a band of bone of roughened texture on the posterior surface (~7 mm wide at its superior end and tapering inferiorly), adjacent to the posterior margin of the glenoid fossa. There is very slight bony lipping along the margin of the fossa. The inferior part of the posterior surface exhibits insect damage. |
| 102 | R. SCA | Axillary border | The middle segment of the axillary border is preserved. The inferior part curves ventrally. There is a bony crest along the ventral margin of the axillary border, curving slightly dorsally at its surperior end. The axillary sulcus is on the dorsal surface. |
| 103 | R. SCA | Inferior angle | The inferiormost part of the inferior angle is preserved. The inferior margin is rounded and blunt. The dorsal and especially ventral surfaces are distorted. |
| 104 | L. SCA | Partial acromion | The acromion is partially preserved, missing the posterolateral corner. There is a bony tubercle on the superior surface near the anterior margin, at the medial edge of the clavicular facet. The acromial shape is approximately symmetrical to its antimere (HAL-VP-9/1-100). The superior and inferior surfaces of the anterior part are partially eroded, as are the anterior margin and the clavicular facet. The anterior margin and inferior surface exhibit insect damage. |
| 105 | L. SCA | Inferior angle | The inferior angle is preserved. The apex is tightly curved (forming a rounded v-shape). The lateral margin curves slightly ventrally and then dorsally near its superior end. The dorsal surface is smooth, whereas the ventral surface exhibits considerable relief (which has been exacerbated by distortion to this surface). The medial and lateral margins are partially eroded, as are the medial parts of the ventral and dorsal surfaces. |
| 106A | R. OCX | Lower portion | This portion joins with HAL-VP-9/1-106B. This portion preserves the inferior part of the ischial tuberosity (the superior part is deeply eroded), with the ischiopubic ramus, the pubic body, and the medialmost part of the iliopubic ramus. The ischial tuberosity is large in absolute dimension (but not markedly so relative to overall os coxal size). The medial extent of the ischial tuberosity terminates in a ridge on the inner surface of the ischium, near the inferior margin. The surface of the inferior margin of the inferior segment of the ischiopubic ramus is highly irregular and porous, with small bony outgrowths. The ischiopubic ramus is thick (i.e., not flattened in dorsoventral dimension). There is a small bony tubercle on the ventral surface of the ischiopubic ramus (near the midpoint of the ramus) in |

| | | | |
|---|---|---|---|
| | | | the area of origin of the *obturator externus*. The subpubic angle appears small, based on a mirrored estimation (see Chapter 4 for discussion of sex estimation). In absolute terms the ischiopubic ramus is very tall and the obturator foramen is large (but not markedly so in relative terms). The pubic body is dorsoventrally thick, with a broad and blunt pubic tubercle (the apex of which is eroded). The medial extent of the iliopubic ramus is very thick, especially in its dorsoventral dimension. There are several small foramina concentrated on the medial half of the ventral surface of the pubic body. The symphyseal surface appears to have been pulled toward the midline and away from the pubic body, with a deep groove separating the body from the symphyseal surface. It is unclear how much of this morphology is the result of bony remodeling during life, and how much is the effect of distortion. If the pulling apart of the symphyseal face from the pubic body is completely due to remodeling, then the degree of lipping is considerable. There is a bony crest (with bony outgrowths on the superior part) extending from the dorsal part of the pubic tubercle to the dorsal margin of the symphyseal surface. The medial part of the pectineal line is preserved as a small bony outgrowth. There is a thin ridge along the dorsal margin of the pubic symphyseal face, and two small bony tubercles near the inferior extent of the symphyseal face (one on the dorsal margin and one on the symphyseal face). The symphyseal surface is deeply eroded. |
| **Suffix** | **Element** | **Element portion** | **Preservational description** |
| 106B | R. OCX | Upper portion | This portion joins with HAL-VP-9/1-106A. Most surfaces of this portion are deeply eroded, with the exception of the central part of the acetabulum. The superior part of the ischial tuberosity is partially preserved, with the base of the ischial spine. The greater sciatic notch is preserved (see Chapter 4 for discussion of sex estimation) but exhibits erosion to its posterior part and insect damage. The auricular surface is nearly complete, missing the posterior and superior margins, but portions of the surface are eroded (see Chapter 4 for discussion of age estimation). There is a shallow hollowing in the area in which a true preauricular sulcus is found. The base of the ilium is preserved but is deeply eroded and fragmented. The posterior part of the acetabulum is preserved, with only the posteriormost part of the acetabular fossa. The superior margin of the acetabulum is nearly completely preserved. Only a small portion of the inferior margin is preserved. The acetabulum is strikingly tall in its vertical dimension, in both relative but especially absolute terms. The lateral margin is deeply eroded. The lunate surface is well preserved, with only very slight distortion (very thin fissures). Only the anteriormost part of the supraacetabular groove is preserved; the groove is shallow. The anterior inferior iliac spine (and the iliac portion superior to that) is not preserved. |
| 107 | R. OCX | Top of Iliac pillar, with gluteal line | This portion preserves the superiormost extent of the iliac pillar, with the iliac tubercle and iliac crest (only the outer lip of the crest is preserved). The superiormost part of the anterior gluteal line is preserved and is moderately developed. Despite that the inner surface of the iliac blade is not preserved, it is clear that the iliac crest is extremely thick near the iliac tubercle. |
| 108 | L. OCX | Ischium with acetabular frag. | This portion preserves the partial left os coxae, including the inferior portion of the ischium, the base of the ischial spine, the lesser sciatic notch, and a small sliver of the inferior part of the lunate surface. All surfaces of this portion are deeply eroded beyond the cortical bone and into the cancellous bone, except for the sliver of the lunate surface and a small portion of the ischial tuberosity. |
| 109 | L. OCX | Ischiopubic ramus | This portion preserves the segment of the ischiopubic ramus adjacent to the pubic body. The inferior margin thins and curves dorsally toward the superior end. All surfaces of this portion are deeply eroded beyond the cortical bone and into the cancellous bone, with the exception of a small segment of the inferior margin. |

| Suffix | Element | Element portion | Preservational description |
|---|---|---|---|
| 110 | OCX | Acetabular frag. | This portion preserves a small sliver of the lunate surface. |
| 111 | ?R. OCX | Iliac blade frag. | This portion preserves a superior part of the iliac blade, including the outer lip of the iliac crest. The crest is partially eroded; the preserved segments of the crest are irregular and exhibit small bony outgrowths. The crest is thick and it thins posteriorly. This portion is posterior to HAL-VP-9/107 but does not join with that portion. The inner surface is partially eroded, exposing the cancellous bone. |
| 112 | R. HUM | Head | The right humeral head is preserved. This portion includes parts of the anatomical neck, and a small inferior portion of the surgical neck (with slight distortion to the anterior surface). Only a small superomedial portion of the greater tubercle is preserved. There is a smooth groove separating the greater and lesser tubercles from the head. The head is vertically oval in superomedial view. The margin of the head is eroded. |
| 113 | R. HUM | Dist. end with shaft | The complete distal humeral end and inferior half of the shaft is preserved. The distal epiphysis is very large relative to the shaft, which is slender. Moving superiorly from the epicondyles, the shaft decreases considerably in mediolateral dimension. The shaft is very straight (exhibiting very little torsion of the medial and lateral borders). The lateral shaft surface near the midshaft position exhibits insect damage, including to the deltoid tuberosity. The tuberosity is a slight bony thickening on the lateral surface of the shaft, angled anteromedially toward its distal end. Despite the insect damage, it appears that the deltoid tuberosity is very weakly developed. The inferior extent of the tuberosity is at the approximate position of estimated midshaft. At the superior extent of the preserved portion, the inferior tip (~5 mm in length) of the crest of the greater tubercle is preserved. The crest is sharp and is slightly distorted (the crest is displaced laterally with matrix in between it and the rest of the shaft). The nutrient foramen is anteriorly adjacent to the medial border, at approximately the position of 1/3 of the estimated total shaft length from the distal end. The posterior surface of the superior half of the preserved shaft exhibits insect damage. The medial epicondyle projects very far medially and is subrectangular in shape. The medial supracondylar crest sharpens as it nears the superior margin of the medial epicondyle. The lateral supracondylar crest is sharper than the medial supracondylar crest at its superior end but is blunter inferiorly. The lateral pillar is very wide relative to the medial pillar. The olecranon fossa is mediolaterally wide, large, and very deep in both absolute and relative terms; it does not exhibit a septal aperture. The capitulum is bulbous and very large relative to the trochlea and is taller than it is wide. The lateral and posterior margins of the capitulum and the medial and lateral margins of the trochlea are partially eroded. The coronoid fossa is small (relative to the size of distal end) and deep. The radial fossa is broader, larger, and shallower than the coronoid fossa. This portion is symmetrical to the corresponding preserved portions of the antimere (HAL-VP-9/1-116). |
| 114 | ? L. HUM | Shaft frag. w/deltoid | This portion preserves part of the humeral shaft. This portion exhibits a smooth bulge that is possibly the superior part of the deltoid tuberosity. |
| 115 | L. HUM | Prox. end | The proximal humeral end with the proximal part of the shaft is preserved. This portion includes the humeral head, the surgical neck, and the greater and lesser tubercles. The anterior and inferior portions of the anatomical neck are also preserved. The proximal shaft is very slender relative to the large size of the humeral head and it thins considerably immediately below the level of the inferior margin of the head. The humeral head is vertically oval in |

| | | | |
|---|---|---|---|
| | | | superomedial view and is approximately symmetrical to its antimere (HAL-VP-9/1-112). The superior and posterior margins of the humeral head and the lateral and posterior surfaces of the greater tubercle are deeply eroded. There is a large foramen immediately inferior and adjacent to the anatomical neck on the anterior surface. The anterior and lateral surfaces of the shaft exhibit insect damage, which extends superiorly through the intertubercular groove. Both the greater and lesser tubercles are large and projecting. The lesser tubercle is elongated and runs from superolateral to inferomedial, terminating in a bony projection at its inferior extent. A smooth groove separates the head from the tubercles. The superior part of the intertubercular groove is very deep (the depth of the inferior part is difficult to assess because of insect damage). There are many foramina in the superior part of the intertubercular groove and especially on the lateral surface of the greater tubercle. The superiormost extent of the crest for the *triceps brachii* is preserved. The crests of the greater and lesser tubercles are visible but have been modified by insect activity, making it difficult to reliably assess the size of the crests, or the width and depth of the intertubercular groove between them. |
| **Suffix** | **Element** | **Element portion** | **Preservational description** |
| 116 | L. HUM | Partial distal end | The distal humeral end is partially preserved. The capitulum is preserved (although the lateral and posterior margins are eroded) and is large relative to the trochlea. The lateral half of the trochlea is preserved, as is the lateral epicondyle (but the superior margin is eroded). There are small bony outgrowths on the inferior extent of the lateral lip of the trochlea. The lateral and superomedial portions of the olecranon are preserved. The olecranon fossa is very deep and wide in absolute and relative terms. The posterior surface of the medial pillar is not preserved. The lateral supracondylar crest is visible but has been modified by insect activity and is eroded. The lateral part of the anterior surface of the distal shaft (proximal to the capitulum) exhibits insect damage. The radial fossa is preserved, although the bone surface is eroded. |
| 117 | L. HUM | Partial shaft | The middle segment of the humeral shaft is preserved. This portion nearly joins with HAL-VP-9/1-116. The shaft is straight and slender. The preserved portion widens mediolaterally at its distal end. The lateral surface of the shaft is slightly eroded, but the deltoid tuberosity is visible as a nearly vertical and very slight bony thickening, with a very thin bony crest at its superior end. Erosion of the shaft surface may have slightly reduced the apparent development of the tuberosity, but it is clear that the tuberosity would have been very weakly developed (erosion is slight). The inferior part of the crest of the greater tubercle is well-defined (as a thin and raised crest of bone); the distalmost extent is eroded. The proximal part of the lateral supracondylar crest is preserved and is well-defined. The superior part of the medial supracondylar crest is preserved and is rounded in shape, and extends proximally to meet the medial border. The inferior margin of the nutrient foramen is preserved and is positioned slightly more anteriorly relative to the medial border than on the right side (HAL-VP-9/1-113), at approximately the same position on the proximodistal axis. A segment of the posterior and medial shaft is missing near midshaft and an anterior segment of the shaft is missing at the proximal end of this portion. Much of the shaft surface exhibits insect damage, especially on the posterior surface of the distal portion, the medial surface of the proximal portion, and the anterior surface near the middle of the preserved portion. |
| 118 | HUM | Shaft frag. | This portion preserves a small part of the humeral shaft. The external shaft surface exhibits insect damage. |

| Suffix | Element | Element portion | Preservational description |
|---|---|---|---|
| 119 | R. RAD | Head | The complete radial head is preserved. The radial head is very large in absolute terms. The radial neck is very thin relative to the size of the head (as observed from the cross-section at the break, immediately inferiorly adjacent to the head). The majority of the lateral surface of the articular circumference is eroded. Portions of the superior articular circumference and the neck exhibit insect damage. |
| 120 | RAD | Shaft frag. | This portion preserves part of the shaft just distal to midshaft. The shaft tapers slightly at one end along the proximodistal axis but is otherwise consistent in shape and size along the length of the fragment. The cross-section is teardrop-shaped. The interosseous crest is blunt (i.e., not particularly sharp). |
| 121 | R. ULN | Proximal end | The complete proximal end with the proximal part of the shaft is preserved (extending to the inferior margin of the ulnar tuberosity). The lateral surface of the olecranon process is deeply eroded, precluding assessment of the olecranon breadth. There are two distinct facets in the trochlear notch (a superior facet and an inferior facet). The medial edge of the inferior facet of the trochlear notch extends far medially, contributing to the waisted appearance of the trochlear notch (i.e., the relatively small breadth between the superior and inferior parts of the trochlear notch). The trochlear articular surface is weakly keeled. There is a well-developed bony ridge extending distally from the medial edge of the inferior facet of the trochlear notch, angling medially as it extends distally. The coronoid process projects further anteriorly than the olecranon process. The trochlear notch is oriented superoanteriorly. The radial notch is very large (in absolute and relative terms) and approximately round. The posterolateral margin of the radial notch is eroded. The ulnar tuberosity is preserved and takes the form of a roughened area distomedial to the coronoid process. The posterior edge of the shaft is narrow and pillar-like. The portion of the shaft with the supinator crest is not preserved. The anterior margin of the medial part of the inferior articular surface of the trochlea is slightly eroded. The medialmost part of the inferior articular surface of the trochlea is missing (appears to have spalled off). The posterior and lateral shaft surfaces exhibit considerable insect damage. There is a flat and smooth calcium carbonate deposit on the radial facet (see Chapter 2 for discussion of taphonomy). |
| 122 | R. ULN | Shaft | The proximal midshaft portion of the ulnar shaft is preserved; the proximal extent of this portion is just distal to the ulnar tuberosity. The shaft is subtriangular at its proximal end, with a larger anteroposterior than mediolateral dimension. The shaft tapers and rounds distally. On the proximal half of this portion the posterior border is rounded (i.e., not sharp). The medial surface of the shaft is very smooth. The shaft curves anteroposteriorly; there is no discernible mediolateral curvature. The nutrient foramen is preserved on the anterior surface of the proximal part of the shaft and opens distally. The entire posterior surface and the distal half of the posterior border exhibit severe insect damage. The interosseous border is almost entirely obliterated by deep insect damage. |
| 123 | L. ULN | Partial proximal end | The proximal ulnar end is partially preserved, including the coronoid process, the radial notch, the inferior portion of the trochlear notch, and the proximal segment of the shaft (extending to the inferior margin of the ulnar tuberosity). The olecranon is not preserved (broken off along the superior margin of the inferior trochlear articular surface). There is slight asymmetry in the shape of the inferior articular surface of the trochlea between the left and right elements (i.e., compared to HAL-VP-9/1-121); the surface of this portion is slightly wider in mediolateral dimension and broader in anteroposterior dimension than HAL-VP-9/1-121, especially near the medial extent (this asymmetry may be exaggerated by erosion to this area on HAL-VP-9/1-121, but erosion clearly does not account |

| | | | |
|---|---|---|---|
| | | | for the full extent of asymmetry). Relative to the right side (HAL-VP-9/1-121), the anterior margin of the inferior articular surface of the trochlea is thickened. There is a deep hollowing posterior to the medial extension of the inferior trochlear articular surface. The margins of the inferior articular surface of the trochlea, and the medial edge of the medial extension of this surface, are eroded. The tip of the coronoid process is broken. The radial notch is large, but the shape is difficult to assess because of erosion to the lateral and inferior margins. There is a slight hollowing distal to the radial notch. A well-developed bony ridge extends distally from the medial edge of the inferior articular surface of the trochlear notch, angling medially and thinning as it extends distally. The ulnar tuberosity is preserved and is immediately inferior to the coronoid process. The supinator crest is well-developed and is long and thin in shape; it extends distally from the posteroinferior corner of the radial notch and has a hollowing posteriorly adjacent to it. The posterior surface of the proximal shaft is narrow, very straight, and pillar-like. The posterior and lateral surfaces of the preserved portion exhibit insect damage. |
| **Suffix** | **Element** | **Element portion** | **Preservational description** |
| 124 | L. ULN | Distal end | The complete distal ulnar end is preserved, with the distalmost segment of the shaft. The shaft is approximately round in cross-section at the break point. The shaft is slender relative to the size of the ulnar head, especially in mediolateral dimension. The articular circumference is tall in proximodistal dimension and flares anteriorly toward the proximal margin; the proximal margin is eroded. The cross-sectional size of the articular circumference decreases slightly distally. The articular circumference is small at its distalmost extent and encircles a roughened bony tubercle that projects distally beyond the level of the articular circumference. The styloid process is large but thin, curving only very slightly medially. There is a very small and shallow pit on the anteromedial surface of the tip of the styloid process. The posterior surface of the styloid process exhibits slight erosion and insect modification. The *extensor carpi ulnaris* groove is deep. There is a bone fragment cemented to the medial surface of the ulnar head, with trabeculae exposed. |
| 125 | L. ULN | Partial shaft | This portion preserves part of the shaft just proximal to the distal end. At the proximal end of the portion, the interosseous border is angular (giving it the appearance of a corner) and it extends distally as a sharp crest, curving posterolaterally, and then thickening and curving anteriorly toward its distal extent where it flattens to become continuous with the shaft surface. The position of greatest development of the interosseous crest is distal relative to the position most often observed in the comparative recent modern human samples. The proximal end of the shaft has an angular appearance and it rounds distally to an approximately circular cross-section at the distal break. Immediately proximal to the point where the interosseous crest flattens there is a small bony ridge along the medial edge of the crest, which may be the pronator ridge; the ridge is small and angles slightly medially toward its distal end. There is a very shallow hollowing anterior to the interosseous crest at its distal end; there is a groove posterior to the interosseous border that is very shallow at the proximal end of the portion and deepens distally, with a slight bony outgrowth in the groove at its distalmost extent. This groove is flanked along its posterior edge by the longitudinal crest (which has a rounded corner-like shape). The longitudinal crest curves anteriorly and becomes continuous with the shaft surface at approximately the same position that the interosseous crest does. There is a small nutrient foramen (opening proximally) near the distal end of the portion. The posterior border is rounded and widens distally. The medial half of the proximal part of the shaft is missing. The medial and posterior shaft surfaces exhibit shallow insect modification. |

| Suffix | Element | Element portion | Preservational description |
|---|---|---|---|
| 126 | ULN | Shaft frag. | This portion preserves a small part of the shaft, including less than half of the shaft cross-section. This portion may include part of the posterior border, based on the tight curvature of the shaft surface and the cortical thickness. |
| 127 | ? ULN | Shaft frag. | This portion preserves a small part of a long bone shaft, likely of an ulna. If this portion is ulnar shaft, it must be from the left side (since it overlaps with the portion preserved of the right shaft, HAL-VP-9/1-122), and from just proximal to the distal midshaft portion (HAL-VP-9/1-125). The shaft is triangular in cross-section and tapers toward one end. If this portion is ulnar shaft, there are slight asymmetries relative to the right side (e.g., the posterior border is sharper than the right side) |
| 128 | R. HAM | | The complete hamate is preserved. The dorsal surface is partially eroded (with trabeculae exposed). The lateral part of the dorsal surface is preserved and is very rugose, with an irregular surface and a large bony tubercle. The hamulus is long in proximodistal dimension, with a thick proximal margin and a sharp and thin distal margin (slightly eroded). There is a small bony tubercle near the distal end of the base of the hamulus, palmar to the facet for the capitate. The hamulus curves medially toward its palmar extent. The palmar surface of the hamulus is roughened and perforated by small foramina. A thin and shallow groove separates the base of the hamulus from the facet for the fifth metacarpal. There is a thin, flat, and smooth calcium carbonate deposit on the palmar portion of the facet for the triquetral, with a flake of bone cemented to the carbonate surface (note that there is a flake of bone missing from the facet for the hamate of the right triquetral, in the corresponding position). There is a small fragment of bone cemented to the palmar margin of the facet for the capitate. |
| 129 | R. Trapezium | | The complete trapezium is preserved. The surfaces of the facets for the second metacarpal and the trapezoid, and most of the margin of the facet for the first metacarpal exhibit slight erosion. There is a very slight bony lip at the margin of the facet for the first metacarpal. The facet for the first metacarpal is large and saddle-shaped, with a larger palmar half. The palmar surface between the trapezial ridge and the facet for the first metacarpal is rugose, with small foramina. The trapezial ridge is moderately developed, has a smooth surface, and is of approximately constant thickness along its length. The trapezial groove is moderately deep. The facet for the second metacarpal is large and round. There is a small elongate bony tubercle between the facets for the first and second metacarpals, on the dorsal side. There is a small bony tubercle between the facets for the first metacarpal and the lunate. There are thin and smooth calcium carbonate deposits on the facets for the scaphoid and the trapezoid, with small flakes of bone adhering to the carbonate surface of each. |
| 130 | R. TRI | | The complete triquetral is preserved. The distal margin and part of the facet for the pisiform are eroded. The facet for the pisiform is concave with very slight lipping around the margins. There is a flake of bone missing from the facet for the hamate, at the position corresponding to the flake of bone adhering to the calcium carbonate deposit on the right hamate (HAL-VP-9/1-128). There is very slight expanding matrix distortion, exhibited by a thin crack running along the length of the facet for the hamate, terminating in a small portion of bone that has been displaced from the facet for the hamate to the facet for the lunate. There is a very deep groove on the nonarticular surface, running approximately along the long axis of the bone, and flanked on its distal side by a ridge; there are many small foramina between this ridge and the margin of the facet for the hamate. |
| 131 | L. LUN | | The complete lunate is preserved. This element is very well-preserved, with only very slight erosion to the dorsal surface. The angle between the facets for the scaphoid and the capitate is wide. The proximalmost extent of the facet |

| | | | |
|---|---|---|---|
| | | | for the scaphoid borders a small elongated bony tubercle. There is a very slight bony lip around the margin of the facet for the scaphoid. There is a calcium carbonate deposit adhering to the facet for the capitate, with a flake of bone cemented to the dorsal part (note that the dorsal margin of the left capitate head, HAL-VP-9/1-132, is missing a flake of bone). |
| **Suffix** | **Element** | **Element portion** | **Preservational description** |
| 132 | L. CAP | | The complete capitate is preserved. This element is very well-preserved, with only slight erosion to the distal corner of the facet for the hamate at the dorsal edge. The head is large, especially in its dorsopalmar dimension. The capitate appears wide in dorsopalmar relative to proximodistal dimension. The facet for the second metacarpal is long and thin, and of approximately constant width along its length. The nonarticular palmar surface is very rugose, and has a thin ridge running along the long axis of the bone. There is a large foramen (laterally) and thin groove (medially) separating the nonarticular palmar surface from the head of the capitate. There is very slight lipping around the margin of the facet for the third metacarpal. There is a thin and smooth calcium carbonate deposit adhering to the facet for the hamate, and to the lateral nonarticular surface; the latter deposit has a flake of bone adhering to its surface. |
| 133 | L. TRI | | The complete triquetral is preserved. The distal margin and part of the facet for the pisiform are eroded. The facet for the pisiform is concave and the margins are slightly eroded. There is a deep groove on the nonarticular surface, running approximately along the long axis of the bone, and flanked on its distal side by a ridge; there are many small foramina between this ridge and the margin of the facet for the hamate. This element is symmetrical to its antimere (HAL-VP-9/1-130). |
| 134 | R. MC2 | Base | The complete base of the second metacarpal is preserved. The palmar and dorsal surfaces of the medial edge are slightly eroded. The base is large, as is the facet for the trapezium. There is a small bony tubercle on the lateral surface of the base (distal and slightly dorsal to the facet for the trapezium), and another just distal to the palmar portion of the facet for the third metacarpal. The nonarticular palmar surface of the base is very rugose. The facet for the capitate is obliquely oriented. The lateral surface of the proximal shaft exhibits insect damage. There is a small flake of bone cemented to the palmar margin of the facet for the third metacarpal. There is a calcium carbonate deposit in the depth of the facet for the trapezoid, with a small flake of bone adhering to the carbonate surface. |
| 135 | R. MC2 | Head + partial shaft | The complete head of the second metacarpal is preserved, with the distal part of the shaft and the dorsomedial half of the midshaft segment. There is slight erosion to the dorsal surface of the head. The head is large. The tubercle on the anterolateral surface just proximal to the margin of the articular surface of the head is well-developed. There is a bony ridge on the palmar portion of the shaft just proximal to the articular margin of the head, terminating in a small tubercle at its distalmost extent. There is a bony lip along the dorsal and distal portions of the medial margin of the head, with a deep groove adjacent to it on its proximal side. There is a very slight and rounded bony outgrowth at the distalmost tip of the head. There is a flat calcium carbonate deposit adhering to the proximal extension of the palmar articular surface of the head on the medial side, with a flake of bone adhering to the carbonate surface. |
| 136 | R. MC3 | | The complete third metacarpal is preserved. The dorsal margin of the head is partially eroded, and a small portion of the dorsal surface of the shaft is missing just proximal to midshaft. The palmar portion of the facet for the capitate is eroded. The head is large and is especially mediolaterally wide relative to its dorsopalmar height. The groove |

| | | | |
|---|---|---|---|
| | | | proximally adjacent to the medial margin of the head is deep. There is a very slight bony tubercle just proximal to the proximal extension of the palmar articular surface of the head on the medial side. The nonarticular palmar surface of the base is rugose and extends into a bony tubercle on the lateral surface. There is a small bony tubercle in the notch of the facet for the second metacarpal. The facet for the second metacarpal is concave. There is a bony tubercle just distal to the styloid process on the lateral margin of the dorsal surface, extending distally as a narrow ridge with a groove adjacent on the palmar side. There is a deep pit-like hollowing medially adjacent to the styloid process on the dorsal surface. The styloid process is mediolaterally wide, but weakly projecting. There are two distinct facets for the fourth metacarpal. There is a small bony thickening on the palmar portion of the medial surface, just distal to the facet for the fourth metacarpal on the palmar half of the base. The facet for the capitate is wider along the dorsal margin; the facet is weakly convex on its palmar half and weakly concave on its dorsal half. The proximal and distal parts of the dorsal surface of the shaft exhibit insect damage. There is a flat and smooth calcium carbonate deposit adhering to the proximal extension of the palmar articular surface of the head on the medial side. There is also a calcium carbonate deposit adhering to the facet for the fourth metacarpal on the palmar half of the base, with a small flake of bone adhering to the carbonate surface. |
| **Suffix** | **Element** | **Element portion** | **Preservational description** |
| 137 | R. MC4 | Base + shaft | The complete base of the fourth metacarpal is preserved, with the proximal part of the shaft and dorsolateral part of the midshaft segment. The facet for the hamate is partially eroded and the dorsal portion is missing. There are two distinct round facets for the third metacarpal, with a deep groove between them. There is a large and blunt tubercle on the lateral surface, just distal to facets for the third metacarpal. The dorsal and medial surfaces of the shaft near the base exhibit insect damage. There is a calcium carbonate deposit adhering to the palmar surface of the base, with a flat flake of bone adhering to the carbonate surface. |
| 138 | L. MC1 | Head | The complete head of the fist metacarpal is preserved, with the distal part of the shaft. This portion is very well preserved. There is a pit-like hollowing on the dorsal surface, immediately proximal to the articular margin of the head. There is a well-developed bony tubercle on the lateral surface, proximal to the articular margin of the head, with a thin groove separating the margin of the head from the tubercle. A thin ridge runs proximally from the bony tubercle along the lateral surface of the shaft. The palmar surface of shaft exhibits very slight keeling. The head and distal shaft are mediolaterally wide. In palmar view, the outline of the distal margin of the head is rectangular, with slightly rounded corners. |
| 139 | L. MC2 | Base | The complete base of the second metacarpal is preserved. The palmar surface of the medial edge is slightly eroded. This portion is approximately symmetrical with its antimere (HAL-VP-9/1-134), with only slight asymmetry at the nonarticular palmar portion of the base. The base is large. There is a large facet for the trapezium. There is a small bony tubercle on the lateral surface of the base (distal and slightly dorsal to the facet for the trapezium), and another just distal to the palmar portion of the facet for the third metacarpal. The nonarticular palmar surface of the base is very rugose. The facet for the capitate is obliquely oriented. There is a calcium carbonate deposit adhering to the medial part of the facet for the trapezoid, with a flake of bone adhering to the carbonate surface. |
| 140 | L. MC2 | Head | The complete head of the second metacarpal is preserved, with the distal part of the shaft. The lateral surface of the head and the proximal margin of the head on the palmar side are slightly eroded. The head is large and is approximately symmetrical with its antimere (HAL-VP-9/1-135), although it is slightly smaller in mediolateral |

| | | | |
|---|---|---|---|
| | | | dimension. The tubercle on the anterolateral surface just proximal to articular margin of the head is well-developed. There is a bony ridge on the palmar portion of the shaft just proximal to the margin of the head, but it lacks the small bony tubercle present on the right element. The medial margin of the head is slightly eroded, but it is nonetheless clear that the bony lip present on the right element along the dorsal and distal portions of the medial margin is either absent or very weak. The groove adjacent to the medial margin of the head on the proximal side is shallower than on the right element. The palmar and medial surfaces of the shaft and the head exhibit slight insect modification. |
| **Suffix** | **Element** | **Element portion** | **Preservational description** |
| 141 | L. MC4 | Head + shaft | The complete head of the fourth metacarpal is preserved, with most of the shaft (missing only the distal segment). There is a small tubercle on the dorsomedial surface just proximal to the articular margin of the head. There is a deep and narrow groove proximally adjacent to the medial margin of the head. The shaft surfaces and the dorsal and palmar surfaces of the head exhibit insect damage. There is a calcium carbonate deposit adhering to the lateral surface of the head, with a flake of bone adhering to the carbonate surface. |
| 142 | L. MC5 | Base + shaft | The complete base of the fifth metacarpal is preserved, with the medial half of the shaft; flaring at the distal end suggests that the preserved portion of the shaft nearly reaches the base of the head. The base is large, with rugose palmar and lateral surfaces. There is a broad tubercle on the palmar surface, extending distally and medially from the palmar margin of the facet for the hamate. There is a large tubercle on the lateral nonarticular surface of the base, with a shallow depression in the center. The dorsal surface of the base is irregular, with a shallow and thin groove distally adjacent to the dorsal margin of the facet for the hamate. There is a small circular pit on the lateral surface just distal to the facet for the fourth metacarpal, which is likely the result of insect modification. |
| 143 | R. MC5 | Head | The head of the fifth metacarpal is nearly complete, missing only the lateral surface. The dorsal surface of the head is partially eroded. There is a well-developed tubercle on the dorsomedial surface, just proximal to the margin of the head. There is a flat and smooth calcium carbonate deposit adhering to the palmar surface of the head. |
| 144 | L. MC3 | Shaft frag. | The midshaft segment of the third metacarpal is preserved. There is a small foramen, opening distally, on the lateral side of the palmar surface, proximal to midshaft. The shaft surfaces exhibit slight insect modification. |
| 145 | PHP | Complete | The complete proximal hand phalanx of the left fifth ray is preserved. The trochlea is slightly wider in mediolateral dimension than the distal shaft. The medial margin of the head projects slightly further distally than the lateral margin. The shaft exhibits very slight curvature, as is typical of recent modern humans. The base is wide, with well-developed tubercles on the lateral and especially the medial margins of the palmar surface. There is a bony tubercle on the lateral surface of the base. There are ridges along the medial and lateral margins of the palmar surface of the shaft, extending distally from the tubercles at the base. The shaft is wide in mediolateral dimension relative to its dorsopalmar dimension. The dorsal surface of the base is partially eroded. The shaft exhibits slight insect modification. The proximal articular surface is concave and has a smooth and concave calcium carbonate deposit adhering to its medial half, with a small flake of bone adhering to the carbonate surface. |
| 146 | PHP | Base + shaft | The proximal hand phalanx of a left ray is partially preserved. This element most likely belongs to the third ray but could also belong to the second ray. This portion is the antimere of HAL-VP-9/1-147. This portion preserves the complete base and shaft, missing only the head. This portion is long in proximodistal dimension. There is slight erosion to the medial side of the dorsal surface of the base. The shaft exhibits very slight curvature, as is typical of |

| | | | |
|---|---|---|---|
| | | | recent modern humans. The base is large with well-developed tubercles on the lateral and especially the medial margins of the palmar surface. There is a ridge extending slightly distally on the palmar surface from the medial tubercle at the base. There is a large bony thickening on the dorsolateral surface of the base. There are well-defined ridges on the medial and lateral margins of the palmar surface near midshaft. The shaft is wide in mediolateral dimension relative to its dorsopalmar dimension. The proximal articular facet is gently concave. The shaft exhibits slight insect modification. There is a flat calcium carbonate deposit adhering to the dorsal surface of the base, with a small flake of bone adhering to the carbonate surface. |
| **Suffix** | **Element** | **Element portion** | **Preservational description** |
| 147 | PHP | Base + shaft | The proximal hand phalanx of a right ray is partially preserved. This element most likely belongs to the third ray but could also belong to the second ray. This portion is the antimere of HAL-VP-9/1-146. This portion preserves the complete base and partial shaft (preserving the proximal segment up to just distal of midshaft). The dorsal surface of the base is partially eroded. There is a small segment of bone missing from middle of the palmar surface of the shaft near midshaft. The shaft exhibits very slight curvature, as is typical of recent modern humans. The base is large with well-developed tubercles on the lateral and especially the medial margins of the palmar surface. There is a ridge extending slightly distally on the palmar surface from the medial tubercle at the base. There is a large bony thickening on the dorsolateral surface of the base. There are well-defined ridges on the medial and lateral margins of the palmar surface near midshaft. The shaft is wide in mediolateral dimension relative to its dorsopalmar dimension. The proximal articular facet is gently concave. The dorsal surface of the shaft exhibits deep insect damage near midshaft. There is a small flake of bone cemented to the lateral tubercle on the palmar surface of the base. |
| 148 | PHP | Base | This portion joins with HAL-VP-9/1-149. The proximal hand phalanx is partially preserved, probably from the left side, and almost certainly from the fourth ray. The base is complete but exhibits erosion to the dorsal and medial surfaces. The base is narrower in mediolateral dimension than HAL-VP-9/1-146. There are bony thickenings on the medial and especially lateral surfaces of the base. There is a tubercle on the lateral margin of the palmar surface (the medial margin is obscured by a calcium carbonate deposit). There is a thin and smooth calcium carbonate deposit on the palmar surface of the base, with a large and thin flake of bone adhering to the carbonate surface (and another more superficial carbonate deposit on the surface of the bone flake). There is also a smooth and concave calcium carbonate deposit adhering to the proximal articular facet, with a concave flake of bone adhering to the carbonate surface. Both the flake of bone and the underlying carbonate deposit correspond in contour to the fourth metacarpal head (HAL-VP-9/1-141). |
| 149 | PHP | Shaft frag. | This portion joins with HAL-VP-9/1-148. This portion preserves the shaft of a proximal hand phalanx, probably from the left side, and almost certainly from the fourth ray. The portion preserves the shaft segment near midshaft. The shaft exhibits very slight curvature, as is typical of recent modern humans. There are well-defined ridges on the medial and lateral margins of the palmar surface of the shaft. The shaft is wide in mediolateral dimension relative to its dorsopalmar dimension. |
| 150 | IHP | Complete | The complete intermediate hand phalanx of the left third ray is preserved. Only a small segment of the dorsomedial shaft surface near midshaft is missing. This portion is the antimere of HAL-VP-9/1-151. The dorsal margin of the base is partially eroded. The trochlea is slightly wider in mediolateral dimension than the adjacent shaft. The shaft |

| | | | |
|---|---|---|---|
| | | | exhibits very slight curvature, as is typical of recent modern humans. The base is very wide, and the shaft tapers considerably toward its distal end. There are well-developed ridges along the medial and lateral margins of the palmar surface near the base, and a broad ridge along the midline of the palmar surface near the base (thinning distally). There are grooves separating the medial and lateral ridges from the midline ridge on the palmar surface of the shaft. There are slight bony thickenings on the medial and lateral surfaces of the base, just distal to the articular surface. The shaft is wide in mediolateral dimension relative to its dorsopalmar dimension. There is a calcium carbonate deposit adhering to the center of the proximal articular facet; the surface of the deposit is smooth, concave, and obliquely-oriented. |
| **Suffix** | **Element** | **Element portion** | **Preservational description** |
| 151 | IHP | Base + shaft | The intermediate hand phalanx of the right third ray is partially preserved. This portion preserves the complete base with the proximal half of the shaft. This portion is the antimere of HAL-VP-9/1-150. The margins of the base are partially eroded. The base is very wide, and the shaft tapers toward its distal end. There are well-developed ridges along the medial and lateral margins of the palmar surface near the base, and a broad ridge along the midline of the palmar surface near the base (thinning distally). There are grooves separating the medial and lateral ridges from the midline ridge on the palmar surface of the shaft. There are slight bony thickenings on the medial and lateral surfaces of the base. The double proximal articular facet has a slightly larger medial facet. In proximal view, the margin of base flares outward, especially along the dorsal margin, with a thin bony ridge encircling the dorsal circumference of the proximal articular surface. The margin of the base is considerably more flared and there is more bone around the margin of facet than observed on the other rays; the proximal facet appears arthritic. Slight lipping is also visible on the antimere of this portion (HAL-VP-9/1-150), but erosion to the margin of the proximal surface of the base of HAL-VP-9/1-150 precludes a comparative assessment of the degree of lipping. There is a very thin but distinct line between the proximal articular surface and the dorsally adjacent lip of bone. The shaft is wide in mediolateral dimension relative to its dorsopalmar dimension. The palmar surface of the shaft exhibits erosion and insect damage. |
| 152 | IHP | Base + shaft | The intermediate hand phalanx of the left second ray is partially preserved. The base is narrower in mediolateral dimension than HAL-VP-9/1-150. The palmar and dorsal margins of the base are partially eroded. The shaft tapers distally. There are weak ridges along the medial and lateral margins of the palmar surface near the base, and a broad ridge along the midline of the palmar surface near the base (thinning distally). There are shallow grooves separating the medial and lateral ridges from the midline ridge on the palmar surface of the shaft. There are slight bony thickenings on the medial and lateral surfaces of the base. The two halves of the double proximal articular facet are approximately equal in size. This portion does not exhibit the arthritic changes observed on the base of HAL-VP-9/1-151. The shaft is wide in mediolateral dimension relative to its dorsopalmar dimension. |
| 153 | IHP | Base + shaft | The intermediate hand phalanx of the left fourth ray is partially preserved. The base is narrower in mediolateral dimension and the shaft is less thick than HAL-VP-9/1-152. There are ridges near the medial and lateral margins of the palmar surface near the base, and a ridge along the midline of the palmar surface near the base (thinning distally). There are grooves separating the medial and lateral ridges from the midline ridge on the palmar surface of the shaft. There are slight bony thickenings on the medial and lateral surfaces of the base. The two halves of the |

| | | | |
|---|---|---|---|
| | | | double proximal articular facet are approximately equal in size. There is a thin bony lip along the medial margin of the proximal facet. The shaft is wide in mediolateral dimension relative to its dorsopalmar dimension. |
| **Suffix** | **Element** | **Element portion** | **Preservational description** |
| 154 | IHP | Base + shaft | The intermediate hand phalanx of the left fifth ray is partially preserved. The base is narrower in mediolateral dimension than HAL-VP-9/1-153. There are slight bony thickenings on the medial and lateral surfaces of the base. The lateral edge of the shaft is more curved (i.e., hollowed) in dorsal view. There is a thin bony lip along the lateral margin of the proximal facet. The shaft is wide in mediolateral dimension relative to its dorsopalmar dimension. Most of the palmar surface and the proximal articular facet is covered with calcium carbonate. There is a carbonate deposit adhering to the central and medial parts of the proximal facet, with a flake of bone adhering to the carbonate surface. There is a flat carbonate deposit adhering to the palmar surface of the base and proximal shaft, with a flat flake of bone adhering to the carbonate surface. |
| 155 | IHP | Head | The head of an intermediate hand phalanx is preserved. This portion likely belongs to the second or third ray. The side is indeterminate. This portion includes the head and distal part of the shaft. The trochlea is preserved but is broken along one of its edges. There is a flat calcium carbonate deposit adhering to the broken edge. There is an irregularly shaped carbonate deposit on the palmar surface of the shaft, immediately proximal to the trochlea and obscuring the proximal part of the trochlea. |
| 156 | ? IHP | Shaft frag. | This portion preserves a small shaft fragment, likely of an intermediate hand phalanx of the fourth or fifth ray. The side is indeterminate. |
| 157 | THP | Complete | The complete terminal hand phalanx of a second, third, or fourth ray is preserved. The side is indeterminate. This portion is well-preserved. The shaft and distal tuberosity are proximodistally elongate and thin in mediolateral dimension relative to the length of the phalanx. The element is long in its maximum dimension, and the shaft is thin in dorsopalmar relative to mediolateral dimension. The shaft tapers in mediolateral dimension toward the distal end. There are bony tubercles on the medial and lateral surfaces of the base. The two halves of the double proximal articular facet are approximately equal in size. There is a thin bony lip along the dorsal margin of the proximal facet. The palmar surfaces of the base and proximal shaft are very irregular, with a broad hollowing along the midline from the proximal edge of the base to approximately midshaft, flanked on the medial and lateral sides by narrow ridges that curve to meet at approximately midshaft. The medial and lateral extensions of the distal tuberosity on the palmar side are thin and project proximally as thin points. |
| 158 | THP Ray 1 | Base + shaft | The terminal hand phalanx of the right first ray is partially preserved. This portion preserves the complete base with most of the shaft. The dorsal and lateral surfaces near the base are eroded. The base is wide, and the shaft tapers distally. There is a bony ridge on the dorsal surface adjacent to the margin of the proximal articular surface. There is a large tubercle on the medial surface of the base. A thin ridge runs along the lateral surface of shaft. The double proximal articular facet has a slightly larger lateral facet. There is a very thin bony lip along the margin of the proximal facet. There is a deep hollowing along the midline on the palmar surface of the base and the proximal shaft; this hollowing is flanked on the medial and lateral sides by two narrow ridges that curve to meet at approximately midshaft. There is a calcium carbonate deposit adhering to the lateral portion of the palmar surface of the base, with a flat flake of bone adhering to the carbonate surface. |

| Suffix | Element | Element portion | Preservational description |
|---|---|---|---|
| 159 | MTT | Shaft frag. | The preserved portion includes part of a metatarsal shaft. The ray and side are indeterminate. The shaft is approximately teardrop-shaped in cross-section. There is a small bony tubercle on the shaft surface and a thin bony ridge running along the length of the shaft. |
| 160 | R. FEM | Proximal end | The complete proximal femoral end is preserved, including only the superior part of the lesser trochanter (which is partially eroded). The proximal end is very large in absolute size, and relative to the shaft cross-sectional size. The femoral head is strikingly large. Small segments of bone are missing from the inferior, anterior, and posterior surfaces near the base of the neck. The posterolateral surface of the greater trochanter is slightly eroded and exhibits slight expanding matrix distortion. The surfaces around the margin of the femoral head are partially eroded, with especially deep erosion to the inferior and anterior surfaces near the margin of the head. A segment of the posterior surface of the head is missing. There is deep erosion to the head near the fovea capitis. The superior surface and margin of the fovea capitis are preserved, with a small bony tubercle adjacent to the anterior margin; the preserved portion of the margin suggest that the fovea capitis is oval or triangular in outline. The femoral neck is long and waisted (in anterior or posterior view). The contour of the superior margin of the neck is deeply concave. There are thin and deep grooves on the superior surface of the neck (running along the long axis of the neck). There are foramina adjacent to the superior margin of the head, on the superior and posterior surfaces of the neck, on the anteromedial surface of the greater trochanter, and on the medial surface of the intertrochanteric crest. The greater trochanter is very large and rugose, with large medially-oriented bony projections at the superior end on the anterior and posterior sides. There is a thin but clearly-defined vertical line on the anterior surface that is likely the intertrochanteric line (at the approximate level of the medial extent of the greater trochanter). At the superior extent of the vertical line on the anterior surface there is a well-developed oval-shaped bony tubercle that slants inferomedially (in the area of attachment of the iliofemoral ligament), with a round patch of thickened and irregular bone inferior to it. There is a round roughened area adjacent to the margin of the head on the anterosuperior surface of the neck. The margin of this roughened area is elevated above the surface of the neck. The trochanteric fossa is very deep. The *obturator externus* groove is very slight, taking the form of a flattened surface on the posterior surface of the neck. The anteromedial surface of the proximal shaft exhibits insect damage. |
| 161 | R. FEM | Partial distal end (lateral condyle) | This portion joins with HAL-VP-9/1-167. The distal femoral end is partially preserved, including the distal segment of the shaft (extending to a position just proximal to where the shaft flares at the distal end). The distal end is very large in absolute terms, and relative to the shaft cross-sectional size. The lateral condyle is preserved, although most of the articular surface is eroded. The lateral epicondyle is preserved, as is a small superolateral portion of the intercondylar fossa with the lateralmost part of the intercondylar line. The proximal part of the medial supracondylar line is visible, although partially eroded. The lateral supracondylar line is well-developed and bulges into a large elongated bony tubercle (proximal to the lateral condyle) before continuing as a broad ridge down the posterolateral edge of the shaft to the posterior projection of the lateral epicondyle, terminating in a well-developed tubercle on the superoposterior portion of the lateral epicondyle. The lateral portion of the popliteal surface is preserved and is broad and slightly hollowed with foramina near the midline. The lateral margin of the patellar lip extends far proximally and sweeps laterally (such that the lateral epicondyle is not visible in anterior view). The lateral condyle is very large in anteroposterior dimension. The popliteal groove is broad and deepens as it curves |

| | | | |
|---|---|---|---|
| | | | anteroinferiorly into a deep impression for the *popliteus*, which continues as a groove anteroinferiorly to meet the articular surface of the lateral condyle. There is a broad groove adjacent to the lateral margin of the condyle on the posterior part of the lateral surface; the lateral margin of the condyle projects laterally as a broad ridge adjacent to the groove. The impression for the lateral head of the *gastrocnemius* is either not clearly visible or is placed inferiorly on the posterior part of the lateral epicondyle. The anterior part of the lateral epicondyle is smooth. The anterior surface of the distal shaft is very flat. There is very slight osteophytic lipping along the lateral margin of the anterior part of the articular surface, with small bony outgrowths along the margin. The anterior surface of the distal shaft exhibits insect damage. |
| **Suffix** | **Element** | **Element portion** | **Preservational description** |
| 162 | R. FEM | Medial condyle | This portion preserves part of the medial condyle; excluding part of the articular surface, most surfaces of this portion are deeply eroded. The posteroinferior part of the medial surface preserved and is very irregular and rugose, with small pit-like depressions. The medial margin of the medial condyle is preserved, as well as the medial part of the popliteal surface (although the surface is completely eroded, with only cancellous bone remaining). |
| 163 | L. FEM | Partial shaft | This portion preserves a distal midshaft segment of the femoral shaft. Most of the anterior surface of the shaft is missing. The anterior surface is rounded in cross-section. The posterolateral and posteromedial surfaces are approximately flat. The shaft is teardrop-shaped in cross-section and is large in anteroposterior relative to mediolateral dimension, in part due to the presence of a well-developed pilaster. A foramen is visible just lateral to the pilaster, opening proximally; the surface of the shaft in this area exhibits deep insect modification, but a thin rod of calcium carbonate is preserved, extending from the foramen beyond the insect-modified surface (preserving the shape of the foramen). The cortical bone is moderately thick. The linea aspera exhibits deep insect damage at its proximal end, but at the distal end the medial and lateral lips are well-defined. At the distal end of the portion, the medial lip of the linea aspera is slightly more well-developed (this may be slightly exaggerated by erosion to the lateral lip, but erosion does not account for the full difference). The linea aspera is well-developed, and the margins preserved are blunt. The proximal part of the shaft exhibits deep insect damage. |
| 164 | L. FEM | Lateral condyle (partial) | This portion preserves the posterior part of the lateral femoral condyle. All surfaces are deeply eroded, and only small portions of the articular and popliteal surfaces are preserved. The preserved portions are symmetrical to the antimere (HAL-VP-9/1-161). A small superior portion of the impression for the *popliteus* is preserved; the lateral epicondyle is otherwise badly eroded. |
| 165 | L. FEM | Medial condyle (partial) | This portion preserves the posteromedial portion of the medial femoral condyle. All surfaces are deeply eroded, with only a small part of the articular surface preserved. The medial part of the popliteal area is preserved, but the surface is eroded, with only cancellous bone remaining. The preserved portions are symmetrical to the antimere (HAL-VP-9/1-162). |
| 166 | L. FEM | Lateral condyle frag. | This portion preserves a long and thin fragment of the anterior part of the lateral femoral condyle. All surfaces are very badly eroded (exposing cancellous bone), with only small portions of the articular surface intact. |
| 167 | R. FEM | Shaft frag. | This portion joins with HAL-VP-9/1-161. This portion preserves a segment of the distal femoral shaft, just proximal to the position where the medial and lateral supracondylar lines meet at the linea aspera. The medial supracondylar line is broader and more well-developed; the lateral supracondylar line is a very thin elevated ridge. The cortical thickness is moderate. The superior part of the medial shaft surface exhibits insect damage. There is slight |

| | | | |
|---|---|---|---|
| | | | expanding matrix distortion on the superior part of the linea aspera, resulting in the posterior displacement of a small shaft fragment. |
| **Suffix** | **Element** | **Element portion** | **Preservational description** |
| 168 | L. FEM | Shaft frag. | This portion preserves a proximal segment of the femoral shaft. The gluteal tuberosity is partially preserved and spirals superolaterally. The surface of the tuberosity is very rugose. The shaft is slightly flattened in anterolateral relative to posteromedial dimension. The shaft surface exhibits deep insect damage, with calcium carbonate deposits adhering to the insect-modified surface. |
| 169 | FEM | Shaft frag. | This portion preserves the anterior portion of the midshaft segment of the femoral shaft. The side is indeterminate. The shaft surface is very smooth and is rounded in cross-section. The external shaft surface exhibits insect damage, with calcium carbonate deposits adhering to the insect-modified surface. |
| 170 | L. FEM | Trochanteric frag. | This portion preserves part of the greater trochanter and a small part of the adjacent shaft. The surface of the trochanteric portion is rugose; the surface of the shaft portion is smooth. This portion is likely the inferior part of the anterolateral surface of the greater trochanter, with the anterior and lateral surfaces of the proximal shaft. The margins of the trochanteric surface extend inferiorly to meet at a point. The shaft surface exhibits considerable insect damage. |
| 171 | ? L. FEM | Trochanteric frag. | This portion preserves a fragment of trochanter. This portion is likely from the left femur since it appears to overlap with the portions preserved of the right proximal femur. The surface is rugose. |
| 172 | FEM shaft fragments | N = 6 | – |
| 173 | R. TIB | Distal end + shaft | The distal tibial end and anterior part of the distal shaft are preserved. The middle segment of the distal end (a rectangular portion at the middle of the distal end along the anteroposterior axis) is not preserved. The medial and posterior margins of the medial malleolus are partially eroded. The posterior, medial, and lateral surfaces of the distal end are slightly eroded. The medial part of the anterior groove is preserved and is deep, with a large bulge of bone superior to it. The anterior groove extends along the margin of the distal articular surface, curving inferiorly toward the tip of the medial malleolus. The anterior colliculus extends only slightly further inferiorly than the posterior colliculus. The intercollicular groove is slight. The posterior groove is weakly excavated. The fibular notch is partially eroded; only a small anteroinferior portion of the distal fibular articular surface is preserved. The medial malleolus is thick in mediolateral dimension. Broad bony ridges extend superiorly and convergently from the anterior and posterior edges of the fibular notch on the medial surface (corresponding to the points of attachment for the anterior and posterior tibiofibular ligaments, respectively); at their superior extent there is a proximodistally elongate bony thickening (for the attachment of the interosseous membrane). The posterior ridge extends superiorly from a large tubercle on the posterolateral surface of the distal end. The lateral portions of the anterior and posterior colliculi are partially eroded. The talar facet is broader in anteroposterior dimension at its lateral end. There are small bony spicules on the lateral part of the anterior margin of the talar facet. The distal articular surface extends very slightly onto the anterior surface of the distal tibia at the lateral edge. The distal end exhibits very slight expanding matrix distortion, resulting in thin carbonate-filled cracks on the talar facet. The anterior surface of this portion is partially eroded and exhibits deep insect modification. |

| Suffix | Element | Element portion | Preservational description |
|---|---|---|---|
| 174 | R. TIB | Post. midshaft | This portion joins with HAL-VP-9/1-175. The following description includes both the HAL-VP-9/1-174 and -175 portions. The proximal segment of the shaft is preserved, with missing segments on the medial and lateral surfaces, and a small missing segment on the posterior surface. The preserved portion extends to the inferior extent of the tibial tuberosity (the bone surface in this area is elevated and irregular with small foramina). There is a small bony spicule extending proximally on the anterior border, just distal to the tibial tuberosity. The interosseous surface is very flat. The medial surface is gently rounded. The anterior crest is rounded at its proximal end and sharpens distally, angling slightly inferolaterally. Small portions of the soleal line are preserved and are moderately developed (some portions are spalled off). The nutrient foramen is preserved (on the vertical line) and extends proximally as a very deep and thin groove. The vertical line is rounded and fades inferiorly. The portion of the shaft preserving the medial crest is not preserved. The distal portion of the interosseous crest is preserved and angles gently posteroinferiorly, with a very slight hollowing anteriorly adjacent near the distal end of the portion. The anteroposterior dimension of the shaft is very large relative to the mediolateral dimension (i.e., the shaft is highly platycnemic). The shaft is very straight. The cortical thickness is moderate, except for the large cortical thickness along the anterior crest. Several portions of the shaft surface, especially the proximal segment, exhibit insect damage. |
| 175 | R. TIB | Anterior part, proximal shaft | This portion joins with HAL-VP-9/1-174. See the description for HAL-VP-9/1-174 (above), which includes both portions. |
| 176 | ? R. TIB | Part of proximal plateau | This portion preserves the posterolateral portion of the proximal tibial end, likely from the right side. This portion includes the posterolateral part of the tibial plateau (although the posterior and lateral margins are badly eroded with only cancellous bone remaining). The plateau thickens in proximo-distal dimension anteriorly. The posterolateral portion of the lateral condyle (with articular surface) is preserved. On the lateral margin of the condyle there is a small circular portion of roughened, porous bone that appears arthritic (angled obliquely relative to the articular surface). A small portion of the posterolateral shaft surface is preserved, with a thin bony ridge running along the posterolateral margin and curving posteroinferiorly. There is a small piece of cancellous bone cemented to the posterior surface of the shaft, just inferomedial to where the superior fibular articular facet would be located. The shaft surface and superior surface of the lateral condyle exhibit insect damage. |
| 177 | L. TIB | Distal end + shaft | This portion joins with HAL-VP-9/1-178. The distal tibial end and distal half of the shaft are preserved. The shaft is missing lateral and posterior segments. The posterior and anterior surfaces of the distal end are partially eroded. The interosseous surface is flat and the medial surface is gently rounded. The anterior crest is rounded distally and sharpens proximally (although the proximal part exhibits extensive insect damage), and angles slightly superomedially at its proximal extent. A segment of the vertical line is visible, slanting slightly anteroinferiorly. The anterior groove is deep and thin and runs along the margin of the distal articular surface, curving inferiorly toward the tip of the medial malleolus. The anterior colliculus extends only slightly further inferiorly than the posterior colliculus. The intercollicular groove is slight. The distal edge of the posterior colliculus is eroded. There are small bony spicules extending from the posterior surface of the anterior colliculus. The posterior groove appears weakly excavated (although this is difficult to assess because of erosion to this area). The surface where the groove for the |

| | | | |
|---|---|---|---|
| | | | *flexor hallucis longus* would be is eroded, however, it is clear that if the groove was present it was weakly excavated. The fibular notch is preserved, although the posterior part of the distal margin is eroded. The distal fibular articular surface is positioned anteriorly in the fibular notch and is a wide crescent-like shape. The medial malleolus is thick in mediolateral dimension. Broad bony ridges extend superiorly and convergently from the tubercles on the anterior and posterior edges of the fibular notch on the medial surface (corresponding to the points of attachment for the anterior and posterior tibiofibular ligaments, respectively); at their superior extent they flank a proximodistally elongate bony thickening (for the attachment of the interosseous membrane). The talar facet is broader in anteroposterior dimension at its lateral end. There is a thin lip of bone on the anterior and posterior margins of the medial part of the talar facet. There are very small bony spicules along the lateral part of the anterior margin of the talar face. There is a thin groove along the lateral side of the posterior colliculus, between the colliculus and the margin of the talar facet, extending slightly posteriorly along the posterior margin of the talar facet. A segment of the vertical line visible, slanting slightly anteroinferiorly. Several portions of the shaft surface, especially the anterior surface of the proximal segment, exhibit insect damage. |
| **Suffix** | **Element** | **Element portion** | **Preservational description** |
| 178 | L. TIB | Anterior proximal shaft | This portion joins with HAL-VP-9/1-177. This portion preserves the anterior half of the proximal segment of the shaft, from the approximate midshaft position to the tibial tuberosity. The inferior part of the tibial tuberosity is elevated and irregular with small foramina, and a slight hollowing adjacent to the lateral edge of the inferior part. The superior part of the tibial tuberosity is eroded. The small preserved anterior portion of the interosseous surface is very flat. The medial surface is gently rounded. The anterior crest is rounded proximally and sharpens distally, angling slightly inferolaterally. The shaft appears highly platycnemic based on the tight curvature of the anterior border. The preserved portion of the shaft is very straight. The cortical thickness increases inferiorly, with the greatest cortical thickness located along the anterior crest. |
| 179 | TIB shaft fragments | N = 6 | – |
| 180 | R. FIB | Distal end | The complete distal fibular end is preserved. There is slight erosion to the anterior, posterior, and lateral surfaces. The distal end is large in anteroposterior relative to mediolateral dimension. The shaft cross-section is approximately triangular in outline. Only the inferiormost extent of the fibular groove is preserved (the superior portion is eroded); the groove extends inferiorly along the medial margin of the lateral malleolus. A small groove interrupts the superomedial margin of the lateral malleolus and continues into the malleolar fossa. The malleolar fossa is very deep. The malleolar articular surface is large, with an anteriorly displaced superior apex and inferior margins that angle sharply inferiorly, tapering to meet at a thin point. The anterior margin of the articular surface is eroded. The inferiormost part of the surface for the interosseous membrane is slightly hollowed and irregular, with small foramina. There is a small bony tubercle on the posteromedial edge, just posterosuperior to the posterior margin of the articular surface. There is a thin ridge of bone along the anterolateral edge of the portion, terminating at its distal extent in a thin bony tubercle on the anteromedial surface (at the level of the superior margin of the articular surface). |

| Suffix | Element | Element portion | Preservational description |
|---|---|---|---|
| 181 | ? R. FIB | Proximal shaft | This portion preserves the proximalmost segment of the fibular shaft, including the fibular neck. This portion is likely from the right side. The base of the fibular head is partially preserved, but the surface is deeply eroded with only cancellous bone remaining. The shaft at the level of the neck is flattened in its approximately anteroposterior dimension. The shaft surface is eroded and exhibits deep insect damage and slight expanding matrix distortion (there are thin cracks running along the length of the shaft). |
| 182 | L. FIB | Distal end | The complete distal fibular end is preserved. Portions of most of the surfaces exhibit erosion. The distal end is large in anteroposterior relative to mediolateral dimension. This portion is noticeably asymmetrical to its antimere (HAL-VP-9/1-180) in its broader anteroposterior dimension. The area around the fibular groove is eroded. A small groove interrupts the superomedial margin of the lateral malleolus and continues into the malleolar fossa. The malleolar fossa is very deep. The malleolar articular surface is large (the anterior and posterior margins are partially eroded), with an anteriorly displaced superior apex and inferior margins that angle sharply inferiorly, tapering to meet at a thin point. The inferiormost part of the surface for the interosseous membrane is preserved but exhibits deep erosion. There is a thin ridge of bone along the anterolateral edge of the portion, terminating at its distal extent in a thin bony tubercle on the anteromedial surface (at the level of the superior margin of the articular surface). |
| 183 | FIB | Shaft frag. | This portion preserves a small segment of the fibular shaft. The side and portion are indeterminate. At one end, the shaft cross-section is teardrop-shaped, with a sharp crest on one side and a tight curve on the opposite side (one surface is convex and the opposite surface is gently concave). The shaft tapers slightly at the other end and is roughly triangular in cross-section; the shaft surface of this end exhibits insect damage. |
| 184 | FIB | Shaft frag. | This portion preserves a small segment of the fibular shaft. The side and portion are indeterminate. At one end, the shaft cross-section is teardrop-shaped, with a sharp crest on one side and a tight curve on the opposite side (both surfaces are weakly convex). One of the shaft surfaces hollows toward the opposite end of this portion, resulting in a cross-section at the opposite end that is approximately teardrop-shaped with a sharp crest on one side and a tight curve on the opposite side, and one weakly concave and one weakly convex shaft surface. The end with two weakly convex surfaces (the former described above) is affected by expanding matrix distortion, with a small shaft segment having been obliquely displaced and cemented in place by a calcium carbonate deposit. Several portions of the shaft surface exhibit insect damage. |
| 185 | FIB shaft fragments | N = 2 | – |
| 186 | R. PAT | | This patella is nearly completely preserved. The base is broken, and the superior and superolateral portions are missing. The anterior surface is partially eroded and exhibits insect damage. The central portion of the articular surface (where the medial and lateral facets meet) is deeply eroded, exposing cancellous bone. The lateral facet is wider than the medial facet in mediolateral dimension. There is very slight bony lipping on the inferolateral margin of the lateral facet (all other margins are eroded); there is a very thin groove superiorly adjacent to the bony lip on the inferior margin of the lateral articular facet. The patella is anteroposteriorly thick in absolute terms. There are very small bony spicules on the posterior surface of the apex. There is a smooth and weakly concave calcium |

| | | | |
|---|---|---|---|
| | | | carbonate deposit on the lateral articular facet, with small flat flakes of bone adhering to the carbonate surface. The curvature suggests that this deposit may preserve the negative impression of the lateral condyle of the femur. |
| **Suffix** | **Element** | **Element portion** | **Preservational description** |
| 187 | L. PAT | | This patella is nearly completely preserved. The base is eroded, and the superior and superolateral portions are missing. The anterior surface is partially eroded and exhibits insect damage. The central portion of the articular surface (where the medial and lateral facets meet) is deeply eroded, exposing cancellous bone. The lateral facet is wider than the medial facet in mediolateral dimension. The patella is anteroposteriorly thick in absolute terms. The margins of the articular facets are eroded. |
| 188 | R. TAL | | The complete talus is preserved. The anteromedial and superior surfaces of the head, and the anterior and medial margins of the superior articular surface are partially eroded. The talus is large in absolute terms. The superior surface of the neck is slightly hollowed. The superior articular surface is broad and nearly square (only slightly longer in anteroposterior dimension), with nearly parallel medial and lateral margins. The lateral process projects strongly laterally, with the lateral malleolar surface appearing to extend to the lateral extent of the process (the lateralmost extent is eroded). The medial malleolar surface is tall at its anterior end and tapers posteriorly. The area anteromedial to the posterior process is bulbous, bulging medially. The groove for the *flexor hallucis longus* is nearly vertical, slanting slightly inferomedially. The anterior margin of the superior articular surface is eroded but appears that it would have been nearly straight across. The anterior and medial subtalar facets are one continuous surface and are very long and thin along their anterolateral-posteromedial axis; at its anterior extent, this long facet meets the facet for the navicular. The posterior subtalar facet is very large, with an irregular surface at its anterolateral margin (possibly indicating bony remodeling). The roof of the sulcus tali is very irregular and exhibits bony outgrowths. There are small bony spicules on the lateral margin of the posterior subtalar facet. The medialmost extent of the posterior subtalar facet terminates in an oval-shaped bony tubercle. There is a thin and smooth calcium carbonate deposit adhering to the anterior subtalar facet, and a second small and smooth deposit near the medial end of the posterior subtalar facet. |
| 189 | R. CAL | | The complete calcaneus is preserved. The medial, lateral, and especially superior surfaces of the tuber, and the posterior and inferior surfaces of the tuberosity exhibit erosion. The calcaneus is strikingly large in most dimensions. The medial and anterior talar facets are continuous as one long and thin facet, curving laterally at the anterior end (the medial and anterior margins are eroded). The superior portion of the medial talar facet is eroded. The inferomedial and superolateral portions of the facet for the cuboid are eroded; there are small bony spicules along the superior margin of the facet. There is a hollowing anteriorly adjacent to the posterior talar facet; the lateral part of the facet surface has a microporous texture that appears to be the result of bony remodeling (and corresponds to the irregular portion of the posterior subtalar facet on the articulating talus). The posterior margin of the posterior talar facet is eroded; there is slight bony lipping on the anteromedial margin. The sustentacular sulcus is weakly hollowed and the margins are weakly defined. The medial and lateral processes of the tuberosity are well-developed as large bony tubercles (the lateral process is only very slightly anterior to the medial process), with bony ridges extending anteriorly from them. The fibular tubercle is visible but eroded, with a small anteroposteriorly elongated tubercle superior to it (also eroded). The calcaneal tuberosity is very large and rugose, with a very well-developed lip on its inferior surface at its anterior edge; the bony lip projects anteroinferiorly. There are small bony outgrowths |

| | | | |
|---|---|---|---|
| | | | on the lateral portion of the posterior surface of the tuberosity. The medial surface of the calcaneal body is gently hollowed (just posteroinferior to the sustentaculum tali). There are many small foramina on all preserved surfaces of the tuber. The inferomedial surface exhibits deep insect damage, just anteroinferior to the medial process of the tuberosity. There is a deep cavity on the inferomedial part of the posterior surface of the tuberosity, just medial to the medial process of the tuberosity (this cavity opens to a large and deep cavern within the tuber); just superolateral to this cavity there is a second smaller cavity (see Chapter 2 for discussion of taphonomy). |
| **Suffix** | **Element** | **Element portion** | **Preservational description** |
| 190 | L. TAL | | The complete talus is preserved. The anteroinferior and superior surfaces of the head, and the anterior, medial, and lateral margins of the superior articular surface are partially eroded. The talus is large in absolute terms. The superior surface of the neck is slightly hollowed. The superior articular surface is broad and nearly square (only slightly longer in anteroposterior dimension), with nearly parallel medial and lateral margins. The lateral process projects strongly laterally (the lateralmost extent is eroded). The medial malleolar surface is tall at its anterior end and tapers posteriorly. The area anteromedial to the posterior process is bulbous, bulging medially. The posterior surface (including the area of the groove for the *flexor hallucis longus*) is eroded. The anterior margin of the superior articular surface is eroded but appears that it would have been nearly straight across. The anterior and medial subtalar facets are one continuous surface and are very long and thin along their anterolateral-posteromedial axis; most of the anterior facet is eroded. The posterior subtalar facet is very large; the posterior part is broken and most of the margin is eroded. The roof of the sulcus tali is irregular and exhibits small bony outgrowths. |
| 191 | L. CAL | | The complete calcaneus is preserved. The superior and lateral surfaces of the tuber are partially eroded. The posterolateral portion of the tuber is missing, and there is a very deep cavity in this region extending deeply into the cancellous bone. The calcaneus is strikingly large in most dimensions. The anterior talar facet is broken; the medial talar facet terminates in a superiorly-oriented point at its superior extent. The superior and lateral portions of the facet for the cuboid are broken. There is a hollowing anteriorly adjacent to the posterior talar facet. The posterior margin of the posterior talar facet is eroded; there is very slight bony lipping on the medial margin. The sustentacular sulcus is wide and weakly hollowed. The medial process of the tuberosity is well-developed as a large bony tubercle (the lateral process is not preserved). The fibular tubercle is well-developed, but the surface is eroded; there is no discernible tubercle superior to the fibular tubercle, unlike on the right-side element. The calcaneal tuberosity is very large and rugose, with a very well-developed lip on its inferior surface at its anterior edge; the bony lip projects anteroinferiorly. This bony lip appears larger on this side relative to the right-side element, but this may be due to differential preservation. There are small bony outgrowths on the lateral portion of the posterior surface of the tuberosity. There are many small foramina on all preserved surfaces of the tuber. The inferior surface of the tuberosity is irregular, exhibiting pitting and small bony outgrowths. |
| 192 | L. NAV | | The complete navicular is preserved. The superomedial surface and the inferolateral portion of the facet for the lateral cuneiform exhibit slight erosion. The navicular is large in absolute size. The tubercle is well-developed and thickens anteriorly. The superomedial surface is irregular with many small foramina. There is a thin and shallow groove along the anterior margin of the superomedial surface (adjacent to the facet for the medial cuneiform), and another along the posterior margin of the superomedial surface. The facet for the medial cuneiform is very large relative to the other cuneiform facets. The plantar surface is very irregular, exhibiting several bony tubercles. There |

| | | | |
|---|---|---|---|
| | | | is a thin groove along the plantar surface of the tubercle. The facet for the talar head is wide in mediolateral dimension, with a small undulation on the plantar margin. There is a smooth and weakly concave calcium carbonate deposit adhering to the facet for the talar head; the shape of the concavity suggests the carbonate may preserve the negative impression of the head of the articulating talus. |
| **Suffix** | **Element** | **Element portion** | **Preservational description** |
| 193 | L. CUB | | The complete cuboid is preserved. The dorsal surface is slightly eroded. The cuboid is large in absolute size. The dorsal surface is irregular with slight bony elevations. The cuboid appears mediolaterally broad relative to its proximodistal length. The cuboid tuberosity is very well-developed (i.e., very thick and elevated). The groove for the *fibularis longus* is moderately deep. There is a thin and shallow groove on the proximal side of the tuberosity, terminating in a hollowing at its lateral extent. The proximal projection is very large and is bulbous on the plantar side. The medial portion of the facet for the fourth metatarsal is broken. The plantar margin of the facet for the fifth metatarsal is eroded; there are very thin bony outgrowths along the lateral margin of this facet. The plantar margin of the facet for the lateral cuneiform is irregular with thin bony extensions toward the plantar surface. The facet for the calcaneus is large in both absolute and relative terms. |
| 194 | R. MT3 | Base | The complete base of the third metatarsal is preserved. The base is large in absolute size. The dorsal surface is partially eroded. The base projects further proximally on the lateral side. There is an irregular bony tubercle on the plantar surface. The facet for the fourth metatarsal is large and elongated in proximodistal dimension; the adjacent nonarticular bone on the plantar side is irregular with small and thin bony outgrowths. The dorsal facet for the second metatarsal is gently convex (the dorsal margin is eroded); there is a calcium carbonate deposit adhering to the medial surface of the base just plantar to the dorsal facet for the second metatarsal, with small flakes of bone adhering to the carbonate surface. There is a small bony tubercle just plantar and distal to the dorsal facet for the second metatarsal. The facet for the lateral cuneiform is nearly flat, very weakly concave, and has a thin and smooth calcium carbonate deposit adhering to its dorsal portion. There is a very slight bony lip on the dorsal and lateral margins of the facet for the lateral cuneiform. |
| 195 | R. MT4 | Base + shaft | The complete base of the fourth metatarsal is preserved, with the anteromedial portion of nearly the complete length of the shaft. The base is large in absolute size. The dorsal and plantar surfaces are partially eroded. The base projects further proximally on the lateral side. The facet for the fifth metatarsal is large and concave. The facet for the third metatarsal is large, flat, and proximodistally elongated, with a very thin groove along its dorsal margin. The plantar portion of the medial surface very irregular, with small bony outgrowths. The plantar surface is very rugose with a large irregular bony tubercle near the proximal extent of the base. The dorsal surface is irregular with a small bony tubercle on the lateral side. The facet for the cuboid is slightly convex along the lateral edge and appears long in dorsoplantar relative to mediolateral dimension. There are small bony spicules at the plantar extent of the lateral margin of the facet for the cuboid. There is a flat calcium carbonate deposit adhering to the lateral surface of the base, from the plantar portion of the facet for the fifth metatarsal to the nonarticular bone distal to the facet; there are small flakes of bone adhering to the carbonate surface. |
| 196 | L. MT1 | Base | The complete base of the first metatarsal is preserved. The medial and dorsal surfaces are slightly eroded. The base is strikingly large in absolute and relative terms. The facet for the medial cuneiform is large and kidney-shaped, with a concave lateral margin and a convex medial margin. There is a rounded ridge of bone along the lateral |

| | | | |
|---|---|---|---|
| | | | surface adjacent to the lateral margin of the facet for the medial cuneiform, terminating in a bony tubercle at its plantar extent. There is a thin ridge of bone along medial surface adjacent to the medial margin of the facet for the medial cuneiform. The lateral surface of the shaft near the base is gently hollowed, with a thin ridge at the lateral edge of the dorsal surface of the shaft. The dorsal part of the medial surface of the shaft near the base is convex and the plantar part is concave, with a sharp ridge running between these two parts along the medial surface. |
| **Suffix** | **Element** | **Element portion** | **Preservational description** |
| 197 | L. MT1 | Head | The complete head of the first metatarsal is preserved. The lateral and dorsal margins are slightly eroded. The head is large in absolute and relative terms; it is very broad in mediolateral relative to dorsoplantar dimension. The shaft thins considerably immediately proximal to the head and is very small in dorsoplantar relative to mediolateral dimension. The lateral part of the dorsal margin of the articular surface is eroded. The lateral margin of the articular surface is eroded. The ridges on the plantar part of the articular surface are very large (i.e., broad and elevated, especially the two medial ridges), with grooves between them; each ridge terminates in a point at its proximalmost extent. There is a thin and proximodistally elongate tubercle on the medial edge of the dorsal surface, just proximal to the articular surface. |
| 198 | L. MT3 | Base | The complete base of the third metatarsal is preserved. The dorsal surface is very slightly eroded. The base is large in absolute size. The base projects further proximally on the lateral side. There is an irregular bony tubercle on the plantar surface. The facet for the fourth metatarsal is large and elongated in proximodistal dimension (although shorter than its antimere); the adjacent nonarticular bone on the plantar side is irregular with small and thin bony outgrowths. The dorsal facet for the second metatarsal is gently convex and has a calcium carbonate deposit adhering to the distal end of the facet on the dorsal side. There is a small bony tubercle just plantar and distal to the dorsal facet for the second metatarsal. The plantar portion of the facet for the lateral cuneiform is slightly eroded; there does not appear to be a second (plantarly-positioned) facet for the second metatarsal. The facet for the lateral cuneiform is nearly flat and is only very weakly concave. |
| 199 | L. MT5 | Base | The complete base of the fifth metatarsal is preserved. This portion is well-preserved. The base is strikingly large in absolute and relative size. The styloid process is very large and bulbous (rounded at its proximal extent). There is a small bony outgrowth on the lateral surface of the base. There is a very thin groove on the dorsal surface, adjacent to the facet for the cuboid. There is a very deep groove on the plantar surface between the styloid process and the facet for the cuboid. There is a large rugose tubercle on the plantar surface, adjacent to the facet for the fourth metatarsal. The proximal portion of the shaft is small in dorsoplantar relative to mediolateral dimension. There is a thin bony lip at the lateral margin of the facet for the cuboid (corresponding in position to the bony outgrowths on the facet for the fifth metatarsal on the cuboid). |
| 200 | L. MT5 | Head | The complete head of the fifth metatarsal is preserved. The size of the head is smaller than expected given the size of the base. The shaft is very slender in dorsoplantar relative to mediolateral dimension. There is a small but very elevated bony tubercle on the medial side of the head. There is a large and blunt tubercle on the lateral side of the head (adjacent to the lateral margin of the articular surface and displaced plantarly), with a second small tubercle just dorsal to it. The articular surface terminates in a point at its proximal extent on the plantar side. The head is twisted medially, as is characteristic of recent modern human fifth metatarsals. |

| Suffix | Element | Element portion | Preservational description |
|---|---|---|---|
| 201 | L. MTT | Head | The complete head of a metatarsal is preserved. This portion may belong to a second, third, or fourth ray; it most likely belongs to a third or fourth ray based on its size relative to HAL-VP-9/1-200. The dorsal and plantar surfaces are partially eroded. The head is very mediolaterally compressed. The distal shaft segment is very slender. There are small bony tubercles on the medial and lateral sides of the head (the medial tubercle is slightly larger and further distal), with thin grooves between the tubercles and the margins of the articular surface. The articular surface tapers into a point at its proximal extent on the plantar surface, along the lateral side of the bone. |
| 202 | MTT | Shaft frag. | This portion preserves a nearly complete metatarsal shaft. The ray and side are indeterminate. The shaft is oval in cross-section. Portions of the shaft surface exhibit insect damage. |
| 203 | PFP | Complete | The complete proximal foot phalanx is preserved. This phalanx is likely from a second or third ray based on its maximum length, but this identification is very tentative since it is difficult to make ray identifications without any other proximal foot phalanges preserved. This phalanx if likely from the right side. The dorsal surface of the head and much of the circumference of the base is eroded. The shaft is very slender, especially relative to the flared base. The proximal articular surface is approximately round. There are two elongated tubercles on the medial and lateral edges of the plantar surface of the base, which continue distally as converging ridges toward midshaft and then diverge to meet the medial and lateral edges of the trochlea. In dorsal view, the left side of the trochlea projects very slightly further distally. Many portions of the bone surface exhibit insect modification. |
| 204 | IFP | Complete | The complete intermediate foot phalanx is preserved. This phalanx is likely from a second or third ray based on the maximum length, but this identification is very tentative since it is difficult to make ray identifications without any other intermediate foot phalanges preserved. The side is indeterminate. The dorsal surface of the trochlea is slightly eroded. The shaft has a waisted appearance and is broad in its mediolateral relative to dorsoplantar dimension. The base is slightly broader than the trochlea in mediolateral dimension. The medial and lateral proximal articular facets are approximately the same size. There are two elongated tubercles on the medial and lateral edges of the plantar surface of the base, which fade distally as they extend convergently (they do not meet). In plantar view, the proximal edge of the plantar portion of the articular surface looks like a bony lip that extends proximally and leans to the right side. In dorsal view, the right side of the trochlea extends slightly further distally than the left side. |
| 205 | MTT | Shaft frag. | This portion preserves a small segment of metatarsal shaft fragment. The ray and side are indeterminate. The shaft is approximately oval in cross-section. |
| 206 | OCX | Acetabular frag. | This portion preserves a small sliver of lunate surface. The precise portion and side are indeterminate. |

**3b**. HAL-VP-9/1520

| Suffix | Element | Element portion | Preservational description |
|---|---|---|---|
| D | R. TIB | Shaft frag. | This portion preserves the midshaft segment of the tibial shaft. The proximalmost portion of the anterior crest is broken off; the step fracture pattern of this break indicates that this is an ancient postmortem fracture (see Chapter 2 for a discussion of taphonomy). The shaft is slender and is extremely narrow in mediolateral dimension. The anterior border is very tightly curved, and the anterior crest is rounded (i.e., not sharp). The anterior border is very straight, with only a very slight sinuous curvature. The shaft is slightly thinner than HAL-VP-9/1, especially in mediolateral dimension. The preserved portion of the shaft is straight. The nutrient foramen is just lateral to the vertical line and is filled with calcium carbonate. The soleal line is long, nearly extending to the popliteal surface, and is very well-developed and rugose. The soleal line angles laterally toward the proximal end and has a groove running along its lateral edge. The medial crest is weakly developed; the interosseous crest is moderately developed (similar to HAL-VP-9/1). The cortical thickness is moderate and is similar to HAL-VP-9/1. |
| E | R. ULN | Shaft frag. | The proximal segment of the ulnar shaft is preserved. The proximal ulnar end is not preserved; the proximal end is broken off at the approximate level of the radial notch. Only the lateralmost extent of the ulnar tuberosity is preserved; the tuberosity cannot be reliably assessed due to breakage in this area. The proximal portion of the interosseous border is preserved and is rounded (i.e., not sharp). The supinator crest is short and sharp and is not as large or thick as HAL-VP-9/1. The posterior border is very tightly curved with a slight hollowing along its lateral edge. The posterior border curves medially toward the proximal end. The shaft is very slender and is small in mediolateral relative to anteroposterior dimension. There is a thin ridge just distal to the supinator crest on the lateral surface and it spirals anteriorly toward the proximal end, toward the ulnar tuberosity. This portion is smaller in overall size and robusticity than HAL-VP-9/1. |
| F | R. HUM | Shaft frag. | The distal segment of the humeral shaft is preserved. The proximalmost extent of the lateral pillar is preserved, as well as the complete medial pillar, the proximal margin of the olecranon fossa, and the proximal margin of the coronoid fossa. The anterior surface of the shaft is more tightly curved (giving it a pillar-like appearance) than HAL-VP-9/1. The anteroposterior dimension of the distal shaft is greater than HAL-VP-9/1; the mediolateral dimension cannot be assessed since the lateral supracondylar crest is broken. The medial pillar is thin (only slightly thicker than HAL-VP-9/1). Based on the preserved proximal and medial margins, the olecranon fossa appears broad and deep. The posterior surface of the shaft just proximal to the olecranon fossa is slightly more convex than HAL-VP-9/1. |
| G | R. CLA | Frag. | This portion preserves a segment of the clavicular shaft near the acromial end. This portion preserves the rugosity for the *deltoideus* along the anterior edge of the superior surface. This portion overlaps with HAL-VP-9/1-96 and is more slender in this individual than HAL-VP-9/1, with a less rectangular cross-section and a more curved inferior surface. The anteroposterior curvature of this portion is greater than in HAL-VP-9/1. |

| Suffix | Element | Element portion | Preservational description |
|---|---|---|---|
| H | R. CLA | Frag. | This portion preserves a segment of the clavicular shaft, including the midshaft portion and the segment medial to midshaft. This portion is just medial to HAL-VP-9/1520-G. This portion preserves the rugosity for the *pectoralis major* as a very rugose area along the anterior half of the inferior surface on the medial half of the preserved portion. The medial end of the subclavian sulcus is preserved as a narrow groove running along the posterior edge of a thin bony ridge that continues medially to meet the rugosity for the *pectoralis major*. This portion likely overlaps with HAL-VP-9/1-98 and is more slender than that portion. |
| I | L. FEM | Shaft frag. | The proximal segment of the femoral shaft is preserved. This portion preserves the inferomedial margin of the lesser trochanter, the medial surface of the inferior part of the neck, and the shaft portion proximal to approximate midshaft. The spiral line is very well-developed, taking the form of a bony ridge; the proximalmost extent of the line exhibits insect damage. The gluteal tuberosity is very rugose with a wide groove running lateral to it; the tuberosity appears more rugose than in HAL-VP-9/1. The shaft surface in the area of the gluteal tuberosity and the spiral line is highly irregular. The spiral line and the gluteal tuberosity converge distally into a very well-developed linea aspera, with distinct medial and lateral lips. The shaft surface anteromedial to the lesser trochanter is deeply hollowed (this appearance is slightly exaggerated by the missing portions of the bone surface in this area). The shaft appears slightly more slender than HAL-VP-9/1. The cortical thickness is moderate and is similar to HAL-VP-9/1. The shaft surface near the lesser trochanter exhibits insect damage. |
| J | R. FEM | Shaft frag. | The proximal segment of the femoral shaft is preserved (the same portion as HAL-VP-9/1520-I, on the opposite side). This portion preserves the inferior part of the spiral line and the gluteal tuberosity near the area where they converge into the linea aspera (but not preserving the actual point of convergence). The shaft surface in the area of the gluteal tuberosity and the spiral line is rugose. The cortical thickness is moderate and appears slightly greater than HAL-VP-9/1. The anterior shaft surface exhibits insect damage. |
| K | HUM | Shaft frag. | This portion preserves a segment of the proximal humeral shaft, likely from the right side. There is an irregular bony ridge that may be the deltoid tuberosity. The shaft thickness is similar to HAL-VP-9/1. The cortical thickness is slightly greater than HAL-VP-9/1. |
| L | FIB | Shaft frag. | This portion preserves a segment of the fibular shaft near midshaft. The side is indeterminate. This shaft portion is considerably thicker than the fibular shaft portions of HAL-VP-9/1, and the cortical bone is also slightly thicker. |
| M | R. ULN | Shaft frag. | This portion preserves a segment of the ulnar shaft, from the level of the greatest development of the interosseous crest to the region of the distal shaft where the shaft begins to flare to meet the distal end. The interosseous crest is well-developed and sharp and runs along the full length of the preserved portion, with a deep hollowing adjacent to it on its posterior side. This hollowing runs along nearly the full length of the interosseous crest, thinning distally then fading toward the distal end. The pronator ridge is slight and is medially adjacent to the interosseous border. The posterior border is more tightly curved and sharper near the proximal end and rounds distally. The interosseous crest is less well-developed at its distal end relative to HAL-VP-9/1. The shaft is more slender than HAL-VP-9/1 and the cortical thickness is similar. |

**3c**. HAL-VP-9/930

| Suffix | Element | Element portion | Preservational description |
|---|---|---|---|
| A | R. HUM | Proximal frag. | The proximal humeral end is preserved, with the proximal part of the shaft. All surfaces of this portion are deeply eroded and there is considerable expanding matrix distortion across most of the portion. The head is large in absolute size and the proximal end is large relative to the slender shaft. The proximal end is smaller than HAL-VP-9/1. The lesser tubercle is partially eroded, but the preserved portion indicates that it was well-developed. The greater tubercle is too deeply eroded to be assessed for size. Despite the distortion, it appears that the head is vertically oval in superomedial view. |
| B | R. ULN | Proximal frag. | The proximal ulnar end is preserved. Most surfaces of this portion are deeply eroded; much of the olecranon and coronoid processes are missing. This proximal ulna is very small relative to HAL-VP-9/1. The trochlear notch appears to open superoanteriorly, but erosion to the anterior parts of the olecranon and coronoid processes make this assessment tentative. Most of the shaft surface just distal to the coronoid process is preserved; the shaft is small in cross-sectional size relative to HAL-VP-9/1. The surface of the radial notch is deeply eroded. |
| C | R. ULN | Distal frag. | The distal ulnar epiphysis is preserved. This portion includes the styloid process and the distalmost portion of the ulnar head. Only the distal edge of the articular circumference is partially preserved; the edges of the circumference are eroded. The distal extent of the *extensor carpi ulnaris* groove is preserved. The medialmost portion of the head is missing. Considering the partial preservation of this element, it is difficult to assess size relative to HAL-VP-9/1, but the preserved portion is similar in size to HAL-VP-9/1. There is a slight hollowing between the ulnar head and the styloid process, but not a deep groove as in HAL-VP-9/1. A thin and rounded ridge extends proximally along the lateral edge of the styloid process. The styloid process is similar in thickness and length to HAL-VP-9/1; the process curves slightly medially and leans slightly posteriorly toward its distal end. The styloid process projects further distally relative to the distal surface of the ulnar head than in HAL-VP-9/1. The distal epiphysis appears to have been unfused or only minimally fused at the time of death, suggesting that this individual was immature. In recent modern humans, the distal ulnar epiphysis tends to fuse between 17 and 20 years of age in males (White, Black, & Folkens, 2012). Because the fusion timing for the distal ulnar epiphysis is generally later than the proximal ulna, and around the same time as the proximal humerus, the unfused status of this portion does not necessarily indicate that these three element portions (collectively catalogued as a single individual, HAL-VP-9/930) do not belong to the same individual. |

**3d**. TAL-VP-7/36

| Suffix | Element | Element portion | Preservational description |
|---|---|---|---|
| H | R. HUM | Distal frag. | The distal humeral end is nearly completely preserved, missing only a few small portions: a plate of bone between the olecranon and coronoid fossae, a plate of bone between the olecranon and radial fossae, and a segment of bone along the superolateral portion of the medial pillar (along the superomedial margin of the olecranon fossa). The missing segments of bone in the olecranon fossa preclude assessment of the presence of a septal aperture, but if present, the aperture would have been very small. The distal end is broad and large, but not as striking in size as HAL-VP-9/1. The medial epicondyle is not as strongly projecting as in HAL-VP-9/1, and the trochlea is smaller in proximodistal and anteroposterior dimensions. The capitulum is considerably smaller than HAL-VP-9/1, especially in proximodistal dimension. The trochlea has a more waisted appearance than HAL-VP-9/1 in proximodistal and anteroposterior dimensions. There is a very slight bony outgrowth on the anterior surface of the lateral lip of the trochlea. There are also small bony outgrowths on the medial and lateral margins of the posterior surface of the trochlea. There is slight erosion to the posterior surface of the medial epicondyle, the lateral surface of the lateral epicondyle, the lateral margin of the capitulum, and the medial margin of the trochlea. The medial pillar is moderately thick (unlike the very thin medial pillar of HAL-VP-9/1). The olecranon fossa is broad and deep, although slightly smaller in mediolateral breadth than HAL-VP-9/1. The medial supracondylar ridge is blunter than in HAL-VP-9/1. The coronoid fossa is moderately deep and broad and extends further proximally than in HAL-VP-9/1, giving it a teardrop shape. The radial fossa is shallow, similar to HAL-VP-9/1. The anterior surface of the distal end (including the area proximal to the radial fossa, and the ridge between the coronoid and radial fossae) is irregular and may have undergone remodeling; this irregularity is also observed along the medial supracondylar crest. |
| I | R. RAD | Distal frag. | The distal radial end is preserved. The anterior surface of the shaft is gently concave. The ulnar notch is nearly flat, exhibiting slight concavity. There is a small bony outgrowth at the posterior margin of the carpal articular surface at the approximate position of the groove for the extensor muscle tendons. The posterior and lateral surfaces are deeply eroded, with cancellous bone exposed. Portions of the distal articular surface are eroded. The surface of the dorsal tubercle is eroded. The grooves for the *extensor carpi radialis*, *extensor pollicis longus*, and extensor muscle tendons are all visible despite erosion to the bone surface. |

**3e**. Individuals represented by a single postcranial element

| Specimen # | Suffix | Element | Element portion | Preservational description |
|---|---|---|---|---|
| BOU-VP-16/100 | - | L. FEM | Shaft frag. | The preserved portion includes the proximal part of the femoral shaft. On the posterior side, the proximalmost portion preserved is at the level of the inferior edge of the lesser trochanter. On the anterior side, the preserved portion extends further proximally, including the inferior part of the femoral neck. The shaft flares medially toward the femoral head, and anteriorly toward the greater trochanter (which is not preserved). This element is moderate in size and cortical thickness (as assessed at the distal break at a position proximal to midshaft). The spiral line is very weakly developed. The superior part of the gluteal tuberosity is not preserved (the external surface of the cortical bone has flaked away). The superior part of the linea aspera is preserved at the position where it meets the gluteal tuberosity. The gluteal tuberosity and the linea aspera angle medially as they extend distally; they are blunt and moderately developed. This area of the shaft exhibits less rugosity than HAL-VP-9/1520-I. The anterior shaft surface at the proximal end is flat, rounding inferiorly; the proximal shaft is slightly anteroposteriorly flattened. The shaft is slightly concave on the posterolateral side, adjacent to the linea aspera. |
| HAL-VP-2/16 | - | RAD | Proximal frag. | The proximal radial end is preserved. This portion is likely from the left side. This portion preserves the radial head and proximal part of the shaft. This individual is considerably smaller than HAL-VP-9/1 in radial head diameter and proximodistal height of the articular circumference. The head to shaft size ratio is not as striking as HAL-VP-9/1 (i.e., the head is not particularly large relative to the proximal shaft). The margins of the articular circumference are partially eroded. A segment of the articular circumference exhibits small round pits, similar to some of the modifications observed in HAL-VP-9/1; these pits may be the result of insect damage. |
| HAL-VP-3/1 | - | R. ULN | Proximal frag. | The proximal ulnar end is preserved. Most surfaces of this portion are deeply eroded, including the coronoid process, the olecranon process, and the radial notch. There is a thin ridge extending from the medial edge of the inferior articular surface of the trochlea, similar to HAL-VP-9/1. This proximal ulna is intermediate in size relative to the other individuals in this sample; it is smaller than HAL-VP-9/1 but larger than HAL-VP-9/930-B. The trochlear notch appears to open slightly superoanteriorly, although this feature is difficult to reliably assess because of the considerable erosion to the anterior parts of the olecranon and coronoid processes. Regardless of the erosion, however, it is still clear that the trochlear notch is not oriented as superiorly as in HAL-VP-9/1. |
| HAL-VP-3/15 | 11 | THP | | A complete terminal hand phalanx is preserved. This element most likely belongs to the first ray. The side cannot be reliably determined, due to distortion (see Chapter 2 for a discussion of |

| | | | | |
|---|---|---|---|---|
| | | | | taphonomy). The shaft flares dramatically near the base (i.e., it does not taper gradually as is more typical of a pollical terminal hand phalanx). The phalanx is long and thin and the tuberosity is narrow. A small segment near midshaft is missing. The edges of the distal tuberosity exhibit slight erosion. |
| **Specimen #** | **Suffix** | **Element** | **Element portion** | **Preservational description** |
| HAL-VP-14/44 | - | FEM | Condyle frag. | This portion preserves part of a femoral condyle. This portion is likely the posteromedial part of the lateral condyle of a left femur. The posterior portion of the articular surface is eroded. The lateral edge of the condyle is not preserved. The medial edge of the articular surface of the condyle is a thin ridge, with a broad hollowing medially adjacent (running along the lateral wall of the intercondylar fossa). |

**3d**. Element abbreviations

| Abbreviation | Element |
|---|---|
| FRO | FRONTAL |
| PAR | PARIETAL |
| OCC | OCCIPITAL |
| TEM | TEMPORAL |
| SPH | SPHENOID |
| MAX | MAXILLA |
| ZYG | ZYGOMATIC |
| NAS | NASAL |
| PAL | PALATINE |
| CRA | CRANIUM |
| VER | VERTEBRA |
| RIB | RIB |
| CLA | CLAVICLE |
| SCA | SCAPULA |
| OCX | OS COXAE |
| HUM | HUMERUS |
| RAD | RADIUS |
| ULN | ULNA |
| HAM | HAMATE |
| TRAPEZIUM | TRAPEZIUM |
| TRI | TRIQUETRAL |
| LUN | LUNATE |
| CAP | CAPITATE |
| MC0 to 5 | METACARPAL 1 TO 5 |
| PHP | PROXIMAL HAND PHALANX |
| IHP | INTERMEDIATE HAND PHALANX |
| THP | TERMINAL HAND PHALANX |
| FEM | FEMUR |
| TIB | TIBIA |
| FIB | FIBULA |
| PAT | PATELLA |
| TAL | TALUS |
| CAL | CALCANEUS |
| NAV | NAVICULAR |
| CUB | CUBOID |
| MTT | METATARSAL |
| MT0 to 5 | METATARSAL 1 TO 5 |
| PFP | PROXIMAL FOOT PHALANX |
| IFP | INTERMEDIATE FOOT PHALANX |
| TFP | TERMINAL FOOT PHALANX |

**Appendix 4** Comparative fossil samples with data sources

The comparative fossils included in this study are listed below with the published sources from which descriptive and metric data were collected. Only the most recent samples, modern humans and Neanderthals, are organized according to taxonomy. All other fossils are organized first according to geographic region and then according to time period. In cases where samples are very limited (<2 individuals), time bins are pooled. It should be noted that the elements listed under "Remains" refer only to those from each site that are considered in the present study.

The modern human and Neanderthal comparative samples are the largest and most comprehensive because they have rich fossil records relative to the earlier samples and are the most relevant to the description of the Late Pleistocene fossils from Halibee (see Chapter 6). The comparative samples included below are not exhaustive, but rather include the most relevant and complete fossils, for which published data are available. Data for some of the more complete Middle and Early Pleistocene fossils were collected to provide a broader context for the Late Pleistocene fossils, and to provide a sense of morphological variation across time and geography.

***Modern Humans***

| Site/Specimen | Geography | Remains | Data reference(s) |
|---|---|---|---|
| Omo (Ethiopia) | Eastern Africa | Partial skeleton, partial tibia and fibula | Day, 1969<br>Pearson et al., 2008a<br>Pearson et al., 2008b<br>Voisin, 2008 |
| Skhul (Israel) | Near East | Seven partial skeletons and isolated postcrania | McCown & Keith, 1939<br>Niewoehner, 2001 |
| Qafzeh (Israel) | Near East | Six partial skeletons | Niewoehner, 2001<br>Vandermeersch, 1981 |
| Klasies River Mouth Caves (South Africa) | Southern Africa | Partial radius, ulna, and first, second, and fifth metatarsals | Churchill et al., 1996<br>Pearson & Grine, 1997<br>Rightmire & Deacon, 1991<br>Rightmire et al., 2006 |
| Nazlet Khater 2 (Egypt) | Northern Africa | Partial skeleton | Crevecoeur, 2012<br>Crevecoeur, 2008<br>Thoma, 1984 |
| Jebel Sahaba (Sudan) | Eastern Africa | 46 partial skeletons | Anderson, 1968<br>Holliday, 2015 |
| Peștera Muierii (Romania) | Eastern Europe | Scapula, tibia, and fibula | Soficaru et al., 2006 |
| Mladeč (Czech Republic) | Central Europe | Postcranial remains of multiple individuals | Trinkaus et al., 2006 |
| Sunghir (Russia) | Eastern Europe | Partial skeleton and partial femur | Trinkaus et al., 2014 |

| Site/Specimen | Geography | Remains | Data reference(s) |
|---|---|---|---|
| Zhoukoudian Upper Cave (China) | Eastern Asia | Isolated femora and a patella | Wu & Poirier, 1995 |
| Liujiang (China) | Eastern Asia | Partial skeleton | Rosenberg, 2002<br>Woo, 1959<br>Wu & Poirier, 1995 |
| Tianyuan (China) | Eastern Asia | Partial skeleton | Shang & Trinkaus, 2010<br>Shang et al., 2007 |
| Lake Mungo 3 (Australia) | Australia | Partial skeleton | Durband et al., 2009 |
| ***Neanderthals*** | | | |
| **Site/Specimen** | **Geography** | **Remains** | **Data references** |
| Amud (Israel) | Near East | Partial skeleton | Endo & Kimura, 1970<br>Trinkaus, 1975 |
| Kebara 2 (Israel) | Near East | Partial skeleton | Bar-Yosef & Vandermeersch, 1991<br>Gómez-Olivencia et al., 2009<br>Rak & Arensburg, 1987 |
| Tabun (Israel) | Near East | One partial skeleton and isolated postcrania | McCown & Keith, 1939 |
| Shanidar (Iraq) | Near East | Seven partial skeletons | Trinkaus, 1983<br>Trinkaus, 1975 |
| Krapina (Croatia) | Central Europe | Postcranial remains of multiple individuals | Bonmatí & Arsuaga, 2007<br>Trinkaus, 2016<br>Trinkaus, 1975 |
| Neanderthal 1 (Germany) | Western Europe | Various postcranial remains | Heim, 1982<br>King, 1864 |
| Spy 2 (Belgium) | Western Europe | Two partial skeletons | Heim, 1982<br>Thoma, 1975 |
| La Chapelle-aux-Saints 1 (France) | Western Europe | Partial skeleton | Gómez-Olivencia, 2013<br>Gómez-Olivencia et al., 2013a<br>Trinkaus, 2011<br>Trinkaus, 1975 |
| La Ferrassie (France) | Western Europe | Two partial skeletons | Heim, 1982<br>Heim, 1976 |
| La Quina (France) | Western Europe | Postcranial remains of multiple individuals | Martin, 1923<br>Trinkaus, 1975 |
| Regourdou 1 (France) | Western Europe | Partial skeleton | Gómez-Olivencia et al., 2013b<br>Meyer et al., 2011<br>Pablos et al., 2019<br>Vandermeersch & Trinkaus, 1995 |

| Site/Specimen | Geography | Remains | Data reference(s) |
|---|---|---|---|
| El Sidrón (Spain) | Western Europe | Two partial skeletons and isolated postcrania | Rosas et al., 2020<br>Rosas et al., 2006 |
| Sima de las Palomas (Spain) | Western Europe | Partial skeleton | Walker et al., 2011a<br>Walker et al., 2011b |
| ***African Late Pleistocene* Homo** | | | |
| **Site/Specimen** | **Geography** | **Remains** | **Data references** |
| Border Cave (South Africa) | Southern Africa | Humeral shaft, proximal ulna | Pearson & Grine, 1996<br>Pfeiffer & Zehr, 1996 |
| Sea Harvest (South Africa) | Southern Africa | Manual distal phalanx | Grine & Klein, 1993 |
| Cave of Hearths (South Africa) | Southern Africa | Radius | Pearson & Grine, 1997<br>Tobias, 1971 |
| Blind River (South Africa) | Southern Africa | Femur | Wang et al., 2008<br>Wells, 1935 |
| ***African Middle Pleistocene* Homo** | | | |
| **Site/Specimen** | **Geography** | **Remains** | **Data references** |
| Bodo (Ethiopia) | Eastern Africa | Distal humerus | Carretero et al., 2009 |
| Baringo Kapthurin (Kenya) | Eastern Africa | Ulna | Solan & Day, 1992 |
| KNM-ER 999 (Kenya) | Eastern Africa | Femur | Day & Leakey, 1974<br>Trinkaus, 1993 |
| OH 28 (Tanzania) | Eastern Africa | Femur and os coxae | Day, 1971<br>Ruff, 2010 |
| Broken Hill (Zambia) | Southern Africa | Humerus, tibia, os coxae | Stringer, 1986<br>Trinkaus, 2012<br>Trinkaus, 2009 |
| Mumbwa Caves [a] (Zambia) | Southern Africa | Two radius fragments, femoral shaft | Pearson et al., 2000 |
| Twin Rivers (Zambia) | Southern Africa | Humerus fragment | Pearson, 2000 |
| Berg Aukas (Namibia) | Southern Africa | Proximal femur | Grine et al., 1995 |
| Hoedjiespunt (South Africa) | Southern Africa | Tibia | Churchill et al., 2000 |
| ***African Early Pleistocene* Homo** | | | |
| **Site/Specimen** | **Geography** | **Remains** | **Data references** |
| Daka (Ethiopia) | Eastern Africa | Three partial femora, partial tibia | Gilbert, 2008 |
| Gona (Ethiopia) | Eastern Africa | Pelvis | Simpson et al., 2008 |

| Site/Specimen | Geography | Remains | Data reference(s) |
|---|---|---|---|
| KNM-WT 15000 (Kenya) | Eastern Africa | Partial skeleton | Walker & Leakey, 1993 |
| KNM-ER 803 (Kenya) | Eastern Africa | Partial skeleton | Day & Leakey, 1974 |
| ***Asian Late and Middle Pleistocene* Homo** | | | |
| **Site/Specimen** | **Geography** | **Remains** | **Data references** |
| Zhoukoudian (China) | Eastern Asia | Postcranial remains of multiple individuals | Wu & Poirier, 1995 |
| Jinniushan (China) | Eastern Asia | Partial skeleton | Lu et al., 2011<br>Lu, 2003<br>Rosenberg et al., 2006 |
| Ngandong (Indonesia) | Southeastern Asia | Two tibiae | Santa Luca, 1980 |
| ***Asian Early Pleistocene* Homo** | | | |
| **Site/Specimen** | **Geography** | **Remains** | **Data references** |
| Dmanisi (Georgia) | Western Asia | Postcranial remains of three individuals | Lordkipanidze et al., 2007 |
| ***European Early and Middle Pleistocene* Homo** | | | |
| **Site/Specimen** | **Geography** | **Remains** | **Data references** |
| Boxgrove (England) | Western Europe | Tibia | Roberts et al., 1994<br>Stringer et al., 1998 |
| Gran Dolina, Atapuerca (Spain) | Western Europe | Postcranial remains of multiple individuals | Bermúdez de Castro et al., 2012<br>Carretero et al., 1999<br>Lorenzo et al., 1999<br>Pablos et al., 2012 |
| Sima de Los Huesos, Atapuerca (Spain) | Western Europe | Postcranial remains of multiple individuals | Arsuaga et al., 2015<br>Arsuaga et al., 1999<br>Bonmatí et al., 2010<br>Carretero et al., 1997<br>Gómez-Olivencia et al., 2007<br>Pablos et al., 2017<br>Pablos et al., 2014<br>Pablos et al., 2013<br>Rodríguez et al., 2016 |
| Arago 44 (France) | Western Europe | Os coxae | Arsuaga et al., 2015 |

[a] Remains from Mumbwa Caves include only those that are of probable or certain Middle Stone Age origin (Pearson et al., 2000). The younger remains from this site are of uncertain antiquity and may derive from the Holocene; they are not included in this study (see Grine, 2016).

**Appendix 5** Measurements of the fossils from the Halibee Member, Dawaitoli Formation, Middle Awash study area

Measurements are reported here for the Late Pleistocene postcranial fossils from the Halibee Member of the Dawaitoli Formation. Measurements are reported first for the HAL-VP-9/1 partial skeleton, followed by the HAL-VP-9/1520 partial skeleton, and then for the individuals with few associated postcranial elements and single postcranial elements. For individuals with suffixed portions, the suffix is included in the heading with the element description. For all measurements collected for the recent modern human comparative samples, measurement references are reported in Appendix 6a and measurement protocols in Appendix 7a. The measurement code is included here for measurements that were also collected for the recent modern human comparative samples.

All reported values are in millimeters (mm) unless otherwise indicated. Estimated measurements are reported in parentheses. The side measured is indicated in the measurement name, or in the column heading. In some cases where breaks permitted the observation of cortical thickness, thicknesses were measured and are also reported below.

---

**Appendix 5: Table of Contents**


**Table A5.1** Vertebral measurements for HAL-VP-9/1
**Table A5.2** Rib measurements for HAL-VP-9/1
**Table A5.3** Clavicle measurements for HAL-VP-9/1
**Table A5.4** Scapula measurements for HAL-VP-9/1
**Table A5.5** Humerus measurements for HAL-VP-9/1
**Table A5.6** Ulna measurements for HAL-VP-9/1
**Table A5.7** Radius measurements for HAL-VP-9/1
**Table A5.8** Carpal measurements for HAL-VP-9/1
**Table A5.9** Metacarpal measurements for HAL-VP-9/1
**Table A5.10** Hand phalanx measurements for HAL-VP-9/1
**Table A5.11** Os coxae and sacrum measurements for HAL-VP-9/1
**Table A5.12** Femur measurements for HAL-VP-9/1
**Table A5.13** Patella measurements for HAL-VP-9/1
**Table A5.14** Tibia measurements for HAL-VP-9/1
**Table A5.15** Fibula measurements for HAL-VP-9/1
**Table A5.16** Tarsal measurements for HAL-VP-9/1
**Table A5.17** Metatarsal measurements for HAL-VP-9/1
**Table A5.18** Foot phalanx measurements for HAL-VP-9/1
**Table A5.19** Measurements for HAL-VP-9/1520
**Table A5.20** Measurements for HAL-VP-9/930
**Table A5.21** Measurements for TAL-VP-7/36
**Table A5.22** Measurements for BOU-VP-16/100
**Table A5.23** Measurements for HAL-VP-2/16
**Table A5.24** Measurements for HAL-VP-3/1
**Table A5.25** Measurements for HAL-VP-3/15


---

**Table A5.1** Vertebral measurements for HAL-VP-9/1

| **Vertebral measurements** | | |
|---|---|---|
| **Fourth cervical vertebra (HAL-VP-9/1-24)** | | |
| **Measurement name** | **Code** | **Value (in mm)** |
| Ventral height of body | CER1_VEN_HEI | 14.9 |
| Superior dorsoventral body diameter | CER2_SUP_DV | 17.6 |
| Superior transverse body diameter | CER3_SUP_TRA | 25.2 |
| Pedicle height (right) | CER4_PED_HEI | 8.9 |
| Dorsal height of body (at midline) | – | 14.3 |
| Inferior dorsoventral body diameter | – | 16.9 |
| Inferior transverse body diameter | – | 22.5 |
| **Fifth cervical vertebra (HAL-VP-9/1-25)** | | |
| **Measurement name** | **Code** | **Value (in mm)** |
| Ventral height of body | CER1_VEN_HEI | 13.3 |
| Superior dorsoventral body diameter | CER2_SUP_DV | 16.9 |
| Superior transverse body diameter | CER3_SUP_TRA | 25.5 |
| Dorsal height of body (at midline) | – | 14.8 |
| Inferior dorsoventral body diameter | – | (14.4) |
| Inferior transverse body diameter | – | 22.8 |
| Height of anterior root of transverse process (right) | – | 11.5 |
| **Sixth cervical vertebra (HAL-VP-9/1-26)** | | |
| **Measurement name** | **Code** | **Value (in mm)** |
| Ventral height of body | CER1_VEN_HEI | 15.1 |
| Superior dorsoventral body diameter | CER2_SUP_DV | 16.0 |
| Superior transverse body diameter | CER3_SUP_TRA | (24.4) |
| Pedicle height (right) | CER4_PED_HEI | 10.0 |
| Dorsal height of body (at midline) | – | 15.9 |
| Inferior dorsoventral body diameter | – | 16.9 |
| Inferior transverse body diameter | – | 25.1 |
| Height of anterior root of transverse process (right) | – | 13.4 |
| **Seventh cervical vertebra (HAL-VP-9/1-27)** | | |
| **Measurement name** | **Code** | **Value (in mm)** |
| Ventral height of body | CER1_VEN_HEI | (16.1) |
| Superior dorsoventral body diameter | CER2_SUP_DV | 17.9 |
| **Middle cervical vertebra (HAL-VP-9/1-28)** | | |

| Measurement name | Code | Value (in mm) |
|---|---|---|
| Maximum dimension of superior articular facet (right) | – | 13.2 |
| Length perpendicular to maximum dimension of superior articular facet (right) | – | 9.2 |
| Maximum dimension of inferior articular facet (right) | – | 14.3 |

**Lower cervical vertebra (HAL-VP-9/1-29)**

| Measurement name | Code | Value |
|---|---|---|
| Mediolateral width at tip of spinous process | – | 7.9 mm |
| Height at tip of spinous process | – | 5.9 mm |
| Length of spinous process | – | 18.6 mm |
| Spinous process angle | – | (136°) |

**Upper thoracic vertebra (HAL-VP-9/1-30)**

| Measurement name | Code | Value |
|---|---|---|
| Ventral height of body | THO1_VEN_HEI | 17.8 mm |
| Superior dorsoventral body diameter | THO2_SUP_DV | (20.5 mm) |
| Superior transverse body diameter | THO3_SUP_TRA | (29.8 mm) |
| Vertebral canal length | THO4_CAN_LEN | 16.9 mm |
| Vertebral canal breadth | THO5_CAN_BRE | (19.5 mm) |
| Vertebral canal index | THO6_CAN_IND | 87.1 |
| Inferior dorsoventral body diameter | – | 21.0 mm |
| Pedicle thickness in transverse plane (right) | – | 10.5 mm |
| Height of lamina (perpendicular to long axis of lamina; right) | – | 20.0 mm |
| Maximum dimension of superior costal facet on body (left) | – | 13.7 mm |

**Upper thoracic vertebra (HAL-VP-9/1-31)**

| Measurement name | Code | Value (in mm) |
|---|---|---|
| Inferior dorsoventral body diameter | – | (23.7) |

**Middle thoracic vertebra (HAL-VP-9/1-32)**

| Measurement name | Code | Value (in mm) |
|---|---|---|
| Dorsal height of body (at midline) | – | (20.1) |

**Middle thoracic vertebra (HAL-VP-9/1-39)**

| Measurement name | Code | Value (in mm) |
|---|---|---|
| Height of lamina (perpendicular to long axis of lamina; right) | – | 13.7 |

**Middle thoracic vertebra (HAL-VP-9/1-42)**

| Measurement name | Code | Value (in mm) |
|---|---|---|

| | | |
|---|---|---|
| Mediolateral width at tip of spinous process | – | 6.8 |
| Height at tip of spinous process | – | 24.5 |

**Middle thoracic vertebra (HAL-VP-9/1-45)**

| Measurement name | Code | Value (in mm) |
|---|---|---|
| Maximum dimension of transverse costal facet (right) | – | 11.9 |
| Length perpendicular to maximum dimension of transverse costal facet (right) | | 8.2 |

**Lower thoracic vertebra (HAL-VP-9/1-44)**

| Measurement name | Code | Value (in mm) |
|---|---|---|
| Mediolateral width of inferior articular facet (right) | – | 10.6 |

**Lower thoracic vertebra (HAL-VP-9/1-35)**

| Measurement name | Code | Value (in mm) |
|---|---|---|
| Pedicle height (right) | THO7_PED_HEI | 21.8 |

**Lower thoracic vertebra (HAL-VP-9/1-41)**

| Measurement name | Code | Value (in mm) |
|---|---|---|
| Mediolateral width at tip of spinous process | – | 5.3 |

**First lumbar vertebra (HAL-VP-9/1-50)**

| Measurement name | Code | Value (in mm) |
|---|---|---|
| Ventral height of body | LUM1_VEN_HEI | (26.3) |
| Superior transverse body diameter | LUM3_SUP_TRA | (47.8) |
| Pedicle height (right) | LUM4_PED_HEI | 15.7 |
| Dorsal height of body (at midline) | – | 31.4 |
| Maximum dimension of superior articular facet (right) | – | 15.3 |
| Maximum dimension of inferior articular facet (right) | – | 14.7 |
| Length from superior margin of superior articular process to inferior margin of inferior articular process (in paracoronal plane) | – | 51.2 |

**Second lumbar vertebra (HAL-VP-9/1-49)**

| Measurement name | Code | Value (in mm) |
|---|---|---|
| Ventral height of body | LUM1_VEN_HEI | (25.0) |
| Superior dorsoventral body diameter | LUM2_SUP_DV | (42.2) |
| Pedicle height (right) | LUM4_PED_HEI | 17.9 |
| Mediolateral width of superior articular facet (right) | – | 14.7 |

**Fourth lumbar vertebra (HAL-VP-9/1-52)**

| Measurement name | Code | Value (in mm) |
|---|---|---|

| | | |
|---|---|---|
| Ventral height of body | LUM1_VEN_HEI | (26.7) |
| Superior dorsoventral body diameter [a] | LUM2_SUP_DV | (37.1) |
| Superior transverse body diameter [a] | LUM3_SUP_TRA | (51.8) |
| Pedicle height (right) | LUM4_PED_HEI | 16.4 |
| Dorsal height of body (at midline) | – | 29.1 |
| Inferior dorsoventral body diameter | – | 35.0 |
| Inferior transverse body diameter | – | 52.8 |

| **Fifth lumbar vertebra (HAL-VP-9/1-53)** | | |
|---|---|---|
| **Measurement name** | **Code** | **Value (in mm)** |
| Ventral height of body | LUM1_VEN_HEI | 27.9 |
| Superior dorsoventral body diameter | LUM2_SUP_DV | 35.7 |
| Superior transverse body diameter | LUM3_SUP_TRA | (52.3) |
| Dorsal height of body (at midline) | – | (23.5) |
| Inferior dorsoventral body diameter | – | 33.7 |
| Inferior transverse body diameter | – | 50.9 |

[a] Measurement was estimated to exclude bony lipping at the margins of the superior surface of the body.

**Table A5.2** Rib measurements for HAL-VP-9/1

| **Rib measurements** | | |
|---|---|---|
| **Right rib head (HAL-VP-9/1-61)** | | |
| **Measurement name** | **Code** | **Value (in mm)** |
| Superoinferior height of head | – | 14.2 |
| Dorsoventral width of head | – | 8.2 |
| Maximum dimension of facet on head | – | 9.7 |
| **Right rib sternal end (HAL-VP-9/1-77)** | | |
| **Measurement name** | **Code** | **Value (in mm)** |
| Superoinferior height of sternal end | – | 15.1 |
| Dorsoventral width of sternal end | – | 10.0 |
| **Right rib sternal end (HAL-VP-9/1-78)** | | |
| **Measurement name** | **Code** | **Value (in mm)** |
| Superoinferior height of sternal end | – | 9.5 |
| Dorsoventral width of sternal end | – | 6.1 |
| **Left rib sternal end (HAL-VP-9/1-93)** | | |

| Measurement name | Code | Value (in mm) |
|---|---|---|
| Superoinferior height of sternal end | – | 16.1 |
| Dorsoventral width of sternal end | – | 11.0 |
| **Left rib sternal end (HAL-VP-9/1-94)** | | |
| **Measurement name** | **Code** | **Value (in mm)** |
| Superoinferior height of sternal end | – | 10.0 |
| Dorsoventral width of sternal end | – | 5.8 |

**Table A5.3** Clavicle measurements for HAL-VP-9/1

| **Clavicle measurements** | | |
|---|---|---|
| **Right clavicle shaft (HAL-VP-9/1-96)** | | |
| **Measurement name** | **Code** | **Value (in mm)** |
| Dorsoventral shaft diameter at midpoint of rugosity for *deltoideus* | – | 19.1 |
| Dorsoventral shaft diameter at medial margin of rugosity for *deltoideus* | – | 16.3 |
| Superoinferior shaft diameter at midpoint of rugosity for *deltoideus* | – | 10.3 |
| **Left clavicle shaft (HAL-VP-9/1-97)** | | |
| **Measurement name** | **Code** | **Value (in mm)** |
| Maximum shaft diameter at lateral margin of costoclavicular impression | – | 15.6 |
| Maximum shaft diameter at position just lateral to midshaft | – | 14.2 |
| Superoinferior shaft diameter at position just lateral to midshaft | – | 11.2 |
| Cortical thickness of inferior shaft (at subclavian sulcus) [a] | – | 2.4 |
| Cortical thickness of superior shaft [a] | – | 2.5 |
| Cortical thickness of posterior shaft [a] | – | 3.1 |
| **Left clavicle shaft (HAL-VP-9/1-98)** | | |
| **Measurement name** | **Code** | **Value (in mm)** |
| Maximum dorsoventral shaft diameter | – | 16.7 |
| Maximum superoinferior shaft diameter | – | 12.7 |

[a] Measurement was taken at the lateral break.

**Table A5.4** Scapula measurements for HAL-VP-9/1

| Scapula measurements | | |
|---|---|---|
| **Right acromion and scapular spine (HAL-VP-9/1-100)** | | |
| **Measurement name** | **Code** | **Value (in mm)** |
| Length of acromion (taken along an axis bisecting the acromion in two halves) | – | 49.4 |
| Maximum thickness of medial part of scapular spine | – | 11.2 |
| Height of clavicular facet | – | 12.5 |
| Width of acromion at posterior margin of clavicular facet | – | 26.3 |
| Width of acromion at anterior margin of clavicular facet | – | 12.7 |
| Minimum thickness at medial end of preserved portion of scapular spine | – | 6.7 |
| Maximum dimension of preserved portion | – | 121.4 |
| **Right partial glenoid fossa (HAL-VP-9/1-101)** | | |
| **Measurement name** | **Code** | **Value (in mm)** |
| Maximum height of preserved portion of glenoid | – | 33.5 |
| **Right axillary border (HAL-VP-9/1-102)** | | |
| **Measurement name** | **Code** | **Value (in mm)** |
| Dorsoventral thickness of axillary border at superior extent of preserved portion | – | 12.8 |
| Dorsoventral thickness of axillary border at inferior extent of preserved portion | – | 4.8 |
| **Right inferior angle (HAL-VP-9/1-103)** | | |
| **Measurement name** | **Code** | **Value (in mm)** |
| Maximum thickness of inferior margin near lateral extent of preserved portion | – | 7.8 |
| Maximum thickness of inferior margin near medial extent of preserved portion | – | 8.4 |
| **Left inferior angle (HAL-VP-9/1-105)** | | |
| **Measurement name** | **Code** | **Value (in mm)** |
| Maximum thickness of inferior margin, just lateral to apex of inferior angle | – | 8.1 |

**Table A5.5** Humerus measurements for HAL-VP-9/1

| Humerus measurements | | |
|---|---|---|
| **Right humeral head (HAL-VP-9/1-112)** | | |
| **Measurement name** | **Code** | **Value (in mm)** |
| Vertical head diameter | HUM9_HEA_DIA | (49.1) |

**Right distal end with shaft (HAL-VP-9/1-113)**

| Measurement name | Code | Value (in mm) |
|---|---|---|
| Humeral midshaft circumference [a] | HUM3_MID_CIR | 68 |
| Maximum midshaft diameter [a] | HUM4_MAX_MID | 22.3 |
| Minimum midshaft diameter [a] | HUM5_MIN_MID | (18.7) |
| Shaft circumference at deltoid tuberosity [a] | HUM6_DEL_CIR | 70.5 |
| Minimum shaft diameter at deltoid tuberosity [a] | HUM7_DEL_MIN | 18.5 |
| Maximum shaft diameter at deltoid tuberosity [a] | HUM8_DEL_MAX | 25.6 |
| Humeral bicondylar breadth | HUM10_BIC_BRE | 70.0 |
| Olecranon fossa breadth | HUM11_FOS_BRE | 29.7 |
| Minimum thickness of medial pillar | HUM12_MED_PIL | 7.9 |
| Minimum thickness of lateral pillar | HUM13_LAT_PIL | 18.00 |
| Mediolateral width of medial epicondyle | HUM14_EPI_ML | 18.7 |
| Mediolateral width of capitulum (in anterior view) | – | 21.0 |
| Height (proximodistal) of capitulum (in anterior view) | – | 25.8 |
| Mediolateral width of trochlea (in anterior view) | – | 26.7 |
| Height (proximodistal) of trochlea (in anterior view) | – | 25.4 |
| Mediolateral width of coronoid fossa | – | 13.9 |
| Mediolateral width of lateral epicondyle (in posterior view) | – | 22.7 |
| Maximum dimension of preserved portion | – | 204.9 |
| Distal articular breadth [b] | – | 47.9 |
| Medial epicondyle projection [c] | – | 46.8 |
| Medial epicondyle breadth [d] | – | 18.5 |
| Lateral epicondyle projection [e] | – | 40.7 |
| Cortical thickness of anterior shaft [f] | – | 5.0 |

**Shaft fragment, probably left side (HAL-VP-9/1-114)**

| Measurement name | Code | Value (in mm) |
|---|---|---|
| Maximum shaft diameter of preserved portion | – | 18.4 |

**Left proximal end (HAL-VP-9/1-115)**

| Measurement name | Code | Value (in mm) |
|---|---|---|
| Vertical head diameter | HUM9_HEA_DIA | 49.5 |
| Maximum diameter between lateral surface of greater tubercle and medial surface of humeral head | – | 52.6 |
| Lesser tubercle breadth [g] | – | 14.6 |
| Cortical thickness of medial proximal shaft [h] | – | 3.7 |

**Left partial shaft (HAL-VP-9/1-117)**

| Measurement name | Code | Value (in mm) |
|---|---|---|
| Shaft circumference at deltoid tuberosity | HUM6_DEL_CIR | 68 |
| Minimum shaft diameter at deltoid tuberosity | HUM7_DEL_MIN | 19.8 |
| Maximum shaft diameter at deltoid tuberosity | HUM8_DEL_MAX | 22.7 |
| Maximum dimension of preserved portion | – | 198.7 |
| Cortical thickness of posterior proximal shaft [i] | – | 4.7 |
| Cortical thickness of anterior distal shaft [j] | – | 5.5 |
| Cortical thickness of anteromedial distal shaft [j] | – | 4.8 |
| Cortical thickness of anterolateral distal shaft [j] | – | 4.7 |
| Cortical thickness of posteromedial distal shaft [j] | – | 5.0 |
| Cortical thickness of posterolateral distal shaft [j] | – | 6.8 |

**Left distal end (HAL-VP-9/1-116)**

| Measurement name | Code | Value (in mm) |
|---|---|---|
| Cortical thickness of posterior distal shaft [k] | – | 4.3 |
| Cortical thickness of anteromedial distal shaft [k] | – | 4.8 |
| Cortical thickness of anterolateral distal shaft [k] | – | 3.8 |

[a] Midshaft and deltoid tuberosity positions were estimated using a small (n<10) modern human reference sample.
[b] See definition for measurement #6 in Carretero, Arsuaga, & Lorenzo, 1997.
[c] See definition for measurement #13 in Carretero, Arsuaga, & Lorenzo, 1997.
[d] See definition for measurement #14 in Carretero, Arsuaga, & Lorenzo, 1997.
[e] See definition for measurement #15 in Carretero, Arsuaga, & Lorenzo, 1997.
[f] Measurement was taken at the proximal break, near midshaft.
[g] See definition for measurement #25 in Carretero, Arsuaga, & Lorenzo, 1997.
[h] Measurement was taken at the distal break.
[i] Measurement was taken at the proximal break.
[j] Measurement was taken at the distal break.
[k] Measurement was taken at the proximal break.

**Table A5.6** Ulna measurements for HAL-VP-9/1

**Ulna measurements**

**Right proximal end (HAL-VP-9/1-121)**

| Measurement name | Code | Value (in mm) |
|---|---|---|
| Anteroposterior thickness at mid-trochlea | ULN6_TRO_THI | 23.1 |
| Coronoid height | ULN7_COR_HEI | 39.4 |
| Olecranon height | ULN8_OLE_HEI | 26.2 |
| Trochlear length | ULN9_TRO_LEN | 27.2 |
| Olecranon length | ULN10_OLE_LEN | 20.9 |
| Radial notch position | ULN11_NOT_POS | 48.2 |

| | | |
|---|---|---|
| Radial notch maximum diameter | ULN12_NOT_MAJ | 23.8 |
| Radial notch diameter perpendicular to maximum diameter | ULN13_NOT_PER | 17.0 |

**Right shaft (HAL-VP-9/1-122)**

| Measurement name | Code | Value (in mm) |
|---|---|---|
| Anteroposterior shaft diameter at nutrient foramen | – | 18.8 |
| Maximum shaft diameter of preserved portion | – | 106.5 |
| Cortical thickness of anterolateral proximal shaft [a] | – | 4.1 |
| Cortical thickness of posterior proximal shaft [b] | – | 4.8 |
| Cortical thickness of anteromedial shaft [c] | – | 4.0 |

**Left partial proximal end (HAL-VP-9/1-123)**

| Measurement name | Code | Value (in mm) |
|---|---|---|
| Coronoid height | ULN7_COR_HEI | 40.4 |
| Radial notch maximum diameter | ULN12_NOT_MAJ | (23.2) |
| Radial notch diameter perpendicular to maximum diameter | ULN13_NOT_PER | (15.2) |
| Anteroposterior shaft diameter at level of inferior margin of radial notch | – | 25.3 |
| Mediolateral shaft diameter at level of inferior margin of radial notch | – | 23.0 |

**Left distal end (HAL-VP-9/1-124)**

| Measurement name | Code | Value (in mm) |
|---|---|---|
| Distal epiphysis maximum breadth excluding styloid process | ULN5_DIS_BRE | 19.0 |
| Mediolateral diameter of styloid process at level of distal margin of articular circumference | – | 6.9 |
| Anteroposterior diameter of styloid process at level of distal margin of articular circumference | – | 5.8 |
| Maximum height (proximodistal) of articular circumference (in anterior view) | – | 12.3 |
| Maximum diameter of distal end (in a transverse plane, including styloid process) | – | 23.5 |
| Cortical thickness of anterior distal shaft [d] | – | 2.0 |
| Cortical thickness of medial distal shaft [d] | – | 2.5 |

**Left partial shaft (HAL-VP-9/1-125)**

| Measurement name | Code | Value (in mm) |
|---|---|---|
| Maximum anteroposterior diameter | ULN3_AP_DIA | 16.2 |
| Maximum mediolateral diameter | ULN4_ML_DIA | 14.1 |
| Ulnar minimum circumference [e] | ULN14_MIN_CIR | 42 |
| Maximum shaft diameter at position with greatest interosseous crest development on preserved portion | – | 17.3 |
| Minimum shaft diameter at position with greatest interosseous crest development on preserved portion | – | 11.4 |

| | | |
|---|---|---|
| Anteroposterior shaft diameter at distal extent of pronator ridge | – | 13.0 |
| Mediolateral shaft diameter at distal extent of pronator ridge | – | 12.8 |
| Maximum dimension of preserved portion | – | 94.7 |
| Cortical thickness of shaft at interosseous crest [f] | – | 6.2 |
| Cortical thickness of anterior distal shaft [g] | – | 3.4 |
| Cortical thickness of posterior distal shaft [g] | – | 2.7 |
| Cortical thickness of medial distal shaft [g] | – | 3.1 |
| Cortical thickness of lateral distal shaft [g] | – | 3.0 |

| **Shaft fragment (HAL-VP-9/1-126)** | | |
|---|---|---|
| **Measurement name** | **Code** | **Value (in mm)** |
| Maximum length of preserved portion (along shaft axis) | – | 25.9 |

| **Shaft fragment (HAL-VP-9/1-127)** | | |
|---|---|---|
| **Measurement name** | **Code** | **Value (in mm)** |
| Maximum dimension of preserved portion | – | 42.5 |
| Maximum shaft diameter of preserved portion | – | 18.5 |
| Minimum shaft diameter of preserved portion | – | 13.1 |

[a] Measurement was taken at the proximal break (just distal to the ulnar tuberosity), near the interosseous crest.
[b] Measurement was taken at the proximal break (just distal to the ulnar tuberosity), at position of the posterior border.
[c] Measurement was taken at the distal break, near the anterior border.
[d] Measurement was taken at the proximal break.
[e] Measurement was taken at position of minimum circumference on the preserved portion. This point is near but just distal to where the minimum circumference is most often observed in recent modern humans, and therefore the reported measurement may be slightly greater than the true minimum circumference.
[f] Measurement was taken at the proximal break.
[g] Measurement was taken at the distal break.

**Table A5.7** Radius measurements for HAL-VP-9/1

| **Radius measurements** | | |
|---|---|---|
| **Right radial head (HAL-VP-9/1-119)** | | |
| **Measurement name** | **Code** | **Value (in mm)** |
| Radial head anteroposterior diameter | RAD6_HEA_AP | (28.4) |
| Radial head circumference | RAD7_HEA_CIR | 88 |
| Maximum cortical thickness of proximal shaft [a] | – | 2.8 |

| **Shaft fragment (HAL-VP-9/1-120)** | | |
|---|---|---|
| **Measurement name** | **Code** | **Value (in mm)** |

| | | |
|---|---|---|
| Maximum shaft diameter of preserved portion | – | 17.6 |
| Minimum shaft diameter of preserved portion | – | 11.7 |
| Cortical thickness at interosseous border [b] | – | 4.0 |
| Cortical thickness at interosseous border [b] | – | 5.3 |

[a] Measurement was taken at the distal break.
[b] Cortical thickness was measured at the interosseous border at both ends of the shaft fragment; because the side and portion of the fragment is indeterminate, the proximodistal directionality is unknown.

---

**Table A5.8** Carpal measurements for HAL-VP-9/1

| **Carpal measurements** | | |
|---|---|---|
| **Right hamate (HAL-VP-9/1-128)** | | |
| **Measurement name** | **Code** | **Value (in mm)** |
| Maximum height | HAM1_MAX_HEI | 26.6 |
| Height of the body | HAM2_BOD_HEI | 14.8 |
| Hamulus projection | HAM3_HAM_PRO | 11.8 |
| Maximum width | HAM4_MAX_WID | 20.7 |
| Maximum width of the distal facets | HAM5_ML_WID | 17.2 |
| Maximum width of the hamulus | HAM6_HAM_WID | 12.6 |
| **Right trapezium (HAL-VP-9/1-129)** | | |
| **Measurement name** | **Code** | **Value (in mm)** |
| Maximum length | TZM1_MAX_LEN | 27.7 |
| Height | TZM2_HEI | 18.1 |
| Maximum length of metacarpal I facet | TZM3_LEN_MC1 | (17.3) |
| Width of metacarpal facet, perpendicular to maximum length | – | 14.1 |
| **Right triquetral (HAL-VP-9/1-130)** | | |
| **Measurement name** | **Code** | **Value (in mm)** |
| Maximum length | TRI1_LEN | (21.5) |
| Maximum width | TRI2_WID | 14.7 |
| Maximum height [a] | – | (17.4) |
| Maximum length of lunate facet [a] | – | (10.4) |
| Maximum length of pisiform facet [a] | – | (10.6) |
| Maximum width of pisiform facet [a] | – | 9.1 |
| Maximum height of hamate facet [a] | – | 15.5 |
| Maximum width of hamate facet [a] | – | 12.5 |

| Left lunate (HAL-VP-9/1-131) | | |
|---|---|---|
| **Measurement name** | **Code** | **Value (in mm)** |
| Maximum length | LUN1_LEN | 19.3 |
| Maximum width | LUN2_BRE | 18.0 |
| Maximum width of triquetral facet [a] | – | 13.1 |
| **Left capitate (HAL-VP-9/1-132)** | | |
| **Measurement name** | **Code** | **Value (in mm)** |
| Maximum height | CAP1_MAX_HEI | 28.3 |
| Maximum width of head | CAP2_WID_HEA | (18.1) |
| Maximum width of distal base | CAP3_WID_BAS | 22.2 |
| Minimum width of head [a] | – | 13.5 |
| Length of tuberosity | – | 17.0 |
| Maximum dimension of facet for metacarpal III | – | (18.3) |
| **Left triquetral (HAL-VP-9/1-133)** | | |
| **Measurement name** | **Code** | **Value (in mm)** |
| Maximum length | TRI1_LEN | 20.6 |
| Maximum width | TRI2_WID | 14.5 |
| Maximum height [a] | – | 17.1 |
| Maximum length of lunate facet [a] | – | (10.0) |
| Maximum width of lunate facet [a] | – | 9.7 |
| Maximum length of pisiform facet [a] | – | (11.4) |
| Maximum width of pisiform facet [a] | – | 8.7 |
| Maximum height of hamate facet [a] | – | 15.6 |
| Maximum width of hamate facet [a] | – | (12.4) |

[a] See Mastrangelo, De Luca, Alemán, & Botella, 2011 for measurement definition.

**Table A5.9** Metacarpal measurements for HAL-VP-9/1

| Metacarpal measurements | | |
|---|---|---|
| **Right second metacarpal base (HAL-VP-9/1-134)** | | |
| **Measurement name** | **Code** | **Value (in mm)** |
| Proximal maximum height | MC5_PRO_HEI | 20.0 |
| Proximal maximum breadth | MC6_PRO_BRE | 19.7 |
| Maximum dimension of capitate facet | – | 10.1 |

| Right second metacarpal head and partial shaft (HAL-VP-9/1-135) | | |
|---|---|---|
| **Measurement name** | **Code** | **Value (in mm)** |
| Distal maximum height | MC7_DIS_HEI | 16.7 |
| Distal maximum breadth | MC8_DIS_BRE | 17.2 |
| **Right third metacarpal (HAL-VP-9/1-136)** | | |
| **Measurement name** | **Code** | **Value (in mm)** |
| Maximum length | MC1_LEN | 74.9 |
| Biomechanical length | MC2_BIO_LEN | 71.1 |
| Midshaft dorsopalmar height | MC3_MID_DP | 9.1 |
| Midshaft mediolateral breadth | MC4_MID_ML | 9.8 |
| Proximal maximum height | MC5_PRO_HEI | 19.4 |
| Proximal maximum breadth | MC6_PRO_BRE | 16.8 |
| Distal maximum height | MC7_DIS_HEI | 14.8 |
| Distal maximum breadth | MC8_DIS_BRE | 17.0 |
| Proximodistal length excluding styloid process | MC9_LEN_EXC | 71.2 |
| Maximum dorsal width of facet for the capitate | MC10_DOR_WID | (13.9) |
| Maximum palmar width of facet for the capitate | MC11_PAL_WID | (9.5) |
| Mediolateral width of facet for the capitate | MC12_FAC_WID | (8.2) |
| Dorsopalmar length of facet for metacarpal II | – | 17.7 |
| Maximum dimension of metacarpal IV dorsal facet | – | 7.1 |
| Proximodistal length of metacarpal IV dorsal facet | – | 6.3 |
| Dorsopalmar length of metacarpal IV dorsal facet | – | 5.9 |
| Maximum dimension of metacarpal IV palmar facet | – | (7.2) |
| Proximodistal length of metacarpal IV palmar facet | – | (7.1) |
| Dorsopalmar length of metacarpal IV palmar facet | – | 6.6 |
| **Right fourth metacarpal base and shaft (HAL-VP-9/1-137)** | | |
| **Measurement name** | **Code** | **Value (in mm)** |
| Proximal maximum height | MC5_PRO_HEI | 15.2 |
| Proximal maximum breadth | MC6_PRO_BRE | 14.2 |
| Maximum dimension of facet for metacarpal V | – | 12.1 |
| Proximodistal length of metacarpal III dorsal facet | – | 6.9 |
| Dorsopalmar length of metacarpal III dorsal facet | – | 6.1 |
| Proximodistal length of metacarpal III palmar facet | – | 6.7 |
| Dorsopalmar length of metacarpal III palmar facet | – | 5.8 |
| **Right fifth metacarpal head (HAL-VP-9/1-143)** | | |
| **Measurement name** | **Code** | **Value (in mm)** |

| | | |
|---|---|---|
| Distal maximum height | MC7_DIS_HEI | 12.4 |
| Distal maximum breadth | MC8_DIS_BRE | 14.1 |

**Left first metacarpal head (HAL-VP-9/1-138)**

| Measurement name | Code | Value (in mm) |
|---|---|---|
| Distal maximum height | MC7_DIS_HEI | 14.0 |
| Distal maximum breadth | MC8_DIS_BRE | 18.3 |
| Cortical thickness of palmar shaft [a] | – | 1.9 |

**Left second metacarpal base (HAL-VP-9/1-139)**

| Measurement name | Code | Value (in mm) |
|---|---|---|
| Proximal maximum height | MC5_PRO_HEI | 19.5 |
| Proximal maximum breadth | MC6_PRO_BRE | 20.5 |
| Maximum dimension of capitate facet | – | 10.6 |
| Maximum dimension of facet for metacarpal III | – | 16.2 |
| Cortical thickness of palmar shaft [b] | – | 2.7 |

**Left second metacarpal head (HAL-VP-9/1-140)**

| Measurement name | Code | Value (in mm) |
|---|---|---|
| Distal maximum height | MC7_DIS_HEI | 15.4 |
| Distal maximum breadth | MC8_DIS_BRE | 15.9 |
| Cortical thickness of dorsal shaft [a] | – | 1.5 |
| Cortical thickness of palmar shaft [a] | – | 2.6 |

**Left third metacarpal shaft (HAL-VP-9/1-144)**

| Measurement name | Code | Value (in mm) |
|---|---|---|
| Midshaft dorsopalmar height [c] | MC3_MID_DP | 8.8 |
| Midshaft mediolateral breadth [c] | MC4_MID_ML | 10.1 |
| Maximum dimension of preserved portion | – | 33.2 |
| Cortical thickness of dorsal shaft [a] | – | 2.8 |
| Cortical thickness of palmar shaft [a] | – | 3.1 |
| Cortical thickness of dorsal shaft [b] | – | 1.3 |
| Cortical thickness of palmolateral shaft [b] | – | 2.0 |
| Cortical thickness of palmomedial shaft [b] | – | 2.2 |

**Left fourth metacarpal head and shaft (HAL-VP-9/1-141)**

| Measurement name | Code | Value (in mm) |
|---|---|---|
| Midshaft dorsopalmar height [d] | MC3_MID_DP | 8.0 |
| Midshaft mediolateral breadth [d] | MC4_MID_ML | 8.4 |
| Distal maximum height | MC7_DIS_HEI | 14.8 |

| | | |
|---|---|---|
| Distal maximum breadth | MC8_DIS_BRE | 15.3 |
| Cortical thickness of dorsal shaft [a] | – | 2.3 |
| Cortical thickness of lateral shaft [a] | – | 2.2 |

| **Left fifth metacarpal base and shaft (HAL-VP-9/1-142)** | | |
|---|---|---|
| **Measurement name** | **Code** | **Value (in mm)** |
| Proximal maximum height | MC5_PRO_HEI | 13.5 |
| Proximal maximum breadth | MC6_PRO_BRE | 14.6 |
| Maximum dimension of facet for metacarpal IV | – | 13.2 |

[a] Measurement was taken at the proximal break.
[b] Measurement was taken at the distal break.
[c] Midshaft position was estimated using the antimere (right metacarpal III: HAL-VP-9/1-136) as a reference.
[d] Midshaft position was estimated using a small (n<10) modern human reference sample.

**Table A5.10** Hand phalanx measurements for HAL-VP-9/1

| **Hand phalanx measurements** | | |
|---|---|---|
| **Proximal hand phalanx of left ray V (HAL-VP-9/1-145)** | | |
| **Measurement name** | **Code** | **Value (in mm)** |
| Maximum length | – | 39.2 |
| Biomechanical length [a] | – | 36.6 |
| Midshaft dorsopalmar height | – | 6.2 |
| Midshaft mediolateral breadth | – | 9.5 |
| Proximal maximum height | – | 11.1 |
| Proximal maximum breadth | – | 16.3 |
| Distal maximum height | – | 7.5 |
| Distal maximum breadth | – | 10.8 |
| Maximum height of proximal articular surface | – | 9.5 |
| Maximum breadth of proximal articular surface | – | 11.7 |

| **Proximal hand phalanx base and shaft, probably of left ray III (HAL-VP-9/1-146)** | | |
|---|---|---|
| **Measurement name** | **Code** | **Value (in mm)** |
| Midshaft dorsopalmar height [b] | – | 7.6 |
| Midshaft mediolateral breadth [b] | – | 11.4 |
| Proximal maximum height | – | 14.0 |
| Proximal maximum breadth | – | 18.4 |
| Maximum height of proximal articular surface | – | 12.4 |
| Maximum breadth of proximal articular surface | – | (14.4) |

| Proximal hand phalanx base and shaft, probably of right ray III (HAL-VP-9/1-147) | | | |
|---|---|---|---|
| | **Measurement name** | **Code** | **Value (in mm)** |
| | Proximal maximum height | – | 13.4 |
| | Proximal maximum breadth | – | 18.7 |
| | Maximum height of proximal articular surface | – | 11.1 |
| | Maximum breadth of proximal articular surface | – | 14.1 |
| | Cortical thickness of palmar shaft [c] | – | 2.4 |
| **Proximal hand phalanx base, probably of left ray IV (HAL-VP-9/1-148)** | | | |
| | **Measurement name** | **Code** | **Value (in mm)** |
| | Proximal maximum breadth | – | 17.3 |
| **Intermediate hand phalanx of left ray III (HAL-VP-9/1-150)** | | | |
| | **Measurement name** | **Code** | **Value (in mm)** |
| | Maximum length | – | 36.1 |
| | Midshaft dorsopalmar height | – | 6.2 |
| | Midshaft mediolateral breadth | – | (10.6) |
| | Proximal maximum height | – | 11.6 |
| | Proximal maximum breadth | – | 16.4 |
| | Distal maximum height | – | 7.3 |
| | Distal maximum breadth | – | 12.5 |
| | Breadth of trochlea at distal margin | – | 10.2 |
| **Intermediate hand phalanx base and shaft of right ray III (HAL-VP-9/1-151)** | | | |
| | **Measurement name** | **Code** | **Value (in mm)** |
| | Proximal maximum height | – | 11.8 |
| | Proximal maximum breadth | – | 16.6 |
| | Maximum height of proximal articular surface | – | 8.6 |
| | Maximum breadth of proximal articular surface | – | 12.2 |
| | Breadth of lateral facet of proximal articular surface | – | 6.1 |
| | Breadth of medial facet of proximal articular surface | – | 6.4 |
| | Cortical thickness of palmar shaft [c] | – | 2.1 |
| | Cortical thickness of dorsal shaft [c] | – | 2.4 |
| **Intermediate hand phalanx base and shaft of left ray II (HAL-VP-9/1-152)** | | | |
| | **Measurement name** | **Code** | **Value (in mm)** |
| | Proximal maximum height | – | 10.2 |
| | Proximal maximum breadth | – | 15.2 |
| | Maximum height of proximal articular surface | – | 8.1 |
| | Maximum breadth of proximal articular surface | – | 12.2 |

| | | |
|---|---|---|
| Breadth of lateral facet of proximal articular surface | – | 6.2 |
| Breadth of medial facet of proximal articular surface | – | 5.8 |

**Intermediate hand phalanx base and shaft of left ray IV (HAL-VP-9/1-153)**

| Measurement name | Code | Value (in mm) |
|---|---|---|
| Proximal maximum height | – | 10.0 |
| Proximal maximum breadth | – | 14.7 |
| Maximum height of proximal articular surface | – | 8.6 |
| Maximum breadth of proximal articular surface | – | 12.0 |
| Breadth of lateral facet of proximal articular surface | – | 5.8 |
| Breadth of medial facet of proximal articular surface | – | 6.5 |

**Intermediate hand phalanx base and shaft of left ray V (HAL-VP-9/1-154)**

| Measurement name | Code | Value (in mm) |
|---|---|---|
| Proximal maximum breadth | – | 13.6 |

**Intermediate hand phalanx head of ray II or III, side indet. (HAL-VP-9/1-155)**

| Measurement name | Code | Value (in mm) |
|---|---|---|
| Breadth of trochlea at distal margin | – | 10.3 |

**Terminal hand phalanx of ray II, III, or IV, side indet. (HAL-VP-9/1-157)**

| Measurement name | Code | Value (in mm) |
|---|---|---|
| Maximum length | THP1_LEN | 21.3 |
| Biomechanical length | THP2_BIO_LEN | 20.4 |
| Midshaft anteroposterior (dorsopalmar) height | THP3_MID_AP | 4.0 |
| Midshaft mediolateral breadth | THP4_MID_ML | 5.8 |
| Proximal anteroposterior (dorsopalmar) height | THP5_PRO_AP | 6.9 |
| Proximal mediolateral breadth | THP6_PRO_ML | 13.0 |
| Distal tuft anteroposterior (dorsopalmar) height | THP7_DIS_AP | 4.1 |
| Distal tuft mediolateral breadth | THP8_DIS_ML | 8.5 |
| Maximum height of proximal articular surface | – | 5.9 |
| Maximum breadth of proximal articular surface | – | 11.0 |

**Terminal hand phalanx base and shaft of right ray I (HAL-VP-9/1-158)**

| Measurement name | Code | Value (in mm) |
|---|---|---|
| Maximum height of proximal articular surface | – | (8.2) |
| Maximum breadth of proximal articular surface | – | 13.0 |
| Breadth of lateral facet of proximal articular surface | – | 6.7 |
| Breadth of medial facet of proximal articular surface | – | 6.2 |
| Cortical thickness of medial shaft [c] | – | 1.3 |

[a] Measurement was taken from the midpoint of the trochlea to the midpoint of the proximal articular surface.
[b] Midshaft position was estimated using the complete proximal hand phalanx from ray V (HAL-VP-9/1-145) as a reference.
[c] Measurement was taken at the distal break.

**Table A5.11** Os coxae and sacrum measurements for HAL-VP-9/1

| **Os coxae and sacrum measurements** | | | |
|---|---|---|---|
| **Right partial ala of sacrum (HAL-VP-9/1-57)** | | | |
| | **Measurement name** | **Code** | **Value (in mm)** |
| | Breadth of ala (from lateral margin of first sacral centrum to lateral margin of ala) | – | 42.3 |
| **Right partial os coxae (HAL-VP-9/1-106A+B)** | | | |
| | **Measurement name** | **Code** | **Value (in mm)** |
| | Maximum diameter from ischium to pubis | OCX2_ISC_PUB | (132.5) |
| | Nonarticular ischial length | OCX5_NA_ISC | 56.8 |
| | Acetabulum diameter | OCX6_ACE_DIA | 59.1 |
| | Dorsoventral diameter of superior pubic ramus at pubic tubercle (taken perpendicular to ramus axis) | – | 17.4 |
| | Minimum cross-sectional diameter of inferior pubic ramus | – | 10.5 |

**Table A5.12** Femur measurements for HAL-VP-9/1

| **Femur measurements** | | | |
|---|---|---|---|
| **Right proximal end (HAL-VP-9/1-160)** | | | |
| | **Measurement name** | **Code** | **Value** |
| | Biomechanical neck length | FEM3_NEC_LEN | 108.9 mm |
| | Vertical head diameter | FEM4_HEA_DIA | (47.6) mm |
| | Anteroposterior head diameter | FEM10_AP_HEA | (51.3) mm |
| | Minimum neck height | FEM11_NEC_HEI | 34.1 mm |
| | Neck angle [a] | FEM12_NEC_ANG | 122.5º |
| | Maximum anteroposterior diameter of greater trochanter | – | 49.0 mm |
| | Minimum neck width (taken in superior view, perpendicular to neck axis) | – | 31.6 mm |
| **Right partial distal end (HAL-VP-9/1-161+167)** | | | |
| | **Measurement name** | **Code** | **Value (in mm)** |
| | Maximum anteroposterior diameter of lateral condyle | – | 74.4 |

| | | |
|---|---|---|
| Maximum mediolateral diameter of lateral condyle (in posterior view) | – | 32.6 |
| Maximum proximodistal diameter of lateral condyle (in posterior view) | – | 42.5 |

| **Left partial shaft (HAL-VP-9/1-163)** | | |
|---|---|---|
| **Measurement name** | **Code** | **Value (in mm)** |
| Maximum anteroposterior shaft diameter [b] | – | (35.0) |
| Maximum mediolateral shaft diameter [b] | – | 29.4 |
| Maximum dimension of preserved portion | – | 134.0 |
| Cortical thickness of medial shaft [c] | – | 6.5 |

| **Shaft fragment (HAL-VP-9/1-169)** | | |
|---|---|---|
| **Measurement name** | **Code** | **Value (in mm)** |
| Maximum shaft diameter of preserved portion (~mediolateral) | – | 30.8 |
| Maximum dimension of preserved portion | – | 68.6 |

[a] A small (n<10) modern human reference sample was used to guide orientation of the proximal femur and identify the shaft axis; the neck angle measurement is likely to be accurate within ±2º.
[b] Measurement was taken just distal to midshaft and proximal to the point on the distal shaft where the medial and lateral lips of the linea aspera begin to diverge.
[c] Measurement was taken at the proximal break.

**Table A5.13** Patella measurements for HAL-VP-9/1

| **Patella measurements** | | |
|---|---|---|
| **Right patella (HAL-VP-9/1-186)** | | |
| **Measurement name** | **Code** | **Value (in mm)** |
| Maximum patellar breadth | PAT2_BRE | 48.4 |
| Maximum thickness | PAT3_THI | 24.9 |
| Mediolateral width of lateral facet | – | 29.5 |
| Mediolateral width of medial facet | – | 23.3 |

| **Left patella (HAL-VP-9/1-187)** | | |
|---|---|---|
| **Measurement name** | **Code** | **Value (in mm)** |
| Maximum patellar height | PAT1_HEI | 42.0 |
| Maximum thickness | PAT3_THI | 24.4 |

**Table A5.14** Tibia measurements for HAL-VP-9/1

**Tibia measurements**

**Right distal end and shaft (HAL-VP-9/1-173)**

| Measurement name | Code | Value (in mm) |
|---|---|---|
| Tibial maximum distal epiphyseal breadth | TIB3_DIS_BRE | 55.9 |
| Distal epiphysis anteroposterior diameter | TIB4_DIS_AP | 44.7 |
| Maximum dimension of preserved portion | – | 146.0 |
| Cortical thickness of anterior shaft [a] | – | 9.3 |

**Right partial shaft (HAL-VP-9/1-174+175)**

| Measurement name | Code | Value |
|---|---|---|
| Tibial anteroposterior midshaft diameter [b] | TIB6_AP_MID | 38.5 mm |
| Tibial mediolateral midshaft diameter [b] | TIB7_ML_MID | (24.3 mm) |
| Tibial circumference at nutrient foramen | TIB9_CIR_NUT | 114 mm |
| Tibial mediolateral shaft diameter at nutrient foramen | TIB10_ML_NUT | 26.0 mm |
| Tibial maximum shaft diameter at nutrient foramen | TIB11_MAX_NUT | 44.2 mm |
| Platycnemic index | TIB12_PLA_IND | 58.8 |
| Maximum dimension of preserved portion | – | 188.2 mm |
| Cortical thickness of anterior shaft [c] | – | 11.8 mm |
| Cortical thickness of posterior shaft [c] | – | 8.1 mm |
| Cortical thickness of medial shaft [c] | – | 3.6 mm |
| Cortical thickness of lateral shaft [c] | – | 4.3 mm |

**Left distal end and shaft (HAL-VP-9/1-177+178)**

| Measurement name | Code | Value (in mm) |
|---|---|---|
| Tibial maximum distal epiphyseal breadth | TIB3_DIS_BRE | 56.3 |
| Distal epiphysis anteroposterior diameter | TIB4_DIS_AP | 43.3 |
| Anteroposterior diameter of distal fibular articular surface | – | 20.6 |
| Maximum diameter of lateral margin of talar articular surface | – | 36.0 |
| Diameter of medial margin of talar articular surface [d] | – | 22.7 |
| Mediolateral diameter of medial malleolus [d] | – | 17.4 |
| Anteroposterior diameter of medial malleolus [d] | – | 28.7 |
| Anteroposterior diameter at midline of horizontal talar articular surface | – | 33.4 |
| Maximum mediolateral width of horizontal talar articular surface | – | 32.0 |

[a] Measurement was taken at the proximal break.
[b] Midshaft position was estimated using a small (n<10) modern human reference sample.
[c] Measurement was taken at the distal break.
[d] Measurement was taken at the level of the horizontal part of the talar articular surface.

**Table A5.15** Fibula measurements for HAL-VP-9/1

| **Fibula measurements** | | | |
|---|---|---|---|
| **Right distal end (HAL-VP-9/1-180)** | | | |
| | **Measurement name** | **Code** | **Value (in mm)** |
| | Maximum proximodistal diameter of malleolar articular surface | FIB3_MAX_ART | 24.2 |
| | Maximum diameter of malleolar articular surface, perpendicular to the max. proximodistal diameter | FIB4_ART_DIA | (22.3) |
| | Maximum distal mediolateral breadth | FIB5_DIS_BRE | 20.3 |
| | Maximum distal anteroposterior diameter | FIB6_DIS_AP | 26.9 |
| **Left distal end (HAL-VP-9/1-182)** | | | |
| | **Measurement name** | **Code** | **Value (in mm)** |
| | Maximum proximodistal diameter of malleolar articular surface | FIB3_MAX_ART | 25.2 |
| | Maximum diameter of malleolar articular surface, perpendicular to the max. proximodistal diameter | FIB4_ART_DIA | (21.6) |
| | Maximum distal mediolateral breadth | FIB5_DIS_BRE | 19.7 |
| | Maximum distal anteroposterior diameter | FIB6_DIS_AP | 28.4 |
| **Shaft fragment (HAL-VP-9/1-183)** | | | |
| | **Measurement name** | **Code** | **Value (in mm)** |
| | Maximum shaft diameter of preserved portion | – | 14.5 |
| | Minimum shaft diameter of preserved portion [a] | – | 7.8 |
| | Maximum dimension of preserved portion | – | 132.7 |
| **Shaft fragment (HAL-VP-9/1-184)** | | | |
| | **Measurement name** | **Code** | **Value (in mm)** |
| | Maximum shaft diameter of preserved portion | – | 14.7 |
| | Minimum shaft diameter of preserved portion [a] | – | 7.1 |
| | Maximum dimension of preserved portion | – | 109.9 |

[a] Measurement was taken at same position as maximum shaft diameter.

**Table A5.16** Tarsal measurements for HAL-VP-9/1

| **Tarsal measurements** |
|---|
| **Right talus (HAL-VP-9/1-188)** |

| Measurement name | Code | Value (in mm) |
|---|---|---|
| Talar length | TAL1_LEN | 59.3 |
| Maximum talar length | TAL2_MAX_LEN | 61.2 |
| Length of head plus neck | TAL3_HEA_NEC | 19.0 |
| Physiological height | TAL4_PHY_HEI | 28.8 |
| Articular breadth | TAL5_ART_BREA | 33.1 |
| Lateral malleolar breadth | TAL6_MAL_BRE | 14.9 |
| Length of the head | TAL7_HEA_LEN | 35.2 |
| Trochlear height | TAL8_TRO_HEI | 11.3 |
| Mediolateral width | TAL9_ML_WID | 51.1 |
| Maximum anteroposterior trochlear length | TAL10_AP_TRO | 41.1 |
| Mediolateral width of talar head | TAL11_ML_HEA | 31.0 |
| Maximum dimension of posterior subtalar facet | TAL12_LEN_FAC | 40.8 |
| Width of posterior subtalar facet [a] | – | (25.1) |
| Maximum length of anterior and medial facets | – | 32.3 |
| Articular breadth [b] | – | (45.8) |
| Lateral malleolar oblique height [c] | – | (30.5) |
| Lateral malleolar length [d] | – | (36.2) |
| Lateral height [e] | – | 32.4 |
| Medial height [f] | – | 35.9 |

**Right calcaneus (HAL-VP-9/1-189)**

| Measurement name | Code | Value (in mm) |
|---|---|---|
| Maximum calcaneal length | CAL1_LEN | 93.4 |
| Posterior calcaneal length | CAL2_POS_LEN | 71.2 |
| Medial breadth | CAL3_MED_BRE | (49.5) |
| Height of the body | CAL4_HEI_BOD | 49.8 |
| Minimum breadth across the body | CAL5_MIN_BRE | 30.3 |
| Dorsoplantar height of cuboid facet | – | 29.9 |
| Maximum diameter of posterior talar facet | – | 29.4 |

**Left talus (HAL-VP-9/1-190)**

| Measurement name | Code | Value (in mm) |
|---|---|---|
| Talar length | TAL1_LEN | 58.2 |
| Length of head plus neck | TAL3_HEA_NEC | (18.7) |
| Physiological height | TAL4_PHY_HEI | 28.7 |
| Articular breadth | TAL5_ART_BREA | 33.5 |
| Length of the head | TAL7_HEA_LEN | 35.4 |
| Trochlear height | TAL8_TRO_HEI | 10.7 |

| | | |
|---|---|---|
| Maximum anteroposterior trochlear length | TAL10_AP_TRO | 38.1 |
| Mediolateral width of talar head | TAL11_ML_HEA | 32.7 |
| Width of posterior subtalar facet [a] | – | 25.0 |
| Lateral height [e] | – | 31.9 |
| Medial height [f] | – | 34.0 |

**Left calcaneus (HAL-VP-9/1-191)**

| Measurement name | Code | Value (in mm) |
|---|---|---|
| Posterior calcaneal length | CAL2_POS_LEN | 72.8 |
| Medial breadth | CAL3_MED_BRE | 47.7 |
| Height of the body | CAL4_HEI_BOD | 51.2 |
| Minimum breadth across the body | CAL5_MIN_BRE | 29.9 |
| Maximum diameter of posterior talar facet | – | 40.6 |

**Left navicular (HAL-VP-9/1-192)**

| Measurement name | Code | Value (in mm) |
|---|---|---|
| Maximum breadth | NAV1_MAX_BRE | 43.7 |
| Maximum length | NAV2_MAX_LEN | 24.2 |
| Maximum height | NAV3_MAX_HEI | 29.0 |
| Maximum diameter of the facet for the talar head | NAV4_TAL_FAC | 32.4 |
| Diameter of facet for talar head, perpendicular to maximum diameter | – | 24.9 |
| Maximum diameter of facet for medial cuneiform | – | 24.7 |
| Maximum diameter of facet for intermediate cuneiform | – | 17.4 |

**Left cuboid (HAL-VP-9/1-193)**

| Measurement name | Code | Value (in mm) |
|---|---|---|
| Maximum breadth | CUB1_MAX_BRE | 32.7 |
| Maximum length | CUB2_MAX_LEN | 38.6 |
| Maximum height | CUB3_MAX_HEI | 28.5 |
| Maximum diameter of the facet for the calcaneus | CUB4_CAL_FAC | 34.0 |
| Height of distal articular surface along margin between facets for fourth and fifth metatarsals | – | 17.0 |
| Length of tuberosity | – | 33.5 |

[a] Measurement was taken perpendicular to maximum dimension of posterior subtalar facet.
[b] See measurement definition for M2b in Pablos et al. 2013.
[c] See measurement definition for M7 in Pablos et al. 2013.
[d] See measurement definition for D4 in Pablos et al. 2013.
[e] See measurement definition for L2 in Pablos et al. 2013.
[f] See measurement definition for M3-1 in Pablos et al. 2013.

**Table A5.17** Metatarsal measurements for HAL-VP-9/1

| **Metatarsal measurements** | | |
|---|---|---|
| **Right third metatarsal base (HAL-VP-9/1-194)** | | |
| **Measurement name** | **Code** | **Value (in mm)** |
| Proximal maximum height | MT5_PRO_HEI | 23.2 |
| Proximal maximum breadth | MT6_PRO_BRE | 16.7 |
| Maximum diameter of facet for fourth metatarsal | – | 12.8 |
| Diameter of facet for fourth metatarsal, perpendicular to maximum diameter | – | 9.4 |
| Dorsoplantar height of proximal articular surface | – | 22.6 |
| **Right fourth metatarsal base and shaft (HAL-VP-9/1-195)** | | |
| **Measurement name** | **Code** | **Value (in mm)** |
| Proximal maximum height | MT5_PRO_HEI | 22.7 |
| Proximal maximum breadth | MT6_PRO_BRE | 14.4 |
| Maximum diameter of the facet for the third metatarsal | – | (13.0) |
| Diameter of the facet for the third metatarsal, perpendicular to maximum diameter | – | 8.9 |
| Maximum dorsoplantar height of proximal articular surface | – | 21.0 |
| Maximum dorsal width of proximal articular surface | – | 12.7 |
| Maximum plantar width of proximal articular surface | – | 13.6 |
| Maximum width of proximal articular surface (along line bisecting surface into dorsal and plantar halves) | – | 12.5 |
| **Left first metatarsal base (HAL-VP-9/1-196)** | | |
| **Measurement name** | **Code** | **Value (in mm)** |
| Proximal maximum height | MT5_PRO_HEI | 32.2 |
| Proximal maximum breadth | MT6_PRO_BRE | 23.3 |
| **Left first metatarsal head (HAL-VP-9/1-197)** | | |
| **Measurement name** | **Code** | **Value (in mm)** |
| Distal maximum height | MT7_DIS_HEI | 20.9 |
| Distal maximum breadth | MT8_DIS_BRE | 23.5 |
| Cortical thickness of dorsal shaft [a] | – | 1.7 |
| Cortical thickness of plantar shaft [a] | – | 2.1 |
| **Left third metatarsal base (HAL-VP-9/1-198)** | | |
| **Measurement name** | **Code** | **Value (in mm)** |
| Proximal maximum height | MT5_PRO_HEI | 22.0 |
| Proximal maximum breadth | MT6_PRO_BRE | 17.2 |

| | | |
|---|---|---|
| Maximum diameter of facet for fourth metatarsal | – | 12.0 |
| Diameter of facet for fourth metatarsal, perpendicular to maximum diameter | – | 9.5 |
| Dorsoplantar height of proximal articular surface | – | (22.3) |

**Left fifth metatarsal base (HAL-VP-9/1-199)**

| Measurement name | Code | Value (in mm) |
|---|---|---|
| Proximal maximum height | MT5_PRO_HEI | 17.6 |
| Proximal maximum breadth | MT6_PRO_BRE | 25.5 |
| Maximum diameter of facet for cuboid (dorsomedial to plantolateral) | – | 21.0 |
| Maximum proximodistal diameter of facet for fourth metatarsal | – | 11.0 |
| Length of ridge dividing the facets for cuboid and fourth metatarsal | – | 13.1 |
| Cortical thickness of medial shaft [b] | – | 3.0 |

**Left fifth metatarsal head (HAL-VP-9/1-200)**

| Measurement name | Code | Value (in mm) |
|---|---|---|
| Distal maximum height | MT7_DIS_HEI | 15.9 |
| Distal maximum breadth | MT8_DIS_BRE | 15.7 |
| Cortical thickness of medial shaft [a] | – | 2.6 |

**Left metatarsal head, ray II, III, or IV (HAL-VP-9/1-201)**

| Measurement name | Code | Value (in mm) |
|---|---|---|
| Distal maximum height | MT7_DIS_HEI | 16.7 |
| Distal maximum breadth | MT8_DIS_BRE | 12.7 |
| Maximum mediolateral breadth of articular surface | – | 10.3 |
| Cortical thickness of medial shaft [a] | – | 2.1 |

**Metatarsal shaft fragment (HAL-VP-9/1-202)**

| Measurement name | Code | Value (in mm) |
|---|---|---|
| Maximum dimension of preserved portion | – | 42.6 |

**Metatarsal shaft fragment (HAL-VP-9/1-205)**

| Measurement name | Code | Value (in mm) |
|---|---|---|
| Maximum dimension of preserved portion | – | 22.4 |
| Maximum shaft diameter | – | 13.7 |
| Minimum shaft diameter, taken at same position as maximum | – | 8.8 |

**Metatarsal shaft fragment (HAL-VP-9/1-159)**

| Measurement name | Code | Value (in mm) |
|---|---|---|
| Maximum dimension of preserved portion | – | 32.6 |

| | | |
|---|---|---|
| Maximum shaft diameter | – | 11.7 |
| Minimum shaft diameter, taken at same position as maximum | – | 8.2 |

[a] Measurement was taken at the proximal break.
[b] Measurement was taken at the distal break.

**Table A5.18** Foot phalanx measurements for HAL-VP-9/1

| **Foot phalanx measurements** | | |
|---|---|---|
| **Proximal foot phalanx (HAL-VP-9/1-203)** | | |
| **Measurement name** | **Code** | **Value (in mm)** |
| Maximum length | – | 33.6 |
| Biomechanical length [a] | – | 30.2 |
| Proximal maximum height | – | 14.3 |
| Proximal maximum breadth | – | 15.6 |
| Distal maximum height | – | 7.0 |
| Distal maximum breadth | – | 10.6 |
| Maximum height of proximal articular surface | – | (12.4) |
| Maximum breadth of proximal articular surface | – | (13.1) |
| **Intermediate foot phalanx (HAL-VP-9/1-204)** | | |
| **Measurement name** | **Code** | **Value (in mm)** |
| Maximum length | – | 18.1 |
| Biomechanical length [a] | – | 16.8 |
| Proximal maximum height | – | 9.4 |
| Proximal maximum breadth | – | 12.0 |
| Distal maximum height | – | 7.2 |
| Distal maximum breadth | – | 10.4 |
| Maximum height of proximal articular surface | – | 7.5 |
| Maximum breadth of proximal articular surface | – | 10.8 |

[a] Measurement was taken from the midpoint of the trochlea to the midpoint of the proximal articular surface.

**Table A5.19** Measurements for HAL-VP-9/1520

| **Measurements of the humerus, ulna, femur, tibia, and fibula shafts of HAL-VP-9/1520** |
|---|
| **Right humeral distal shaft (HAL-VP-9/1520-F)** |

| Measurement name | Code | Value (in mm) |
|---|---|---|
| Minimum thickness of medial pillar | HUM12_MED_PIL | 8.9 |
| Cortical thickness of anterior distal shaft [a] | – | 6.1 |
| Cortical thickness of anterolateral distal shaft [a] | – | 4.8 |
| Cortical thickness of anteromedial distal shaft [a] | – | 5.6 |
| Cortical thickness of posterior distal shaft [a] | – | 6.0 |

**Humeral proximal shaft, probably right side (HAL-VP-9/1520-K)**

| Measurement name | Code | Value (in mm) |
|---|---|---|
| Shaft circumference at deltoid tuberosity | HUM6_DEL_CIR | 66.5 |
| Minimum shaft diameter at deltoid tuberosity | HUM7_DEL_MIN | 18.8 |
| Maximum shaft diameter at deltoid tuberosity | HUM8_DEL_MAX | 21.4 |

**Right ulnar proximal shaft (HAL-VP-9/1520-E)**

| Measurement name | Code | Value (in mm) |
|---|---|---|
| Anteroposterior shaft diameter at approximately 1/3 of the shaft length from the proximal end | – | 17.7 |
| Mediolateral shaft diameter at approximately 1/3 of the shaft length from the proximal end | – | 13.9 |

**Right ulnar shaft (HAL-VP-9/1520-M)**

| Measurement name | Code | Value (in mm) |
|---|---|---|
| Maximum anteroposterior diameter | ULN3_AP_DIA | 17.8 |
| Maximum mediolateral diameter | ULN4_ML_DIA | 14.9 |
| Ulnar minimum circumference | ULN14_MIN_CIR | 38 |
| Anteroposterior shaft diameter at distal extent of pronator ridge | – | 12.0 |
| Mediolateral shaft diameter at distal extent of pronator ridge | – | 11.4 |
| Maximum dimension of preserved portion | – | 152.4 |

**Left femoral proximal shaft (HAL-VP-9/1520-I)**

| Measurement name | Code | Value |
|---|---|---|
| Femoral midshaft circumference [b] | FEM6_MID_CIR | 96.0 mm |
| Femoral anteroposterior midshaft diameter [b] | FEM7_AP_MID | 32.9 mm |
| Femoral mediolateral midshaft diameter [b] | FEM8_ML_MID | 28.5 mm |
| Platymeric index [b] | FEM9_PLA_IND | 115.4 |
| Cortical thickness of posterior shaft (at pilaster) [c] | – | 12.8 mm |
| Cortical thickness of posterolateral shaft [c] | – | 6.9 mm |

**Right tibial shaft (HAL-VP-9/1520-D)**

| Measurement name | Code | Value |
|---|---|---|
| Tibial anteroposterior midshaft diameter [d] | TIB6_AP_MID | 34.6 mm |

| | | |
|---|---|---|
| Tibial mediolateral midshaft diameter [d] | TIB7_ML_MID | 21.5 mm |
| Tibial midshaft circumference [d] | TIB8_MID_CIR | 89.5 mm |
| Tibial circumference at nutrient foramen | TIB9_CIR_NUT | 101.0 mm |
| Tibial mediolateral shaft diameter at nutrient foramen | TIB10_ML_NUT | 22.1 mm |
| Tibial maximum shaft diameter at nutrient foramen | TIB11_MAX_NUT | 40.2 mm |
| Platycnemic index | TIB12_PLA_IND | 55.0 |

**Fibular shaft (HAL-VP-9/1520-L)**

| Measurement name | Code | Value (in mm) |
|---|---|---|
| Maximum shaft diameter of preserved portion | – | 18.5 |
| Minimum shaft diameter of preserved portion | – | 10.7 |
| Maximum dimension of preserved portion | – | 113.4 |

[a] Measurement was taken at the proximal break.
[b] Measurement was taken ~30 mm proximal to midshaft, which was estimated using a small (n<10) modern human reference sample.
[c] Measurement was taken at the distal break, proximal to midshaft.
[d] Midshaft position was estimated using a small (n<10) modern human reference sample.

---

**Table A5.20** Measurements for HAL-VP-9/930

**Measurements of the proximal humerus and distal ulna of HAL-VP-9/930**

**Right proximal humerus (HAL-VP-9/930-A)**

| Measurement name | Code | Value (in mm) |
|---|---|---|
| Vertical head diameter | HUM9_HEA_DIA | (45.2) |

**Right distal ulna (HAL-VP-9/930-C)**

| Measurement name | Code | Value (in mm) |
|---|---|---|
| Mediolateral diameter of styloid process [a] | – | 7.3 |
| Anteroposterior diameter of styloid process [a] | – | 6.9 |
| Maximum diameter of distal epiphysis (including styloid) [b] | – | 19.9 |

[a] Measurement was taken at the level of the distal edge of the articular circumference.
[b] It should be noted that this measurement is not equivalent to the maximum diameter of the distal end as it is usually reported, since only the distal epiphysis is preserved and it does not include the articular circumference.

---

**Table A5.21** Measurements for TAL-VP-7/36

**Measurements of the distal humerus and distal radius of TAL-VP-7/36**

| Right distal radius (TAL-VP-7/36-I) | | |
|---|---|---|
| **Measurement name** | **Code** | **Value (in mm)** |
| Radial maximum distal epiphyseal breadth | RAD8_DIS_BRE | 31.6 |
| Distal epiphyseal anteroposterior diameter | RAD9_DIS_AP | 20.5 |
| Maximum anteroposterior diameter of ulnar notch | – | 14.9 |
| Maximum mediolateral diameter of carpal articular surface | – | 28.5 |
| Maximum anteroposterior diameter of carpal articular surface | – | 17.2 |
| Maximum length of preserved portion (measured along shaft long axis) | – | 39.3 |
| **Right distal humerus (TAL-VP-7/36-H)** | | |
| **Measurement name** | **Code** | **Value (in mm)** |
| Humeral bicondylar breadth | HUM10_BIC_BRE | 62.5 |
| Olecranon fossa breadth | HUM11_FOS_BRE | 28.1 |
| Minimum thickness of medial pillar | HUM12_ MED_PIL | 12.9 |
| Minimum thickness of lateral pillar | HUM13_LAT_PIL | 16.7 |
| Mediolateral width of medial epicondyle | HUM14_EPI_ML | 17.0 |
| Mediolateral width of capitulum [a] | – | 19.5 |
| Proximodistal height of capitulum [a] | – | 21.2 |
| Mediolateral width of trochlea [a] | – | 27.1 |
| Proximodistal height of trochlea [a] | – | 24.6 |
| Mediolateral width of coronoid fossa | – | 16.4 |
| Mediolateral width of lateral epicondyle [b] | – | 17.4 |
| Maximum length of preserved portion (measured along shaft long axis) | – | 64.8 |
| Cortical thickness of anterior distal shaft [c] | – | 5.3 |
| Cortical thickness of posterior distal shaft [c] | – | 3.7 |
| Cortical thickness of anterolateral distal shaft [c] | – | 4.8 |
| Cortical thickness of anteromedial distal shaft [c] | – | 5.2 |
| Cortical thickness of posterolateral distal shaft [c] | – | 8.1 |
| Cortical thickness of posteromedial distal shaft [c] | – | 8.5 |

[a] Measurement was taken in anterior view.
[b] Measurement was taken in posterior view.
[c] Measurement was taken at the proximal break.

**Table A5.22** Measurements for BOU-VP-16/100

| Measurements of the BOU-VP-16/100 femoral proximal shaft |
|---|

| Left femoral proximal shaft | | |
|---|---|---|
| **Measurement name** | **Code** | **Value (in mm)** |
| Anteroposterior shaft diameter [a] | – | 24.8 |
| Mediolateral shaft diameter [a] | – | 26.0 |
| Cortical thickness [b] | – | 10.4 |

[a] Measurement was taken at the superior extent of the preserved portion of the linea aspera.
[b] Measurement was taken at the distal break, proximal to midshaft and just posteromedial to the linea aspera.

---

**Table A5.23** Measurements for HAL-VP-2/16

| Measurements of the HAL-VP-2/16 proximal radius | | |
|---|---|---|
| **Proximal radius, probably left side** | | |
| **Measurement name** | **Code** | **Value (in mm)** |
| Radial head anteroposterior diameter [a] | RAD6_HEA_AP | (23.1) |
| Radial head circumference | RAD7_HEA_CIR | 73 |
| Maximum cortical thickness of proximal shaft [b] | – | 2.1 |

[a] The anteroposterior axis was estimated using a small (n<10) modern human reference sample, and assuming that this element is from the left side.
[b] Measurement was taken at the distal break.

---

**Table A5.24** Measurements for HAL-VP-3/1

| Measurements of the HAL-VP-3/1 proximal ulna | | |
|---|---|---|
| **Right proximal ulna** | | |
| **Measurement name** | **Code** | **Value (in mm)** |
| Anteroposterior thickness at mid-trochlea | ULN6_TRO_THI | 17.2 |

---

**Table A5.25** Measurements for HAL-VP-3/15

| Measurements of the HAL-VP-3/15 terminal hand phalanx | | |
|---|---|---|
| Terminal hand phalanx, probably ray I (HAL-VP-3/15-11) | | |
| **Measurement name** | **Code** | **Value (in mm)** |
| Maximum length | THP1_LEN | (22.5) |
| Biomechanical length | THP2_BIO_LEN | (20.9) |

| | | |
|---|---|---|
| Midshaft anteroposterior (dorsopalmar) height | THP3_MID_AP | 4.0 |
| Proximal anteroposterior (dorsopalmar) height | THP5_PRO_AP | (6.8) |
| Distal tuft anteroposterior (dorsopalmar) height | THP7_DIS_AP | 4.2 |
| Distal tuft mediolateral breadth | THP8_DIS_ML | (8.6) |
| Maximum height of proximal articular surface | – | (5.7) |

**Appendix 6** Definitions and sources of measurements

All measurements and nonmetric observations that were collected for the comparative recent modern human samples are included in this Appendix as sections **6a** and **6b**, respectively.

---

**6a**. Metric data

M# refers to the measurement in the Martin system, as relayed by Bräuer (1988). In cases where the measurement definition employed deviates from published definitions, the reader is directed to the measurement protocols reported in Appendix 7. Measurement definitions are reported in tabular format, organized by anatomical region as follows:

**Table A6.1** Vertebral measurements
**Table A6.2** Measurements of the shoulder girdle
**Table A6.3** Measurements of the arm elements
**Table A6.4** Carpal measurements
**Table A6.5** Metacarpal measurements
**Table A6.6** Terminal hand phalanx measurements
**Table A6.7** Measurements of the pelvic girdle
**Table A6.8** Measurements of the leg elements
**Table A6.9** Tarsal measurements
**Table A6.10** Metatarsal measurements
**Table A6.11** Terminal foot phalanx measurements

---

**Table A6.1** Vertebral measurements

| Code | Bräuer (1988) | Reference | Definition |
|---|---|---|---|
| ***Cervical vertebrae*** | | | |
| **CER1_VEN_HEI** | M1 | - | Ventral height of the body |
| **CER2_SUP_DV** | M4 | See Appendix 7 | Superior dorsoventral body diameter |
| **CER3_SUP_TRA** | M7 | - | Superior transverse body diameter |
| **CER4_PED_HEI** | - | Walker & Leakey, 1993 (p. 98) | Pedicle height |
| ***Thoracic vertebrae*** | | | |
| **THO1_VEN_HEI** | M1 | - | Ventral height of the body |
| **THO2_SUP_DV** | M4 | See Appendix 7 | Superior dorsoventral body diameter |
| **THO3_SUP_TRA** | M7 | - | Superior transverse body diameter |
| **THO4_CAN_LEN** | M10 | - | Vertebral canal length |
| **THO5_CAN_BRE** | M11 | - | Vertebral canal breadth |
| **THO6_CAN_IND** | p. 194 | - | Vertebral canal index |
| **THO7_PED_HEI** | - | Walker & Leakey, 1993 (p. 98) | Pedicle height |
| ***Lumbar vertebrae*** | | | |
| **LUM1_VEN_HEI** | M1 | - | Ventral height of the body |
| **LUM2_SUP_DV** | M4 | See Appendix 7 | Superior dorsoventral body diameter |
| **LUM3_SUP_TRA** | M7 | - | Superior transverse body diameter |
| **LUM4_PED_HEI** | - | Walker & Leakey, 1993 (p. 98) | Pedicle height |

**Table A6.2** Measurements of the shoulder girdle

| Code | Bräuer (1988) | Reference | Definition |
|---|---|---|---|
| ***Clavicle*** | | | |
| **CLA1_LEN** | M1 | Buikstra & Ubelaker, 1994 (#35) | Maximum clavicular length |
| ***Scapula*** | | | |
| **SCA1_MAX_LEN** | M1 | Buikstra & Ubelaker, 1994 (#38) | Maximum length |
| **SCA2_BRE** | M2 | Buikstra & Ubelaker, 1994 (#39) | Morphological breadth |
| **SCA3_IND** | - | Bass, 2005 (p. 117) | Scapular index |

**Table A6.3** Measurements of the arm elements

| Code | Bräuer (1988) | Reference | Definition |
|---|---|---|---|
| ***Humerus*** | | | |
| **HUM1_MAX_LEN** | M1 | Buikstra & Ubelaker, 1994 (#40) | Maximum humeral length |
| **HUM2_BIO_LEN** | - | Trinkaus, Churchill, Ruff, & Vandermeersch, 1999 (p. 756) | Humeral biomechanical length |
| **HUM3_MID_CIR** | M7a | - | Humeral midshaft circumference |
| **HUM4_MAX_MID** | M5 | Buikstra & Ubelaker, 1994 (#43) | Maximum midshaft diameter |
| **HUM5_MIN_MID** | M6 | Buikstra & Ubelaker, 1994 (#44) | Minimum midshaft diameter |
| **HUM6_DEL_CIR** | - | See Appendix 7 | Shaft circumference at deltoid tuberosity |
| **HUM7_DEL_MIN** | M6a | - | Minimum shaft diameter at deltoid tuberosity |
| **HUM8_DEL_MAX** | - | See Appendix 7 | Maximum shaft diameter at deltoid tuberosity |
| **HUM9_HEA_DIA** | M10 | Buikstra & Ubelaker, 1994 (#42) | Vertical head diameter |
| **HUM10_BIC_BRE** | M4 | Buikstra & Ubelaker, 1994 (#41) | Humeral bicondylar breadth |

| Code | Bräuer (1988) | Reference | Definition |
|---|---|---|---|
| **HUM11_FOS_BRE** | - | Carretero, Arsuaga, & Lorenzo, 1997 (#16) | Olecranon fossa breadth |
| **HUM12_MED_PIL** | - | Carretero, Arsuaga, & Lorenzo, 1997 (#18) | Minimum thickness of medial pillar |
| **HUM13_LAT_PIL** | - | Carretero, Arsuaga, & Lorenzo, 1997 (#19) | Minimum thickness of lateral pillar |
| **HUM14_EPI_ML** | - | See Appendix 7 | Mediolateral width of medial epicondyle |
| **HUM15_PRO_BRE** | - | Carretero, Arsuaga, & Lorenzo, 1997 (#2) | Mediolateral width of proximal end |
| ***Radius*** | | | |
| **RAD1_LEN** | - | See Appendix 7 | Maximum radial length |
| **RAD2_BIO_LEN** | - | Trinkaus, Churchill, Ruff, & Vandermeersch, 1999 (p. 756-757) | Radial biomechanical length |
| **RAD3_MID_CIR** | M5 (5) | - | Radial midshaft circumference |
| **RAD4_AP_MID** | M5a | Buikstra & Ubelaker, 1994 (#46) | Radial anteroposterior midshaft diameter |
| **RAD5_ML_MID** | M4a | Buikstra & Ubelaker, 1994 (#47) | Radial mediolateral midshaft diameter |
| **RAD6_HEA_AP** | M5 (1) | - | Radial head anteroposterior diameter |
| **RAD7_HEA_CIR** | M5 (3) | - | Radial head circumference |
| **RAD8_DIS_BRE** | M5 (6) | - | Radial maximum distal epiphyseal breadth |
| **RAD9_DIS_AP** | - | See Appendix 7 | Distal epiphysis anteroposterior diameter |
| ***Ulna*** | | | |
| **ULN1_LEN** | M1 | Buikstra & Ubelaker, 1994 (#48) | Maximum ulnar length |
| **ULN2_BIO_LEN** | - | Trinkaus, Churchill, Ruff, & Vandermeersch, 1999 (p. 756) | Ulnar biomechanical length |
| **ULN3_AP_DIA** | M11 | Buikstra & Ubelaker, 1994 (#49) | Maximum anteroposterior diameter |
| **ULN4_ML_DIA** | M12 | Buikstra & Ubelaker, 1994 (#50) | Maximum mediolateral diameter |
| **ULN5_DIS_BRE** | - | McHenry, Corruccini, & Howell, 1976 (#3) | Distal epiphysis maximum breadth excluding styloid process |
| **ULN6_TRO_THI** | - | See Appendix 7 | Anteroposterior thickness at mid-trochlea |

| Code | Bräuer (1988) | Reference | Definition |
|---|---|---|---|
| **ULN7_COR_HEI** | M7d | McHenry, Corruccini, & Howell, 1976 (#8) | Coronoid height |
| **ULN8_OLE_HEI** | M7 | McHenry, Corruccini, & Howell, 1976 (#9) | Olecranon height |
| **ULN9_TRO_LEN** | - | McHenry, Corruccini, & Howell, 1976 (#10) | Trochlear length |
| **ULN10_OLE_LEN** | - | McHenry, Corruccini, & Howell, 1976 (#12) | Olecranon length |
| **ULN11_NOT_POS** | - | See Appendix 7 | Radial notch position |
| **ULN12_NOT_MAJ** | - | See Appendix 7 | Radial notch maximum diameter |
| **ULN13_NOT_PER** | - | See Appendix 7 | Radial notch diameter perpendicular to maximum diameter |
| **ULN14_MIN_CIR** | M3 | Buikstra & Ubelaker, 1994 (#52) | Ulnar minimum circumference |

**Table A6.4** Carpal measurements

| Code | Bräuer (1988) | Reference | Definition |
|---|---|---|---|
| ***Lunate*** | | | |
| **LUN1_LEN** | - | Sulzmann, Buckberry, & Pastor, 2008 (p. 253) | Maximum length |
| **LUN2_BRE** | - | Sulzmann, Buckberry, & Pastor, 2008 (p. 253) | Maximum width |
| ***Triquetral*** | | | |
| **TRI1_LEN** | - | Sulzmann, Buckberry, & Pastor, 2008 (p. 253-254) | Maximum length |
| **TRI2_WID** | - | Sulzmann, Buckberry, & Pastor, 2008 (p. 254) | Maximum width |
| ***Trapezium*** | | | |
| **TZM1_MAX_LEN** | - | Sulzmann, Buckberry, & Pastor, 2008 (p. 256) | Maximum length |
| **TZM2_HEI** | - | Sulzmann, Buckberry, & Pastor, 2008 (p. 256) | Height |
| **TZM3_LEN_MC1** | - | Sulzmann, Buckberry, & Pastor, 2008 (p. 256) | Maximum length of metacarpal I facet |

| Code | Bräuer (1988) | Reference | Definition |
|---|---|---|---|
| *Capitate* | | | |
| **CAP1_MAX_HEI** | - | Sulzmann, Buckberry, & Pastor, 2008 (p. 255) | Maximum height |
| **CAP2_WID_HEA** | - | Sulzmann, Buckberry, & Pastor, 2008 (p. 255) | Maximum width of head |
| **CAP3_WID_BAS** | - | Sulzmann, Buckberry, & Pastor, 2008 (= "maximum length of distal base", p. 255) | Maximum width of distal base |
| *Hamate* | | | |
| **HAM1_MAX_HEI** | - | Sulzmann, Buckberry, & Pastor, 2008 (p. 255) | Maximum height |
| **HAM2_BOD_HEI** | - | Sulzmann, Buckberry, & Pastor, 2008 (p. 255) | Height of the body |
| **HAM3_HAM_PRO** | - | See Appendix 7 | Hamulus projection |
| **HAM4_MAX_WID** | - | Sulzmann, Buckberry, & Pastor, 2008 (p. 255) | Maximum width |
| **HAM5_ML_WID** | - | Sulzmann, Buckberry, & Pastor, 2008 (p. 256) | Maximum width of the distal facets |
| **HAM6_HAM_WID** | - | Sulzmann, Buckberry, & Pastor, 2008 (p. 255-256) | Maximum width of the hamulus |

**Table A6.5** Metacarpal measurements

| Code | Bräuer (1988) | Reference | Definition |
|---|---|---|---|
| *Metacarpals* | | | |
| **MC1_LEN** | - | Bush, Lovejoy, Johanson, & Coppens, 1982 (p. 667) | Maximum length |
| **MC2_BIO_LEN** | M2 | - | Biomechanical length |
| **MC3_MID_DP** | M7 | Bush, Lovejoy, Johanson, & Coppens, 1982 (p. 667) | Midshaft dorsopalmar height |
| **MC4_MID_ML** | M6 | Bush, Lovejoy, Johanson, & Coppens, 1982 (p. 667) | Midshaft mediolateral breadth |
| **MC5_PRO_HEI** | M10 | Bush, Lovejoy, Johanson, & Coppens, 1982 (p. 667) | Proximal maximum height |
| **MC6_PRO_BRE** | M8 | Bush, Lovejoy, Johanson, & Coppens, 1982 (p. 667) | Proximal maximum breadth |

| Code | Bräuer (1988) | Reference | Definition |
|---|---|---|---|
| **MC7_DIS_HEI** | M11 | Bush, Lovejoy, Johanson, & Coppens, 1982 (p. 667) | Distal maximum height |
| **MC8_DIS_BRE** | M9 | Bush, Lovejoy, Johanson, & Coppens, 1982 (p. 667) | Distal maximum breadth |
| ***Metacarpal III*** | | | |
| **MC9_LEN_EXC** | - | See Appendix 7 | Proximodistal length excluding styloid process |
| **MC10_DOR_WID** | - | See Appendix 7 | Maximum dorsal width of facet for the capitate |
| **MC11_PAL_WID** | - | See Appendix 7 | Maximum palmar width of facet for the capitate |
| **MC12_FAC_WID** | - | See Appendix 7 | Mediolateral width of facet for the capitate |

**Table A6.6** Terminal hand phalanx measurements

| Code | Bräuer (1988) | Reference | Definition |
|---|---|---|---|
| ***Terminal hand phalanges*** | | | |
| **THP1_LEN** | - | Bush, Lovejoy, Johanson, & Coppens, 1982 (p. 667) | Maximum length |
| **THP2_BIO_LEN** | - | Bush, Lovejoy, Johanson, & Coppens, 1982 (p. 667) | Biomechanical length |
| **THP3_MID_AP** | M7 | Bush, Lovejoy, Johanson, & Coppens, 1982 (p. 668) | Midshaft anteroposterior (dorsopalmar) height |
| **THP4_MID_ML** | M6 | Bush, Lovejoy, Johanson, & Coppens, 1982 (p. 668) | Midshaft mediolateral breadth |
| **THP5_PRO_AP** | M10 | Bush, Lovejoy, Johanson, & Coppens, 1982 (p. 668) | Proximal anteroposterior (dorsopalmar) height |
| **THP6_PRO_ML** | M8 | Bush, Lovejoy, Johanson, & Coppens, 1982 (p. 668) | Proximal mediolateral breadth |
| **THP7_DIS_AP** | M11 | Bush, Lovejoy, Johanson, & Coppens, 1982 (p. 667-668) | Distal tuft anteroposterior (dorsopalmar) height |
| **THP8_DIS_ML** | M9 | Bush, Lovejoy, Johanson, & Coppens, 1982 (p. 667-668) | Distal tuft mediolateral breadth |

**Table A6.7** Measurements of the pelvic girdle

| Code | Bräuer (1988) | Reference | Definition |
|---|---|---|---|
| ***Sacrum*** | | | |
| **SAC1_BRE** | M5 | Buikstra & Ubelaker, 1994 (#54) | Maximum breadth |
| **SAC2_ANT_HEI** | M2 | Buikstra & Ubelaker, 1994 (#53) | Maximum anterior height |
| **SAC3_IND** | - | Bass, 2005 (p. 109) | Sacral index |
| ***Os coxae*** | | | |
| **OCX1_HEI** | - | Arsuaga & Carretero, 1994 (#2) | Os coxae height |
| **OCX2_ISC_PUB** | - | Arsuaga & Carretero, 1994 (#1) | Maximum diameter from ischium to pubis |
| **OCX3_PUB_LEN** | - | McCown & Keith, 1939 (p. 90) | Pubic length |
| **OCX4_ACE_LEN** | - | Arsuaga & Carretero, 1994 (#10) | Acetabulosymphyseal length |
| **OCX5_NA_ISC** | - | Arsuaga & Carretero, 1994 (#13) | Nonarticular ischial length |
| **OCX6_ACE_DIA** | - | Arsuaga & Carretero, 1994 (#34) | Acetabulum diameter |
| **OCX7_ACE_HEI** | M22 | - | Acetabular height |

**Table A6.8** Measurements of the leg elements

| Code | Bräuer (1988) | Reference | Definition |
|---|---|---|---|
| ***Femur*** | | | |
| **FEM1_LEN** | M1 | Buikstra & Ubelaker, 1994 (#60) | Maximum femoral length |
| **FEM2_EPI_BRE** | M21 | Buikstra & Ubelaker, 1994 (#62) | Femoral epicondylar breadth |
| **FEM3_NEC_LEN** | | McHenry & Corruccini, 1978 (#6) | Biomechanical neck length |
| **FEM4_HEA_DIA** | - | See Appendix 7 | Vertical head diameter |

| Code | Bräuer (1988) | Reference | Definition |
|---|---|---|---|
| **FEM5_BIO_LEN** | - | Trinkaus, Churchill, Ruff, & Vandermeersch, 1999 (p. 757) | Femoral biomechanical length |
| **FEM6_MID_CIR** | M8 | Buikstra & Ubelaker, 1994 (#68) | Femoral midshaft circumference |
| **FEM7_AP_MID** | M6 | Buikstra & Ubelaker, 1994 (#66) | Femoral anteroposterior midshaft diameter |
| **FEM8_ML_MID** | M7 | Buikstra & Ubelaker, 1994 (#67) | Femoral mediolateral midshaft diameter |
| **FEM9_PLA_IND** | p. 220 | - | Platymeric index |
| **FEM10_AP_HEA** | | Ruff et al., 2006 (p. 93) | Anteroposterior head diameter |
| **FEM11_NEC_HEI** | - | McHenry & Corruccini, 1978 (#2) | Minimum neck height |
| **FEM12_NEC_ANG** | M29 | - | Neck angle |
| ***Patella*** | | | |
| **PAT1_HEI** | M1 | - | Maximum patellar height |
| **PAT2_BRE** | M2 | - | Maximum patellar breadth |
| **PAT3_THI** | M3 | - | Maximum thickness |
| ***Tibia*** | | | |
| **TIB1_LEN** | M1a | - | Maximum tibial length |
| **TIB2_PRO_BRE** | M3 | Buikstra & Ubelaker, 1994 (#70) | Tibial max. prox. epiphyseal breadth |
| **TIB3_DIS_BRE** | M6 | Buikstra & Ubelaker, 1994 (#71) | Tibial maximum distal epiphyseal breadth |
| **TIB4_DIS_AP** | M7 | - | Distal epiphysis anteroposterior diameter |
| **TIB5_BIO_LEN** | | Trinkaus, Churchill, Ruff, & Vandermeersch, 1999 (p. 757) | Tibial biomechanical length |
| **TIB6_AP_MID** | M8 | - | Tibial anteroposterior midshaft diameter |
| **TIB7_ML_MID** | M9 | - | Tibial mediolateral midshaft diameter |
| **TIB8_MID_CIR** | M10 | - | Tibial midshaft circumference |
| **TIB9_CIR_NUT** | M10a | Buikstra & Ubelaker, 1994 (#74) | Tibial circumference at nutrient foramen |

| Code | Bräuer (1988) | Reference | Definition |
|---|---|---|---|
| **TIB10_ML_NUT** | M9a | Buikstra & Ubelaker, 1994 (#73) | Tibial mediolateral shaft diameter at nutrient foramen |
| **TIB11_MAX_NUT** | - | Buikstra & Ubelaker, 1994 (#72) | Tibial maximum shaft diameter at nutrient foramen |
| **TIB12_PLA_IND** | p. 222 | Bass, 2005 (p. 247) | Platycnemic index |
| ***Fibula*** | | | |
| **FIB1_LEN** | M1 | Buikstra & Ubelaker, 1994 (#75) | Maximum fibular length |
| **FIB2_MID_CIR** | M4 | | Fibular midshaft circumference |
| **FIB3_MAX_ART** | - | See Appendix 7 | Maximum proximodistal diameter of malleolar articular surface |
| **FIB4_ART_DIA** | - | See Appendix 7 | Maximum diameter of the malleolar articular surface, perpendicular to the maximum proximodistal diameter |
| **FIB5_DIS_BRE** | M4 (2) | - | Maximum distal mediolateral breadth |
| **FIB6_DIS_AP** | - | See Appendix 7 | Maximum distal anteroposterior diameter |

**Table A6.9** Tarsal measurements

| Code | Bräuer (1988) | Reference | Definition |
|---|---|---|---|
| ***Talus*** | | | |
| **TAL1_LEN** | M1 | - | Talar length |
| **TAL2_MAX_LEN** | M1a | - | Maximum talar length |
| **TAL3_HEA_NEC** | M8 | - | Length of head plus neck |
| **TAL4_PHY_HEI** | M3b | - | Physiological height |
| **TAL5_ART_BRE** | M5 | - | Articular breadth |

| Code | Bräuer (1988) | Reference | Definition |
|---|---|---|---|
| **TAL6_MAL_BRE** | M7a | - | Lateral malleolar breadth |
| **TAL7_HEA_LEN** | M9 | - | Length of the head |
| **TAL8_TRO_HEI** | M6 | - | Trochlear height |
| **TAL9_ML_WID** | M2 | - | Mediolateral width |
| **TAL10_AP_TRO** | - | See Appendix 7 | Maximum anteroposterior trochlear length |
| **TAL11_ML_HEA** | - | See Appendix 7 | Mediolateral width of talar head |
| **TAL12_LEN_FAC** | M12 | - | Maximum dimension of posterior subtalar facet |
| ***Calcaneus*** | | | |
| **CAL1_LEN** | M1 | Buikstra & Ubelaker, 1994 (#77) | Maximum calcaneal length |
| **CAL2_POS_LEN** | M5 | - | Posterior calcaneal length |
| **CAL3_MED_BRE** | M2 | Buikstra & Ubelaker, 1994 (#78) | Medial breadth (across the sustentaculum tali) |
| **CAL4_HEI_BOD** | M7 | - | Height of the body |
| **CAL5_MIN_BRE** | M3 | - | Minimum breadth across the body |
| ***Cuboid*** | | | |
| **CUB1_MAX_BRE** | - | Harris & Case, 2012 (=CubBrd) | Maximum breadth |
| **CUB2_MAX_LEN** | - | Harris & Case, 2012 (=CubLg) | Maximum length |
| **CUB3_MAX_HEI** | - | Harris & Case, 2012 (=CubHt) | Maximum height |
| **CUB4_CAL_FAC** | - | See Appendix 7 | Maximum diameter of the facet for the calcaneus |
| ***Navicular*** | | | |
| **NAV1_MAX_BRE** | M1 | Harris & Case, 2012 (=NavBrd) | Maximum breadth |
| **NAV2_MAX_LEN** | | Harris & Case, 2012 (=NavLg) | Maximum length |
| **NAV3_MAX_HEI** | M2 | - | Maximum height |

| Code | Bräuer (1988) | Reference | Definition |
|---|---|---|---|
| **NAV4_TAL_FAC** | | See Appendix 7 | Maximum diameter of the facet for the talar head |

**Table A6.10** Metatarsal measurements

| Code | Bräuer (1988) | Reference | Definition |
|---|---|---|---|
| ***Metatarsals*** | | | |
| **MT1_LEN** | M2 (rays II-V) | See Appendix 7 | Maximum metatarsal length |
| **MT2_BIO_LEN** | M1 (ray I); M1b (rays II-V) | Trinkaus, 1978 (p. 17) | Biomechanical length |
| **MT3_MID_DP** | M4 | - | Midshaft dorsoplantar height |
| **MT4_MID_ML** | M3 | - | Midshaft mediolateral breadth |
| **MT5_PRO_HEI** | M7a | Trinkaus, 1978 (p. 17) | Proximal maximum height |
| **MT6_PRO_BRE** | M6a | Trinkaus, 1978 (p. 17) | Proximal maximum breadth |
| **MT7_DIS_HEI** | M9a | Trinkaus, 1978 (p. 18) | Distal maximum height |
| **MT8_DIS_BRE** | M8a | Trinkaus, 1978 (p. 18) | Distal maximum breadth |

**Table A6.11** Terminal foot phalanx measurements

| Code | Bräuer (1988) | Reference | Definition |
|---|---|---|---|
| ***Terminal foot phalanges*** | | | |
| **TFP1_LEN** | M1 | - | Maximum length |
| **TFP2_BIO_LEN** | M1a | Trinkaus, 1978 (p. 17) | Biomechanical length |

| Code | Bräuer (1988) | Reference | Definition |
|---|---|---|---|
| **TFP3_MID_AP** | M3 | - | Midshaft anteroposterior (dorsoplantar) height |
| **TFP4_MID_ML** | M2 | - | Midshaft mediolateral breadth |
| **TFP5_PRO_AP** | M3a | Trinkaus, 1978 (p. 17) | Proximal anteroposterior (dorsoplantar) height |
| **TFP6_PRO_ML** | M2a | Trinkaus, 1978 (p. 17) | Proximal mediolateral breadth |
| **TFP7_DIS_AP** | M3b | Trinkaus, 1978 (p. 18) | Distal tuft anteroposterior (dorsoplantar) height |
| **TFP8_DIS_ML** | M2b | Trinkaus, 1978 (p. 18) | Distal tuft mediolateral breadth |

**6b**. Nonmetric data

| Trait | Reference |
|---|---|
| ***Scapula*** | |
| **Axillary sulcus** | Trinkaus, 1977 (p. 231-233) |
| ***Humerus*** | |
| **Humeral head shape** | Carretero, Arsuaga, & Lorenzo, 1997 (p. 365) |
| **Olecranon fossa relative size** | See Appendix 7 |
| **Olecranon fossa depth** | See Appendix 7 |
| ***Ulna*** | |
| **Ulnar trochlear notch form** | Buikstra & Ubelaker, 1994 (p. 94) |
| **Ulnar trochlear notch orientation** | Trinkaus, 1983 (p. 238-239) |
| ***Tibia*** | |
| **Squatting facets on the tibia** | Buikstra & Ubelaker, 1994 (p. 94) |
| ***Talus*** | |
| **Squatting facets on the talus** | Buikstra & Ubelaker, 1994 (p. 94) |
| **Talar trochlear shape** | See Appendix 7 |
| **Inferior talar articular surface** | Finnegan, 1978 (#23) |
| ***Calcaneus*** | |
| **Anterior calcaneal facets** | Buikstra & Ubelaker, 1994 (p. 94) |

**Appendix 7** Measurement protocols for comparative data collection

---

**7a**. METRIC DATA

Measurement protocols are detailed below by anatomical element. Some measurement descriptions are adapted from White, Black, & Folkens (2012). Carpal measurement descriptions are adapted from Sulzmann, Buckberry, & Pastor (2008). Some tarsal measurement descriptions are adapted from Harris & Case (2012). See Appendix 6a for measurement references.

## CERVICAL VERTEBRAE

**1. CER1_VEN_HEI**: Ventral height of the body

Hold the vertebra with the ventral surface facing upwards, and the spinous process pointing toward the table. Keep the vertebral body perpendicular to the table. With a sliding caliper, measure the craniocaudal dimension of the ventral border of the body at midline.

**2. CER2_SUP_DV**: Superior dorsoventral body diameter

Hold the vertebra with the superior surface facing upward and the spinous process pointing to the left. Hold the vertebral body parallel to the table. With a sliding caliper, measure the maximum anteroposterior dimension of the superior surface of the vertebral body, including the annular rings. While the ventral point is taken at midline, the dorsal point is extended by the right and left projections of the vertebral disk surface.

**3. CER3_SUP_TRA**: Superior transverse body diameter

Hold the vertebra with the superior surface facing upward, the ventral side near you, and the spinous process pointing away from you. Hold the vertebral body parallel to the table. With a sliding caliper, measure the maximum transverse dimension of the superior surface of the vertebral body, including the annular rings.

**4. CER4_PED_HEI**: Pedicle height

Hold the vertebra with the body perpendicular to the table, the spinous process pointed toward you, and the ventral surface facing away from you. With a sliding caliper equipped with inner points (angled away from you at 45º from the surface of the table), measure the minimum height of the right pedicle along a line perpendicular to the plane of the body.

## THORACIC VERTEBRAE

**1. THO1_VEN_HEI**: Ventral height of the body

Hold the vertebra with the ventral surface facing upwards, and the spinous process pointing toward the table. Keep the vertebral body perpendicular to the table. With a sliding caliper, measure the craniocaudal dimension of the ventral border of the body at midline.

**2. THO2_SUP_DV**: Superior dorsoventral body diameter

Hold the vertebra with the superior surface facing upward and the spinous process pointing to the left. Hold the vertebral body parallel to the table. With a sliding caliper, measure the maximum anteroposterior dimension of the superior surface of the vertebral body, including the annular rings. While the ventral point is taken at midline, the dorsal point is extended by the right and left projections of the vertebral disk surface.

**3. THO3_SUP_TRA**: Superior transverse body diameter

Hold the vertebra with the superior surface facing upward, the ventral side near you, and the spinous process pointing away from you. Hold the vertebral body parallel to the table. With a sliding caliper, measure the maximum transverse dimension of the superior surface of the vertebral body, including the annular rings.

**4. THO4_CAN_LEN**: Vertebral canal length

Holding the spinous process with your left hand, hold the plane of the body perpendicular to the surface of the table with the ventral surface to the right and the superior surface facing you. With a sliding caliper, measure the maximum dorsoventral diameter of the cranial end of the vertebral canal using the inner (spreading) jaws of the caliper.

**5. THO5_CAN_BRE**: Vertebral canal breadth

Hold the vertebra with the plane of the body perpendicular to the surface of the table, the spinous process pointing up, the ventral surface near the table surface, and the superior surface facing you. With a sliding caliper, measure the maximum mediolateral diameter of the cranial end of the vertebral canal using the inner (spreading) jaws of the caliper.

**6. THO6_CAN_IND**: Vertebral canal index

Calculated as: (vertebral canal length / vertebral canal breadth) x 100

**7. THO7_PED_HEI**: Pedicle height

Hold the vertebra with the body perpendicular to the table, the spinous process pointed toward you, and the ventral surface facing away from you. With a sliding caliper (angled away from you at 45º from the surface of the table), measure the minimum height of the right pedicle along a line perpendicular to the plane of the body.

## LUMBAR VERTEBRAE

**1. LUM1_VEN_HEI**: Ventral height of the body

Hold the vertebra with the ventral surface facing upwards, and the spinous process pointing toward the table. Keep the vertebral body perpendicular to the table. With a sliding caliper, measure the craniocaudal dimension of the ventral border of the body at midline.

**2. LUM2_SUP_DV**: Superior dorsoventral body diameter

Hold the vertebra with the superior surface facing upward and the spinous process pointing to the left. Hold the vertebral body parallel to the table. With a sliding caliper, measure the maximum anteroposterior dimension of the superior surface of the vertebral body, including

the annular rings. While the ventral point is taken at midline, the dorsal point is extended by the right and left projections of the vertebral disk surface.

**3. LUM3_SUP_TRA**: Superior transverse body diameter

Hold the vertebra with the superior surface facing upward, the ventral side near you, and the spinous process pointing away from you. Hold the vertebral body parallel to the table. With a sliding caliper, measure the maximum transverse dimension of the superior surface of the vertebral body, including the annular rings.

**4. LUM4_PED_HEI**: Pedicle height

Hold the vertebra with the body perpendicular to the table, the spinous process pointed toward you, and the ventral surface facing away from you. With a standard sliding caliper (angled away from you at 45º from the surface of the table), or a sliding caliper with inner points, measure the minimum height of the right pedicle along a line perpendicular to the plane of the body.

## CLAVICLE

**1. CLA1_LEN**: Maximum clavicular length

Place the sternal end of the clavicle against the stationary end of the osteometric board, with the inferior surface of the bone facing down. Place the adjustable end of the board against the acromial end of the bone and record the measurement.

## SCAPULA

**1. SCA1_MAX_LEN**: Maximum length

Place the inferior angle of the scapula against the stationary end of the osteometric board, with the ventral surface of the bone facing down. Place the adjustable end (the short block of wood) of the board against the superior angle of the bone and record the measurement.

**2. SCA2_BRE**: Morphological breadth

Place the scapula on the table with the ventral surface facing down, and the inferior angle pointing away from you. With a sliding caliper, measure the distance between the midpoint of the dorsal margin of the glenoid fossa and the point midway between the two ridges of the scapular spine on the medial border (measuring from point to point, not just framing the diameter).

**3. SCA3_IND**: Scapular index

Calculated as: (morphological breadth / maximum length) x 100

## HUMERUS

**1. HUM1_MAX_LEN**: Maximum humeral length

Place the top of the humeral head against the stationary end of the osteometric board, with the posterior surface of the bone facing down. Place the adjustable end of the board against the most distant point on the distal humerus, making sure the long axis of the bone is parallel to the long axis of the board.

**2. HUM2_BIO_LEN**: Humeral biomechanical length

Place the humerus on the table with the posterior side facing down, the head to the left, and the distal end to the right. Using a spreading caliper, measure from the superiormost point of the top of the humeral head to the most distal point on the lateral lip of the trochlea. Calculate the midshaft value (50% of biomechanical length) and enter it in column "HUM2A_BIO_MID".

**3. HUM3_MID_CIR**: Humeral midshaft circumference

Place the humerus on the table with the posterior surface facing down, the head to the left, and the distal end to the right. Determine the location of midshaft (measuring to 50% of humeral biomechanical length from the humeral head with a spreading caliper) and use a flexible cloth tape to determine the circumference at that location.

**4. HUM4_MAX_MID**: Maximum midshaft diameter

Place the humerus on the table with the posterior surface facing down, the head to the left, and the distal end to the right. Determine the location of midshaft (measuring to 50% of humeral biomechanical length from the humeral head with a spreading caliper). Grasp the bone at the midshaft location and hold the bone upright with the distal end on the table and the long axis of the shaft perpendicular to the surface of the table. Use a sliding caliper to determine the largest cross-sectional dimension at the midshaft point, making sure to take the measurement perpendicular to the long axis of the shaft.

**5. HUM5_MIN_MID**: Minimum midshaft diameter

Place the humerus on the table with the posterior surface facing down, the head to the left, and the distal end to the right. Determine the location of midshaft (measuring to 50% of humeral biomechanical length from the humeral head with a spreading caliper). Grasp the bone at the midshaft location and hold the bone upright with the distal end on the table and the long axis of the shaft perpendicular to the surface of the table. Use a sliding caliper to determine the smallest cross-sectional dimension at the midshaft point, making sure to take the measurement perpendicular to the long axis of the shaft.

**6. HUM6_DEL_CIR**: Shaft circumference at deltoid tuberosity

Hold the humerus upright with the distal end on the table and the long axis of the shaft perpendicular to the surface of the table. Identify the midpoint of the deltoid tuberosity, and use a flexible cloth tape to determine the circumference at that location.

**7. HUM7_DEL_MIN**: Minimum shaft diameter at deltoid tuberosity

Hold the humerus upright with the distal end on the table and the long axis of the shaft perpendicular to the surface of the table. Identify the midpoint of the deltoid tuberosity, and use a sliding caliper to measure the smallest dimension perpendicular to the long axis of the shaft.

**8. HUM8_DEL_MAX**: Maximum shaft diameter at deltoid tuberosity

Hold the humerus upright with the distal end on the table and the long axis of the shaft perpendicular to the surface of the table. Identify the midpoint of the deltoid tuberosity, and use a sliding caliper to measure the largest dimension perpendicular to the long axis of the shaft.

**9. HUM9_HEA_DIA**: Vertical head diameter

Hold the humerus on the table with the lateral side down, the head to the left, and the distal end to the right, such that a paracoronal plane is perpendicular to the surface of the table. Using a sliding caliper, measure the greatest distance between the margins of the head in a paracoronal plane.

**10. HUM10_BIC_BRE**: Humeral bicondylar breadth

Place the humerus on the table with the posterior side down, the head pointing away from you, and the distal end nearest to you. Using a sliding caliper, measure the greatest distance between the medial and lateral epicondyles (not necessarily touching the bone, but framing the maximum diameter with the calipers parallel to the surface of the table), making sure to keep the jaws of the caliper parallel to the long axis of the humeral shaft.

**11. HUM11_FOS_BRE**: Olecranon fossa breadth

Place the humerus on the table with the anterior side facing down, the head pointing away from you, and the distal end nearest to you. Using the inner (spreading) jaws of a sliding caliper, measure the maximum distance across the olecranon fossa, perpendicular to the axis of the shaft, making sure to keep the jaws of the caliper parallel to the surface of the table.

**12. HUM12_MED_PIL**: Minimum thickness of medial pillar

Place the humerus on the table with the anterior side facing down, the head pointing away from you, and the distal end nearest to you. Using a sliding caliper, measure the minimum thickness of the medial pillar, taking the measurement perpendicular to the axis of the medial pillar and making sure to take the measurement while looking down from directly above the bone, keeping the caliper jaws parallel to the surface of the table.

**13. HUM13_LAT_PIL**: Minimum thickness of lateral pillar

Place the humerus on the table with the anterior side facing down, the head pointing away from you, and the distal end nearest to you. Using a sliding caliper, measure the minimum thickness of the lateral pillar, taking the measurement perpendicular to the axis of the lateral pillar and making sure to take the measurement while looking down from directly above the bone, keeping the caliper jaws parallel to the surface of the table.

**14. HUM14_EPI_ML**: Mediolateral width of medial epicondyle

Place the humerus on the table with the anterior side facing down, the head pointing away from you, and the distal end nearest to you. Using a sliding caliper, measure the maximum distance between the medial margin of the olecranon fossa and the most distant point on the medial epicondyle, making sure to keep the caliper jaws parallel to the coronal plane.

**15. HUM15_PRO_BRE**: Mediolateral width of proximal end

While standing, place the medialmost point of the humeral head against the stationary end of an osteometric board, with the posterior surface of the bone facing down. Place the

adjustable end of the board against the lateralmost point of the greater tubercle, making sure the long axis of the bone is perpendicular to the long axis of the board.

## RADIUS

**1. RAD1_LEN**: Maximum radial length

Place the head of the radius against the stationary end of the osteometric board, with the posterior surface of the bone facing down. Place the adjustable end of the board against the most distal point of the styloid process, making sure that the long axis of the bone is parallel to the long axis of the board.

**2. RAD2_BIO_LEN**: Radial biomechanical length

Place the radius on the table surface, with the head to the left and the distal end to the right. Using a spreading caliper, measure the distance between the center (deepest point) of the radial head and the deepest point of the carpal (or distal radial) articular surface. Calculate the midshaft value (50% of biomechanical length) and enter it in column "RAD2A_BIO_MID".

**3. RAD3_MID_CIR**: Radial midshaft circumference

Place the radius on the table with the posterior surface facing down, the head to the left, and the distal end to the right. Determine the location of midshaft (measuring to 50% of radial biomechanical length from the radial head with a spreading caliper). Grasp the bone at the midshaft location and hold the bone upright with the distal end on the table and the long axis of the shaft perpendicular to the surface of the table. Use a flexible cloth tape to determine the minimum circumference at that the midshaft location.

**4. RAD4_AP_MID**: Radial anteroposterior midshaft diameter

Place the radius on the table with the posterior surface facing down, the head to the left, and the distal end to the right. Determine the location of midshaft (measuring to 50% of radial biomechanical length from the radial head with a spreading caliper). Grasp the bone at the midshaft location and hold the bone upright with the distal end on the table and the long axis of the shaft perpendicular to the surface of the table. Use a sliding caliper to measure the anteroposterior diameter at the midshaft location, making sure to take the measurement perpendicular to the long axis of the bone.

**5. RAD5_ML_MID**: Radial mediolateral midshaft diameter

Place the radius on the table with the posterior surface facing down, the head to the left, and the distal end to the right. Determine the location of midshaft (measuring to 50% of radial biomechanical length from the radial head with a spreading caliper). Grasp the bone at the midshaft location and hold the bone upright with the distal end on the table and the long axis of the shaft perpendicular to the surface of the table. Use a sliding caliper to measure the mediolateral diameter at the midshaft location, making sure to take the measurement perpendicular to the long axis of the bone.

**6. RAD6_HEA_AP**: Radial head anteroposterior diameter

Hold the radius such that you are looking at the proximal surface of the head, like you are looking down the long axis of the shaft, with the anterior surface facing to the right. Using a sliding caliper, measure the anteroposterior diameter of the head of the radius.

**7. RAD7_HEA_CIR**: Radial head circumference

Hold the radius such that you are looking at the proximal surface of the head, like you are looking down the long axis of the shaft, with the anterior surface facing down. Use a flexible cloth tape to determine the circumference of the radial head.

**8. RAD8_DIS_BRE**: Radial maximum distal epiphyseal breadth

While standing, place the lateralmost point of the distal epiphysis against the end of an osteometric board, with the posterior surface of the bone facing down. Place the adjustable end of the board against the medialmost point of the distal epiphysis, making sure the long axis of the bone is perpendicular to the long axis of the board.

**9. RAD9_DIS_AP**: Distal epiphysis anteroposterior diameter

While standing, place the posteriormost point of the distal epiphysis against the stationary end of an osteometric board, with the medial surface of the bone facing down. Place the adjustable end of the board against the anteriormost point of the distal epiphysis, making sure the long axis of the bone is perpendicular to the long axis of the board.

## ULNA

**1. ULN1_LEN**: Maximum ulnar length

Place the olecranon against the stationary end of an osteometric board, with the lateral surface of the bone facing down. Place the adjustable end of the board against the most distal point of the styloid process, making sure that the long axis of the bone is parallel to the long axis of the board.

**2. ULN2_BIO_LEN**: Ulnar biomechanical length

Place the ulna on the table surface with the olecranon to the right, the distal end to the left, and the lateral surface facing up. With a spreading caliper or a large sliding caliper, measure the distance between the proximodistal midpoint of the trochlear notch and the centerpoint of the distal head, making sure to take the measurement in a plane parallel to the long axis of the bone.

**3. ULN3_AP_DIA**: Maximum anteroposterior diameter

Determine the point along the shaft where the interosseous crest has its greatest development. Grasp the bone at this location and hold the bone upright with the distal end on the table and the long axis of the shaft perpendicular to the surface of the table. Use a sliding caliper to measure the anteroposterior diameter at this point, keeping the caliper jaws perpendicular to the anteroposterior axis, and making sure to take the measurement in a plane perpendicular to the long axis of the bone.

**4. ULN4_ML_DIA**: Maximum mediolateral diameter

Determine the point along the shaft where the interosseous crest has its greatest development. Grasp the bone at this location and hold the bone upright with the distal end on the table and the long axis of the shaft perpendicular to the surface of the table. Use a sliding caliper to measure the mediolateral diameter at this point, keeping the caliper jaws parallel to the anteroposterior axis, making sure to take the measurement in a plane perpendicular to the long axis of the bone.

**5. ULN5_DIS_BRE**: Distal epiphysis maximum breadth excluding styloid process

Hold the ulna such that you are looking at the distal surface of the head, like you are looking down the long axis of the shaft. Using a sliding caliper, measure the largest diameter of the head of the distal epiphysis (excluding the styloid process), making sure to take the measurement in a plane perpendicular to the long axis of the bone (not necessarily touching the bone, but framing the maximum diameter).

**6. ULN6_TRO_THI**: Anteroposterior thickness at mid-trochlea

Place the ulna on the table surface with the olecranon to the right, the distal end to the left, and the lateral surface facing up. Using a sliding caliper, measure the minimum anteroposterior thickness near the mid-point of the trochlea, making sure to take the measurement in a plane perpendicular to the long axis of the bone.

**7. ULN7_COR_HEI**: Coronoid height

Place the ulna on the table surface with the olecranon to the right, the distal end to the left, and the lateral surface facing up. Using a sliding caliper, measure the distance from the dorsal surface of the shaft to the tip of the coronoid process, making sure to take the measurement in a plane perpendicular to the long axis of the bone.

**8. ULN8_OLE_HEI**: Olecranon height

Place the ulna on the table surface with the olecranon to the right, the distal end to the left, and the lateral surface facing up. Using a sliding caliper, measure the distance from the dorsal surface of the shaft to the tip of the olecranon process, making sure to take the measurement in a plane perpendicular to the long axis of the bone.

**9. ULN9_TRO_LEN**: Trochlear length

Place the ulna on the table surface with the olecranon to the right, the distal end to the left, and the lateral surface facing up. Using the spreading jaws of the caliper, measure the distance between the tip of the olecranon process and the tip of the coronoid process.

**10. ULN10_OLE_LEN**: Olecranon length

Place the ulna on the table surface with the olecranon to the right, the distal end to the left, and the lateral surface facing up. Using a sliding caliper, measure the distance between mid-trochlea (at the proximodistal midpoint of the trochlear notch) and the proximal-most point of the olecranon process, making sure to take the measurement in a plane parallel to the long axis of the bone.

**11. ULN11_NOT_POS**: Radial notch position

Place the ulna on the table surface with the olecranon to the right, the distal end to the left, and the lateral surface facing up. Using a sliding caliper, measure the distance between the most proximal point of the olecranon and the distal border of the radial notch, making sure to take the measurement in a plane parallel to the long axis of the bone (not necessarily touching the bone, but framing the maximum diameter).

**12. ULN12_NOT_MAJ**: Radial notch maximum diameter

Place the ulna on the table surface with the olecranon to the right, the distal end to the left, and the lateral surface facing up. Using a sliding caliper, measure the maximum diameter of the radial notch (not necessarily touching the bone, but framing the maximum diameter).

**13. ULN13_NOT_PER**: Radial notch diameter perpendicular to maximum diameter

Place the ulna on the table surface with the olecranon to the right, the distal end to the left, and the lateral surface facing up. Using a sliding caliper, measure the maximum dimension of the radial notch along a line perpendicular to the maximum diameter (not necessarily touching the bone, but framing the maximum diameter).

**14. ULN14_MIN_CIR**: Ulnar minimum circumference

Holding the bone upright with the proximal end on the table and the long axis of the shaft perpendicular to the surface of the table, use a measuring tape to measure the minimum circumference of the shaft (usually near the distal end of the shaft).

## LUNATE

**1. LUN1_LEN**: Maximum length

Hold the lunate with the facet for the triquetral facing up, and the "horns" pointed to the right. Place both "horns" flat against one of the sliding caliper arms, then close the other caliper arm on to the most extended point on the rounded medial side while keeping both the element and the calipers parallel to the table.

**2. LUN2_BRE**: Maximum width

Place the dorsal surface of the lunate against one of the sliding caliper arms. Slowly close the other arm until it comes into contact with the most palmar point of the palmar surface, holding both the element and calipers parallel to the table.

## TRIQUETRAL

**1. TRI1_LEN**: Maximum length

Hold the triquetral with the facet for the hamate facing up, with the facet for the pisiform to the left. Using a sliding caliper, measure the maximum diameter of the bone in this view.

**2. TRI2_WID**: Maximum width

Hold the triquetral with the facet for the hamate facing up, with the facet for the pisiform to the left. Using a sliding caliper, place the stationary arm of the caliper flat against the pisiform facet and measure to the most projecting dorsal point.

## TRAPEZIUM

**1. TZM1_MAX_LEN**: Maximum length

Hold the trapezium with the trapezial (palmar) ridge to the right, the facet for the metacarpal I facing down, and the long axis of the bone parallel to the table. Holding the sliding caliper jaws parallel to the table, measure from the most projecting point of the metacarpal II facet to the most projecting point of the trapezial (palmar) ridge.

**2. TZM2_HEI**: Height

Hold the trapezium with the facet for the MCI facing to the right, the MCII facet facing away from you, and the trapezial (palmar) ridge facing you. Holding the sliding caliper jaws parallel to the table, measure the maximum distance between the palmar margin of the MCI facet and the ridge dividing the trapezoid and scaphoid facets.

**3. TZM3_LEN_MC1**: Maximum length of metacarpal I facet

Hold the trapezium with the MCI facet facing up, and the facet for the MCII pointing towards the left. Holding the sliding caliper jaws parallel to the table, measure the greatest dimension of the MCI facet along the long axis of the facet.

## CAPITATE

**1. CAP1_MAX_HEI**: Maximum height

Hold the capitate with the facet for the hamate side facing up and held parallel to the table surface, the nonarticular palmar surface facing away from you, and the base facing to the left. Measure the maximum dimension from the most projecting point on the "styloid process" (on the edge adjacent to the facet for the hamate) to the furthest point on the head, keeping the sliding caliper jaws parallel to the surface of the table.

**2. CAP2_WID_HEA**: Maximum width of head

Hold the capitate with the head facing up and the edge with "styloid process" (on the edge adjacent to the facet for the hamate) facing to the left. Measure the maximum dimension of the head, keeping the jaws of the sliding caliper parallel to the surface of the table.

**3. CAP3_WID_BAS**: Maximum width of distal base

Hold the capitate with the base facing up and the edge with "styloid process" (on the edge adjacent to the facet for the hamate) facing to the left. Measure the maximum dimension of the base (including nonarticular bone), keeping the jaws of the sliding caliper parallel to the surface of the table.

## HAMATE

**1. HAM1_MAX_HEI**: Maximum height

Hold the hamate with the facet for the triquetral facing up, with the hamulus pointing to the right and the facets for metacarpals IV and V facing away from you. Using a sliding caliper and keeping the jaws parallel to the surface of the table, measure the distance from the most dorsal point on the dorsal base to the most palmar point on the hamulus.

**2. HAM2_BOD_HEI**: Height of the body

Hold the hamate with the facet for the capitate facing up (and parallel to the surface of the table), the facets for metacarpals IV and V facing away from you, and the hamulus pointing to the left. Using a sliding caliper and keeping the jaws parallel to the surface of the table, measure the maximum height of the body (from the most dorsal point on the dorsal base to the most palmar point on the body, excluding the hamulus).

**3. HAM3_HAM_PRO**: Hamulus projection

Calculated as: Maximum height – Height of the body = (HAM1_MAX_HEI – HAM2_BOD_HEI)

**4. HAM4_MAX_WID**: Maximum width

Hold the hamate with the facet for the triquetral facing up, with the hamulus pointing away from you and the facets for metacarpals IV and V facing to the left. Place the stationary jaw of a sliding caliper against the most distal point of the hamulus and the most distal point of the dorsal base. Measure the distance to the proximalmost point.

**5. HAM5_ML_WID**: Maximum width of the distal facets

Hold the hamate with the facets for metacarpals IV and V facing up (and parallel to the surface of the table), the facet for the triquetral to the right, and the hamulus pointing away from you. Keeping the sliding caliper jaws parallel to the surface of the table, measure the maximum width of the facets from the medial margin of the facet for metacarpal V to the lateral margin of the facet for metacarpal IV.

**6. HAM6_HAM_WID**: Maximum width of the hamulus

Hold the hamate with the facets for metacarpals IV and V facing to the left, the facet for the triquetral to the right, and the hamulus pointing up such that the full breadth of the hamulus is in view. Using a sliding caliper, measure the maximum width of the hamulus.

## METACARPALS

**1. MC1_LEN**: Maximum length

Hold the metacarpal with the shaft parallel to the surface of the table, the distal end to the left, and the proximal end to the right, with the dorsal surface facing up. With a sliding caliper kept parallel to the long axis of the diaphysis, measure the maximum length of the metacarpal.

**2. MC2_BIO_LEN**: Biomechanical length

Hold the metacarpal with the shaft parallel to the surface of the table, the distal end to the left, and the proximal end to the right, with the dorsal surface facing up. Using a sliding caliper with inner points, measure the distance from the center of the carpal articular surface to the distalmost point on the metacarpal head. Calculate the midshaft value (50% of biomechanical length) and enter it in column "MC2A_BIO_MID".

**3. MC3_MID_DP**: Midshaft dorsopalmar height

Hold the metacarpal with the shaft parallel to the surface of the table, the distal end to the left, and the proximal end to the right, with the dorsal surface facing up. Determine the location of midshaft (measuring to 50% of biomechanical length with a spreading caliper). Mark the location of midshaft with string, and reorient the bone upright with the proximal end on the table and the long axis of the shaft perpendicular to the surface of the table, with the dorsal side facing to the left, and the palmar side to the right. At the midshaft point, use a sliding caliper to measure the greatest dorsopalmar dimension, making sure to keep the caliper jaws parallel to the surface of the table.

**4. MC4_MID_ML**: Midshaft mediolateral breadth

Hold the metacarpal with the shaft parallel to the surface of the table, the distal end to the left, and the proximal end to the right, with the dorsal surface facing up. Determine the location of midshaft (measuring to 50% of biomechanical length with a spreading caliper). Mark the location of midshaft with string, and reorient the bone upright with the proximal end on the table and the long axis of the shaft perpendicular to the surface of the table, with the dorsal side facing away from you, and the palmar side facing you. At the midshaft point, use a sliding caliper to measure the greatest mediolateral dimension, making sure to keep the caliper jaws parallel to the surface of the table.

**5. MC5_PRO_HEI**: Proximal maximum height

Hold the metacarpal with the long axis perpendicular to the surface of the table, the proximal surface facing up, the dorsal side to the left, and the palmar side to the right. Measure the maximum dorsopalmar diameter of the proximal end of the metacarpal, including both articular and non-articular surface, making sure to keep the caliper jaws parallel to the table (not necessarily contacting the bone, but framing the maximum dimension).

**6. MC6_PRO_BRE**: Proximal maximum breadth

Hold the metacarpal with the long axis perpendicular to the surface of the table, the proximal surface facing up, the dorsal surface facing away from you, and the palmar surface nearest to you. Measure the maximum mediolateral diameter of the proximal end of the metacarpal, including both articular and non-articular surface, making sure to keep the caliper jaws parallel to the table (not necessarily contacting the bone, but framing the maximum dimension).

**7. MC7_DIS_HEI**: Distal maximum height

Hold the metacarpal with the long axis perpendicular to the surface of the table, the distal surface facing up, the dorsal side to the left, and the palmar side to the right. Measure the greatest dorsopalmar height of the distal end of the metacarpal, making sure to keep the caliper jaws parallel to the table (not necessarily contacting the bone, but framing the maximum dimension).

**8. MC8_DIS_BRE**: Distal maximum breadth

Hold the metacarpal with the long axis perpendicular to the surface of the table, the distal surface facing up, the dorsal surface facing away from you, and the palmar surface nearest to you. Measure the largest mediolateral measurement of the distal end of the metacarpal, making sure to keep the caliper jaws parallel to the table (not necessarily contacting the bone, but framing the maximum dimension).

**9. MC9_LEN_EXC**: Proximodistal length excluding styloid process (MC3 only)

Hold the metacarpal with the shaft parallel to the surface of the table, the distal end to the left, and the proximal end to the right, with the dorsal surface facing up. Measure the distance from the distalmost point to the proximalmost point on the line bisecting the proximal articular surface into dorsal and palmar halves, making sure to keep the caliper jaws parallel to the surface of the table.

**10. MC10_DOR_WID**: Maximum dorsal width of facet for the capitate (MC3 only)

Hold the metacarpal with the long axis perpendicular to the surface of the table, the proximal surface facing up, the dorsal surface facing away from you, and the palmar surface nearest to you. Measure the maximum diameter along the dorsal edge of the facet for the capitate, making sure to keep the caliper jaws parallel to the table.

**11. MC11_PAL_WID**: Maximum palmar width of facet for the capitate (MC3 only)

Hold the metacarpal with the long axis perpendicular to the surface of the table, the proximal surface facing up, the palmar surface facing away from you, and the dorsal surface nearest to you. Measure the maximum diameter along the palmar edge of the facet for the capitate, making sure to keep the caliper jaws parallel to the table.

**12. MC12_FAC_WID**: Mediolateral width of facet for the capitate (MC3 only)

Hold the metacarpal with the long axis perpendicular to the surface of the table, the proximal surface facing up, the palmar surface facing away from you, and the dorsal surface nearest to you. Measure the maximum diameter along the line bisecting the facet for the capitate into dorsal and palmar halves, making sure to keep the caliper jaws parallel to the table.

## TERMINAL HAND PHALANGES

**1. THP1_LEN**: Maximum length

With the sliding caliper jaws perpendicular to the long axis of the phalangeal diaphysis and in a paracoronal plane, measure the maximum length of the phalanx.

**2. THP2_BIO_LEN**: Biomechanical length

Using a sliding caliper with at least one inside point, measure from the depth of the proximal facet to the distalmost point on the apical tuft. Calculate the midshaft value (50% of biomechanical length) and enter it in column “THP2A_BIO_MID”.

**3. THP3_MID_AP**: Midshaft anteroposterior (dorsopalmar) height

Using a sliding caliper (with no inside points), measure to 50% of biomechanical length from the distalmost point on the apical tuft and mark the location with a string. Reorient the bone such that the tuft is pointing away from you and the palmar surface is facing to the left. At the midshaft location, measure the greatest dorsopalmar dimension, keeping the caliper jaws perpendicular to the long axis of the phalanx.

**4. THP4_MID_ML**: Midshaft mediolateral breadth

Using a sliding caliper (with no inside points), measure to 50% of biomechanical length from the distalmost point on the apical tuft and mark the location with a string. Reorient the bone such that the tuft is pointing away from you and the palmar surface is facing down. At the midshaft location, measure the greatest mediolateral dimension, keeping the caliper jaws perpendicular to the long axis of the phalanx.

**5. THP5_PRO_AP**: Proximal anteroposterior (dorsopalmar) height

Hold the phalanx with the apical tuft pointing toward the table such that the axis of the bone is perpendicular to the surface of the table, with the palmar surface facing to the right. Using a sliding caliper and keeping the jaws parallel to the surface of the table, measure the greatest dorsopalmar dimension of the proximal end of the phalanx.

**6. THP6_PRO_ML**: Proximal mediolateral breadth

Hold the phalanx with the apical tuft pointing toward the table such that the axis of the bone is perpendicular to the surface of the table, with the palmar surface facing you. Using a sliding caliper and keeping the jaws parallel to the surface of the table, measure the greatest mediolateral dimension of the proximal end of the phalanx.

**7. THP7_DIS_AP**: Distal tuft anteroposterior (dorsopalmar) height

Hold the phalanx with the apical tuft pointing up such that the axis of the bone is perpendicular to the surface of the table, with the palmar surface facing to the right. Using a sliding caliper and keeping the jaws parallel to the surface of the table, measure the greatest dorsopalmar dimension of the distal tuft.

**8. THP8_DIS_ML**: Distal tuft mediolateral breadth

Hold the phalanx with the apical tuft pointing up such that the axis of the bone is perpendicular to the surface of the table, with the palmar surface facing you. Using a sliding caliper and keeping the jaws parallel to the surface of the table, measure the greatest mediolateral dimension of the distal tuft.

## SACRUM

**1. SAC1_BRE**: Maximum breadth

Hold the sacrum perpendicular to the table with the superior surface facing up, the inferior end pointing away from you, and the ventral surface facing you. Use a sliding caliper to determine the greatest breadth of the first sacral vertebra (including the alae), keeping the jaws of the caliper parallel to the table.

**2. SAC2_ANT_HEI**: Maximum anterior height

Place the sacrum on the table with the ventral surface facing up, the superior end to the left, and the inferior end to the right. Place the stationary jaw of the sliding caliper on the ventral midline point of the sacral promontory, and then extend the adjustable jaw to the midline of the inferoventral midline point of the last sacral vertebral body, keeping the jaws of the caliper parallel to the table.

**3. SAC3_IND**: Sacral index

Calculated as: (maximum breadth / maximum anterior height) x 100

## OS COXAE

**1. OCX1_HEI**: Os coxae height

While standing, place the iliac crest against the stationary end of the osteometric board, holding the os coxae such that the acetabulum is facing up and the bone (including the pubis) is resting on the board, and place the adjustable end of the board against the ischiopubic ramus. Record the maximum distance between the iliac crest and the ischiopubic ramus.

**2. OCX2_ISC_PUB**: Maximum diameter from ischium to pubis

While standing, hold the os coxae with the ilium nearest you, the acetabulum facing down toward the table, the ischium and the anterior portion of the ilium resting on the table, and the pubis and ischium away from you. Adjust the bone such that you can see the maximum dimension from the ischium to the pubis and take the measurement, keeping the caliper jaws parallel to the surface of the table.

**3. OCX3_PUB_LEN**: Pubic length

Hold the os coxae at the ischium with the acetabulum facing up, the posterior portion of the ilium resting on the table, and the pubis nearest to you. Spread the sliding caliper fully open, and place the stationary jaw of the caliper at the point along the superior margin of the acetabulum closest to the center of the triradiate suture. Carefully narrow the caliper until the second jaw contacts the most distant point on the superior part of the pubic body.

**4. OCX4_ACE_LEN**: Acetabulosymphyseal length

Hold the os coxae at the ischium with the acetabulum facing up, the posterior portion of the ilium resting on the table, and the pubis nearest to you. Open the sliding caliper (with inner points), place the stationary jaw on the point on the lunate surface closest to the pubic symphysis, and carefully narrow the caliper until the second jaw contacts the superiormost point on the pubic symphysis.

**5. OCX5_NA_ISC**: Nonarticular ischial length

Hold the os coxae on the table with the acetabulum facing up, the ilium to the left, and the ischium to the right. Measure the distance between the point where the axis of the body of the ischium crosses the inferior acetabular margin and the point where the axis of the body of the ischium crosses the surface of the ischial tuberosity, holding the caliper jaws parallel to the table.

**6. OCX6_ACE_DIA**: Acetabulum diameter

Hold the os coxae with the ilium resting on the table, the acetabulum facing you, and the pubis pointing up. Using the inside spreading jaws of a sliding caliper, place the stationary jaw on the acetabular margin where the axis of the ischial body intersects the superior margin. Carefully spread the caliper until the second jaw contacts inferior margin, at the point where the axis of the ischial body intersects the inferior margin.

**7. OCX7_ACE_HEI**: Acetabular height

Hold the os coxae with the ilium resting on the table, the acetabulum facing you, and the pubis pointing up. Using the inside spreading jaws of a sliding caliper, place the stationary jaw on the edge of the lunate surface (not the acetabular margin) immediately beneath the anterior inferior iliac spine. Carefully spread the caliper until the second jaw contacts the most distant point on the lunate surface.

## FEMUR

**1. FEM1_LEN**: Maximum femoral length

While standing, place the top of the femoral head against the stationary end of the osteometric board, with the posterior surface of the bone facing down. Place the adjustable end of the board against the most distant point on the farthest condyle, making sure the long axis of the bone is parallel to the long axis of the board.

**2. FEM2_EPI_BRE**: Femoral epicondylar breadth

While standing, place the lateralmost point of the lateral epicondyle against the stationary end of an osteometric board, with the posterior surface of the bone facing down. Place the adjustable end of the board against the medialmost point of the medial epicondyle, making sure the long axis of the bone is perpendicular to the long axis of the board.

**3. FEM3_NEC_LEN**: Biomechanical neck length

While standing, place the lateralmost point of the greater trochanter against the stationary end of an osteometric board, with the anterior surface of the bone facing down and the femoral head and greater trochanter resting against the board. Place the adjustable end of the board against the medialmost point of the femoral head, making sure the long axis of the bone is perpendicular to the long axis of the board.

**4. FEM4_HEA_DIA**: Vertical head diameter

While standing, place the top of the femoral head against the stationary end of the osteometric board, with the posterior surface of the bone facing down, and the long axis of the bone parallel to the long axis of the board. Place the adjustable end of the board against the inferiormost point of the femoral head.

**5. FEM5_BIO_LEN**: Femoral biomechanical length

Place the femur on the table with the posterior surface facing down, the head to the left, and the distal end to the right. Using a large sliding caliper, place the stationary jaw on the inferiormost point of the superior femoral neck, and then measure the distances to: 1) the

distalmost point of the medial condyle (enter this value in column “FEM5A_BIO_LEN”); and 2) the distalmost point of the lateral condyle (enter this value in column “FEM5B_BIO_LEN”). Biomechanical length is the average of these two distances. Calculate the midshaft value (50% of biomechanical length) and enter it in column “FEM5C_BIO_MID”.

**6. FEM6_MID_CIR**: Femoral midshaft circumference

Place the femur on the table with the posterior surface facing down, the head to the left, and the distal end to the right. Determine the location of midshaft (measuring to 50% of femoral biomechanical length from the inferiormost point of the superior femoral neck with a large sliding caliper), mark it with a piece of string, and use a flexible cloth tape to determine the circumference at that location.

**7. FEM7_AP_MID**: Femoral anteroposterior midshaft diameter

Place the femur on the table with the posterior surface facing down, the head to the left, and the distal end to the right. Determine the location of midshaft (measuring to 50% of femoral biomechanical length with a large sliding caliper) and mark it with a piece of string. Reorient the bone to an upright position with the distal end on the table and the long axis of the shaft perpendicular to the surface of the table, with the medial surface facing you. While standing, use a sliding caliper to measure the anteroposterior diameter at the midshaft location, making sure to take the measurement perpendicular to the long axis of the bone and keeping the jaws of the caliper parallel to the table surface.

**8. FEM8_ML_MID**: Femoral mediolateral midshaft diameter

Place the femur on the table with the posterior surface facing down, the head to the left, and the distal end to the right. Determine the location of midshaft (measuring to 50% of femoral biomechanical length with a large sliding caliper) and mark it with a piece of string. Reorient the bone to an upright position with the distal end on the table and the long axis of the shaft perpendicular to the surface of the table, with the posterior surface facing you. While standing, use a sliding caliper to measure the mediolateral diameter at the midshaft location, making sure to take the measurement perpendicular to the long axis of the bone and keeping the jaws of the caliper parallel to the table surface.

**9. FEM9_PLA_IND**: Platymeric index

Calculated as: (anteroposterior midshaft diameter / mediolateral midshaft diameter) x 100

**10. FEM10_AP_HEA**: Anteroposterior head diameter

Hold the femur with the lateral surface facing down such that the coronal plane is perpendicular to the surface of the table, with the distal end away from you, and the proximal end nearest you. Using a sliding caliper, measure the maximum anteroposterior dimension, keeping the caliper jaws parallel to the surface of the table, and aligned with the long axis of the shaft.

**11. FEM11_NEC_HEI**: Minimum neck height

Place the femur on the table with the anterior surface facing down, with the distal end away from you and to the right, such that you are looking down the long axis of the neck of the

femur. Using a sliding caliper and keeping the jaws perpendicular to the surface of the table, measure the minimum height of the neck, taken perpendicular to its long axis.

**12. FEM12_NEC_ANG**: Neck angle

Place the femur on the table with the anterior surface facing down, the head pointing away from you, and the distal end to nearest to you. While standing and looking down from directly above the where the shaft and neck axes intersect, align one arm of the digital protractor with the long axis of the shaft, and align the other arm with the shaft of the femoral neck.

## PATELLA

**1. PAT1_HEI**: Maximum patellar height

While standing, place the superior margin of the patella against the stationary end of the osteometric board, with the anterior surface of the bone facing down, and the superoinferior axis of the bone parallel to the long axis of the board. Place the adjustable end of the board against the apex.

**2. PAT2_BRE**: Maximum patellar breadth

While standing, place the medial margin of the patella against the stationary end of the osteometric board, with the anterior surface of the bone facing down. Place the adjustable end of the board against the lateral margin of the patella, making sure to take the measurement perpendicular to the maximum patellar height.

**3. PAT3_THI**: Maximum thickness

Hold the patella with the superior surface facing up, the articular surface facing to the left, and the lateral surface facing you. Place the stationary arm of a sliding caliper against the ridge dividing the medial and lateral articular facets and move the adjustable arm until it contacts the ventral surface of the patella, making sure to take the measurement in a parasagittal plane.

## TIBIA

**1. TIB1_LEN**: Maximum tibial length

While standing, place the top of the intercondylar eminence against the stationary end of the osteometric board, with the posterior surface of the bone facing down. Place the adjustable end of the board against the most distant point on the medial malleolus, making sure the long axis of the bone is parallel to the long axis of the board.

**2. TIB2_PRO_BRE**: Tibial maximum proximal epiphyseal breadth

While standing, place the medialmost point of the tibial plateau against the stationary end of an osteometric board, with the posterior surface of the bone facing down. Position the bone such that the flat anterior surface of the distal end of the tibia is parallel to the surface of the table. Place the adjustable end of the board against the lateralmost point of the tibial plateau, making sure the long axis of the bone is perpendicular to the long axis of the board.

**3. TIB3_DIS_BRE**: Tibial maximum distal epiphyseal breadth

While standing, place the lateralmost point of the distal epiphysis against the stationary end of an osteometric board, with the posterior surface of the bone facing down. Place the adjustable end of the board against the medialmost point of the medial malleolus, making sure the long axis of the bone is perpendicular to the long axis of the board.

**4. TIB4_DIS_AP**: Distal epiphysis anteroposterior diameter

While standing, place the anteriormost point of the distal epiphysis against the stationary end of an osteometric board, with the lateral surface of the bone facing down. Place the adjustable end of the board against the posteriormost point of the distal epiphysis, making sure the long axis of the bone is perpendicular to the long axis of the board.

**5. TIB5_BIO_LEN**: Tibial biomechanical length

Place the tibia on the table with the posterior surface facing down, the proximal end to the left, and the distal end to the right. Using a spreading caliper, place one jaw on the center point of the talar articular surface, and then measure the distances to: 1) the center point of the medial condyle (enter this value in column "TIB5A_BIO_LEN"); and 2) the center point of the lateral condyle (enter this value in column "TIB5B_BIO_LEN"). Biomechanical length is the average of these two distances. Calculate the midshaft value (50% of biomechanical length) and enter it in column "TIB5C_BIO_MID".

**6. TIB6_AP_MID**: Tibial anteroposterior midshaft diameter

Place the tibia on the table with the posterior surface facing down, the proximal end to the left, and the distal end to the right. Determine the location of midshaft (measuring to 50% of tibial biomechanical length from the centerpoint of the talar articular surface with a spreading caliper) and mark it with a piece of string. Reorient the bone to an upright position with the distal end on the table and the long axis of the shaft perpendicular to the surface of the table, with the medial surface facing you. While standing, use a sliding caliper to measure the anteroposterior diameter at the midshaft location, making sure to take the measurement perpendicular to the long axis of the bone and keeping the jaws of the caliper parallel to the table surface.

**7. TIB7_ML_MID**: Tibial mediolateral midshaft diameter

Place the tibia on the table with the posterior surface facing down, the proximal end to the left, and the distal end to the right. Determine the location of midshaft (measuring to 50% of tibial biomechanical length from the centerpoint of the talar articular surface with a spreading caliper) and mark it with a piece of string. Reorient the bone to an upright position with the distal end on the table and the long axis of the shaft perpendicular to the surface of the table, with the posterior surface facing you. While standing, use a sliding caliper to measure the mediolateral diameter at the midshaft location, making sure to take the measurement perpendicular to the long axis of the bone and keeping the jaws of the caliper parallel to the table surface.

**8. TIB8_MID_CIR**: Tibial midshaft circumference

Place the tibia on the table with the posterior surface facing down, the proximal end to the left, and the distal end to the right. Determine the location of midshaft (measuring to 50% of tibial biomechanical length from the centerpoint of the talar articular surface with a spreading

caliper), mark it with a piece of string, and use a flexible cloth tape to determine the circumference at that location.

**9. TIB9_CIR_NUT**: Tibial circumference at nutrient foramen

Place the tibia on the table with the lateral surface facing up, the proximal end to the left, and the distal end to the right. Determine the location of the nutrient foramen and use a flexible cloth tape to determine the circumference at that location (at the most distal extent of the foramen).

**10. TIB10_ML_NUT**: Tibial mediolateral shaft diameter at nutrient foramen

Place the tibia on the table with the lateral surface facing up, the proximal end to the left, and the distal end to the right. Determine the location of the nutrient foramen and mark it with a piece of string (at the most distal extent of the foramen). Reorient the bone to an upright position with the distal end on the table and the long axis of the shaft perpendicular to the surface of the table, with the posterior surface facing you. While standing, use a sliding caliper to measure the greatest mediolateral dimension of the shaft at the level of the nutrient foramen, making sure to measure along a paracoronal plane while keeping the jaws of the caliper parallel to the table surface.

**11. TIB11_MAX_NUT**: Tibial maximum shaft diameter at nutrient foramen

Place the tibia on the table with the lateral surface facing up, the proximal end to the left, and the distal end to the right. Determine the location of the nutrient foramen and mark it with a piece of string (at the most distal extent of the foramen). Reorient the bone to an upright position with the distal end on the table and the long axis of the shaft perpendicular to the surface of the table, with the lateral surface facing you. While standing, use a sliding caliper to measure the greatest distance from the anterior border to the posterior surface at the level of the nutrient foramen, making sure to measure along a parasagittal plane while keeping the jaws of the caliper parallel to the table surface.

**12. TIB12_PLA_IND**: Platycnemic index

Calculated as: (mediolateral shaft diameter at nutrient foramen / maximum shaft diameter at nutrient foramen) x 100

## FIBULA

**1. FIB1_LEN**: Maximum fibular length

While standing, place the top of the styloid process against the stationary end of the osteometric board, with the medial surface of the bone facing down. Place the adjustable end of the board against the most distant point on the lateral malleolus, making sure the long axis of the bone is parallel to the long axis of the board. Calculate the midshaft value (50% of maximum length) and enter it in column “FIB1A_LEN_MID”.

**2. FIB2_MID_CIR**: Fibular midshaft circumference

Place the fibula on the table with the medial surface facing down, the proximal end to the left, and the distal end to the right. Determine the location of midshaft (measuring to 50% of

fibular maximum length from the superiormost point on the styloid process with a large sliding caliper), mark it with a piece of string, and use a flexible cloth tape to determine the circumference at that location (making sure to hold the tape against the bone surface).

**3. FIB3_MAX_ART**: Maximum proximodistal diameter of malleolar articular surface

Hold the fibula above the table with the proximal end to the left and resting on the table, the medial surface facing up, the distal end held such that the malleolar articular surface is approximately parallel to the surface of the table. Looking down at the bone from directly above and keeping the caliper jaws parallel to the surface of the table and perpendicular to the long axis of the shaft, measure the distance from the proximalmost to the distalmost point on the malleolar articular surface.

**4. FIB4_ART_DIA**: Maximum diameter of the malleolar articular surface, perpendicular to the maximum proximodistal diameter

Hold the fibula above the table with the proximal end pointing away from you and resting on the table, the medial surface facing up, the distal end held such that the malleolar articular surface is approximately parallel to the surface of the table. Looking down at the bone from directly above and keeping the caliper jaws parallel to the surface of the table and parallel to the long axis of the shaft, measure the maximum dimension across the malleolar articular surface along a line perpendicular to the maximum proximodistal diameter (FIB3_MAX_ART).

**5. FIB5_DIS_BRE**: Maximum distal mediolateral breadth

While standing, place the lateralmost point of the distal epiphysis against the stationary end of an osteometric board, with the posterior surface of the bone facing down. Place the adjustable end of the board against the medialmost point of the distal epiphysis, making sure the long axis of the bone is perpendicular to the long axis of the board.

**6. FIB6_DIS_AP**: Maximum distal anteroposterior diameter

While standing, place the anteriormost point of the distal epiphysis against the stationary end of an osteometric board, with the lateral surface of the bone facing down. Place the adjustable end of the board against the posteriormost point of the distal epiphysis, making sure the long axis of the bone is perpendicular to the long axis of the board.

## TALUS

**1. TAL1_LEN**: Talar length

Hold the talus with the lateral malleolar surface facing away from you, the posterior subtalar facet facing down, and the medial malleolar surface facing you. With the caliper jaws perpendicular to the table, measure from the depth of the groove for the flexor hallucis longus to the anteriormost point on the talar head.

**2. TAL2_MAX_LEN**: Maximum talar length

Place the anteriormost point of the talar head against the stationary end of the osteometric board, with the inferior surface of the bone facing down. Place the adjustable end of the board against the most posterior point.

**3. TAL3_HEA_NEC**: Length of head plus neck

Place the talus on the surface of the table, with the talar head pointing to the right and the superior surface facing up. Identify the point at which a line bisecting the superior articular surface of the trochlea intersects the anterior margin of the trochlea. Using a sliding caliper and keeping the jaws parallel to the surface of the table, measure the distance from the anterior edge of the trochlea to the most distal point of the head, taken parallel to the long axis of the head and neck.

**4. TAL4_PHY_HEI**: Physiological height

Place the talus on a thin, flat piece of wood, with the superior surface facing down and resting on the wood (resting on the head and the two superiormost points of the trochlea). Using a sliding caliper with inner points, measure from the superiormost point on the posterior subtalar facet to the opposite side of the piece of wood along a line perpendicular to the piece of wood (enter this value in column "TAL4A_PHY_HEI"). Subtract the thickness of the wood (enter this value in column "TAL4B_PHY_HEI").

**5. TAL5_ART_BRE**: Articular breadth

Hold the talus with the trochlea facing superiorly and the talar head pointing away from you. Holding the caliper jaws parallel to the table, measure the widest mediolateral distance of the trochlea (excluding the lateral process), perpendicular to the long axis.

**6. TAL6_MAL_BRE**: Lateral malleolar breadth

Hold the talus with the trochlea facing superiorly and the talar head pointing away from you. Holding the caliper jaws parallel to the table, measure the widest mediolateral distance of the lateral malleolar process from the lateral edge of the superior articular surface of the trochlea to the lateralmost point of the lateral process.

**7. TAL7_HEA_LEN**: Length of the head

Hold the talus with the head facing up and the lateral process pointing toward you, such that the long axis of the head is oriented left-to-right. Using a sliding caliper, measure the distance between the most projecting points on the medial and lateral margins of the articular surface of the head.

**8. TAL8_TRO_HEI**: Trochlear height

Hold the talus with the medial surface facing up and the head pointing away from you. Using a sliding caliper and keeping the jaws parallel to the table, measure the distance between the highest point of the trochlea along the medial margin, and the line connecting the the two endpoints of the curve of the trochlea.

**9. TAL9_ML_WID**: Mediolateral width

Place the talus on an osteometric board, with the inferior surface facing down and the medial surface (both the medial malleolar surface and the talar head) against the stationary end of the board. Move the adjustable end of the board until it comes into contact with the lateral process of the lateral malleolar surface.

**10. TAL10_AP_TRO**: Maximum anteroposterior trochlear length

Place the talus on the surface of the table with the trochlea facing up and the talar head pointing to the left. Holding the caliper jaws parallel to the table and perpendicular to the anteroposterior axis, measure the diameter between the anteriormost and posteriormost points of the trochlea.

**11. TAL11_ML_HEA**: Mediolateral width of talar head

Hold the talus with the anteroposterior axis perpendicular to the table surface, the talar head pointing up, and the superior surface facing away from you. Looking at the talus from directly above, measure the widest mediolateral distance of the talar head (making sure not to include the neck).

**12. TAL12_LEN_FAC**: Maximum dimension of posterior subtalar facet

Hold the talus on the surface of the table with the inferior surface facing up and the talar head pointing away from you. Holding the caliper jaws parallel to the surface of the table, measure the diameter of the posterior subtalar facet along the long axis of the facet, keeping the caliper jaws perpendicular to the long axis of the facet.

## CALCANEUS

**1. CAL1_LEN**: Maximum calcaneal length

Place the posteriormost point of the calcaneal tuberosity against the stationary end of the osteometric board, with the inferior surface of the bone facing down. Place the adjustable end of the board against the most anterior point.

ALTERNATE (CALIPER): Hold the calcaneus parallel to the table, with the cuboid facet facing to the left, the calcaneal tuberosity pointing to the right, with the lateral surface facing up. Holding the calipers parallel to the table, measure the distance from the anteriormost to the posteriormost point.

**2. CAL2_POS_LEN**: Posterior calcaneal length

Place the calcaneus on the table with the plantar surface facing down and the medial surface facing you. Holding the caliper jaws parallel to the table and looking down at the bone from directly above, place the stationary jaw of the caliper on the anteriormost point of the posterior talar facet, and close the caliper until you reach a superoinferior line tangential to the posteriormost surface of the calcaneal tuberosity, measuring along the long axis of the bone.

**3. CAL3_MED_BRE**: Medial breadth (across the sustentaculum tali)

Place the calcaneus on the table with the long axis parallel to the table, the plantar surface on the table, and the calcaneal tuberosity nearest you. Stabilize the calcaneus with your left hand, and measure from the most medial point on the sustentaculum tali to the most lateral portion of the talar articular surface, holding the caliper jaws parallel to the table.

**4. CAL4_HEI_BOD**: Height of the body

Hold the calcaneus on the surface of the table with the medial surface facing up and the calcaneal tuberosity pointing away from you. Looking down at the bone from directly above and holding the caliper jaws parallel to the table, measure from the most plantar point on the calcaneal tuberosity to the most superior point of the corpus calcanei, making sure to keep the jaws of the caliper parallel to the long axis of the calcaneus.

**5. CAL5_MIN_BRE**: Minimum breadth across the body

Hold the calcaneus with the superior surface facing up and the calcaneal tuberosity pointing away from you, with your pointer finger on the tuber calcanei and thumb on the facet for the cuboid. Looking down at the bone from directly above, measure the smallest transverse diameter across the body, holding the caliper jaws perpendicular to the table and taking the measurement along a line perpendicular to the long axis of the bone. This dimension with be located approximately midway between the talar articular surface and the posteriormost extent of the tuber calcanei.

## CUBOID

**1. CUB1_MAX_BRE**: Maximum breadth

Place the cuboid on the osteometric board with the plantar surface facing up and the superior surface facing down, with the medial edge against the stationary end (contacting the stationary end at two points). Move the adjustable end to contact the lateralmost point of the lateral edge of the bone.

**2. CUB2_MAX_LEN**: Maximum length

Place the cuboid on the osteometric board with the medial surface facing down and the distal edge against the stationary end (contacting the stationary end at two points). Move the adjustable end to contact the most proximal point of the cuboid beak.

**3. CUB3_MAX_HEI**: Maximum height

Place the cuboid on the osteometric board with the medial surface facing down and the long axis perpendicular to the long axis of the board, with the superior surface against the stationary end (contacting the stationary end at two points). Move the adjustable end to contact the plantarmost point on the plantar surface.

**4. CUB4_CAL_FAC**: Maximum diameter of the facet for the calcaneus

Hold the cuboid with the superior surface facing you and the plantar surface facing away from you, with the calcaneal facet facing up and held roughly parallel to the table surface. Looking down at the bone from directly above and holding the caliper jaws parallel to the table, measure the maximum dimension of the calcaneal facet.

## NAVICULAR

**1. NAV1_MAX_BRE**: Maximum breadth

Place the navicular on the osteometric board with the proximal surface facing down and the lateral edge of the bone against the stationary end of the board (contacting the stationary end at two points). Move the adjustable end to contact the most medial point on the navicular tuberosity.

**2. NAV2_MAX_LEN**: Maximum length

Place the navicular on the osteometric board with the plantar surface facing down, the medial tuberosity contacting the base of the board, and the proximal surface against the stationary end of the board (contacting the stationary end at two points, at the medial and lateral ends). Move the adjustable end to contact the most distal point.

**3. NAV3_MAX_HEI**: Maximum height

Place the navicular on the osteometric board with the proximal surface facing down and the distal articular surfaces facing up. Place the plantar surface of the bone against the stationary end of the board (contacting the stationary end at two points). Move the adjustable end to contact the most superior point.

**4. NAV4_TAL_FAC**: Maximum diameter of the facet for the talar head

Holding the navicular with the facet for the talar head facing up and the medial tuberosity pointing to the left, measure the maximum diameter of the facet for the talar head, making sure to keep the caliper jaws parallel to the surface of the table.

## METATARSALS

**1. MT1_LEN**: Maximum metatarsal length

Hold the metatarsal with the shaft parallel to the surface of the table, the distal end to the left, and the proximal end to the right, with the dorsal surface facing up. With a sliding caliper kept parallel to the long axis of the diaphysis, measure the maximum length of the metatarsal.

**2. MT2_BIO_LEN**: Biomechanical length

Hold the metatarsal with the shaft parallel to the surface of the table, the distal end to the left, and the proximal end to the right, with the dorsal surface facing up. Using a sliding caliper with inner points, measure the distance from the center of the tarsal articular surface to the distalmost point on the metatarsal head. Calculate the midshaft value (50% of biomechanical length) and enter it in column “MT2A_BIO_MID”.

**3. MT3_MID_DP**: Midshaft dorsoplantar height

Hold the metatarsal with the shaft parallel to the surface of the table, the distal end to the left, and the proximal end to the right, with the dorsal surface facing up. Determine the location of midshaft (measuring to 50% of biomechanical length with a spreading caliper). Mark the location of midshaft with string, and reorient the bone upright with the proximal end on the table and the long axis of the shaft perpendicular to the surface of the table, with the dorsal side facing to the left, and the plantar side to the right. At the midshaft point, use a sliding caliper to measure the greatest dorsoplantar dimension, making sure to keep the caliper jaws parallel to the surface of the table.

**4. MT4_MID_ML**: Midshaft mediolateral breadth

Hold the metatarsal with the shaft parallel to the surface of the table, the distal end to the left, and the proximal end to the right, with the dorsal surface facing up. Determine the location of midshaft (measuring to 50% of biomechanical length with a spreading caliper). Mark the location of midshaft with string, and reorient the bone upright with the proximal end on the table and the long axis of the shaft perpendicular to the surface of the table, with the dorsal side facing away from you, and the plantar side facing you. At the midshaft point, use a sliding caliper to measure the greatest mediolateral dimension, making sure to keep the caliper jaws parallel to the surface of the table.

**5. MT5_PRO_HEI**: Proximal maximum height

Hold the metatarsal with the long axis perpendicular to the surface of the table, the proximal surface facing up, the dorsal side to the left, and the plantar side to the right. Measure the maximum dorsoplantar diameter of the proximal end of the metatarsal, including both articular and non-articular surface, making sure to keep the caliper jaws parallel to the table (not necessarily contacting the bone, but framing the maximum dimension).

**6. MT6_PRO_BRE**: Proximal maximum breadth

Hold the metatarsal with the long axis perpendicular to the surface of the table, the proximal surface facing up, the dorsal surface facing away from you, and the plantar surface nearest to you. Measure the maximum mediolateral diameter of the proximal end of the metatarsal, including both articular and non-articular surface, making sure to keep the caliper jaws parallel to the table (not necessarily contacting the bone, but framing the maximum dimension).

**7. MT7_DIS_HEI**: Distal maximum height

Hold the metatarsal with the long axis perpendicular to the surface of the table, the distal surface facing up, the dorsal side to the left, and the plantar side to the right. Measure the greatest dorsoplantar height of the distal end of the metatarsal, making sure to keep the caliper jaws parallel to the table (not necessarily contacting the bone, but framing the maximum dimension).

**8. MT8_DIS_BRE**: Distal maximum breadth

Hold the metatarsal with the long axis perpendicular to the surface of the table, the distal surface facing up, the dorsal surface facing away from you, and the plantar surface nearest to you. Measure the largest mediolateral measurement of the distal end of the metatarsal, making sure to keep the caliper jaws parallel to the table (not necessarily contacting the bone, but framing the maximum dimension).

## TERMINAL FOOT PHALANGES

**1. TFP1_LEN**: Maximum length

With the sliding caliper jaws perpendicular to the long axis of the phalangeal diaphysis and in a paracoronal plane, measure the maximum length of the phalanx.

**2. TFP2_BIO_LEN**: Biomechanical length

Using a sliding caliper with at least one inside point, measure from the depth of the proximal facet to the distalmost point on the apical tuft. Calculate the midshaft value (50% of biomechanical length) and enter it in column "TFP2A_BIO_MID".

**3. TFP3_MID_AP**: Midshaft anteroposterior (dorsoplantar) height

Using a sliding caliper (with no inside points), measure to 50% of biomechanical length from the distalmost point on the apical tuft and mark the location with a string. Reorient the bone such that the tuft is pointing away from you and the plantar surface is facing to the left. At the midshaft location, measure the greatest dorsoplantar dimension, keeping the caliper jaws perpendicular to the long axis of the phalanx.

**4. TFP4_MID_ML**: Midshaft mediolateral breadth

Using a sliding caliper (with no inside points), measure to 50% of biomechanical length from the distalmost point on the apical tuft and mark the location with a string. Reorient the bone such that the tuft is pointing away from you and the plantar surface is facing down. At the midshaft location, measure the greatest mediolateral dimension, keeping the caliper jaws perpendicular to the long axis of the phalanx.

**5. TFP5_PRO_AP**: Proximal anteroposterior (dorsoplantar) height

Hold the phalanx with the apical tuft pointing toward the table such that the axis of the bone is perpendicular to the surface of the table, with the plantar surface facing to the right. Using a sliding caliper and keeping the jaws parallel to the surface of the table, measure the greatest dorsoplantar dimension of the proximal end of the phalanx.

**6. TFP6_PRO_ML**: Proximal mediolateral breadth

Hold the phalanx with the apical tuft pointing toward the table such that the axis of the bone is perpendicular to the surface of the table, with the plantar surface facing you. Using a sliding caliper and keeping the jaws parallel to the surface of the table, measure the greatest mediolateral dimension of the proximal end of the phalanx.

**7. TFP7_DIS_AP**: Distal tuft anteroposterior (dorsoplantar) height

Hold the phalanx with the apical tuft pointing up such that the axis of the bone is perpendicular to the surface of the table, with the plantar surface facing to the right. Using a sliding caliper and keeping the jaws parallel to the surface of the table, measure the greatest dorsoplantar dimension of the distal tuft.

**8. TFP8_DIS_ML**: Distal tuft mediolateral breadth

Hold the phalanx with the apical tuft pointing up such that the axis of the bone is perpendicular to the surface of the table, with the plantar surface facing you. Using a sliding caliper and keeping the jaws parallel to the surface of the table, measure the greatest mediolateral dimension of the distal tuft.

---

**7b**. NONMETRIC DATA

Nonmetric data collection protocols are detailed below by anatomical element. References for the assessed nonmetric traits are listed in Appendix 6b. Eleven nonmetric traits were assessed for the comparative recent modern human individuals. Both sides were assessed when preservation allowed. In cases where the nonmetric scores were different for the right and left sides, both scores were recorded and the individual noted as asymmetrical for the nonmetric trait in question.

## SCAPULA

**Axillary sulcus**

Observe the axillary border of the scapula and record whether the axillary sulcus is placed on the ***ventral*** surface, the ***dorsal*** surface, distributed approximately evenly across both (i.e., ***bisulcate***), or distributed across both with the majority on the ventral side (i.e., ***bisulcate, with the majority on the ventral side***).

## HUMERUS

**Humeral head shape**

Observe the humeral head in superomedial view and record whether the head shape is ***horizontally oval***, ***slightly horizontally oval***, ***round***, ***slightly vertically oval***, or ***vertically oval***.

**Olecranon fossa relative size**

Observe the posterior surface of the distal end of the humerus and record whether the size of the olecranon fossa is ***very small***, ***small***, ***moderate***, ***large***, or ***very large*** relative to general humeral size.

**Olecranon fossa depth**

Observe the posterior surface of the distal end of the humerus and record whether the depth of the olecranon fossa is ***very shallow***, ***shallow***, ***moderate***, ***deep***, or ***very deep***.

## ULNA

**Ulnar trochlear notch form**

Observe the proximal ulna in anterosuperior view and record whether the trochlear facets are ***completely continuous***, ***continuous at the lateral edge***, ***continuous at the medial edge***, ***continuous at the medial and lateral edges***, or ***two distinct facets***. In cases where the facets meet at the depth of the trochlear notch but are divided by a bony ridge, score the individual as having ***two distinct facets***.

**Ulnar trochlear notch orientation**

Observe the proximal ulna in lateral view and record whether the trochlear notch opens ***anteriorly***, ***slightly superoanteriorly***, or ***superoanteriorly***.

## TIBIA

### Squatting facets on the tibia

Observe the anterior surface of the distal tibia and record whether at least one squatting facet is ***present*** or ***absent***. In cases where the talar facet extends very slightly onto the anterior surface of the distal end, but does not present as a well-developed facet, record the trait as ***slight***. In cases where the presence of a squatting facet cannot be reliably assessed (e.g., in pathological individuals) record the trait as ***indeterminate***.

## TALUS

### Squatting facets on the talus

Observe the superior surface of the talar neck and record whether at least one squatting facet is ***present*** or ***absent***. In cases where the presence of a squatting facet cannot be reliably assessed (e.g., in pathological individuals) record the trait as ***indeterminate***.

### Talar trochlear shape

Observe the trochlea of the talus in superior view and record whether the trochlear surface (in outline) ***tapers posteriorly***, ***tapers slightly posteriorly***, is ***broad***, is ***broad and tapers posteriorly***, is ***broad and tapers slightly posteriorly***, is ***square***, is ***long***, or is ***long and tapers slightly posteriorly.***

### Inferior talar articular surface

Observe the inferior surface of the talus and record whether the anterior and medial subtalar facets are ***distinct***, ***continuous***, or ***the anterior facet is absent***.

## CALCANEUS

### Anterior calcaneal facets

Observe the calcaneus in superior view and record whether the anterior and medial talar facets are ***distinct***, ***continuous***, or ***the anterior facet is absent***.

**Appendix 8** Nonmetric observations for the HAL-VP-9/1 partial skeleton

The nonmetric observations reported below include the set of eleven traits that were assessed for the comparative modern human samples (each indicated with an asterisk); see Appendix 6b for references and Appendix 7b for data collection protocols. In addition to these eleven traits, several other standard nonmetrics were also assessed for the HAL-VP-9/1 skeleton, following definitions from Buikstra and Ubelaker (1994) and Finnegan (1978).

| Trait | Right side | Left side |
|---|---|---|
| ***Scapula*** | | |
| **Axillary sulcus *** | Dorsal | – |
| **Accessory acromial articular facet** | Absent | Absent |
| ***Humerus*** | | |
| **Humeral head shape *** | Vertically oval | Vertically oval |
| **Olecranon fossa relative size *** | Very large | Very large |
| **Olecranon fossa depth *** | Very deep | Very deep |
| **Septal aperture** | Absent | – |
| **Supracondyloid process** | Absent | – |
| ***Ulna*** | | |
| **Ulnar trochlear notch form *** | Two distinct facets | – |
| **Ulnar trochlear notch orientation *** | Opens superoanteriorly | – |
| ***Os coxae*** | | |
| **Acetabular crease** | Absent | – |
| **Preauricular sulcus** | Shallow hollowing [a] | – |
| ***Femur*** | | |
| **Plaque formation** | Present | – |
| **Exostosis in trochanteric fossa** | Absent | – |
| ***Tibia*** | | |
| **Squatting facets on the tibia *** | Slight [b] | Absent |
| ***Talus*** | | |
| **Squatting facets on the talus *** | Indet. [c] | Indet. [c] |
| **Talar trochlear shape *** | Square | Square |
| **Inferior talar articular surface *** | Continuous | Continuous |

| Trait | Right side | Left side |
|---|---|---|
| **Lateral talar extension** | Absent | Absent |
| ***Calcaneus*** | | |
| **Anterior calcaneal facets *** | Continuous | Continuous |

[a] The right os coxae displays a very shallow hollowing in the area in which a true preauricular sulcus is found.
[b] The distal articular surface extends slightly onto the anterior surface of the distal tibia at the lateral edge; the middle portion of anterior margin is missing and therefore cannot be assessed.
[c] It appears unlikely that squatting facets are present on the talus, but erosion to this area precludes confident assessment.

**Appendix 9** Summary statistics for comparative modern human measurements

Summary statistics are reported below for each measurement collected from the five comparative modern human samples. For measurement definitions and references, see Appendix 6. For measurement protocols, see Appendix 7. All mean values and standard deviations are reported in millimeters except for indices and the femoral neck-shaft angle measurements, the latter of which are reported in degrees. Values are reported for males, females, and the total combined sample for each of the modern human groups. Some of the hand and foot bone measurements for the Levantine sample (Jordan) have combined sample sizes that are greater than the combined number of males and females; these combined sample sizes include unassociated elements of indeterminate sex that were measured to increase sample sizes, since many of the associated skeletal remains were missing hand and foot elements as a result of the secondary burial of these individuals (see Chapter 3). Abbreviations used below include: N (sample size), SD (standard deviation), CV (coefficient of variation), M (male), and F (female).

---

**Appendix 9: Table of Contents**

**Table A9.1** Summary statistics for measurements of the third cervical vertebra
**Table A9.2** Summary statistics for measurements of the fourth cervical vertebra
**Table A9.3** Summary statistics for measurements of the fifth cervical vertebra
**Table A9.4** Summary statistics for measurements of the sixth cervical vertebra
**Table A9.5** Summary statistics for measurements of the seventh cervical vertebra
**Table A9.6** Summary statistics for measurements of the first thoracic vertebra
**Table A9.7** Summary statistics for measurements of the second thoracic vertebra
**Table A9.8** Summary statistics for measurements of the third thoracic vertebra
**Table A9.9** Summary statistics for measurements of the fourth thoracic vertebra
**Table A9.10** Summary statistics for measurements of the fifth thoracic vertebra
**Table A9.11** Summary statistics for measurements of the sixth thoracic vertebra
**Table A9.12** Summary statistics for measurements of the seventh thoracic vertebra
**Table A9.13** Summary statistics for measurements of the eighth thoracic vertebra
**Table A9.14** Summary statistics for measurements of the ninth thoracic vertebra
**Table A9.15** Summary statistics for measurements of the tenth thoracic vertebra
**Table A9.16** Summary statistics for measurements of the eleventh thoracic vertebra
**Table A9.17** Summary statistics for measurements of the twelfth thoracic vertebra
**Table A9.18** Summary statistics for measurements of the first lumbar vertebra

**Table A9.19** Summary statistics for measurements of the second lumbar vertebra
**Table A9.20** Summary statistics for measurements of the third lumbar vertebra
**Table A9.21** Summary statistics for measurements of the fourth lumbar vertebra
**Table A9.22** Summary statistics for measurements of the fifth lumbar vertebra
**Table A9.23** Summary statistics for measurements of the clavicle and scapula
**Table A9.24** Summary statistics for measurements of the humerus
**Table A9.25** Summary statistics for measurements of the radius
**Table A9.26** Summary statistics for measurements of the ulna
**Table A9.27** Summary statistics for measurements of the lunate and triquetral
**Table A9.28** Summary statistics for measurements of the trapezium
**Table A9.29** Summary statistics for measurements of the capitate
**Table A9.30** Summary statistics for measurements of the hamate
**Table A9.31** Summary statistics for measurements of the first metacarpal
**Table A9.32** Summary statistics for measurements of the second metacarpal
**Table A9.33** Summary statistics for measurements of the third metacarpal
**Table A9.34** Summary statistics for measurements of the fourth metacarpal
**Table A9.35** Summary statistics for measurements of the fifth metacarpal
**Table A9.36** Summary statistics for measurements of the terminal hand phalanx of ray I
**Table A9.37** Summary statistics for measurements of the terminal hand phalanx of ray II
**Table A9.38** Summary statistics for measurements of the terminal hand phalanx of ray III
**Table A9.39** Summary statistics for measurements of the terminal hand phalanx of ray IV
**Table A9.40** Summary statistics for measurements of the terminal hand phalanx of ray V
**Table A9.41** Summary statistics for measurements of the sacrum
**Table A9.42** Summary statistics for measurements of the os coxae
**Table A9.43** Summary statistics for measurements of the femur
**Table A9.44** Summary statistics for measurements of the patella
**Table A9.45** Summary statistics for measurements of the tibia
**Table A9.46** Summary statistics for measurements of the fibula
**Table A9.47** Summary statistics for measurements of the talus
**Table A9.48** Summary statistics for measurements of the calcaneus
**Table A9.49** Summary statistics for measurements of the cuboid
**Table A9.50** Summary statistics for measurements of the navicular
**Table A9.51** Summary statistics for measurements of the first metatarsal

**Table A9.52** Summary statistics for measurements of the second metatarsal
**Table A9.53** Summary statistics for measurements of the third metatarsal
**Table A9.54** Summary statistics for measurements of the fourth metatarsal
**Table A9.55** Summary statistics for measurements of the fifth metatarsal
**Table A9.56** Summary statistics for measurements of the terminal foot phalanx of ray I

**Table A9.1** Summary statistics for measurements of the third cervical vertebra

| | | Third cervical vertebra | | | | | | | | | | | | | | | |
|---|---|---|---|---|---|---|---|---|---|---|---|---|---|---|---|---|---|
| | | CER1_VEN_HEI | | | | CER2_SUP_DV | | | | CER3_SUP_TRA | | | | CER4_PED_HEI | | | |
| **Sample** | **Sex** | **N** | **Mean** | **SD** | **CV** | **N** | **Mean** | **SD** | **CV** | **N** | **Mean** | **SD** | **CV** | **N** | **Mean** | **SD** | **CV** |
| Southern Africa (Zulu) | Combined | 30 | 11.7 | 1.3 | 11.0 | 30 | 16.5 | 1.3 | 7.9 | 28 | 20.4 | 1.6 | 8.0 | 30 | 6.3 | 1.0 | 15.6 |
| | M | 14 | 12.4 | 1.5 | 12.0 | 14 | 16.7 | 1.3 | 7.9 | 12 | 21.5 | 1.4 | 6.6 | 14 | 6.8 | 1.1 | 15.4 |
| | F | 16 | 11.2 | 0.8 | 7.0 | 16 | 16.2 | 1.3 | 7.9 | 16 | 19.5 | 1.2 | 6.1 | 16 | 5.8 | 0.6 | 9.9 |
| Northeastern Africa (Egypt) | Combined | 16 | 12.7 | 1.1 | 8.2 | 18 | 15.9 | 1.5 | 9.2 | 15 | 20.2 | 1.3 | 6.3 | 19 | 6.1 | 0.8 | 12.6 |
| | M | 10 | 13.1 | 1.2 | 8.9 | 10 | 16.4 | 1.7 | 10.4 | 9 | 20.9 | 1.0 | 5.0 | 11 | 6.3 | 0.8 | 12.2 |
| | F | 6 | 12.2 | 0.5 | 3.7 | 8 | 15.3 | 0.9 | 5.9 | 6 | 19.2 | 0.9 | 4.6 | 8 | 5.8 | 0.7 | 11.9 |
| Levant (Jordan) | Combined | 9 | 12.4 | 1.2 | 9.6 | 10 | 16.5 | 0.9 | 5.3 | 9 | 20.5 | 2.1 | 10.3 | 10 | 6.3 | 1.0 | 15.4 |
| | M | 4 | 12.9 | 0.9 | 7.2 | 4 | 16.8 | 1.0 | 6.0 | 4 | 21.2 | 1.6 | 7.6 | 4 | 7.0 | 0.9 | 13.2 |
| | F | 5 | 12.1 | 1.4 | 11.3 | 6 | 16.2 | 0.8 | 4.8 | 5 | 20.0 | 2.5 | 12.5 | 6 | 5.8 | 0.7 | 12.8 |
| Western Europe (Portugal) | Combined | 25 | 13.8 | 1.6 | 11.7 | 26 | 15.3 | 1.4 | 9.3 | 24 | 20.4 | 2.0 | 9.7 | 28 | 6.6 | 1.0 | 14.9 |
| | M | 13 | 14.4 | 1.6 | 11.1 | 13 | 16.2 | 1.4 | 8.5 | 13 | 21.4 | 1.9 | 8.9 | 15 | 6.9 | 1.0 | 13.7 |
| | F | 12 | 13.2 | 1.4 | 10.7 | 13 | 14.4 | 0.8 | 5.5 | 11 | 19.2 | 1.3 | 6.7 | 13 | 6.2 | 0.9 | 14.5 |
| North America (CA, U.S.A.) | Combined | 24 | 11.8 | 1.4 | 11.8 | 25 | 16.1 | 1.5 | 9.6 | 24 | 22.7 | 1.4 | 6.3 | 25 | 6.9 | 0.7 | 9.8 |
| | M | 14 | 12.6 | 1.0 | 8.0 | 15 | 16.5 | 1.5 | 9.3 | 14 | 22.8 | 1.8 | 8.0 | 15 | 7.1 | 0.5 | 6.9 |
| | F | 10 | 10.6 | 1.0 | 9.5 | 10 | 15.5 | 1.4 | 9.0 | 10 | 22.6 | 0.6 | 2.8 | 10 | 6.6 | 0.8 | 12.1 |

**Table A9.2** Summary statistics for measurements of the fourth cervical vertebra

| | | Fourth cervical vertebra | | | | | | | | | | | | | | | |
|---|---|---|---|---|---|---|---|---|---|---|---|---|---|---|---|---|---|
| | | CER1_VEN_HEI | | | | CER2_SUP_DV | | | | CER3_SUP_TRA | | | | CER4_PED_HEI | | | |
| **Sample** | **Sex** | **N** | **Mean** | **SD** | **CV** | **N** | **Mean** | **SD** | **CV** | **N** | **Mean** | **SD** | **CV** | **N** | **Mean** | **SD** | **CV** |
| Southern Africa (Zulu) | Combined | 30 | 11.7 | 1.2 | 9.9 | 28 | 16.3 | 1.0 | 6.4 | 27 | 21.2 | 1.8 | 8.6 | 30 | 6.6 | 0.8 | 12.6 |
| | M | 13 | 12.3 | 1.4 | 11.2 | 12 | 16.5 | 0.9 | 5.5 | 12 | 21.9 | 2.2 | 10.1 | 14 | 7.1 | 0.8 | 11.1 |
| | F | 17 | 11.2 | 0.6 | 5.5 | 16 | 16.2 | 1.1 | 7.1 | 15 | 20.6 | 1.2 | 5.8 | 16 | 6.2 | 0.6 | 10.4 |
| Northeastern Africa (Egypt) | Combined | 15 | 11.9 | 0.8 | 6.4 | 15 | 15.9 | 1.3 | 8.2 | 15 | 21.1 | 1.2 | 5.7 | 19 | 6.6 | 0.8 | 12.2 |
| | M | 8 | 12.3 | 0.9 | 7.1 | 7 | 16.8 | 1.5 | 8.6 | 6 | 21.9 | 1.1 | 5.2 | 10 | 6.9 | 0.7 | 9.7 |
| | F | 7 | 11.5 | 0.4 | 3.2 | 8 | 15.2 | 0.4 | 3.0 | 9 | 20.5 | 1.0 | 4.6 | 9 | 6.3 | 0.8 | 13.4 |
| Levant (Jordan) | Combined | 10 | 11.6 | 1.3 | 11.0 | 10 | 16.8 | 0.9 | 5.5 | 10 | 20.8 | 1.7 | 8.4 | 10 | 6.5 | 1.1 | 17.2 |
| | M | 4 | 12.0 | 1.2 | 10.2 | 4 | 17.0 | 0.5 | 3.2 | 4 | 21.9 | 1.5 | 6.7 | 4 | 7.3 | 0.7 | 9.5 |
| | F | 6 | 11.4 | 1.4 | 12.0 | 6 | 16.7 | 1.2 | 7.0 | 6 | 20.0 | 1.5 | 7.7 | 6 | 6.0 | 1.1 | 17.9 |
| Western Europe (Portugal) | Combined | 21 | 13.3 | 1.5 | 11.4 | 18 | 15.9 | 1.4 | 9.0 | 17 | 21.9 | 1.6 | 7.2 | 21 | 6.9 | 0.7 | 9.9 |
| | M | 11 | 14.4 | 1.1 | 7.5 | 11 | 16.7 | 1.2 | 7.3 | 10 | 22.9 | 1.2 | 5.2 | 13 | 7.2 | 0.5 | 7.4 |
| | F | 10 | 12.1 | 0.8 | 6.9 | 7 | 14.8 | 0.9 | 6.4 | 7 | 20.5 | 0.7 | 3.6 | 8 | 6.5 | 0.7 | 10.4 |
| North America (CA, U.S.A.) | Combined | 22 | 12.0 | 1.1 | 9.4 | 23 | 17.0 | 1.3 | 7.8 | 24 | 23.8 | 1.8 | 7.6 | 24 | 7.0 | 0.6 | 9.2 |
| | M | 15 | 12.4 | 1.1 | 8.5 | 15 | 17.4 | 1.3 | 7.7 | 16 | 24.2 | 2.0 | 8.4 | 16 | 7.1 | 0.7 | 9.6 |
| | F | 7 | 11.1 | 0.6 | 5.4 | 8 | 16.1 | 0.8 | 4.8 | 8 | 23.2 | 1.2 | 5.0 | 8 | 6.7 | 0.5 | 7.4 |

**Table A9.3** Summary statistics for measurements of the fifth cervical vertebra

| | | Fifth cervical vertebra | | | | | | | | | | | | | | | |
|---|---|---|---|---|---|---|---|---|---|---|---|---|---|---|---|---|---|
| | | CER1_VEN_HEI | | | | CER2_SUP_DV | | | | CER3_SUP_TRA | | | | CER4_PED_HEI | | | |
| **Sample** | **Sex** | **N** | **Mean** | **SD** | **CV** | **N** | **Mean** | **SD** | **CV** | **N** | **Mean** | **SD** | **CV** | **N** | **Mean** | **SD** | **CV** |
| Southern Africa (Zulu) | Combined | 31 | 11.2 | 1.1 | 9.7 | 28 | 16.0 | 1.0 | 6.2 | 27 | 21.8 | 1.6 | 7.4 | 31 | 6.3 | 0.8 | 12.8 |
| | M | 15 | 11.6 | 1.3 | 11.3 | 12 | 16.3 | 0.8 | 5.1 | 13 | 22.4 | 1.7 | 7.7 | 15 | 6.6 | 0.9 | 14.1 |
| | F | 16 | 10.9 | 0.8 | 6.9 | 16 | 15.8 | 1.1 | 6.8 | 14 | 21.1 | 1.3 | 6.0 | 16 | 5.9 | 0.5 | 7.8 |
| Northeastern Africa (Egypt) | Combined | 14 | 11.7 | 1.2 | 10.0 | 13 | 15.8 | 1.3 | 8.4 | 15 | 22.0 | 1.6 | 7.4 | 18 | 6.1 | 1.1 | 18.7 |
| | M | 8 | 12.2 | 1.0 | 8.4 | 6 | 16.5 | 1.7 | 10.5 | 7 | 22.9 | 1.4 | 6.3 | 9 | 6.3 | 1.0 | 15.6 |
| | F | 6 | 10.9 | 1.0 | 8.7 | 7 | 15.3 | 0.5 | 3.2 | 8 | 21.3 | 1.5 | 7.1 | 9 | 5.8 | 1.3 | 21.8 |
| Levant (Jordan) | Combined | 7 | 10.9 | 1.2 | 11.1 | 10 | 16.0 | 1.3 | 8.2 | 11 | 21.9 | 2.2 | 9.9 | 11 | 6.6 | 0.6 | 9.6 |
| | M | 3 | 11.0 | 1.3 | 12.0 | 4 | 16.5 | 1.2 | 7.4 | 5 | 23.4 | 2.1 | 9.1 | 5 | 7.0 | 0.4 | 6.1 |
| | F | 4 | 10.8 | 1.3 | 12.2 | 6 | 15.7 | 1.4 | 8.8 | 6 | 20.7 | 1.4 | 6.7 | 6 | 6.3 | 0.6 | 9.8 |
| Western Europe (Portugal) | Combined | 19 | 12.5 | 1.4 | 11.3 | 15 | 15.6 | 1.5 | 9.9 | 16 | 21.8 | 1.5 | 6.7 | 24 | 6.3 | 0.8 | 12.9 |
| | M | 9 | 13.5 | 0.9 | 6.7 | 8 | 16.6 | 1.5 | 9.0 | 8 | 22.5 | 1.5 | 6.6 | 12 | 6.8 | 0.8 | 12.2 |
| | F | 10 | 11.5 | 1.0 | 8.9 | 7 | 14.5 | 0.4 | 2.6 | 8 | 21.1 | 1.1 | 5.3 | 12 | 5.9 | 0.5 | 8.4 |
| North America (CA, U.S.A.) | Combined | 21 | 11.3 | 1.0 | 9.3 | 21 | 16.6 | 1.7 | 10.4 | 22 | 25.0 | 1.5 | 6.0 | 24 | 6.6 | 0.8 | 12.6 |
| | M | 13 | 11.5 | 1.0 | 8.5 | 13 | 17.0 | 1.8 | 10.7 | 14 | 25.1 | 1.5 | 6.0 | 15 | 6.6 | 0.9 | 13.6 |
| | F | 8 | 10.9 | 1.1 | 10.0 | 8 | 15.8 | 1.3 | 8.1 | 8 | 24.7 | 1.6 | 6.3 | 9 | 6.5 | 0.7 | 11.2 |

**Table A9.4** Summary statistics for measurements of the sixth cervical vertebra

| | | Sixth cervical vertebra | | | | | | | | | | | | | | | |
|---|---|---|---|---|---|---|---|---|---|---|---|---|---|---|---|---|---|
| | | CER1_VEN_HEI | | | | CER2_SUP_DV | | | | CER3_SUP_TRA | | | | CER4_PED_HEI | | | |
| **Sample** | **Sex** | **N** | **Mean** | **SD** | **CV** | **N** | **Mean** | **SD** | **CV** | **N** | **Mean** | **SD** | **CV** | **N** | **Mean** | **SD** | **CV** |
| Southern Africa (Zulu) | Combined | 31 | 11.3 | 0.9 | 8.0 | 29 | 16.6 | 1.3 | 7.9 | 30 | 23.1 | 1.8 | 7.8 | 32 | 6.3 | 0.8 | 12.4 |
| | M | 14 | 11.5 | 1.2 | 10.3 | 12 | 16.9 | 1.2 | 7.0 | 15 | 24.0 | 1.7 | 7.1 | 15 | 6.5 | 0.9 | 14.5 |
| | F | 17 | 11.1 | 0.5 | 4.9 | 17 | 16.4 | 1.4 | 8.4 | 15 | 22.2 | 1.4 | 6.4 | 17 | 6.1 | 0.6 | 9.2 |
| Northeastern Africa (Egypt) | Combined | 16 | 11.7 | 1.1 | 9.5 | 12 | 16.8 | 1.6 | 9.5 | 16 | 23.7 | 2.0 | 8.3 | 18 | 6.1 | 0.9 | 14.1 |
| | M | 8 | 12.0 | 1.3 | 10.7 | 7 | 17.1 | 1.9 | 11.0 | 7 | 24.8 | 1.3 | 5.1 | 10 | 6.1 | 0.9 | 14.2 |
| | F | 8 | 11.4 | 0.9 | 8.1 | 5 | 16.4 | 1.2 | 7.0 | 9 | 22.9 | 2.1 | 9.2 | 8 | 6.2 | 0.9 | 14.9 |
| Levant (Jordan) | Combined | 9 | 11.5 | 1.4 | 12.3 | 11 | 17.4 | 1.7 | 9.7 | 12 | 23.9 | 1.7 | 7.1 | 11 | 6.4 | 1.0 | 15.8 |
| | M | 4 | 12.0 | 1.4 | 11.5 | 5 | 17.7 | 1.4 | 7.9 | 5 | 24.9 | 1.0 | 4.2 | 5 | 6.7 | 1.3 | 18.8 |
| | F | 5 | 11.1 | 1.4 | 13.0 | 6 | 17.2 | 2.0 | 11.6 | 7 | 23.3 | 1.8 | 7.9 | 6 | 6.1 | 0.7 | 12.1 |
| Western Europe (Portugal) | Combined | 19 | 12.5 | 1.2 | 9.9 | 12 | 16.7 | 1.2 | 7.2 | 12 | 23.7 | 2.1 | 8.8 | 19 | 6.1 | 1.0 | 16.9 |
| | M | 10 | 13.1 | 1.2 | 9.1 | 7 | 17.2 | 1.3 | 7.4 | 7 | 24.4 | 2.4 | 9.7 | 10 | 6.4 | 0.9 | 14.7 |
| | F | 9 | 11.8 | 0.9 | 7.7 | 5 | 16.0 | 0.7 | 4.2 | 5 | 22.8 | 1.4 | 6.0 | 9 | 5.7 | 1.1 | 18.6 |
| North America (CA, U.S.A.) | Combined | 24 | 10.9 | 1.0 | 9.4 | 22 | 17.7 | 1.6 | 9.2 | 24 | 27.1 | 2.6 | 9.6 | 25 | 6.6 | 0.7 | 10.5 |
| | M | 16 | 11.2 | 0.9 | 7.6 | 14 | 18.4 | 1.4 | 7.4 | 15 | 27.2 | 2.5 | 9.3 | 16 | 6.5 | 0.7 | 11.3 |
| | F | 8 | 10.3 | 1.1 | 10.8 | 8 | 16.6 | 1.5 | 8.9 | 9 | 26.8 | 2.8 | 10.6 | 9 | 6.7 | 0.6 | 9.2 |

**Table A9.5** Summary statistics for measurements of the seventh cervical vertebra

| | | Seventh cervical vertebra | | | | | | | | | | | | | | | |
|---|---|---|---|---|---|---|---|---|---|---|---|---|---|---|---|---|---|
| | | CER1_VEN_HEI | | | | CER2_SUP_DV | | | | CER3_SUP_TRA | | | | CER4_PED_HEI | | | |
| **Sample** | **Sex** | **N** | **Mean** | **SD** | **CV** | **N** | **Mean** | **SD** | **CV** | **N** | **Mean** | **SD** | **CV** | **N** | **Mean** | **SD** | **CV** |
| Southern Africa (Zulu) | Combined | 32 | 12.9 | 1.0 | 7.8 | 31 | 17.1 | 1.3 | 7.6 | 30 | 25.0 | 1.9 | 7.4 | 32 | 7.1 | 0.9 | 12.0 |
| | M | 15 | 13.3 | 1.1 | 8.3 | 14 | 17.6 | 1.4 | 7.9 | 14 | 26.0 | 1.6 | 6.1 | 15 | 7.5 | 0.8 | 11.1 |
| | F | 17 | 12.5 | 0.8 | 6.2 | 17 | 16.6 | 1.0 | 6.3 | 16 | 24.1 | 1.6 | 6.7 | 17 | 6.8 | 0.8 | 11.3 |
| Northeastern Africa (Egypt) | Combined | 18 | 13.6 | 1.4 | 10.3 | 17 | 17.6 | 1.4 | 7.7 | 15 | 26.3 | 1.5 | 5.7 | 21 | 6.4 | 0.8 | 12.4 |
| | M | 9 | 13.9 | 1.8 | 12.8 | 8 | 18.1 | 1.7 | 9.2 | 7 | 26.9 | 1.3 | 5.0 | 11 | 6.4 | 0.9 | 13.7 |
| | F | 9 | 13.2 | 0.8 | 6.4 | 9 | 17.2 | 0.9 | 5.2 | 8 | 25.8 | 1.5 | 6.0 | 10 | 6.4 | 0.7 | 11.5 |
| Levant (Jordan) | Combined | 8 | 13.1 | 1.6 | 12.3 | 9 | 18.2 | 1.3 | 7.3 | 11 | 25.4 | 1.4 | 5.6 | 12 | 6.4 | 0.7 | 10.9 |
| | M | 3 | 14.3 | 1.2 | 8.1 | 4 | 18.8 | 1.1 | 6.1 | 5 | 26.5 | 0.7 | 2.5 | 5 | 6.9 | 0.8 | 11.4 |
| | F | 5 | 12.4 | 1.5 | 12.1 | 5 | 17.8 | 1.4 | 7.9 | 6 | 24.5 | 1.3 | 5.1 | 7 | 6.1 | 0.5 | 8.0 |
| Western Europe (Portugal) | Combined | 21 | 14.0 | 1.3 | 9.3 | 14 | 17.5 | 1.5 | 8.6 | 14 | 25.6 | 1.7 | 6.5 | 23 | 6.5 | 0.9 | 13.7 |
| | M | 11 | 14.6 | 1.1 | 7.5 | 8 | 18.2 | 1.3 | 7.0 | 8 | 26.4 | 1.3 | 5.0 | 12 | 7.1 | 0.4 | 6.3 |
| | F | 10 | 13.3 | 1.2 | 8.8 | 6 | 16.6 | 1.4 | 8.3 | 6 | 24.6 | 1.5 | 6.3 | 11 | 5.9 | 0.9 | 15.3 |
| North America (CA, U.S.A.) | Combined | 27 | 13.0 | 1.2 | 8.8 | 22 | 18.8 | 1.5 | 7.8 | 26 | 29.6 | 2.1 | 7.2 | 28 | 7.4 | 0.6 | 8.2 |
| | M | 17 | 13.4 | 1.0 | 7.2 | 13 | 19.4 | 1.2 | 6.4 | 16 | 30.3 | 2.0 | 6.6 | 18 | 7.6 | 0.6 | 7.9 |
| | F | 10 | 12.4 | 1.2 | 9.7 | 9 | 17.9 | 1.4 | 7.7 | 10 | 28.5 | 1.9 | 6.7 | 10 | 7.0 | 0.4 | 6.1 |

**Table A9.6** Summary statistics for measurements of the first thoracic vertebra

| | | First thoracic vertebra | | | | | | | | | | | | | | | |
|---|---|---|---|---|---|---|---|---|---|---|---|---|---|---|---|---|---|
| | | THO1_VEN_HEI | | | | THO2_SUP_DV | | | | THO3_SUP_TRA | | | | THO4_CAN_LEN | | | |
| **Sample** | **Sex** | **N** | **Mean** | **SD** | **CV** | **N** | **Mean** | **SD** | **CV** | **N** | **Mean** | **SD** | **CV** | **N** | **Mean** | **SD** | **CV** |
| Southern Africa (Zulu) | Combined | 30 | 14.9 | 1.0 | 6.5 | 31 | 17.9 | 1.5 | 8.6 | 29 | 26.3 | 2.0 | 7.7 | 30 | 12.8 | 1.2 | 9.8 |
| | M | 14 | 15.3 | 0.9 | 5.6 | 15 | 18.6 | 1.8 | 9.6 | 13 | 27.9 | 1.3 | 4.6 | 15 | 13.1 | 1.3 | 10.2 |
| | F | 16 | 14.5 | 0.9 | 6.5 | 16 | 17.4 | 1.0 | 5.8 | 16 | 25.0 | 1.4 | 5.7 | 15 | 12.4 | 1.1 | 8.7 |
| Northeastern Africa (Egypt) | Combined | 16 | 15.2 | 1.1 | 7.3 | 14 | 18.3 | 1.6 | 8.8 | 16 | 27.5 | 2.1 | 7.8 | 19 | 13.5 | 1.2 | 8.9 |
| | M | 8 | 15.6 | 0.9 | 6.0 | 7 | 19.0 | 1.6 | 8.2 | 8 | 29.0 | 1.9 | 6.4 | 10 | 13.9 | 1.2 | 8.8 |
| | F | 8 | 14.9 | 1.2 | 8.3 | 7 | 17.6 | 1.4 | 8.1 | 8 | 26.1 | 1.2 | 4.6 | 9 | 13.2 | 1.1 | 8.6 |
| Levant (Jordan) | Combined | 8 | 14.3 | 1.7 | 11.8 | 10 | 18.6 | 1.8 | 9.6 | 11 | 27.0 | 1.5 | 5.6 | 11 | 12.6 | 0.7 | 5.3 |
| | M | 2 | 16.6 | 1.2 | 7.3 | 4 | 19.6 | 1.6 | 8.0 | 4 | 28.2 | 1.3 | 4.6 | 4 | 12.8 | 0.8 | 6.0 |
| | F | 6 | 13.6 | 1.0 | 7.7 | 6 | 17.9 | 1.7 | 9.5 | 7 | 26.4 | 1.3 | 4.8 | 7 | 12.6 | 0.7 | 5.3 |
| Western Europe (Portugal) | Combined | 24 | 15.9 | 1.4 | 8.5 | 23 | 18.2 | 1.5 | 8.0 | 23 | 26.7 | 1.8 | 6.8 | 26 | 14.3 | 1.0 | 6.7 |
| | M | 9 | 16.8 | 1.0 | 6.3 | 9 | 19.4 | 1.3 | 6.9 | 12 | 27.5 | 2.1 | 7.7 | 12 | 14.6 | 0.9 | 6.0 |
| | F | 15 | 15.3 | 1.2 | 8.1 | 14 | 17.4 | 1.0 | 5.6 | 11 | 25.9 | 1.1 | 4.1 | 14 | 14.1 | 1.0 | 7.0 |
| North America (CA, U.S.A.) | Combined | 27 | 15.3 | 1.2 | 7.7 | 25 | 19.7 | 1.3 | 6.6 | 28 | 28.9 | 2.0 | 6.8 | 27 | 15.0 | 1.2 | 7.7 |
| | M | 17 | 15.7 | 1.2 | 7.9 | 16 | 20.1 | 1.0 | 5.0 | 17 | 29.9 | 1.7 | 5.8 | 16 | 15.2 | 1.1 | 7.3 |
| | F | 10 | 14.7 | 0.8 | 5.4 | 9 | 18.9 | 1.5 | 7.9 | 11 | 27.4 | 1.3 | 4.6 | 11 | 14.8 | 1.2 | 8.4 |

**Table A9.6, Continued** Summary statistics for measurements of the first thoracic vertebra

| | | First thoracic vertebra | | | | | | | | | | | |
|---|---|---|---|---|---|---|---|---|---|---|---|---|---|
| | | THO5_CAN_BRE | | | | THO6_CAN_IND | | | | THO7_PED_HEI | | | |
| **Sample** | **Sex** | **N** | **Mean** | **SD** | **CV** | **N** | **Mean** | **SD** | **CV** | **N** | **Mean** | **SD** | **CV** |
| Southern Africa (Zulu) | Combined | 30 | 20.2 | 1.8 | 8.7 | 30 | 63.4 | 6.6 | 10.3 | 31 | 9.9 | 1.0 | 10.3 |
| | M | 15 | 21.3 | 1.4 | 6.6 | 15 | 61.8 | 7.1 | 11.5 | 15 | 10.4 | 1.1 | 10.3 |
| | F | 15 | 19.1 | 1.3 | 6.9 | 15 | 65.1 | 5.7 | 8.8 | 16 | 9.4 | 0.7 | 7.6 |
| Northeastern Africa (Egypt) | Combined | 19 | 20.0 | 1.5 | 7.6 | 19 | 67.9 | 5.7 | 8.4 | 19 | 9.4 | 1.1 | 11.3 |
| | M | 10 | 20.5 | 1.6 | 7.7 | 10 | 67.9 | 5.7 | 8.4 | 10 | 9.8 | 0.8 | 7.8 |
| | F | 9 | 19.5 | 1.3 | 6.9 | 9 | 67.9 | 6.0 | 8.8 | 9 | 9.0 | 1.3 | 13.9 |
| Levant (Jordan) | Combined | 11 | 19.8 | 1.2 | 6.0 | 11 | 64.3 | 5.5 | 8.5 | 10 | 8.6 | 0.9 | 10.0 |
| | M | 4 | 19.9 | 1.4 | 6.8 | 4 | 64.3 | 5.7 | 8.8 | 4 | 9.1 | 0.9 | 9.4 |
| | F | 7 | 19.7 | 1.2 | 6.1 | 7 | 64.3 | 5.8 | 9.1 | 6 | 8.3 | 0.7 | 9.0 |
| Western Europe (Portugal) | Combined | 27 | 20.3 | 1.5 | 7.2 | 25 | 70.7 | 4.9 | 7.0 | 27 | 9.2 | 1.1 | 11.9 |
| | M | 12 | 20.9 | 1.5 | 7.3 | 11 | 69.4 | 5.7 | 8.2 | 12 | 9.9 | 1.0 | 10.5 |
| | F | 15 | 19.9 | 1.3 | 6.5 | 14 | 71.7 | 4.2 | 5.8 | 15 | 8.6 | 0.8 | 8.9 |
| North America (CA, U.S.A.) | Combined | 28 | 20.2 | 1.3 | 6.2 | 27 | 74.7 | 5.4 | 7.3 | 29 | 8.8 | 0.7 | 8.2 |
| | M | 16 | 20.2 | 1.3 | 6.5 | 16 | 75.4 | 4.6 | 6.0 | 18 | 9.1 | 0.7 | 8.2 |
| | F | 12 | 20.1 | 1.2 | 6.1 | 11 | 73.8 | 6.6 | 9.0 | 11 | 8.5 | 0.6 | 6.5 |

**Table A9.7** Summary statistics for measurements of the second thoracic vertebra

| | | Second thoracic vertebra | | | | | | | | | | | | | | | |
|---|---|---|---|---|---|---|---|---|---|---|---|---|---|---|---|---|---|
| | | THO1_VEN_HEI | | | | THO2_SUP_DV | | | | THO3_SUP_TRA | | | | THO4_CAN_LEN | | | |
| **Sample** | **Sex** | **N** | **Mean** | **SD** | **CV** | **N** | **Mean** | **SD** | **CV** | **N** | **Mean** | **SD** | **CV** | **N** | **Mean** | **SD** | **CV** |
| Southern Africa (Zulu) | Combined | 29 | 16.6 | 1.2 | 7.1 | 30 | 19.5 | 1.9 | 9.6 | 30 | 26.3 | 2.5 | 9.7 | 31 | 13.0 | 1.3 | 9.9 |
| | M | 13 | 17.4 | 1.0 | 5.7 | 14 | 20.5 | 2.0 | 9.8 | 14 | 27.8 | 1.8 | 6.6 | 16 | 13.5 | 1.5 | 10.9 |
| | F | 16 | 16.0 | 1.0 | 6.0 | 16 | 18.5 | 1.1 | 5.9 | 16 | 24.9 | 2.3 | 9.3 | 15 | 12.5 | 0.9 | 7.0 |
| Northeastern Africa (Egypt) | Combined | 17 | 16.8 | 1.0 | 6.0 | 16 | 20.3 | 1.6 | 8.1 | 20 | 27.2 | 1.9 | 6.9 | 20 | 14.0 | 1.3 | 8.9 |
| | M | 10 | 16.9 | 1.1 | 6.4 | 10 | 20.7 | 1.7 | 8.4 | 11 | 28.4 | 1.4 | 4.9 | 11 | 14.5 | 1.3 | 8.7 |
| | F | 7 | 16.7 | 0.9 | 5.6 | 6 | 19.6 | 1.3 | 6.7 | 9 | 25.9 | 1.5 | 5.6 | 9 | 13.4 | 1.0 | 7.2 |
| Levant (Jordan) | Combined | 10 | 15.9 | 1.3 | 7.9 | 10 | 19.8 | 1.9 | 9.5 | 10 | 26.4 | 1.8 | 6.7 | 10 | 13.9 | 0.6 | 4.6 |
| | M | 4 | 17.0 | 1.0 | 6.1 | 4 | 21.0 | 1.4 | 6.5 | 4 | 28.0 | 1.2 | 4.1 | 4 | 13.9 | 0.3 | 2.1 |
| | F | 6 | 15.1 | 0.8 | 5.1 | 6 | 19.1 | 1.9 | 9.9 | 6 | 25.4 | 1.4 | 5.4 | 6 | 13.9 | 0.8 | 5.9 |
| Western Europe (Portugal) | Combined | 26 | 17.4 | 1.5 | 8.4 | 24 | 19.8 | 1.6 | 8.0 | 27 | 27.0 | 2.0 | 7.2 | 28 | 14.8 | 1.1 | 7.7 |
| | M | 12 | 18.1 | 1.3 | 7.0 | 10 | 20.6 | 1.7 | 8.1 | 12 | 28.0 | 2.0 | 7.3 | 13 | 15.0 | 1.0 | 7.0 |
| | F | 14 | 16.7 | 1.3 | 7.8 | 14 | 19.3 | 1.3 | 6.8 | 15 | 26.2 | 1.5 | 5.9 | 15 | 14.5 | 1.2 | 8.2 |
| North America (CA, U.S.A.) | Combined | 22 | 17.0 | 1.3 | 7.8 | 22 | 21.0 | 1.5 | 7.1 | 23 | 27.8 | 2.1 | 7.5 | 26 | 15.4 | 1.2 | 8.1 |
| | M | 12 | 17.5 | 1.5 | 8.4 | 12 | 21.9 | 0.9 | 4.2 | 12 | 29.0 | 1.6 | 5.4 | 14 | 15.7 | 1.0 | 6.4 |
| | F | 10 | 16.5 | 0.9 | 5.4 | 10 | 19.9 | 1.3 | 6.8 | 11 | 26.4 | 1.7 | 6.4 | 12 | 15.1 | 1.5 | 9.8 |

**Table A9.7, Continued** Summary statistics for measurements of the second thoracic vertebra

| | | Second thoracic vertebra | | | | | | | | | | | |
|---|---|---|---|---|---|---|---|---|---|---|---|---|---|
| | | THO5_CAN_BRE | | | | THO6_CAN_IND | | | | THO7_PED_HEI | | | |
| **Sample** | **Sex** | **N** | **Mean** | **SD** | **CV** | **N** | **Mean** | **SD** | **CV** | **N** | **Mean** | **SD** | **CV** |
| Southern Africa (Zulu) | Combined | 31 | 16.9 | 1.5 | 9.1 | 31 | 77.3 | 7.5 | 9.6 | 32 | 11.5 | 1.2 | 10.5 |
| | M | 16 | 17.8 | 1.5 | 8.2 | 16 | 76.2 | 8.6 | 11.3 | 16 | 12.2 | 1.1 | 8.9 |
| | F | 15 | 16.0 | 1.0 | 6.4 | 15 | 78.6 | 6.0 | 7.7 | 16 | 10.9 | 1.0 | 8.8 |
| Northeastern Africa (Egypt) | Combined | 20 | 17.4 | 1.5 | 8.4 | 20 | 80.8 | 8.2 | 10.1 | 20 | 11.0 | 1.0 | 9.2 |
| | M | 11 | 17.9 | 1.3 | 7.1 | 11 | 81.5 | 9.2 | 11.3 | 11 | 11.2 | 0.8 | 6.8 |
| | F | 9 | 16.8 | 1.5 | 9.0 | 9 | 80.0 | 7.3 | 9.1 | 9 | 10.8 | 1.3 | 11.8 |
| Levant (Jordan) | Combined | 10 | 17.1 | 1.2 | 7.2 | 10 | 81.8 | 7.9 | 9.6 | 10 | 9.9 | 0.9 | 9.5 |
| | M | 4 | 17.7 | 1.4 | 7.9 | 4 | 78.6 | 5.2 | 6.6 | 4 | 10.2 | 1.1 | 10.7 |
| | F | 6 | 16.7 | 1.0 | 6.1 | 6 | 83.9 | 9.1 | 10.8 | 6 | 9.7 | 0.9 | 8.9 |
| Western Europe (Portugal) | Combined | 29 | 17.5 | 1.4 | 8.1 | 28 | 85.0 | 6.8 | 8.0 | 28 | 11.5 | 1.3 | 11.1 |
| | M | 14 | 18.1 | 1.6 | 8.8 | 13 | 83.6 | 7.8 | 9.3 | 13 | 12.3 | 1.3 | 10.5 |
| | F | 15 | 16.9 | 0.9 | 5.6 | 15 | 86.2 | 5.9 | 6.8 | 15 | 10.9 | 0.9 | 8.4 |
| North America (CA, U.S.A.) | Combined | 25 | 17.4 | 1.1 | 6.2 | 25 | 88.7 | 5.7 | 6.5 | 28 | 11.0 | 1.6 | 14.3 |
| | M | 14 | 17.6 | 1.1 | 6.3 | 14 | 89.5 | 5.2 | 5.8 | 16 | 11.4 | 1.6 | 14.3 |
| | F | 11 | 17.2 | 1.1 | 6.2 | 11 | 87.6 | 6.4 | 7.4 | 12 | 10.4 | 1.3 | 12.9 |

**Table A9.8** Summary statistics for measurements of the third thoracic vertebra

| | | Third thoracic vertebra | | | | | | | | | | | | | | | |
|---|---|---|---|---|---|---|---|---|---|---|---|---|---|---|---|---|---|
| | | THO1_VEN_HEI | | | | THO2_SUP_DV | | | | THO3_SUP_TRA | | | | THO4_CAN_LEN | | | |
| **Sample** | **Sex** | **N** | **Mean** | **SD** | **CV** | **N** | **Mean** | **SD** | **CV** | **N** | **Mean** | **SD** | **CV** | **N** | **Mean** | **SD** | **CV** |
| Southern Africa (Zulu) | Combined | 30 | 17.2 | 1.5 | 8.6 | 29 | 21.1 | 1.7 | 7.9 | 30 | 25.8 | 2.4 | 9.5 | 30 | 13.2 | 1.1 | 8.4 |
| | M | 16 | 17.9 | 1.2 | 7.0 | 15 | 22.1 | 1.5 | 6.8 | 16 | 27.1 | 1.5 | 5.7 | 16 | 13.6 | 1.2 | 8.6 |
| | F | 14 | 16.4 | 1.3 | 8.2 | 14 | 20.1 | 1.0 | 5.2 | 14 | 24.3 | 2.5 | 10.2 | 14 | 12.8 | 0.9 | 7.0 |
| Northeastern Africa (Egypt) | Combined | 15 | 17.3 | 0.7 | 4.1 | 15 | 21.7 | 1.7 | 8.0 | 18 | 25.9 | 2.2 | 8.6 | 18 | 14.2 | 1.3 | 9.1 |
| | M | 8 | 17.6 | 0.6 | 3.7 | 8 | 22.8 | 1.2 | 5.2 | 9 | 27.2 | 2.4 | 8.8 | 9 | 14.6 | 1.2 | 8.4 |
| | F | 7 | 16.8 | 0.5 | 3.0 | 7 | 20.4 | 1.3 | 6.3 | 9 | 24.7 | 1.2 | 4.9 | 9 | 13.7 | 1.2 | 9.0 |
| Levant (Jordan) | Combined | 10 | 17.3 | 1.6 | 9.2 | 9 | 21.0 | 1.9 | 8.9 | 10 | 25.7 | 1.8 | 6.9 | 9 | 14.2 | 0.6 | 4.1 |
| | M | 4 | 18.9 | 1.1 | 5.7 | 3 | 22.0 | 0.5 | 2.1 | 4 | 26.8 | 1.3 | 5.0 | 3 | 14.2 | 0.9 | 6.3 |
| | F | 6 | 16.3 | 0.8 | 4.9 | 6 | 20.4 | 2.1 | 10.2 | 6 | 25.0 | 1.8 | 7.1 | 6 | 14.2 | 0.5 | 3.3 |
| Western Europe (Portugal) | Combined | 23 | 17.5 | 1.2 | 6.8 | 24 | 21.7 | 1.7 | 8.0 | 26 | 26.1 | 2.0 | 7.6 | 26 | 14.7 | 1.1 | 7.3 |
| | M | 10 | 18.1 | 1.0 | 5.7 | 10 | 23.0 | 1.7 | 7.3 | 12 | 26.6 | 2.6 | 9.8 | 11 | 15.0 | 1.0 | 6.8 |
| | F | 13 | 17.1 | 1.2 | 6.9 | 14 | 20.7 | 0.9 | 4.5 | 14 | 25.7 | 1.2 | 4.6 | 15 | 14.4 | 1.1 | 7.4 |
| North America (CA, U.S.A.) | Combined | 23 | 17.9 | 1.2 | 6.9 | 20 | 22.1 | 1.5 | 6.9 | 23 | 26.9 | 1.7 | 6.2 | 24 | 15.0 | 1.0 | 6.6 |
| | M | 13 | 18.3 | 1.1 | 5.9 | 11 | 23.1 | 0.9 | 3.8 | 13 | 27.9 | 1.6 | 5.7 | 14 | 15.0 | 0.6 | 4.0 |
| | F | 10 | 17.5 | 1.3 | 7.6 | 9 | 20.9 | 1.2 | 5.7 | 10 | 25.7 | 0.8 | 3.1 | 10 | 15.0 | 1.4 | 9.4 |

**Table A9.8, Continued** Summary statistics for measurements of the third thoracic vertebra

| | | Third thoracic vertebra | | | | | | | | | | | |
|---|---|---|---|---|---|---|---|---|---|---|---|---|---|
| | | THO5_CAN_BRE | | | | THO6_CAN_IND | | | | THO7_PED_HEI | | | |
| **Sample** | **Sex** | **N** | **Mean** | **SD** | **CV** | **N** | **Mean** | **SD** | **CV** | **N** | **Mean** | **SD** | **CV** |
| Southern Africa (Zulu) | Combined | 30 | 15.8 | 1.5 | 9.7 | 30 | 84.4 | 7.6 | 9.0 | 31 | 12.0 | 1.3 | 10.5 |
| | M | 16 | 16.5 | 1.4 | 8.4 | 16 | 82.6 | 7.0 | 8.5 | 16 | 12.7 | 1.2 | 9.7 |
| | F | 14 | 14.9 | 1.2 | 8.0 | 14 | 86.4 | 8.0 | 9.3 | 15 | 11.4 | 0.9 | 8.1 |
| Northeastern Africa (Egypt) | Combined | 18 | 16.5 | 1.4 | 8.5 | 18 | 86.2 | 8.0 | 9.2 | 19 | 11.2 | 1.2 | 10.6 |
| | M | 9 | 17.1 | 1.4 | 8.4 | 9 | 86.2 | 9.7 | 11.2 | 10 | 11.7 | 1.0 | 8.1 |
| | F | 9 | 15.9 | 1.1 | 7.1 | 9 | 86.3 | 6.4 | 7.4 | 9 | 10.7 | 1.2 | 11.5 |
| Levant (Jordan) | Combined | 10 | 16.1 | 1.2 | 7.4 | 9 | 88.4 | 6.8 | 7.7 | 10 | 10.5 | 1.2 | 11.0 |
| | M | 4 | 16.5 | 1.5 | 9.3 | 3 | 85.7 | 4.8 | 5.6 | 4 | 11.2 | 1.4 | 12.7 |
| | F | 6 | 15.9 | 1.0 | 6.1 | 6 | 89.8 | 7.6 | 8.5 | 6 | 10.0 | 0.7 | 7.0 |
| Western Europe (Portugal) | Combined | 28 | 16.3 | 1.3 | 8.1 | 26 | 90.5 | 7.2 | 7.9 | 28 | 12.3 | 1.4 | 11.5 |
| | M | 13 | 16.6 | 1.3 | 8.1 | 11 | 90.8 | 8.2 | 9.1 | 13 | 13.2 | 1.1 | 8.1 |
| | F | 15 | 16.0 | 1.3 | 8.1 | 15 | 90.3 | 6.6 | 7.3 | 15 | 11.5 | 1.2 | 10.5 |
| North America (CA, U.S.A.) | Combined | 24 | 16.9 | 2.9 | 16.9 | 24 | 83.6 | 28.7 | 34.4 | 24 | 11.3 | 1.0 | 9.0 |
| | M | 14 | 17.0 | 3.3 | 19.4 | 14 | 85.1 | 26.4 | 31.0 | 14 | 11.6 | 1.1 | 9.9 |
| | F | 10 | 16.8 | 2.3 | 13.6 | 10 | 81.4 | 33.1 | 40.6 | 10 | 11.0 | 0.7 | 6.4 |

**Table A9.9** Summary statistics for measurements of the fourth thoracic vertebra

| | | Fourth thoracic vertebra | | | | | | | | | | | | | | | |
|---|---|---|---|---|---|---|---|---|---|---|---|---|---|---|---|---|---|
| | | THO1_VEN_HEI | | | | THO2_SUP_DV | | | | THO3_SUP_TRA | | | | THO4_CAN_LEN | | | |
| **Sample** | **Sex** | **N** | **Mean** | **SD** | **CV** | **N** | **Mean** | **SD** | **CV** | **N** | **Mean** | **SD** | **CV** | **N** | **Mean** | **SD** | **CV** |
| Southern Africa (Zulu) | Combined | 30 | 17.1 | 1.4 | 8.2 | 30 | 22.7 | 2.0 | 8.9 | 30 | 25.0 | 2.3 | 9.3 | 30 | 13.4 | 1.1 | 8.5 |
| | M | 14 | 17.8 | 1.3 | 7.3 | 14 | 24.0 | 1.8 | 7.5 | 14 | 26.8 | 1.7 | 6.4 | 15 | 13.5 | 1.3 | 9.5 |
| | F | 16 | 16.4 | 1.2 | 7.1 | 16 | 21.6 | 1.5 | 6.9 | 16 | 23.5 | 1.7 | 7.1 | 15 | 13.2 | 1.0 | 7.5 |
| Northeastern Africa (Egypt) | Combined | 13 | 17.6 | 1.2 | 6.6 | 14 | 22.2 | 1.8 | 8.0 | 14 | 26.6 | 2.1 | 7.9 | 18 | 14.7 | 1.2 | 8.3 |
| | M | 8 | 18.0 | 0.9 | 4.9 | 8 | 22.7 | 1.9 | 8.5 | 8 | 27.5 | 2.4 | 8.7 | 9 | 15.2 | 0.8 | 5.5 |
| | F | 5 | 16.9 | 1.3 | 7.7 | 6 | 21.4 | 1.4 | 6.4 | 6 | 25.4 | 0.8 | 3.1 | 9 | 14.2 | 1.4 | 9.6 |
| Levant (Jordan) | Combined | 10 | 17.2 | 1.5 | 8.5 | 11 | 22.7 | 2.3 | 10.3 | 11 | 25.8 | 2.2 | 8.4 | 11 | 14.2 | 0.9 | 6.2 |
| | M | 4 | 18.7 | 0.7 | 3.7 | 5 | 24.2 | 1.2 | 5.1 | 5 | 27.1 | 0.8 | 2.8 | 5 | 14.0 | 1.3 | 9.3 |
| | F | 6 | 16.2 | 0.8 | 5.0 | 6 | 21.5 | 2.4 | 11.3 | 6 | 24.7 | 2.4 | 9.7 | 6 | 14.4 | 0.4 | 2.6 |
| Western Europe (Portugal) | Combined | 22 | 17.7 | 1.4 | 7.9 | 19 | 23.2 | 2.1 | 9.0 | 23 | 26.2 | 2.0 | 7.5 | 22 | 15.3 | 1.4 | 9.1 |
| | M | 10 | 18.4 | 1.3 | 6.8 | 10 | 24.4 | 1.9 | 7.9 | 12 | 27.2 | 2.1 | 7.6 | 12 | 15.3 | 1.4 | 9.3 |
| | F | 12 | 17.1 | 1.3 | 7.4 | 9 | 21.9 | 1.3 | 6.0 | 11 | 25.1 | 1.1 | 4.6 | 10 | 15.3 | 1.4 | 9.4 |
| North America (CA, U.S.A.) | Combined | 20 | 18.1 | 1.7 | 9.6 | 18 | 23.6 | 1.1 | 4.7 | 19 | 27.1 | 2.8 | 10.3 | 22 | 14.8 | 1.0 | 6.8 |
| | M | 12 | 18.3 | 1.7 | 9.1 | 11 | 24.3 | 0.7 | 3.0 | 11 | 27.4 | 1.8 | 6.4 | 13 | 14.9 | 0.9 | 6.1 |
| | F | 8 | 17.6 | 1.8 | 10.3 | 7 | 22.6 | 0.8 | 3.5 | 8 | 26.7 | 3.9 | 14.7 | 9 | 14.7 | 1.2 | 8.0 |

**Table A9.9, Continued** Summary statistics for measurements of the fourth thoracic vertebra

| | | Fourth thoracic vertebra | | | | | | | | | | | |
|---|---|---|---|---|---|---|---|---|---|---|---|---|---|
| | | THO5_CAN_BRE | | | | THO6_CAN_IND | | | | THO7_PED_HEI | | | |
| **Sample** | **Sex** | **N** | **Mean** | **SD** | **CV** | **N** | **Mean** | **SD** | **CV** | **N** | **Mean** | **SD** | **CV** |
| Southern Africa (Zulu) | Combined | 30 | 15.0 | 1.6 | 10.9 | 30 | 89.6 | 8.9 | 9.9 | 30 | 12.0 | 1.4 | 12.1 |
| | M | 15 | 15.8 | 1.6 | 9.9 | 15 | 85.5 | 7.5 | 8.8 | 15 | 12.9 | 1.2 | 9.2 |
| | F | 15 | 14.2 | 1.3 | 9.0 | 15 | 93.6 | 8.6 | 9.1 | 15 | 11.1 | 1.2 | 10.4 |
| Northeastern Africa (Egypt) | Combined | 18 | 16.0 | 1.5 | 9.1 | 18 | 92.2 | 6.4 | 7.0 | 18 | 11.1 | 1.0 | 9.1 |
| | M | 9 | 16.7 | 1.4 | 8.2 | 9 | 91.5 | 7.7 | 8.4 | 9 | 11.5 | 0.8 | 6.8 |
| | F | 9 | 15.3 | 1.2 | 8.1 | 9 | 92.8 | 5.3 | 5.7 | 9 | 10.7 | 1.1 | 10.3 |
| Levant (Jordan) | Combined | 11 | 15.9 | 1.0 | 6.4 | 11 | 89.7 | 7.6 | 8.4 | 11 | 10.9 | 1.6 | 14.5 |
| | M | 5 | 15.9 | 1.4 | 8.8 | 5 | 88.4 | 10.8 | 12.2 | 5 | 12.2 | 1.3 | 10.8 |
| | F | 6 | 15.9 | 0.7 | 4.5 | 6 | 90.8 | 4.3 | 4.7 | 6 | 9.9 | 0.9 | 9.0 |
| Western Europe (Portugal) | Combined | 24 | 16.1 | 1.6 | 9.8 | 22 | 94.3 | 9.1 | 9.6 | 29 | 11.9 | 1.2 | 10.4 |
| | M | 13 | 16.2 | 1.7 | 10.4 | 12 | 94.7 | 10.8 | 11.4 | 14 | 12.7 | 0.9 | 6.8 |
| | F | 11 | 16.1 | 1.5 | 9.4 | 10 | 93.9 | 7.1 | 7.6 | 15 | 11.2 | 1.2 | 10.2 |
| North America (CA, U.S.A.) | Combined | 22 | 15.6 | 0.8 | 5.2 | 22 | 95.3 | 5.3 | 5.6 | 22 | 10.8 | 0.8 | 7.3 |
| | M | 13 | 15.7 | 0.8 | 4.9 | 13 | 95.2 | 5.5 | 5.8 | 13 | 11.1 | 0.9 | 7.8 |
| | F | 9 | 15.4 | 0.9 | 5.7 | 9 | 95.6 | 5.3 | 5.5 | 9 | 10.4 | 0.5 | 4.5 |

**Table A9.10** Summary statistics for measurements of the fifth thoracic vertebra

| | | Fifth thoracic vertebra | | | | | | | | | | | | | | | |
|---|---|---|---|---|---|---|---|---|---|---|---|---|---|---|---|---|---|
| | | THO1_VEN_HEI | | | | THO2_SUP_DV | | | | THO3_SUP_TRA | | | | THO4_CAN_LEN | | | |
| **Sample** | **Sex** | **N** | **Mean** | **SD** | **CV** | **N** | **Mean** | **SD** | **CV** | **N** | **Mean** | **SD** | **CV** | **N** | **Mean** | **SD** | **CV** |
| Southern Africa (Zulu) | Combined | 30 | 17.1 | 1.4 | 8.3 | 31 | 23.8 | 2.0 | 8.6 | 31 | 25.5 | 2.3 | 8.9 | 30 | 13.6 | 1.0 | 7.4 |
| | M | 14 | 17.8 | 1.3 | 7.3 | 15 | 25.1 | 1.6 | 6.4 | 15 | 27.1 | 1.7 | 6.2 | 15 | 13.9 | 1.2 | 8.5 |
| | F | 16 | 16.4 | 1.2 | 7.3 | 16 | 22.5 | 1.6 | 6.9 | 16 | 24.0 | 1.6 | 6.9 | 15 | 13.3 | 0.8 | 5.7 |
| Northeastern Africa (Egypt) | Combined | 16 | 17.5 | 1.1 | 6.1 | 15 | 24.2 | 2.1 | 8.7 | 12 | 27.3 | 2.6 | 9.4 | 18 | 14.8 | 1.1 | 7.2 |
| | M | 10 | 17.9 | 0.8 | 4.7 | 10 | 24.9 | 2.0 | 8.0 | 9 | 28.1 | 2.5 | 8.8 | 10 | 15.2 | 0.9 | 6.1 |
| | F | 6 | 16.9 | 1.2 | 7.3 | 5 | 22.8 | 1.7 | 7.5 | 3 | 24.9 | 0.8 | 3.0 | 8 | 14.4 | 1.1 | 7.9 |
| Levant (Jordan) | Combined | 9 | 17.9 | 1.8 | 9.8 | 10 | 23.8 | 2.3 | 9.8 | 10 | 26.5 | 2.4 | 9.2 | 11 | 14.3 | 1.6 | 11.4 |
| | M | 4 | 19.5 | 1.1 | 5.6 | 5 | 25.6 | 1.2 | 4.8 | 5 | 28.3 | 0.8 | 3.0 | 5 | 13.8 | 2.4 | 17.5 |
| | F | 5 | 16.7 | 1.0 | 5.8 | 5 | 22.1 | 1.8 | 8.0 | 5 | 24.6 | 1.9 | 7.8 | 6 | 14.6 | 0.5 | 3.7 |
| Western Europe (Portugal) | Combined | 20 | 17.9 | 1.3 | 7.3 | 20 | 24.7 | 2.0 | 8.2 | 21 | 27.0 | 2.1 | 7.9 | 20 | 15.2 | 1.3 | 8.6 |
| | M | 10 | 18.7 | 1.0 | 5.2 | 9 | 26.0 | 2.1 | 8.3 | 10 | 28.6 | 1.6 | 5.6 | 10 | 15.4 | 1.4 | 9.2 |
| | F | 10 | 17.1 | 1.1 | 6.4 | 11 | 23.5 | 1.0 | 4.4 | 11 | 25.5 | 1.3 | 5.1 | 10 | 15.0 | 1.2 | 8.3 |
| North America (CA, U.S.A.) | Combined | 17 | 18.2 | 1.9 | 10.3 | 16 | 24.0 | 1.8 | 7.4 | 18 | 27.3 | 1.9 | 6.8 | 16 | 14.8 | 1.0 | 6.9 |
| | M | 11 | 18.7 | 1.7 | 9.2 | 10 | 24.6 | 1.6 | 6.6 | 11 | 28.5 | 1.2 | 4.3 | 9 | 15.0 | 0.7 | 4.4 |
| | F | 6 | 17.3 | 1.9 | 11.0 | 6 | 22.9 | 1.5 | 6.8 | 7 | 25.5 | 0.7 | 2.8 | 7 | 14.6 | 1.4 | 9.5 |

**Table A9.10, Continued** Summary statistics for measurements of the fifth thoracic vertebra

| | | Fifth thoracic vertebra | | | | | | | | | | | |
|---|---|---|---|---|---|---|---|---|---|---|---|---|---|
| | | THO5_CAN_BRE | | | | THO6_CAN_IND | | | | THO7_PED_HEI | | | |
| **Sample** | **Sex** | **N** | **Mean** | **SD** | **CV** | **N** | **Mean** | **SD** | **CV** | **N** | **Mean** | **SD** | **CV** |
| Southern Africa (Zulu) | Combined | 30 | 14.7 | 1.5 | 10.5 | 30 | 93.2 | 9.1 | 9.8 | 30 | 11.9 | 1.6 | 13.1 |
| | M | 15 | 15.5 | 1.5 | 9.8 | 15 | 90.2 | 7.9 | 8.8 | 15 | 12.8 | 1.4 | 11.3 |
| | F | 15 | 14.0 | 1.2 | 8.6 | 15 | 96.2 | 9.5 | 9.8 | 15 | 11.0 | 1.1 | 10.3 |
| Northeastern Africa (Egypt) | Combined | 18 | 16.3 | 1.3 | 8.3 | 18 | 91.2 | 6.8 | 7.5 | 18 | 11.2 | 0.9 | 8.1 |
| | M | 10 | 16.9 | 1.3 | 7.4 | 10 | 89.9 | 7.6 | 8.4 | 10 | 11.7 | 0.7 | 6.4 |
| | F | 8 | 15.5 | 1.1 | 6.9 | 8 | 92.9 | 5.8 | 6.2 | 8 | 10.6 | 0.8 | 7.2 |
| Levant (Jordan) | Combined | 11 | 16.0 | 1.1 | 7.2 | 11 | 89.7 | 12.0 | 13.4 | 11 | 10.8 | 1.4 | 12.6 |
| | M | 5 | 16.0 | 1.5 | 9.1 | 5 | 87.2 | 17.5 | 20.1 | 5 | 11.9 | 1.0 | 8.8 |
| | F | 6 | 16.0 | 1.0 | 6.0 | 6 | 91.8 | 5.8 | 6.3 | 6 | 9.9 | 0.7 | 7.5 |
| Western Europe (Portugal) | Combined | 21 | 16.2 | 1.9 | 12.0 | 20 | 93.2 | 8.8 | 9.4 | 28 | 12.0 | 1.3 | 10.8 |
| | M | 10 | 16.5 | 2.2 | 13.5 | 10 | 93.9 | 10.1 | 10.8 | 14 | 12.6 | 1.1 | 8.4 |
| | F | 11 | 16.0 | 1.7 | 10.8 | 10 | 92.6 | 7.8 | 8.4 | 14 | 11.3 | 1.2 | 10.6 |
| North America (CA, U.S.A.) | Combined | 18 | 15.4 | 0.8 | 5.0 | 16 | 95.9 | 7.0 | 7.3 | 19 | 10.5 | 0.9 | 9.0 |
| | M | 10 | 15.5 | 0.8 | 4.9 | 9 | 96.3 | 6.9 | 7.1 | 11 | 10.9 | 1.0 | 9.5 |
| | F | 8 | 15.3 | 0.8 | 5.3 | 7 | 95.3 | 7.7 | 8.1 | 8 | 10.1 | 0.6 | 5.9 |

**Table A9.11** Summary statistics for measurements of the sixth thoracic vertebra

| | | Sixth thoracic vertebra | | | | | | | | | | | | | | | |
|---|---|---|---|---|---|---|---|---|---|---|---|---|---|---|---|---|---|
| | | THO1_VEN_HEI | | | | THO2_SUP_DV | | | | THO3_SUP_TRA | | | | THO4_CAN_LEN | | | |
| **Sample** | **Sex** | **N** | **Mean** | **SD** | **CV** | **N** | **Mean** | **SD** | **CV** | **N** | **Mean** | **SD** | **CV** | **N** | **Mean** | **SD** | **CV** |
| Southern Africa (Zulu) | Combined | 31 | 17.3 | 1.6 | 9.3 | 30 | 24.9 | 2.1 | 8.4 | 31 | 26.4 | 2.2 | 8.2 | 30 | 13.7 | 1.0 | 7.6 |
| | M | 15 | 18.1 | 1.6 | 8.8 | 14 | 26.3 | 1.5 | 5.8 | 15 | 27.9 | 1.6 | 5.8 | 15 | 13.9 | 1.2 | 8.7 |
| | F | 16 | 16.6 | 1.3 | 8.0 | 16 | 23.6 | 1.7 | 7.1 | 16 | 24.9 | 1.5 | 6.1 | 15 | 13.5 | 0.9 | 6.3 |
| Northeastern Africa (Egypt) | Combined | 16 | 18.3 | 1.2 | 6.5 | 17 | 25.4 | 2.2 | 8.6 | 13 | 27.8 | 2.7 | 9.8 | 19 | 14.7 | 1.3 | 9.1 |
| | M | 10 | 18.8 | 0.9 | 4.8 | 10 | 26.5 | 1.9 | 7.0 | 7 | 29.2 | 3.0 | 10.2 | 10 | 15.0 | 1.3 | 8.4 |
| | F | 6 | 17.3 | 1.0 | 6.0 | 7 | 24.0 | 1.8 | 7.7 | 6 | 26.1 | 1.2 | 4.4 | 9 | 14.3 | 1.4 | 9.6 |
| Levant (Jordan) | Combined | 8 | 18.2 | 1.6 | 8.9 | 9 | 24.9 | 1.9 | 7.5 | 9 | 27.0 | 2.9 | 10.9 | 9 | 14.9 | 0.9 | 5.7 |
| | M | 3 | 19.8 | 0.6 | 3.2 | 4 | 26.3 | 1.6 | 6.1 | 4 | 29.3 | 1.8 | 6.0 | 4 | 15.2 | 1.1 | 6.9 |
| | F | 5 | 17.3 | 1.2 | 6.9 | 5 | 23.8 | 1.3 | 5.4 | 5 | 25.2 | 2.4 | 9.5 | 5 | 14.7 | 0.7 | 4.9 |
| Western Europe (Portugal) | Combined | 17 | 17.6 | 1.2 | 6.8 | 18 | 26.4 | 2.2 | 8.2 | 21 | 28.6 | 2.1 | 7.3 | 22 | 15.4 | 1.5 | 9.6 |
| | M | 8 | 18.1 | 0.7 | 3.6 | 8 | 27.9 | 2.2 | 7.8 | 10 | 30.0 | 1.9 | 6.4 | 11 | 15.8 | 1.6 | 10.1 |
| | F | 9 | 17.1 | 1.4 | 8.2 | 10 | 25.3 | 1.4 | 5.4 | 11 | 27.3 | 1.3 | 4.6 | 11 | 15.1 | 1.3 | 8.9 |
| North America (CA, U.S.A.) | Combined | 17 | 19.3 | 1.5 | 8.0 | 18 | 25.4 | 1.4 | 5.3 | 18 | 28.5 | 1.9 | 6.8 | 18 | 14.8 | 0.7 | 5.0 |
| | M | 11 | 19.8 | 1.5 | 7.4 | 11 | 25.8 | 1.5 | 5.8 | 11 | 29.7 | 1.2 | 4.2 | 10 | 15.0 | 0.5 | 3.7 |
| | F | 6 | 18.5 | 1.3 | 7.2 | 7 | 24.8 | 0.8 | 3.4 | 7 | 26.5 | 0.9 | 3.5 | 8 | 14.6 | 0.9 | 6.3 |

**Table A9.11, Continued** Summary statistics for measurements of the sixth thoracic vertebra

| | | Sixth thoracic vertebra | | | | | | | | | | | |
|---|---|---|---|---|---|---|---|---|---|---|---|---|---|
| | | THO5_CAN_BRE | | | | THO6_CAN_IND | | | | THO7_PED_HEI | | | |
| **Sample** | **Sex** | **N** | **Mean** | **SD** | **CV** | **N** | **Mean** | **SD** | **CV** | **N** | **Mean** | **SD** | **CV** |
| Southern Africa (Zulu) | Combined | 30 | 14.7 | 1.6 | 11.0 | 30 | 94.1 | 10.9 | 11.6 | 30 | 12.0 | 1.4 | 11.9 |
| | M | 15 | 15.5 | 1.6 | 10.4 | 15 | 90.1 | 9.5 | 10.5 | 15 | 12.8 | 1.3 | 9.8 |
| | F | 15 | 13.9 | 1.2 | 8.5 | 15 | 98.1 | 11.2 | 11.4 | 15 | 11.1 | 1.0 | 9.4 |
| Northeastern Africa (Egypt) | Combined | 19 | 16.2 | 1.3 | 8.1 | 19 | 91.2 | 7.9 | 8.6 | 19 | 11.3 | 1.1 | 9.6 |
| | M | 10 | 16.9 | 1.0 | 6.1 | 10 | 89.4 | 8.0 | 9.0 | 10 | 11.8 | 1.0 | 8.5 |
| | F | 9 | 15.4 | 1.1 | 7.4 | 9 | 93.3 | 7.6 | 8.1 | 9 | 10.8 | 1.0 | 9.3 |
| Levant (Jordan) | Combined | 9 | 15.9 | 1.1 | 7.1 | 9 | 93.8 | 7.4 | 7.9 | 9 | 10.9 | 1.5 | 13.8 |
| | M | 4 | 16.2 | 1.5 | 9.0 | 4 | 94.2 | 8.2 | 8.7 | 4 | 12.0 | 1.4 | 11.7 |
| | F | 5 | 15.8 | 1.0 | 6.1 | 5 | 93.5 | 7.7 | 8.3 | 5 | 10.0 | 0.9 | 9.1 |
| Western Europe (Portugal) | Combined | 23 | 16.1 | 1.9 | 11.7 | 22 | 95.6 | 8.2 | 8.6 | 27 | 12.2 | 1.3 | 10.9 |
| | M | 11 | 16.4 | 2.2 | 13.1 | 11 | 96.4 | 7.1 | 7.4 | 14 | 13.1 | 0.9 | 7.0 |
| | F | 12 | 15.9 | 1.6 | 10.4 | 11 | 94.7 | 9.4 | 9.9 | 13 | 11.3 | 1.0 | 9.1 |
| North America (CA, U.S.A.) | Combined | 19 | 15.5 | 1.0 | 6.4 | 18 | 96.2 | 6.0 | 6.2 | 19 | 11.0 | 0.8 | 7.6 |
| | M | 11 | 15.8 | 0.9 | 5.6 | 10 | 95.8 | 6.4 | 6.7 | 11 | 11.4 | 0.9 | 7.9 |
| | F | 8 | 15.1 | 1.0 | 6.8 | 8 | 96.7 | 5.8 | 6.0 | 8 | 10.6 | 0.5 | 4.5 |

**Table A9.12** Summary statistics for measurements of the seventh thoracic vertebra

| | | Seventh thoracic vertebra | | | | | | | | | | | | | | | |
|---|---|---|---|---|---|---|---|---|---|---|---|---|---|---|---|---|---|
| | | THO1_VEN_HEI | | | | THO2_SUP_DV | | | | THO3_SUP_TRA | | | | THO4_CAN_LEN | | | |
| **Sample** | **Sex** | **N** | **Mean** | **SD** | **CV** | **N** | **Mean** | **SD** | **CV** | **N** | **Mean** | **SD** | **CV** | **N** | **Mean** | **SD** | **CV** |
| Southern Africa (Zulu) | Combined | 31 | 17.8 | 1.5 | 8.5 | 30 | 26.0 | 2.3 | 8.8 | 30 | 27.7 | 2.3 | 8.1 | 30 | 13.7 | 1.0 | 7.6 |
| | M | 15 | 18.5 | 1.5 | 8.3 | 14 | 27.5 | 1.8 | 6.7 | 14 | 29.3 | 1.6 | 5.6 | 15 | 14.1 | 1.1 | 7.9 |
| | F | 16 | 17.2 | 1.2 | 6.9 | 16 | 24.7 | 1.9 | 7.6 | 16 | 26.3 | 1.8 | 6.7 | 15 | 13.4 | 0.9 | 6.6 |
| Northeastern Africa (Egypt) | Combined | 14 | 18.8 | 1.0 | 5.4 | 16 | 26.6 | 2.4 | 8.9 | 13 | 29.2 | 2.1 | 7.2 | 18 | 14.8 | 1.2 | 8.0 |
| | M | 10 | 19.1 | 0.8 | 4.1 | 10 | 27.6 | 2.3 | 8.2 | 9 | 29.9 | 2.1 | 7.0 | 10 | 15.1 | 1.2 | 7.8 |
| | F | 4 | 18.1 | 1.3 | 7.4 | 6 | 25.0 | 1.5 | 5.9 | 4 | 27.6 | 0.9 | 3.4 | 8 | 14.5 | 1.2 | 8.2 |
| Levant (Jordan) | Combined | 8 | 18.5 | 1.5 | 8.3 | 8 | 25.7 | 1.9 | 7.6 | 9 | 28.5 | 3.0 | 10.6 | 9 | 15.1 | 0.7 | 4.8 |
| | M | 3 | 20.3 | 0.4 | 2.1 | 4 | 27.0 | 1.7 | 6.4 | 4 | 30.8 | 2.1 | 6.9 | 4 | 15.3 | 0.9 | 6.0 |
| | F | 5 | 17.5 | 0.6 | 3.2 | 4 | 24.5 | 1.2 | 5.0 | 5 | 26.6 | 2.3 | 8.5 | 5 | 15.0 | 0.6 | 4.1 |
| Western Europe (Portugal) | Combined | 16 | 18.3 | 1.4 | 7.9 | 16 | 27.5 | 2.3 | 8.2 | 18 | 29.5 | 1.8 | 6.0 | 19 | 15.1 | 1.2 | 8.0 |
| | M | 8 | 18.7 | 0.8 | 4.1 | 8 | 28.9 | 2.1 | 7.2 | 8 | 31.0 | 1.5 | 5.0 | 9 | 15.0 | 0.9 | 6.2 |
| | F | 8 | 17.9 | 1.9 | 10.6 | 8 | 26.2 | 1.6 | 6.1 | 10 | 28.4 | 0.9 | 3.3 | 10 | 15.2 | 1.5 | 9.6 |
| North America (CA, U.S.A.) | Combined | 18 | 19.7 | 1.3 | 6.6 | 18 | 26.2 | 1.7 | 6.5 | 17 | 29.7 | 2.4 | 8.1 | 19 | 14.6 | 0.9 | 6.0 |
| | M | 10 | 20.0 | 1.4 | 7.1 | 11 | 26.9 | 1.7 | 6.5 | 11 | 31.1 | 1.5 | 4.8 | 11 | 14.8 | 0.7 | 4.8 |
| | F | 8 | 19.3 | 1.1 | 5.6 | 7 | 25.2 | 1.1 | 4.2 | 6 | 27.1 | 1.3 | 4.7 | 8 | 14.4 | 1.0 | 7.3 |

**Table A9.12, Continued** Summary statistics for measurements of the seventh thoracic vertebra

| | | Seventh thoracic vertebra | | | | | | | | | | | |
|---|---|---|---|---|---|---|---|---|---|---|---|---|---|
| | | THO5_CAN_BRE | | | | THO6_CAN_IND | | | | THO7_PED_HEI | | | |
| **Sample** | **Sex** | **N** | **Mean** | **SD** | **CV** | **N** | **Mean** | **SD** | **CV** | **N** | **Mean** | **SD** | **CV** |
| Southern Africa (Zulu) | Combined | 30 | 14.8 | 1.7 | 11.5 | 30 | 93.9 | 10.1 | 10.8 | 30 | 12.3 | 1.4 | 11.5 |
| | M | 15 | 15.6 | 1.7 | 10.9 | 15 | 90.9 | 9.5 | 10.5 | 15 | 13.1 | 1.3 | 9.8 |
| | F | 15 | 13.9 | 1.2 | 8.7 | 15 | 96.8 | 10.2 | 10.5 | 15 | 11.6 | 1.2 | 10.0 |
| Northeastern Africa (Egypt) | Combined | 18 | 16.3 | 1.4 | 8.5 | 18 | 91.2 | 7.2 | 7.9 | 18 | 11.7 | 1.0 | 8.9 |
| | M | 10 | 16.9 | 1.2 | 6.9 | 10 | 89.6 | 7.9 | 8.8 | 10 | 12.0 | 1.2 | 9.9 |
| | F | 8 | 15.6 | 1.3 | 8.6 | 8 | 93.2 | 6.2 | 6.6 | 8 | 11.3 | 0.7 | 5.9 |
| Levant (Jordan) | Combined | 10 | 16.2 | 1.3 | 8.2 | 9 | 94.2 | 6.9 | 7.4 | 10 | 11.2 | 1.6 | 14.5 |
| | M | 4 | 16.1 | 1.5 | 9.0 | 4 | 95.0 | 5.4 | 5.7 | 4 | 12.3 | 1.5 | 12.1 |
| | F | 6 | 16.3 | 1.4 | 8.4 | 5 | 93.5 | 8.5 | 9.1 | 6 | 10.4 | 1.3 | 12.3 |
| Western Europe (Portugal) | Combined | 21 | 15.8 | 1.4 | 9.0 | 19 | 94.8 | 6.7 | 7.1 | 26 | 12.4 | 1.4 | 11.1 |
| | M | 9 | 15.7 | 1.1 | 7.1 | 9 | 95.6 | 6.6 | 6.9 | 13 | 13.4 | 1.0 | 7.3 |
| | F | 12 | 15.8 | 1.7 | 10.5 | 10 | 94.1 | 7.1 | 7.6 | 13 | 11.5 | 1.0 | 8.7 |
| North America (CA, U.S.A.) | Combined | 19 | 15.5 | 1.1 | 7.1 | 19 | 94.7 | 5.2 | 5.5 | 22 | 11.1 | 0.9 | 8.6 |
| | M | 11 | 15.9 | 0.8 | 5.1 | 11 | 93.7 | 4.7 | 5.1 | 13 | 11.2 | 1.0 | 8.6 |
| | F | 8 | 15.0 | 1.3 | 8.5 | 8 | 96.0 | 5.9 | 6.1 | 9 | 10.8 | 0.9 | 8.6 |

**Table A9.13** Summary statistics for measurements of the eighth thoracic vertebra

| | | Eighth thoracic vertebra | | | | | | | | | | | | | | | |
|---|---|---|---|---|---|---|---|---|---|---|---|---|---|---|---|---|---|
| | | THO1_VEN_HEI | | | | THO2_SUP_DV | | | | THO3_SUP_TRA | | | | THO4_CAN_LEN | | | |
| **Sample** | **Sex** | **N** | **Mean** | **SD** | **CV** | **N** | **Mean** | **SD** | **CV** | **N** | **Mean** | **SD** | **CV** | **N** | **Mean** | **SD** | **CV** |
| Southern Africa (Zulu) | Combined | 30 | 18.6 | 1.6 | 8.7 | 29 | 26.4 | 2.3 | 8.8 | 29 | 28.8 | 2.5 | 8.6 | 29 | 13.5 | 1.1 | 8.1 |
| | M | 14 | 19.5 | 1.7 | 8.7 | 13 | 27.9 | 1.9 | 6.9 | 13 | 30.5 | 2.1 | 6.7 | 14 | 14.0 | 1.1 | 7.8 |
| | F | 16 | 17.9 | 1.1 | 6.4 | 16 | 25.3 | 2.0 | 7.8 | 16 | 27.4 | 1.9 | 6.8 | 15 | 13.0 | 0.9 | 6.8 |
| Northeastern Africa (Egypt) | Combined | 15 | 19.3 | 1.5 | 8.0 | 15 | 27.5 | 2.1 | 7.6 | 13 | 30.4 | 2.1 | 6.9 | 18 | 14.8 | 1.2 | 8.0 |
| | M | 8 | 20.0 | 1.2 | 5.9 | 9 | 28.3 | 1.9 | 6.8 | 8 | 31.2 | 2.0 | 6.5 | 10 | 15.2 | 1.0 | 6.3 |
| | F | 7 | 18.4 | 1.5 | 8.3 | 6 | 26.3 | 1.9 | 7.4 | 5 | 29.1 | 1.6 | 5.6 | 8 | 14.3 | 1.3 | 9.1 |
| Levant (Jordan) | Combined | 9 | 18.5 | 1.9 | 10.3 | 10 | 27.4 | 2.4 | 8.7 | 9 | 29.3 | 2.7 | 9.2 | 10 | 14.8 | 0.9 | 5.8 |
| | M | 3 | 20.7 | 0.4 | 2.0 | 4 | 29.4 | 2.3 | 7.7 | 4 | 31.2 | 1.6 | 5.2 | 3 | 15.7 | 0.9 | 5.6 |
| | F | 6 | 17.4 | 1.1 | 6.5 | 6 | 26.1 | 1.4 | 5.4 | 5 | 27.7 | 2.4 | 8.7 | 7 | 14.4 | 0.5 | 3.8 |
| Western Europe (Portugal) | Combined | 16 | 18.7 | 1.6 | 8.3 | 15 | 29.0 | 2.4 | 8.3 | 15 | 31.6 | 1.7 | 5.4 | 21 | 15.0 | 1.1 | 7.6 |
| | M | 8 | 19.2 | 1.5 | 7.8 | 8 | 30.3 | 2.4 | 7.9 | 8 | 32.5 | 1.7 | 5.1 | 10 | 15.0 | 1.0 | 6.6 |
| | F | 8 | 18.2 | 1.5 | 8.5 | 7 | 27.6 | 1.7 | 6.1 | 7 | 30.5 | 1.0 | 3.4 | 11 | 15.0 | 1.3 | 8.7 |
| North America (CA, U.S.A.) | Combined | 22 | 20.6 | 1.4 | 7.0 | 20 | 27.1 | 2.0 | 7.2 | 21 | 31.3 | 2.6 | 8.3 | 20 | 14.6 | 1.0 | 6.8 |
| | M | 14 | 21.0 | 1.3 | 6.2 | 12 | 27.7 | 2.0 | 7.2 | 14 | 32.6 | 2.0 | 6.0 | 12 | 14.8 | 0.7 | 4.9 |
| | F | 8 | 19.9 | 1.5 | 7.4 | 8 | 26.3 | 1.7 | 6.6 | 7 | 28.8 | 1.7 | 5.9 | 8 | 14.3 | 1.3 | 9.0 |

**Table A9.13, Continued** Summary statistics for measurements of the eighth thoracic vertebra

| | | Eighth thoracic vertebra | | | | | | | | | | | |
|---|---|---|---|---|---|---|---|---|---|---|---|---|---|
| | | THO5_CAN_BRE | | | | THO6_CAN_IND | | | | THO7_PED_HEI | | | |
| **Sample** | **Sex** | **N** | **Mean** | **SD** | **CV** | **N** | **Mean** | **SD** | **CV** | **N** | **Mean** | **SD** | **CV** |
| Southern Africa (Zulu) | Combined | 29 | 15.1 | 1.9 | 12.3 | 29 | 90.5 | 10.5 | 11.6 | 30 | 12.7 | 1.4 | 10.8 |
| | M | 14 | 16.2 | 1.7 | 10.2 | 14 | 86.8 | 8.6 | 9.9 | 14 | 13.4 | 1.3 | 9.4 |
| | F | 15 | 14.0 | 1.4 | 9.7 | 15 | 93.9 | 11.2 | 11.9 | 16 | 12.0 | 1.1 | 9.1 |
| Northeastern Africa (Egypt) | Combined | 18 | 16.4 | 1.5 | 9.3 | 18 | 90.7 | 8.2 | 9.0 | 18 | 12.2 | 1.3 | 10.9 |
| | M | 10 | 16.9 | 1.2 | 6.9 | 10 | 90.2 | 7.4 | 8.2 | 10 | 12.9 | 1.4 | 10.6 |
| | F | 8 | 15.7 | 1.7 | 11.0 | 8 | 91.4 | 9.6 | 10.5 | 8 | 11.4 | 0.8 | 7.0 |
| Levant (Jordan) | Combined | 11 | 16.3 | 1.2 | 7.3 | 10 | 91.4 | 5.8 | 6.3 | 11 | 11.3 | 1.3 | 11.7 |
| | M | 4 | 16.6 | 1.5 | 9.1 | 3 | 95.2 | 5.8 | 6.1 | 4 | 12.6 | 0.9 | 7.3 |
| | F | 7 | 16.1 | 1.1 | 6.5 | 7 | 89.8 | 5.4 | 6.0 | 7 | 10.6 | 0.8 | 7.8 |
| Western Europe (Portugal) | Combined | 21 | 16.1 | 1.5 | 9.4 | 21 | 93.6 | 5.8 | 6.2 | 26 | 12.5 | 1.3 | 10.1 |
| | M | 10 | 16.3 | 1.4 | 8.8 | 10 | 92.5 | 4.4 | 4.7 | 13 | 13.3 | 0.7 | 5.5 |
| | F | 11 | 15.9 | 1.6 | 10.1 | 11 | 94.6 | 6.9 | 7.3 | 13 | 11.7 | 1.2 | 10.3 |
| North America (CA, U.S.A.) | Combined | 21 | 15.6 | 1.0 | 6.2 | 20 | 93.7 | 5.1 | 5.5 | 23 | 11.6 | 0.9 | 7.9 |
| | M | 13 | 15.8 | 0.7 | 4.7 | 12 | 94.2 | 4.7 | 5.0 | 14 | 11.8 | 1.0 | 8.4 |
| | F | 8 | 15.4 | 1.3 | 8.4 | 8 | 93.0 | 6.0 | 6.4 | 9 | 11.4 | 0.8 | 7.2 |

**Table A9.14** Summary statistics for measurements of the ninth thoracic vertebra

| | | Ninth thoracic vertebra | | | | | | | | | | | | | | | |
|---|---|---|---|---|---|---|---|---|---|---|---|---|---|---|---|---|---|
| | | THO1_VEN_HEI | | | | THO2_SUP_DV | | | | THO3_SUP_TRA | | | | THO4_CAN_LEN | | | |
| **Sample** | **Sex** | **N** | **Mean** | **SD** | **CV** | **N** | **Mean** | **SD** | **CV** | **N** | **Mean** | **SD** | **CV** | **N** | **Mean** | **SD** | **CV** |
| Southern Africa (Zulu) | Combined | 29 | 19.3 | 1.6 | 8.2 | 28 | 26.8 | 2.6 | 9.8 | 26 | 30.1 | 2.5 | 8.2 | 28 | 13.6 | 1.0 | 7.5 |
| | M | 13 | 19.8 | 1.8 | 9.2 | 12 | 28.7 | 2.2 | 7.8 | 12 | 31.7 | 2.2 | 6.9 | 13 | 13.9 | 1.0 | 7.4 |
| | F | 16 | 18.9 | 1.3 | 6.7 | 16 | 25.4 | 1.9 | 7.6 | 14 | 28.8 | 1.9 | 6.6 | 15 | 13.3 | 0.9 | 7.1 |
| Northeastern Africa (Egypt) | Combined | 17 | 20.7 | 1.5 | 7.4 | 16 | 28.3 | 2.9 | 10.1 | 14 | 31.4 | 2.4 | 7.7 | 18 | 14.6 | 1.3 | 8.7 |
| | M | 9 | 21.5 | 1.0 | 4.7 | 9 | 29.6 | 2.9 | 9.7 | 7 | 32.6 | 2.6 | 7.9 | 10 | 15.0 | 1.0 | 6.6 |
| | F | 8 | 19.8 | 1.5 | 7.7 | 7 | 26.7 | 2.0 | 7.3 | 7 | 30.2 | 1.7 | 5.5 | 8 | 14.0 | 1.4 | 9.9 |
| Levant (Jordan) | Combined | 12 | 19.8 | 1.5 | 7.6 | 11 | 28.1 | 2.8 | 10.0 | 11 | 30.7 | 2.6 | 8.5 | 11 | 14.2 | 0.7 | 5.1 |
| | M | 4 | 21.5 | 0.6 | 2.9 | 4 | 30.6 | 2.5 | 8.3 | 4 | 32.7 | 1.7 | 5.1 | 4 | 14.4 | 0.6 | 4.3 |
| | F | 8 | 19.0 | 1.1 | 5.6 | 7 | 26.6 | 1.8 | 6.8 | 7 | 29.6 | 2.4 | 8.2 | 7 | 14.1 | 0.8 | 5.7 |
| Western Europe (Portugal) | Combined | 15 | 19.6 | 1.4 | 7.2 | 14 | 29.5 | 2.7 | 9.3 | 14 | 33.5 | 2.5 | 7.6 | 21 | 15.2 | 1.2 | 8.0 |
| | M | 7 | 20.2 | 1.3 | 6.4 | 7 | 31.4 | 2.6 | 8.2 | 7 | 35.3 | 2.4 | 6.8 | 11 | 15.3 | 1.4 | 9.0 |
| | F | 8 | 19.1 | 1.4 | 7.2 | 7 | 27.6 | 1.2 | 4.4 | 7 | 31.8 | 1.0 | 3.0 | 10 | 15.0 | 1.1 | 7.2 |
| North America (CA, U.S.A.) | Combined | 24 | 21.0 | 1.7 | 8.0 | 23 | 28.0 | 2.2 | 8.0 | 22 | 32.4 | 2.6 | 8.1 | 18 | 14.3 | 1.1 | 7.6 |
| | M | 14 | 21.9 | 1.3 | 5.8 | 14 | 28.8 | 2.1 | 7.1 | 13 | 34.0 | 2.1 | 6.1 | 11 | 14.7 | 0.8 | 5.1 |
| | F | 10 | 19.8 | 1.4 | 7.0 | 9 | 26.7 | 2.0 | 7.5 | 9 | 30.2 | 1.6 | 5.3 | 7 | 13.8 | 1.3 | 9.7 |

**Table A9.14, Continued** Summary statistics for measurements of the ninth thoracic vertebra

| | | Ninth thoracic vertebra | | | | | | | | | | | |
|---|---|---|---|---|---|---|---|---|---|---|---|---|---|
| | | THO5_CAN_BRE | | | | THO6_CAN_IND | | | | THO7_PED_HEI | | | |
| **Sample** | **Sex** | **N** | **Mean** | **SD** | **CV** | **N** | **Mean** | **SD** | **CV** | **N** | **Mean** | **SD** | **CV** |
| Southern Africa (Zulu) | Combined | 28 | 15.3 | 1.9 | 12.5 | 28 | 89.9 | 10.5 | 11.7 | 28 | 13.5 | 1.4 | 10.6 |
| | M | 13 | 16.3 | 1.7 | 10.6 | 13 | 86.0 | 8.3 | 9.7 | 13 | 14.1 | 1.2 | 8.8 |
| | F | 15 | 14.4 | 1.6 | 11.4 | 15 | 93.2 | 11.3 | 12.1 | 15 | 12.9 | 1.4 | 10.7 |
| Northeastern Africa (Egypt) | Combined | 18 | 16.4 | 1.6 | 9.7 | 18 | 89.4 | 7.3 | 8.1 | 18 | 13.0 | 1.3 | 9.8 |
| | M | 10 | 17.0 | 1.4 | 8.1 | 10 | 89.2 | 8.0 | 9.0 | 10 | 13.6 | 1.1 | 8.4 |
| | F | 8 | 15.6 | 1.6 | 10.2 | 8 | 89.8 | 6.8 | 7.6 | 8 | 12.3 | 1.1 | 8.9 |
| Levant (Jordan) | Combined | 10 | 16.6 | 1.2 | 7.0 | 10 | 86.1 | 7.5 | 8.7 | 11 | 12.6 | 1.6 | 12.9 |
| | M | 4 | 17.0 | 1.5 | 9.1 | 4 | 85.1 | 6.7 | 7.9 | 4 | 13.4 | 0.5 | 4.1 |
| | F | 6 | 16.3 | 0.9 | 5.4 | 6 | 86.8 | 8.5 | 9.8 | 7 | 12.1 | 1.9 | 15.5 |
| Western Europe (Portugal) | Combined | 22 | 16.5 | 1.8 | 10.7 | 21 | 92.3 | 6.0 | 6.5 | 25 | 13.6 | 1.5 | 11.3 |
| | M | 11 | 16.7 | 2.2 | 13.2 | 11 | 92.2 | 6.9 | 7.5 | 11 | 14.5 | 1.2 | 8.5 |
| | F | 11 | 16.2 | 1.2 | 7.5 | 10 | 92.4 | 5.2 | 5.6 | 14 | 12.9 | 1.3 | 10.4 |
| North America (CA, U.S.A.) | Combined | 21 | 15.1 | 1.0 | 6.5 | 18 | 95.5 | 6.3 | 6.6 | 24 | 12.4 | 0.7 | 6.0 |
| | M | 11 | 15.3 | 0.6 | 3.8 | 11 | 96.3 | 5.3 | 5.5 | 14 | 12.6 | 0.7 | 5.8 |
| | F | 10 | 14.9 | 1.3 | 8.7 | 7 | 94.3 | 7.8 | 8.3 | 10 | 12.1 | 0.7 | 5.5 |

**Table A9.15** Summary statistics for measurements of the tenth thoracic vertebra

| | | Tenth thoracic vertebra | | | | | | | | | | | | | | | |
|---|---|---|---|---|---|---|---|---|---|---|---|---|---|---|---|---|---|
| | | THO1_VEN_HEI | | | | THO2_SUP_DV | | | | THO3_SUP_TRA | | | | THO4_CAN_LEN | | | |
| **Sample** | **Sex** | **N** | **Mean** | **SD** | **CV** | **N** | **Mean** | **SD** | **CV** | **N** | **Mean** | **SD** | **CV** | **N** | **Mean** | **SD** | **CV** |
| Southern Africa (Zulu) | Combined | 29 | 20.8 | 1.6 | 7.5 | 29 | 27.7 | 2.6 | 9.2 | 28 | 31.8 | 2.9 | 9.1 | 28 | 13.7 | 1.3 | 9.6 |
| | M | 14 | 21.6 | 1.5 | 7.0 | 14 | 29.4 | 2.0 | 6.8 | 14 | 33.6 | 2.4 | 7.2 | 14 | 13.9 | 1.3 | 9.2 |
| | F | 15 | 20.0 | 1.2 | 6.0 | 15 | 26.0 | 1.8 | 7.1 | 14 | 29.9 | 2.1 | 6.9 | 14 | 13.4 | 1.3 | 10.0 |
| Northeastern Africa (Egypt) | Combined | 16 | 21.2 | 1.8 | 8.4 | 13 | 28.0 | 2.2 | 7.8 | 15 | 33.8 | 2.1 | 6.3 | 17 | 14.4 | 1.3 | 8.7 |
| | M | 8 | 22.5 | 1.0 | 4.3 | 8 | 29.0 | 1.7 | 5.8 | 9 | 34.8 | 2.1 | 6.0 | 10 | 15.0 | 1.0 | 6.7 |
| | F | 8 | 19.8 | 1.3 | 6.5 | 5 | 26.5 | 2.2 | 8.3 | 6 | 32.2 | 1.0 | 3.0 | 7 | 13.5 | 1.1 | 8.1 |
| Levant (Jordan) | Combined | 10 | 20.3 | 1.2 | 6.1 | 10 | 27.5 | 1.5 | 5.6 | 11 | 32.2 | 2.6 | 8.1 | 12 | 14.1 | 1.0 | 6.7 |
| | M | 2 | 22.0 | 0.1 | 0.3 | 3 | 28.8 | 0.7 | 2.3 | 4 | 34.2 | 1.4 | 4.0 | 4 | 14.5 | 1.1 | 7.5 |
| | F | 8 | 19.8 | 1.0 | 4.8 | 7 | 26.9 | 1.5 | 5.4 | 7 | 31.1 | 2.5 | 8.0 | 8 | 14.0 | 0.9 | 6.5 |
| Western Europe (Portugal) | Combined | 18 | 21.3 | 1.7 | 8.0 | 16 | 29.6 | 2.8 | 9.6 | 18 | 35.4 | 3.3 | 9.2 | 20 | 14.9 | 0.8 | 5.4 |
| | M | 10 | 21.9 | 1.3 | 6.0 | 8 | 31.4 | 2.7 | 8.5 | 9 | 38.0 | 2.5 | 6.5 | 11 | 15.0 | 0.7 | 4.6 |
| | F | 8 | 20.5 | 1.9 | 9.3 | 8 | 27.8 | 1.7 | 5.9 | 9 | 32.9 | 1.2 | 3.5 | 9 | 14.8 | 1.0 | 6.4 |
| North America (CA, U.S.A.) | Combined | 23 | 21.1 | 1.7 | 7.9 | 20 | 29.8 | 2.4 | 8.1 | 24 | 34.9 | 3.3 | 9.3 | 20 | 14.8 | 0.9 | 6.3 |
| | M | 13 | 21.8 | 1.5 | 7.0 | 11 | 30.9 | 1.9 | 6.2 | 14 | 36.8 | 2.4 | 6.5 | 12 | 15.0 | 0.7 | 4.4 |
| | F | 10 | 20.1 | 1.4 | 6.8 | 9 | 28.4 | 2.3 | 8.1 | 10 | 32.2 | 2.2 | 7.0 | 8 | 14.5 | 1.2 | 8.4 |

**Table A9.15, Continued** Summary statistics for measurements of the tenth thoracic vertebra

| | | Tenth thoracic vertebra | | | | | | | | | | | |
|---|---|---|---|---|---|---|---|---|---|---|---|---|---|
| | | THO5_CAN_BRE | | | | THO6_CAN_IND | | | | THO7_PED_HEI | | | |
| **Sample** | **Sex** | **N** | **Mean** | **SD** | **CV** | **N** | **Mean** | **SD** | **CV** | **N** | **Mean** | **SD** | **CV** |
| Southern Africa (Zulu) | Combined | 28 | 15.5 | 1.9 | 12.2 | 28 | 89.2 | 10.9 | 12.3 | 28 | 15.5 | 1.3 | 8.3 |
| | M | 14 | 16.4 | 1.5 | 9.3 | 14 | 85.1 | 8.7 | 10.2 | 14 | 16.0 | 1.3 | 8.1 |
| | F | 14 | 14.6 | 1.8 | 12.5 | 14 | 93.2 | 11.7 | 12.6 | 14 | 14.9 | 1.0 | 7.0 |
| Northeastern Africa (Egypt) | Combined | 18 | 16.6 | 1.4 | 8.4 | 17 | 87.0 | 6.6 | 7.6 | 18 | 15.1 | 1.2 | 7.8 |
| | M | 10 | 17.1 | 1.3 | 7.5 | 10 | 87.8 | 7.9 | 9.0 | 10 | 15.2 | 1.0 | 6.6 |
| | F | 8 | 15.9 | 1.3 | 8.3 | 7 | 85.7 | 4.2 | 4.9 | 8 | 14.9 | 1.4 | 9.5 |
| Levant (Jordan) | Combined | 12 | 16.6 | 1.4 | 8.4 | 12 | 85.8 | 7.6 | 8.9 | 12 | 14.0 | 1.3 | 9.6 |
| | M | 4 | 17.0 | 1.8 | 10.9 | 4 | 85.6 | 7.6 | 8.9 | 4 | 14.8 | 0.8 | 5.1 |
| | F | 8 | 16.4 | 1.2 | 7.3 | 8 | 85.8 | 8.2 | 9.5 | 8 | 13.6 | 1.4 | 10.6 |
| Western Europe (Portugal) | Combined | 21 | 16.2 | 1.5 | 9.0 | 20 | 92.4 | 7.9 | 8.6 | 26 | 15.8 | 1.8 | 11.6 |
| | M | 11 | 16.2 | 1.8 | 11.0 | 11 | 93.7 | 9.3 | 10.0 | 12 | 17.0 | 1.3 | 7.8 |
| | F | 10 | 16.2 | 1.1 | 6.7 | 9 | 90.9 | 6.0 | 6.6 | 14 | 14.7 | 1.5 | 10.4 |
| North America (CA, U.S.A.) | Combined | 22 | 15.3 | 1.0 | 6.3 | 20 | 97.5 | 6.8 | 7.0 | 24 | 14.8 | 0.9 | 6.3 |
| | M | 12 | 15.4 | 0.6 | 3.7 | 12 | 97.9 | 6.1 | 6.2 | 14 | 15.1 | 0.9 | 6.1 |
| | F | 10 | 15.1 | 1.3 | 8.6 | 8 | 97.0 | 8.2 | 8.5 | 10 | 14.4 | 0.8 | 5.8 |

**Table A9.16** Summary statistics for measurements of the eleventh thoracic vertebra

| | | Eleventh thoracic vertebra | | | | | | | | | | | | | | | |
|---|---|---|---|---|---|---|---|---|---|---|---|---|---|---|---|---|---|
| | | THO1_VEN_HEI | | | | THO2_SUP_DV | | | | THO3_SUP_TRA | | | | THO4_CAN_LEN | | | |
| **Sample** | **Sex** | **N** | **Mean** | **SD** | **CV** | **N** | **Mean** | **SD** | **CV** | **N** | **Mean** | **SD** | **CV** | **N** | **Mean** | **SD** | **CV** |
| Southern Africa (Zulu) | Combined | 33 | 21.2 | 1.5 | 7.0 | 33 | 28.7 | 2.2 | 7.8 | 31 | 35.1 | 2.9 | 8.3 | 32 | 14.1 | 1.4 | 9.9 |
| | M | 16 | 21.9 | 1.5 | 6.7 | 16 | 30.4 | 1.6 | 5.1 | 15 | 37.1 | 2.5 | 6.8 | 16 | 14.2 | 1.5 | 10.5 |
| | F | 17 | 20.5 | 1.2 | 5.7 | 17 | 27.1 | 1.4 | 5.3 | 16 | 33.2 | 1.7 | 5.2 | 16 | 14.1 | 1.3 | 9.6 |
| Northeastern Africa (Egypt) | Combined | 16 | 22.1 | 1.3 | 5.7 | 14 | 29.1 | 2.1 | 7.2 | 13 | 37.0 | 2.0 | 5.3 | 18 | 14.8 | 1.3 | 8.9 |
| | M | 8 | 22.9 | 1.0 | 4.2 | 7 | 29.8 | 1.4 | 4.7 | 8 | 37.6 | 2.3 | 6.1 | 9 | 15.1 | 1.0 | 6.3 |
| | F | 8 | 21.2 | 0.9 | 4.4 | 7 | 28.4 | 2.5 | 8.9 | 5 | 36.0 | 0.7 | 1.9 | 9 | 14.5 | 1.6 | 11.1 |
| Levant (Jordan) | Combined | 11 | 20.3 | 1.7 | 8.1 | 11 | 28.7 | 2.5 | 8.6 | 12 | 34.9 | 2.7 | 7.8 | 13 | 14.4 | 1.3 | 8.8 |
| | M | 3 | 21.3 | 1.8 | 8.4 | 4 | 30.8 | 2.2 | 7.2 | 4 | 37.1 | 1.6 | 4.3 | 4 | 14.4 | 1.0 | 7.1 |
| | F | 8 | 19.9 | 1.5 | 7.7 | 7 | 27.5 | 1.7 | 6.2 | 8 | 33.8 | 2.5 | 7.5 | 9 | 14.4 | 1.4 | 9.9 |
| Western Europe (Portugal) | Combined | 18 | 21.9 | 1.9 | 8.9 | 14 | 31.1 | 3.0 | 9.6 | 13 | 37.5 | 3.2 | 8.4 | 20 | 15.4 | 0.8 | 5.1 |
| | M | 10 | 22.4 | 1.3 | 5.8 | 8 | 32.6 | 3.2 | 9.9 | 7 | 38.9 | 3.6 | 9.3 | 11 | 15.4 | 0.7 | 4.6 |
| | F | 8 | 21.3 | 2.5 | 11.7 | 6 | 29.3 | 1.2 | 4.0 | 6 | 35.9 | 1.6 | 4.5 | 9 | 15.4 | 0.9 | 6.1 |
| North America (CA, U.S.A.) | Combined | 19 | 21.1 | 1.7 | 8.1 | 18 | 32.1 | 2.3 | 7.1 | 22 | 37.6 | 2.8 | 7.4 | 17 | 14.9 | 0.9 | 5.9 |
| | M | 13 | 21.5 | 1.7 | 7.9 | 12 | 32.6 | 2.1 | 6.5 | 13 | 39.3 | 1.9 | 4.8 | 12 | 15.2 | 0.6 | 3.8 |
| | F | 6 | 20.4 | 1.6 | 7.7 | 6 | 31.1 | 2.4 | 7.8 | 9 | 35.0 | 1.7 | 4.8 | 5 | 14.1 | 1.0 | 7.3 |

**Table A9.16, Continued** Summary statistics for measurements of the eleventh thoracic vertebra

| | | Eleventh thoracic vertebra | | | | | | | | | | | |
|---|---|---|---|---|---|---|---|---|---|---|---|---|---|
| | | THO5_CAN_BRE | | | | THO6_CAN_IND | | | | THO7_PED_HEI | | | |
| **Sample** | **Sex** | **N** | **Mean** | **SD** | **CV** | **N** | **Mean** | **SD** | **CV** | **N** | **Mean** | **SD** | **CV** |
| Southern Africa (Zulu) | Combined | 32 | 16.2 | 2.0 | 12.3 | 32 | 88.3 | 10.9 | 12.4 | 32 | 16.6 | 1.4 | 8.4 |
| | M | 16 | 16.8 | 1.9 | 11.5 | 16 | 85.2 | 10.2 | 11.9 | 16 | 17.3 | 1.2 | 6.7 |
| | F | 16 | 15.6 | 1.9 | 12.4 | 16 | 91.3 | 11.1 | 12.2 | 16 | 15.8 | 1.2 | 7.9 |
| Northeastern Africa (Egypt) | Combined | 18 | 18.1 | 1.5 | 8.5 | 18 | 81.8 | 6.5 | 8.0 | 18 | 17.1 | 1.2 | 7.0 |
| | M | 9 | 18.3 | 1.3 | 6.8 | 9 | 82.7 | 4.8 | 5.9 | 9 | 17.6 | 0.9 | 5.1 |
| | F | 9 | 17.9 | 1.8 | 10.2 | 9 | 80.9 | 8.1 | 10.0 | 9 | 16.6 | 1.3 | 7.8 |
| Levant (Jordan) | Combined | 13 | 17.3 | 1.9 | 11.0 | 13 | 83.3 | 8.2 | 9.8 | 13 | 15.6 | 1.4 | 9.2 |
| | M | 4 | 17.6 | 2.4 | 13.9 | 4 | 82.4 | 8.8 | 10.7 | 4 | 16.6 | 1.0 | 6.3 |
| | F | 9 | 17.2 | 1.8 | 10.3 | 9 | 83.8 | 8.4 | 10.1 | 9 | 15.2 | 1.4 | 9.5 |
| Western Europe (Portugal) | Combined | 20 | 17.3 | 1.6 | 9.1 | 20 | 89.7 | 8.9 | 10.0 | 27 | 17.6 | 1.8 | 10.4 |
| | M | 11 | 17.3 | 1.6 | 9.3 | 11 | 89.4 | 9.1 | 10.2 | 14 | 18.6 | 1.5 | 8.1 |
| | F | 9 | 17.3 | 1.6 | 9.5 | 9 | 89.9 | 9.2 | 10.3 | 13 | 16.6 | 1.6 | 9.4 |
| North America (CA, U.S.A.) | Combined | 20 | 16.2 | 1.0 | 6.1 | 16 | 92.5 | 6.1 | 6.6 | 22 | 16.4 | 1.5 | 9.3 |
| | M | 12 | 16.2 | 0.7 | 4.1 | 11 | 93.6 | 6.1 | 6.5 | 14 | 16.8 | 1.3 | 7.6 |
| | F | 8 | 16.1 | 1.4 | 8.6 | 5 | 89.9 | 5.8 | 6.4 | 8 | 15.7 | 1.8 | 11.4 |

**Table A9.17** Summary statistics for measurements of the twelfth thoracic vertebra

| | | Twelfth thoracic vertebra | | | | | | | | | | | | | | | |
|---|---|---|---|---|---|---|---|---|---|---|---|---|---|---|---|---|---|
| | | THO1_VEN_HEI | | | | THO2_SUP_DV | | | | THO3_SUP_TRA | | | | THO4_CAN_LEN | | | |
| **Sample** | **Sex** | **N** | **Mean** | **SD** | **CV** | **N** | **Mean** | **SD** | **CV** | **N** | **Mean** | **SD** | **CV** | **N** | **Mean** | **SD** | **CV** |
| Southern Africa (Zulu) | Combined | 32 | 22.2 | 1.6 | 7.4 | 32 | 29.8 | 2.3 | 7.6 | 32 | 38.5 | 3.0 | 7.8 | 31 | 15.0 | 1.5 | 10.0 |
| | M | 15 | 22.8 | 1.9 | 8.2 | 15 | 31.4 | 1.7 | 5.3 | 15 | 40.6 | 2.5 | 6.3 | 15 | 15.3 | 1.6 | 10.8 |
| | F | 17 | 21.7 | 1.3 | 5.8 | 17 | 28.5 | 1.8 | 6.4 | 17 | 36.6 | 2.0 | 5.4 | 16 | 14.7 | 1.3 | 9.1 |
| Northeastern Africa (Egypt) | Combined | 18 | 23.4 | 1.4 | 6.0 | 17 | 30.9 | 2.1 | 6.7 | 17 | 39.4 | 1.9 | 4.7 | 19 | 15.7 | 1.4 | 8.6 |
| | M | 9 | 24.0 | 1.3 | 5.5 | 8 | 31.7 | 1.1 | 3.5 | 9 | 40.4 | 1.5 | 3.8 | 10 | 16.3 | 1.0 | 6.2 |
| | F | 9 | 22.7 | 1.2 | 5.5 | 9 | 30.1 | 2.5 | 8.2 | 8 | 38.3 | 1.6 | 4.1 | 9 | 15.0 | 1.5 | 9.7 |
| Levant (Jordan) | Combined | 13 | 22.8 | 1.4 | 6.1 | 13 | 30.5 | 2.3 | 7.6 | 13 | 37.8 | 3.0 | 8.0 | 12 | 15.5 | 1.2 | 7.9 |
| | M | 4 | 23.8 | 0.3 | 1.3 | 5 | 31.9 | 2.0 | 6.4 | 5 | 40.6 | 1.8 | 4.5 | 5 | 15.5 | 0.8 | 5.2 |
| | F | 9 | 22.4 | 1.5 | 6.6 | 8 | 29.7 | 2.2 | 7.4 | 8 | 36.0 | 2.2 | 6.1 | 7 | 15.5 | 1.5 | 9.9 |
| Western Europe (Portugal) | Combined | 17 | 23.0 | 2.1 | 9.3 | 14 | 32.0 | 3.8 | 11.9 | 14 | 41.1 | 2.7 | 6.6 | 23 | 16.8 | 1.0 | 6.1 |
| | M | 9 | 23.8 | 1.1 | 4.8 | 8 | 33.6 | 4.0 | 11.9 | 8 | 42.9 | 2.0 | 4.7 | 11 | 16.9 | 0.9 | 5.3 |
| | F | 8 | 22.1 | 2.7 | 12.1 | 6 | 29.8 | 2.3 | 7.6 | 6 | 38.8 | 1.5 | 4.0 | 12 | 16.7 | 1.2 | 6.9 |
| North America (CA, U.S.A.) | Combined | 23 | 23.3 | 1.8 | 7.7 | 21 | 33.4 | 2.7 | 8.0 | 24 | 41.5 | 3.2 | 7.6 | 22 | 16.4 | 1.1 | 6.7 |
| | M | 13 | 23.7 | 1.6 | 6.6 | 11 | 34.8 | 2.3 | 6.7 | 15 | 43.2 | 2.7 | 6.1 | 14 | 16.5 | 1.1 | 6.6 |
| | F | 10 | 22.9 | 2.0 | 8.8 | 10 | 31.8 | 2.2 | 6.9 | 9 | 38.6 | 1.3 | 3.3 | 8 | 16.3 | 1.2 | 7.3 |

**Table A9.17, Continued** Summary statistics for measurements of the twelfth thoracic vertebra

| | | Twelfth thoracic vertebra | | | | | | | | | | | |
|---|---|---|---|---|---|---|---|---|---|---|---|---|---|
| | | THO5_CAN_BRE | | | | THO6_CAN_IND | | | | THO7_PED_HEI | | | |
| **Sample** | **Sex** | **N** | **Mean** | **SD** | **CV** | **N** | **Mean** | **SD** | **CV** | **N** | **Mean** | **SD** | **CV** |
| Southern Africa (Zulu) | Combined | 31 | 18.4 | 2.2 | 12.2 | 31 | 82.0 | 9.4 | 11.5 | 31 | 16.7 | 1.6 | 9.8 |
| | M | 15 | 19.0 | 2.4 | 12.5 | 15 | 81.1 | 9.4 | 11.6 | 15 | 17.6 | 0.7 | 4.0 |
| | F | 16 | 17.9 | 2.0 | 11.4 | 16 | 82.9 | 9.6 | 11.6 | 16 | 15.9 | 1.9 | 11.6 |
| Northeastern Africa (Egypt) | Combined | 20 | 20.8 | 1.8 | 8.4 | 19 | 75.3 | 6.1 | 8.1 | 20 | 16.0 | 1.4 | 8.6 |
| | M | 10 | 21.1 | 1.3 | 6.1 | 10 | 77.2 | 3.9 | 5.0 | 10 | 16.4 | 1.2 | 7.5 |
| | F | 10 | 20.5 | 2.1 | 10.4 | 9 | 73.3 | 7.6 | 10.4 | 10 | 15.6 | 1.4 | 9.2 |
| Levant (Jordan) | Combined | 12 | 19.7 | 1.8 | 9.4 | 12 | 79.3 | 7.3 | 9.2 | 12 | 15.7 | 1.7 | 10.6 |
| | M | 5 | 20.0 | 2.5 | 12.3 | 5 | 78.5 | 10.7 | 13.6 | 5 | 16.9 | 1.0 | 5.8 |
| | F | 7 | 19.5 | 1.4 | 7.4 | 7 | 79.9 | 4.6 | 5.7 | 7 | 14.9 | 1.6 | 10.7 |
| Western Europe (Portugal) | Combined | 25 | 20.3 | 1.7 | 8.6 | 23 | 84.1 | 8.3 | 9.8 | 27 | 17.1 | 1.6 | 9.5 |
| | M | 13 | 20.8 | 1.9 | 9.0 | 11 | 82.9 | 7.7 | 9.3 | 14 | 17.8 | 1.5 | 8.3 |
| | F | 12 | 19.7 | 1.5 | 7.5 | 12 | 85.2 | 9.0 | 10.5 | 13 | 16.4 | 1.5 | 8.9 |
| North America (CA, U.S.A.) | Combined | 25 | 18.5 | 1.3 | 7.1 | 22 | 88.4 | 8.2 | 9.3 | 26 | 16.6 | 1.5 | 9.0 |
| | M | 14 | 18.6 | 1.2 | 6.7 | 14 | 88.8 | 8.5 | 9.6 | 15 | 17.2 | 1.1 | 6.5 |
| | F | 11 | 18.4 | 1.5 | 8.0 | 8 | 87.7 | 8.2 | 9.3 | 11 | 15.8 | 1.6 | 10.1 |

**Table A9.18** Summary statistics for measurements of the first lumbar vertebra

| | | First lumbar vertebra | | | | | | | | | | | | | | | |
|---|---|---|---|---|---|---|---|---|---|---|---|---|---|---|---|---|---|
| | | LUM1_VEN_HEI | | | | LUM2_SUP_DV | | | | LUM3_SUP_TRA | | | | LUM4_PED_HEI | | | |
| **Sample** | **Sex** | **N** | **Mean** | **SD** | **CV** | **N** | **Mean** | **SD** | **CV** | **N** | **Mean** | **SD** | **CV** | **N** | **Mean** | **SD** | **CV** |
| Southern Africa (Zulu) | Combined | 33 | 24.1 | 1.6 | 6.6 | 33 | 31.0 | 2.4 | 7.7 | 33 | 40.9 | 3.3 | 8.1 | 33 | 15.9 | 1.7 | 10.8 |
| | M | 16 | 24.0 | 1.8 | 7.6 | 16 | 32.7 | 1.6 | 4.8 | 16 | 43.3 | 2.5 | 5.8 | 16 | 16.9 | 1.4 | 8.1 |
| | F | 17 | 24.2 | 1.4 | 5.7 | 17 | 29.3 | 1.7 | 5.9 | 17 | 38.7 | 2.3 | 5.8 | 17 | 14.9 | 1.4 | 9.1 |
| Northeastern Africa (Egypt) | Combined | 19 | 24.9 | 1.1 | 4.3 | 18 | 32.5 | 2.5 | 7.6 | 18 | 41.6 | 2.7 | 6.4 | 21 | 14.7 | 1.1 | 7.3 |
| | M | 10 | 25.2 | 1.0 | 3.9 | 10 | 33.4 | 2.4 | 7.2 | 10 | 43.1 | 2.5 | 5.7 | 11 | 15.0 | 1.2 | 7.9 |
| | F | 9 | 24.5 | 1.1 | 4.4 | 8 | 31.4 | 2.1 | 6.8 | 8 | 39.8 | 1.6 | 4.0 | 10 | 14.5 | 0.9 | 6.4 |
| Levant (Jordan) | Combined | 13 | 24.2 | 1.4 | 5.7 | 13 | 31.4 | 2.5 | 8.0 | 11 | 39.9 | 3.1 | 7.8 | 13 | 14.1 | 1.0 | 6.9 |
| | M | 5 | 24.9 | 1.8 | 7.4 | 5 | 33.8 | 1.4 | 4.0 | 5 | 42.3 | 2.5 | 5.9 | 5 | 14.6 | 1.1 | 7.8 |
| | F | 8 | 23.8 | 0.9 | 4.0 | 8 | 29.9 | 1.7 | 5.7 | 6 | 38.0 | 2.1 | 5.6 | 8 | 13.8 | 0.7 | 5.4 |
| Western Europe (Portugal) | Combined | 22 | 25.1 | 1.8 | 7.2 | 18 | 33.8 | 3.6 | 10.6 | 18 | 44.2 | 3.2 | 7.3 | 29 | 15.8 | 1.5 | 9.4 |
| | M | 13 | 25.1 | 1.6 | 6.5 | 11 | 35.3 | 3.6 | 10.3 | 13 | 45.5 | 2.7 | 5.9 | 15 | 16.6 | 1.4 | 8.4 |
| | F | 9 | 25.1 | 2.2 | 8.6 | 7 | 31.4 | 1.9 | 6.0 | 5 | 40.9 | 2.0 | 4.9 | 14 | 14.9 | 1.1 | 7.1 |
| North America (CA, U.S.A.) | Combined | 27 | 25.3 | 1.7 | 6.6 | 24 | 34.5 | 2.4 | 6.9 | 25 | 43.6 | 4.1 | 9.4 | 29 | 15.4 | 1.4 | 8.8 |
| | M | 14 | 25.8 | 1.9 | 7.4 | 12 | 35.9 | 2.2 | 6.0 | 13 | 46.9 | 2.4 | 5.2 | 15 | 15.9 | 1.1 | 7.2 |
| | F | 13 | 24.8 | 1.3 | 5.1 | 12 | 33.1 | 1.7 | 5.1 | 12 | 40.1 | 1.9 | 4.6 | 14 | 14.8 | 1.4 | 9.3 |

**Table A9.19** Summary statistics for measurements of the second lumbar vertebra

| | | Second lumbar vertebra | | | | | | | | | | | | | | | |
|---|---|---|---|---|---|---|---|---|---|---|---|---|---|---|---|---|---|
| | | LUM1_VEN_HEI | | | | LUM2_SUP_DV | | | | LUM3_SUP_TRA | | | | LUM4_PED_HEI | | | |
| **Sample** | **Sex** | **N** | **Mean** | **SD** | **CV** | **N** | **Mean** | **SD** | **CV** | **N** | **Mean** | **SD** | **CV** | **N** | **Mean** | **SD** | **CV** |
| Southern Africa (Zulu) | Combined | 31 | 24.8 | 1.7 | 6.7 | 32 | 32.1 | 2.8 | 8.8 | 32 | 42.9 | 3.7 | 8.6 | 32 | 15.4 | 1.6 | 10.1 |
| | M | 14 | 24.8 | 1.9 | 7.7 | 15 | 34.3 | 1.9 | 5.4 | 15 | 45.8 | 2.5 | 5.6 | 15 | 16.3 | 1.6 | 9.7 |
| | F | 17 | 24.9 | 1.5 | 6.0 | 17 | 30.2 | 2.1 | 6.8 | 17 | 40.3 | 2.3 | 5.7 | 17 | 14.6 | 1.1 | 7.3 |
| Northeastern Africa (Egypt) | Combined | 19 | 25.8 | 1.5 | 5.8 | 15 | 33.8 | 3.0 | 8.8 | 16 | 44.6 | 3.0 | 6.6 | 21 | 14.0 | 1.1 | 7.9 |
| | M | 9 | 26.3 | 1.2 | 4.6 | 8 | 35.1 | 2.6 | 7.4 | 8 | 46.6 | 2.5 | 5.3 | 10 | 14.2 | 1.3 | 9.3 |
| | F | 10 | 25.3 | 1.7 | 6.5 | 7 | 32.4 | 2.9 | 8.9 | 8 | 42.6 | 1.8 | 4.3 | 11 | 13.8 | 0.9 | 6.4 |
| Levant (Jordan) | Combined | 13 | 25.0 | 1.7 | 6.9 | 13 | 32.9 | 2.4 | 7.4 | 11 | 42.3 | 3.0 | 7.2 | 13 | 13.9 | 1.6 | 11.7 |
| | M | 5 | 26.1 | 1.6 | 6.3 | 5 | 34.7 | 1.3 | 3.9 | 3 | 45.4 | 0.8 | 1.7 | 4 | 15.2 | 0.5 | 3.0 |
| | F | 8 | 24.4 | 1.4 | 5.9 | 8 | 31.7 | 2.3 | 7.2 | 8 | 41.1 | 2.7 | 6.6 | 9 | 13.4 | 1.7 | 12.7 |
| Western Europe (Portugal) | Combined | 23 | 26.3 | 1.9 | 7.2 | 19 | 33.6 | 3.4 | 10.1 | 20 | 45.4 | 3.0 | 6.7 | 29 | 14.6 | 1.4 | 9.9 |
| | M | 13 | 26.8 | 1.0 | 3.7 | 9 | 35.8 | 3.2 | 8.8 | 12 | 46.9 | 2.5 | 5.4 | 15 | 15.2 | 1.5 | 9.7 |
| | F | 10 | 25.6 | 2.6 | 10.0 | 10 | 31.7 | 2.2 | 7.1 | 8 | 43.2 | 2.3 | 5.4 | 14 | 14.1 | 1.2 | 8.6 |
| North America (CA, U.S.A.) | Combined | 26 | 26.1 | 1.7 | 6.6 | 27 | 34.9 | 2.7 | 7.7 | 28 | 46.5 | 4.0 | 8.6 | 30 | 14.8 | 1.0 | 6.7 |
| | M | 14 | 26.4 | 1.9 | 7.4 | 15 | 36.5 | 2.2 | 6.0 | 16 | 49.4 | 2.5 | 5.1 | 18 | 14.9 | 1.0 | 6.6 |
| | F | 12 | 25.8 | 1.4 | 5.5 | 12 | 33.0 | 1.8 | 5.6 | 12 | 42.7 | 1.8 | 4.3 | 12 | 14.5 | 1.0 | 6.9 |

**Table A9.20** Summary statistics for measurements of the third lumbar vertebra

| | | Third lumbar vertebra | | | | | | | | | | | | | | | |
|---|---|---|---|---|---|---|---|---|---|---|---|---|---|---|---|---|---|
| | | LUM1_VEN_HEI | | | | LUM2_SUP_DV | | | | LUM3_SUP_TRA | | | | LUM4_PED_HEI | | | |
| **Sample** | **Sex** | **N** | **Mean** | **SD** | **CV** | **N** | **Mean** | **SD** | **CV** | **N** | **Mean** | **SD** | **CV** | **N** | **Mean** | **SD** | **CV** |
| Southern Africa (Zulu) | Combined | 29 | 25.1 | 1.5 | 6.0 | 30 | 33.0 | 2.9 | 8.7 | 31 | 45.5 | 4.0 | 8.8 | 31 | 15.3 | 1.8 | 11.8 |
| | M | 15 | 24.8 | 1.7 | 7.0 | 15 | 34.7 | 2.0 | 5.9 | 16 | 48.4 | 2.9 | 5.9 | 16 | 16.0 | 1.8 | 11.3 |
| | F | 14 | 25.5 | 1.2 | 4.8 | 15 | 31.3 | 2.6 | 8.3 | 15 | 42.5 | 2.5 | 5.9 | 15 | 14.5 | 1.4 | 10.0 |
| Northeastern Africa (Egypt) | Combined | 18 | 26.1 | 1.6 | 6.1 | 17 | 33.6 | 2.6 | 7.7 | 16 | 46.8 | 3.4 | 7.2 | 22 | 13.7 | 1.1 | 8.3 |
| | M | 9 | 26.4 | 1.9 | 7.2 | 9 | 34.7 | 2.6 | 7.4 | 8 | 49.0 | 2.8 | 5.8 | 12 | 13.9 | 1.1 | 7.7 |
| | F | 9 | 25.9 | 1.3 | 5.0 | 8 | 32.4 | 2.1 | 6.5 | 8 | 44.6 | 2.2 | 4.9 | 10 | 13.4 | 1.2 | 9.0 |
| Levant (Jordan) | Combined | 14 | 24.9 | 1.5 | 6.1 | 14 | 33.9 | 2.1 | 6.2 | 12 | 45.8 | 3.2 | 7.1 | 14 | 13.8 | 1.2 | 9.0 |
| | M | 5 | 25.8 | 1.8 | 6.9 | 5 | 35.3 | 1.0 | 2.9 | 5 | 47.7 | 3.1 | 6.5 | 5 | 14.5 | 0.9 | 5.9 |
| | F | 9 | 24.4 | 1.2 | 4.7 | 9 | 33.1 | 2.2 | 6.5 | 7 | 44.4 | 2.8 | 6.2 | 9 | 13.5 | 1.3 | 9.8 |
| Western Europe (Portugal) | Combined | 24 | 26.7 | 1.7 | 6.5 | 19 | 33.6 | 3.2 | 9.6 | 20 | 47.8 | 3.1 | 6.4 | 28 | 14.3 | 1.8 | 12.3 |
| | M | 14 | 27.3 | 1.3 | 4.6 | 9 | 35.7 | 3.5 | 9.9 | 12 | 49.6 | 2.4 | 4.9 | 15 | 15.2 | 1.7 | 11.3 |
| | F | 10 | 25.9 | 2.0 | 7.8 | 10 | 31.8 | 1.1 | 3.6 | 8 | 45.2 | 1.7 | 3.9 | 13 | 13.2 | 1.1 | 8.5 |
| North America (CA, U.S.A.) | Combined | 29 | 26.7 | 1.6 | 5.9 | 29 | 36.6 | 2.8 | 7.5 | 28 | 48.7 | 4.2 | 8.6 | 33 | 13.8 | 1.0 | 7.5 |
| | M | 15 | 27.1 | 1.5 | 5.4 | 17 | 37.7 | 2.7 | 7.1 | 15 | 51.6 | 3.4 | 6.7 | 19 | 13.9 | 1.2 | 8.4 |
| | F | 14 | 26.2 | 1.6 | 6.0 | 12 | 35.0 | 2.1 | 6.0 | 13 | 45.4 | 2.0 | 4.5 | 14 | 13.6 | 0.8 | 6.1 |

**Table A9.21** Summary statistics for measurements of the fourth lumbar vertebra

| | | Fourth lumbar vertebra | | | | | | | | | | | | | | | |
|---|---|---|---|---|---|---|---|---|---|---|---|---|---|---|---|---|---|
| | | LUM1_VEN_HEI | | | | LUM2_SUP_DV | | | | LUM3_SUP_TRA | | | | LUM4_PED_HEI | | | |
| **Sample** | **Sex** | **N** | **Mean** | **SD** | **CV** | **N** | **Mean** | **SD** | **CV** | **N** | **Mean** | **SD** | **CV** | **N** | **Mean** | **SD** | **CV** |
| Southern Africa (Zulu) | Combined | 31 | 24.8 | 1.4 | 5.7 | 30 | 33.8 | 3.2 | 9.6 | 32 | 48.1 | 4.3 | 9.0 | 32 | 14.3 | 1.6 | 11.6 |
| | M | 16 | 24.4 | 1.4 | 5.9 | 15 | 35.9 | 2.8 | 7.7 | 16 | 51.2 | 3.1 | 6.0 | 16 | 14.7 | 1.8 | 12.2 |
| | F | 15 | 25.3 | 1.3 | 5.1 | 15 | 31.8 | 2.3 | 7.3 | 16 | 44.9 | 2.9 | 6.5 | 16 | 13.8 | 1.4 | 10.3 |
| Northeastern Africa (Egypt) | Combined | 18 | 26.5 | 1.9 | 7.2 | 14 | 32.9 | 2.5 | 7.5 | 16 | 48.4 | 3.0 | 6.2 | 22 | 13.0 | 1.7 | 13.4 |
| | M | 9 | 26.3 | 1.8 | 6.9 | 6 | 33.9 | 2.3 | 6.8 | 7 | 50.8 | 2.4 | 4.8 | 11 | 13.3 | 1.5 | 11.5 |
| | F | 9 | 26.7 | 2.1 | 7.7 | 8 | 32.1 | 2.4 | 7.6 | 9 | 46.4 | 1.8 | 3.9 | 11 | 12.6 | 2.0 | 15.4 |
| Levant (Jordan) | Combined | 15 | 25.2 | 1.4 | 5.5 | 15 | 34.1 | 2.8 | 8.2 | 11 | 47.8 | 2.9 | 6.1 | 15 | 12.8 | 1.6 | 12.8 |
| | M | 6 | 26.0 | 1.3 | 5.0 | 6 | 35.8 | 2.8 | 7.8 | 5 | 49.5 | 2.4 | 4.8 | 6 | 13.7 | 1.5 | 10.6 |
| | F | 9 | 24.7 | 1.2 | 5.0 | 9 | 32.9 | 2.2 | 6.8 | 6 | 46.4 | 2.7 | 5.8 | 9 | 12.2 | 1.6 | 12.7 |
| Western Europe (Portugal) | Combined | 22 | 26.7 | 1.7 | 6.2 | 15 | 33.5 | 2.9 | 8.6 | 16 | 50.3 | 3.4 | 6.7 | 28 | 13.3 | 1.3 | 9.5 |
| | M | 12 | 27.1 | 1.3 | 4.7 | 7 | 35.1 | 3.2 | 9.1 | 11 | 51.5 | 3.3 | 6.4 | 15 | 13.9 | 1.2 | 8.5 |
| | F | 10 | 26.1 | 2.0 | 7.5 | 8 | 32.1 | 1.8 | 5.6 | 5 | 47.6 | 1.6 | 3.4 | 13 | 12.7 | 1.1 | 8.5 |
| North America (CA, U.S.A.) | Combined | 28 | 27.1 | 1.4 | 5.3 | 28 | 36.2 | 2.5 | 7.0 | 31 | 51.1 | 4.3 | 8.3 | 28 | 12.8 | 1.3 | 10.0 |
| | M | 17 | 27.1 | 1.5 | 5.5 | 16 | 37.0 | 2.6 | 7.0 | 18 | 53.9 | 3.1 | 5.7 | 16 | 13.0 | 1.3 | 10.2 |
| | F | 11 | 27.0 | 1.5 | 5.4 | 12 | 35.0 | 2.0 | 5.8 | 13 | 47.3 | 2.2 | 4.7 | 12 | 12.4 | 1.2 | 9.5 |

**Table A9.22** Summary statistics for measurements of the fifth lumbar vertebra

| | | Fifth lumbar vertebra | | | | | | | | | | | | | | | |
|---|---|---|---|---|---|---|---|---|---|---|---|---|---|---|---|---|---|
| | | LUM1_VEN_HEI | | | | LUM2_SUP_DV | | | | LUM3_SUP_TRA | | | | LUM4_PED_HEI | | | |
| **Sample** | **Sex** | **N** | **Mean** | **SD** | **CV** | **N** | **Mean** | **SD** | **CV** | **N** | **Mean** | **SD** | **CV** | **N** | **Mean** | **SD** | **CV** |
| Southern Africa (Zulu) | Combined | 31 | 25.4 | 1.6 | 6.2 | 30 | 33.9 | 2.8 | 8.2 | 32 | 50.8 | 4.2 | 8.2 | 32 | 11.7 | 1.6 | 13.4 |
| | M | 15 | 25.4 | 1.8 | 7.2 | 14 | 35.6 | 2.5 | 7.0 | 16 | 53.6 | 3.1 | 5.9 | 16 | 11.9 | 1.7 | 14.4 |
| | F | 16 | 25.4 | 1.4 | 5.4 | 16 | 32.4 | 2.1 | 6.6 | 16 | 47.9 | 3.0 | 6.3 | 16 | 11.5 | 1.4 | 12.4 |
| Northeastern Africa (Egypt) | Combined | 17 | 27.4 | 1.6 | 5.8 | 13 | 33.6 | 2.4 | 7.3 | 12 | 50.3 | 2.9 | 5.7 | 19 | 10.9 | 1.8 | 16.9 |
| | M | 8 | 27.7 | 1.6 | 5.6 | 5 | 34.7 | 2.6 | 7.6 | 5 | 52.6 | 2.5 | 4.8 | 8 | 12.2 | 2.0 | 16.8 |
| | F | 9 | 27.1 | 1.7 | 6.1 | 8 | 32.9 | 2.2 | 6.7 | 7 | 48.7 | 1.9 | 3.9 | 11 | 10.0 | 1.0 | 10.0 |
| Levant (Jordan) | Combined | 13 | 26.0 | 1.6 | 6.0 | 12 | 34.3 | 2.9 | 8.4 | 12 | 50.1 | 3.7 | 7.4 | 13 | 10.8 | 1.4 | 12.5 |
| | M | 5 | 26.6 | 0.8 | 3.1 | 5 | 35.8 | 3.7 | 10.4 | 5 | 51.1 | 4.4 | 8.7 | 5 | 10.8 | 1.2 | 10.8 |
| | F | 8 | 25.6 | 1.8 | 7.1 | 7 | 33.2 | 1.6 | 4.8 | 7 | 49.4 | 3.3 | 6.7 | 8 | 10.9 | 1.5 | 14.2 |
| Western Europe (Portugal) | Combined | 24 | 27.3 | 1.9 | 6.9 | 16 | 33.2 | 3.1 | 9.5 | 16 | 50.9 | 2.7 | 5.3 | 29 | 12.0 | 1.7 | 14.6 |
| | M | 11 | 27.3 | 1.5 | 5.4 | 7 | 35.3 | 3.5 | 9.8 | 9 | 52.6 | 2.3 | 4.4 | 14 | 12.6 | 1.9 | 14.9 |
| | F | 13 | 27.2 | 2.2 | 8.3 | 9 | 31.5 | 1.4 | 4.6 | 7 | 48.7 | 1.1 | 2.3 | 15 | 11.4 | 1.4 | 12.3 |
| North America (CA, U.S.A.) | Combined | 26 | 28.6 | 1.9 | 6.8 | 29 | 35.9 | 2.7 | 7.5 | 32 | 52.9 | 3.8 | 7.3 | 25 | 11.8 | 1.0 | 8.8 |
| | M | 15 | 29.0 | 1.9 | 6.4 | 18 | 36.4 | 2.5 | 6.9 | 19 | 55.0 | 3.0 | 5.5 | 14 | 11.8 | 0.9 | 7.5 |
| | F | 11 | 28.1 | 2.0 | 7.2 | 11 | 34.9 | 2.8 | 8.1 | 13 | 49.8 | 2.7 | 5.4 | 11 | 11.8 | 1.3 | 10.7 |

**Table A9.23** Summary statistics for measurements of the clavicle and scapula

| | | Clavicle | | | | Scapula | | | | | | | | | | | |
|---|---|---|---|---|---|---|---|---|---|---|---|---|---|---|---|---|---|
| | | CLA1_LEN | | | | SCA1_MAX_LEN | | | | SCA2_BRE | | | | SCA3_IND | | | |
| **Sample** | **Sex** | **N** | **Mean** | **SD** | **CV** | **N** | **Mean** | **SD** | **CV** | **N** | **Mean** | **SD** | **CV** | **N** | **Mean** | **SD** | **CV** |
| Southern Africa (Zulu) | Combined | 30 | 143.0 | 10.5 | 7.3 | 27 | 146.6 | 11.5 | 7.9 | 31 | 98.1 | 7.6 | 7.7 | 27 | 66.9 | 4.4 | 6.5 |
| | M | 13 | 149.7 | 9.2 | 6.1 | 12 | 155.0 | 11.1 | 7.2 | 15 | 103.7 | 4.9 | 4.8 | 12 | 67.1 | 3.8 | 5.7 |
| | F | 17 | 138.0 | 8.6 | 6.2 | 15 | 139.9 | 6.5 | 4.6 | 16 | 92.9 | 5.8 | 6.2 | 15 | 66.7 | 4.9 | 7.3 |
| Northeastern Africa (Egypt) | Combined | 22 | 144.2 | 10.0 | 6.9 | 4 | 142.6 | 20.2 | 14.2 | 14 | 101.2 | 6.6 | 6.5 | 4 | 71.6 | 10.8 | 15.0 |
| | M | 12 | 149.6 | 7.7 | 5.1 | 2 | 157.6 | 5.2 | 3.3 | 9 | 103.9 | 5.8 | 5.6 | 2 | 66.7 | 3.4 | 5.1 |
| | F | 10 | 137.6 | 8.6 | 6.2 | 2 | 127.6 | 17.3 | 13.5 | 5 | 96.2 | 4.9 | 5.1 | 2 | 76.6 | 15.5 | 20.2 |
| Levant (Jordan) | Combined | 18 | 135.9 | 9.9 | 7.3 | 0 | – | – | – | 8 | 94.5 | 6.9 | 7.3 | 0 | – | – | – |
| | M | 7 | 144.3 | 7.6 | 5.2 | 0 | – | – | – | 5 | 99.0 | 3.5 | 3.6 | 0 | – | – | – |
| | F | 11 | 130.6 | 7.4 | 5.6 | 0 | – | – | – | 3 | 87.1 | 3.0 | 3.5 | 0 | – | – | – |
| Western Europe (Portugal) | Combined | 29 | 144.6 | 11.3 | 7.8 | 21 | 148.7 | 13.0 | 8.7 | 29 | 100.8 | 9.0 | 8.9 | 21 | 68.3 | 3.9 | 5.7 |
| | M | 14 | 152.0 | 9.3 | 6.1 | 11 | 155.9 | 11.1 | 7.1 | 15 | 106.4 | 7.5 | 7.0 | 11 | 69.4 | 3.4 | 4.9 |
| | F | 15 | 137.7 | 8.3 | 6.0 | 10 | 140.7 | 10.1 | 7.2 | 14 | 94.7 | 6.1 | 6.4 | 10 | 67.1 | 4.2 | 6.3 |
| North America (CA, U.S.A.) | Combined | 31 | 148.8 | 12.0 | 8.0 | 6 | 149.7 | 13.8 | 9.2 | 12 | 103.6 | 6.4 | 6.2 | 6 | 69.9 | 3.9 | 5.6 |
| | M | 18 | 156.4 | 8.8 | 5.6 | 2 | 165.4 | 3.0 | 1.8 | 6 | 106.8 | 6.6 | 6.2 | 2 | 67.7 | 2.4 | 3.6 |
| | F | 13 | 138.3 | 6.6 | 4.7 | 4 | 141.9 | 8.4 | 5.9 | 6 | 100.4 | 4.6 | 4.6 | 4 | 71.0 | 4.4 | 6.2 |

**Table A9.24** Summary statistics for measurements of the humerus

| | | Humerus | | | | | | | | | | | | | | | |
|---|---|---|---|---|---|---|---|---|---|---|---|---|---|---|---|---|---|
| | | HUM1_MAX_LEN | | | | HUM2_BIO_LEN | | | | HUM3_MID_CIR | | | | HUM4_MAX_MID | | | |
| **Sample** | **Sex** | **N** | **Mean** | **SD** | **CV** | **N** | **Mean** | **SD** | **CV** | **N** | **Mean** | **SD** | **CV** | **N** | **Mean** | **SD** | **CV** |
| Southern Africa (Zulu) | Combined | 34 | 308.0 | 16.1 | 5.2 | 34 | 302.5 | 15.9 | 5.2 | 34 | 66.1 | 6.2 | 9.4 | 34 | 22.1 | 2.0 | 9.2 |
| | M | 17 | 314.0 | 17.4 | 5.5 | 17 | 308.2 | 17.4 | 5.7 | 17 | 69.8 | 5.6 | 8.0 | 17 | 23.1 | 2.0 | 8.8 |
| | F | 17 | 301.9 | 12.4 | 4.1 | 17 | 296.8 | 12.1 | 4.1 | 17 | 62.5 | 4.4 | 7.1 | 17 | 21.0 | 1.4 | 6.9 |
| Northeastern Africa (Egypt) | Combined | 25 | 309.5 | 22.0 | 7.1 | 26 | 304.9 | 20.9 | 6.9 | 26 | 59.9 | 6.2 | 10.4 | 26 | 20.5 | 2.3 | 11.3 |
| | M | 14 | 323.0 | 15.2 | 4.7 | 14 | 317.2 | 14.5 | 4.6 | 14 | 63.7 | 5.1 | 8.0 | 14 | 21.7 | 2.1 | 9.7 |
| | F | 11 | 292.3 | 16.6 | 5.7 | 12 | 290.6 | 18.2 | 6.3 | 12 | 55.5 | 4.2 | 7.6 | 12 | 18.9 | 1.5 | 8.1 |
| Levant (Jordan) | Combined | 27 | 289.7 | 16.8 | 5.8 | 23 | 285.8 | 13.3 | 4.7 | 22 | 60.2 | 4.2 | 7.0 | 22 | 20.7 | 1.6 | 7.7 |
| | M | 14 | 300.5 | 11.4 | 3.8 | 12 | 293.9 | 12.1 | 4.1 | 11 | 62.3 | 4.1 | 6.6 | 11 | 21.1 | 1.6 | 7.7 |
| | F | 13 | 278.1 | 13.8 | 5.0 | 11 | 277.0 | 8.1 | 2.9 | 11 | 58.1 | 3.3 | 5.7 | 11 | 20.2 | 1.5 | 7.5 |
| Western Europe (Portugal) | Combined | 30 | 308.6 | 22.9 | 7.4 | 30 | 302.9 | 22.6 | 7.5 | 30 | 68.3 | 6.0 | 8.7 | 30 | 22.7 | 1.9 | 8.4 |
| | M | 15 | 322.6 | 17.2 | 5.3 | 15 | 316.7 | 17.0 | 5.4 | 15 | 72.6 | 4.8 | 6.7 | 15 | 23.9 | 1.8 | 7.7 |
| | F | 15 | 294.6 | 19.4 | 6.6 | 15 | 289.0 | 18.9 | 6.5 | 15 | 64.1 | 3.5 | 5.5 | 15 | 21.5 | 1.1 | 5.3 |
| North America (CA, U.S.A.) | Combined | 35 | 317.2 | 17.5 | 5.5 | 36 | 312.2 | 17.0 | 5.4 | 36 | 63.8 | 5.6 | 8.8 | 36 | 22.4 | 1.9 | 8.4 |
| | M | 20 | 325.3 | 14.3 | 4.4 | 21 | 319.2 | 14.3 | 4.5 | 21 | 66.7 | 4.8 | 7.2 | 21 | 23.2 | 1.7 | 7.3 |
| | F | 15 | 306.4 | 15.8 | 5.1 | 15 | 302.2 | 15.6 | 5.2 | 15 | 59.7 | 3.9 | 6.5 | 15 | 21.2 | 1.5 | 7.1 |

**Table A9.24, Continued** Summary statistics for measurements of the humerus

| | | Humerus | | | | | | | | | | | | | | | |
|---|---|---|---|---|---|---|---|---|---|---|---|---|---|---|---|---|---|
| | | HUM5_MIN_MID | | | | HUM6_DEL_CIR | | | | HUM7_DEL_MIN | | | | HUM8_DEL_MAX | | | |
| **Sample** | **Sex** | **N** | **Mean** | **SD** | **CV** | **N** | **Mean** | **SD** | **CV** | **N** | **Mean** | **SD** | **CV** | **N** | **Mean** | **SD** | **CV** |
| Southern Africa (Zulu) | Combined | 34 | 17.2 | 1.9 | 11.1 | 34 | 67.9 | 6.9 | 10.2 | 34 | 17.8 | 2.2 | 12.5 | 34 | 22.6 | 2.3 | 10.2 |
| | M | 17 | 18.3 | 1.5 | 8.0 | 17 | 71.8 | 6.7 | 9.3 | 17 | 19.1 | 2.0 | 10.4 | 17 | 23.8 | 2.4 | 10.0 |
| | F | 17 | 16.1 | 1.6 | 10.3 | 17 | 63.9 | 4.5 | 7.1 | 17 | 16.4 | 1.5 | 9.3 | 17 | 21.4 | 1.5 | 6.9 |
| Northeastern Africa (Egypt) | Combined | 26 | 15.2 | 1.9 | 12.2 | 27 | 61.8 | 6.7 | 10.8 | 27 | 16.3 | 2.2 | 13.6 | 27 | 20.5 | 2.3 | 11.4 |
| | M | 14 | 16.2 | 1.5 | 9.1 | 13 | 66.3 | 5.6 | 8.4 | 13 | 17.8 | 1.9 | 10.7 | 13 | 22.1 | 2.0 | 9.2 |
| | F | 12 | 14.0 | 1.6 | 11.2 | 14 | 57.6 | 4.6 | 8.0 | 14 | 14.9 | 1.5 | 10.2 | 14 | 19.1 | 1.6 | 8.4 |
| Levant (Jordan) | Combined | 22 | 15.4 | 1.2 | 7.7 | 33 | 62.7 | 6.1 | 9.8 | 33 | 16.9 | 2.1 | 12.2 | 33 | 21.0 | 2.0 | 9.6 |
| | M | 11 | 16.1 | 1.0 | 6.4 | 17 | 66.4 | 5.1 | 7.8 | 17 | 18.5 | 1.4 | 7.4 | 17 | 22.0 | 1.8 | 8.3 |
| | F | 11 | 14.6 | 0.8 | 5.4 | 16 | 58.7 | 4.5 | 7.6 | 16 | 15.3 | 1.3 | 8.3 | 16 | 19.9 | 1.6 | 8.2 |
| Western Europe (Portugal) | Combined | 30 | 17.4 | 1.8 | 10.1 | 30 | 71.2 | 6.7 | 9.4 | 30 | 18.5 | 2.2 | 11.6 | 30 | 23.1 | 2.2 | 9.5 |
| | M | 15 | 18.5 | 1.3 | 7.3 | 15 | 75.9 | 5.6 | 7.3 | 15 | 20.1 | 1.8 | 8.8 | 15 | 24.7 | 1.7 | 6.9 |
| | F | 15 | 16.3 | 1.4 | 8.6 | 15 | 66.5 | 3.7 | 5.6 | 15 | 17.0 | 1.2 | 7.1 | 15 | 21.6 | 1.4 | 6.7 |
| North America (CA, U.S.A.) | Combined | 36 | 16.3 | 1.5 | 9.2 | 39 | 65.8 | 6.7 | 10.1 | 39 | 17.8 | 1.8 | 10.3 | 39 | 22.3 | 2.0 | 8.9 |
| | M | 21 | 17.2 | 1.1 | 6.4 | 21 | 69.4 | 6.0 | 8.7 | 21 | 18.9 | 1.5 | 7.8 | 21 | 23.3 | 1.8 | 7.8 |
| | F | 15 | 15.0 | 0.8 | 5.6 | 18 | 61.6 | 4.8 | 7.8 | 18 | 16.5 | 1.3 | 8.0 | 18 | 21.2 | 1.6 | 7.6 |

**Table A9.24, Continued** Summary statistics for measurements of the humerus

| | | Humerus | | | | | | | | | | | | | | | |
|---|---|---|---|---|---|---|---|---|---|---|---|---|---|---|---|---|---|
| | | HUM9_HEA_DIA | | | | HUM10_BIC_BRE | | | | HUM11_FOS_BRE | | | | HUM12_MED_PIL | | | |
| **Sample** | **Sex** | **N** | **Mean** | **SD** | **CV** | **N** | **Mean** | **SD** | **CV** | **N** | **Mean** | **SD** | **CV** | **N** | **Mean** | **SD** | **CV** |
| Southern Africa (Zulu) | Combined | 34 | 41.2 | 3.4 | 8.2 | 34 | 58.7 | 4.7 | 8.0 | 34 | 24.8 | 1.7 | 7.0 | 34 | 10.5 | 2.5 | 24.2 |
| | M | 17 | 43.5 | 2.6 | 5.9 | 17 | 61.8 | 4.3 | 7.0 | 17 | 24.9 | 2.1 | 8.3 | 17 | 11.8 | 2.6 | 22.2 |
| | F | 17 | 38.9 | 2.3 | 5.9 | 17 | 55.6 | 2.6 | 4.6 | 17 | 24.6 | 1.4 | 5.6 | 17 | 9.1 | 1.6 | 17.5 |
| Northeastern Africa (Egypt) | Combined | 27 | 41.5 | 3.9 | 9.3 | 27 | 58.3 | 5.1 | 8.8 | 28 | 24.0 | 2.2 | 9.1 | 28 | 9.7 | 2.3 | 23.3 |
| | M | 14 | 44.4 | 2.4 | 5.5 | 13 | 62.6 | 3.3 | 5.3 | 14 | 25.0 | 1.8 | 7.3 | 14 | 10.9 | 1.7 | 15.8 |
| | F | 13 | 38.5 | 2.5 | 6.5 | 14 | 54.3 | 2.6 | 4.7 | 14 | 23.0 | 2.1 | 9.1 | 14 | 8.4 | 2.1 | 24.4 |
| Levant (Jordan) | Combined | 28 | 40.7 | 2.9 | 7.0 | 25 | 57.3 | 4.5 | 7.9 | 33 | 23.9 | 1.8 | 7.7 | 32 | 9.8 | 1.7 | 17.5 |
| | M | 14 | 42.7 | 2.4 | 5.7 | 13 | 61.0 | 2.2 | 3.6 | 17 | 25.0 | 1.6 | 6.6 | 17 | 10.9 | 1.5 | 13.5 |
| | F | 14 | 38.7 | 1.6 | 4.0 | 12 | 53.2 | 2.1 | 3.9 | 16 | 22.7 | 1.2 | 5.3 | 15 | 8.7 | 1.1 | 13.3 |
| Western Europe (Portugal) | Combined | 28 | 43.9 | 3.6 | 8.2 | 30 | 58.5 | 5.1 | 8.7 | 30 | 24.1 | 2.2 | 9.2 | 30 | 11.3 | 1.9 | 16.7 |
| | M | 15 | 46.4 | 2.2 | 4.8 | 15 | 61.8 | 4.3 | 6.9 | 15 | 25.6 | 2.0 | 7.7 | 15 | 12.4 | 1.6 | 13.3 |
| | F | 13 | 41.0 | 2.6 | 6.3 | 15 | 55.2 | 3.6 | 6.4 | 15 | 22.6 | 1.3 | 5.7 | 15 | 10.2 | 1.5 | 14.3 |
| North America (CA, U.S.A.) | Combined | 39 | 45.2 | 3.3 | 7.4 | 38 | 60.2 | 4.3 | 7.1 | 39 | 25.8 | 2.2 | 8.5 | 40 | 9.7 | 2.0 | 21.1 |
| | M | 20 | 47.6 | 2.8 | 5.9 | 19 | 63.6 | 3.3 | 5.2 | 20 | 27.4 | 1.7 | 6.2 | 20 | 10.2 | 1.9 | 19.0 |
| | F | 19 | 42.7 | 1.4 | 3.3 | 19 | 56.9 | 1.5 | 2.7 | 19 | 24.2 | 1.3 | 5.5 | 20 | 9.2 | 2.1 | 22.5 |

**Table A9.24, Continued** Summary statistics for measurements of the humerus

| | | Humerus | | | | | | | | | | | |
|---|---|---|---|---|---|---|---|---|---|---|---|---|---|
| | | HUM13_LAT_PIL | | | | HUM14_EPI_ML | | | | HUM15_PRO_BRE | | | |
| **Sample** | **Sex** | **N** | **Mean** | **SD** | **CV** | **N** | **Mean** | **SD** | **CV** | **N** | **Mean** | **SD** | **CV** |
| Southern Africa (Zulu) | Combined | 34 | 17.0 | 2.1 | 12.6 | 34 | 16.2 | 2.7 | 16.7 | 34 | 46.5 | 3.1 | 6.7 |
| | M | 17 | 18.0 | 2.5 | 13.9 | 17 | 17.9 | 2.5 | 14.0 | 17 | 48.6 | 2.6 | 5.3 |
| | F | 17 | 16.1 | 1.1 | 7.1 | 17 | 14.5 | 1.7 | 11.7 | 17 | 44.4 | 2.0 | 4.5 |
| Northeastern Africa (Egypt) | Combined | 28 | 16.0 | 2.1 | 12.9 | 27 | 15.8 | 2.2 | 13.9 | 24 | 46.8 | 4.0 | 8.6 |
| | M | 14 | 17.6 | 1.3 | 7.7 | 13 | 17.3 | 1.6 | 9.2 | 13 | 49.8 | 2.5 | 5.0 |
| | F | 14 | 14.5 | 1.4 | 9.8 | 14 | 14.4 | 1.7 | 11.8 | 11 | 43.2 | 1.9 | 4.5 |
| Levant (Jordan) | Combined | 27 | 15.4 | 1.7 | 11.1 | 28 | 16.2 | 2.2 | 13.9 | 25 | 46.3 | 3.1 | 6.8 |
| | M | 13 | 15.8 | 1.8 | 11.4 | 14 | 17.9 | 1.6 | 9.2 | 12 | 48.5 | 3.0 | 6.2 |
| | F | 14 | 15.0 | 1.6 | 10.6 | 14 | 14.4 | 1.2 | 8.4 | 13 | 44.3 | 1.5 | 3.4 |
| Western Europe (Portugal) | Combined | 30 | 16.6 | 2.1 | 12.4 | 30 | 15.2 | 2.6 | 16.8 | 30 | 47.6 | 3.6 | 7.6 |
| | M | 15 | 17.7 | 1.6 | 9.2 | 15 | 16.2 | 2.9 | 17.9 | 15 | 50.5 | 2.4 | 4.7 |
| | F | 15 | 15.4 | 1.8 | 11.9 | 15 | 14.2 | 1.7 | 12.3 | 15 | 44.7 | 1.9 | 4.2 |
| North America (CA, U.S.A.) | Combined | 40 | 16.5 | 1.3 | 7.7 | 39 | 16.3 | 1.9 | 11.7 | 39 | 49.5 | 3.3 | 6.7 |
| | M | 21 | 17.3 | 1.2 | 6.8 | 20 | 16.9 | 2.3 | 13.4 | 20 | 52.0 | 2.6 | 5.1 |
| | F | 19 | 15.7 | 0.8 | 5.2 | 19 | 15.8 | 1.3 | 8.4 | 19 | 46.9 | 1.3 | 2.8 |

**Table A9.25** Summary statistics for measurements of the radius

| | | Radius | | | | | | | | | | | | | | | |
|---|---|---|---|---|---|---|---|---|---|---|---|---|---|---|---|---|---|
| | | RAD1_LEN | | | | RAD2_BIO_LEN | | | | RAD3_MID_CIR | | | | RAD4_AP_MID | | | |
| **Sample** | **Sex** | **N** | **Mean** | **SD** | **CV** | **N** | **Mean** | **SD** | **CV** | **N** | **Mean** | **SD** | **CV** | **N** | **Mean** | **SD** | **CV** |
| Southern Africa (Zulu) | Combined | 34 | 244.3 | 15.4 | 6.3 | 34 | 231.1 | 14.9 | 6.4 | 34 | 43.2 | 4.2 | 9.7 | 34 | 11.9 | 1.3 | 10.8 |
| | M | 17 | 252.2 | 15.3 | 6.1 | 17 | 238.4 | 15.0 | 6.3 | 17 | 45.9 | 3.8 | 8.4 | 17 | 12.9 | 1.1 | 8.7 |
| | F | 17 | 236.4 | 10.9 | 4.6 | 17 | 223.8 | 10.9 | 4.9 | 17 | 40.5 | 2.4 | 5.9 | 17 | 11.0 | 0.6 | 5.3 |
| Northeastern Africa (Egypt) | Combined | 25 | 240.1 | 17.4 | 7.2 | 25 | 226.9 | 16.5 | 7.3 | 25 | 39.9 | 4.4 | 11.1 | 25 | 10.8 | 1.4 | 12.5 |
| | M | 13 | 252.3 | 11.0 | 4.3 | 13 | 238.4 | 10.6 | 4.4 | 13 | 43.1 | 3.6 | 8.3 | 13 | 11.7 | 1.0 | 8.8 |
| | F | 12 | 227.0 | 12.8 | 5.6 | 12 | 214.5 | 12.2 | 5.7 | 12 | 36.5 | 2.0 | 5.6 | 12 | 9.9 | 1.0 | 9.7 |
| Levant (Jordan) | Combined | 19 | 224.1 | 15.4 | 6.9 | 22 | 213.9 | 15.1 | 7.1 | 21 | 40.2 | 3.9 | 9.6 | 21 | 11.0 | 1.3 | 11.6 |
| | M | 8 | 239.4 | 7.5 | 3.1 | 9 | 229.1 | 6.3 | 2.8 | 9 | 43.0 | 3.4 | 7.9 | 9 | 11.9 | 1.0 | 8.1 |
| | F | 11 | 213.0 | 8.1 | 3.8 | 13 | 203.5 | 9.1 | 4.5 | 12 | 38.1 | 2.8 | 7.3 | 12 | 10.3 | 1.0 | 10.1 |
| Western Europe (Portugal) | Combined | 30 | 227.8 | 19.8 | 8.7 | 30 | 215.3 | 19.2 | 8.9 | 30 | 44.4 | 4.2 | 9.4 | 30 | 11.7 | 1.4 | 11.6 |
| | M | 15 | 240.9 | 16.8 | 7.0 | 15 | 227.3 | 16.9 | 7.4 | 15 | 47.4 | 3.3 | 6.9 | 15 | 12.8 | 0.9 | 7.4 |
| | F | 15 | 214.8 | 12.8 | 6.0 | 15 | 203.4 | 13.1 | 6.4 | 15 | 41.4 | 2.4 | 5.8 | 15 | 10.7 | 0.8 | 7.1 |
| North America (CA, U.S.A.) | Combined | 41 | 247.1 | 16.7 | 6.8 | 41 | 232.8 | 15.8 | 6.8 | 40 | 40.9 | 4.3 | 10.4 | 41 | 11.7 | 1.0 | 8.6 |
| | M | 21 | 257.9 | 13.1 | 5.1 | 21 | 242.8 | 12.7 | 5.2 | 21 | 42.7 | 4.7 | 11.1 | 21 | 12.4 | 0.9 | 7.3 |
| | F | 20 | 235.7 | 11.8 | 5.0 | 20 | 222.4 | 11.4 | 5.1 | 19 | 39.0 | 2.7 | 6.8 | 20 | 11.1 | 0.6 | 5.6 |

**Table A9.25, Continued** Summary statistics for measurements of the radius

| | | Radius | | | | | | | | | | | | | | | |
|---|---|---|---|---|---|---|---|---|---|---|---|---|---|---|---|---|---|
| | | RAD5_ML_MID | | | | RAD6_HEA_AP | | | | RAD7_HEA_CIR | | | | RAD8_DIS_BRE | | | |
| **Sample** | **Sex** | **N** | **Mean** | **SD** | **CV** | **N** | **Mean** | **SD** | **CV** | **N** | **Mean** | **SD** | **CV** | **N** | **Mean** | **SD** | **CV** |
| Southern Africa (Zulu) | Combined | 34 | 14.7 | 1.8 | 12.4 | 27 | 21.4 | 1.7 | 7.9 | 25 | 68.7 | 5.3 | 7.8 | 34 | 32.7 | 2.1 | 6.3 |
| | M | 17 | 15.5 | 1.8 | 11.7 | 13 | 22.6 | 1.5 | 6.4 | 11 | 73.3 | 4.1 | 5.5 | 17 | 34.1 | 1.8 | 5.3 |
| | F | 17 | 13.8 | 1.4 | 9.8 | 14 | 20.3 | 1.0 | 4.7 | 14 | 65.2 | 3.0 | 4.5 | 17 | 31.3 | 1.2 | 3.8 |
| Northeastern Africa (Egypt) | Combined | 25 | 13.7 | 1.9 | 13.6 | 18 | 21.0 | 2.0 | 9.7 | 13 | 64.8 | 5.5 | 8.5 | 24 | 31.5 | 3.1 | 9.7 |
| | M | 13 | 15.0 | 1.5 | 10.3 | 8 | 22.5 | 1.3 | 5.7 | 6 | 69.3 | 4.2 | 6.1 | 11 | 34.1 | 1.7 | 5.1 |
| | F | 12 | 12.2 | 0.7 | 5.6 | 10 | 19.8 | 1.6 | 8.2 | 7 | 60.9 | 2.9 | 4.7 | 13 | 29.2 | 1.9 | 6.4 |
| Levant (Jordan) | Combined | 22 | 14.0 | 1.6 | 11.3 | 15 | 20.3 | 1.9 | 9.3 | 8 | 65.0 | 4.0 | 6.2 | 23 | 31.4 | 2.8 | 9.0 |
| | M | 9 | 14.8 | 1.6 | 10.8 | 6 | 21.8 | 2.0 | 9.2 | 5 | 67.2 | 3.0 | 4.5 | 11 | 33.6 | 2.2 | 6.6 |
| | F | 13 | 13.4 | 1.3 | 9.8 | 9 | 19.3 | 1.0 | 5.1 | 3 | 61.4 | 2.7 | 4.4 | 12 | 29.3 | 1.3 | 4.6 |
| Western Europe (Portugal) | Combined | 30 | 15.2 | 1.7 | 11.0 | 29 | 21.3 | 2.0 | 9.6 | 23 | 68.9 | 6.5 | 9.4 | 30 | 31.5 | 3.0 | 9.4 |
| | M | 15 | 16.2 | 1.4 | 8.6 | 15 | 22.8 | 1.4 | 6.3 | 13 | 73.1 | 5.1 | 7.0 | 15 | 33.5 | 2.4 | 7.2 |
| | F | 15 | 14.1 | 1.2 | 8.8 | 14 | 19.7 | 1.2 | 6.0 | 10 | 63.6 | 3.2 | 5.1 | 15 | 29.4 | 1.8 | 6.2 |
| North America (CA, U.S.A.) | Combined | 41 | 14.4 | 1.3 | 8.7 | 31 | 22.6 | 1.5 | 6.5 | 25 | 69.8 | 4.3 | 6.1 | 36 | 32.9 | 2.0 | 6.2 |
| | M | 21 | 14.7 | 1.3 | 8.6 | 17 | 23.5 | 1.2 | 5.2 | 14 | 72.7 | 3.0 | 4.1 | 16 | 34.5 | 1.7 | 4.8 |
| | F | 20 | 14.0 | 1.1 | 8.1 | 14 | 21.5 | 0.8 | 3.6 | 11 | 66.2 | 2.5 | 3.8 | 20 | 31.5 | 1.1 | 3.4 |

**Table A9.25, Continued** Summary statistics for measurements of the radius

| | | Radius | | | |
|---|---|---|---|---|---|
| | | RAD9_DIS_AP | | | |
| **Sample** | **Sex** | **N** | **Mean** | **SD** | **CV** |
| Southern Africa (Zulu) | Combined | 33 | 23.8 | 1.7 | 7.0 |
| | M | 16 | 25.0 | 1.1 | 4.5 |
| | F | 17 | 22.7 | 1.3 | 5.6 |
| Northeastern Africa (Egypt) | Combined | 23 | 22.9 | 2.0 | 8.9 |
| | M | 11 | 24.4 | 1.5 | 6.0 |
| | F | 12 | 21.6 | 1.5 | 6.8 |
| Levant (Jordan) | Combined | 17 | 22.1 | 1.6 | 7.2 |
| | M | 8 | 23.0 | 1.4 | 6.1 |
| | F | 9 | 21.3 | 1.4 | 6.4 |
| Western Europe (Portugal) | Combined | 30 | 24.1 | 2.3 | 9.5 |
| | M | 15 | 25.4 | 1.7 | 6.7 |
| | F | 15 | 22.7 | 2.1 | 9.0 |
| North America (CA, U.S.A.) | Combined | 31 | 25.1 | 1.2 | 4.8 |
| | M | 13 | 25.6 | 0.9 | 3.6 |
| | F | 18 | 24.7 | 1.2 | 5.0 |

**Table A9.26** Summary statistics for measurements of the ulna

| | | Ulna | | | | | | | | | | | | | | | |
|---|---|---|---|---|---|---|---|---|---|---|---|---|---|---|---|---|---|
| | | ULN1_LEN | | | | ULN2_BIO_LEN | | | | ULN3_AP_DIA | | | | ULN4_ML_DIA | | | |
| **Sample** | **Sex** | **N** | **Mean** | **SD** | **CV** | **N** | **Mean** | **SD** | **CV** | **N** | **Mean** | **SD** | **CV** | **N** | **Mean** | **SD** | **CV** |
| Southern Africa (Zulu) | Combined | 34 | 262.4 | 15.5 | 5.9 | 34 | 238.2 | 14.7 | 6.2 | 34 | 15.6 | 1.8 | 11.4 | 34 | 13.5 | 1.4 | 10.3 |
| | M | 17 | 269.9 | 15.9 | 5.9 | 17 | 245.1 | 15.3 | 6.2 | 17 | 16.2 | 1.8 | 11.0 | 17 | 14.3 | 0.9 | 6.4 |
| | F | 17 | 254.9 | 11.2 | 4.4 | 17 | 231.4 | 10.5 | 4.5 | 17 | 15.1 | 1.7 | 11.0 | 17 | 12.6 | 1.3 | 9.9 |
| Northeastern Africa (Egypt) | Combined | 27 | 258.7 | 18.1 | 7.0 | 27 | 233.7 | 16.5 | 7.1 | 27 | 14.0 | 1.9 | 13.8 | 27 | 12.2 | 1.4 | 11.7 |
| | M | 14 | 271.0 | 12.3 | 4.5 | 14 | 245.1 | 10.9 | 4.4 | 14 | 15.3 | 1.8 | 11.8 | 14 | 13.0 | 1.2 | 9.0 |
| | F | 13 | 245.5 | 13.4 | 5.5 | 13 | 221.5 | 12.1 | 5.5 | 13 | 12.6 | 0.8 | 6.4 | 13 | 11.2 | 1.0 | 9.2 |
| Levant (Jordan) | Combined | 19 | 245.6 | 17.0 | 6.9 | 19 | 221.4 | 15.3 | 6.9 | 31 | 14.0 | 1.6 | 11.1 | 31 | 12.9 | 1.3 | 10.4 |
| | M | 8 | 262.4 | 8.2 | 3.1 | 8 | 236.6 | 7.4 | 3.1 | 16 | 14.6 | 1.4 | 9.6 | 16 | 13.8 | 1.1 | 7.7 |
| | F | 11 | 233.4 | 9.1 | 3.9 | 11 | 210.3 | 8.0 | 3.8 | 15 | 13.4 | 1.5 | 11.5 | 15 | 11.9 | 0.8 | 6.8 |
| Western Europe (Portugal) | Combined | 26 | 249.3 | 20.1 | 8.1 | 29 | 223.6 | 19.1 | 8.5 | 30 | 15.5 | 2.1 | 13.3 | 30 | 13.3 | 2.0 | 14.7 |
| | M | 15 | 259.0 | 18.4 | 7.1 | 15 | 234.6 | 17.6 | 7.5 | 15 | 16.8 | 1.9 | 11.0 | 15 | 14.8 | 1.5 | 10.0 |
| | F | 11 | 236.1 | 14.4 | 6.1 | 14 | 211.8 | 12.7 | 6.0 | 15 | 14.3 | 1.4 | 9.6 | 15 | 11.8 | 1.0 | 8.7 |
| North America (CA, U.S.A.) | Combined | 36 | 268.6 | 17.8 | 6.6 | 37 | 240.7 | 16.9 | 7.0 | 39 | 16.0 | 1.7 | 10.5 | 39 | 13.9 | 1.1 | 8.2 |
| | M | 18 | 279.7 | 14.9 | 5.3 | 19 | 250.8 | 14.4 | 5.8 | 20 | 16.5 | 1.6 | 9.6 | 20 | 14.4 | 1.1 | 7.8 |
| | F | 18 | 257.5 | 13.0 | 5.0 | 18 | 230.1 | 12.4 | 5.4 | 19 | 15.5 | 1.6 | 10.6 | 19 | 13.4 | 0.9 | 7.0 |

**Table A9.26, Continued** Summary statistics for measurements of the ulna

| | | Ulna | | | | | | | | | | | | | | | |
|---|---|---|---|---|---|---|---|---|---|---|---|---|---|---|---|---|---|
| | | ULN5_DIS_BRE | | | | ULN6_TRO_THI | | | | ULN7_COR_HEI | | | | ULN8_OLE_HEI | | | |
| **Sample** | **Sex** | **N** | **Mean** | **SD** | **CV** | **N** | **Mean** | **SD** | **CV** | **N** | **Mean** | **SD** | **CV** | **N** | **Mean** | **SD** | **CV** |
| Southern Africa (Zulu) | Combined | 33 | 16.4 | 1.6 | 9.9 | 34 | 18.2 | 1.7 | 9.2 | 34 | 34.1 | 2.5 | 7.4 | 34 | 23.7 | 1.8 | 7.5 |
| | M | 17 | 17.2 | 1.2 | 6.9 | 17 | 18.6 | 1.8 | 9.7 | 17 | 35.6 | 2.6 | 7.2 | 17 | 24.7 | 1.7 | 7.0 |
| | F | 16 | 15.5 | 1.6 | 10.1 | 17 | 17.7 | 1.4 | 8.1 | 17 | 32.6 | 1.4 | 4.2 | 17 | 22.7 | 1.2 | 5.3 |
| Northeastern Africa (Egypt) | Combined | 26 | 15.7 | 1.4 | 8.9 | 28 | 17.6 | 1.4 | 8.1 | 27 | 32.0 | 2.3 | 7.1 | 28 | 24.4 | 2.4 | 9.8 |
| | M | 13 | 16.6 | 1.2 | 7.1 | 14 | 18.3 | 1.1 | 6.2 | 13 | 33.4 | 1.5 | 4.4 | 14 | 25.7 | 2.3 | 8.9 |
| | F | 13 | 14.8 | 1.0 | 6.7 | 14 | 16.8 | 1.4 | 8.1 | 14 | 30.7 | 2.1 | 6.8 | 14 | 23.2 | 1.8 | 7.7 |
| Levant (Jordan) | Combined | 22 | 15.6 | 1.3 | 8.1 | 32 | 17.4 | 1.6 | 9.1 | 29 | 31.0 | 2.4 | 7.8 | 30 | 24.7 | 2.0 | 8.2 |
| | M | 10 | 16.4 | 1.1 | 7.0 | 19 | 18.0 | 1.6 | 8.8 | 17 | 32.1 | 2.1 | 6.5 | 18 | 25.9 | 1.5 | 5.8 |
| | F | 12 | 14.9 | 1.0 | 6.5 | 13 | 16.4 | 1.0 | 6.1 | 12 | 29.4 | 2.0 | 6.7 | 12 | 22.9 | 1.1 | 5.0 |
| Western Europe (Portugal) | Combined | 28 | 16.5 | 2.3 | 13.9 | 30 | 18.8 | 1.8 | 9.3 | 29 | 33.8 | 3.0 | 9.0 | 29 | 23.6 | 1.6 | 6.6 |
| | M | 13 | 17.5 | 2.3 | 13.3 | 15 | 20.1 | 1.4 | 7.2 | 14 | 36.1 | 2.6 | 7.3 | 14 | 24.6 | 1.1 | 4.6 |
| | F | 15 | 15.6 | 1.9 | 12.3 | 15 | 17.6 | 0.9 | 5.1 | 15 | 31.6 | 1.3 | 4.0 | 15 | 22.7 | 1.4 | 6.1 |
| North America (CA, U.S.A.) | Combined | 29 | 17.7 | 1.5 | 8.5 | 39 | 19.4 | 1.5 | 7.9 | 37 | 36.0 | 2.7 | 7.5 | 36 | 26.3 | 1.8 | 6.7 |
| | M | 14 | 18.3 | 1.8 | 10.1 | 20 | 19.9 | 1.6 | 8.0 | 20 | 37.5 | 2.6 | 6.9 | 19 | 27.3 | 1.5 | 5.6 |
| | F | 15 | 17.2 | 0.9 | 5.1 | 19 | 18.8 | 1.3 | 6.8 | 17 | 34.3 | 1.6 | 4.8 | 17 | 25.3 | 1.4 | 5.6 |

**Table A9.26, Continued** Summary statistics for measurements of the ulna

| | | Ulna | | | | | | | | | | | | | | | |
|---|---|---|---|---|---|---|---|---|---|---|---|---|---|---|---|---|---|
| | | ULN9_TRO_LEN | | | | ULN10_OLE_LEN | | | | ULN11_NOT_POS | | | | ULN12_NOT_MAJ | | | |
| **Sample** | **Sex** | **N** | **Mean** | **SD** | **CV** | **N** | **Mean** | **SD** | **CV** | **N** | **Mean** | **SD** | **CV** | **N** | **Mean** | **SD** | **CV** |
| Southern Africa (Zulu) | Combined | 34 | 22.6 | 2.1 | 9.4 | 34 | 18.8 | 1.6 | 8.5 | 33 | 38.7 | 2.7 | 7.0 | 34 | 19.1 | 1.8 | 9.4 |
| | M | 17 | 23.9 | 1.9 | 7.9 | 17 | 19.5 | 1.7 | 8.6 | 16 | 40.5 | 2.5 | 6.1 | 17 | 19.7 | 1.4 | 7.3 |
| | F | 17 | 21.4 | 1.6 | 7.4 | 17 | 18.1 | 1.2 | 6.5 | 17 | 37.0 | 1.7 | 4.7 | 17 | 18.6 | 2.0 | 10.8 |
| Northeastern Africa (Egypt) | Combined | 28 | 20.9 | 1.8 | 8.4 | 28 | 18.8 | 1.6 | 8.4 | 28 | 38.2 | 3.3 | 8.7 | 20 | 17.8 | 1.8 | 9.9 |
| | M | 14 | 21.6 | 1.4 | 6.6 | 14 | 19.7 | 1.4 | 7.1 | 14 | 40.3 | 2.8 | 7.0 | 9 | 19.1 | 1.0 | 5.2 |
| | F | 14 | 20.2 | 1.8 | 9.0 | 14 | 17.8 | 1.1 | 6.1 | 14 | 36.0 | 2.1 | 5.9 | 11 | 16.7 | 1.5 | 9.0 |
| Levant (Jordan) | Combined | 29 | 20.3 | 1.7 | 8.4 | 32 | 18.5 | 1.5 | 8.1 | 30 | 38.1 | 3.3 | 8.6 | 29 | 17.4 | 1.7 | 9.8 |
| | M | 17 | 21.0 | 1.6 | 7.5 | 19 | 19.4 | 0.9 | 4.8 | 17 | 40.3 | 2.3 | 5.7 | 15 | 18.3 | 1.4 | 7.4 |
| | F | 12 | 19.3 | 1.4 | 7.1 | 13 | 17.2 | 1.2 | 6.9 | 13 | 35.2 | 1.9 | 5.3 | 14 | 16.4 | 1.5 | 9.0 |
| Western Europe (Portugal) | Combined | 30 | 21.3 | 2.4 | 11.0 | 29 | 18.5 | 1.5 | 8.1 | 29 | 38.2 | 3.4 | 8.8 | 29 | 17.7 | 2.2 | 12.3 |
| | M | 15 | 23.1 | 1.4 | 6.3 | 14 | 19.2 | 1.1 | 5.9 | 14 | 40.5 | 2.3 | 5.7 | 14 | 19.1 | 2.2 | 11.4 |
| | F | 15 | 19.6 | 1.7 | 8.6 | 15 | 17.9 | 1.5 | 8.6 | 15 | 36.2 | 2.9 | 8.0 | 15 | 16.4 | 1.3 | 7.7 |
| North America (CA, U.S.A.) | Combined | 37 | 22.8 | 1.9 | 8.5 | 39 | 21.2 | 1.6 | 7.6 | 39 | 39.9 | 2.9 | 7.1 | 20 | 16.8 | 1.9 | 11.2 |
| | M | 19 | 24.2 | 1.4 | 6.0 | 20 | 22.1 | 1.4 | 6.3 | 20 | 41.6 | 2.7 | 6.5 | 8 | 18.1 | 2.0 | 11.4 |
| | F | 18 | 21.4 | 1.3 | 5.9 | 19 | 20.2 | 1.2 | 6.0 | 19 | 38.1 | 1.7 | 4.4 | 12 | 16.0 | 1.3 | 8.1 |

**Table A9.26, Continued** Summary statistics for measurements of the ulna

| | | Ulna | | | | | | | |
|---|---|---|---|---|---|---|---|---|---|
| | | ULN13_NOT_PER | | | | ULN14_MIN_CIR | | | |
| **Sample** | **Sex** | **N** | **Mean** | **SD** | **CV** | **N** | **Mean** | **SD** | **CV** |
| Southern Africa (Zulu) | Combined | 33 | 11.9 | 1.4 | 12.1 | 34 | 36.7 | 2.9 | 7.9 |
| | M | 16 | 12.7 | 1.1 | 8.9 | 17 | 38.2 | 2.8 | 7.2 |
| | F | 17 | 11.2 | 1.4 | 12.1 | 17 | 35.2 | 2.2 | 6.2 |
| Northeastern Africa (Egypt) | Combined | 22 | 10.5 | 1.5 | 14.0 | 28 | 33.3 | 2.9 | 8.8 |
| | M | 10 | 11.6 | 1.3 | 10.8 | 14 | 35.3 | 2.5 | 7.0 |
| | F | 12 | 9.6 | 1.0 | 10.3 | 14 | 31.2 | 1.6 | 5.1 |
| Levant (Jordan) | Combined | 31 | 10.7 | 1.5 | 14.0 | 29 | 34.5 | 2.5 | 7.4 |
| | M | 17 | 11.6 | 1.4 | 11.9 | 16 | 35.9 | 1.9 | 5.4 |
| | F | 14 | 9.7 | 0.9 | 9.0 | 13 | 32.8 | 2.1 | 6.4 |
| Western Europe (Portugal) | Combined | 27 | 10.8 | 1.9 | 17.2 | 30 | 37.1 | 3.6 | 9.8 |
| | M | 13 | 11.9 | 1.7 | 14.1 | 15 | 39.2 | 3.6 | 9.2 |
| | F | 14 | 9.8 | 1.4 | 14.4 | 15 | 35.0 | 2.2 | 6.2 |
| North America (CA, U.S.A.) | Combined | 33 | 10.3 | 1.3 | 12.8 | 38 | 37.1 | 2.7 | 7.3 |
| | M | 15 | 11.3 | 1.1 | 9.6 | 20 | 38.1 | 2.9 | 7.6 |
| | F | 18 | 9.5 | 0.9 | 9.8 | 18 | 35.9 | 1.9 | 5.3 |

**Table A9.27** Summary statistics for measurements of the lunate and triquetral

| | | Lunate | | | | | | | | Triquetral | | | | | | | |
|---|---|---|---|---|---|---|---|---|---|---|---|---|---|---|---|---|---|
| | | LUN1_LEN | | | | LUN2_BRE | | | | TRI1_LEN | | | | TRI2_WID | | | |
| **Sample** | **Sex** | **N** | **Mean** | **SD** | **CV** | **N** | **Mean** | **SD** | **CV** | **N** | **Mean** | **SD** | **CV** | **N** | **Mean** | **SD** | **CV** |
| Southern Africa (Zulu) | Combined | 26 | 15.9 | 1.3 | 8.0 | 28 | 16.9 | 1.1 | 6.5 | 27 | 17.9 | 1.4 | 7.9 | 28 | 13.6 | 1.0 | 7.3 |
| | M | 11 | 16.4 | 1.3 | 7.8 | 12 | 17.5 | 1.1 | 6.3 | 13 | 18.2 | 1.5 | 8.3 | 13 | 14.0 | 0.9 | 6.5 |
| | F | 15 | 15.5 | 1.2 | 7.5 | 16 | 16.5 | 0.9 | 5.6 | 14 | 17.7 | 1.3 | 7.6 | 15 | 13.2 | 0.9 | 6.9 |
| Northeastern Africa (Egypt) | Combined | 15 | 16.4 | 2.1 | 12.8 | 17 | 17.3 | 1.6 | 9.2 | 15 | 17.4 | 1.3 | 7.4 | 15 | 13.0 | 1.3 | 9.6 |
| | M | 12 | 16.7 | 2.2 | 13.1 | 13 | 17.8 | 1.5 | 8.3 | 10 | 17.7 | 1.3 | 7.2 | 10 | 13.3 | 1.2 | 9.4 |
| | F | 3 | 15.0 | 0.9 | 5.7 | 4 | 15.7 | 0.7 | 4.3 | 5 | 16.6 | 1.1 | 6.7 | 5 | 12.6 | 1.3 | 10.2 |
| Levant (Jordan) | Combined | 16 | 15.9 | 1.5 | 9.6 | 16 | 17.3 | 1.0 | 5.7 | 13 | 18.4 | 1.2 | 6.8 | 14 | 13.8 | 0.9 | 6.2 |
| | M | 3 | 16.8 | 0.3 | 1.7 | 3 | 18.2 | 1.2 | 6.4 | 2 | 19.3 | 0.0 | 0.0 | 3 | 14.3 | 0.2 | 1.2 |
| | F | 3 | 14.0 | 1.2 | 8.4 | 3 | 16.5 | 0.2 | 0.9 | 2 | 17.6 | 0.4 | 2.0 | 2 | 13.3 | 0.8 | 5.9 |
| Western Europe (Portugal) | Combined | 21 | 15.3 | 1.6 | 10.6 | 22 | 16.8 | 1.3 | 8.0 | 20 | 18.1 | 1.7 | 9.3 | 21 | 13.7 | 1.0 | 7.5 |
| | M | 10 | 16.3 | 1.2 | 7.3 | 10 | 17.9 | 0.7 | 3.8 | 10 | 19.2 | 1.6 | 8.2 | 10 | 14.3 | 0.9 | 6.6 |
| | F | 11 | 14.4 | 1.4 | 9.9 | 12 | 15.9 | 1.1 | 6.7 | 10 | 17.1 | 1.0 | 5.9 | 11 | 13.2 | 0.8 | 6.4 |
| North America (CA, U.S.A.) | Combined | 8 | 15.6 | 1.3 | 8.6 | 9 | 17.5 | 1.0 | 5.7 | 3 | 17.9 | 0.7 | 3.9 | 3 | 14.1 | 0.3 | 2.5 |
| | M | 4 | 15.5 | 2.0 | 13.0 | 5 | 17.8 | 1.3 | 7.1 | 2 | 18.1 | 0.8 | 4.7 | 2 | 14.2 | 0.4 | 3.0 |
| | F | 4 | 15.7 | 0.3 | 1.7 | 4 | 17.2 | 0.5 | 2.8 | 1 | 17.5 | – | – | 1 | 13.9 | – | – |

**Table A9.28** Summary statistics for measurements of the trapezium

| | | Trapezium | | | | | | | | | | | |
|---|---|---|---|---|---|---|---|---|---|---|---|---|---|
| | | TZM1_MAX_LEN | | | | TZM2_HEI | | | | TZM3_LEN_MC1 | | | |
| **Sample** | **Sex** | **N** | **Mean** | **SD** | **CV** | **N** | **Mean** | **SD** | **CV** | **N** | **Mean** | **SD** | **CV** |
| Southern Africa (Zulu) | Combined | 30 | 23.5 | 1.8 | 7.8 | 30 | 16.9 | 1.4 | 8.3 | 30 | 15.1 | 1.4 | 9.3 |
| | M | 15 | 24.4 | 1.8 | 7.2 | 15 | 17.3 | 1.4 | 8.3 | 15 | 15.9 | 1.3 | 8.2 |
| | F | 15 | 22.6 | 1.4 | 6.3 | 15 | 16.4 | 1.3 | 7.7 | 15 | 14.3 | 1.0 | 7.1 |
| Northeastern Africa (Egypt) | Combined | 13 | 22.7 | 1.7 | 7.4 | 14 | 16.3 | 1.3 | 7.7 | 13 | 13.8 | 1.3 | 9.4 |
| | M | 9 | 23.3 | 1.3 | 5.6 | 10 | 16.6 | 1.3 | 7.8 | 9 | 14.4 | 1.1 | 7.8 |
| | F | 4 | 21.5 | 2.0 | 9.1 | 4 | 15.7 | 1.1 | 6.9 | 4 | 12.6 | 0.6 | 4.9 |
| Levant (Jordan) | Combined | 14 | 23.2 | 2.2 | 9.4 | 14 | 16.7 | 1.4 | 8.1 | 12 | 14.6 | 1.6 | 11.1 |
| | M | 3 | 24.6 | 0.9 | 3.5 | 3 | 17.2 | 1.3 | 7.6 | 1 | 15.8 | – | – |
| | F | 3 | 21.2 | 1.2 | 5.8 | 3 | 15.6 | 0.7 | 4.5 | 3 | 13.5 | 0.8 | 5.8 |
| Western Europe (Portugal) | Combined | 22 | 23.0 | 1.8 | 7.8 | 21 | 17.2 | 1.6 | 9.1 | 19 | 14.4 | 1.2 | 8.3 |
| | M | 11 | 24.4 | 1.1 | 4.7 | 12 | 18.0 | 1.2 | 6.7 | 10 | 15.1 | 1.0 | 6.8 |
| | F | 11 | 21.5 | 1.0 | 4.5 | 9 | 16.2 | 1.5 | 9.1 | 9 | 13.6 | 0.8 | 6.1 |
| North America (CA, U.S.A.) | Combined | 4 | 24.1 | 1.5 | 6.1 | 5 | 18.0 | 0.8 | 4.3 | 5 | 15.3 | 1.2 | 7.6 |
| | M | 3 | 24.3 | 1.7 | 7.2 | 4 | 18.2 | 0.8 | 4.2 | 4 | 15.7 | 1.1 | 6.9 |
| | F | 1 | 23.5 | – | – | 1 | 17.3 | – | – | 1 | 14.1 | – | – |

**Table A9.29** Summary statistics for measurements of the capitate

| | | Capitate | | | | | | | | | | | |
|---|---|---|---|---|---|---|---|---|---|---|---|---|---|
| | | CAP1_MAX_HEI | | | | CAP2_WID_HEA | | | | CAP3_WID_BAS | | | |
| **Sample** | **Sex** | **N** | **Mean** | **SD** | **CV** | **N** | **Mean** | **SD** | **CV** | **N** | **Mean** | **SD** | **CV** |
| Southern Africa (Zulu) | Combined | 31 | 25.4 | 1.9 | 7.5 | 31 | 14.5 | 1.3 | 8.8 | 31 | 18.9 | 1.3 | 7.0 |
| | M | 14 | 26.7 | 1.3 | 5.0 | 14 | 15.1 | 1.1 | 7.4 | 14 | 20.0 | 1.1 | 5.6 |
| | F | 17 | 24.3 | 1.6 | 6.5 | 17 | 14.0 | 1.2 | 8.7 | 17 | 18.1 | 0.8 | 4.5 |
| Northeastern Africa (Egypt) | Combined | 20 | 25.3 | 1.8 | 7.1 | 20 | 13.7 | 1.3 | 9.4 | 20 | 19.5 | 1.6 | 8.3 |
| | M | 13 | 26.2 | 1.5 | 5.6 | 13 | 14.3 | 1.1 | 8.0 | 13 | 20.5 | 1.0 | 4.8 |
| | F | 7 | 23.6 | 1.0 | 4.1 | 7 | 12.7 | 0.8 | 6.6 | 7 | 17.8 | 0.9 | 5.2 |
| Levant (Jordan) | Combined | 14 | 26.2 | 2.3 | 8.8 | 16 | 13.7 | 1.2 | 8.8 | 15 | 20.0 | 1.8 | 9.2 |
| | M | 2 | 27.2 | 0.7 | 2.6 | 3 | 15.0 | 0.9 | 5.8 | 3 | 20.5 | 1.7 | 8.4 |
| | F | 2 | 24.7 | 1.7 | 6.9 | 3 | 12.6 | 0.6 | 5.0 | 2 | 19.5 | 0.8 | 4.0 |
| Western Europe (Portugal) | Combined | 26 | 25.6 | 2.5 | 9.7 | 27 | 14.2 | 1.5 | 10.7 | 26 | 19.1 | 1.8 | 9.5 |
| | M | 13 | 27.4 | 1.8 | 6.6 | 13 | 15.2 | 1.1 | 7.2 | 13 | 20.5 | 1.3 | 6.6 |
| | F | 13 | 23.7 | 1.5 | 6.4 | 14 | 13.2 | 1.2 | 9.1 | 13 | 17.7 | 0.9 | 5.0 |
| North America (CA, U.S.A.) | Combined | 15 | 26.0 | 1.1 | 4.4 | 16 | 14.2 | 0.9 | 6.7 | 16 | 19.7 | 1.0 | 4.8 |
| | M | 9 | 26.6 | 0.8 | 3.2 | 10 | 14.3 | 1.0 | 7.1 | 10 | 19.9 | 1.0 | 4.9 |
| | F | 6 | 24.9 | 0.6 | 2.6 | 6 | 14.0 | 0.9 | 6.1 | 6 | 19.3 | 0.8 | 4.3 |

**Table A9.30** Summary statistics for measurements of the hamate

| | | Hamate | | | | | | | | | | | | | | | |
|---|---|---|---|---|---|---|---|---|---|---|---|---|---|---|---|---|---|
| | | HAM1_MAX_HEI | | | | HAM2_BOD_HEI | | | | HAM3_HAM_PRO | | | | HAM4_MAX_WID | | | |
| **Sample** | **Sex** | **N** | **Mean** | **SD** | **CV** | **N** | **Mean** | **SD** | **CV** | **N** | **Mean** | **SD** | **CV** | **N** | **Mean** | **SD** | **CV** |
| Southern Africa (Zulu) | Combined | 32 | 22.0 | 2.0 | 9.1 | 32 | 13.2 | 0.9 | 7.1 | 32 | 8.8 | 1.5 | 16.6 | 32 | 20.5 | 1.8 | 8.9 |
| | M | 15 | 23.4 | 1.3 | 5.6 | 15 | 13.8 | 0.9 | 6.3 | 15 | 9.6 | 0.9 | 9.1 | 15 | 21.3 | 1.5 | 7.0 |
| | F | 17 | 20.9 | 1.7 | 8.4 | 17 | 12.7 | 0.7 | 5.7 | 17 | 8.1 | 1.5 | 19.0 | 17 | 19.8 | 1.9 | 9.5 |
| Northeastern Africa (Egypt) | Combined | 18 | 22.0 | 2.2 | 10.2 | 18 | 13.4 | 1.2 | 9.0 | 18 | 8.7 | 1.3 | 14.6 | 17 | 20.0 | 1.8 | 9.2 |
| | M | 12 | 23.0 | 2.0 | 8.6 | 12 | 14.0 | 0.9 | 6.3 | 12 | 9.0 | 1.3 | 14.1 | 11 | 20.6 | 2.0 | 9.8 |
| | F | 6 | 20.0 | 1.2 | 6.0 | 6 | 12.1 | 0.5 | 4.0 | 6 | 7.9 | 1.0 | 12.2 | 6 | 18.8 | 0.6 | 3.1 |
| Levant (Jordan) | Combined | 15 | 20.7 | 1.7 | 8.5 | 16 | 13.5 | 1.0 | 7.3 | 15 | 7.2 | 1.3 | 18.2 | 14 | 19.6 | 1.8 | 9.4 |
| | M | 2 | 22.0 | 1.1 | 5.1 | 3 | 14.2 | 0.8 | 5.6 | 2 | 7.7 | 0.1 | 0.9 | 2 | 21.8 | 2.0 | 9.1 |
| | F | 3 | 20.2 | 2.4 | 11.7 | 3 | 12.9 | 1.0 | 7.4 | 3 | 7.3 | 1.9 | 26.3 | 2 | 17.1 | 0.2 | 1.2 |
| Western Europe (Portugal) | Combined | 22 | 21.9 | 1.9 | 8.9 | 22 | 13.1 | 1.1 | 8.8 | 22 | 8.9 | 1.2 | 13.9 | 22 | 19.8 | 2.3 | 11.7 |
| | M | 11 | 23.3 | 1.6 | 6.7 | 11 | 14.0 | 0.8 | 5.5 | 11 | 9.3 | 1.4 | 14.6 | 11 | 21.4 | 1.9 | 8.7 |
| | F | 11 | 20.5 | 1.1 | 5.3 | 11 | 12.2 | 0.5 | 4.5 | 11 | 8.4 | 1.0 | 11.3 | 11 | 18.2 | 1.5 | 8.3 |
| North America (CA, U.S.A.) | Combined | 6 | 21.8 | 0.9 | 4.0 | 7 | 13.6 | 0.7 | 5.2 | 6 | 8.1 | 0.5 | 6.1 | 5 | 20.4 | 1.5 | 7.5 |
| | M | 3 | 21.7 | 0.4 | 1.7 | 4 | 13.7 | 0.6 | 4.7 | 3 | 7.8 | 0.4 | 4.5 | 3 | 20.7 | 2.1 | 9.9 |
| | F | 3 | 21.8 | 1.3 | 6.0 | 3 | 13.4 | 0.9 | 6.8 | 3 | 8.4 | 0.4 | 5.2 | 2 | 20.0 | 0.5 | 2.5 |

**Table A9.30, Continued** Summary statistics for measurements of the hamate

| | | Hamate | | | | | | | |
|---|---|---|---|---|---|---|---|---|---|
| | | HAM5_ML_WID | | | | HAM6_HAM_WID | | | |
| **Sample** | **Sex** | **N** | **Mean** | **SD** | **CV** | **N** | **Mean** | **SD** | **CV** |
| Southern Africa (Zulu) | Combined | 32 | 15.0 | 1.2 | 7.7 | 32 | 9.6 | 1.6 | 16.6 |
| | M | 15 | 15.5 | 0.7 | 4.5 | 15 | 10.2 | 1.7 | 16.3 |
| | F | 17 | 14.6 | 1.4 | 9.2 | 17 | 9.1 | 1.4 | 15.0 |
| Northeastern Africa (Egypt) | Combined | 16 | 14.9 | 0.8 | 5.3 | 18 | 10.0 | 1.0 | 10.0 |
| | M | 10 | 15.3 | 0.7 | 4.9 | 12 | 10.1 | 1.1 | 11.4 |
| | F | 6 | 14.4 | 0.5 | 3.5 | 6 | 9.8 | 0.7 | 6.7 |
| Levant (Jordan) | Combined | 12 | 15.1 | 1.1 | 7.4 | 16 | 9.3 | 1.5 | 16.5 |
| | M | 1 | 14.7 | – | – | 3 | 11.0 | 0.4 | 4.0 |
| | F | 2 | 14.3 | 1.9 | 13.4 | 3 | 8.9 | 2.3 | 25.4 |
| Western Europe (Portugal) | Combined | 21 | 14.6 | 1.4 | 9.8 | 22 | 10.3 | 1.5 | 14.4 |
| | M | 10 | 15.4 | 1.4 | 9.2 | 11 | 10.9 | 1.7 | 15.4 |
| | F | 11 | 13.9 | 1.0 | 7.5 | 11 | 9.6 | 1.0 | 10.0 |
| North America (CA, U.S.A.) | Combined | 6 | 14.8 | 0.5 | 3.5 | 8 | 9.9 | 1.4 | 14.4 |
| | M | 3 | 14.5 | 0.4 | 2.8 | 3 | 9.8 | 0.8 | 8.3 |
| | F | 3 | 15.1 | 0.5 | 3.1 | 5 | 10.0 | 2.1 | 20.9 |

**Table A9.31** Summary statistics for measurements of the first metacarpal

| | | First metacarpal | | | | | | | | | | | | | | | |
|---|---|---|---|---|---|---|---|---|---|---|---|---|---|---|---|---|---|
| | | MC1_LEN | | | | MC2_BIO_LEN | | | | MC3_MID_DP | | | | MC4_MID_ML | | | |
| **Sample** | **Sex** | **N** | **Mean** | **SD** | **CV** | **N** | **Mean** | **SD** | **CV** | **N** | **Mean** | **SD** | **CV** | **N** | **Mean** | **SD** | **CV** |
| Southern Africa (Zulu) | Combined | 33 | 45.0 | 2.6 | 5.7 | 33 | 42.9 | 2.6 | 6.0 | 33 | 9.0 | 0.8 | 8.3 | 33 | 11.9 | 1.1 | 9.4 |
| | M | 16 | 46.1 | 2.8 | 6.1 | 16 | 44.0 | 2.8 | 6.3 | 16 | 9.5 | 0.7 | 7.2 | 16 | 12.6 | 0.8 | 6.8 |
| | F | 17 | 43.9 | 1.8 | 4.1 | 17 | 41.8 | 1.9 | 4.5 | 17 | 8.5 | 0.4 | 5.2 | 17 | 11.3 | 1.0 | 9.0 |
| Northeastern Africa (Egypt) | Combined | 20 | 45.4 | 3.7 | 8.2 | 21 | 43.9 | 3.5 | 8.0 | 21 | 7.8 | 0.9 | 12.0 | 21 | 11.0 | 1.1 | 10.0 |
| | M | 13 | 47.6 | 2.7 | 5.7 | 13 | 45.7 | 2.4 | 5.2 | 13 | 8.2 | 0.9 | 10.6 | 13 | 11.5 | 1.2 | 10.1 |
| | F | 7 | 41.4 | 0.7 | 1.8 | 8 | 40.9 | 3.2 | 7.7 | 8 | 7.1 | 0.6 | 8.0 | 8 | 10.4 | 0.6 | 5.3 |
| Levant (Jordan) | Combined | 13 | 44.3 | 2.6 | 6.0 | 13 | 42.2 | 2.5 | 6.0 | 13 | 8.8 | 0.8 | 8.7 | 13 | 11.5 | 0.8 | 6.8 |
| | M | 4 | 46.3 | 2.5 | 5.5 | 4 | 43.9 | 2.6 | 6.0 | 4 | 9.2 | 0.8 | 8.2 | 4 | 11.7 | 0.9 | 7.5 |
| | F | 3 | 43.4 | 2.9 | 6.8 | 3 | 41.5 | 3.1 | 7.4 | 3 | 8.1 | 0.5 | 6.4 | 3 | 11.2 | 0.3 | 2.9 |
| Western Europe (Portugal) | Combined | 29 | 44.8 | 3.6 | 8.0 | 29 | 42.5 | 3.4 | 8.0 | 29 | 8.3 | 0.9 | 10.8 | 29 | 11.8 | 1.5 | 12.7 |
| | M | 15 | 46.8 | 2.8 | 6.0 | 15 | 44.3 | 2.7 | 6.1 | 15 | 8.9 | 0.6 | 7.1 | 15 | 12.7 | 1.3 | 10.0 |
| | F | 14 | 42.6 | 3.1 | 7.2 | 14 | 40.6 | 3.0 | 7.5 | 14 | 7.7 | 0.7 | 9.3 | 14 | 10.9 | 1.2 | 10.7 |
| North America (CA, U.S.A.) | Combined | 26 | 45.6 | 3.0 | 6.5 | 26 | 43.7 | 2.8 | 6.4 | 26 | 8.9 | 0.8 | 9.2 | 26 | 11.1 | 0.6 | 5.3 |
| | M | 15 | 46.5 | 3.3 | 7.1 | 15 | 44.5 | 3.1 | 6.9 | 15 | 9.1 | 0.8 | 9.2 | 15 | 11.0 | 0.7 | 6.3 |
| | F | 11 | 44.2 | 1.6 | 3.7 | 11 | 42.4 | 1.8 | 4.3 | 11 | 8.4 | 0.6 | 6.8 | 11 | 11.2 | 0.4 | 3.2 |

**Table A9.31, Continued** Summary statistics for measurements of the first metacarpal

| | | First metacarpal | | | | | | | | | | | | | | | |
|---|---|---|---|---|---|---|---|---|---|---|---|---|---|---|---|---|---|
| | | MC5_PRO_HEI | | | | MC6_PRO_BRE | | | | MC7_DIS_HEI | | | | MC8_DIS_BRE | | | |
| **Sample** | **Sex** | **N** | **Mean** | **SD** | **CV** | **N** | **Mean** | **SD** | **CV** | **N** | **Mean** | **SD** | **CV** | **N** | **Mean** | **SD** | **CV** |
| Southern Africa (Zulu) | Combined | 33 | 15.3 | 1.3 | 8.4 | 33 | 15.3 | 1.4 | 9.2 | 33 | 12.7 | 0.8 | 6.3 | 33 | 15.4 | 1.1 | 7.3 |
| | M | 16 | 16.1 | 1.2 | 7.5 | 16 | 16.2 | 1.2 | 7.4 | 16 | 13.2 | 0.6 | 4.7 | 16 | 16.0 | 1.2 | 7.4 |
| | F | 17 | 14.5 | 0.8 | 5.5 | 17 | 14.6 | 1.1 | 7.9 | 17 | 12.4 | 0.8 | 6.2 | 17 | 14.9 | 0.8 | 5.1 |
| Northeastern Africa (Egypt) | Combined | 20 | 14.9 | 1.4 | 9.2 | 21 | 15.5 | 1.4 | 9.2 | 21 | 13.3 | 1.4 | 10.8 | 21 | 15.4 | 1.3 | 8.5 |
| | M | 13 | 15.5 | 1.2 | 8.0 | 13 | 15.9 | 1.4 | 8.8 | 13 | 14.1 | 0.9 | 6.3 | 13 | 16.0 | 1.2 | 7.2 |
| | F | 7 | 13.7 | 0.6 | 4.1 | 8 | 14.8 | 1.3 | 8.5 | 8 | 11.9 | 1.0 | 8.4 | 8 | 14.3 | 0.7 | 5.1 |
| Levant (Jordan) | Combined | 13 | 15.4 | 1.2 | 7.6 | 13 | 15.6 | 1.4 | 9.2 | 11 | 12.9 | 1.0 | 8.1 | 13 | 15.5 | 1.1 | 7.0 |
| | M | 4 | 16.1 | 0.4 | 2.6 | 4 | 16.6 | 1.0 | 5.8 | 2 | 14.2 | 1.9 | 13.5 | 4 | 15.7 | 0.7 | 4.4 |
| | F | 3 | 14.5 | 0.2 | 1.2 | 3 | 15.0 | 0.7 | 4.3 | 3 | 12.2 | 0.4 | 3.6 | 3 | 14.7 | 0.9 | 5.8 |
| Western Europe (Portugal) | Combined | 25 | 15.6 | 1.5 | 9.7 | 28 | 15.5 | 1.3 | 8.1 | 26 | 13.5 | 1.3 | 9.4 | 28 | 15.7 | 1.5 | 9.5 |
| | M | 14 | 16.5 | 1.1 | 6.6 | 15 | 16.2 | 1.1 | 6.6 | 14 | 14.0 | 1.2 | 8.3 | 14 | 16.7 | 1.2 | 7.0 |
| | F | 11 | 14.4 | 1.1 | 7.9 | 13 | 14.8 | 1.0 | 6.9 | 12 | 12.8 | 1.1 | 8.3 | 14 | 14.7 | 1.1 | 7.4 |
| North America (CA, U.S.A.) | Combined | 25 | 15.5 | 1.1 | 6.8 | 26 | 15.1 | 0.9 | 6.1 | 22 | 13.9 | 1.1 | 8.0 | 23 | 15.8 | 1.2 | 7.3 |
| | M | 14 | 15.6 | 1.3 | 8.4 | 15 | 15.3 | 1.1 | 7.0 | 13 | 14.4 | 1.1 | 7.7 | 14 | 16.1 | 1.2 | 7.7 |
| | F | 11 | 15.3 | 0.5 | 3.3 | 11 | 14.9 | 0.6 | 4.1 | 9 | 13.3 | 0.8 | 6.0 | 9 | 15.2 | 0.8 | 5.3 |

**Table A9.32** Summary statistics for measurements of the second metacarpal

| | | Second metacarpal | | | | | | | | | | | | | | | |
|---|---|---|---|---|---|---|---|---|---|---|---|---|---|---|---|---|---|
| | | MC1_LEN | | | | MC2_BIO_LEN | | | | MC3_MID_DP | | | | MC4_MID_ML | | | |
| **Sample** | **Sex** | **N** | **Mean** | **SD** | **CV** | **N** | **Mean** | **SD** | **CV** | **N** | **Mean** | **SD** | **CV** | **N** | **Mean** | **SD** | **CV** |
| Southern Africa (Zulu) | Combined | 33 | 67.1 | 3.6 | 5.4 | 33 | 64.6 | 3.5 | 5.4 | 33 | 9.2 | 0.9 | 9.6 | 33 | 8.4 | 0.6 | 7.3 |
| | M | 16 | 68.1 | 3.7 | 5.5 | 16 | 65.5 | 3.5 | 5.4 | 16 | 9.7 | 0.8 | 8.7 | 16 | 8.6 | 0.6 | 6.5 |
| | F | 17 | 66.2 | 3.3 | 5.0 | 17 | 63.8 | 3.3 | 5.2 | 17 | 8.8 | 0.7 | 7.9 | 17 | 8.1 | 0.6 | 7.0 |
| Northeastern Africa (Egypt) | Combined | 21 | 68.0 | 4.6 | 6.8 | 21 | 65.5 | 4.4 | 6.8 | 21 | 8.2 | 0.8 | 10.2 | 21 | 7.9 | 1.2 | 14.9 |
| | M | 13 | 70.4 | 2.8 | 4.0 | 13 | 67.8 | 2.6 | 3.8 | 13 | 8.7 | 0.6 | 7.3 | 13 | 8.4 | 1.2 | 14.7 |
| | F | 8 | 64.1 | 4.2 | 6.6 | 8 | 61.9 | 4.5 | 7.2 | 8 | 7.6 | 0.7 | 9.2 | 8 | 7.2 | 0.4 | 5.9 |
| Levant (Jordan) | Combined | 10 | 65.1 | 3.5 | 5.4 | 10 | 62.6 | 3.3 | 5.3 | 10 | 8.7 | 0.8 | 9.1 | 10 | 8.2 | 0.9 | 11.2 |
| | M | 2 | 68.7 | 3.7 | 5.4 | 2 | 66.0 | 3.5 | 5.3 | 2 | 9.3 | 0.7 | 7.6 | 2 | 9.0 | 1.8 | 20.4 |
| | F | 2 | 62.4 | 0.9 | 1.5 | 2 | 60.1 | 0.8 | 1.4 | 2 | 8.1 | 0.8 | 9.7 | 2 | 7.7 | 0.3 | 3.7 |
| Western Europe (Portugal) | Combined | 29 | 66.3 | 5.3 | 8.0 | 29 | 63.1 | 5.0 | 7.9 | 29 | 9.0 | 0.8 | 9.0 | 29 | 8.7 | 0.9 | 10.8 |
| | M | 15 | 68.9 | 5.1 | 7.4 | 15 | 65.4 | 4.9 | 7.5 | 15 | 9.4 | 0.7 | 7.7 | 15 | 9.4 | 0.5 | 4.8 |
| | F | 14 | 63.6 | 4.2 | 6.6 | 14 | 60.7 | 3.8 | 6.3 | 14 | 8.6 | 0.7 | 7.8 | 14 | 8.0 | 0.7 | 8.5 |
| North America (CA, U.S.A.) | Combined | 31 | 68.6 | 3.7 | 5.4 | 31 | 65.9 | 3.8 | 5.8 | 31 | 9.0 | 0.6 | 7.2 | 31 | 8.4 | 0.7 | 8.3 |
| | M | 16 | 70.5 | 3.7 | 5.2 | 16 | 67.8 | 3.8 | 5.7 | 16 | 9.2 | 0.6 | 6.2 | 16 | 8.6 | 0.7 | 8.6 |
| | F | 15 | 66.6 | 2.5 | 3.8 | 15 | 63.9 | 2.6 | 4.1 | 15 | 8.8 | 0.7 | 7.7 | 15 | 8.1 | 0.6 | 6.9 |

**Table A9.32, Continued** Summary statistics for measurements of the second metacarpal

| | | Second metacarpal | | | | | | | | | | | | | | | |
|---|---|---|---|---|---|---|---|---|---|---|---|---|---|---|---|---|---|
| | | MC5_PRO_HEI | | | | MC6_PRO_BRE | | | | MC7_DIS_HEI | | | | MC8_DIS_BRE | | | |
| **Sample** | **Sex** | **N** | **Mean** | **SD** | **CV** | **N** | **Mean** | **SD** | **CV** | **N** | **Mean** | **SD** | **CV** | **N** | **Mean** | **SD** | **CV** |
| Southern Africa (Zulu) | Combined | 33 | 16.1 | 1.4 | 8.7 | 33 | 17.0 | 1.5 | 8.9 | 33 | 14.1 | 1.2 | 8.4 | 33 | 14.3 | 1.0 | 7.3 |
| | M | 16 | 16.8 | 1.0 | 6.2 | 16 | 17.8 | 1.6 | 8.8 | 16 | 14.8 | 1.2 | 7.9 | 16 | 15.0 | 0.9 | 6.0 |
| | F | 17 | 15.4 | 1.4 | 9.3 | 17 | 16.2 | 1.0 | 5.9 | 17 | 13.5 | 0.8 | 6.1 | 17 | 13.8 | 0.8 | 5.9 |
| Northeastern Africa (Egypt) | Combined | 21 | 16.1 | 1.5 | 9.5 | 21 | 17.3 | 1.5 | 8.5 | 22 | 13.5 | 1.2 | 8.5 | 21 | 14.6 | 1.4 | 9.3 |
| | M | 13 | 16.9 | 1.2 | 7.3 | 13 | 18.0 | 1.2 | 6.7 | 13 | 14.1 | 0.9 | 6.7 | 13 | 15.5 | 0.8 | 5.1 |
| | F | 8 | 14.7 | 0.8 | 5.5 | 8 | 16.2 | 1.2 | 7.6 | 9 | 12.6 | 0.8 | 6.5 | 8 | 13.3 | 0.9 | 7.0 |
| Levant (Jordan) | Combined | 12 | 16.7 | 1.3 | 7.7 | 12 | 17.4 | 1.4 | 8.3 | 11 | 14.0 | 0.8 | 5.9 | 11 | 14.4 | 1.2 | 8.3 |
| | M | 3 | 16.8 | 0.5 | 3.1 | 3 | 18.6 | 0.9 | 4.6 | 3 | 14.8 | 0.6 | 4.1 | 3 | 15.3 | 0.8 | 5.5 |
| | F | 3 | 15.4 | 1.2 | 7.7 | 3 | 16.0 | 0.8 | 4.8 | 2 | 13.5 | 1.3 | 9.4 | 2 | 13.4 | 0.6 | 4.8 |
| Western Europe (Portugal) | Combined | 29 | 16.4 | 1.4 | 8.5 | 28 | 17.7 | 1.7 | 9.8 | 27 | 14.4 | 1.2 | 8.1 | 29 | 15.1 | 1.4 | 9.5 |
| | M | 15 | 17.3 | 1.1 | 6.5 | 14 | 18.6 | 1.2 | 6.6 | 14 | 15.0 | 1.1 | 7.6 | 15 | 16.0 | 1.0 | 6.1 |
| | F | 14 | 15.5 | 1.0 | 6.5 | 14 | 16.9 | 1.8 | 10.7 | 13 | 13.9 | 0.9 | 6.5 | 14 | 14.1 | 1.1 | 8.0 |
| North America (CA, U.S.A.) | Combined | 33 | 16.8 | 1.2 | 7.3 | 36 | 17.6 | 1.1 | 6.3 | 29 | 14.2 | 0.8 | 5.3 | 30 | 14.8 | 0.7 | 4.9 |
| | M | 18 | 17.3 | 1.2 | 6.8 | 21 | 18.1 | 1.0 | 5.5 | 14 | 14.5 | 0.8 | 5.7 | 15 | 15.3 | 0.5 | 3.6 |
| | F | 15 | 16.1 | 0.9 | 5.6 | 15 | 16.9 | 0.8 | 4.8 | 15 | 13.9 | 0.6 | 4.1 | 15 | 14.4 | 0.6 | 3.9 |

**Table A9.33** Summary statistics for measurements of the third metacarpal

| | | Third metacarpal | | | | | | | | | | | | | | | |
|---|---|---|---|---|---|---|---|---|---|---|---|---|---|---|---|---|---|
| | | MC1_LEN | | | | MC2_BIO_LEN | | | | MC3_MID_DP | | | | MC4_MID_ML | | | |
| **Sample** | **Sex** | **N** | **Mean** | **SD** | **CV** | **N** | **Mean** | **SD** | **CV** | **N** | **Mean** | **SD** | **CV** | **N** | **Mean** | **SD** | **CV** |
| Southern Africa (Zulu) | Combined | 33 | 66.1 | 3.5 | 5.3 | 33 | 62.6 | 3.4 | 5.5 | 33 | 9.6 | 0.9 | 9.6 | 33 | 8.2 | 0.5 | 6.2 |
| | M | 16 | 66.9 | 4.1 | 6.1 | 16 | 63.5 | 3.6 | 5.7 | 16 | 10.0 | 1.0 | 10.4 | 16 | 8.5 | 0.5 | 5.9 |
| | F | 17 | 65.3 | 2.8 | 4.3 | 17 | 61.7 | 3.1 | 5.1 | 17 | 9.1 | 0.5 | 5.8 | 17 | 8.0 | 0.4 | 5.3 |
| Northeastern Africa (Egypt) | Combined | 19 | 65.9 | 4.6 | 7.0 | 19 | 61.8 | 4.2 | 6.8 | 19 | 8.5 | 0.8 | 9.3 | 19 | 7.9 | 0.9 | 11.5 |
| | M | 11 | 68.2 | 3.1 | 4.5 | 11 | 64.0 | 2.8 | 4.4 | 11 | 8.9 | 0.5 | 5.2 | 11 | 8.4 | 0.9 | 10.8 |
| | F | 8 | 62.8 | 4.7 | 7.5 | 8 | 58.8 | 4.1 | 7.0 | 8 | 7.9 | 0.8 | 9.6 | 8 | 7.3 | 0.5 | 7.2 |
| Levant (Jordan) | Combined | 12 | 64.9 | 3.0 | 4.7 | 12 | 60.2 | 3.1 | 5.1 | 12 | 8.4 | 0.7 | 8.0 | 12 | 8.2 | 0.7 | 8.1 |
| | M | 4 | 68.1 | 2.8 | 4.1 | 4 | 63.4 | 1.9 | 3.0 | 4 | 8.9 | 0.9 | 10.0 | 4 | 8.8 | 0.7 | 8.0 |
| | F | 3 | 63.6 | 2.5 | 3.9 | 3 | 59.5 | 3.4 | 5.8 | 3 | 8.0 | 0.4 | 4.7 | 3 | 8.0 | 0.8 | 9.3 |
| Western Europe (Portugal) | Combined | 30 | 65.1 | 5.1 | 7.8 | 30 | 60.5 | 4.7 | 7.7 | 30 | 9.2 | 1.0 | 10.6 | 30 | 8.6 | 0.9 | 10.5 |
| | M | 15 | 67.2 | 4.9 | 7.3 | 15 | 62.7 | 4.5 | 7.2 | 15 | 9.9 | 0.7 | 7.5 | 15 | 9.1 | 0.7 | 7.4 |
| | F | 15 | 62.9 | 4.3 | 6.9 | 15 | 58.4 | 3.9 | 6.7 | 15 | 8.5 | 0.6 | 7.4 | 15 | 8.1 | 0.8 | 10.0 |
| North America (CA, U.S.A.) | Combined | 36 | 66.9 | 3.8 | 5.7 | 35 | 62.9 | 3.4 | 5.4 | 35 | 9.5 | 0.6 | 6.7 | 35 | 7.9 | 0.5 | 6.0 |
| | M | 20 | 68.2 | 4.2 | 6.2 | 20 | 64.4 | 3.6 | 5.6 | 20 | 9.7 | 0.6 | 6.1 | 20 | 8.1 | 0.5 | 6.1 |
| | F | 16 | 65.2 | 2.6 | 3.9 | 15 | 61.1 | 2.0 | 3.3 | 15 | 9.2 | 0.6 | 6.4 | 15 | 7.7 | 0.4 | 4.6 |

**Table A9.33, Continued** Summary statistics for measurements of the third metacarpal

| | | Third metacarpal | | | | | | | | | | | | | | | |
|---|---|---|---|---|---|---|---|---|---|---|---|---|---|---|---|---|---|
| | | MC5_PRO_HEI | | | | MC6_PRO_BRE | | | | MC7_DIS_HEI | | | | MC8_DIS_BRE | | | |
| **Sample** | **Sex** | **N** | **Mean** | **SD** | **CV** | **N** | **Mean** | **SD** | **CV** | **N** | **Mean** | **SD** | **CV** | **N** | **Mean** | **SD** | **CV** |
| Southern Africa (Zulu) | Combined | 33 | 16.3 | 1.3 | 7.7 | 33 | 13.7 | 1.0 | 7.3 | 33 | 13.9 | 0.8 | 6.1 | 33 | 14.4 | 1.0 | 7.2 |
| | M | 16 | 17.0 | 1.1 | 6.3 | 16 | 14.2 | 1.0 | 6.9 | 16 | 14.5 | 0.6 | 4.3 | 16 | 15.0 | 1.0 | 6.4 |
| | F | 17 | 15.7 | 1.1 | 7.0 | 17 | 13.2 | 0.8 | 5.8 | 17 | 13.3 | 0.7 | 5.1 | 17 | 13.8 | 0.7 | 5.3 |
| Northeastern Africa (Egypt) | Combined | 19 | 16.0 | 1.2 | 7.8 | 19 | 13.2 | 1.1 | 8.0 | 20 | 13.3 | 1.1 | 8.3 | 20 | 14.3 | 1.2 | 8.7 |
| | M | 11 | 16.8 | 0.7 | 3.9 | 11 | 13.7 | 0.9 | 6.9 | 11 | 14.0 | 0.9 | 6.3 | 11 | 15.1 | 1.1 | 7.2 |
| | F | 8 | 14.8 | 0.9 | 6.1 | 8 | 12.5 | 0.8 | 6.3 | 9 | 12.5 | 0.8 | 6.3 | 9 | 13.4 | 0.7 | 5.1 |
| Levant (Jordan) | Combined | 11 | 15.6 | 0.9 | 5.8 | 9 | 13.4 | 0.9 | 6.9 | 12 | 13.4 | 0.9 | 7.1 | 12 | 13.7 | 0.9 | 6.5 |
| | M | 3 | 16.5 | 0.7 | 4.0 | 1 | 14.1 | – | – | 4 | 14.1 | 0.8 | 5.5 | 4 | 14.6 | 0.8 | 5.5 |
| | F | 3 | 15.1 | 0.8 | 5.5 | 3 | 12.7 | 0.9 | 6.8 | 3 | 12.3 | 0.2 | 1.7 | 3 | 13.6 | 0.7 | 4.8 |
| Western Europe (Portugal) | Combined | 30 | 16.5 | 1.3 | 8.0 | 30 | 14.0 | 1.2 | 8.4 | 28 | 14.0 | 1.1 | 8.0 | 29 | 14.6 | 1.3 | 8.9 |
| | M | 15 | 17.5 | 1.0 | 5.6 | 15 | 14.7 | 1.0 | 6.9 | 14 | 14.8 | 0.7 | 4.5 | 14 | 15.6 | 1.0 | 6.6 |
| | F | 15 | 15.6 | 0.8 | 5.2 | 15 | 13.3 | 0.8 | 6.0 | 14 | 13.2 | 0.9 | 6.8 | 15 | 13.7 | 0.8 | 6.0 |
| North America (CA, U.S.A.) | Combined | 33 | 16.9 | 1.0 | 5.9 | 34 | 14.1 | 0.9 | 6.5 | 35 | 14.5 | 0.9 | 6.0 | 36 | 14.3 | 0.8 | 5.4 |
| | M | 18 | 17.5 | 0.9 | 4.9 | 19 | 14.3 | 1.0 | 6.6 | 19 | 14.9 | 0.9 | 6.1 | 20 | 14.6 | 0.8 | 5.4 |
| | F | 15 | 16.3 | 0.7 | 4.4 | 15 | 13.7 | 0.8 | 5.6 | 16 | 14.1 | 0.6 | 4.3 | 16 | 14.0 | 0.6 | 4.6 |

**Table A9.33, Continued** Summary statistics for measurements of the third metacarpal

| | | Third metacarpal | | | | | | | | | | | | | | | |
|---|---|---|---|---|---|---|---|---|---|---|---|---|---|---|---|---|---|
| | | MC9_LEN_EXC | | | | MC10_DOR_WID | | | | MC11_PAL_WID | | | | MC12_FAC_WID | | | |
| **Sample** | **Sex** | **N** | **Mean** | **SD** | **CV** | **N** | **Mean** | **SD** | **CV** | **N** | **Mean** | **SD** | **CV** | **N** | **Mean** | **SD** | **CV** |
| Southern Africa (Zulu) | Combined | 33 | 62.9 | 3.4 | 5.5 | 33 | 12.3 | 0.8 | 6.8 | 33 | 7.2 | 1.3 | 17.5 | 33 | 8.1 | 0.6 | 7.8 |
| | M | 16 | 63.8 | 3.6 | 5.7 | 16 | 12.7 | 0.8 | 6.4 | 16 | 7.6 | 1.5 | 20.4 | 16 | 8.3 | 0.7 | 7.9 |
| | F | 17 | 62.0 | 3.1 | 5.0 | 17 | 11.9 | 0.7 | 5.6 | 17 | 6.9 | 0.8 | 12.1 | 17 | 7.9 | 0.5 | 6.9 |
| Northeastern Africa (Egypt) | Combined | 19 | 62.2 | 4.3 | 6.9 | 18 | 11.9 | 1.1 | 9.2 | 18 | 8.0 | 1.2 | 15.1 | 18 | 7.9 | 0.9 | 11.6 |
| | M | 11 | 64.3 | 2.8 | 4.4 | 11 | 12.5 | 0.8 | 6.7 | 11 | 8.5 | 1.0 | 11.9 | 10 | 8.4 | 0.9 | 11.2 |
| | F | 8 | 59.2 | 4.3 | 7.3 | 7 | 10.9 | 0.7 | 6.5 | 7 | 7.1 | 1.0 | 14.0 | 8 | 7.3 | 0.5 | 6.3 |
| Levant (Jordan) | Combined | 12 | 60.6 | 3.0 | 4.9 | 7 | 12.6 | 0.8 | 6.0 | 7 | 8.2 | 0.6 | 6.8 | 10 | 8.2 | 0.6 | 7.2 |
| | M | 4 | 63.8 | 2.0 | 3.1 | 1 | 12.2 | – | – | 1 | 8.4 | – | – | 2 | 8.9 | 0.1 | 0.8 |
| | F | 3 | 59.8 | 3.1 | 5.2 | 2 | 12.5 | 0.9 | 7.4 | 3 | 7.8 | 0.2 | 2.0 | 3 | 8.0 | 0.6 | 6.9 |
| Western Europe (Portugal) | Combined | 30 | 60.7 | 4.7 | 7.7 | 30 | 11.8 | 1.5 | 12.4 | 28 | 8.0 | 1.2 | 14.8 | 30 | 7.9 | 0.8 | 10.7 |
| | M | 15 | 62.9 | 4.5 | 7.1 | 15 | 12.7 | 1.1 | 8.4 | 14 | 8.5 | 1.3 | 15.5 | 15 | 8.3 | 0.8 | 9.4 |
| | F | 15 | 58.6 | 3.9 | 6.6 | 15 | 10.8 | 1.1 | 10.2 | 14 | 7.5 | 0.8 | 10.9 | 15 | 7.5 | 0.7 | 9.7 |
| North America (CA, U.S.A.) | Combined | 35 | 63.6 | 3.4 | 5.3 | 30 | 13.2 | 0.9 | 6.8 | 27 | 8.0 | 1.0 | 12.4 | 32 | 8.3 | 0.6 | 7.1 |
| | M | 20 | 64.9 | 3.6 | 5.6 | 15 | 13.6 | 0.7 | 5.2 | 13 | 8.5 | 1.0 | 12.4 | 17 | 8.6 | 0.5 | 5.5 |
| | F | 15 | 61.8 | 2.1 | 3.4 | 15 | 12.8 | 0.9 | 7.3 | 14 | 7.6 | 0.8 | 10.1 | 15 | 8.0 | 0.5 | 6.7 |

**Table A9.34** Summary statistics for measurements of the fourth metacarpal

| | | Fourth metacarpal | | | | | | | | | | | | | | | |
|---|---|---|---|---|---|---|---|---|---|---|---|---|---|---|---|---|---|
| | | MC1_LEN | | | | MC2_BIO_LEN | | | | MC3_MID_DP | | | | MC4_MID_ML | | | |
| **Sample** | **Sex** | **N** | **Mean** | **SD** | **CV** | **N** | **Mean** | **SD** | **CV** | **N** | **Mean** | **SD** | **CV** | **N** | **Mean** | **SD** | **CV** |
| Southern Africa (Zulu) | Combined | 33 | 56.7 | 3.0 | 5.4 | 33 | 55.9 | 2.9 | 5.2 | 33 | 8.1 | 0.7 | 9.1 | 33 | 6.7 | 0.5 | 8.0 |
| | M | 16 | 57.4 | 3.1 | 5.4 | 16 | 56.5 | 2.9 | 5.2 | 16 | 8.4 | 0.9 | 10.7 | 16 | 7.0 | 0.6 | 8.6 |
| | F | 17 | 56.1 | 2.9 | 5.2 | 17 | 55.4 | 2.9 | 5.2 | 17 | 7.8 | 0.4 | 5.6 | 17 | 6.5 | 0.4 | 5.9 |
| Northeastern Africa (Egypt) | Combined | 21 | 56.6 | 4.0 | 7.1 | 21 | 55.5 | 3.9 | 7.1 | 21 | 6.8 | 0.8 | 12.4 | 21 | 6.3 | 0.7 | 11.2 |
| | M | 13 | 58.7 | 2.5 | 4.3 | 13 | 57.5 | 2.4 | 4.2 | 13 | 7.2 | 0.7 | 9.7 | 13 | 6.6 | 0.7 | 10.3 |
| | F | 8 | 53.2 | 3.6 | 6.8 | 8 | 52.2 | 3.8 | 7.3 | 8 | 6.1 | 0.6 | 9.1 | 8 | 5.8 | 0.5 | 8.5 |
| Levant (Jordan) | Combined | 9 | 54.0 | 2.5 | 4.6 | 8 | 53.2 | 2.1 | 4.0 | 8 | 7.4 | 1.0 | 12.9 | 8 | 6.4 | 0.6 | 9.9 |
| | M | 1 | 55.5 | – | – | 1 | 53.8 | – | – | 1 | 8.6 | – | – | 1 | 7.4 | – | – |
| | F | 2 | 52.3 | 1.0 | 1.9 | 1 | 51.9 | – | – | 1 | 7.6 | – | – | 1 | 5.8 | – | – |
| Western Europe (Portugal) | Combined | 28 | 55.5 | 4.4 | 7.9 | 28 | 54.4 | 4.1 | 7.6 | 28 | 7.5 | 0.7 | 9.4 | 28 | 6.9 | 0.8 | 11.1 |
| | M | 15 | 57.4 | 3.9 | 6.8 | 15 | 56.1 | 3.7 | 6.6 | 15 | 7.9 | 0.6 | 7.3 | 15 | 7.1 | 0.7 | 10.4 |
| | F | 13 | 53.4 | 4.0 | 7.5 | 13 | 52.5 | 3.8 | 7.3 | 13 | 7.0 | 0.5 | 6.7 | 13 | 6.5 | 0.7 | 10.3 |
| North America (CA, U.S.A.) | Combined | 26 | 58.0 | 3.4 | 5.9 | 26 | 56.9 | 3.3 | 5.8 | 26 | 7.7 | 0.5 | 6.6 | 26 | 6.4 | 0.6 | 9.0 |
| | M | 13 | 59.6 | 3.7 | 6.2 | 13 | 58.5 | 3.5 | 6.0 | 13 | 7.9 | 0.4 | 4.5 | 13 | 6.5 | 0.5 | 7.3 |
| | F | 13 | 56.3 | 2.2 | 3.9 | 13 | 55.3 | 2.2 | 3.9 | 13 | 7.6 | 0.6 | 7.7 | 13 | 6.3 | 0.7 | 10.5 |

**Table A9.34, Continued** Summary statistics for measurements of the fourth metacarpal

| | | Fourth metacarpal | | | | | | | | | | | | | | | |
|---|---|---|---|---|---|---|---|---|---|---|---|---|---|---|---|---|---|
| | | MC5_PRO_HEI | | | | MC6_PRO_BRE | | | | MC7_DIS_HEI | | | | MC8_DIS_BRE | | | |
| **Sample** | **Sex** | **N** | **Mean** | **SD** | **CV** | **N** | **Mean** | **SD** | **CV** | **N** | **Mean** | **SD** | **CV** | **N** | **Mean** | **SD** | **CV** |
| Southern Africa (Zulu) | Combined | 33 | 12.4 | 0.9 | 7.6 | 33 | 12.1 | 1.0 | 8.2 | 33 | 12.7 | 0.8 | 6.6 | 33 | 12.2 | 0.9 | 7.7 |
| | M | 16 | 12.8 | 0.9 | 6.9 | 16 | 12.4 | 1.0 | 7.7 | 16 | 13.3 | 0.7 | 5.0 | 16 | 12.6 | 0.9 | 7.0 |
| | F | 17 | 12.0 | 0.8 | 7.0 | 17 | 11.8 | 1.0 | 8.3 | 17 | 12.2 | 0.6 | 5.0 | 17 | 11.9 | 0.9 | 7.4 |
| Northeastern Africa (Egypt) | Combined | 21 | 11.8 | 1.2 | 10.2 | 20 | 12.0 | 1.1 | 9.3 | 21 | 12.1 | 1.1 | 9.0 | 21 | 12.2 | 1.2 | 10.1 |
| | M | 13 | 12.4 | 1.1 | 9.0 | 12 | 12.7 | 0.7 | 5.4 | 13 | 12.7 | 0.8 | 6.6 | 13 | 12.8 | 1.1 | 8.4 |
| | F | 8 | 11.0 | 0.8 | 7.2 | 8 | 10.9 | 0.5 | 4.2 | 8 | 11.2 | 0.8 | 6.9 | 8 | 11.2 | 0.6 | 5.7 |
| Levant (Jordan) | Combined | 9 | 12.3 | 1.3 | 10.3 | 10 | 12.5 | 0.9 | 7.1 | 8 | 12.1 | 1.1 | 9.2 | 8 | 12.2 | 1.2 | 9.9 |
| | M | 1 | 14.2 | – | – | 1 | 13.1 | – | – | 1 | 13.3 | – | – | 1 | 14.2 | – | – |
| | F | 2 | 11.5 | 0.3 | 2.5 | 3 | 11.9 | 1.0 | 8.3 | 1 | 11.1 | – | – | 1 | 12.0 | – | – |
| Western Europe (Portugal) | Combined | 28 | 12.2 | 1.1 | 8.7 | 28 | 12.3 | 1.3 | 10.4 | 27 | 12.3 | 1.1 | 9.1 | 26 | 12.6 | 1.0 | 7.8 |
| | M | 15 | 12.8 | 0.9 | 7.1 | 15 | 13.1 | 1.1 | 8.4 | 15 | 13.1 | 0.7 | 5.3 | 14 | 13.1 | 0.8 | 6.2 |
| | F | 13 | 11.6 | 0.9 | 7.5 | 13 | 11.5 | 0.9 | 7.6 | 12 | 11.4 | 0.8 | 7.4 | 12 | 11.9 | 0.8 | 6.8 |
| North America (CA, U.S.A.) | Combined | 25 | 11.9 | 0.8 | 7.0 | 27 | 12.1 | 0.9 | 7.4 | 26 | 12.8 | 0.7 | 5.3 | 26 | 12.4 | 0.8 | 6.2 |
| | M | 12 | 12.3 | 1.0 | 8.3 | 14 | 12.6 | 0.9 | 6.9 | 14 | 13.1 | 0.6 | 4.5 | 14 | 12.6 | 0.8 | 6.7 |
| | F | 13 | 11.6 | 0.4 | 3.8 | 13 | 11.6 | 0.6 | 5.0 | 12 | 12.5 | 0.7 | 5.3 | 12 | 12.1 | 0.5 | 4.5 |

**Table A9.35** Summary statistics for measurements of the fifth metacarpal

| | | Fifth metacarpal | | | | | | | | | | | | | | | |
|---|---|---|---|---|---|---|---|---|---|---|---|---|---|---|---|---|---|
| | | MC1_LEN | | | | MC2_BIO_LEN | | | | MC3_MID_DP | | | | MC4_MID_ML | | | |
| **Sample** | **Sex** | **N** | **Mean** | **SD** | **CV** | **N** | **Mean** | **SD** | **CV** | **N** | **Mean** | **SD** | **CV** | **N** | **Mean** | **SD** | **CV** |
| Southern Africa (Zulu) | Combined | 33 | 52.0 | 2.7 | 5.3 | 33 | 51.0 | 2.8 | 5.4 | 33 | 7.1 | 0.6 | 8.8 | 33 | 8.1 | 0.7 | 8.1 |
| | M | 16 | 52.7 | 2.7 | 5.1 | 16 | 51.7 | 2.7 | 5.1 | 16 | 7.4 | 0.6 | 8.6 | 16 | 8.6 | 0.5 | 5.8 |
| | F | 17 | 51.3 | 2.7 | 5.3 | 17 | 50.4 | 2.8 | 5.5 | 17 | 6.8 | 0.5 | 6.8 | 17 | 7.7 | 0.5 | 6.5 |
| Northeastern Africa (Egypt) | Combined | 19 | 52.5 | 3.9 | 7.3 | 20 | 51.3 | 3.8 | 7.4 | 19 | 6.4 | 0.7 | 10.8 | 20 | 7.2 | 0.9 | 12.8 |
| | M | 12 | 54.6 | 2.6 | 4.7 | 12 | 53.3 | 2.6 | 4.8 | 11 | 6.6 | 0.6 | 8.6 | 12 | 7.6 | 0.8 | 10.9 |
| | F | 7 | 48.8 | 2.7 | 5.6 | 8 | 48.3 | 3.4 | 7.1 | 8 | 6.1 | 0.7 | 12.3 | 8 | 6.7 | 0.8 | 12.7 |
| Levant (Jordan) | Combined | 11 | 50.9 | 2.5 | 4.8 | 11 | 49.7 | 2.3 | 4.5 | 11 | 6.5 | 0.7 | 10.1 | 11 | 7.7 | 0.7 | 8.8 |
| | M | 2 | 50.7 | 2.1 | 4.0 | 2 | 49.1 | 1.6 | 3.2 | 2 | 7.1 | 1.1 | 15.9 | 2 | 8.3 | 1.1 | 13.6 |
| | F | 3 | 49.3 | 3.2 | 6.5 | 3 | 48.4 | 3.1 | 6.4 | 3 | 6.2 | 0.8 | 12.0 | 3 | 7.6 | 0.8 | 10.8 |
| Western Europe (Portugal) | Combined | 27 | 51.8 | 3.6 | 6.9 | 27 | 50.3 | 3.5 | 7.0 | 27 | 6.8 | 0.7 | 9.8 | 27 | 7.7 | 0.8 | 10.4 |
| | M | 13 | 53.2 | 3.6 | 6.9 | 13 | 51.7 | 3.5 | 6.8 | 13 | 7.1 | 0.6 | 8.8 | 13 | 8.2 | 0.7 | 8.2 |
| | F | 14 | 50.4 | 3.1 | 6.1 | 14 | 49.0 | 3.1 | 6.2 | 14 | 6.4 | 0.5 | 7.5 | 14 | 7.3 | 0.7 | 9.1 |
| North America (CA, U.S.A.) | Combined | 26 | 52.9 | 2.7 | 5.1 | 26 | 52.1 | 2.8 | 5.3 | 25 | 7.3 | 0.7 | 8.9 | 25 | 7.9 | 0.7 | 9.1 |
| | M | 14 | 54.0 | 2.7 | 4.9 | 14 | 53.2 | 2.9 | 5.4 | 13 | 7.5 | 0.7 | 9.5 | 13 | 8.2 | 0.6 | 7.8 |
| | F | 12 | 51.6 | 2.2 | 4.2 | 12 | 50.9 | 2.2 | 4.2 | 12 | 7.2 | 0.6 | 8.2 | 12 | 7.5 | 0.6 | 8.0 |

**Table A9.35, Continued** Summary statistics for measurements of the fifth metacarpal

| | | Fifth metacarpal | | | | | | | | | | | | | | | |
|---|---|---|---|---|---|---|---|---|---|---|---|---|---|---|---|---|---|
| | | MC5_PRO_HEI | | | | MC6_PRO_BRE | | | | MC7_DIS_HEI | | | | MC8_DIS_BRE | | | |
| **Sample** | **Sex** | **N** | **Mean** | **SD** | **CV** | **N** | **Mean** | **SD** | **CV** | **N** | **Mean** | **SD** | **CV** | **N** | **Mean** | **SD** | **CV** |
| Southern Africa (Zulu) | Combined | 33 | 10.9 | 1.0 | 9.1 | 33 | 13.2 | 1.2 | 8.9 | 33 | 11.5 | 0.9 | 7.5 | 33 | 11.5 | 0.8 | 6.8 |
| | M | 16 | 11.3 | 0.7 | 6.5 | 16 | 13.8 | 1.0 | 7.0 | 16 | 12.0 | 0.6 | 5.0 | 16 | 11.9 | 0.7 | 5.8 |
| | F | 17 | 10.6 | 1.1 | 10.2 | 17 | 12.6 | 1.0 | 8.2 | 17 | 10.9 | 0.7 | 6.2 | 17 | 11.2 | 0.7 | 6.7 |
| Northeastern Africa (Egypt) | Combined | 21 | 11.3 | 1.1 | 9.8 | 21 | 13.7 | 1.3 | 9.6 | 20 | 11.2 | 0.9 | 8.1 | 20 | 11.8 | 0.9 | 8.1 |
| | M | 13 | 11.7 | 0.7 | 5.9 | 13 | 14.3 | 1.2 | 8.1 | 12 | 11.6 | 0.8 | 6.8 | 12 | 12.1 | 0.9 | 7.1 |
| | F | 8 | 10.6 | 1.3 | 12.5 | 8 | 12.8 | 1.0 | 8.0 | 8 | 10.6 | 0.7 | 6.6 | 8 | 11.3 | 0.9 | 8.2 |
| Levant (Jordan) | Combined | 12 | 11.4 | 0.9 | 7.7 | 12 | 14.1 | 1.1 | 7.8 | 11 | 11.2 | 0.9 | 7.7 | 11 | 11.7 | 1.0 | 8.4 |
| | M | 3 | 12.2 | 0.3 | 2.2 | 3 | 14.4 | 1.6 | 11.2 | 2 | 11.8 | 0.8 | 6.6 | 2 | 12.8 | 1.4 | 11.0 |
| | F | 3 | 10.7 | 1.3 | 11.7 | 3 | 13.4 | 0.4 | 2.6 | 3 | 10.3 | 0.3 | 2.6 | 3 | 11.3 | 0.5 | 4.0 |
| Western Europe (Portugal) | Combined | 27 | 11.4 | 1.2 | 10.8 | 27 | 13.1 | 1.0 | 7.6 | 27 | 11.4 | 0.9 | 8.2 | 26 | 12.0 | 0.8 | 6.7 |
| | M | 13 | 12.0 | 1.2 | 9.7 | 13 | 13.7 | 0.9 | 6.3 | 13 | 12.1 | 0.9 | 7.3 | 13 | 12.4 | 0.7 | 6.0 |
| | F | 14 | 10.7 | 0.9 | 8.7 | 14 | 12.5 | 0.7 | 5.8 | 14 | 10.8 | 0.5 | 4.4 | 13 | 11.5 | 0.5 | 4.6 |
| North America (CA, U.S.A.) | Combined | 24 | 11.1 | 0.8 | 7.3 | 24 | 13.2 | 0.9 | 6.5 | 24 | 11.8 | 0.7 | 6.1 | 24 | 11.8 | 0.8 | 6.5 |
| | M | 12 | 11.2 | 0.8 | 6.8 | 12 | 13.6 | 0.9 | 6.6 | 12 | 12.2 | 0.7 | 6.1 | 12 | 12.3 | 0.5 | 4.2 |
| | F | 12 | 10.9 | 0.8 | 7.8 | 12 | 12.8 | 0.7 | 5.1 | 12 | 11.4 | 0.5 | 4.3 | 12 | 11.4 | 0.7 | 6.0 |

**Table A9.36** Summary statistics for measurements of the terminal hand phalanx of ray I

| | | Terminal hand phalanx of first ray | | | | | | | | | | | | | | | |
|---|---|---|---|---|---|---|---|---|---|---|---|---|---|---|---|---|---|
| | | THP1_LEN | | | | THP2_BIO_LEN | | | | THP3_MID_AP | | | | THP4_MID_ML | | | |
| **Sample** | **Sex** | **N** | **Mean** | **SD** | **CV** | **N** | **Mean** | **SD** | **CV** | **N** | **Mean** | **SD** | **CV** | **N** | **Mean** | **SD** | **CV** |
| Southern Africa (Zulu) | Combined | 30 | 22.9 | 1.4 | 6.1 | 30 | 21.4 | 1.4 | 6.7 | 30 | 4.8 | 0.6 | 13.4 | 30 | 7.7 | 0.8 | 10.2 |
| | M | 15 | 23.7 | 1.2 | 5.2 | 15 | 22.1 | 1.3 | 5.7 | 15 | 5.1 | 0.7 | 13.3 | 15 | 8.0 | 0.8 | 9.7 |
| | F | 15 | 22.2 | 1.1 | 5.0 | 15 | 20.6 | 1.2 | 5.8 | 15 | 4.4 | 0.4 | 8.6 | 15 | 7.3 | 0.6 | 8.4 |
| Northeastern Africa (Egypt) | Combined | 13 | 22.6 | 2.7 | 11.9 | 13 | 20.6 | 2.8 | 13.4 | 13 | 4.3 | 0.6 | 13.5 | 13 | 7.6 | 1.0 | 12.7 |
| | M | 9 | 23.8 | 1.6 | 6.9 | 9 | 21.8 | 1.8 | 8.1 | 9 | 4.5 | 0.6 | 12.8 | 9 | 7.9 | 0.8 | 10.8 |
| | F | 4 | 19.9 | 2.9 | 14.4 | 4 | 18.1 | 3.1 | 17.3 | 4 | 3.9 | 0.4 | 9.7 | 4 | 6.9 | 1.0 | 14.3 |
| Levant (Jordan) | Combined | 10 | 22.6 | 1.8 | 8.1 | 10 | 20.8 | 1.5 | 7.3 | 10 | 4.4 | 0.4 | 9.2 | 9 | 7.4 | 0.8 | 11.0 |
| | M | 2 | 22.3 | 0.0 | 0.0 | 2 | 20.5 | 0.1 | 0.3 | 2 | 4.6 | 0.2 | 4.7 | 1 | 8.0 | – | – |
| | F | 3 | 21.3 | 2.6 | 12.3 | 3 | 19.7 | 2.2 | 11.1 | 3 | 4.2 | 0.8 | 18.3 | 3 | 6.8 | 1.0 | 15.2 |
| Western Europe (Portugal) | Combined | 16 | 22.6 | 1.9 | 8.3 | 16 | 20.8 | 1.7 | 8.1 | 16 | 4.6 | 0.5 | 11.8 | 16 | 7.5 | 1.0 | 13.2 |
| | M | 7 | 24.0 | 1.9 | 7.8 | 7 | 22.1 | 1.3 | 6.1 | 7 | 4.9 | 0.6 | 11.5 | 7 | 7.9 | 1.2 | 15.1 |
| | F | 9 | 21.6 | 1.1 | 5.0 | 9 | 19.8 | 1.2 | 5.9 | 9 | 4.3 | 0.4 | 9.4 | 9 | 7.1 | 0.6 | 8.8 |
| North America (CA, U.S.A.) | Combined | 3 | 24.0 | 0.7 | 3.0 | 3 | 22.3 | 0.9 | 4.1 | 3 | 5.1 | 0.3 | 5.9 | 3 | 8.0 | 0.6 | 7.5 |
| | M | 3 | 24.0 | 0.7 | 3.0 | 3 | 22.3 | 0.9 | 4.1 | 3 | 5.1 | 0.3 | 5.9 | 3 | 8.0 | 0.6 | 7.5 |
| | F | 0 | – | – | – | 0 | – | – | – | 0 | – | – | – | 0 | – | – | – |

**Table A9.36, Continued** Summary statistics for measurements of the terminal hand phalanx of ray I

| | | Terminal hand phalanx of first ray | | | | | | | | | | | | | | | |
|---|---|---|---|---|---|---|---|---|---|---|---|---|---|---|---|---|---|
| | | THP5_PRO_AP | | | | THP6_PRO_ML | | | | THP7_DIS_AP | | | | THP8_DIS_ML | | | |
| **Sample** | **Sex** | **N** | **Mean** | **SD** | **CV** | **N** | **Mean** | **SD** | **CV** | **N** | **Mean** | **SD** | **CV** | **N** | **Mean** | **SD** | **CV** |
| Southern Africa (Zulu) | Combined | 29 | 8.4 | 0.7 | 7.8 | 29 | 14.4 | 1.2 | 8.3 | 29 | 3.8 | 0.4 | 10.2 | 29 | 9.9 | 1.0 | 9.7 |
| | M | 15 | 8.8 | 0.6 | 6.3 | 15 | 15.1 | 1.0 | 6.7 | 15 | 3.9 | 0.4 | 10.6 | 15 | 10.3 | 0.9 | 8.9 |
| | F | 14 | 8.0 | 0.4 | 5.4 | 14 | 13.6 | 0.8 | 5.6 | 14 | 3.6 | 0.3 | 8.1 | 14 | 9.5 | 0.9 | 9.2 |
| Northeastern Africa (Egypt) | Combined | 13 | 8.7 | 0.8 | 9.1 | 13 | 14.8 | 1.4 | 9.5 | 13 | 3.5 | 0.4 | 12.1 | 13 | 9.7 | 1.1 | 11.4 |
| | M | 9 | 8.9 | 0.6 | 6.9 | 9 | 15.2 | 1.0 | 6.6 | 9 | 3.6 | 0.4 | 11.3 | 9 | 10.0 | 0.8 | 8.2 |
| | F | 4 | 8.3 | 1.0 | 12.7 | 4 | 13.8 | 1.8 | 13.4 | 4 | 3.4 | 0.5 | 13.9 | 4 | 8.9 | 1.4 | 15.4 |
| Levant (Jordan) | Combined | 10 | 8.6 | 0.8 | 9.1 | 10 | 14.6 | 1.3 | 9.0 | 10 | 3.7 | 0.4 | 11.6 | 9 | 9.4 | 1.2 | 13.2 |
| | M | 2 | 8.9 | 0.0 | 0.0 | 2 | 15.2 | 0.4 | 2.8 | 2 | 3.7 | 0.5 | 13.6 | 1 | 9.0 | – | – |
| | F | 3 | 8.2 | 1.1 | 13.1 | 3 | 13.7 | 1.2 | 8.9 | 3 | 3.5 | 0.6 | 17.1 | 3 | 8.8 | 1.5 | 17.0 |
| Western Europe (Portugal) | Combined | 17 | 8.6 | 0.5 | 6.0 | 17 | 14.6 | 1.5 | 10.5 | 17 | 3.9 | 0.6 | 14.9 | 17 | 9.8 | 1.6 | 16.7 |
| | M | 8 | 8.9 | 0.4 | 4.3 | 8 | 15.7 | 1.2 | 7.4 | 8 | 4.3 | 0.7 | 15.3 | 8 | 10.7 | 2.0 | 18.8 |
| | F | 9 | 8.3 | 0.5 | 5.8 | 9 | 13.7 | 1.2 | 8.5 | 9 | 3.6 | 0.3 | 7.6 | 9 | 9.1 | 0.7 | 7.8 |
| North America (CA, U.S.A.) | Combined | 3 | 8.7 | 0.6 | 7.0 | 3 | 14.4 | 0.9 | 6.2 | 3 | 4.0 | 0.2 | 5.0 | 3 | 9.7 | 1.2 | 12.1 |
| | M | 3 | 8.7 | 0.6 | 7.0 | 3 | 14.4 | 0.9 | 6.2 | 3 | 4.0 | 0.2 | 5.0 | 3 | 9.7 | 1.2 | 12.1 |
| | F | 0 | – | – | – | 0 | – | – | – | 0 | – | – | – | 0 | – | – | – |

**Table A9.37** Summary statistics for measurements of the terminal hand phalanx of ray II

| | | Terminal hand phalanx of second ray | | | | | | | | | | | | | | | |
|---|---|---|---|---|---|---|---|---|---|---|---|---|---|---|---|---|---|
| | | THP1_LEN | | | | THP2_BIO_LEN | | | | THP3_MID_AP | | | | THP4_MID_ML | | | |
| **Sample** | **Sex** | **N** | **Mean** | **SD** | **CV** | **N** | **Mean** | **SD** | **CV** | **N** | **Mean** | **SD** | **CV** | **N** | **Mean** | **SD** | **CV** |
| Southern Africa (Zulu) | Combined | 18 | 17.2 | 1.6 | 9.2 | 18 | 16.2 | 1.4 | 8.8 | 18 | 3.6 | 0.5 | 13.0 | 18 | 5.1 | 0.6 | 11.3 |
| | M | 8 | 18.2 | 1.6 | 8.8 | 8 | 17.1 | 1.3 | 7.8 | 8 | 4.0 | 0.4 | 10.4 | 8 | 5.3 | 0.7 | 12.4 |
| | F | 10 | 16.4 | 1.1 | 6.6 | 10 | 15.5 | 1.0 | 6.7 | 10 | 3.4 | 0.3 | 10.2 | 10 | 5.0 | 0.5 | 9.4 |
| Northeastern Africa (Egypt) | Combined | 1 | 17.1 | – | – | 1 | 16.5 | – | – | 1 | 3.0 | – | – | 1 | 4.2 | – | – |
| | M | 1 | 17.1 | – | – | 1 | 16.5 | – | – | 1 | 3.0 | – | – | 1 | 4.2 | – | – |
| | F | 0 | – | – | – | 0 | – | – | – | 0 | – | – | – | 0 | – | – | – |
| Levant (Jordan) | Combined | 1 | 17.0 | – | – | 1 | 16.0 | – | – | 1 | 3.4 | – | – | 1 | 4.4 | – | – |
| | M | 0 | – | – | – | 0 | – | – | – | 0 | – | – | – | 0 | – | – | – |
| | F | 1 | 17.0 | – | – | 1 | 16.0 | – | – | 1 | 3.4 | – | – | 1 | 4.4 | – | – |
| Western Europe (Portugal) | Combined | 4 | 17.2 | 0.7 | 4.2 | 4 | 16.2 | 0.3 | 1.8 | 4 | 3.6 | 0.5 | 14.5 | 4 | 4.8 | 0.4 | 7.8 |
| | M | 1 | 17.0 | – | – | 1 | 16.1 | – | – | 1 | 4.1 | – | – | 1 | 5.3 | – | – |
| | F | 3 | 17.3 | 0.9 | 5.1 | 3 | 16.2 | 0.4 | 2.2 | 3 | 3.5 | 0.5 | 14.8 | 3 | 4.6 | 0.2 | 4.5 |
| North America (CA, U.S.A.) | Combined | 0 | – | – | – | 0 | – | – | – | 0 | – | – | – | 0 | – | – | – |
| | M | 0 | – | – | – | 0 | – | – | – | 0 | – | – | – | 0 | – | – | – |
| | F | 0 | – | – | – | 0 | – | – | – | 0 | – | – | – | 0 | – | – | – |

**Table A9.37, Continued** Summary statistics for measurements of the terminal hand phalanx of ray II

| | | Terminal hand phalanx of second ray | | | | | | | | | | | | | | | |
|---|---|---|---|---|---|---|---|---|---|---|---|---|---|---|---|---|---|
| | | THP5_PRO_AP | | | | THP6_PRO_ML | | | | THP7_DIS_AP | | | | THP8_DIS_ML | | | |
| **Sample** | **Sex** | **N** | **Mean** | **SD** | **CV** | **N** | **Mean** | **SD** | **CV** | **N** | **Mean** | **SD** | **CV** | **N** | **Mean** | **SD** | **CV** |
| Southern Africa (Zulu) | Combined | 18 | 6.2 | 0.7 | 12.0 | 18 | 10.2 | 1.1 | 10.5 | 18 | 3.5 | 0.6 | 16.1 | 18 | 7.6 | 1.0 | 13.6 |
| | M | 8 | 6.4 | 0.9 | 13.3 | 8 | 10.7 | 1.3 | 12.3 | 8 | 3.8 | 0.7 | 17.4 | 8 | 7.9 | 1.3 | 17.0 |
| | F | 10 | 5.9 | 0.6 | 9.6 | 10 | 9.7 | 0.6 | 6.1 | 10 | 3.3 | 0.4 | 12.2 | 10 | 7.4 | 0.7 | 9.7 |
| Northeastern Africa (Egypt) | Combined | 1 | 5.3 | – | – | 1 | 9.5 | – | – | 1 | 3.3 | – | – | 1 | 6.9 | – | – |
| | M | 1 | 5.3 | – | – | 1 | 9.5 | – | – | 1 | 3.3 | – | – | 1 | 6.9 | – | – |
| | F | 0 | – | – | – | 0 | – | – | – | 0 | – | – | – | 0 | – | – | – |
| Levant (Jordan) | Combined | 1 | 6.2 | – | – | 1 | 10.3 | – | – | 1 | 3.6 | – | – | 1 | 6.5 | – | – |
| | M | 0 | – | – | – | 0 | – | – | – | 0 | – | – | – | 0 | – | – | – |
| | F | 1 | 6.2 | – | – | 1 | 10.3 | – | – | 1 | 3.6 | – | – | 1 | 6.5 | – | – |
| Western Europe (Portugal) | Combined | 4 | 6.5 | 0.5 | 7.7 | 4 | 10.3 | 1.0 | 10.0 | 4 | 3.7 | 0.5 | 13.1 | 4 | 7.1 | 0.9 | 13.2 |
| | M | 1 | 6.6 | – | – | 1 | 10.8 | – | – | 1 | 3.8 | – | – | 1 | 8.0 | – | – |
| | F | 3 | 6.4 | 0.6 | 9.4 | 3 | 10.1 | 1.2 | 11.7 | 3 | 3.7 | 0.6 | 16.0 | 3 | 6.8 | 0.9 | 13.3 |
| North America (CA, U.S.A.) | Combined | 0 | – | – | – | 0 | – | – | – | 0 | – | – | – | 0 | – | – | – |
| | M | 0 | – | – | – | 0 | – | – | – | 0 | – | – | – | 0 | – | – | – |
| | F | 0 | – | – | – | 0 | – | – | – | 0 | – | – | – | 0 | – | – | – |

**Table A9.38** Summary statistics for measurements of the terminal hand phalanx of ray III

| | | Terminal hand phalanx of third ray | | | | | | | | | | | | | | | |
|---|---|---|---|---|---|---|---|---|---|---|---|---|---|---|---|---|---|
| | | THP1_LEN | | | | THP2_BIO_LEN | | | | THP3_MID_AP | | | | THP4_MID_ML | | | |
| **Sample** | **Sex** | **N** | **Mean** | **SD** | **CV** | **N** | **Mean** | **SD** | **CV** | **N** | **Mean** | **SD** | **CV** | **N** | **Mean** | **SD** | **CV** |
| Southern Africa (Zulu) | Combined | 19 | 18.3 | 1.3 | 7.3 | 19 | 17.1 | 1.2 | 7.3 | 19 | 3.9 | 0.6 | 14.4 | 19 | 5.5 | 0.6 | 11.5 |
| | M | 8 | 18.9 | 1.3 | 7.1 | 8 | 17.8 | 1.2 | 6.7 | 8 | 4.3 | 0.6 | 14.1 | 8 | 5.8 | 0.7 | 12.6 |
| | F | 11 | 17.8 | 1.2 | 6.6 | 11 | 16.7 | 1.1 | 6.7 | 11 | 3.6 | 0.3 | 8.0 | 11 | 5.3 | 0.5 | 9.4 |
| Northeastern Africa (Egypt) | Combined | 1 | 19.4 | – | – | 1 | 18.6 | – | – | 1 | 3.2 | – | – | 1 | 5.0 | – | – |
| | M | 1 | 19.4 | – | – | 1 | 18.6 | – | – | 1 | 3.2 | – | – | 1 | 5.0 | – | – |
| | F | 0 | – | – | – | 0 | – | – | – | 0 | – | – | – | 0 | – | – | – |
| Levant (Jordan) | Combined | 1 | 17.0 | – | – | 1 | 16.3 | – | – | 1 | 3.1 | – | – | 1 | 4.1 | – | – |
| | M | 0 | – | – | – | 0 | – | – | – | 0 | – | – | – | 0 | – | – | – |
| | F | 1 | 17.0 | – | – | 1 | 16.3 | – | – | 1 | 3.1 | – | – | 1 | 4.1 | – | – |
| Western Europe (Portugal) | Combined | 5 | 17.8 | 0.6 | 3.4 | 5 | 16.6 | 0.6 | 3.7 | 5 | 3.9 | 0.4 | 10.6 | 5 | 5.2 | 0.3 | 6.7 |
| | M | 2 | 18.0 | 1.1 | 5.9 | 2 | 16.4 | 1.0 | 6.0 | 2 | 4.2 | 0.1 | 1.7 | 2 | 5.5 | 0.1 | 2.6 |
| | F | 3 | 17.7 | 0.3 | 1.8 | 3 | 16.7 | 0.4 | 2.6 | 3 | 3.8 | 0.5 | 13.7 | 3 | 5.0 | 0.3 | 6.4 |
| North America (CA, U.S.A.) | Combined | 0 | – | – | – | 0 | – | – | – | 0 | – | – | – | 0 | – | – | – |
| | M | 0 | – | – | – | 0 | – | – | – | 0 | – | – | – | 0 | – | – | – |
| | F | 0 | – | – | – | 0 | – | – | – | 0 | – | – | – | 0 | – | – | – |

**Table A9.38, Continued** Summary statistics for measurements of the terminal hand phalanx of ray III

| | | Terminal hand phalanx of third ray | | | | | | | | | | | | | | | |
|---|---|---|---|---|---|---|---|---|---|---|---|---|---|---|---|---|---|
| | | THP5_PRO_AP | | | | THP6_PRO_ML | | | | THP7_DIS_AP | | | | THP8_DIS_ML | | | |
| **Sample** | **Sex** | **N** | **Mean** | **SD** | **CV** | **N** | **Mean** | **SD** | **CV** | **N** | **Mean** | **SD** | **CV** | **N** | **Mean** | **SD** | **CV** |
| Southern Africa (Zulu) | Combined | 19 | 6.7 | 0.7 | 11.1 | 19 | 11.0 | 1.0 | 9.4 | 19 | 3.9 | 0.4 | 11.3 | 19 | 8.1 | 0.8 | 10.3 |
| | M | 8 | 7.2 | 0.8 | 10.8 | 8 | 11.7 | 1.3 | 11.0 | 8 | 4.2 | 0.4 | 10.2 | 8 | 8.4 | 1.0 | 12.5 |
| | F | 11 | 6.4 | 0.5 | 8.6 | 11 | 10.5 | 0.4 | 4.1 | 11 | 3.6 | 0.2 | 6.5 | 11 | 7.9 | 0.6 | 8.0 |
| Northeastern Africa (Egypt) | Combined | 1 | 5.8 | – | – | 1 | 10.0 | – | – | 1 | 3.9 | – | – | 1 | 7.6 | – | – |
| | M | 1 | 5.8 | – | – | 1 | 10.0 | – | – | 1 | 3.9 | – | – | 1 | 7.6 | – | – |
| | F | 0 | – | – | – | 0 | – | – | – | 0 | – | – | – | 0 | – | – | – |
| Levant (Jordan) | Combined | 1 | 5.6 | – | – | 1 | 10.0 | – | – | 1 | 3.9 | – | – | 1 | 6.2 | – | – |
| | M | 0 | – | – | – | 0 | – | – | – | 0 | – | – | – | 0 | – | – | – |
| | F | 1 | 5.6 | – | – | 1 | 10.0 | – | – | 1 | 3.9 | – | – | 1 | 6.2 | – | – |
| Western Europe (Portugal) | Combined | 5 | 6.8 | 0.6 | 9.2 | 5 | 11.1 | 1.0 | 8.9 | 5 | 4.0 | 0.5 | 12.4 | 5 | 7.6 | 0.9 | 12.1 |
| | M | 2 | 7.1 | 0.1 | 2.0 | 2 | 11.7 | 0.8 | 6.7 | 2 | 4.2 | 0.1 | 3.4 | 2 | 8.5 | 0.3 | 3.3 |
| | F | 3 | 6.6 | 0.8 | 11.8 | 3 | 10.7 | 1.0 | 9.8 | 3 | 3.9 | 0.7 | 16.8 | 3 | 7.1 | 0.7 | 9.4 |
| North America (CA, U.S.A.) | Combined | 0 | – | – | – | 0 | – | – | – | 0 | – | – | – | 0 | – | – | – |
| | M | 0 | – | – | – | 0 | – | – | – | 0 | – | – | – | 0 | – | – | – |
| | F | 0 | – | – | – | 0 | – | – | – | 0 | – | – | – | 0 | – | – | – |

**Table A9.39** Summary statistics for measurements of the terminal hand phalanx of ray IV

| | | Terminal hand phalanx of fourth ray | | | | | | | | | | | | | | | |
|---|---|---|---|---|---|---|---|---|---|---|---|---|---|---|---|---|---|
| | | THP1_LEN | | | | THP2_BIO_LEN | | | | THP3_MID_AP | | | | THP4_MID_ML | | | |
| **Sample** | **Sex** | **N** | **Mean** | **SD** | **CV** | **N** | **Mean** | **SD** | **CV** | **N** | **Mean** | **SD** | **CV** | **N** | **Mean** | **SD** | **CV** |
| Southern Africa (Zulu) | Combined | 19 | 17.9 | 1.2 | 6.6 | 19 | 17.0 | 1.1 | 6.7 | 19 | 3.7 | 0.5 | 12.8 | 19 | 5.1 | 0.6 | 11.7 |
| | M | 8 | 18.5 | 0.9 | 5.1 | 8 | 17.5 | 0.8 | 4.5 | 8 | 4.0 | 0.4 | 9.8 | 8 | 5.4 | 0.5 | 8.8 |
| | F | 11 | 17.5 | 1.2 | 6.9 | 11 | 16.6 | 1.2 | 7.5 | 11 | 3.4 | 0.4 | 10.6 | 11 | 4.9 | 0.6 | 12.3 |
| Northeastern Africa (Egypt) | Combined | 1 | 18.5 | – | – | 1 | 17.6 | – | – | 1 | 3.3 | – | – | 1 | 4.9 | – | – |
| | M | 1 | 18.5 | – | – | 1 | 17.6 | – | – | 1 | 3.3 | – | – | 1 | 4.9 | – | – |
| | F | 0 | – | – | – | 0 | – | – | – | 0 | – | – | – | 0 | – | – | – |
| Levant (Jordan) | Combined | 1 | 16.4 | – | – | 1 | 15.6 | – | – | 1 | 3.2 | – | – | 1 | 4.1 | – | – |
| | M | 0 | – | – | – | 0 | – | – | – | 0 | – | – | – | 0 | – | – | – |
| | F | 1 | 16.4 | – | – | 1 | 15.6 | – | – | 1 | 3.2 | – | – | 1 | 4.1 | – | – |
| Western Europe (Portugal) | Combined | 5 | 17.4 | 0.7 | 4.2 | 5 | 16.5 | 1.0 | 5.9 | 5 | 3.6 | 0.3 | 8.3 | 5 | 4.7 | 0.3 | 5.8 |
| | M | 2 | 17.3 | 0.7 | 4.1 | 2 | 16.5 | 0.8 | 5.1 | 2 | 3.7 | 0.1 | 1.9 | 2 | 5.0 | 0.2 | 4.3 |
| | F | 3 | 17.5 | 0.9 | 5.1 | 3 | 16.5 | 1.2 | 7.5 | 3 | 3.5 | 0.4 | 11.4 | 3 | 4.5 | 0.2 | 3.4 |
| North America (CA, U.S.A.) | Combined | 0 | – | – | – | 0 | – | – | – | 0 | – | – | – | 0 | – | – | – |
| | M | 0 | – | – | – | 0 | – | – | – | 0 | – | – | – | 0 | – | – | – |
| | F | 0 | – | – | – | 0 | – | – | – | 0 | – | – | – | 0 | – | – | – |

**Table A9.39, Continued** Summary statistics for measurements of the terminal hand phalanx of ray IV

| | | Terminal hand phalanx of fourth ray | | | | | | | | | | | | | | | |
|---|---|---|---|---|---|---|---|---|---|---|---|---|---|---|---|---|---|
| | | THP5_PRO_AP | | | | THP6_PRO_ML | | | | THP7_DIS_AP | | | | THP8_DIS_ML | | | |
| **Sample** | **Sex** | **N** | **Mean** | **SD** | **CV** | **N** | **Mean** | **SD** | **CV** | **N** | **Mean** | **SD** | **CV** | **N** | **Mean** | **SD** | **CV** |
| Southern Africa (Zulu) | Combined | 19 | 6.2 | 0.6 | 9.1 | 19 | 10.3 | 0.8 | 7.5 | 19 | 3.7 | 0.4 | 11.2 | 19 | 7.6 | 0.9 | 11.2 |
| | M | 8 | 6.6 | 0.5 | 8.3 | 8 | 10.8 | 0.7 | 6.6 | 8 | 3.8 | 0.4 | 10.2 | 8 | 7.9 | 0.8 | 10.1 |
| | F | 11 | 5.9 | 0.4 | 6.6 | 11 | 9.9 | 0.6 | 6.1 | 11 | 3.7 | 0.5 | 12.4 | 11 | 7.4 | 0.9 | 11.9 |
| Northeastern Africa (Egypt) | Combined | 1 | 6.1 | – | – | 1 | 10.3 | – | – | 1 | 4.1 | – | – | 1 | 7.4 | – | – |
| | M | 1 | 6.1 | – | – | 1 | 10.3 | – | – | 1 | 4.1 | – | – | 1 | 7.4 | – | – |
| | F | 0 | – | – | – | 0 | – | – | – | 0 | – | – | – | 0 | – | – | – |
| Levant (Jordan) | Combined | 1 | 5.7 | – | – | 1 | 9.6 | – | – | 1 | 3.1 | – | – | 1 | 5.5 | – | – |
| | M | 0 | – | – | – | 0 | – | – | – | 0 | – | – | – | 0 | – | – | – |
| | F | 1 | 5.7 | – | – | 1 | 9.6 | – | – | 1 | 3.1 | – | – | 1 | 5.5 | – | – |
| Western Europe (Portugal) | Combined | 5 | 6.2 | 0.5 | 8.0 | 5 | 10.4 | 0.6 | 6.0 | 5 | 3.6 | 0.4 | 10.6 | 5 | 6.9 | 0.8 | 10.9 |
| | M | 2 | 6.4 | 0.3 | 4.4 | 2 | 11.0 | 0.4 | 3.2 | 2 | 3.8 | 0.6 | 17.0 | 2 | 7.6 | 0.8 | 10.3 |
| | F | 3 | 6.1 | 0.6 | 10.5 | 3 | 10.0 | 0.4 | 3.5 | 3 | 3.4 | 0.2 | 4.4 | 3 | 6.5 | 0.4 | 5.4 |
| North America (CA, U.S.A.) | Combined | 0 | – | – | – | 0 | – | – | – | 0 | – | – | – | 0 | – | – | – |
| | M | 0 | – | – | – | 0 | – | – | – | 0 | – | – | – | 0 | – | – | – |
| | F | 0 | – | – | – | 0 | – | – | – | 0 | – | – | – | 0 | – | – | – |

**Table A9.40** Summary statistics for measurements of the terminal hand phalanx of ray V

| | | Terminal hand phalanx of fifth ray | | | | | | | | | | | | | | | |
|---|---|---|---|---|---|---|---|---|---|---|---|---|---|---|---|---|---|
| | | THP1_LEN | | | | THP2_BIO_LEN | | | | THP3_MID_AP | | | | THP4_MID_ML | | | |
| **Sample** | **Sex** | **N** | **Mean** | **SD** | **CV** | **N** | **Mean** | **SD** | **CV** | **N** | **Mean** | **SD** | **CV** | **N** | **Mean** | **SD** | **CV** |
| Southern Africa (Zulu) | Combined | 22 | 16.1 | 1.5 | 9.4 | 22 | 15.2 | 1.3 | 8.7 | 22 | 3.2 | 0.4 | 12.4 | 22 | 3.9 | 0.5 | 11.9 |
| | M | 10 | 17.1 | 1.3 | 7.8 | 10 | 16.1 | 1.1 | 6.6 | 10 | 3.5 | 0.4 | 12.2 | 10 | 4.2 | 0.5 | 11.9 |
| | F | 12 | 15.2 | 1.1 | 7.1 | 12 | 14.4 | 1.0 | 6.6 | 12 | 3.1 | 0.3 | 9.9 | 12 | 3.7 | 0.4 | 9.5 |
| Northeastern Africa (Egypt) | Combined | 4 | 17.6 | 1.0 | 5.8 | 4 | 16.8 | 1.0 | 5.9 | 4 | 3.0 | 0.4 | 12.5 | 4 | 4.0 | 0.3 | 7.4 |
| | M | 4 | 17.6 | 1.0 | 5.8 | 4 | 16.8 | 1.0 | 5.9 | 4 | 3.0 | 0.4 | 12.5 | 4 | 4.0 | 0.3 | 7.4 |
| | F | 0 | – | – | – | 0 | – | – | – | 0 | – | – | – | 0 | – | – | – |
| Levant (Jordan) | Combined | 3 | 15.9 | 0.5 | 3.3 | 3 | 15.4 | 0.4 | 2.7 | 3 | 3.0 | 0.2 | 6.9 | 3 | 3.6 | 0.4 | 12.1 |
| | M | 1 | 16.3 | – | – | 1 | 15.5 | – | – | 1 | 3.1 | – | – | 1 | 4.1 | – | – |
| | F | 2 | 15.7 | 0.6 | 3.6 | 2 | 15.3 | 0.6 | 3.7 | 2 | 3.0 | 0.3 | 9.4 | 2 | 3.4 | 0.1 | 2.1 |
| Western Europe (Portugal) | Combined | 5 | 16.3 | 0.6 | 3.8 | 5 | 15.1 | 0.3 | 2.2 | 5 | 3.2 | 0.3 | 9.8 | 5 | 3.8 | 0.3 | 6.7 |
| | M | 2 | 16.2 | 0.3 | 1.7 | 2 | 15.3 | 0.1 | 0.9 | 2 | 3.3 | 0.1 | 4.3 | 2 | 3.9 | 0.1 | 3.6 |
| | F | 3 | 16.3 | 0.9 | 5.2 | 3 | 14.9 | 0.4 | 2.4 | 3 | 3.1 | 0.4 | 12.9 | 3 | 3.7 | 0.3 | 7.9 |
| North America (CA, U.S.A.) | Combined | 1 | 14.8 | – | – | 1 | 14.1 | – | – | 1 | 3.1 | – | – | 1 | 3.8 | – | – |
| | M | 0 | – | – | – | 0 | – | – | – | 0 | – | – | – | 0 | – | – | – |
| | F | 1 | 14.8 | – | – | 1 | 14.1 | – | – | 1 | 3.1 | – | – | 1 | 3.8 | – | – |

**Table A9.40, Continued** Summary statistics for measurements of the terminal hand phalanx of ray V

| | | Terminal hand phalanx of fifth ray | | | | | | | | | | | | | | | |
|---|---|---|---|---|---|---|---|---|---|---|---|---|---|---|---|---|---|
| | | THP5_PRO_AP | | | | THP6_PRO_ML | | | | THP7_DIS_AP | | | | THP8_DIS_ML | | | |
| **Sample** | **Sex** | **N** | **Mean** | **SD** | **CV** | **N** | **Mean** | **SD** | **CV** | **N** | **Mean** | **SD** | **CV** | **N** | **Mean** | **SD** | **CV** |
| Southern Africa (Zulu) | Combined | 22 | 5.6 | 0.7 | 12.3 | 22 | 8.9 | 0.8 | 8.7 | 22 | 3.4 | 0.4 | 11.0 | 22 | 5.9 | 0.9 | 14.7 |
| | M | 10 | 6.0 | 0.6 | 10.8 | 10 | 9.5 | 0.7 | 7.2 | 10 | 3.5 | 0.3 | 9.9 | 10 | 6.1 | 1.1 | 17.2 |
| | F | 12 | 5.2 | 0.5 | 9.8 | 12 | 8.5 | 0.5 | 6.0 | 12 | 3.3 | 0.4 | 11.4 | 12 | 5.7 | 0.6 | 11.3 |
| Northeastern Africa (Egypt) | Combined | 4 | 5.8 | 0.5 | 8.2 | 4 | 9.8 | 0.7 | 7.2 | 4 | 3.6 | 0.1 | 2.8 | 4 | 6.0 | 0.4 | 7.3 |
| | M | 4 | 5.8 | 0.5 | 8.2 | 4 | 9.8 | 0.7 | 7.2 | 4 | 3.6 | 0.1 | 2.8 | 4 | 6.0 | 0.4 | 7.3 |
| | F | 0 | – | – | – | 0 | – | – | – | 0 | – | – | – | 0 | – | – | – |
| Levant (Jordan) | Combined | 3 | 5.9 | 0.7 | 11.2 | 3 | 8.7 | 0.5 | 5.6 | 3 | 3.2 | 0.1 | 1.8 | 3 | 5.5 | 0.7 | 12.0 |
| | M | 1 | 6.5 | – | – | 1 | 9.3 | – | – | 1 | 3.3 | – | – | 1 | 5.1 | – | – |
| | F | 2 | 5.7 | 0.6 | 11.3 | 2 | 8.5 | 0.1 | 0.8 | 2 | 3.2 | 0.0 | 0.0 | 2 | 5.8 | 0.8 | 13.5 |
| Western Europe (Portugal) | Combined | 4 | 5.6 | 0.5 | 9.8 | 4 | 9.2 | 0.6 | 6.8 | 5 | 3.5 | 0.3 | 9.7 | 5 | 5.8 | 0.6 | 10.6 |
| | M | 2 | 5.8 | 0.2 | 3.7 | 2 | 9.5 | 0.4 | 4.5 | 2 | 3.7 | 0.0 | 0.0 | 2 | 6.3 | 0.5 | 7.9 |
| | F | 2 | 5.4 | 0.8 | 15.7 | 2 | 8.8 | 0.7 | 8.0 | 3 | 3.3 | 0.4 | 10.9 | 3 | 5.4 | 0.5 | 8.7 |
| North America (CA, U.S.A.) | Combined | 1 | 4.8 | – | – | 1 | 8.2 | – | – | 1 | 3.4 | – | – | 1 | 5.1 | – | – |
| | M | 0 | – | – | – | 0 | – | – | – | 0 | – | – | – | 0 | – | – | – |
| | F | 1 | 4.8 | – | – | 1 | 8.2 | – | – | 1 | 3.4 | – | – | 1 | 5.1 | – | – |

**Table A9.41** Summary statistics for measurements of the sacrum

| | | Sacrum | | | | | | | | | | | |
|---|---|---|---|---|---|---|---|---|---|---|---|---|---|
| | | SAC1_BRE | | | | SAC2_ANT_HEI | | | | SAC3_IND | | | |
| **Sample** | **Sex** | **N** | **Mean** | **SD** | **CV** | **N** | **Mean** | **SD** | **CV** | **N** | **Mean** | **SD** | **CV** |
| Southern Africa (Zulu) | Combined | 28 | 107.7 | 7.2 | 6.7 | 19 | 100.0 | 9.6 | 9.6 | 18 | 106.4 | 9.6 | 9.0 |
| | M | 14 | 107.2 | 6.0 | 5.6 | 9 | 104.9 | 10.9 | 10.4 | 9 | 102.2 | 10.0 | 9.7 |
| | F | 14 | 108.1 | 8.5 | 7.9 | 10 | 95.6 | 5.8 | 6.1 | 9 | 110.5 | 7.7 | 7.0 |
| Northeastern Africa (Egypt) | Combined | 23 | 111.1 | 7.3 | 6.6 | 14 | 95.9 | 9.1 | 9.5 | 13 | 115.7 | 7.1 | 6.1 |
| | M | 11 | 110.3 | 7.0 | 6.4 | 7 | 98.3 | 9.0 | 9.2 | 7 | 114.1 | 7.4 | 6.5 |
| | F | 12 | 111.9 | 7.8 | 7.0 | 7 | 93.5 | 9.1 | 9.8 | 6 | 117.5 | 6.9 | 5.9 |
| Levant (Jordan) | Combined | 22 | 110.1 | 6.7 | 6.1 | 22 | 95.9 | 9.1 | 9.5 | 19 | 113.7 | 9.1 | 8.0 |
| | M | 12 | 108.8 | 7.0 | 6.5 | 11 | 99.7 | 4.8 | 4.8 | 10 | 108.6 | 3.6 | 3.3 |
| | F | 10 | 111.6 | 6.4 | 5.7 | 11 | 92.1 | 10.9 | 11.8 | 9 | 119.5 | 10.0 | 8.4 |
| Western Europe (Portugal) | Combined | 23 | 114.5 | 5.7 | 4.9 | 17 | 101.4 | 10.4 | 10.3 | 15 | 113.1 | 10.1 | 9.0 |
| | M | 10 | 116.3 | 6.3 | 5.4 | 8 | 105.3 | 8.4 | 7.9 | 8 | 108.9 | 9.9 | 9.1 |
| | F | 13 | 113.1 | 4.9 | 4.4 | 9 | 97.9 | 11.3 | 11.5 | 7 | 117.8 | 8.7 | 7.4 |
| North America (CA, U.S.A.) | Combined | 24 | 122.2 | 7.0 | 5.7 | 17 | 107.2 | 13.2 | 12.3 | 15 | 114.4 | 10.8 | 9.4 |
| | M | 13 | 120.8 | 7.5 | 6.2 | 8 | 110.3 | 15.9 | 14.4 | 8 | 110.7 | 13.5 | 12.2 |
| | F | 11 | 123.9 | 6.2 | 5.0 | 9 | 104.4 | 10.4 | 9.9 | 7 | 118.6 | 4.7 | 4.0 |

**Table A9.42** Summary statistics for measurements of the os coxae

| | | Os coxae | | | | | | | | | | | | | | | |
|---|---|---|---|---|---|---|---|---|---|---|---|---|---|---|---|---|---|
| | | OCX1_HEI | | | | OCX2_ISC_PUB | | | | OCX3_PUB_LEN | | | | OCX4_ACE_LEN | | | |
| **Sample** | **Sex** | **N** | **Mean** | **SD** | **CV** | **N** | **Mean** | **SD** | **CV** | **N** | **Mean** | **SD** | **CV** | **N** | **Mean** | **SD** | **CV** |
| Southern Africa (Zulu) | Combined | 33 | 194.8 | 12.2 | 6.3 | 33 | 112.0 | 5.8 | 5.2 | 33 | 75.9 | 5.5 | 7.2 | 33 | 65.6 | 4.6 | 7.1 |
| | M | 17 | 198.8 | 13.4 | 6.7 | 17 | 112.1 | 5.7 | 5.1 | 17 | 74.7 | 6.4 | 8.6 | 17 | 64.0 | 4.6 | 7.3 |
| | F | 16 | 190.5 | 9.4 | 4.9 | 16 | 111.9 | 6.1 | 5.5 | 16 | 77.2 | 4.2 | 5.4 | 16 | 67.3 | 4.1 | 6.1 |
| Northeastern Africa (Egypt) | Combined | 22 | 202.5 | 14.4 | 7.1 | 20 | 118.6 | 6.3 | 5.3 | 20 | 81.3 | 3.8 | 4.7 | 19 | 70.2 | 3.0 | 4.3 |
| | M | 12 | 212.6 | 8.0 | 3.8 | 11 | 121.6 | 4.5 | 3.7 | 11 | 81.7 | 3.5 | 4.3 | 10 | 70.2 | 2.5 | 3.5 |
| | F | 10 | 190.4 | 10.2 | 5.4 | 9 | 115.0 | 6.4 | 5.6 | 9 | 80.7 | 4.3 | 5.3 | 9 | 70.3 | 3.6 | 5.2 |
| Levant (Jordan) | Combined | 20 | 199.6 | 12.6 | 6.3 | 18 | 114.2 | 6.4 | 5.6 | 21 | 77.9 | 4.7 | 6.0 | 20 | 67.6 | 4.2 | 6.3 |
| | M | 13 | 205.3 | 9.7 | 4.7 | 13 | 114.5 | 6.9 | 6.0 | 13 | 78.2 | 5.1 | 6.5 | 12 | 67.3 | 4.0 | 5.9 |
| | F | 7 | 188.8 | 10.4 | 5.5 | 5 | 113.7 | 5.2 | 4.6 | 8 | 77.3 | 4.1 | 5.4 | 8 | 68.1 | 4.8 | 7.1 |
| Western Europe (Portugal) | Combined | 20 | 207.0 | 14.3 | 6.9 | 17 | 117.3 | 6.8 | 5.8 | 18 | 84.2 | 5.8 | 6.9 | 17 | 69.8 | 4.4 | 6.4 |
| | M | 11 | 215.5 | 11.9 | 5.5 | 10 | 118.4 | 8.0 | 6.8 | 11 | 85.6 | 6.4 | 7.4 | 10 | 70.0 | 5.4 | 7.8 |
| | F | 9 | 196.7 | 9.6 | 4.9 | 7 | 115.8 | 4.7 | 4.1 | 7 | 82.0 | 4.5 | 5.5 | 7 | 69.6 | 2.8 | 4.1 |
| North America (CA, U.S.A.) | Combined | 25 | 212.3 | 11.5 | 5.4 | 22 | 125.7 | 7.3 | 5.8 | 22 | 86.6 | 5.2 | 6.0 | 27 | 73.6 | 4.8 | 6.5 |
| | M | 13 | 219.0 | 11.3 | 5.2 | 11 | 123.9 | 9.3 | 7.5 | 13 | 85.3 | 5.5 | 6.4 | 14 | 71.7 | 4.6 | 6.5 |
| | F | 12 | 205.1 | 6.2 | 3.0 | 11 | 127.4 | 4.4 | 3.4 | 9 | 88.6 | 4.3 | 4.9 | 13 | 75.6 | 4.2 | 5.5 |

**Table A9.42, Continued** Summary statistics for measurements of the os coxae

| | | Os coxae | | | | | | | | | | | |
|---|---|---|---|---|---|---|---|---|---|---|---|---|---|
| | | OCX5_NA_ISC | | | | OCX6_ACE_DIA | | | | OCX7_ACE_HEI | | | |
| **Sample** | **Sex** | **N** | **Mean** | **SD** | **CV** | **N** | **Mean** | **SD** | **CV** | **N** | **Mean** | **SD** | **CV** |
| Southern Africa (Zulu) | Combined | 33 | 46.2 | 4.1 | 8.9 | 33 | 51.0 | 3.2 | 6.3 | 34 | 49.0 | 2.9 | 5.8 |
| | M | 17 | 47.6 | 4.8 | 10.0 | 17 | 52.7 | 2.7 | 5.1 | 17 | 50.6 | 2.3 | 4.6 |
| | F | 16 | 44.7 | 2.6 | 5.9 | 16 | 49.2 | 2.8 | 5.7 | 17 | 47.4 | 2.4 | 5.1 |
| Northeastern Africa (Egypt) | Combined | 30 | 45.9 | 4.0 | 8.8 | 30 | 50.0 | 4.4 | 8.8 | 30 | 47.6 | 4.1 | 8.6 |
| | M | 15 | 48.2 | 2.8 | 5.8 | 15 | 53.3 | 3.1 | 5.9 | 15 | 50.8 | 2.9 | 5.7 |
| | F | 15 | 43.6 | 3.9 | 8.9 | 15 | 46.8 | 2.8 | 5.9 | 15 | 44.4 | 2.3 | 5.1 |
| Levant (Jordan) | Combined | 31 | 45.0 | 3.3 | 7.4 | 34 | 51.1 | 3.8 | 7.5 | 34 | 48.4 | 3.3 | 6.8 |
| | M | 17 | 47.0 | 3.0 | 6.4 | 20 | 53.3 | 2.8 | 5.3 | 20 | 50.3 | 2.2 | 4.4 |
| | F | 14 | 42.6 | 1.8 | 4.1 | 14 | 47.8 | 2.6 | 5.4 | 14 | 45.6 | 2.4 | 5.2 |
| Western Europe (Portugal) | Combined | 27 | 49.8 | 5.4 | 10.8 | 29 | 51.4 | 4.6 | 8.9 | 29 | 48.7 | 4.2 | 8.7 |
| | M | 14 | 52.5 | 5.4 | 10.3 | 14 | 54.9 | 3.7 | 6.7 | 14 | 52.2 | 2.9 | 5.5 |
| | F | 13 | 46.9 | 3.5 | 7.4 | 15 | 48.1 | 2.3 | 4.8 | 15 | 45.4 | 2.1 | 4.7 |
| North America (CA, U.S.A.) | Combined | 31 | 50.0 | 2.6 | 5.3 | 36 | 52.7 | 3.3 | 6.2 | 36 | 48.8 | 3.2 | 6.6 |
| | M | 16 | 50.9 | 2.8 | 5.6 | 18 | 54.7 | 3.2 | 5.8 | 19 | 50.6 | 2.9 | 5.8 |
| | F | 15 | 49.1 | 2.1 | 4.3 | 18 | 50.6 | 1.8 | 3.6 | 17 | 46.8 | 2.4 | 5.0 |

**Table A9.43** Summary statistics for measurements of the femur

| | | Femur | | | | | | | | | | | | | | | |
|---|---|---|---|---|---|---|---|---|---|---|---|---|---|---|---|---|---|
| | | FEM1_LEN | | | | FEM2_EPI_BRE | | | | FEM3_NEC_LEN | | | | FEM4_HEA_DIA | | | |
| **Sample** | **Sex** | **N** | **Mean** | **SD** | **CV** | **N** | **Mean** | **SD** | **CV** | **N** | **Mean** | **SD** | **CV** | **N** | **Mean** | **SD** | **CV** |
| Southern Africa (Zulu) | Combined | 34 | 435.9 | 20.3 | 4.7 | 33 | 76.0 | 4.8 | 6.3 | 34 | 83.8 | 6.4 | 7.6 | 34 | 40.6 | 2.7 | 6.7 |
| | M | 17 | 441.3 | 21.4 | 4.9 | 17 | 79.5 | 3.3 | 4.2 | 17 | 87.7 | 5.4 | 6.2 | 17 | 42.5 | 1.9 | 4.5 |
| | F | 17 | 430.5 | 18.1 | 4.2 | 16 | 72.2 | 2.9 | 4.0 | 17 | 79.8 | 4.6 | 5.8 | 17 | 38.7 | 2.0 | 5.2 |
| Northeastern Africa (Egypt) | Combined | 26 | 429.3 | 25.3 | 5.9 | 24 | 75.5 | 5.3 | 7.1 | 25 | 86.6 | 8.3 | 9.5 | 23 | 40.2 | 3.9 | 9.7 |
| | M | 14 | 442.4 | 19.0 | 4.3 | 14 | 78.9 | 3.0 | 3.8 | 13 | 91.8 | 7.2 | 7.8 | 12 | 42.6 | 3.4 | 7.9 |
| | F | 12 | 414.0 | 23.7 | 5.7 | 10 | 70.8 | 4.1 | 5.7 | 12 | 81.0 | 5.2 | 6.4 | 11 | 37.5 | 2.3 | 6.2 |
| Levant (Jordan) | Combined | 29 | 413.7 | 22.6 | 5.5 | 20 | 76.5 | 4.4 | 5.8 | 31 | 85.9 | 7.1 | 8.3 | 31 | 41.3 | 3.5 | 8.5 |
| | M | 15 | 429.3 | 16.3 | 3.8 | 12 | 79.2 | 3.0 | 3.8 | 16 | 91.7 | 4.3 | 4.7 | 17 | 43.6 | 2.7 | 6.1 |
| | F | 14 | 397.0 | 15.3 | 3.9 | 8 | 72.6 | 3.0 | 4.2 | 15 | 79.8 | 3.4 | 4.2 | 14 | 38.6 | 2.3 | 5.9 |
| Western Europe (Portugal) | Combined | 29 | 429.8 | 32.4 | 7.5 | 30 | 78.4 | 6.5 | 8.3 | 29 | 88.6 | 6.1 | 6.9 | 29 | 41.3 | 3.7 | 9.0 |
| | M | 14 | 452.3 | 22.7 | 5.0 | 15 | 82.8 | 4.9 | 5.9 | 14 | 92.6 | 4.5 | 4.9 | 14 | 43.9 | 2.3 | 5.2 |
| | F | 15 | 408.8 | 25.4 | 6.2 | 15 | 74.0 | 4.6 | 6.2 | 15 | 84.8 | 4.9 | 5.8 | 15 | 38.8 | 3.1 | 8.1 |
| North America (CA, U.S.A.) | Combined | 31 | 444.7 | 23.3 | 5.2 | 32 | 79.3 | 5.1 | 6.5 | 37 | 89.8 | 5.3 | 5.9 | 35 | 42.5 | 2.8 | 6.7 |
| | M | 19 | 455.8 | 21.1 | 4.6 | 17 | 82.9 | 4.0 | 4.8 | 21 | 92.5 | 4.5 | 4.9 | 19 | 43.8 | 2.6 | 5.9 |
| | F | 12 | 427.1 | 14.0 | 3.3 | 15 | 75.1 | 2.4 | 3.2 | 16 | 86.4 | 4.2 | 4.9 | 16 | 40.9 | 2.3 | 5.6 |

**Table A9.43, Continued** Summary statistics for measurements of the femur

| | | Femur | | | | | | | | | | | | | | | |
|---|---|---|---|---|---|---|---|---|---|---|---|---|---|---|---|---|---|
| | | FEM5_BIO_LEN | | | | FEM6_MID_CIR | | | | FEM7_AP_MID | | | | FEM8_ML_MID | | | |
| **Sample** | **Sex** | **N** | **Mean** | **SD** | **CV** | **N** | **Mean** | **SD** | **CV** | **N** | **Mean** | **SD** | **CV** | **N** | **Mean** | **SD** | **CV** |
| Southern Africa (Zulu) | Combined | 34 | 409.2 | 19.6 | 4.8 | 34 | 85.3 | 5.3 | 6.2 | 34 | 28.7 | 2.2 | 7.6 | 34 | 25.0 | 1.8 | 7.4 |
| | M | 17 | 414.6 | 21.1 | 5.1 | 17 | 88.6 | 5.0 | 5.6 | 17 | 29.6 | 2.2 | 7.3 | 17 | 26.1 | 1.7 | 6.5 |
| | F | 17 | 403.9 | 16.9 | 4.2 | 17 | 82.1 | 3.3 | 4.0 | 17 | 27.8 | 1.9 | 6.7 | 17 | 23.9 | 1.3 | 5.3 |
| Northeastern Africa (Egypt) | Combined | 27 | 403.1 | 23.8 | 5.9 | 27 | 82.5 | 6.8 | 8.3 | 27 | 27.2 | 2.7 | 9.9 | 27 | 24.5 | 2.3 | 9.6 |
| | M | 14 | 416.1 | 17.4 | 4.2 | 14 | 86.5 | 6.4 | 7.4 | 14 | 28.6 | 2.6 | 9.2 | 14 | 25.7 | 2.1 | 8.3 |
| | F | 13 | 389.2 | 22.2 | 5.7 | 13 | 78.2 | 4.3 | 5.4 | 13 | 25.8 | 1.9 | 7.5 | 13 | 23.3 | 2.0 | 8.6 |
| Levant (Jordan) | Combined | 30 | 388.5 | 21.1 | 5.4 | 30 | 85.0 | 8.8 | 10.4 | 30 | 27.7 | 3.3 | 12.1 | 30 | 25.8 | 2.4 | 9.4 |
| | M | 15 | 404.0 | 14.8 | 3.7 | 15 | 91.1 | 7.8 | 8.5 | 15 | 29.8 | 3.0 | 10.0 | 15 | 27.5 | 1.4 | 5.1 |
| | F | 15 | 373.0 | 13.7 | 3.7 | 15 | 78.8 | 4.5 | 5.7 | 15 | 25.6 | 2.2 | 8.6 | 15 | 24.0 | 2.0 | 8.1 |
| Western Europe (Portugal) | Combined | 30 | 403.9 | 29.0 | 7.2 | 30 | 90.1 | 8.0 | 8.8 | 30 | 29.3 | 3.3 | 11.4 | 30 | 26.5 | 2.2 | 8.3 |
| | M | 15 | 421.4 | 24.6 | 5.8 | 15 | 95.9 | 6.6 | 6.9 | 15 | 31.4 | 3.2 | 10.1 | 15 | 28.0 | 1.9 | 6.8 |
| | F | 15 | 386.4 | 21.9 | 5.7 | 15 | 84.3 | 3.9 | 4.6 | 15 | 27.3 | 2.0 | 7.4 | 15 | 25.0 | 1.2 | 4.9 |
| North America (CA, U.S.A.) | Combined | 32 | 418.9 | 22.6 | 5.4 | 32 | 85.0 | 6.5 | 7.6 | 32 | 27.9 | 3.1 | 11.2 | 32 | 26.1 | 1.7 | 6.5 |
| | M | 19 | 430.8 | 19.7 | 4.6 | 19 | 88.8 | 4.4 | 5.0 | 19 | 29.7 | 2.4 | 8.1 | 19 | 26.9 | 1.3 | 4.8 |
| | F | 13 | 401.5 | 13.7 | 3.4 | 13 | 79.3 | 4.6 | 5.8 | 13 | 25.2 | 1.8 | 7.1 | 13 | 24.9 | 1.5 | 5.9 |

**Table A9.43, Continued** Summary statistics for measurements of the femur

| | | Femur | | | | | | | | | | | | | | | |
|---|---|---|---|---|---|---|---|---|---|---|---|---|---|---|---|---|---|
| | | FEM9_PLA_IND | | | | FEM10_AP_HEA | | | | FEM11_NEC_HEI | | | | FEM12_NEC_ANG | | | |
| **Sample** | **Sex** | **N** | **Mean** | **SD** | **CV** | **N** | **Mean** | **SD** | **CV** | **N** | **Mean** | **SD** | **CV** | **N** | **Mean** | **SD** | **CV** |
| Southern Africa (Zulu) | Combined | 34 | 115.0 | 8.9 | 7.8 | 33 | 42.9 | 3.1 | 7.1 | 34 | 29.3 | 2.3 | 7.8 | 34 | 126.5 | 2.8 | 2.2 |
| | M | 17 | 113.4 | 7.9 | 7.0 | 16 | 45.0 | 2.3 | 5.2 | 17 | 30.7 | 2.2 | 7.1 | 17 | 126.6 | 2.9 | 2.3 |
| | F | 17 | 116.5 | 9.8 | 8.4 | 17 | 41.0 | 2.3 | 5.6 | 17 | 27.8 | 1.3 | 4.5 | 17 | 126.4 | 2.8 | 2.2 |
| Northeastern Africa (Egypt) | Combined | 26 | 111.5 | 10.1 | 9.1 | 24 | 42.6 | 3.8 | 9.0 | 26 | 28.6 | 3.2 | 11.3 | 26 | 123.8 | 4.6 | 3.7 |
| | M | 13 | 111.7 | 8.6 | 7.7 | 13 | 45.4 | 2.5 | 5.5 | 14 | 30.8 | 2.4 | 7.9 | 14 | 123.4 | 4.6 | 3.8 |
| | F | 13 | 111.2 | 11.7 | 10.6 | 11 | 39.3 | 1.8 | 4.7 | 12 | 26.0 | 1.8 | 7.0 | 12 | 124.3 | 4.7 | 3.8 |
| Levant (Jordan) | Combined | 30 | 107.8 | 9.7 | 9.0 | 30 | 42.8 | 3.3 | 7.8 | 36 | 29.5 | 2.6 | 8.8 | 34 | 123.9 | 2.8 | 2.2 |
| | M | 15 | 108.4 | 8.7 | 8.0 | 16 | 45.1 | 2.2 | 5.0 | 20 | 31.2 | 1.9 | 6.1 | 19 | 123.4 | 2.6 | 2.1 |
| | F | 15 | 107.2 | 11.0 | 10.2 | 14 | 40.1 | 2.1 | 5.2 | 16 | 27.4 | 1.7 | 6.0 | 15 | 124.6 | 3.0 | 2.4 |
| Western Europe (Portugal) | Combined | 30 | 110.7 | 8.8 | 7.9 | 30 | 43.3 | 3.9 | 8.9 | 29 | 30.9 | 3.1 | 10.1 | 30 | 126.9 | 5.2 | 4.1 |
| | M | 15 | 112.1 | 8.8 | 7.9 | 15 | 46.2 | 2.5 | 5.3 | 14 | 32.9 | 2.9 | 8.9 | 15 | 128.9 | 3.8 | 3.0 |
| | F | 15 | 109.3 | 8.8 | 8.1 | 15 | 40.4 | 2.5 | 6.2 | 15 | 29.1 | 2.0 | 6.9 | 15 | 124.9 | 5.7 | 4.6 |
| North America (CA, U.S.A.) | Combined | 32 | 106.7 | 8.9 | 8.3 | 35 | 45.2 | 3.2 | 7.0 | 39 | 30.3 | 2.1 | 7.0 | 37 | 129.1 | 4.5 | 3.5 |
| | M | 19 | 110.4 | 9.0 | 8.1 | 18 | 47.3 | 2.7 | 5.8 | 21 | 31.5 | 1.8 | 5.9 | 21 | 129.5 | 4.8 | 3.7 |
| | F | 13 | 101.2 | 5.3 | 5.3 | 17 | 43.0 | 1.7 | 4.0 | 18 | 28.9 | 1.5 | 5.2 | 16 | 128.4 | 4.1 | 3.2 |

**Table A9.44** Summary statistics for measurements of the patella

| | | Patella | | | | | | | | | | | |
|---|---|---|---|---|---|---|---|---|---|---|---|---|---|
| | | PAT1_HEI | | | | PAT2_BRE | | | | PAT3_THI | | | |
| **Sample** | **Sex** | **N** | **Mean** | **SD** | **CV** | **N** | **Mean** | **SD** | **CV** | **N** | **Mean** | **SD** | **CV** |
| Southern Africa (Zulu) | Combined | 25 | 39.5 | 3.8 | 9.5 | 25 | 41.7 | 2.9 | 7.0 | 25 | 19.0 | 1.7 | 9.0 |
| | M | 9 | 42.2 | 3.8 | 9.0 | 9 | 43.5 | 2.7 | 6.1 | 9 | 20.1 | 1.9 | 9.7 |
| | F | 16 | 38.0 | 2.8 | 7.5 | 16 | 40.7 | 2.6 | 6.4 | 16 | 18.4 | 1.2 | 6.7 |
| Northeastern Africa (Egypt) | Combined | 23 | 40.9 | 3.3 | 8.1 | 25 | 43.0 | 3.8 | 8.9 | 23 | 20.0 | 1.3 | 6.7 |
| | M | 13 | 42.5 | 2.9 | 6.8 | 14 | 43.8 | 3.8 | 8.7 | 13 | 20.6 | 1.4 | 6.6 |
| | F | 10 | 38.7 | 2.5 | 6.5 | 11 | 42.0 | 3.8 | 9.1 | 10 | 19.3 | 0.9 | 4.6 |
| Levant (Jordan) | Combined | 22 | 44.6 | 20.8 | 46.6 | 24 | 42.4 | 3.3 | 7.8 | 25 | 19.4 | 1.4 | 7.1 |
| | M | 12 | 41.7 | 2.4 | 5.8 | 14 | 44.1 | 3.0 | 6.9 | 14 | 20.2 | 1.1 | 5.6 |
| | F | 10 | 48.2 | 31.3 | 64.8 | 10 | 39.9 | 1.8 | 4.4 | 11 | 18.3 | 0.9 | 4.7 |
| Western Europe (Portugal) | Combined | 22 | 40.1 | 3.3 | 8.3 | 22 | 43.2 | 3.3 | 7.7 | 22 | 19.8 | 1.9 | 9.7 |
| | M | 11 | 42.3 | 2.6 | 6.0 | 11 | 44.8 | 2.8 | 6.2 | 11 | 20.4 | 1.7 | 8.2 |
| | F | 11 | 37.9 | 2.5 | 6.6 | 11 | 41.6 | 3.2 | 7.6 | 11 | 19.1 | 2.0 | 10.5 |
| North America (CA, U.S.A.) | Combined | 27 | 41.4 | 3.2 | 7.7 | 28 | 42.0 | 3.3 | 7.9 | 27 | 19.4 | 1.7 | 8.6 |
| | M | 11 | 43.7 | 3.4 | 7.8 | 12 | 44.0 | 3.8 | 8.7 | 11 | 20.6 | 1.7 | 8.4 |
| | F | 16 | 39.9 | 1.9 | 4.7 | 16 | 40.5 | 1.9 | 4.8 | 16 | 18.5 | 1.0 | 5.3 |

**Table A9.45** Summary statistics for measurements of the tibia

| | | Tibia | | | | | | | | | | | | | | | |
|---|---|---|---|---|---|---|---|---|---|---|---|---|---|---|---|---|---|
| | | TIB1_LEN | | | | TIB2_PRO_BRE | | | | TIB3_DIS_BRE | | | | TIB4_DIS_AP | | | |
| **Sample** | **Sex** | **N** | **Mean** | **SD** | **CV** | **N** | **Mean** | **SD** | **CV** | **N** | **Mean** | **SD** | **CV** | **N** | **Mean** | **SD** | **CV** |
| Southern Africa (Zulu) | Combined | 34 | 372.9 | 22.3 | 6.0 | 33 | 69.8 | 4.2 | 6.0 | 34 | 49.2 | 3.4 | 6.9 | 34 | 37.7 | 2.7 | 7.1 |
| | M | 17 | 376.9 | 27.3 | 7.2 | 17 | 72.8 | 3.1 | 4.2 | 17 | 51.5 | 2.9 | 5.7 | 17 | 39.6 | 1.9 | 4.9 |
| | F | 17 | 369.0 | 15.8 | 4.3 | 16 | 66.6 | 2.5 | 3.8 | 17 | 47.0 | 2.1 | 4.5 | 17 | 35.8 | 1.9 | 5.3 |
| Northeastern Africa (Egypt) | Combined | 26 | 360.0 | 24.6 | 6.8 | 19 | 68.6 | 5.0 | 7.3 | 17 | 48.4 | 3.0 | 6.2 | 26 | 37.7 | 3.6 | 9.5 |
| | M | 13 | 371.7 | 20.5 | 5.5 | 10 | 72.2 | 3.3 | 4.6 | 9 | 50.2 | 2.3 | 4.5 | 13 | 40.2 | 3.4 | 8.4 |
| | F | 13 | 348.4 | 23.4 | 6.7 | 9 | 64.5 | 2.9 | 4.6 | 8 | 46.5 | 2.5 | 5.5 | 13 | 35.3 | 1.5 | 4.3 |
| Levant (Jordan) | Combined | 23 | 352.8 | 25.8 | 7.3 | 14 | 67.8 | 5.0 | 7.3 | 14 | 48.4 | 3.4 | 7.1 | 27 | 37.8 | 3.0 | 8.0 |
| | M | 12 | 372.8 | 17.2 | 4.6 | 6 | 71.7 | 3.9 | 5.5 | 5 | 52.2 | 1.8 | 3.4 | 13 | 39.8 | 2.9 | 7.4 |
| | F | 11 | 330.8 | 11.2 | 3.4 | 8 | 65.0 | 3.6 | 5.5 | 9 | 46.3 | 2.0 | 4.2 | 14 | 35.9 | 1.5 | 4.1 |
| Western Europe (Portugal) | Combined | 30 | 358.2 | 31.2 | 8.7 | 28 | 71.6 | 6.2 | 8.6 | 30 | 49.9 | 4.0 | 7.9 | 30 | 39.0 | 3.2 | 8.2 |
| | M | 15 | 376.3 | 27.8 | 7.4 | 14 | 76.3 | 3.9 | 5.1 | 15 | 52.9 | 2.5 | 4.7 | 15 | 41.0 | 2.7 | 6.6 |
| | F | 15 | 340.1 | 23.2 | 6.8 | 14 | 66.9 | 4.0 | 5.9 | 15 | 46.9 | 2.7 | 5.7 | 15 | 37.0 | 2.3 | 6.2 |
| North America (CA, U.S.A.) | Combined | 31 | 371.7 | 22.5 | 6.1 | 19 | 74.4 | 5.6 | 7.5 | 26 | 50.4 | 3.7 | 7.3 | 27 | 38.0 | 2.7 | 7.0 |
| | M | 14 | 386.8 | 19.0 | 4.9 | 11 | 77.8 | 4.4 | 5.6 | 12 | 53.1 | 3.5 | 6.5 | 13 | 39.6 | 2.1 | 5.4 |
| | F | 17 | 359.3 | 17.0 | 4.7 | 8 | 69.8 | 3.2 | 4.5 | 14 | 48.1 | 1.9 | 3.9 | 14 | 36.5 | 2.3 | 6.2 |

**Table A9.45, Continued** Summary statistics for measurements of the tibia

| | | Tibia | | | | | | | | | | | | | | | |
|---|---|---|---|---|---|---|---|---|---|---|---|---|---|---|---|---|---|
| | | TIB5_BIO_LEN | | | | TIB6_AP_MID | | | | TIB7_ML_MID | | | | TIB8_MID_CIR | | | |
| **Sample** | **Sex** | **N** | **Mean** | **SD** | **CV** | **N** | **Mean** | **SD** | **CV** | **N** | **Mean** | **SD** | **CV** | **N** | **Mean** | **SD** | **CV** |
| Southern Africa (Zulu) | Combined | 34 | 351.0 | 21.3 | 6.1 | 34 | 29.7 | 3.0 | 10.0 | 34 | 22.2 | 2.2 | 10.1 | 34 | 82.9 | 6.9 | 8.3 |
| | M | 17 | 354.3 | 25.8 | 7.3 | 17 | 31.3 | 2.7 | 8.6 | 17 | 22.7 | 2.2 | 9.9 | 17 | 86.7 | 6.2 | 7.2 |
| | F | 17 | 347.8 | 15.7 | 4.5 | 17 | 28.0 | 2.3 | 8.1 | 17 | 21.6 | 2.1 | 9.9 | 17 | 79.2 | 5.3 | 6.7 |
| Northeastern Africa (Egypt) | Combined | 26 | 339.3 | 24.3 | 7.1 | 26 | 27.7 | 2.5 | 9.0 | 26 | 19.3 | 1.8 | 9.4 | 26 | 76.6 | 6.0 | 7.9 |
| | M | 13 | 351.8 | 18.7 | 5.3 | 13 | 28.8 | 2.5 | 8.6 | 13 | 20.1 | 1.7 | 8.3 | 13 | 79.8 | 5.2 | 6.5 |
| | F | 13 | 326.7 | 23.1 | 7.1 | 13 | 26.6 | 2.0 | 7.7 | 13 | 18.6 | 1.7 | 9.3 | 13 | 73.4 | 5.1 | 6.9 |
| Levant (Jordan) | Combined | 23 | 327.7 | 22.7 | 6.9 | 22 | 28.3 | 2.8 | 9.8 | 23 | 20.4 | 1.9 | 9.4 | 22 | 77.7 | 7.1 | 9.1 |
| | M | 11 | 346.9 | 15.1 | 4.4 | 11 | 30.4 | 1.6 | 5.1 | 11 | 21.5 | 1.3 | 6.0 | 11 | 83.1 | 4.4 | 5.3 |
| | F | 12 | 310.0 | 10.6 | 3.4 | 11 | 26.2 | 2.0 | 7.8 | 12 | 19.3 | 1.8 | 9.5 | 11 | 72.3 | 4.6 | 6.3 |
| Western Europe (Portugal) | Combined | 30 | 335.7 | 30.2 | 9.0 | 30 | 29.1 | 3.0 | 10.2 | 30 | 21.7 | 2.4 | 11.0 | 30 | 83.6 | 8.5 | 10.1 |
| | M | 15 | 353.2 | 26.9 | 7.6 | 15 | 31.3 | 2.5 | 7.9 | 15 | 23.3 | 2.1 | 8.9 | 15 | 90.2 | 5.9 | 6.6 |
| | F | 15 | 318.2 | 22.6 | 7.1 | 15 | 27.0 | 1.5 | 5.5 | 15 | 20.1 | 1.3 | 6.6 | 15 | 76.9 | 4.4 | 5.7 |
| North America (CA, U.S.A.) | Combined | 33 | 349.7 | 21.0 | 6.0 | 32 | 30.6 | 3.3 | 10.6 | 33 | 20.5 | 1.6 | 7.8 | 32 | 83.0 | 7.3 | 8.8 |
| | M | 16 | 361.6 | 18.2 | 5.0 | 16 | 33.2 | 2.2 | 6.7 | 16 | 21.3 | 1.3 | 6.3 | 16 | 88.4 | 5.3 | 6.0 |
| | F | 17 | 338.5 | 17.1 | 5.0 | 16 | 28.1 | 1.9 | 6.6 | 17 | 19.6 | 1.4 | 7.1 | 16 | 77.5 | 4.1 | 5.3 |

**Table A9.45, Continued** Summary statistics for measurements of the tibia

| | | Tibia | | | | | | | | | | | | | | | |
|---|---|---|---|---|---|---|---|---|---|---|---|---|---|---|---|---|---|
| | | TIB9_CIR_NUT | | | | TIB10_ML_NUT | | | | TIB11_MAX_NUT | | | | TIB12_PLA_IND | | | |
| **Sample** | **Sex** | **N** | **Mean** | **SD** | **CV** | **N** | **Mean** | **SD** | **CV** | **N** | **Mean** | **SD** | **CV** | **N** | **Mean** | **SD** | **CV** |
| Southern Africa (Zulu) | Combined | 32 | 93.3 | 7.9 | 8.4 | 33 | 24.3 | 2.1 | 8.5 | 32 | 34.2 | 3.3 | 9.5 | 32 | 71.5 | 5.9 | 8.3 |
| | M | 15 | 98.1 | 7.3 | 7.5 | 16 | 24.9 | 2.0 | 7.9 | 15 | 36.2 | 3.0 | 8.3 | 15 | 69.4 | 5.0 | 7.1 |
| | F | 17 | 89.2 | 5.7 | 6.4 | 17 | 23.8 | 2.1 | 8.6 | 17 | 32.5 | 2.3 | 7.2 | 17 | 73.4 | 6.2 | 8.4 |
| Northeastern Africa (Egypt) | Combined | 27 | 85.0 | 7.0 | 8.2 | 27 | 21.2 | 2.0 | 9.3 | 27 | 32.3 | 3.2 | 10.0 | 27 | 66.2 | 6.2 | 9.4 |
| | M | 14 | 88.5 | 6.1 | 6.8 | 14 | 22.2 | 2.0 | 9.0 | 14 | 33.6 | 2.9 | 8.7 | 14 | 66.4 | 7.0 | 10.5 |
| | F | 13 | 81.3 | 6.0 | 7.4 | 13 | 20.2 | 1.4 | 7.0 | 13 | 30.8 | 3.0 | 9.6 | 13 | 66.0 | 5.6 | 8.4 |
| Levant (Jordan) | Combined | 31 | 87.4 | 9.0 | 10.2 | 32 | 22.5 | 2.0 | 9.1 | 32 | 32.8 | 3.9 | 11.8 | 32 | 68.9 | 5.4 | 7.8 |
| | M | 17 | 93.2 | 6.7 | 7.2 | 17 | 23.7 | 1.5 | 6.3 | 17 | 35.4 | 2.9 | 8.2 | 17 | 67.2 | 4.6 | 6.9 |
| | F | 14 | 80.3 | 5.6 | 7.0 | 15 | 21.1 | 1.7 | 7.9 | 15 | 29.8 | 2.4 | 8.1 | 15 | 70.9 | 5.6 | 7.9 |
| Western Europe (Portugal) | Combined | 30 | 95.9 | 9.8 | 10.2 | 30 | 24.4 | 3.0 | 12.2 | 30 | 34.5 | 3.9 | 11.2 | 30 | 70.7 | 4.8 | 6.8 |
| | M | 15 | 103.3 | 7.5 | 7.2 | 15 | 26.3 | 2.7 | 10.4 | 15 | 37.3 | 3.0 | 8.1 | 15 | 70.6 | 5.5 | 7.8 |
| | F | 15 | 88.5 | 5.1 | 5.7 | 15 | 22.4 | 1.6 | 7.3 | 15 | 31.7 | 2.2 | 7.0 | 15 | 70.9 | 4.2 | 5.9 |
| North America (CA, U.S.A.) | Combined | 33 | 91.1 | 7.9 | 8.6 | 32 | 22.3 | 1.8 | 8.2 | 32 | 34.0 | 3.4 | 9.9 | 32 | 65.8 | 3.8 | 5.8 |
| | M | 15 | 97.3 | 5.7 | 5.9 | 15 | 23.6 | 1.3 | 5.6 | 15 | 36.5 | 2.6 | 7.2 | 15 | 64.7 | 3.4 | 5.3 |
| | F | 18 | 86.0 | 5.3 | 6.2 | 17 | 21.2 | 1.4 | 6.8 | 17 | 31.8 | 2.1 | 6.8 | 17 | 66.7 | 4.0 | 5.9 |

**Table A9.46** Summary statistics for measurements of the fibula

| | | Fibula | | | | | | | | | | | | | | | |
|---|---|---|---|---|---|---|---|---|---|---|---|---|---|---|---|---|---|
| | | FIB1_LEN | | | | FIB2_MID_CIR | | | | FIB3_MAX_ART | | | | FIB4_ART_DIA | | | |
| **Sample** | **Sex** | **N** | **Mean** | **SD** | **CV** | **N** | **Mean** | **SD** | **CV** | **N** | **Mean** | **SD** | **CV** | **N** | **Mean** | **SD** | **CV** |
| Southern Africa (Zulu) | Combined | 33 | 361.7 | 22.5 | 6.2 | 33 | 45.0 | 4.9 | 10.9 | 34 | 20.8 | 1.5 | 7.3 | 32 | 18.0 | 1.8 | 10.0 |
| | M | 16 | 366.3 | 27.6 | 7.5 | 16 | 48.3 | 3.9 | 8.2 | 17 | 21.2 | 1.4 | 6.6 | 17 | 18.8 | 1.6 | 8.2 |
| | F | 17 | 357.3 | 15.9 | 4.4 | 17 | 41.9 | 3.6 | 8.6 | 17 | 20.3 | 1.6 | 7.8 | 15 | 17.0 | 1.6 | 9.3 |
| Northeastern Africa (Egypt) | Combined | 23 | 349.8 | 24.7 | 7.1 | 22 | 43.4 | 4.3 | 9.9 | 21 | 21.0 | 1.8 | 8.7 | 20 | 18.8 | 1.4 | 7.2 |
| | M | 13 | 364.7 | 19.2 | 5.3 | 12 | 44.3 | 4.4 | 9.9 | 11 | 21.6 | 1.9 | 8.8 | 10 | 18.8 | 1.9 | 9.9 |
| | F | 10 | 332.0 | 18.0 | 5.4 | 10 | 42.3 | 4.2 | 9.9 | 10 | 20.3 | 1.6 | 7.9 | 10 | 18.8 | 0.7 | 3.5 |
| Levant (Jordan) | Combined | 7 | 337.4 | 21.2 | 6.3 | 6 | 42.9 | 2.6 | 6.1 | 20 | 21.3 | 2.2 | 10.5 | 20 | 19.2 | 1.8 | 9.5 |
| | M | 4 | 350.0 | 19.7 | 5.6 | 4 | 43.9 | 2.3 | 5.2 | 10 | 22.5 | 2.2 | 9.8 | 10 | 20.5 | 1.3 | 6.5 |
| | F | 3 | 320.6 | 5.7 | 1.8 | 2 | 40.7 | 2.1 | 5.2 | 10 | 20.1 | 1.6 | 7.9 | 10 | 17.9 | 1.2 | 6.9 |
| Western Europe (Portugal) | Combined | 29 | 349.3 | 31.6 | 9.1 | 29 | 45.7 | 5.1 | 11.2 | 27 | 21.1 | 1.8 | 8.7 | 26 | 18.1 | 1.6 | 8.9 |
| | M | 14 | 368.7 | 27.2 | 7.4 | 14 | 48.4 | 5.3 | 10.9 | 13 | 21.7 | 1.5 | 6.9 | 13 | 18.4 | 1.9 | 10.2 |
| | F | 15 | 331.1 | 24.1 | 7.3 | 15 | 43.1 | 3.5 | 8.0 | 14 | 20.6 | 2.1 | 9.9 | 13 | 17.8 | 1.3 | 7.3 |
| North America (CA, U.S.A.) | Combined | 27 | 357.8 | 19.9 | 5.5 | 27 | 45.8 | 4.8 | 10.4 | 28 | 21.5 | 1.8 | 8.2 | 29 | 17.6 | 1.3 | 7.3 |
| | M | 13 | 370.1 | 17.6 | 4.8 | 13 | 48.3 | 5.5 | 11.4 | 13 | 21.2 | 1.9 | 9.1 | 13 | 18.2 | 1.1 | 6.3 |
| | F | 14 | 346.4 | 14.6 | 4.2 | 14 | 43.5 | 2.4 | 5.5 | 15 | 21.8 | 1.6 | 7.5 | 16 | 17.2 | 1.3 | 7.4 |

**Table A9.46, Continued** Summary statistics for measurements of the fibula

| | | Fibula | | | | | | | |
|---|---|---|---|---|---|---|---|---|---|
| | | FIB5_DIS_BRE | | | | FIB6_DIS_AP | | | |
| **Sample** | **Sex** | **N** | **Mean** | **SD** | **CV** | **N** | **Mean** | **SD** | **CV** |
| Southern Africa (Zulu) | Combined | 34 | 20.1 | 1.7 | 8.4 | 34 | 25.7 | 2.3 | 9.0 |
| | M | 17 | 21.1 | 1.1 | 5.2 | 17 | 27.0 | 2.2 | 8.0 |
| | F | 17 | 19.1 | 1.6 | 8.4 | 17 | 24.4 | 1.7 | 6.8 |
| Northeastern Africa (Egypt) | Combined | 22 | 21.0 | 1.5 | 7.1 | 21 | 25.5 | 1.7 | 6.6 |
| | M | 11 | 21.2 | 1.3 | 6.2 | 11 | 26.2 | 2.0 | 7.8 |
| | F | 11 | 20.7 | 1.7 | 8.1 | 10 | 24.8 | 0.8 | 3.2 |
| Levant (Jordan) | Combined | 17 | 20.8 | 1.8 | 8.6 | 17 | 25.9 | 1.7 | 6.5 |
| | M | 9 | 21.7 | 1.6 | 7.5 | 9 | 26.9 | 1.4 | 5.3 |
| | F | 8 | 19.7 | 1.4 | 7.0 | 8 | 24.9 | 1.3 | 5.3 |
| Western Europe (Portugal) | Combined | 29 | 19.6 | 1.8 | 9.1 | 29 | 26.1 | 2.0 | 7.8 |
| | M | 15 | 20.4 | 1.9 | 9.2 | 15 | 27.3 | 1.9 | 7.0 |
| | F | 14 | 18.7 | 1.2 | 6.3 | 14 | 24.8 | 1.2 | 4.9 |
| North America (CA, U.S.A.) | Combined | 27 | 22.6 | 1.4 | 6.3 | 29 | 27.1 | 1.7 | 6.4 |
| | M | 11 | 23.5 | 1.4 | 5.8 | 13 | 28.3 | 1.6 | 5.8 |
| | F | 16 | 22.0 | 1.1 | 5.0 | 16 | 26.2 | 1.1 | 4.4 |

**Table A9.47** Summary statistics for measurements of the talus

| | | Talus | | | | | | | | | | | | | | | |
|---|---|---|---|---|---|---|---|---|---|---|---|---|---|---|---|---|---|
| | | TAL1_LEN | | | | TAL2_MAX_LEN | | | | TAL3_HEA_NEC | | | | TAL4_PHY_HEI | | | |
| **Sample** | **Sex** | **N** | **Mean** | **SD** | **CV** | **N** | **Mean** | **SD** | **CV** | **N** | **Mean** | **SD** | **CV** | **N** | **Mean** | **SD** | **CV** |
| Southern Africa (Zulu) | Combined | 32 | 49.3 | 3.8 | 7.7 | 32 | 55.1 | 4.3 | 7.7 | 32 | 21.4 | 2.3 | 10.7 | 32 | 24.2 | 2.2 | 9.1 |
| | M | 16 | 51.6 | 3.0 | 5.8 | 16 | 57.5 | 3.2 | 5.6 | 16 | 22.3 | 2.0 | 9.1 | 16 | 25.5 | 2.0 | 7.7 |
| | F | 16 | 47.0 | 3.2 | 6.7 | 16 | 52.6 | 3.8 | 7.2 | 16 | 20.5 | 2.2 | 10.9 | 16 | 23.0 | 1.6 | 7.1 |
| Northeastern Africa (Egypt) | Combined | 25 | 49.3 | 3.5 | 7.2 | 23 | 55.4 | 4.1 | 7.4 | 24 | 20.7 | 1.9 | 9.4 | 23 | 23.9 | 2.1 | 8.7 |
| | M | 14 | 51.6 | 2.4 | 4.6 | 14 | 57.8 | 3.0 | 5.2 | 13 | 21.4 | 1.6 | 7.6 | 12 | 25.0 | 1.8 | 7.1 |
| | F | 11 | 46.4 | 2.4 | 5.1 | 9 | 51.8 | 2.6 | 5.1 | 11 | 19.9 | 2.1 | 10.3 | 11 | 22.6 | 1.7 | 7.3 |
| Levant (Jordan) | Combined | 15 | 50.2 | 2.7 | 5.4 | 13 | 55.5 | 3.3 | 6.0 | 15 | 21.4 | 2.4 | 11.3 | 15 | 24.1 | 1.9 | 7.9 |
| | M | 7 | 51.2 | 2.4 | 4.8 | 5 | 56.0 | 2.1 | 3.7 | 7 | 22.1 | 2.0 | 9.1 | 7 | 24.5 | 2.2 | 8.8 |
| | F | 1 | 47.3 | – | – | 1 | 53.5 | – | – | 1 | 19.5 | – | – | 1 | 21.8 | – | – |
| Western Europe (Portugal) | Combined | 30 | 52.3 | 4.8 | 9.2 | 30 | 57.3 | 5.1 | 8.9 | 27 | 23.1 | 2.7 | 11.9 | 30 | 24.9 | 3.0 | 11.9 |
| | M | 15 | 55.8 | 3.5 | 6.2 | 15 | 61.1 | 3.3 | 5.4 | 14 | 24.0 | 2.1 | 8.8 | 15 | 26.6 | 2.2 | 8.4 |
| | F | 15 | 48.8 | 3.2 | 6.5 | 15 | 53.5 | 3.3 | 6.2 | 13 | 22.0 | 3.1 | 13.9 | 15 | 23.2 | 2.6 | 11.1 |
| North America (CA, U.S.A.) | Combined | 30 | 50.7 | 3.5 | 6.9 | 30 | 55.2 | 4.1 | 7.4 | 30 | 23.0 | 1.8 | 7.9 | 31 | 25.0 | 1.7 | 6.7 |
| | M | 14 | 53.3 | 3.1 | 5.8 | 14 | 58.1 | 3.3 | 5.7 | 14 | 24.1 | 1.9 | 7.8 | 14 | 25.9 | 1.6 | 6.4 |
| | F | 16 | 48.4 | 1.9 | 3.9 | 16 | 52.6 | 2.7 | 5.1 | 16 | 22.0 | 1.0 | 4.6 | 17 | 24.2 | 1.3 | 5.4 |

**Table A9.47, Continued** Summary statistics for measurements of the talus

| | | Talus | | | | | | | | | | | | | | | |
|---|---|---|---|---|---|---|---|---|---|---|---|---|---|---|---|---|---|
| | | TAL5_ART_BRE | | | | TAL6_MAL_BRE | | | | TAL7_HEA_LEN | | | | TAL8_TRO_HEI | | | |
| **Sample** | **Sex** | **N** | **Mean** | **SD** | **CV** | **N** | **Mean** | **SD** | **CV** | **N** | **Mean** | **SD** | **CV** | **N** | **Mean** | **SD** | **CV** |
| Southern Africa (Zulu) | Combined | 32 | 29.7 | 2.2 | 7.4 | 31 | 10.9 | 1.4 | 12.6 | 32 | 30.5 | 2.8 | 9.4 | 32 | 9.3 | 1.3 | 14.1 |
| | M | 16 | 30.9 | 2.2 | 7.0 | 16 | 11.1 | 1.4 | 13.0 | 16 | 32.0 | 2.2 | 7.0 | 16 | 9.9 | 1.2 | 12.4 |
| | F | 16 | 28.4 | 1.4 | 5.1 | 15 | 10.7 | 1.3 | 12.5 | 16 | 28.9 | 2.5 | 8.8 | 16 | 8.7 | 1.2 | 13.4 |
| Northeastern Africa (Egypt) | Combined | 25 | 30.0 | 2.4 | 8.0 | 17 | 10.3 | 1.4 | 13.5 | 22 | 31.4 | 2.8 | 8.8 | 22 | 8.8 | 1.0 | 10.8 |
| | M | 14 | 31.4 | 2.2 | 7.0 | 10 | 10.3 | 1.5 | 14.5 | 12 | 32.7 | 2.7 | 8.3 | 12 | 9.2 | 1.0 | 10.8 |
| | F | 11 | 28.3 | 1.3 | 4.5 | 7 | 10.4 | 1.3 | 13.0 | 10 | 29.9 | 2.0 | 6.8 | 10 | 8.3 | 0.7 | 8.0 |
| Levant (Jordan) | Combined | 14 | 31.2 | 1.9 | 6.2 | 9 | 11.6 | 1.3 | 11.3 | 12 | 33.2 | 1.9 | 5.8 | 14 | 8.8 | 0.8 | 9.1 |
| | M | 6 | 32.2 | 1.4 | 4.3 | 3 | 11.5 | 1.3 | 11.1 | 4 | 33.9 | 1.9 | 5.5 | 6 | 9.0 | 0.9 | 10.5 |
| | F | 1 | 28.6 | – | – | 0 | – | – | – | 1 | 30.4 | – | – | 1 | 10.0 | – | – |
| Western Europe (Portugal) | Combined | 30 | 30.4 | 2.6 | 8.5 | 28 | 11.1 | 2.1 | 18.6 | 29 | 31.3 | 3.2 | 10.3 | 27 | 8.8 | 1.4 | 16.3 |
| | M | 15 | 32.2 | 2.1 | 6.6 | 15 | 11.9 | 2.1 | 17.4 | 14 | 33.5 | 3.0 | 9.0 | 14 | 9.3 | 1.5 | 16.4 |
| | F | 15 | 28.7 | 1.6 | 5.6 | 13 | 10.2 | 1.7 | 16.7 | 15 | 29.2 | 1.6 | 5.6 | 13 | 8.2 | 1.1 | 13.9 |
| North America (CA, U.S.A.) | Combined | 31 | 31.5 | 1.8 | 5.6 | 27 | 12.4 | 0.9 | 7.3 | 30 | 31.5 | 2.3 | 7.3 | 29 | 10.3 | 1.0 | 9.5 |
| | M | 14 | 33.2 | 1.0 | 3.1 | 13 | 12.5 | 0.9 | 7.1 | 14 | 33.1 | 2.2 | 6.6 | 13 | 10.9 | 1.0 | 8.8 |
| | F | 17 | 30.1 | 0.8 | 2.8 | 14 | 12.4 | 0.9 | 7.7 | 16 | 30.1 | 1.2 | 4.0 | 16 | 9.8 | 0.7 | 6.7 |

**Table A9.47, Continued** Summary statistics for measurements of the talus

| | | Talus | | | | | | | | | | | | | | | |
|---|---|---|---|---|---|---|---|---|---|---|---|---|---|---|---|---|---|
| | | TAL9_ML_WID | | | | TAL10_AP_TRO | | | | TAL11_ML_HEA | | | | TAL12_LEN_FAC | | | |
| **Sample** | **Sex** | **N** | **Mean** | **SD** | **CV** | **N** | **Mean** | **SD** | **CV** | **N** | **Mean** | **SD** | **CV** | **N** | **Mean** | **SD** | **CV** |
| Southern Africa (Zulu) | Combined | 32 | 41.0 | 2.8 | 6.8 | 32 | 31.3 | 2.7 | 8.6 | 32 | 27.6 | 2.8 | 10.0 | 31 | 30.5 | 2.3 | 7.7 |
| | M | 16 | 42.7 | 2.4 | 5.7 | 16 | 33.1 | 1.9 | 5.6 | 16 | 29.2 | 2.5 | 8.6 | 15 | 32.0 | 2.1 | 6.6 |
| | F | 16 | 39.2 | 1.9 | 4.9 | 16 | 29.6 | 2.2 | 7.5 | 16 | 26.1 | 2.2 | 8.3 | 16 | 29.2 | 1.7 | 5.9 |
| Northeastern Africa (Egypt) | Combined | 19 | 40.7 | 3.2 | 7.9 | 25 | 32.3 | 2.9 | 9.0 | 21 | 27.8 | 2.4 | 8.7 | 17 | 30.3 | 2.2 | 7.1 |
| | M | 12 | 42.4 | 2.6 | 6.1 | 14 | 33.9 | 2.4 | 7.2 | 11 | 29.0 | 2.1 | 7.2 | 10 | 31.1 | 2.2 | 7.2 |
| | F | 7 | 38.0 | 2.1 | 5.5 | 11 | 30.4 | 2.3 | 7.5 | 10 | 26.4 | 2.1 | 7.8 | 7 | 29.1 | 1.5 | 5.1 |
| Levant (Jordan) | Combined | 11 | 42.7 | 3.0 | 6.9 | 15 | 32.3 | 1.7 | 5.2 | 11 | 29.0 | 2.1 | 7.2 | 10 | 32.0 | 2.9 | 9.1 |
| | M | 3 | 43.2 | 2.2 | 5.0 | 7 | 32.8 | 2.1 | 6.5 | 3 | 29.4 | 1.1 | 3.6 | 2 | 32.5 | 2.5 | 7.8 |
| | F | 1 | 38.5 | – | – | 1 | 30.4 | – | – | 1 | 26.3 | – | – | 3 | 29.2 | 0.5 | 1.6 |
| Western Europe (Portugal) | Combined | 28 | 41.5 | 3.5 | 8.4 | 30 | 33.3 | 3.8 | 11.4 | 29 | 27.9 | 2.5 | 9.1 | 30 | 30.9 | 2.7 | 8.8 |
| | M | 15 | 43.7 | 2.6 | 6.0 | 15 | 35.8 | 2.7 | 7.6 | 14 | 29.5 | 2.2 | 7.5 | 15 | 33.0 | 1.8 | 5.3 |
| | F | 13 | 39.0 | 2.6 | 6.6 | 15 | 30.8 | 2.9 | 9.4 | 15 | 26.4 | 1.9 | 7.0 | 15 | 28.9 | 1.8 | 6.3 |
| North America (CA, U.S.A.) | Combined | 29 | 43.4 | 2.6 | 5.9 | 29 | 30.1 | 2.7 | 9.1 | 29 | 27.7 | 2.6 | 9.4 | 28 | 32.1 | 2.3 | 7.2 |
| | M | 14 | 44.8 | 2.0 | 4.5 | 14 | 31.5 | 2.5 | 7.8 | 13 | 29.9 | 1.7 | 5.5 | 13 | 34.1 | 1.4 | 4.1 |
| | F | 15 | 42.1 | 2.4 | 5.8 | 15 | 28.7 | 2.3 | 8.1 | 16 | 26.0 | 1.8 | 7.0 | 15 | 30.4 | 1.4 | 4.5 |

**Table A9.48** Summary statistics for measurements of the calcaneus

| | | Calcaneus | | | | | | | | | | | | | | | |
|---|---|---|---|---|---|---|---|---|---|---|---|---|---|---|---|---|---|
| | | CAL1_LEN | | | | CAL2_POS_LEN | | | | CAL3_MED_BRE | | | | CAL4_HEI_BOD | | | |
| **Sample** | **Sex** | **N** | **Mean** | **SD** | **CV** | **N** | **Mean** | **SD** | **CV** | **N** | **Mean** | **SD** | **CV** | **N** | **Mean** | **SD** | **CV** |
| Southern Africa (Zulu) | Combined | 32 | 77.5 | 4.2 | 5.4 | 32 | 55.9 | 3.1 | 5.6 | 31 | 40.9 | 3.2 | 7.9 | 31 | 41.9 | 3.1 | 7.3 |
| | M | 16 | 79.7 | 4.2 | 5.2 | 16 | 56.7 | 3.7 | 6.6 | 16 | 42.6 | 3.0 | 7.0 | 16 | 43.4 | 3.2 | 7.5 |
| | F | 16 | 75.3 | 3.0 | 3.9 | 16 | 55.1 | 2.2 | 4.0 | 15 | 39.0 | 2.3 | 5.9 | 15 | 40.3 | 1.9 | 4.7 |
| Northeastern Africa (Egypt) | Combined | 23 | 77.7 | 5.9 | 7.5 | 23 | 54.6 | 4.7 | 8.6 | 24 | 39.5 | 2.6 | 6.7 | 21 | 41.1 | 3.0 | 7.4 |
| | M | 12 | 81.3 | 4.4 | 5.4 | 12 | 57.2 | 3.6 | 6.3 | 13 | 41.0 | 2.2 | 5.3 | 11 | 42.8 | 2.9 | 6.9 |
| | F | 11 | 73.8 | 4.7 | 6.4 | 11 | 51.8 | 4.1 | 7.9 | 11 | 37.7 | 1.9 | 5.1 | 10 | 39.2 | 1.8 | 4.7 |
| Levant (Jordan) | Combined | 16 | 78.2 | 5.1 | 6.5 | 17 | 55.7 | 3.8 | 6.7 | 15 | 41.5 | 2.4 | 5.9 | 4 | 38.1 | 2.1 | 5.6 |
| | M | 5 | 80.9 | 5.8 | 7.1 | 6 | 56.6 | 3.7 | 6.6 | 5 | 43.3 | 1.6 | 3.8 | 1 | 39.4 | – | – |
| | F | 2 | 73.8 | 7.6 | 10.3 | 2 | 52.4 | 7.7 | 14.7 | 1 | 37.3 | – | – | 2 | 36.4 | 1.2 | 3.3 |
| Western Europe (Portugal) | Combined | 29 | 79.8 | 7.5 | 9.4 | 30 | 57.0 | 4.6 | 8.1 | 30 | 40.1 | 3.6 | 8.9 | 26 | 43.8 | 3.6 | 8.2 |
| | M | 15 | 84.1 | 6.3 | 7.4 | 15 | 59.2 | 3.6 | 6.0 | 15 | 42.7 | 2.8 | 6.6 | 14 | 45.7 | 3.3 | 7.3 |
| | F | 14 | 75.2 | 5.8 | 7.8 | 15 | 54.8 | 4.6 | 8.5 | 15 | 37.5 | 2.1 | 5.5 | 12 | 41.6 | 2.6 | 6.2 |
| North America (CA, U.S.A.) | Combined | 31 | 78.5 | 4.7 | 6.0 | 32 | 55.7 | 4.1 | 7.4 | 33 | 41.0 | 2.3 | 5.6 | 31 | 44.7 | 3.1 | 7.0 |
| | M | 16 | 82.0 | 3.5 | 4.2 | 16 | 58.8 | 3.0 | 5.1 | 17 | 42.2 | 2.4 | 5.8 | 16 | 47.1 | 2.1 | 4.4 |
| | F | 15 | 74.7 | 2.3 | 3.0 | 16 | 52.6 | 2.3 | 4.4 | 16 | 39.7 | 1.3 | 3.3 | 15 | 42.1 | 1.5 | 3.6 |

**Table A9.48, Continued** Summary statistics for measurements of the calcaneus

| | | Calcaneus | | | |
|---|---|---|---|---|---|
| | | CAL5_MIN_BRE | | | |
| **Sample** | **Sex** | **N** | **Mean** | **SD** | **CV** |
| Southern Africa (Zulu) | Combined | 32 | 28.6 | 3.0 | 10.4 |
| | M | 16 | 30.1 | 3.2 | 10.5 |
| | F | 16 | 27.2 | 2.0 | 7.3 |
| Northeastern Africa (Egypt) | Combined | 23 | 28.2 | 1.9 | 6.9 |
| | M | 12 | 29.0 | 2.0 | 7.1 |
| | F | 11 | 27.3 | 1.5 | 5.3 |
| Levant (Jordan) | Combined | 13 | 29.1 | 2.3 | 7.7 |
| | M | 3 | 31.8 | 2.4 | 7.5 |
| | F | 2 | 27.3 | 0.6 | 2.3 |
| Western Europe (Portugal) | Combined | 30 | 27.2 | 2.8 | 10.3 |
| | M | 15 | 28.9 | 2.7 | 9.2 |
| | F | 15 | 25.5 | 1.8 | 7.0 |
| North America (CA, U.S.A.) | Combined | 29 | 28.1 | 2.0 | 7.0 |
| | M | 16 | 28.9 | 2.0 | 7.0 |
| | F | 13 | 27.2 | 1.4 | 5.2 |

**Table A9.49** Summary statistics for measurements of the cuboid

| | | Cuboid | | | | | | | | | | | | | | | |
|---|---|---|---|---|---|---|---|---|---|---|---|---|---|---|---|---|---|
| | | CUB1_MAX_BRE | | | | CUB2_MAX_LEN | | | | CUB3_MAX_HEI | | | | CUB4_CAL_FAC | | | |
| **Sample** | **Sex** | **N** | **Mean** | **SD** | **CV** | **N** | **Mean** | **SD** | **CV** | **N** | **Mean** | **SD** | **CV** | **N** | **Mean** | **SD** | **CV** |
| Southern Africa (Zulu) | Combined | 32 | 27.4 | 1.8 | 6.6 | 30 | 36.1 | 2.8 | 7.8 | 33 | 24.6 | 1.9 | 7.7 | 31 | 25.6 | 2.2 | 8.6 |
| | M | 15 | 27.9 | 1.9 | 6.9 | 15 | 37.5 | 2.7 | 7.2 | 16 | 25.6 | 1.9 | 7.4 | 15 | 26.3 | 2.5 | 9.4 |
| | F | 17 | 26.9 | 1.6 | 5.9 | 15 | 34.7 | 2.2 | 6.4 | 17 | 23.8 | 1.5 | 6.2 | 16 | 25.0 | 1.8 | 7.1 |
| Northeastern Africa (Egypt) | Combined | 16 | 27.5 | 2.4 | 8.9 | 19 | 35.7 | 2.9 | 8.0 | 18 | 24.7 | 2.1 | 8.6 | 16 | 25.6 | 2.5 | 9.6 |
| | M | 9 | 28.7 | 2.6 | 8.9 | 11 | 37.5 | 2.5 | 6.7 | 10 | 26.1 | 1.8 | 7.0 | 10 | 27.0 | 1.9 | 7.2 |
| | F | 7 | 25.9 | 0.8 | 3.3 | 8 | 33.4 | 1.1 | 3.2 | 8 | 23.0 | 0.8 | 3.4 | 6 | 23.2 | 0.8 | 3.5 |
| Levant (Jordan) | Combined | 14 | 27.8 | 1.5 | 5.3 | 17 | 36.0 | 3.2 | 8.8 | 17 | 25.2 | 1.5 | 6.0 | 11 | 26.6 | 2.1 | 8.1 |
| | M | 3 | 28.7 | 0.7 | 2.5 | 5 | 37.8 | 2.6 | 6.9 | 5 | 25.9 | 1.3 | 4.9 | 2 | 27.9 | 0.5 | 1.8 |
| | F | 2 | 26.3 | 2.0 | 7.5 | 3 | 33.4 | 3.5 | 10.5 | 3 | 23.3 | 1.5 | 6.3 | 2 | 24.1 | 1.3 | 5.3 |
| Western Europe (Portugal) | Combined | 29 | 28.2 | 2.9 | 10.3 | 30 | 37.5 | 3.7 | 9.8 | 30 | 25.1 | 2.1 | 8.4 | 29 | 25.4 | 2.2 | 8.8 |
| | M | 14 | 30.1 | 2.4 | 7.9 | 15 | 39.6 | 3.2 | 8.0 | 15 | 26.6 | 1.5 | 5.8 | 14 | 26.9 | 1.8 | 6.9 |
| | F | 15 | 26.4 | 2.1 | 8.0 | 15 | 35.3 | 2.8 | 7.8 | 15 | 23.7 | 1.6 | 6.7 | 15 | 24.0 | 1.6 | 6.7 |
| North America (CA, U.S.A.) | Combined | 20 | 28.4 | 2.6 | 9.0 | 20 | 36.4 | 2.6 | 7.1 | 20 | 24.2 | 2.2 | 9.0 | 17 | 27.7 | 2.2 | 7.8 |
| | M | 8 | 30.3 | 2.6 | 8.5 | 8 | 38.4 | 2.9 | 7.5 | 8 | 25.8 | 2.0 | 7.6 | 7 | 29.5 | 1.7 | 5.7 |
| | F | 12 | 27.1 | 1.6 | 6.0 | 12 | 35.1 | 1.2 | 3.5 | 12 | 23.2 | 1.7 | 7.1 | 10 | 26.5 | 1.5 | 5.6 |

**Table A9.50** Summary statistics for measurements of the navicular

| | | Navicular | | | | | | | | | | | | | | | |
|---|---|---|---|---|---|---|---|---|---|---|---|---|---|---|---|---|---|
| | | NAV1_MAX_BRE | | | | NAV2_MAX_LEN | | | | NAV3_MAX_HEI | | | | NAV4_TAL_FAC | | | |
| **Sample** | **Sex** | **N** | **Mean** | **SD** | **CV** | **N** | **Mean** | **SD** | **CV** | **N** | **Mean** | **SD** | **CV** | **N** | **Mean** | **SD** | **CV** |
| Southern Africa (Zulu) | Combined | 32 | 39.6 | 3.0 | 7.5 | 32 | 21.1 | 1.7 | 8.2 | 32 | 27.1 | 2.4 | 8.9 | 32 | 27.5 | 2.2 | 7.8 |
| | M | 15 | 40.8 | 2.7 | 6.6 | 15 | 21.4 | 1.8 | 8.5 | 15 | 28.0 | 2.3 | 8.3 | 15 | 28.7 | 1.9 | 6.5 |
| | F | 17 | 38.5 | 2.8 | 7.4 | 17 | 20.8 | 1.6 | 7.9 | 17 | 26.2 | 2.2 | 8.3 | 17 | 26.4 | 1.8 | 6.9 |
| Northeastern Africa (Egypt) | Combined | 19 | 39.2 | 2.5 | 6.4 | 18 | 21.8 | 2.1 | 9.8 | 19 | 28.0 | 3.1 | 11.2 | 18 | 27.3 | 2.1 | 7.6 |
| | M | 11 | 40.1 | 2.0 | 5.1 | 11 | 22.7 | 2.2 | 9.5 | 11 | 28.6 | 3.7 | 13.1 | 11 | 28.3 | 1.8 | 6.5 |
| | F | 8 | 38.1 | 2.8 | 7.2 | 7 | 20.4 | 1.3 | 6.2 | 8 | 27.3 | 2.1 | 7.7 | 7 | 25.6 | 1.3 | 5.2 |
| Levant (Jordan) | Combined | 15 | 39.3 | 2.5 | 6.3 | 17 | 21.5 | 1.9 | 8.7 | 17 | 28.6 | 0.9 | 3.2 | 15 | 28.7 | 2.7 | 9.4 |
| | M | 4 | 41.1 | 1.3 | 3.3 | 5 | 22.2 | 2.4 | 11.0 | 5 | 28.8 | 1.0 | 3.6 | 5 | 28.9 | 2.0 | 7.0 |
| | F | 3 | 36.7 | 1.3 | 3.6 | 3 | 20.3 | 1.2 | 6.1 | 3 | 28.4 | 1.1 | 4.0 | 2 | 25.7 | 0.6 | 2.2 |
| Western Europe (Portugal) | Combined | 26 | 39.3 | 3.3 | 8.4 | 30 | 21.3 | 2.2 | 10.2 | 28 | 26.3 | 2.5 | 9.4 | 29 | 27.6 | 2.7 | 9.6 |
| | M | 14 | 41.3 | 2.9 | 7.0 | 15 | 22.5 | 2.1 | 9.3 | 14 | 27.9 | 2.0 | 7.2 | 14 | 29.6 | 2.3 | 7.9 |
| | F | 12 | 36.9 | 1.8 | 4.8 | 15 | 20.2 | 1.6 | 7.9 | 14 | 24.6 | 1.7 | 6.8 | 15 | 25.9 | 1.4 | 5.4 |
| North America (CA, U.S.A.) | Combined | 23 | 38.8 | 2.7 | 7.0 | 22 | 20.5 | 1.8 | 8.9 | 21 | 29.4 | 3.1 | 10.4 | 24 | 28.1 | 1.8 | 6.5 |
| | M | 12 | 39.7 | 3.1 | 7.7 | 12 | 20.9 | 2.0 | 9.6 | 12 | 29.8 | 3.9 | 13.0 | 13 | 29.2 | 1.4 | 4.9 |
| | F | 11 | 37.8 | 1.9 | 5.1 | 10 | 19.9 | 1.5 | 7.5 | 9 | 28.9 | 1.5 | 5.1 | 11 | 26.9 | 1.5 | 5.5 |

**Table A9.51** Summary statistics for measurements of the first metatarsal

| | | First metatarsal | | | | | | | | | | | | | | | |
|---|---|---|---|---|---|---|---|---|---|---|---|---|---|---|---|---|---|
| | | MT1_LEN | | | | MT2_BIO_LEN | | | | MT3_MID_DP | | | | MT4_MID_ML | | | |
| **Sample** | **Sex** | **N** | **Mean** | **SD** | **CV** | **N** | **Mean** | **SD** | **CV** | **N** | **Mean** | **SD** | **CV** | **N** | **Mean** | **SD** | **CV** |
| Southern Africa (Zulu) | Combined | 33 | 62.0 | 3.8 | 6.1 | 33 | 59.4 | 3.6 | 6.1 | 33 | 13.4 | 0.9 | 6.4 | 33 | 13.6 | 1.1 | 7.9 |
| | M | 16 | 63.3 | 4.5 | 7.2 | 16 | 60.6 | 4.3 | 7.1 | 16 | 13.7 | 0.9 | 6.3 | 16 | 14.2 | 1.0 | 6.9 |
| | F | 17 | 60.8 | 2.4 | 4.0 | 17 | 58.2 | 2.5 | 4.3 | 17 | 13.1 | 0.8 | 5.8 | 17 | 13.1 | 0.9 | 6.8 |
| Northeastern Africa (Egypt) | Combined | 20 | 61.0 | 4.6 | 7.5 | 21 | 58.9 | 4.1 | 7.0 | 20 | 12.1 | 1.4 | 11.2 | 20 | 13.0 | 1.4 | 10.6 |
| | M | 12 | 63.7 | 3.2 | 5.0 | 12 | 61.2 | 2.8 | 4.6 | 11 | 13.0 | 1.0 | 7.7 | 11 | 13.9 | 1.1 | 8.3 |
| | F | 8 | 57.1 | 3.3 | 5.7 | 9 | 55.8 | 3.5 | 6.3 | 9 | 11.0 | 0.8 | 7.4 | 9 | 11.9 | 0.6 | 5.4 |
| Levant (Jordan) | Combined | 12 | 58.4 | 4.2 | 7.1 | 13 | 56.7 | 3.8 | 6.8 | 13 | 13.0 | 1.1 | 8.6 | 13 | 13.6 | 1.1 | 7.7 |
| | M | 3 | 61.7 | 6.2 | 10.0 | 4 | 59.5 | 4.8 | 8.0 | 4 | 13.3 | 1.3 | 10.1 | 4 | 14.1 | 1.3 | 9.6 |
| | F | 3 | 56.9 | 4.7 | 8.3 | 3 | 55.1 | 4.5 | 8.2 | 3 | 13.0 | 0.8 | 5.9 | 3 | 12.9 | 0.8 | 5.9 |
| Western Europe (Portugal) | Combined | 29 | 62.5 | 4.8 | 7.7 | 30 | 59.4 | 4.6 | 7.8 | 30 | 13.4 | 1.5 | 10.9 | 30 | 13.3 | 1.6 | 12.0 |
| | M | 15 | 65.0 | 3.9 | 6.1 | 15 | 61.8 | 3.9 | 6.3 | 15 | 14.2 | 1.2 | 8.6 | 15 | 14.4 | 1.0 | 7.0 |
| | F | 14 | 59.9 | 4.3 | 7.2 | 15 | 57.0 | 4.1 | 7.1 | 15 | 12.5 | 1.2 | 9.4 | 15 | 12.2 | 1.3 | 10.8 |
| North America (CA, U.S.A.) | Combined | 26 | 60.8 | 4.4 | 7.3 | 26 | 58.1 | 4.2 | 7.2 | 26 | 13.2 | 1.1 | 8.5 | 26 | 13.7 | 1.2 | 8.9 |
| | M | 12 | 63.8 | 3.8 | 5.9 | 12 | 60.7 | 3.7 | 6.2 | 12 | 13.8 | 1.2 | 8.5 | 12 | 14.3 | 1.3 | 9.0 |
| | F | 14 | 58.3 | 3.3 | 5.7 | 14 | 55.8 | 3.2 | 5.7 | 14 | 12.6 | 0.6 | 5.2 | 14 | 13.1 | 0.9 | 6.5 |

**Table A9.51, Continued** Summary statistics for measurements of the first metatarsal

| | | First metatarsal | | | | | | | | | | | | | | | |
|---|---|---|---|---|---|---|---|---|---|---|---|---|---|---|---|---|---|
| | | MT5_PRO_HEI | | | | MT6_PRO_BRE | | | | MT7_DIS_HEI | | | | MT8_DIS_BRE | | | |
| **Sample** | **Sex** | **N** | **Mean** | **SD** | **CV** | **N** | **Mean** | **SD** | **CV** | **N** | **Mean** | **SD** | **CV** | **N** | **Mean** | **SD** | **CV** |
| Southern Africa (Zulu) | Combined | 32 | 28.0 | 1.9 | 6.8 | 32 | 19.5 | 1.6 | 8.3 | 33 | 19.0 | 1.3 | 7.0 | 33 | 20.8 | 1.4 | 6.9 |
| | M | 16 | 29.2 | 1.7 | 5.9 | 16 | 20.6 | 1.4 | 6.8 | 16 | 19.7 | 1.0 | 5.2 | 16 | 21.7 | 1.2 | 5.6 |
| | F | 16 | 26.9 | 1.3 | 4.9 | 16 | 18.5 | 1.0 | 5.3 | 17 | 18.3 | 1.2 | 6.6 | 17 | 20.0 | 1.1 | 5.6 |
| Northeastern Africa (Egypt) | Combined | 20 | 27.6 | 2.0 | 7.4 | 14 | 19.9 | 1.9 | 9.8 | 19 | 18.5 | 1.8 | 9.5 | 18 | 20.5 | 1.6 | 7.7 |
| | M | 11 | 28.9 | 1.3 | 4.4 | 8 | 20.9 | 1.9 | 9.2 | 11 | 19.6 | 1.4 | 7.3 | 10 | 21.6 | 1.1 | 5.0 |
| | F | 9 | 26.0 | 1.6 | 6.2 | 6 | 18.6 | 1.0 | 5.2 | 8 | 17.0 | 0.7 | 4.1 | 8 | 19.2 | 0.9 | 4.5 |
| Levant (Jordan) | Combined | 11 | 28.1 | 1.7 | 6.0 | 8 | 19.9 | 1.4 | 7.2 | 13 | 19.2 | 2.1 | 10.9 | 13 | 21.0 | 1.8 | 8.5 |
| | M | 3 | 29.3 | 1.1 | 3.7 | 1 | 21.9 | – | – | 4 | 21.3 | 1.9 | 9.1 | 4 | 22.5 | 2.1 | 9.5 |
| | F | 3 | 27.3 | 1.5 | 5.4 | 2 | 19.2 | 1.1 | 5.5 | 3 | 17.2 | 1.8 | 10.5 | 3 | 19.8 | 0.8 | 3.9 |
| Western Europe (Portugal) | Combined | 29 | 28.9 | 2.3 | 7.9 | 29 | 20.0 | 1.8 | 9.0 | 29 | 19.6 | 1.8 | 9.1 | 27 | 21.4 | 1.9 | 8.8 |
| | M | 14 | 30.5 | 1.6 | 5.4 | 14 | 21.3 | 1.2 | 5.8 | 14 | 20.8 | 1.4 | 6.6 | 13 | 22.2 | 1.4 | 6.5 |
| | F | 15 | 27.3 | 1.6 | 5.7 | 15 | 18.8 | 1.3 | 7.2 | 15 | 18.4 | 1.3 | 7.1 | 14 | 20.6 | 1.9 | 9.3 |
| North America (CA, U.S.A.) | Combined | 24 | 28.1 | 1.9 | 6.9 | 21 | 20.3 | 1.7 | 8.2 | 25 | 21.6 | 1.7 | 8.0 | 24 | 21.7 | 1.7 | 7.7 |
| | M | 12 | 29.2 | 2.0 | 7.0 | 10 | 21.2 | 1.4 | 6.8 | 13 | 22.7 | 1.6 | 7.0 | 12 | 22.8 | 1.5 | 6.7 |
| | F | 12 | 26.9 | 1.0 | 3.6 | 11 | 19.5 | 1.5 | 7.6 | 12 | 20.4 | 0.8 | 4.1 | 12 | 20.7 | 1.0 | 5.0 |

**Table A9.52** Summary statistics for measurements of the second metatarsal

| | | Second metatarsal | | | | | | | | | | | | | | | |
|---|---|---|---|---|---|---|---|---|---|---|---|---|---|---|---|---|---|
| | | MT1_LEN | | | | MT2_BIO_LEN | | | | MT3_MID_DP | | | | MT4_MID_ML | | | |
| **Sample** | **Sex** | **N** | **Mean** | **SD** | **CV** | **N** | **Mean** | **SD** | **CV** | **N** | **Mean** | **SD** | **CV** | **N** | **Mean** | **SD** | **CV** |
| Southern Africa (Zulu) | Combined | 33 | 73.8 | 4.2 | 5.7 | 33 | 70.6 | 3.9 | 5.6 | 33 | 9.0 | 1.0 | 10.9 | 33 | 8.1 | 1.1 | 13.6 |
| | M | 16 | 75.0 | 5.1 | 6.8 | 16 | 71.7 | 4.8 | 6.7 | 16 | 9.2 | 1.1 | 12.0 | 16 | 8.6 | 1.2 | 13.7 |
| | F | 17 | 72.7 | 2.9 | 3.9 | 17 | 69.5 | 2.6 | 3.7 | 17 | 8.8 | 0.8 | 9.3 | 17 | 7.7 | 0.8 | 10.6 |
| Northeastern Africa (Egypt) | Combined | 19 | 74.7 | 6.0 | 8.0 | 19 | 71.2 | 6.1 | 8.6 | 19 | 8.6 | 0.9 | 10.2 | 19 | 7.9 | 0.7 | 9.5 |
| | M | 11 | 77.8 | 4.5 | 5.8 | 11 | 74.3 | 4.9 | 6.6 | 11 | 9.1 | 0.7 | 7.9 | 11 | 8.1 | 0.7 | 8.7 |
| | F | 8 | 70.3 | 5.1 | 7.3 | 8 | 66.8 | 4.9 | 7.4 | 8 | 8.0 | 0.6 | 7.5 | 8 | 7.6 | 0.8 | 10.1 |
| Levant (Jordan) | Combined | 12 | 71.3 | 3.4 | 4.8 | 12 | 67.6 | 3.1 | 4.6 | 12 | 8.6 | 0.7 | 8.7 | 12 | 7.8 | 0.6 | 7.4 |
| | M | 3 | 73.3 | 1.9 | 2.7 | 3 | 68.5 | 1.8 | 2.7 | 3 | 9.0 | 0.8 | 9.1 | 3 | 8.0 | 0.3 | 4.0 |
| | F | 3 | 68.3 | 3.8 | 5.6 | 3 | 65.4 | 4.3 | 6.5 | 3 | 8.3 | 0.5 | 6.4 | 3 | 7.1 | 0.3 | 4.0 |
| Western Europe (Portugal) | Combined | 30 | 74.1 | 5.5 | 7.4 | 30 | 70.2 | 5.4 | 7.8 | 30 | 8.9 | 0.9 | 10.5 | 30 | 7.6 | 1.0 | 12.9 |
| | M | 15 | 76.8 | 5.4 | 7.0 | 15 | 72.9 | 5.5 | 7.5 | 15 | 9.1 | 1.0 | 11.5 | 15 | 7.8 | 1.1 | 13.9 |
| | F | 15 | 71.3 | 4.0 | 5.6 | 15 | 67.4 | 4.0 | 5.9 | 15 | 8.7 | 0.8 | 9.2 | 15 | 7.4 | 0.9 | 11.7 |
| North America (CA, U.S.A.) | Combined | 24 | 74.0 | 4.0 | 5.4 | 24 | 70.6 | 3.8 | 5.3 | 24 | 9.1 | 0.6 | 6.8 | 24 | 8.1 | 0.8 | 10.1 |
| | M | 11 | 75.9 | 4.5 | 5.9 | 11 | 72.3 | 4.3 | 5.9 | 11 | 9.3 | 0.7 | 7.2 | 11 | 8.1 | 0.9 | 11.6 |
| | F | 13 | 72.5 | 2.9 | 4.1 | 13 | 69.2 | 2.6 | 3.8 | 13 | 8.9 | 0.5 | 5.6 | 13 | 8.0 | 0.7 | 9.2 |

**Table A9.52, Continued** Summary statistics for measurements of the second metatarsal

| | | Second metatarsal | | | | | | | | | | | | | | | |
|---|---|---|---|---|---|---|---|---|---|---|---|---|---|---|---|---|---|
| | | MT5_PRO_HEI | | | | MT6_PRO_BRE | | | | MT7_DIS_HEI | | | | MT8_DIS_BRE | | | |
| **Sample** | **Sex** | **N** | **Mean** | **SD** | **CV** | **N** | **Mean** | **SD** | **CV** | **N** | **Mean** | **SD** | **CV** | **N** | **Mean** | **SD** | **CV** |
| Southern Africa (Zulu) | Combined | 33 | 20.1 | 1.7 | 8.4 | 33 | 14.8 | 1.3 | 8.8 | 33 | 14.8 | 1.0 | 7.1 | 33 | 11.5 | 1.1 | 9.4 |
| | M | 16 | 21.1 | 1.7 | 8.2 | 16 | 15.1 | 1.3 | 8.7 | 16 | 15.2 | 1.0 | 6.5 | 16 | 11.6 | 1.3 | 10.9 |
| | F | 17 | 19.3 | 1.1 | 5.6 | 17 | 14.4 | 1.2 | 8.5 | 17 | 14.4 | 0.9 | 6.6 | 17 | 11.5 | 0.9 | 8.1 |
| Northeastern Africa (Egypt) | Combined | 14 | 19.9 | 1.6 | 8.0 | 17 | 15.7 | 1.8 | 11.2 | 18 | 14.5 | 1.5 | 10.3 | 18 | 11.8 | 1.2 | 10.0 |
| | M | 8 | 20.9 | 1.1 | 5.1 | 10 | 16.7 | 1.7 | 10.2 | 10 | 15.5 | 1.1 | 7.0 | 10 | 12.5 | 0.9 | 7.1 |
| | F | 6 | 18.6 | 1.1 | 5.8 | 7 | 14.4 | 0.6 | 3.9 | 8 | 13.3 | 0.9 | 6.6 | 8 | 10.9 | 0.9 | 8.1 |
| Levant (Jordan) | Combined | 10 | 20.4 | 1.2 | 5.7 | 12 | 15.8 | 1.3 | 8.2 | 11 | 14.7 | 1.5 | 10.0 | 11 | 11.7 | 0.8 | 6.6 |
| | M | 2 | 20.6 | 0.4 | 2.1 | 3 | 16.3 | 0.5 | 3.0 | 2 | 16.1 | 0.9 | 5.7 | 2 | 12.0 | 0.6 | 5.3 |
| | F | 2 | 18.4 | 0.3 | 1.5 | 3 | 14.4 | 1.2 | 8.0 | 3 | 13.5 | 1.2 | 9.2 | 3 | 11.6 | 0.9 | 8.0 |
| Western Europe (Portugal) | Combined | 29 | 20.8 | 1.8 | 8.5 | 29 | 16.1 | 1.7 | 10.4 | 30 | 15.0 | 1.5 | 10.2 | 29 | 11.6 | 1.1 | 9.2 |
| | M | 14 | 22.1 | 1.7 | 7.5 | 14 | 16.9 | 1.7 | 9.9 | 15 | 16.1 | 1.2 | 7.3 | 15 | 11.7 | 1.2 | 9.9 |
| | F | 15 | 19.7 | 1.0 | 4.9 | 15 | 15.4 | 1.4 | 9.0 | 15 | 14.0 | 1.0 | 7.3 | 14 | 11.4 | 1.0 | 8.5 |
| North America (CA, U.S.A.) | Combined | 23 | 21.5 | 1.3 | 6.1 | 25 | 16.0 | 1.0 | 6.5 | 21 | 15.7 | 1.5 | 9.6 | 23 | 12.1 | 0.9 | 7.2 |
| | M | 11 | 22.2 | 1.3 | 5.9 | 12 | 16.6 | 0.9 | 5.6 | 10 | 16.6 | 1.6 | 9.8 | 11 | 12.4 | 1.0 | 7.9 |
| | F | 12 | 20.8 | 0.9 | 4.4 | 13 | 15.4 | 0.8 | 5.2 | 11 | 14.9 | 0.8 | 5.1 | 12 | 11.8 | 0.6 | 5.5 |

**Table A9.53** Summary statistics for measurements of the third metatarsal

| | | Third metatarsal | | | | | | | | | | | | | | | |
|---|---|---|---|---|---|---|---|---|---|---|---|---|---|---|---|---|---|
| | | MT1_LEN | | | | MT2_BIO_LEN | | | | MT3_MID_DP | | | | MT4_MID_ML | | | |
| **Sample** | **Sex** | **N** | **Mean** | **SD** | **CV** | **N** | **Mean** | **SD** | **CV** | **N** | **Mean** | **SD** | **CV** | **N** | **Mean** | **SD** | **CV** |
| Southern Africa (Zulu) | Combined | 33 | 70.3 | 4.1 | 5.9 | 33 | 68.3 | 4.0 | 5.9 | 33 | 9.1 | 0.9 | 9.8 | 33 | 7.8 | 0.8 | 10.1 |
| | M | 16 | 71.4 | 4.9 | 6.8 | 16 | 69.1 | 4.8 | 7.0 | 16 | 9.4 | 1.1 | 11.1 | 16 | 8.1 | 0.8 | 9.9 |
| | F | 17 | 69.3 | 3.1 | 4.4 | 17 | 67.5 | 3.1 | 4.6 | 17 | 8.8 | 0.6 | 7.0 | 17 | 7.5 | 0.6 | 8.6 |
| Northeastern Africa (Egypt) | Combined | 18 | 69.0 | 5.6 | 8.2 | 18 | 67.1 | 5.8 | 8.7 | 17 | 8.4 | 0.9 | 11.0 | 17 | 7.4 | 0.7 | 9.5 |
| | M | 10 | 72.6 | 4.8 | 6.6 | 10 | 70.9 | 4.8 | 6.7 | 10 | 9.0 | 0.8 | 8.8 | 10 | 7.6 | 0.6 | 7.5 |
| | F | 8 | 64.4 | 2.2 | 3.4 | 8 | 62.3 | 2.5 | 4.0 | 7 | 7.7 | 0.5 | 6.6 | 7 | 7.0 | 0.8 | 10.9 |
| Levant (Jordan) | Combined | 11 | 67.6 | 4.8 | 7.1 | 11 | 65.5 | 4.8 | 7.3 | 11 | 9.1 | 1.1 | 12.0 | 11 | 7.9 | 0.4 | 5.5 |
| | M | 3 | 71.5 | 4.0 | 5.6 | 3 | 69.9 | 4.0 | 5.8 | 3 | 10.2 | 0.9 | 8.9 | 3 | 7.9 | 0.5 | 6.2 |
| | F | 3 | 64.5 | 4.6 | 7.1 | 3 | 62.3 | 4.5 | 7.2 | 3 | 8.1 | 0.6 | 7.4 | 3 | 7.8 | 0.4 | 4.8 |
| Western Europe (Portugal) | Combined | 29 | 68.8 | 5.4 | 7.9 | 29 | 66.7 | 5.5 | 8.2 | 29 | 8.8 | 0.9 | 10.6 | 29 | 7.1 | 0.8 | 11.7 |
| | M | 15 | 71.3 | 5.4 | 7.5 | 15 | 69.2 | 5.5 | 7.9 | 15 | 9.1 | 1.0 | 11.4 | 15 | 7.5 | 0.9 | 11.6 |
| | F | 14 | 66.1 | 4.1 | 6.2 | 14 | 64.1 | 4.2 | 6.5 | 14 | 8.5 | 0.7 | 8.4 | 14 | 6.7 | 0.5 | 7.8 |
| North America (CA, U.S.A.) | Combined | 26 | 70.1 | 4.1 | 5.8 | 26 | 68.3 | 3.9 | 5.7 | 26 | 9.2 | 0.8 | 8.3 | 26 | 7.4 | 0.7 | 9.3 |
| | M | 13 | 71.5 | 4.4 | 6.2 | 13 | 69.6 | 4.3 | 6.1 | 13 | 9.3 | 0.8 | 8.5 | 13 | 7.5 | 0.7 | 8.7 |
| | F | 13 | 68.7 | 3.4 | 4.9 | 13 | 67.1 | 3.1 | 4.6 | 13 | 9.0 | 0.7 | 8.0 | 13 | 7.4 | 0.7 | 10.1 |

**Table A9.53, Continued** Summary statistics for measurements of the third metatarsal

| | | Third metatarsal | | | | | | | | | | | | | | | |
|---|---|---|---|---|---|---|---|---|---|---|---|---|---|---|---|---|---|
| | | MT5_PRO_HEI | | | | MT6_PRO_BRE | | | | MT7_DIS_HEI | | | | MT8_DIS_BRE | | | |
| **Sample** | **Sex** | **N** | **Mean** | **SD** | **CV** | **N** | **Mean** | **SD** | **CV** | **N** | **Mean** | **SD** | **CV** | **N** | **Mean** | **SD** | **CV** |
| Southern Africa (Zulu) | Combined | 31 | 19.5 | 1.6 | 8.1 | 32 | 13.9 | 1.1 | 8.1 | 33 | 14.5 | 1.1 | 7.4 | 33 | 10.1 | 0.8 | 8.1 |
| | M | 16 | 20.4 | 1.6 | 7.7 | 16 | 14.1 | 1.2 | 8.8 | 16 | 15.1 | 1.0 | 6.8 | 16 | 10.3 | 1.0 | 9.6 |
| | F | 15 | 18.5 | 0.9 | 4.7 | 16 | 13.8 | 1.0 | 7.5 | 17 | 13.9 | 0.7 | 5.2 | 17 | 10.0 | 0.6 | 6.4 |
| Northeastern Africa (Egypt) | Combined | 16 | 19.4 | 1.3 | 6.7 | 19 | 14.0 | 1.6 | 11.3 | 18 | 13.7 | 1.2 | 8.8 | 15 | 10.2 | 1.0 | 9.5 |
| | M | 9 | 20.1 | 1.2 | 6.2 | 11 | 14.9 | 1.5 | 9.8 | 10 | 14.4 | 0.8 | 5.5 | 9 | 10.7 | 0.9 | 8.8 |
| | F | 7 | 18.4 | 0.6 | 3.0 | 8 | 12.8 | 0.6 | 4.9 | 8 | 12.8 | 1.0 | 7.6 | 6 | 9.6 | 0.6 | 6.3 |
| Levant (Jordan) | Combined | 12 | 20.3 | 1.4 | 6.8 | 13 | 14.3 | 1.1 | 7.5 | 12 | 14.0 | 1.2 | 8.9 | 12 | 10.7 | 0.7 | 6.8 |
| | M | 3 | 20.8 | 1.0 | 4.7 | 4 | 15.1 | 1.1 | 7.6 | 3 | 14.9 | 0.9 | 6.0 | 3 | 11.2 | 0.2 | 1.5 |
| | F | 3 | 19.4 | 2.3 | 12.0 | 3 | 13.4 | 1.1 | 8.5 | 3 | 13.1 | 1.6 | 12.6 | 3 | 10.5 | 0.6 | 5.4 |
| Western Europe (Portugal) | Combined | 29 | 20.0 | 1.7 | 8.6 | 30 | 14.0 | 1.2 | 8.9 | 25 | 14.6 | 1.5 | 10.1 | 26 | 10.2 | 0.9 | 8.4 |
| | M | 15 | 21.0 | 1.6 | 7.4 | 15 | 14.3 | 1.2 | 8.3 | 13 | 15.6 | 1.1 | 6.9 | 14 | 10.3 | 1.0 | 9.6 |
| | F | 14 | 18.9 | 1.1 | 5.9 | 15 | 13.7 | 1.3 | 9.2 | 12 | 13.5 | 0.9 | 6.9 | 12 | 10.0 | 0.7 | 6.9 |
| North America (CA, U.S.A.) | Combined | 24 | 21.4 | 1.5 | 7.2 | 26 | 14.0 | 1.0 | 7.4 | 24 | 15.2 | 1.2 | 7.8 | 26 | 10.8 | 0.7 | 6.7 |
| | M | 13 | 22.0 | 1.6 | 7.1 | 14 | 14.3 | 1.0 | 6.8 | 12 | 15.8 | 1.3 | 8.3 | 13 | 11.0 | 0.9 | 7.9 |
| | F | 11 | 20.7 | 1.2 | 5.9 | 12 | 13.5 | 1.0 | 7.1 | 12 | 14.7 | 0.8 | 5.2 | 13 | 10.5 | 0.4 | 4.2 |

**Table A9.54** Summary statistics for measurements of the fourth metatarsal

| | | Fourth metatarsal | | | | | | | | | | | | | | | |
|---|---|---|---|---|---|---|---|---|---|---|---|---|---|---|---|---|---|
| | | MT1_LEN | | | | MT2_BIO_LEN | | | | MT3_MID_DP | | | | MT4_MID_ML | | | |
| **Sample** | **Sex** | **N** | **Mean** | **SD** | **CV** | **N** | **Mean** | **SD** | **CV** | **N** | **Mean** | **SD** | **CV** | **N** | **Mean** | **SD** | **CV** |
| Southern Africa (Zulu) | Combined | 33 | 68.8 | 4.5 | 6.5 | 33 | 66.3 | 4.1 | 6.2 | 33 | 10.0 | 1.0 | 10.5 | 33 | 8.0 | 1.0 | 12.1 |
| | M | 16 | 69.7 | 4.9 | 7.0 | 16 | 67.0 | 4.7 | 7.0 | 16 | 10.4 | 1.3 | 12.4 | 16 | 8.3 | 1.1 | 13.7 |
| | F | 17 | 67.9 | 4.1 | 6.0 | 17 | 65.7 | 3.5 | 5.3 | 17 | 9.7 | 0.7 | 6.8 | 17 | 7.8 | 0.7 | 8.9 |
| Northeastern Africa (Egypt) | Combined | 19 | 67.9 | 5.3 | 7.9 | 19 | 65.7 | 5.4 | 8.2 | 19 | 9.1 | 1.0 | 10.7 | 19 | 7.8 | 0.8 | 10.8 |
| | M | 11 | 71.3 | 4.0 | 5.6 | 11 | 69.2 | 3.9 | 5.6 | 11 | 9.3 | 1.1 | 11.6 | 11 | 8.2 | 0.8 | 9.2 |
| | F | 8 | 63.2 | 2.6 | 4.0 | 8 | 60.8 | 2.3 | 3.8 | 8 | 8.9 | 0.8 | 9.3 | 8 | 7.3 | 0.7 | 9.0 |
| Levant (Jordan) | Combined | 11 | 65.3 | 5.0 | 7.7 | 13 | 63.3 | 4.9 | 7.7 | 13 | 9.5 | 1.1 | 12.1 | 13 | 8.5 | 0.9 | 10.8 |
| | M | 4 | 68.2 | 4.5 | 6.6 | 4 | 66.5 | 4.4 | 6.6 | 4 | 9.9 | 0.4 | 3.8 | 4 | 9.1 | 0.9 | 10.2 |
| | F | 1 | 59.8 | – | – | 3 | 60.1 | 3.1 | 5.2 | 3 | 10.1 | 2.1 | 21.0 | 3 | 8.2 | 0.7 | 8.0 |
| Western Europe (Portugal) | Combined | 29 | 66.9 | 5.2 | 7.7 | 29 | 64.6 | 4.8 | 7.4 | 29 | 9.3 | 1.0 | 10.9 | 29 | 7.9 | 1.1 | 13.5 |
| | M | 14 | 69.6 | 4.6 | 6.7 | 14 | 66.9 | 4.4 | 6.6 | 14 | 9.6 | 1.3 | 13.0 | 14 | 8.3 | 1.0 | 12.1 |
| | F | 15 | 64.5 | 4.5 | 7.0 | 15 | 62.4 | 4.1 | 6.6 | 15 | 9.1 | 0.7 | 7.6 | 15 | 7.5 | 1.0 | 13.7 |
| North America (CA, U.S.A.) | Combined | 25 | 68.1 | 4.0 | 5.9 | 25 | 66.3 | 3.8 | 5.7 | 24 | 9.0 | 0.7 | 8.3 | 24 | 8.0 | 0.8 | 9.8 |
| | M | 12 | 69.3 | 4.7 | 6.8 | 12 | 67.6 | 4.4 | 6.6 | 12 | 9.2 | 0.7 | 7.5 | 12 | 8.2 | 0.9 | 10.4 |
| | F | 13 | 66.9 | 2.9 | 4.4 | 13 | 65.0 | 2.6 | 4.0 | 12 | 8.8 | 0.8 | 8.8 | 12 | 7.8 | 0.7 | 8.9 |

**Table A9.54, Continued** Summary statistics for measurements of the fourth metatarsal

| | | Fourth metatarsal | | | | | | | | | | | | | | | |
|---|---|---|---|---|---|---|---|---|---|---|---|---|---|---|---|---|---|
| | | MT5_PRO_HEI | | | | MT6_PRO_BRE | | | | MT7_DIS_HEI | | | | MT8_DIS_BRE | | | |
| **Sample** | **Sex** | **N** | **Mean** | **SD** | **CV** | **N** | **Mean** | **SD** | **CV** | **N** | **Mean** | **SD** | **CV** | **N** | **Mean** | **SD** | **CV** |
| Southern Africa (Zulu) | Combined | 33 | 17.4 | 1.5 | 8.9 | 33 | 13.5 | 1.0 | 7.1 | 33 | 13.6 | 1.1 | 7.9 | 33 | 10.1 | 0.8 | 7.6 |
| | M | 16 | 18.2 | 1.6 | 8.6 | 16 | 13.6 | 1.1 | 8.3 | 16 | 14.2 | 1.0 | 7.2 | 16 | 10.3 | 1.0 | 9.3 |
| | F | 17 | 16.7 | 1.2 | 7.2 | 17 | 13.4 | 0.8 | 5.9 | 17 | 13.0 | 0.8 | 5.8 | 17 | 9.9 | 0.5 | 5.0 |
| Northeastern Africa (Egypt) | Combined | 20 | 17.5 | 1.9 | 10.8 | 21 | 13.0 | 1.4 | 11.0 | 17 | 13.1 | 1.2 | 9.1 | 17 | 10.1 | 1.1 | 11.0 |
| | M | 12 | 18.2 | 2.0 | 11.0 | 12 | 13.5 | 1.3 | 10.0 | 9 | 13.8 | 0.9 | 6.3 | 9 | 10.5 | 1.1 | 10.2 |
| | F | 8 | 16.4 | 1.0 | 6.1 | 9 | 12.3 | 1.3 | 10.4 | 8 | 12.3 | 0.9 | 7.6 | 8 | 9.7 | 1.1 | 11.0 |
| Levant (Jordan) | Combined | 12 | 17.7 | 1.2 | 6.6 | 13 | 13.2 | 0.7 | 5.6 | 12 | 14.0 | 1.5 | 10.6 | 11 | 10.6 | 0.6 | 5.9 |
| | M | 4 | 19.0 | 1.0 | 5.0 | 5 | 13.4 | 0.7 | 5.0 | 4 | 14.7 | 0.6 | 3.8 | 4 | 11.1 | 0.3 | 2.9 |
| | F | 2 | 17.0 | 0.0 | 0.0 | 2 | 12.5 | 1.3 | 10.8 | 2 | 13.4 | 2.0 | 14.8 | 1 | 10.6 | – | – |
| Western Europe (Portugal) | Combined | 26 | 17.3 | 1.4 | 8.2 | 28 | 13.7 | 1.4 | 10.2 | 22 | 13.8 | 1.3 | 9.5 | 23 | 10.0 | 0.8 | 8.5 |
| | M | 14 | 18.0 | 0.9 | 4.8 | 14 | 14.6 | 1.3 | 9.0 | 13 | 14.5 | 1.1 | 7.5 | 13 | 10.1 | 0.8 | 8.3 |
| | F | 12 | 16.5 | 1.5 | 9.3 | 14 | 12.8 | 0.9 | 6.7 | 9 | 12.7 | 0.8 | 6.3 | 10 | 9.7 | 0.9 | 8.8 |
| North America (CA, U.S.A.) | Combined | 27 | 18.4 | 1.6 | 8.8 | 28 | 13.7 | 1.3 | 9.4 | 23 | 14.6 | 1.4 | 9.8 | 23 | 10.4 | 0.8 | 8.0 |
| | M | 12 | 19.5 | 1.7 | 8.8 | 13 | 14.2 | 1.4 | 10.0 | 12 | 15.3 | 1.5 | 9.8 | 12 | 10.7 | 0.9 | 8.6 |
| | F | 15 | 17.5 | 0.9 | 4.9 | 15 | 13.3 | 1.0 | 7.8 | 11 | 13.8 | 0.8 | 6.1 | 11 | 10.0 | 0.5 | 4.9 |

**Table A9.55** Summary statistics for measurements of the fifth metatarsal

| | | Fifth metatarsal | | | | | | | | | | | | | | | |
|---|---|---|---|---|---|---|---|---|---|---|---|---|---|---|---|---|---|
| | | MT1_LEN | | | | MT2_BIO_LEN | | | | MT3_MID_DP | | | | MT4_MID_ML | | | |
| **Sample** | **Sex** | **N** | **Mean** | **SD** | **CV** | **N** | **Mean** | **SD** | **CV** | **N** | **Mean** | **SD** | **CV** | **N** | **Mean** | **SD** | **CV** |
| Southern Africa (Zulu) | Combined | 33 | 69.1 | 4.5 | 6.6 | 33 | 62.6 | 4.0 | 6.4 | 33 | 9.7 | 1.1 | 10.9 | 33 | 9.9 | 0.9 | 9.4 |
| | M | 16 | 70.7 | 4.6 | 6.5 | 16 | 63.5 | 4.7 | 7.3 | 16 | 10.2 | 1.1 | 10.7 | 16 | 9.9 | 0.8 | 7.8 |
| | F | 17 | 67.7 | 4.2 | 6.2 | 17 | 61.7 | 3.2 | 5.2 | 17 | 9.2 | 0.7 | 7.9 | 17 | 9.9 | 1.1 | 11.0 |
| Northeastern Africa (Egypt) | Combined | 20 | 69.2 | 5.6 | 8.1 | 20 | 61.9 | 4.8 | 7.7 | 19 | 8.5 | 0.8 | 9.7 | 20 | 9.5 | 1.4 | 15.0 |
| | M | 11 | 72.8 | 3.8 | 5.2 | 11 | 64.4 | 3.6 | 5.7 | 10 | 8.6 | 0.7 | 8.7 | 11 | 10.2 | 1.2 | 11.6 |
| | F | 9 | 64.9 | 4.3 | 6.7 | 9 | 58.7 | 4.2 | 7.2 | 9 | 8.4 | 0.9 | 11.3 | 9 | 8.7 | 1.3 | 14.9 |
| Levant (Jordan) | Combined | 11 | 63.7 | 3.7 | 5.7 | 11 | 57.6 | 3.9 | 6.8 | 11 | 8.7 | 0.8 | 9.7 | 11 | 9.6 | 1.0 | 10.5 |
| | M | 2 | 65.6 | 3.3 | 5.0 | 2 | 59.3 | 0.1 | 0.2 | 2 | 9.2 | 0.8 | 8.5 | 2 | 9.6 | 0.4 | 3.7 |
| | F | 3 | 61.2 | 2.7 | 4.5 | 3 | 55.7 | 4.7 | 8.3 | 3 | 9.4 | 0.5 | 4.9 | 3 | 8.7 | 1.2 | 14.1 |
| Western Europe (Portugal) | Combined | 26 | 68.5 | 6.2 | 9.1 | 29 | 60.7 | 5.1 | 8.5 | 29 | 8.0 | 1.0 | 12.8 | 29 | 10.6 | 1.3 | 12.3 |
| | M | 14 | 71.5 | 5.7 | 8.0 | 14 | 63.3 | 4.7 | 7.4 | 14 | 8.5 | 1.0 | 11.8 | 14 | 11.4 | 1.3 | 11.7 |
| | F | 12 | 65.0 | 4.9 | 7.5 | 15 | 58.4 | 4.5 | 7.7 | 15 | 7.5 | 0.8 | 10.9 | 15 | 9.8 | 0.7 | 6.8 |
| North America (CA, U.S.A.) | Combined | 27 | 68.1 | 4.0 | 5.8 | 28 | 62.2 | 3.1 | 4.9 | 28 | 8.4 | 0.9 | 10.8 | 28 | 9.7 | 1.0 | 9.9 |
| | M | 12 | 70.5 | 4.2 | 6.0 | 13 | 63.9 | 3.2 | 5.1 | 13 | 9.1 | 0.9 | 10.0 | 13 | 10.0 | 1.1 | 10.6 |
| | F | 15 | 66.2 | 2.6 | 3.9 | 15 | 60.7 | 2.1 | 3.4 | 15 | 7.9 | 0.4 | 5.1 | 15 | 9.4 | 0.8 | 8.1 |

**Table A9.55, Continued** Summary statistics for measurements of the fifth metatarsal

| | | Fifth metatarsal | | | | | | | | | | | | | | | |
|---|---|---|---|---|---|---|---|---|---|---|---|---|---|---|---|---|---|
| | | MT5_PRO_HEI | | | | MT6_PRO_BRE | | | | MT7_DIS_HEI | | | | MT8_DIS_BRE | | | |
| **Sample** | **Sex** | **N** | **Mean** | **SD** | **CV** | **N** | **Mean** | **SD** | **CV** | **N** | **Mean** | **SD** | **CV** | **N** | **Mean** | **SD** | **CV** |
| Southern Africa (Zulu) | Combined | 33 | 14.2 | 1.5 | 10.3 | 33 | 18.9 | 1.7 | 9.2 | 32 | 12.7 | 1.1 | 8.4 | 32 | 10.7 | 1.1 | 10.0 |
| | M | 16 | 15.0 | 1.5 | 10.1 | 16 | 19.1 | 2.1 | 10.8 | 16 | 13.2 | 1.1 | 8.5 | 16 | 10.8 | 1.1 | 10.5 |
| | F | 17 | 13.5 | 1.1 | 7.8 | 17 | 18.6 | 1.4 | 7.3 | 16 | 12.1 | 0.7 | 6.0 | 16 | 10.7 | 1.0 | 9.7 |
| Northeastern Africa (Egypt) | Combined | 20 | 13.9 | 1.4 | 9.7 | 20 | 18.3 | 2.1 | 11.3 | 18 | 12.4 | 1.4 | 11.5 | 19 | 10.7 | 1.0 | 9.6 |
| | M | 11 | 14.5 | 1.2 | 8.6 | 11 | 19.1 | 2.1 | 10.9 | 10 | 13.1 | 1.4 | 10.3 | 10 | 11.1 | 1.1 | 10.0 |
| | F | 9 | 13.2 | 1.1 | 8.4 | 9 | 17.3 | 1.6 | 9.5 | 8 | 11.5 | 1.0 | 8.7 | 9 | 10.2 | 0.7 | 6.9 |
| Levant (Jordan) | Combined | 13 | 14.9 | 0.9 | 5.9 | 13 | 18.6 | 1.6 | 8.3 | 11 | 12.8 | 1.8 | 13.9 | 11 | 11.1 | 0.8 | 6.8 |
| | M | 4 | 15.1 | 0.6 | 4.2 | 4 | 18.6 | 1.2 | 6.3 | 2 | 13.1 | 0.3 | 2.2 | 2 | 10.7 | 0.1 | 1.3 |
| | F | 3 | 14.5 | 0.7 | 5.1 | 3 | 17.5 | 0.9 | 4.9 | 3 | 11.9 | 2.7 | 22.4 | 3 | 11.7 | 0.7 | 6.0 |
| Western Europe (Portugal) | Combined | 27 | 14.4 | 1.5 | 10.7 | 28 | 19.0 | 2.3 | 12.2 | 16 | 12.7 | 1.3 | 10.1 | 18 | 11.2 | 1.2 | 10.6 |
| | M | 14 | 15.2 | 1.5 | 9.7 | 14 | 19.9 | 2.3 | 11.7 | 10 | 13.2 | 1.1 | 8.6 | 10 | 11.8 | 1.0 | 8.9 |
| | F | 13 | 13.5 | 1.0 | 7.7 | 14 | 18.1 | 2.0 | 11.0 | 6 | 11.8 | 1.0 | 8.3 | 8 | 10.4 | 0.9 | 8.8 |
| North America (CA, U.S.A.) | Combined | 29 | 15.1 | 1.3 | 8.8 | 28 | 19.6 | 1.7 | 8.9 | 24 | 13.6 | 1.1 | 8.4 | 26 | 11.2 | 0.9 | 8.1 |
| | M | 13 | 16.1 | 1.2 | 7.2 | 12 | 21.0 | 1.7 | 8.3 | 11 | 14.5 | 0.6 | 4.5 | 12 | 11.8 | 0.9 | 7.3 |
| | F | 16 | 14.3 | 0.8 | 5.4 | 16 | 18.5 | 0.7 | 3.9 | 13 | 12.9 | 0.9 | 7.2 | 14 | 10.7 | 0.6 | 5.7 |

**Table A9.56** Summary statistics for measurements of the terminal foot phalanx of ray I

| | | Terminal foot phalanx of first ray | | | | | | | | | | | | | | | |
|---|---|---|---|---|---|---|---|---|---|---|---|---|---|---|---|---|---|
| | | TFP1_LEN | | | | TFP2_BIO_LEN | | | | TFP3_MID_AP | | | | TFP4_MID_ML | | | |
| **Sample** | **Sex** | **N** | **Mean** | **SD** | **CV** | **N** | **Mean** | **SD** | **CV** | **N** | **Mean** | **SD** | **CV** | **N** | **Mean** | **SD** | **CV** |
| Southern Africa (Zulu) | Combined | 31 | 23.5 | 1.7 | 7.3 | 31 | 21.1 | 1.5 | 7.0 | 31 | 7.5 | 1.0 | 13.2 | 31 | 9.5 | 1.2 | 12.7 |
| | M | 15 | 24.4 | 1.7 | 7.1 | 15 | 21.8 | 1.5 | 6.7 | 15 | 7.7 | 1.0 | 13.5 | 15 | 10.3 | 0.8 | 8.0 |
| | F | 16 | 22.6 | 1.2 | 5.3 | 16 | 20.5 | 1.2 | 6.0 | 16 | 7.4 | 1.0 | 12.9 | 16 | 8.7 | 1.0 | 11.0 |
| Northeastern Africa (Egypt) | Combined | 12 | 24.6 | 1.9 | 7.8 | 14 | 22.7 | 2.1 | 9.3 | 14 | 6.6 | 0.6 | 9.3 | 14 | 10.0 | 1.1 | 10.9 |
| | M | 8 | 25.3 | 1.9 | 7.6 | 10 | 23.4 | 2.0 | 8.7 | 10 | 6.7 | 0.6 | 9.1 | 10 | 10.3 | 1.1 | 10.5 |
| | F | 4 | 23.1 | 0.8 | 3.4 | 4 | 20.9 | 0.9 | 4.2 | 4 | 6.2 | 0.5 | 8.0 | 4 | 9.1 | 0.3 | 3.6 |
| Levant (Jordan) | Combined | 11 | 24.6 | 1.3 | 5.1 | 11 | 22.2 | 1.2 | 5.6 | 11 | 6.2 | 0.8 | 12.2 | 11 | 10.2 | 0.9 | 8.6 |
| | M | 3 | 23.7 | 0.8 | 3.4 | 3 | 21.7 | 0.4 | 1.7 | 3 | 6.3 | 0.9 | 14.7 | 3 | 10.5 | 0.4 | 4.2 |
| | F | 3 | 24.0 | 1.7 | 7.2 | 3 | 21.0 | 1.2 | 5.7 | 3 | 5.8 | 1.1 | 18.5 | 3 | 9.5 | 0.5 | 5.3 |
| Western Europe (Portugal) | Combined | 20 | 24.6 | 2.3 | 9.3 | 21 | 22.4 | 2.1 | 9.5 | 18 | 6.3 | 0.9 | 14.7 | 20 | 9.1 | 1.4 | 14.8 |
| | M | 10 | 25.9 | 1.7 | 6.4 | 10 | 23.6 | 1.3 | 5.6 | 8 | 6.3 | 1.2 | 19.0 | 9 | 9.8 | 1.5 | 15.7 |
| | F | 10 | 23.4 | 2.3 | 9.6 | 11 | 21.4 | 2.3 | 10.6 | 10 | 6.4 | 0.7 | 11.2 | 11 | 8.6 | 1.0 | 11.2 |
| North America (CA, U.S.A.) | Combined | 4 | 27.1 | 1.5 | 5.6 | 4 | 24.4 | 1.4 | 5.7 | 4 | 7.6 | 0.4 | 4.7 | 4 | 11.8 | 1.0 | 8.2 |
| | M | 3 | 27.7 | 1.1 | 4.0 | 3 | 25.0 | 0.6 | 2.4 | 3 | 7.5 | 0.4 | 4.8 | 3 | 11.7 | 1.2 | 9.9 |
| | F | 1 | 25.2 | – | – | 1 | 22.4 | – | – | 1 | 7.9 | – | – | 1 | 12.1 | – | – |

**Table A9.56, Continued** Summary statistics for measurements of the terminal foot phalanx of ray I

| | | Terminal foot phalanx of first ray | | | | | | | | | | | | | | | |
|---|---|---|---|---|---|---|---|---|---|---|---|---|---|---|---|---|---|
| | | TFP5_PRO_AP | | | | TFP6_PRO_ML | | | | TFP7_DIS_AP | | | | TFP8_DIS_ML | | | |
| **Sample** | **Sex** | **N** | **Mean** | **SD** | **CV** | **N** | **Mean** | **SD** | **CV** | **N** | **Mean** | **SD** | **CV** | **N** | **Mean** | **SD** | **CV** |
| Southern Africa (Zulu) | Combined | 31 | 10.0 | 0.8 | 8.4 | 31 | 18.6 | 1.4 | 7.6 | 31 | 6.6 | 0.9 | 13.2 | 31 | 12.0 | 1.4 | 11.5 |
| | M | 15 | 10.5 | 0.8 | 7.9 | 15 | 19.6 | 1.1 | 5.4 | 15 | 6.7 | 1.1 | 16.4 | 15 | 12.6 | 1.3 | 10.1 |
| | F | 16 | 9.5 | 0.5 | 5.2 | 16 | 17.7 | 1.0 | 5.5 | 16 | 6.4 | 0.6 | 8.7 | 16 | 11.6 | 1.3 | 11.5 |
| Northeastern Africa (Egypt) | Combined | 11 | 10.4 | 1.1 | 10.5 | 12 | 19.1 | 1.7 | 9.1 | 12 | 6.2 | 0.9 | 14.6 | 12 | 11.9 | 1.4 | 11.9 |
| | M | 7 | 11.0 | 0.8 | 7.1 | 8 | 19.8 | 1.3 | 6.5 | 8 | 6.4 | 1.0 | 16.2 | 8 | 12.4 | 1.4 | 11.5 |
| | F | 4 | 9.4 | 0.7 | 7.2 | 4 | 17.7 | 1.8 | 10.3 | 4 | 5.9 | 0.5 | 8.5 | 4 | 11.1 | 1.1 | 9.5 |
| Levant (Jordan) | Combined | 11 | 10.4 | 0.7 | 7.0 | 10 | 18.8 | 1.4 | 7.6 | 11 | 6.2 | 0.5 | 8.6 | 10 | 12.3 | 1.2 | 10.0 |
| | M | 3 | 10.5 | 1.0 | 9.6 | 2 | 18.2 | 0.8 | 4.3 | 3 | 6.3 | 0.3 | 4.8 | 2 | 12.2 | 0.1 | 0.6 |
| | F | 3 | 10.5 | 0.9 | 8.9 | 3 | 18.5 | 1.0 | 5.5 | 3 | 5.9 | 0.8 | 13.5 | 3 | 11.6 | 1.4 | 11.9 |
| Western Europe (Portugal) | Combined | 21 | 10.4 | 1.0 | 9.3 | 18 | 19.4 | 1.9 | 9.7 | 20 | 6.9 | 0.9 | 13.0 | 19 | 12.2 | 1.5 | 12.3 |
| | M | 11 | 10.8 | 0.9 | 8.3 | 11 | 20.1 | 1.9 | 9.5 | 10 | 7.1 | 1.0 | 14.5 | 10 | 12.8 | 1.5 | 11.9 |
| | F | 10 | 9.9 | 0.9 | 8.8 | 7 | 18.4 | 1.3 | 7.3 | 10 | 6.8 | 0.8 | 11.5 | 9 | 11.6 | 1.2 | 10.6 |
| North America (CA, U.S.A.) | Combined | 4 | 11.3 | 1.3 | 11.9 | 4 | 20.0 | 1.1 | 5.6 | 4 | 6.2 | 0.3 | 4.0 | 4 | 13.0 | 0.9 | 6.8 |
| | M | 3 | 11.6 | 1.5 | 12.7 | 3 | 20.2 | 1.3 | 6.3 | 3 | 6.2 | 0.3 | 4.8 | 3 | 13.0 | 1.1 | 8.3 |
| | F | 1 | 10.4 | – | – | 1 | 19.3 | – | – | 1 | 6.1 | – | – | 1 | 13.1 | – | – |